



**TECHNISCHE  
UNIVERSITÄT  
WIEN**

Vienna University of Technology

## **DISSERTATION**

# **"Porous Mo and Nb Preforms for Micro and Nanocrystalline Silicide - Refractory Metal Functionally Graded Materials"**

durchgeführt zum Zwecke der Erlangung des akademischen Grades einer Doktorin der technischen Wissenschaften unter der Leitung von

Univ.Prof. Dipl.-Ing. Dr.techn. Herbert Danninger  
E 164  
Institut für chemische Technologie und Analytik

Eingereicht an der Technischen Universität Wien  
Fakultät für Technische Chemie

durch  
Dipl.-Ing Ewa Dadal  
Matrikelnummer 0326049  
Davidgasse 41/12, 1100 Wien

Wien, am 3.3.2014





## Acknowledgment

I would like to begin by thanking the EU for enabling to start the SILTRANS Project and by supporting it with money. A very special word of thanks goes to my supervisor Prof. Danninger for giving me the opportunity to work on this project, for guiding and supporting me. Thank you for believing in me and for teaching me. At this point, I also want to thank my co-supervisor Dr. Christian Gierl-Mayer for his support in technical problems and his fruitful discussions about the work and the world.

Dr. Susanne Strobl I would like to thank for her help during metallographical sample preparation, during polishing and etching, and for her patient support during some experiments.

I want to thank also Wolfgang Tomischko for the repair work of the Bähr Dilatometer. Also for the new construction of the "semi automatic resistance meter" which enabled me and many other colleagues an easier measurement of conductivity of specimens.

For the measurement and characterisation by XRD of many specimens I want to thank DI Mariana Pantazi and Prof. Kubel.

The technical workshop, especially Marius Mayer and Johannes Frank, I would like to thank for the rebuilding of some furnaces and further equipment I needed during my work and for the provided grinding equipment.

Last but not least, a particularly thanks to the work groups "Hochleistungskeramik" and "Metallkunde" for the possibility of using their equipment like the CIP or some furnaces.

I would like to thank at that point my colleagues from the office, for a very funny time, a lot of laughing and for amusing lunch breaks. I want also to thank Maryam Jalilizyaeian for her helping hand during sample preparation and characterisation. Further on, I like to thank also my trainee Kinga Kaniewska, who came three times during summer holidays to help me in the lab. She learned very quickly, so it was possible to let her work independently which let me save a lot of time. Special thanks go to Armineh Avakemian, my dear friend, for her physical and mental support and for the very chilly lunch breaks in the park with her and Jessie (our lovely office dog). I'm really glad that I won such a lovely friend like her.

At least I want to thank my lovely family and my boyfriend Roman Hochenauer that they supported me very much during the last period of the PhD thesis, during the writing of the work. My parents cooked lunch for me and my boyfriend was taking care of running of our household so I could focus completely on my work.



## Kurzfassung

Ziel dieser Arbeit war das Herstellen von porösen Mo- und Nb-Vorkörpern, die in einem weiteren Schritt mit Si infiltriert werden können. Da beide Metalle zwar hochwarmfest, aber bei hohen Temperaturen nicht oxidationsbeständig sind, sollte durch die Infiltration und Reaktion mit Si eine gradierte Silizidschicht am Substrat aufgebaut werden, die es vor weiterer Oxidation schützt. Neben der Porengröße der offenen Poren im Probenkörper ist auch die spezifische Oberfläche ausschlaggebend für eine erfolgreiche Infiltration mit Silizium, da die Reaktion zwischen Molybdän und Silizium sehr exotherm verläuft. Im Weiteren ist wichtig, dass die Infiltration noch vor der Reaktion stattfindet, da sonst die Poren blockiert werden. Neben der Herstellung poröser Körper wurde auch die Reaktivität mit Si untersucht.

Die Versuche wurden mit einem kommerziell erhältlichen Mo-Pulver, das als ein Pulver mit Partikelgröße  $<63\mu\text{m}$  verkauft wurde, durchgeführt.

In den ersten Versuchen wurden Probenkörper über eine Press- und Sinterroute hergestellt. Diese wurden zur Charakterisierung des Einflusses von Pressdruck, Sinter Temperatur und der Pulverfraktion auf die Eigenschaften der Sinterkörper wie Dichte, offene Porosität oder die Härte untersucht. Sinterkörper, die 38 % offene Porosität aufwiesen, wurden an den Projektpartner ATL für CVI Versuche gesendet. Nach der Infiltration wurden die Proben mittels RFA auf ihren Si- und O-Gehalt an der TU Wien charakterisiert und wiesen einen Si Gehalt von 0,4-0,9 % Si im Querschnitt auf. Am Lichtmikroskop und am REM konnte man im Querschnitt sehen, dass die Probe nicht durchgängig mit Si infiltriert war. Nur am Rand wurde eine Silizidschicht identifiziert.

In weiteren Versuchen wurden auch Proben mit Gradientenporosität hergestellt. Dazu wurde das Mo-Pulver in Fraktionen gesiebt. Es stellte sich aber heraus, dass die nominell unterschiedlichen Fraktionen recht einheitlich aus sehr feinen Partikeln bestanden. Aus diesem Grund war es nicht möglich, eine Abgrenzung zwischen den Schichten in einer Probe zu erkennen, und somit auch war kein Unterschied in der Porengröße zu erkennen.

Der Einfluss von Nickel als Sinteraktivator wurde auch untersucht. Aus der Literatur war bereits bekannt, dass durch die Zugabe von Nickel die Sinter Temperatur und -dauer verkürzt werden können. Auf der anderen Seite darf nicht außer Acht gelassen werden, dass durch den Nickelzusatz die Hochtemperaturfestigkeit des Molybdäns verloren geht. Nichts desto trotz wurden Mo Proben mit 0,1 gew% Ni dotiert und die Auswirkung auf die Dichte, offene Porosität und Härte untersucht. Es wurden auch Mo-Proben mit höheren Ni-Gehalten untersucht und der Einfluss auf die physikalischen und mechanischen Eigenschaften des Materials untersucht. Durch die Dotierung mit unterschiedlichen Ni-Gehalten war es möglich, Mo-Proben mit stufenweiser Gradientenporosität herzustellen.

In weiteren Versuchen wurde ein organisches Wachs (Kenolube P11) als Platzhalter verwendet, das mit dem Mo Pulver mitgepresst, aber vor dem Sinterversuch durch einen Entbinderungsschritt wieder entfernt wurde. Somit wurden Proben mit großer und offener Porosität hergestellt. Es wurde beobachtet, dass zu hohe Gehalte an Wachs zu Rissbildung während des Entbinderns führten. So hergestellte Probenkörper wurden für Infiltrationsversuche zu ATL (für CVI) gesendet und danach wieder auf der TU Wien charakterisiert. Man konnte beobachten, dass die Proben kaum Si enthielten, was darauf zurückzuführen war, dass die offenen Poren immer noch zu klein waren und nicht genug Si eindringen konnte.

Des weiteren wurden auch Sinterversuche mit losen Pulverschüttungen durchgeführt. Das lose Mo-Pulver wurde dabei mit unterschiedlichen Ni-Gehalten in einem  $\text{Al}_2\text{O}_3$

Tiegel gesintert. So hergestellte Proben wurden an den Partner IMSAS für weitere Infiltrationsversuche gesendet, wobei die Probenkörper während der Infiltrationsversuche mit flüssigem Si komplett desintegrierten. Grund waren die zu schwachen Sinterkontakte und die hoch exotherme Reaktion zwischen Mo und Si.

Als eine Alternative wurde versucht, einen Mo-Metallschwamm herzustellen. Dabei wurde ein PU-Schwamm in eine Polymer - Metall Mischung eingetaucht, danach getrocknet und das Polymer durch einen anschließenden Sinterprozess zersetzt und die Metallstruktur verstärkt. Die resultierende Struktur zeigte jedoch kaum Zusammenhalt, da während der Zersetzung des Polymers ein Teil des Molybdäns zu Karbiden umgewandelt wurde.

In einem anderen Teil der Arbeit wurden Versuche zur Charakterisierung der Reaktivität zwischen Mo und Si durchgeführt. Dazu wurden Mo - Presslinge mit unterschiedlichen Gehalten an Si gepresst und mit einem Si - wafer auf der Oberfläche, der als Si-Quelle für Infiltration diente, gesintert. Die Proben waren jedoch nach der Infiltration sehr fragil. Weiters wurde die Reaktivität von Mo mit unterschiedlichen Si-Gehalten auf der DTA gemessen und ausgewertet. Exotherme Peaks kennzeichneten die Reaktion zwischen Mo und Si. Mit steigendem Si Gehalt wurden diese zu höheren Temperaturen verschoben und nahmen an Intensität zu.

Da gezeigt werden konnte, dass das drucklose Sintern keinen Erfolg brachte, wurden im weiteren Verlauf heißgepresste Probenkörper aus Mo und Si hergestellt und die physikalischen und mechanischen Eigenschaften charakterisiert. Es konnte gezeigt werden, dass das Heißpressen eine gute Methode ist, dichte Mo-Silizid Proben zu erzielen; auch gradierte Körper mit lokal variierendem Si-Gehalt ließen sich herstellen.

Bei weiteren Versuchen wurde ein sehr grobes Mo-Pulver verwendet, wodurch die spezifische Oberfläche der Mo-Körper verringert und die Dicke der Sinterkontakte erhöht werden kann. Für die ersten Versuche wurde ein grobes Pulver angekauft. Da Probenkörper aus dem groben Mo infiltriert werden konnten, ohne dass sie desintegrierten, wurde versucht, solch ein grobes Pulver selbst herzustellen. Dazu wurden Reduktionsversuche mit  $\text{MoO}_2$  zwischen 900 und 1100 °C in trockener und feuchter  $\text{H}_2$  Atmosphäre durchgeführt. Die resultierende Partikelgröße der Mo Partikel überschritt jedoch nicht  $\sim 5\mu\text{m}$ .

Aus früheren Versuchen für W war bekannt, dass geringe Mengen an LiOH nach der Reduktion zu größeren W Partikeln führen. Versuche, bei denen  $\text{MoO}_2$  mit LiOH dotiert und danach reduziert wurde, wurden durchgeführt. Auch hier war die resultierende Partikelgröße nicht höher als  $\sim 5\mu\text{m}$ . D.h. die Maßnahmen, die bei der Reduktion von W-Oxiden zu groben W-Pulvern führen, versagen bei Mo.

Es wurde auch die Oxidationsstabilität von Mo-Proben, die mit Si infiltriert wurden, in Verbrennungsgasen untersucht. Dabei wurden die von den Projektpartnern mit Si infiltrierten Proben bei 1100 °C und 3h Haltedauer Verbrennungsgasen ausgesetzt. Bei den meisten Proben war der Masserverlust höher als 19 gew%. Den geringsten Masseverlust hatte eine Probe, die aus gebündelten und anschließend infiltrierten Mo-Drähten bestand. Weiters wurden auch heißgepresste Mo-Si Proben, die zuvor auf der TUW hergestellt wurden, getestet. Den geringsten Masseverlust von 5% erlitten Proben, die den höchsten Gehalt an  $\text{MoSi}_2$  (37% Si) aufwiesen.

Neben Versuchen mit Mo wurden auch Nb-Probenkörper gesintert und charakterisiert, sowohl vor als auch nach den Infiltrationsversuchen. Auch hier wurden die meisten Proben bei der anschließenden Si-Infiltration aufgrund stark exothermer Reaktion zerstört. Es wurde auch die Reaktivität von Nb mit Si auf DTA/TG getestet, da Experimente zuvor zeigten, dass die Sinteraktivität sehr niedrig ist. Es konnte anhand der DTA Ergebnisse gezeigt werden, dass mit steigendem Si-Gehalt auch die Reaktivität stieg.

Aufgrund mangelnder Literatur über das Sinterverhalten von Mo, das gemeinsam mit Nb gesintert wird, wurden Untersuchungen durchgeführt, in denen der O- und C-Gehalt gesinterter Mo-Nb-Körper bestimmt wurde. Es konnte gezeigt werden, dass mit steigendem Gehalt an Nb in den Proben der gemessene Sauerstoffgehalt höher war. Grund dafür war der interne Gettereffekt, bei dem der Sauerstoff, der vom Mo kam, durch Nb gefangen wurde und so das Material nicht vollständig reduziert werden konnte.

Im Allgemeinen kann gesagt werden, dass die Herstellung von Mo- bzw. Nb-Vorkörpern mit gradierter Porosität, die durch eine Silizidschicht geschützt sind, prinzipiell möglich ist. Eine wichtige Voraussetzung dafür ist, dass die Vorkörper grobe Poren und eine niedrige spezifische Oberfläche haben, ansonsten kommt es während der Infiltration mit Si zu Desintegration aufgrund der stark exothermen Reaktion.



## Abstract

The aim of the work was the preparation of porous Mo and Nb bodies which could be infiltrated by Si. Both refractory metals suffer from poor oxidation resistance at high temperatures. By infiltration with Si and further reaction of Si with the substrate metal, a silicide protective layer was generated. For a successful infiltration not only the size of the open pores but also the specific surface is important, due to the strongly exothermic reaction between Mo and Si. The infiltration with Si has to take place before reaction. Beside the preparation of porous Mo and Nb preforms, also the reactivity with Si was investigated.

The work started with a Mo powder which was stored at TUW. It was a Plansee SE Mo powder with a particle size designated as  $<63\text{ }\mu\text{m}$ , but in fact virtually  $<25\text{ }\mu\text{m}$ . After the Mo powder from Plansee SE was consumed a very similar Mo powder from Chemie Metall was used. The powder shape and size were characterised by SEM.

The aim of the first experiments was to prepare specimens by the press-and-sinter route and to evaluate the influence of compacting pressure, sintering temperature and starting powder fraction on the properties of the sintered Mo specimens such as density, open porosity and hardness. Specimens which contained about 38 % open porosity were sent to the partner ATL for chemical vapour infiltration (CVI) and characterised on TUW for their Si and O content by XRF. About 0.4-0.9 % Si could be measured in the specimens but no continuous infiltrated cross section was observed on LOM or SEM. Only near the surface a silicide layer was observed.

Some Mo bodies with gradient porosity have also been prepared by building up a layer-structured specimen. The layers were prepared from powder fractions sieved from commercially available Mo powder (designated as  $\leq 63\text{ }\mu\text{m}$ ). Due to the fact, that the sieved powders contained mostly very fine particles of similar size, no interface between the layers was observed and therefore no difference in pore size between the layers.

Furthermore, the influence of Ni as sintering activator was investigated. It is well known from the literature that by doping Mo with Ni the sintering temperature and time required for a given sintering effect can be decreased. On the other hand Ni deteriorates the high temperature properties of Mo. Nevertheless, the influence of sintering temperature on density, open porosity and hardness were studied with a 0.1 wt% Ni doped Mo specimen. Furthermore also the influence of varying Ni content in Mo on physical and mechanical properties of the materials were investigated. By doping Mo with different amounts of Ni, layered specimens with stepwise graded porosity were prepared.

Infiltration experiments with liquid Si by IMSAS showed that the rapid formation of silicides tended to block the pores, thus preventing further infiltration. Furthermore, the highly exothermic and violent reaction easily resulted in disintegration of the Mo bodies. To enable Si infiltration of Mo bodies without blocking of pores, it was tried to increase the size of open pores in the Mo bodies, e.g. by introducing a space holder into the molybdenum specimens. An organic wax (Kenolube P11) was mixed with Mo in different ratios. After pressing of the specimens the wax was burnt out. The remaining porous structure was sintered afterwards to strengthen the interparticle contacts. The high amount of organic wax was detrimental resulting in cracks during debinding. The specimens thus prepared were sent to project partners for CVI (at ATL) and characterised after infiltration by TUW. Barely any Si or silicides could be measured in the cross section, which could be related to still too small and narrow open pores.

Beside the space holder method, loose powder (gravity) sintering was carried out. Mo powder was poured into an  $\text{Al}_2\text{O}_3$  cup, without pressing, and was sintered. Ni as sintering activator was added to improve the sintering. Such prepared specimens were infiltrated with liquid Si by IMSAS which however resulted in total disintegration due to weak sintering contacts and the highly exothermic reaction between Mo and Si.

Metal sponge, as a further alternative, was manufactured by dipping a polymer sponge (PU) into a polymer - metal (Mo) mixture, drying, thermal decomposition of the polymer and sintering. However it showed that the Mo was at least partly transformed into carbide, and the resulting structures were intolerably brittle.

One part of the work was the examination of the reactions between Mo and Si. Molybdenum specimens with different amounts of Si powder have been mixed, pressed and sintered. In part an Si wafer was placed on top of each sample, as a silicon source for infiltration. In general it showed that the reaction resulted in pronounced expansion, i.e. increased porosity, and in very fragile specimens. Also two-layered specimens with one layer out of pure Mo and the second one containing Si have been studied for sintering behaviour and diffusion of Si (from the Si containing layer) into the plain Mo layer. The reaction between Mo and Si was studied by DTA analysis of Mo specimens containing different amounts of Si (5; 15; 37 wt%) showing a high exothermic peak for Mo-Si reaction the intensity of which was increasing with higher amounts of Si in Mo.

Since pressureless sintering of Mo-Si mixes had shown to be ineffective, pressure assisted sintering in a hot press was carried out to enhance sintering between Mo and Si and decrease porosity. Mo with different amounts of Si was hot pressed, and the physical and mechanical properties of the sintered bodies were tested. It was also tried to combine Mo with different amounts of Si to a sandwich specimen, where each layer contained another amount of Si. In fact it showed that virtually dense specimens could be obtained, pressure assisted reactive sintering thus being an attractive way to manufacture dense Mo-silicide specimens.

To decrease the specific surface of Mo preforms – thus lowering the reactivity towards liquid Si - and increase the thickness of the sintering contacts, further investigation was focused on preparation of Mo specimen from coarse powders. First, specimens were prepared from a commercially available but very expensive Mo. Since these results were satisfying, Si infiltration being possible without disintegration, coarse Mo powder was prepared at TUW from a commercially available fine one, which was much cheaper, by pressing, sintering and crushing.

Also other options to prepare coarse Mo have been tested, e.g. by varying the reduction parameters.  $\text{MoO}_2$  powder was reduced in a dry and in a further experiment in a humid  $\text{H}_2$  atmosphere at different temperatures between 900 and 1100 °C. From W manufacturing it is known that humid atmosphere results in markedly coarser powder; the experiments with  $\text{MoO}_2$  however showed that the difference between dry and humid atmosphere is insignificant in the case of Mo. The particle size of the Mo particles after reduction in dry and in humid atmosphere did not exceed ~ 5  $\mu\text{m}$  with consistent particle size for humid reduced powder.

From previous experiments with tungsten it is also known that by addition of LiOH followed by reduction, the resulting W powder could be coarsened. Due to the similarity between tungsten and molybdenum, reduction experiments of  $\text{MoO}_2$  doped with LiOH have been carried out and the resulting powder characterised on SEM. Once more, however, it showed that results from W cannot be transferred to Mo, Li doping being found to be ineffective with Mo.



The oxidation stability of Mo specimens infiltrated with Si by CVI or liquid Si was tested in oxidizing atmosphere at 1100 °C for 3 h, a test device being established that enabled testing in combustion gases. The first specimen was an Mo (with low amount of Si) laser sintered specimen which lost about 92 wt% of its weight during the stability experiment in oxidizing atmosphere. The second laser sintered Mo specimen was infiltrated with liquid Si-Mg-Al (while Mg and Al evaporated). Mg and Al were added to dilute the melt and thus lower the reactivity between Mo and Si. They were tested for their oxidation behaviour at TUW. The specimen lost about 19 wt% of its weight during the experiment in oxidizing atmosphere. Bundled Mo wires encapsulated and infiltrated with liquid Si by IMSAS have also been tested for their oxidation stability. The lowest material loss of about 1,55 wt%, was observed in this case. Furthermore, TUW hot pressed Mo + 3-37 wt% Si specimens were characterised after testing in oxidizing atmosphere. With increasing amount of Si the material loss during the experiment in oxidizing atmosphere was decreasing. In the case of to the highest amount of MoSi<sub>2</sub> in the specimen, only 5 wt% were lost.

Parallel to Mo specimens, also Nb specimens were prepared by pressing at different pressures and sintering afterwards. After characterisation of the resulting densities, open porosities and hardness, the specimens were sent to partners for infiltration and TUW characterised these specimens afterwards. Also here, the specimens were partly destroyed due to the exothermic reaction with Si. Due to the low sinterability of the Nb-Si specimens the reactivity was also tested in some DTA/TG experiments. It was observed that the reactivity was increasing with increasing content of Si.

Due to the fact that there was no literature found about the sintering of Mo with Nb mixtures (in one material) some experiments investigating the carbon and oxygen content of the resulting specimens were carried out. Both, the sintering of Nb-Mo powder mixtures was carried out and two layer specimens, where one layer was out of Mo and the second one was out of Nb, have been prepared and characterised. The two layer specimens separated in the interface. Furthermore with increasing content of Nb in the mixed specimens, the oxygen content of the specimens increased due to internal getter effect where the reduced oxygen from Mo was captured by Nb.

In general it showed that manufacturing of Mo or Nb base specimens which are protected against oxidation by a silicide surface layer with graded transition into the core can be done by infiltration; however a principal requirement is that the performs contain relatively coarse pores with wide pore channels and a low specific surface; otherwise the violent exothermic reaction between the substrate and liquid Si easily results in disintegration.



## Table of contents

<b>1</b>	<b>LITERATURE .....</b>	<b>17</b>
1.1	HIGH TEMPERATURE MATERIALS .....	17
1.2	MOLYBDENUM .....	19
1.2.1	<i>Properties</i> .....	19
1.2.2	<i>Reduction of molybdenum oxide</i> .....	21
1.2.3	<i>Activated and liquid phase sintering</i> .....	24
1.2.3.1	Molybdenum and nickel .....	26
1.3	MOLYBDENUM AND SILICON .....	28
1.3.1	<i>Molybdenum silicides</i> .....	28
1.3.1.1	Properties .....	31
1.3.1.2	Oxidation mechanism .....	31
1.3.1.3	Wetting and infiltration .....	33
1.3.1.3.1	Coatings of silicon on molybdenum.....	35
1.3.2	<i>Molybdenum silicides and boron</i> .....	36
1.4	NIOBIUM .....	40
1.4.1	<i>Properties</i> .....	40
1.5	NIOBIUM AND SILICON.....	42
1.6	SINTERING OF Nb-MO-SILICIDES .....	43
<b>2</b>	<b>SAMPLE PREPARATION AND CHARACTERISATION METHODS.....</b>	<b>46</b>
2.1	PREPARATION .....	46
2.1.1	<i>Starting powders used</i> .....	46
2.1.1.1	Molybdenum from Plansee.....	46
2.1.1.2	Molybdenum from Chemie Metall.....	46
2.1.1.3	Molybdenum powder from Goodfellow .....	47
2.1.1.4	MoO <sub>2</sub> from Chemie Metall (CM).....	48
2.1.1.5	Niobium powder from H. C. Starck - Amperit 30/10 µm.....	49
2.1.1.6	Silicon from Ecka .....	50
2.1.1.7	Nickel powder .....	50
2.1.1.8	Space holder - wax Kenolube P11 .....	51
2.1.2	<i>Manufacturing of samples</i> .....	51
2.1.2.1	Mixing of powders .....	51
2.1.2.2	Pressing.....	51
2.1.2.3	Sintering.....	52
2.1.2.4	Infiltration of Mo and Nb specimens by partners .....	55
2.1.2.5	Metallographic preparation .....	55
2.1.3	<i>Measurement of physical and mechanical properties</i> .....	56
2.1.3.1	Measurement of the density .....	56
2.1.3.1.1	Green density .....	56
2.1.3.1.2	Sintered density .....	56
2.1.3.2	Measurement of the He – pycnometer density .....	57
2.1.3.3	Measurement of the porosity .....	57
2.1.3.4	Measurement of the pore size with Hg porosimetry .....	58
2.1.3.5	Measurement of the electrical conductivity .....	58
2.1.3.6	Carbon analysis by LECO .....	59
2.1.3.7	Oxygen analysis by LECO .....	59
2.1.3.8	DTA analysis .....	59
2.1.3.9	Dilatometry .....	60
2.1.3.10	XRF analysis.....	60
2.1.3.11	SEM and EDAX.....	61
2.1.3.12	Determination of Vickers hardness.....	61
2.1.3.13	Measurement of the impact strength.....	62
2.1.3.14	Measurement of the 3-point bending strength .....	62
<b>3</b>	<b>RESULTS.....</b>	<b>63</b>
3.1	MO SPECIMENS FROM COMMERCIALY AVAILABLE MO .....	63
3.1.1	<i>Influence of some factors on density and porosity of molybdenum samples</i> .....	63

3.1.1.1	Influence of compacting pressure .....	64
3.1.1.2	Influence of the sintering temperature .....	66
3.1.1.2.1	LOM images of Mo samples from Mo fraction < 45 µm sintered at different temperatures .....	67
3.1.1.3	Different powder fractions .....	68
3.1.1.4	Resulting hardness .....	70
3.1.1.5	Open porosity measured by Hg porosimetry .....	72
3.1.1.5.1	Uniaxially pressed samples .....	72
3.1.1.5.2	Cold isostatically pressed samples .....	74
3.1.1.6	Characterisation by LOM and SEM .....	75
3.1.1.7	Dilatometry .....	77
3.1.2	<i>Preparation of layered samples for gradient porosity</i> .....	80
3.1.2.1	Multiple layer samples .....	80
3.1.2.1.1	LOM images of multilayer samples after sintering at 1300 °C for 120/ min soaking period .....	82
3.1.3	<i>Characterisation of samples after Si CVI treatment</i> .....	83
3.1.3.1	LOM images .....	86
3.1.3.2	Scanning electron microscope (SEM) investigations .....	88
3.1.4	<i>Summary: molybdenum samples prepared from commercially available Mo</i> .....	89
3.1.5	<i>Molybdenum with Ni as sintering activator</i> .....	92
3.1.5.1	Influence of Ni content on the open porosity in Mo bodies .....	92
3.1.5.1.1	Influence of sintering temperature on Mo doped with 0.1 wt% Ni .....	92
3.1.5.1.2	Influence of different amounts of Ni on the physical and mechanical properties of Mo .....	93
3.1.5.2	Molybdenum with different amounts of Ni introduced in aqueous solution .....	102
3.1.5.2.1	Summary: Mo samples with Ni as sintering activator .....	103
3.1.5.3	Porous layered samples with different amounts of Ni .....	104
3.1.5.4	Two-layer samples with high amount of sintering activator .....	108
3.1.5.5	Summary .....	110
3.1.6	<i>Preparation of highly porous molybdenum samples with bigger open pores</i> .....	111
3.1.6.1	Molybdenum with wax as space holder .....	112
3.1.6.2	Characterisation of space holder samples after Si treatment by ATL .....	114
3.1.6.2.1	Light optical microscopy .....	114
3.1.6.2.2	SEM .....	115
3.1.6.2.3	Elemental mapping .....	116
3.1.6.2.4	Microhardness .....	117
3.1.6.3	Loose powder (gravity) sintering .....	117
3.1.6.4	Very porous molybdenum sponge preparation .....	119
3.1.6.5	Summary: preparation of high porosity molybdenum samples .....	120
3.2	<b>MOLYBDENUM WITH SI</b> .....	121
3.2.1	<i>Reactivity of molybdenum with different amounts of Si</i> .....	121
3.2.1.1	Different wt % Si and Si wafer .....	121
3.2.1.1.1	XRD .....	122
3.2.1.1.2	Light optical microscopy .....	123
3.2.1.2	Diffusion of Si in Mo-Si multilayer samples .....	128
3.2.1.2.1	Light optical microscopy .....	128
3.2.1.2.2	SEM and mapping .....	130
3.2.1.3	Reactivity of molybdenum with silicon measured by DTA .....	131
3.2.1.4	Activation of sintering in Mo-Si compacts .....	134
3.2.1.4.1	SEM of powders .....	134
3.2.1.4.2	LOM .....	135
3.2.1.4.3	Density, open porosity and hardness .....	136
3.2.1.5	Summary - examination of reactivity between Mo and Si .....	136
3.2.2	<i>Pressure-assisted sintering at higher temperatures</i> .....	137
3.2.2.1	Mo + x wt% Si after hot pressing at 1800 °C and 50 kN .....	137
3.2.2.1.1	Physical and mechanical properties .....	138
3.2.2.1.2	XRD .....	139
3.2.2.1.3	LOM .....	140
3.2.2.1.4	SEM with mapping .....	141
3.2.2.1.5	Summary .....	142
3.2.2.2	Sandwich – structured sample after hot pressing of [Mo / Mo+15%Si / 37%Si] .....	142
3.2.2.2.1	LOM .....	143
3.2.2.2.2	SEM .....	145
3.2.2.2.3	Hardness .....	146
3.2.2.2.4	Summary .....	147
3.3	<b>MO SPECIMENS PREPARED FROM COARSE POWDER</b> .....	147

3.3.1	<i>Molybdenum from Goodfellow</i>	148
3.3.1.1	Characterisation of samples from coarse Mo powder	148
3.3.1.1.1	LOM	148
3.3.1.2	Si penetration of compacts from coarse Mo powder	149
3.3.1.2.1	SEM-EDAX of sample with Si powder pressed on it	150
3.3.1.2.2	SEM-EDAX of sample with Si wafer placed on the top of the surface	150
3.3.1.3	Mixtures of Goodfellow coarse Mo and fine grained Mo (CM)	151
3.3.1.3.1	Mechanical properties	152
3.3.1.4	Characterisation of samples after Si treatment by partners	154
3.3.1.4.1	LOM	154
3.3.1.4.2	SEM	155
3.3.1.4.3	EDAX	156
3.3.1.4.4	Hardness	157
3.3.1.5	Compacts from bimodal Mo powders infiltrated with Si by IMSAS	158
3.3.1.5.1	LOM	158
3.3.1.5.2	SEM	160
3.3.1.5.3	EDAX analysis	161
3.3.1.5.4	Mapping	162
3.3.1.6	Summary: molybdenum samples from Goodfellow powder < 355 $\mu\text{m}$	162
3.3.2	<i>Preparation of coarse molybdenum powders and samples</i>	164
3.3.2.1	Reduction of $\text{MoO}_2$	164
3.3.2.1.1	In dry $\text{H}_2$ atmosphere	164
3.3.2.1.2	In humid $\text{H}_2$ atmosphere	166
3.3.2.2	Reduction of LiOH doped $\text{MoO}_2$	171
3.3.2.3	Granulation of Mo (CM) with camphor and Ni	171
3.3.3	<i>Powder prepared from presintered Mo(CM) powder compacts</i>	174
3.3.3.1	Preparation	174
3.3.3.2	LOM	175
3.3.3.3	SEM	176
3.3.4	<i>Sample preparation from coarse Mo powder</i>	176
3.3.4.1	Properties of the samples	177
3.3.4.2	Light microscopy	178
3.3.4.3	Addition of Si in different contents	178
3.3.4.3.1	Characterisation of density and open porosity	178
3.3.4.3.2	LOM	179
3.3.4.4	Summary of specimens prepared from coarse Mo powder	181
3.3.5	<i>Characterisation of samples after Si treatment by partners</i>	182
3.3.5.1	Specimens from bimodal mixtures of coarse and fine Mo powders	183
3.3.5.1.1	Open porosity	183
3.3.5.1.2	Hardness	186
3.3.5.1.3	LOM	187
3.3.6	<i>Testing of FGM for oxidation resistance</i>	189
3.3.6.1	First specimen from KE (batch 1427_12)	190
3.3.6.1.1	Characterisation before oxidation	190
3.3.6.1.2	During oxidation	191
3.3.6.1.3	After oxidation	191
3.3.6.2	Summary	194
3.3.6.3	Second specimen - EPFL specimen 5	194
3.3.6.3.1	Characterisation before oxidation	194
3.3.6.3.2	During oxidation	195
3.3.6.3.3	After oxidation	195
3.3.6.4	Summary	200
3.3.6.5	third specimen - IMSAS sample	201
3.3.6.5.1	Characterisation before oxidation	201
3.3.6.5.2	Characterisation after oxidation	202
3.3.6.6	Summary	204
3.3.6.7	Fourth specimen: oxidation resistance of Mo + x*wt% Si hot pressed at 1800 °C with 50 kN	205
3.4	<b>NIOBIUM PREFORMS</b>	207
3.4.1	<i>Sintering</i>	207
3.4.1.1	Dilatometry	207
3.4.1.2	Light microscopy	208
3.4.1.3	Light microscopy	211
3.4.2	<i>Reactivity with Si</i>	212
3.4.2.1	Microstructures	215

3.4.2.2	DTA/TG analysis of Nb + x*wt% Si .....	215
3.4.3	<i>Si infiltration of Nb preforms by partners</i> .....	218
3.4.3.1	LOM .....	218
3.4.3.2	SEM and elemental mapping.....	218
3.4.4	<i>Summary and discussion of Niobium</i> .....	219
3.5	SINTERING OF NIOBIUM – MOLYBDENUM COMPACTS .....	221
3.5.1	<i>Appearance of specimens</i> .....	222
3.5.2	<i>Carbon measurement</i> .....	223
3.5.2.1	Mixed powder samples .....	223
3.5.2.2	Two layer samples .....	223
3.5.3	<i>Oxygen measurement</i> .....	223
3.5.3.1	Mixed powder samples .....	223
3.5.3.2	Two layer samples .....	224
3.5.4	<i>Hardness of the mixed samples</i> .....	224
3.5.5	<i>Hardness for the two layer samples</i> .....	225
3.5.6	<i>Summary and discussion of niobium-molybdenum specimens</i> .....	226
4	<b>SUMMARY OF THE WORK</b> .....	227
5	<b>REFERENCES</b> .....	241
6	<b>LIST OF ABBREVIATIONS</b> .....	253

# 1 Literature

## 1.1 High temperature materials

There are many high temperature materials which can be used at higher working temperatures such as refractory metals or materials like graphite, carbides, oxides or nitrides. A main criterion is the stability in oxidizing atmosphere.

The development of many technical fields is strongly restricted by the limits of current structural materials. The high-tech applications working in extreme conditions and environments such as aircraft and automobile engines, space vehicles, high temperature or high pressure fusion or chemical reactors require efficient performance, dramatically improved materials able to withstand complex loading conditions. For such applications many loading factors are combined, like high temperature, corrosion (oxidation) attack and multiaxial dynamically changing forces. Furthermore, requirements like availability of techniques for cost effective production of net shape (also very complex) structural parts should be fulfilled [1,2]. Materials for high temperature applications can be summarised in a few materials which have some advantages but also some disadvantages which may disqualify these materials for specific applications at higher temperatures.

There are graphite and other carbon-based materials which are widely used as high temperature structural materials. Their advantages are that they are dimensionally stable, strong at high temperature, easy to machine, lightweight, and relatively inexpensive. However, they degrade rapidly at temperatures above 800°C in oxidizing atmospheres. Coatings that protect carbon-based materials from oxidation are an attractive option, but thermal expansion differences between coatings and the substrates, along with high temperature reactions, make this an impractical solution for many applications.

There are also diborides and carbides of the early transition metals (e.g., Zr, Hf, Ta). Their thermal and chemical stability makes them candidates for use in extreme environments like in hypersonic flight (1400°C and above, in air), atmospheric re-entry (2000°C and above, in monoatomic O and N), and rocket propulsion (3000°C and above, in reactive chemical vapours). These materials have melting temperature above 3000°C, retain their strength at temperatures above 1200°C, exhibit good thermal shock resistance, and can be modified with additives such as SiC to promote oxidation resistance. The borides and carbides have excellent erosion resistance under extreme heat flux and gas velocity conditions and have also been tested in a variety of propulsion applications. The major limitation to their use is a lack of affordable, reproducible manufacturing processes. Other candidate materials include ceramic oxides, nitrides, refractory metals or their silicides [3].

Although oxides are inherently stable in an oxidizing environment and can be fabricated by manufacturing-friendly processes such as powder forming and pressureless sintering, they suffer from lack of thermal shock resistance, low fracture toughness and poor creep resistance at elevated temperatures.

Nitrides of the early transition metals have shown promise as structural materials with high thermal conductivities, thermal shock resistance, and strength, but these materials have not been investigated to the same extent as the borides and carbides.

Ni based superalloys still remain as the most reliable and widely used material systems for many high temperature applications. They exhibit excellent creep strength, oxidation resistance, and fracture toughness [4]. However, their fundamental limitation is their melting point. Since advanced superalloys melt at temperatures in the range of 1350°C, significant strengthening can be obtained only at temperatures below 1150°C, which is as much as 150 K lower than requirements defined by designers of efficient and clean aircraft or modern industrial turbines [5,6]. One key aspect of such nickel superalloys is that the many design requirements can be satisfied with a multiphase microstructure. For Ni – based superalloys, the  $\gamma$  phase (face - centred - cubic Ni solid solution) acts as a matrix that holds together the other phases dispersed within it. More than a half of this matrix is a precipitate of nickel, aluminum and titanium which is mainly the  $\gamma'$  phase ( $\text{Ni}_3\text{Al}$ ) that strengthens the superalloy. Another phase is the  $\gamma''$  which acts as a strengthening phase in poly-crystal superalloys. This phase is a body-centred tetragonal (BCT) structured phase which is metastable and only provides strength to the material up to a temperature of 650 °C. Above this temperature, the  $\gamma''$ -phase instead transforms into  $\delta$ -phase, and the high strength of the superalloys is lost. This is the reason why such poly-crystalline superalloys are used only for turbine disc applications where the temperature is not as high as for turbine blades [7]. Phases  $\gamma$  and  $\gamma'$  have extensive solubility for transition metal alloying which increases the melting temperature and adds strength at higher temperatures. The oxidation resistance is supplied by Al and Cr which form  $\text{Al}_2\text{O}_3$  and  $\text{Cr}_2\text{O}_3$  surface layers, which are the protective layers passivating the material against oxidation/hot gas corrosion [8,9,10].

The next group are the refractory metals. Refractory metals are readily formed to shape, have high thermal shock resistance and have high fracture toughness. Mo and Nb, for example, satisfy many of the requirements for engine applications. One big disadvantage is that both metals suffer from poor oxidation resistance. The oxide layer that forms on Nb,  $\text{Nb}_2\text{O}_5$ , does not protect the metal from further oxidation. For Mo it is the  $\text{MoO}_3$  oxide which is formed, and it is volatile above about 700 °C [8]. It was observed by TUW that the volatilization starts already at about 400 °C. They are also limited by low creep resistance at elevated temperatures. In addition, most of them have high densities and cost.

Refractory metal (Mo, Nb) silicides have been explored during the last decade, and they show promising oxidation resistance [8]. They are able to create stable and renewing oxide at the surface and thus protect material from further corrosion. A key difference between Nb/Mo and the nickel superalloys is that oxidation resistance cannot rely on  $\text{Al}_2\text{O}_3$ . At 1300 °C and above, silica ( $\text{SiO}_2$ ) which grows slowly acts as oxidation protection. Both the Nb and Mo base systems have a body-centred-cubic solid-solution phase that functions like the  $\gamma$  phase in Ni superalloys. In the Mo base alloys, whose typical composition includes boron, silicide and borosilicide phases are also present and act like the  $\gamma'$  phase in superalloys. For Nb base alloys, the chemistry is more complex and includes other transition metals, such as Cr, Ti and Hf. The oxidation behaviour is more complex, too. At present, Nb base systems can serve in uncooled applications up to about 1200°C, and the Mo base systems can offer capability to above 1300°C [8] and even above 1600 °C for  $\text{MoSi}_2$  heating elements.

Their main problem is the high ductile-brittle transition temperature (DBTT) ~1100 K [11], limited creep resistance above 1500 K [12], low oxidation resistance at moderate temperatures (due to “peeling” behaviour) and in sulphuric environments. Manufacturing of complex parts can also be difficult. The oxidation behaviour of Mo



and Nb parts with and without Si, as relevant materials for the described work, will be discussed in the following chapters.

## 1.2 Molybdenum

The principal ore of molybdenum is molybdenite which in its purified form is molybdenum disulphide. In addition to the disulphide also oxides and molybdates (in tetragonal and monoclinic form) are occurring in the nature [13]. Molybdenum is mined by two procedures, the underground and the open pit. Ore processing takes place by crushing, ball milling and flotation [14]. For the removal of Cu from the ore,  $\text{Fe}_2(\text{SO}_4)_3$  is used.

There are two grades of Mo, the technical one and the ferromolybdenum. The technical grade Mo is processed by roasting of the oxide and the ferromolybdenum by thermite process. Mo-metal has to be prepared from chemically pure oxide or molybdate. There are many trace impurities in the  $\text{MoO}_3$  which affect the properties of the final product, for example the W which is undesirable in the fabrication of fine Mo glass-metal joints in electronic tube [16]. Silica is thought to have an adverse effect on recovery from hot working.

The shape and size of the starting powder is the deciding factor for the resulting porosity of the pressed body. The coarser the initial powder, the more porosity will result after pressing and sintering. It was mentioned in Gmelin [17] that coarse Mo powders (60 - 100  $\mu\text{m}$  and bigger) can be prepared only by one way. It is not possible to prepare such coarse powders from  $\text{MoO}_3$  by the reduction in  $\text{H}_2$ . A fine Mo powder is rolled to strips and after presintering at 1400 °C the strips are crushed to achieve the desired particle size.

### 1.2.1 Properties

Molybdenum is located in the group VI of the periodic table. Its refractory properties reflect the high strength of interatomic bonding resulting from the efficient overlap of the 4d - orbitals and the number of bonding electrons available. In such a structure the d-electrons exist in an energy band and the cohesion of the metal is determined by the extent of the filling. In the case of Mo the d-band is split into high and low energy bands, the latter giving rise to a high density of states and low Fermi energy which favours the bcc to the fcc structure [13], [18].

By the addition of elements like Re it is possible to increase the strain hardening of the Mo material. High Re Mo-Re alloys obtain their low temperature ductility enhancement from the activation of deformation twinning [19]. The recrystallization temperature and creep resistance at elevated temperatures can be influenced by doping Mo with rare earth metals due to formation of interlocking grains which impede the slipping of boundaries [20].

Mo has a melting point of 2610 °C which makes it a high temperature strength material. It has a relatively good thermal conductivity of 142 W/mK at 20°C [21,22]. Because of the high electrical conductivity Mo can be used for many electrical applications. Sintering in case of Mo occurs in the solid state by heating to temperatures below the

melting point of 2610 °C in a protective atmosphere of hydrogen. To obtain Mo specimens with nearly dense structure it requires long time sintering [23]. Another possibility is spark plasma sintering [24,25] or explosive consolidation of molybdenum [26]. Sintering of Mo is dominated by the volume diffusion process with associated activation energy of 405 kJ/ mol [27]. This high activation energy explains the need for high sintering temperatures, in the range of 1800 - 2000 °C. Some sintering activators can be used such as Ni, Pd or Pt which lower the sintering temperature to 1200 - 1400 °C. Furthermore, Hiraoka et al. [28] found that the yield strength is decreasing with small additions of Group VIII elements such as iron, cobalt, nickel or palladium. The decrease of the yield strength takes place due to the difference in the number of (s + d) electrons between molybdenum and the alloy element. The effect of the difference in the atomic size between molybdenum and the alloy element was secondary and minor.

Garg et al. [23] described the influence of the compacting pressure on the sintering behaviour. The finer Mo powder exhibits higher densification than the coarser powder at all compaction pressures. Furthermore, it could be shown that samples compacted at higher pressures show faster densification than samples pressed at lower pressures. Increasing the compaction pressure causes several simultaneous changes in the green structure. The number of interparticle contacts increases, the neck size increases and more dislocations are introduced. Thus less work of sintering is required to achieve the same densification at higher compaction pressure than at lower one. Therefore, the required sintering temperature decreases with increasing compaction pressure [23]. Majumdar et al. [29] agree with [23] that during sintering grain boundary diffusion and volume diffusion occur, which results in isothermal densification. In the work of Majumdar et al. [29] the activation energy for the isothermal sintering of pure Mo is found to be 407 kJ mol<sup>-1</sup> between 1500 °C and 1800 °C.

The mechanism during sintering was observed and detailed described by Blaschko et al. [30]. There are three stages of sintering beginning with growing of necks between adjacent powder particles due to large gradients of curvature in their neighbourhood. During this phase the dominating mechanisms mostly are such as to reduce the inner surface of the sintered body by rounding the pores while its density remains nearly unchanged. The intermediate stage is characterized by the increased importance of mechanisms affecting the density of the aggregate. The pores still are linked by an interconnecting network of channels. The pore shape is changing slowly. The distance between centres of neighbouring grains decreases, and the cross-sections of the pore connections gradually narrow. Finally the channels of the network pinch off and leave isolated pores of approximately spherical shape. In the last stage coarsening of the grains takes place [30]. These three stages of sintering were already described by Schatt et al. [31]

The micro - morphology of the Mo powder is a determining factor for further properties of the compacts prepared from such a powder. An et al. [32] studied the influence of powder micro - morphology on further properties of the compacts and presented two powders of which one is a standard Mo powder (commercially available) and a second one was a reduced monodisperse powder. It could be observed that specimens from powder which has uniform particle size distribution and less agglomeration show higher yield and room temperature mechanical properties, excellent high-temperature performance and better isotropy. On the other hand Poster [33] could show for tungsten that a wide particle size distribution has a positive influence on pressing. A reason might be the particle agglomeration which causes a decreasing in sintering activity which results in a lag of sintering of the aggregates compared to the rest of the particles. Kim et al. [34] researched on sintering behaviour of molybdenum nanopowders in comparison to that of commercial Mo powder. In the case of the Mo nanopowder,

shrinkage started at a lower temperature of about 600 °C, while the starting temperature of shrinkage for commercial powder was 1000 °C. Final relative densities of the sintered samples were 94% for the nanopowder and 74% for the commercial powder. These results indicate that particle size strongly influences the sintering behaviour, and thus, enhanced sinterability can be realized by using nanopowder. Nanopowder requires less sintering time or lower temperature for densification to occur to the same extent as with commercial powder. On the polished surface of the compacts the grain size of the sintered body prepared from Mo nanopowder was finer than that prepared from commercial Mo powder. These mean grain sizes were measured to be about 1.4 and 6.2  $\mu\text{m}$ , respectively.

The influence of lubricants on the density of Mo green bodies was characterised by Du et al. [35]. By the addition of lubricants such as EBS lubricant (Microwax C) the green density of Mo can be enhanced dramatically without residue. Furthermore, the compact quality can be improved, and defects like delaminating and cracks can be avoided.

There are many applications for Mo but some of them are for example as pins in incandescent lamps, hooks and eyes as supports for the tungsten filaments, Mo ribbon in halogen lamps. Mo wire is also used in electronic tubes for vacuum tight connections through borosilicate glass. Due to the fact that Mo has about the same thermal expansion as silicon, it has found applications in transistors and semiconductor elements. The most common application of Mo, reported by Burman et al. [16], remains that as an alloy element in irons and steels, as well as to some heat and corrosion resistant alloys, which generally do not demand the high purity of metallic Mo, but can tolerate less refined ferromolybdenum or molybdic oxide additions. The principal molybdenum alloy commercially available is the TZM Mo (0.5 % Ti and 0.08 % Zr and a small amount of C) which has superior hot strength and resistance to recrystallization or softening compared with unalloyed metallic molybdenum. The vast majority of engineering applications of molybdenum metal make use of its high melting temperature, high strength and stiffness especially at elevated temperatures, resistance to chemical corrosion in many media, or the excellent thermal and electrical properties. Another important application of Mo is for sputtering targets for flat screens which is produced e.g. by Plansee Group.

### **1.2.2 Reduction of molybdenum oxide**

Molybdenum metal has to be prepared from chemically pure oxide or molybdate. The morphology of molybdenum powder depends on whether the metal is prepared from the sublimed trioxide  $\text{MoO}_3$  or from the ammonium dimolybdate  $(\text{NH}_4)_2\text{Mo}_2\text{O}_7$  and on the agents used for the reduction process. As a result of the differences in powder morphology, densities of sintered products differ, and recrystallization temperatures, strength and ductility are affected.  $\text{MoO}_3$  reduced in the first step in  $\text{NH}_3$  ( $\text{MoO}_3 \rightarrow \text{MoO}_2$ ) and in the second step in  $\text{H}_2$  ( $\text{MoO}_2 \rightarrow \text{Mo}$ ) result in  $\text{MoO}_2$  cubes. The  $\text{NH}_3$  promotes the formation of  $\text{MoO}_2$  cubes that yield faceted, dense metal particles. When only  $\text{H}_2$  is present,  $\text{MoO}_3$  is reduced to form needles and platelets of  $\text{MoO}_2$  that are further reduced to porous, irregularly shaped metal particles [36].

From these two described methods for metal powder preparation, mostly it is prepared by the reduction of  $\text{MoO}_3$  with hydrogen [37] and this is usually carried out in two

stages. In the first step  $\text{MoO}_3 + \text{H}_2 \rightarrow \text{MoO}_2 + \text{H}_2\text{O}$  while in the second stage  $\text{MoO}_2 + 2 \text{H}_2 \rightarrow \text{Mo} + 2 \text{H}_2\text{O}$ . The first reduction step at low temperature is needed because in other case  $\text{MoO}_3$  will sublime in next step carried out by the reverse flow of the atmosphere. Hydrogen easily reduces  $\text{MoO}_3$  to  $\text{MoO}_2$ , but the reduction of  $\text{MoO}_2$  to  $\text{Mo}$  is more difficult since the standard free energy for the oxidation  $\text{Mo}$  to  $\text{MoO}_2$  and  $\text{H}_2$  to  $\text{H}_2\text{O}$  per mole  $\text{O}_2$  are clearly similar. This is however only valid under standard conditions, for an atmosphere in which  $\text{H}_2\text{O}/\text{H}_2=1$ . In real reduction atmospheres the removal of the formed  $\text{H}_2\text{O}$  determines the reaction rate. The two stage reaction is generally favoured because it avoids the formation of a coarse metal powder through the action of  $\text{H}_2\text{O}$  vapour produced during the reaction. These results could not be confirmed by our experiments. Reduction in humid atmosphere resulted in coarser particles with uniform shape. The relatively low temperature and the use of a dilute hydrogen stream produced in the second stage reduces the risk of volatilisation as the reaction is strongly exothermic. Haber et al. [38] claimed in their study that the movement of oxygen during reduction proceeds by the formation of shear planes in the  $\text{Mo-O}$  layers. This ensures a very rapid transport of oxide ions in the lattice, the adsorption of the reducing agent becoming the rate-determining step (this was however an observation at one single particle - not a loose powder bed) .

For the determination of the particle size of the final powder, the conditions of reduction such as temperature, soaking period,  $\text{H}_2$  flow, dilution partial pressure of water vapour and bed depth of feedstock are critical factors. The initial reduction occurs at around  $600^\circ\text{C}$  and the final reduction at  $950\text{-}1100^\circ\text{C}$  [13].

Braithwaite et al. [22] summarised that there are three stages of reduction. At first chemisorption of hydrogen on the surface takes place followed by desorption of water to create anion vacancies. Second, diffusion of vacancies from the surface into the bulk takes place. Finally in the third step salination of the crystal lattice with defects followed by nucleation of the new phase takes place. The rate determining step in the first reduction process is the diffusion of the anion vacancies into the interior of the crystal. Since the activation energies of the first and second stage reductions are the same, the rate controlling factor of  $\text{MoO}_2 \rightarrow \text{Mo}$  is the diffusion of  $\text{O}^{2-}$  through the  $\text{MoO}_2$  lattice. Also Thöni et al. [39] described the reduction process and vacancies movement in their work and the results can be compared to Braithwaite's.

Braithwaite et al. [22] reported that the first reduction step to  $\text{MoO}_2$  should be carried out between  $600 - 700^\circ\text{C}$  in hydrogen (with 100 l/min) while  $\sim 520^\circ\text{C}$  have been reported in Gmelin [17]. Braithwaite et al. described experiments in a batch furnace while the reduction process described in Gmelin was carried out in a TGA. The reaction temperature in the batch furnace should be cooled down to  $300^\circ\text{C}$  (still in  $\text{H}_2$ ) and after 150 min the furnace can be cooled down and the reaction gas can be switched to  $\text{N}_2$ . The physical properties of the resulting brown  $\text{MoO}_2$  are important as they determine more than anything else the quality of the final  $\text{Mo}$  powder. In the second reduction process the dioxide is transferred to a second continuous hydrogen reduction furnace. This is a very critical stage for the determination of the particle size distribution of the  $\text{Mo}$  powder. Generally it can be said that the two stage process yields a product with high chemical purity, and one that is low in oxygen and nitrogen. During the process, excess hydrogen is maintained to remove water produced during the reduction process. Residual water may prevent the complete reduction of the oxides. Schulmeyer et al. [40] investigated the accurate phases occurring during the reduction of  $\text{MoO}_3$  in  $\text{H}_2$ . In the first reduction step from  $\text{MoO}_3$  to  $\text{MoO}_2$  an intermediate phase occurs, the  $\text{Mo}_4\text{O}_{11}$ . The reaction path is  $\text{MoO}_3 \rightarrow \text{Mo}_4\text{O}_{11} \rightarrow \text{MoO}_2$  via chemical vapour transport. Depending on

the local partial pressure of  $\text{H}_2\text{O}$  during reduction, the formed  $\text{Mo}_4\text{O}_{11}$  and  $\text{MoO}_2$  exhibit different size distributions and shapes of the grains. The  $\text{MoO}_2$  platelet dimensions of  $<2\text{ }\mu\text{m}$  were observed independently of reduction conditions in the first stage. For the second reduction step from  $\text{MoO}_2 \rightarrow \text{Mo}$  no intermediate phase was observed. The Mo product particle size and size distribution is determined by stage two reduction. Furthermore, the stage-two reduction requires very dry  $\text{H}_2$  to achieve complete conversion. Temperature,  $\text{H}_2$  flow rate and dew point, powder bed depth are the key parameters. Stage-one reduction can be achieved by using wet  $\text{H}_2$  [40,41,42,43].

Dobos et al. [44] have observed the behaviour of  $\text{MoO}_3$  during heat treatment in vacuum (instead as described in  $\text{H}_2$ ). It could be observed that the native  $\text{MoO}_3$  on a Mo specimen surface dissociates, and a layer of suboxides forms on the surface which was measured with XPS during the experiment. This layer hinders the further dissociation of the surface and the reaction speed decreases after the initial phase. Furthermore, the author observed that in the initial phase of the heat treatment the oxide layer ( $\text{MoO}_3$ ) has lost some oxygen either by the dissociation, reduction or by evaporation, which was not clarified. The  $\text{MoO}_3$  might also been evaporated and not dissolved.

Some reduction experiments of a fine grained Mo ( $\sim 4,5\text{ }\mu\text{m}$  particle size, with oxides on Mo surface due to storage and handling) have been carried out on a dilatometer/MS coupling by Edtmaier et al. [45]. In these experiments the first step reduction ( $\text{MoO}_3 \rightarrow \text{MoO}_2$ ) was finished at  $400\text{ }^\circ\text{C}$  while the second step reduction ( $\text{MoO}_2 \rightarrow \text{Mo}$ ) at  $750 - 800\text{ }^\circ\text{C}$  in dry hydrogen. This temperature is shifted to a higher temperature of  $850 - 900\text{ }^\circ\text{C}$  for  $\text{H}_2$  dew point  $0^\circ\text{C}$  (i.e. in humid  $\text{H}_2$  atmosphere).

By the hydrogen reduction and ball-milling of  $\text{MoO}_3$  it is possible to prepare a nano-sized Mo powder of  $10\text{ nm}$  by a  $20\text{ h}$  ball-milling process and it increased to  $60\text{ nm}$  after reduction at  $800\text{ }^\circ\text{C}$  in hydrogen as was described by Kim et al. [46,47]. The peak temperature for the reduction was shifted to lower temperatures by increasing the milling time. The reduction process of  $\text{MoO}_3 \rightarrow \text{MoO}_2$  is more dependent on the initial particle size while the second reduction step of  $\text{MoO}_2 \rightarrow \text{Mo}$  is less affected by this parameter. The temperature of the peak for the reaction of  $\text{MoO}_3 \rightarrow \text{MoO}_2$  was more shifted to lower temperatures than that for the reaction of  $\text{MoO}_2 \rightarrow \text{Mo}$ . This is due to the fact that the transformation steps for the reaction of  $\text{MoO}_3 \rightarrow \text{MoO}_2$  take place via chemical vapour transport. The nano sized Mo powder has a lower starting temperature for densification and higher value for linear shrinkage at  $1400\text{ }^\circ\text{C}$  than the commercial powder due to the decrease in particle size with a starting green density of  $60\%$  of the theoretical density. Savin et al. [48] mentioned in their work that molybdenum particles reduced with hydrogen at  $800\text{--}900^\circ\text{C}$  correspond to the size of the starting oxide particles. At temperatures of  $1100\text{ }^\circ\text{C} - 1200\text{ }^\circ\text{C}$ , the Mo particles begin to grow so that the resulting Mo particles are bigger than the starting oxide powder. Increase in temperature results in coarser reduced particles.

Due to the chemical similarity between molybdenum and tungsten it was therefore stated and argued that vapour-phase transport via volatile hydroxides, as observed for W, should also be considered for Mo. A brief summary of tungsten reduction, and influence of impurities or doped elements on the reduction of tungsten and subsequently that of molybdenum, is given here. Haubner gives us an overview of tungsten reduction [49]. The reduction starts with  $\text{WO}_3$  and goes through  $\text{WO}_{2.95} \rightarrow \text{WO}_{2.9} \rightarrow \text{WO}_{2.7} \rightarrow \text{WO}_2 \rightarrow \text{W}$ . The tungsten reduction is controlled by the  $\text{H}_2\text{O}$  diffusion out of the powder bed and by the reduction rate (production of  $\text{H}_2\text{O}$ ). In the first reduction steps



the reaction is controlled by the transport of  $\text{H}_2\text{O}$  out of the powder bed. The reaction takes place near the thermodynamic equilibrium. After nucleation no further nuclei are formed and big rosettes of  $\text{WO}_2$  are formed. The reduction of  $\text{WO}_2 \rightarrow \text{W}$  is not in the thermodynamic equilibrium, a lot of  $\text{H}_2\text{O}$  diffuses out of the powder bed so that the reaction is far away from the thermodynamic equilibrium. This results in a high nucleation rate. Many crystals are the result. In general it can be said that for the nucleation and grain growth the proportion between reaction and diffusion rate of  $\text{H}_2\text{O}$  is of importance. The reduction rate is affected by the temperature while the diffusion rate is affected by the height of the powder bed. With increased water vapour content and higher temperature more volatile  $\text{WO}_2(\text{OH})_2$  is formed (each W atom is oxidized and afterwards reduced for three times on the way from  $\text{WO}_3$  to W) which is adsorbed on energetically favourable crystal faces, forming bigger grains as a result.

The reduction temperatures start at 380 °C for the  $\text{WO}_3$  to  $\text{WO}_{2.9}$  reduction and go up to 900 °C for the  $\text{WO}_{2.75}$  to  $\text{WO}_2$  reduction and end at 575 °C for the  $\text{WO}_2$  to W reduction step [50]. Very similar results for the reduction temperature and for the reduced phases have been reported by Hellmer et al. [51].

It was also reported by Haubner [52] that the addition of impurities such as LiOH to W oxides promotes grain growth during reduction while evaporating without Li residues. In the first reduction steps to  $\text{WO}_2$  no morphological differences between doped and undoped tungsten could be seen. In the last reduction step from  $\text{WO}_2$  to W an increase in the reaction rate could be observed. That results in a higher reduction rate by the alkaline metals which increase on the other side the water production. By the increase of water also the number of nuclei is decreasing. This results in a small amount of new nuclei but of a bigger size of the crystals [52,53]. In some further work by Danninger et al. [54,55,56] the influence of Lithium and also of some other impurities on the properties of W and W alloys was studied.

### 1.2.3 Activated and liquid phase sintering

The temperature and time for sintering of Mo compacts can be decreased by the addition of small amounts of the VIII (iron and platinum group) elements. Thereby the diffusion and shrinkage processes are accelerated, which is called “activated sintering”. Palladium is reported as the most effective activator, but usually nickel is chosen as sintering activator due to costs and properties as described in the literature below. German et al. [57] found that the transition in behaviour from nonactivated to activated sintering occurs at a coating thickness of approximately one monolayer. An optimal behaviour is associated with approximately four monolayers of activator. Higher amounts of activator have been observed to hinder the densification process [57].

Corti [58] gave a wide review of models for activated sintering of refractory metals with VIII group elements. Hayden and Brophy [59] reported that the sintering kinetics in terms of the process controlling mechanism in their carrier phase model of activated sintering, which applies also to liquid phase sintering, showed that for all the platinum group metals examined, the sintering rate was not dependent upon composition, but was proportional to the cube root of time, except for rhodium in a low shrinkage regime. This time dependence was interpreted in terms of the diffusion controlled transport of tungsten in the interface between the W and platinum group metal coating layer.

There were three models described of activated sintering. The first was described by Hayden and Brophy [59] where tungsten is diffusing through the activator phase away from the line joining the centres of adjacent particles, to be deposited elsewhere on the particles as indicated by the arrows in fig. 1.1- a. The rate controlling step is found to be

either refractory metal diffusion at the interface with the activation layer or refractory metal solution in the activator layer. The model of Toth and Lockington [60] claims that the dissolution of tungsten on the tungsten - activator interface is followed by volume diffusion outwards through the activator layer and subsequent surface diffusion, this being the rate controlling step. Diffusion through the activator layer to the contact point between adjacent particles results in the formation of sintering necks (fig. 1.1-b). Samsonov and Jakowlev [61] proposed that activated sintering was a consequence of the electronic structure stabilisation of the refractory metal caused by the additive metal. They based this approach on the argument that a metallic system containing partially filled d-subshells becomes more stable as the number of d5 and d10 electron configurations increase. The refractory element acts as an electron donor, and this case of electron transfer gives rise to the high solubility in the activating element. A proposal by German et al. [57,62,27] takes this model further and applies the Engel-Brewer [63] theory to the prediction of the activation energies for the diffusion of refractory metals through the activator layer. In this model the activator has a role in providing enhanced grain boundary diffusion of refractory metal (fig. 1.1 - c).

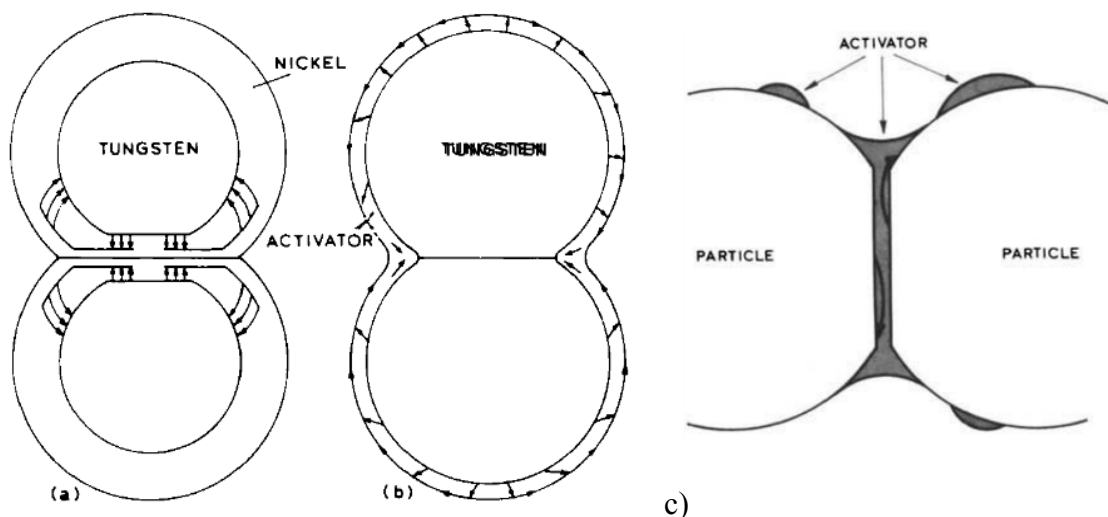


**fig. 1.1.: three models of activated sintering; model described by a) Hayden and Brophy; b) Toth and Lockington; c) German and Munir**

Furthermore, the solubility of Ni and Mo can be observed very well in fig. 1.2. It can be seen that there is about 40 wt % solubility of Mo in Ni. There is just a very small solubility of Ni in Mo of about 2 wt% at 1362 °C.

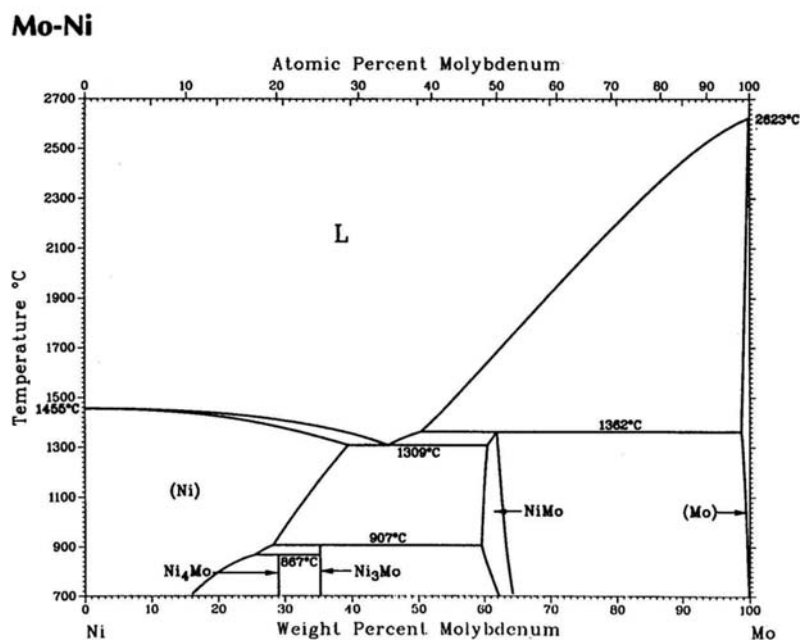


fig. 1.2.: Binary system Mo-Ni (ASM Handbook Vol. 3)

### 1.2.3.1 Molybdenum and nickel

By the addition of 0,5 - 1 % Ni to Mo it is possible to attain sintered densities of 90 % already at sintering temperatures of 1300 °C. Above 1500 °C this effect is decreasing while the determining factor is the solubility of Ni in Mo. The kinetics of sintering Mo doped with 0.5 - 0.75 % Ni at 1100 - 1400 °C is accelerated by the diffusion at the grain boundaries. Lejbrandt et al. [64] have explained in their work that with increasing content of Ni (up to 0.4 at% Ni) the degree of densification increases. Up to 1400 - 1500 °C the densification increases with higher sintering temperature. Above this limit, any further rise of the temperature no longer causes a clear cut increase in density due to the fact that Ni melts already at 1455°C. There is furthermore a relationship between activator particle size and the sintering of Mo. The finer the nickel particles the stronger is the effect on Mo densification. This effect was observed between 1000 °C and 1400 °C, i.e. in the temperature range of solid state sintering. At 1455 °C (the melting temperature of nickel), molybdenum sintering in the presence of liquid state starts, and the effect of Ni grain size becomes less evident. (the heating rate in Lejbrandt's experiments was 25°C/min; in the opinion of this author, the eutectic temperature of 1319 °C can be "skipped" and the melting point of Ni is the key factor. Lejbrandt et al. [64] observed furthermore that at lower temperatures the Ni occurs in the form of foreign inclusions between the Mo grains. At higher T°C (>1000 °C), diffusion of the Mo into the Ni becomes more intense (the partial diffusion coefficients are: Mo in Ni at 1000 °C is  $5 \cdot 10^{-12}$  cm<sup>2</sup>/sec and the diffusion coefficient of Ni in Mo at the same temperature is  $7 \cdot 10^{-13}$  cm<sup>2</sup>/sec). At about 1455°C the Ni melts and wets the Mo surfaces. In experiments where a coarse Ni was used large pores are left which disappear during sintering at higher T. Nickel forms a thin layer of liquid on the Mo surface, which is a good mass transport medium during sintering [64,65]. Hwang et al. [66] described in their work that there is a  $\delta$ -NiMo intermetallic compound film, about 2 nm thick, at the grain boundaries which was also confirmed by Raevskaya et al. [67]. In this work it was also mentioned that beneath  $\delta$ -NiMo there are also  $\gamma$ -Ni<sub>3</sub>Mo and  $\beta$ -



$\text{Ni}_4\text{Mo}$  which are formed at 700 °C but above 1000 °C they are not stable anymore. Only the  $\delta\text{-NiMo}$  remains stable above 700 °C until 1362 °C. This  $\delta\text{-NiMo}$  couple serves as a short-circuit diffusion path and causes the activated sintering of Ni-doped Mo. On the other hand this  $\delta\text{-NiMo}$  intermetallic compound is the reason for the lower ductility of Ni-doped Mo at higher temperatures [66]. In a further work Hwang et al. [68] observed, that by the addition of 1,5 wt% Ni the density of Mo compacts increased from 82,4 to 95,5 % when sintered at 1300 °C and 1370 °C. By replacing 0,5 wt% of Ni by Cu, the sintered density of the Mo-1wt%Ni-0,5wt%Cu compact increased to 99,1%. The sintered density of 97.3 % could be increased to 99.1% at 1300 °C sintering. The addition of copper lowers the melting point from 1360 °C, the peritectic temperature of Mo-Ni, to 1270°C. It also enhances the sintering during heating in the solid state. Although copper has little solubility in molybdenum, and vice versa, it aids nickel in enhancing the sintering which results in improved density due to better wetting on Mo particles. A very low ductility of the compact was observed due to the brittleness of the Mo-Ni intermetallic compound. Furthermore, Hiraoka et al. [28] could find that the addition of group VIII elements, especially Ni, decreased the yield strength of Mo (these Mo - Ni alloys have been fully recrystallized at 1773 K). This effect of Ni addition is attributed primarily to the difference in the number of (s+d)-electrons between the alloy element and molybdenum. The difference in the atomic size between Ni and Mo has a positive, though minor, effect on the yield strength [28,17]. Cao et al. [69] could investigate the diffusion behaviour of Mo and Ni and found that the diffusion coefficient of Mo in  $\delta\text{-NiMo}$  in the Mo-Ni system is about 106 times bigger than that of the self diffusion of Mo.

In fig. 1.3 the influence of the Ni content on mechanical and electrical properties of sintered tungsten is demonstrated. The density and hardness are increasing with higher amount of Ni while the electrical resistance is decreasing.

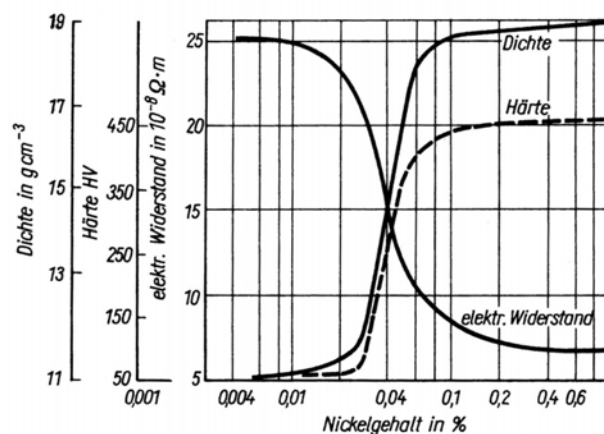


fig. 1.3.: Properties of sintered W-Ni with varying Ni content, sintered at 1300°C; W.Schatt: Sinteraktivierung im System W-Ni: Einfluss von geringen Ni-Zusätzen [164]

An example was given in Gmelin's Handbook [17] where a 2  $\mu\text{m}$  Mo powder with 0.5 wt% Ni was sintered for 30 min at 1300 °C and reached 90 % relative density. This can be explained by the fact that the diffusion of Mo through the Ni films/coatings is much quicker than the self diffusion (volume diffusion) of Mo without Ni. Higher sintered densities were achieved in specimens where the used powder was already reduced with a sintering activator. The efficiency of a sintering activator can only be observed where a minimum ratio of 0.5 % Ni as sintering activator has been added. By the addition of higher ratios of Ni in Mo the sintering activator is accumulating at the grain boundaries

as intermetallic phases, resulting in embrittlement. This results described in Gmelin [17] were also achieved by Smith et al. [70].

German et al. [27] sintered Mo with 13 different transition metal additives between 1000 - 1350 °C and confirmed that next to Pd, Ni is the most effective sintering activator for Mo. He also could find that the sintering is predicted by a grain boundary heterodiffusion model. Also for tungsten, which is chemically similar to Mo, Ni was the most effective sintering activator.

## 1.3 Molybdenum and silicon

### 1.3.1 Molybdenum silicides

There are three stable silicides. The first one is the cubic  $\text{Mo}_3\text{Si}$  which decomposes at 2025 °C. This phase is formed peritectically by a reaction between liquid Si and Mo at 2025 °C. The second is the tetragonal  $\text{Mo}_5\text{Si}_3$  with melting point at 2180°C. The third one is the tetragonal  $\alpha\text{-MoSi}_2$  which transforms to hexagonal  $\beta\text{-MoSi}_2$  at 1900 °C and melts at 2020°C [22]. The phase diagram for the system Mo-Si is given in fig. 1.4 [22]. It can be seen that  $\text{Mo}_3\text{Si}$  and  $\text{MoSi}_2$  are line compounds whereas  $\text{Mo}_5\text{Si}_3$  shows a wider stability range. The disilicide is the most interesting industrially.  $\text{Mo}_3\text{Si}$  and  $\text{Mo}_5\text{Si}_3$  suffer from poor oxidation resistance. Analysis of the electron structure of  $\text{MoSi}_2$  indicates that the d-state of the metal in  $\text{MoSi}_2$  has vacant sites as is the case with Mo itself. The comparatively large diameter of the Si atom precludes the formation of an interstitial structure.

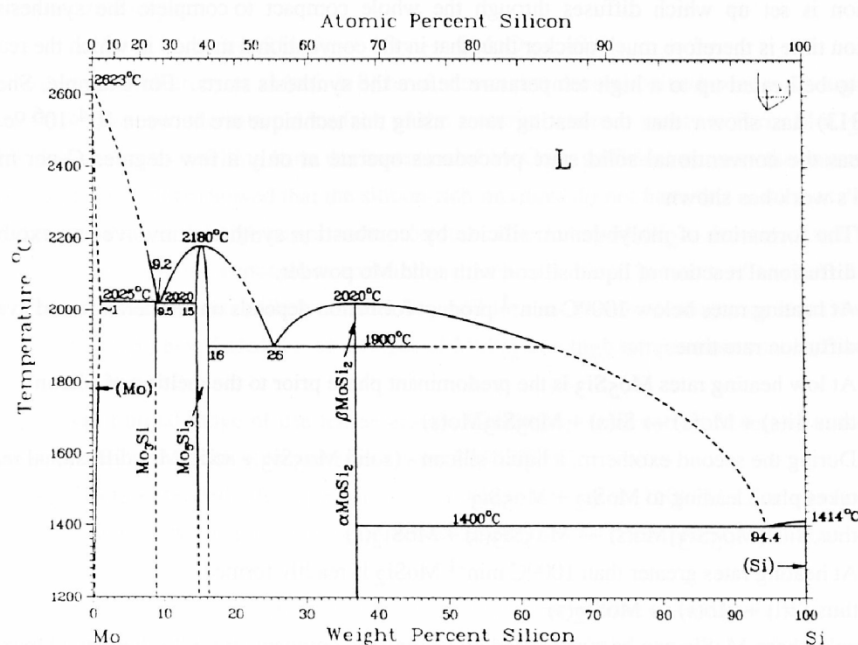


fig. 1.4.: phase diagram of the Mo - Si system [94BRA]

The disilicide can be prepared in several ways. It is now produced either by a thermite process or by combustion synthesis. The mechanism of the thermite reaction consists of a reduction of  $\text{MoO}_3$  by Al to  $\text{MoO}_2$  followed by a simultaneous oxidation of Al to  $\text{Al}_2\text{O}_3$  and synthesis reaction between reduced  $\text{MoO}_2$  and Si to form  $\text{MoSi}_2$ . The rate determining step is found to be the reduction of  $\text{MoO}_3$  by Al and oxidation of Al to  $\text{Al}_2\text{O}_3$  [22].

Another way for preparation is the combustion synthesis where all powdered reactants are mixed and pressed together and ignited using an ignition coil. The reaction is very quick and highly exothermic. The formation of molybdenum silicide by combustion synthesis involves an exothermic diffusional reaction of liquid silicon with solid Mo powder [22].

At heating rates  $>100^\circ\text{C}/\text{min}$ ,  $\text{MoSi}_2$  is readily formed ( $2\text{Si} + \text{Mo} \rightarrow \text{MoSi}_2$ ). One disadvantage is the generation of cracks due to the violent reaction and pores due to Kirkendall effects [71]. Some authors were dealing with different methods to produce  $\text{MoSi}_2$ . Yao et al. [71] listed some methods like the mechanical alloying by high energy milling of Mo and Si powders, and a mechanically induced self-propagating reaction is responsible for the  $\text{MoSi}_2$  formation. A further way for  $\text{MoSi}_2$  preparation is the CVD process (chemical vapour deposition) wherein vapour phase reactants form a coating which is deposited on a heated molybdenum surface. The source of silicon can be  $\text{SiH}_4$ ,  $\text{SiH}_2\text{Cl}_2$  or  $\text{SiCl}_4$ . Substrate cleanliness is very important in order to prevent any difficulties during subsequent processing steps such as annealing or contact metallization. Also a consolidation of molybdenum disilicide is possible by powder metallurgy by sintering and in a further step by hot pressing or in one step by HIP (hot isostatic pressing) [72]. However, according to experimental observations of one of the partners in the current project, it was not possible to convert all silicides into the most stable form  $\text{MoSi}_2$  by HIP, and  $\text{MoSi}_2$  was also resistant to densification by HIP. Ignat et al. [73] reported also about laser cladding of Mo and Si.

In an annealing experiment between  $1400 - 1600^\circ\text{C}$  with Mo and Si diffusion couples, Byun et al. [74] could show that the dominant diffusing element in the  $\text{MoSi}_2$ ,  $\text{Mo}_5\text{Si}_3$  and  $\text{Mo}_3\text{Si}$  phases is Si. In some further annealing experiments Tortorici et. al. [75] could demonstrate that  $\text{MoSi}_2$  and  $\text{Mo}_5\text{Si}_3$  form a diffusion zone while the thickness of the  $\text{MoSi}_2$  zone was one to two orders of magnitude larger than that of the  $\text{Mo}_5\text{Si}_3$  layer. The  $\text{MoSi}_2$  layer exhibited a columnar microstructure with evidence of texture and preferential growth (parabolic growth was observed in his further work [76]) of grains in the direction of diffusion. The Si to Mo ratio across the layer varied approximately within the range of 1,9 to 2.

Yoon et al. [77] described that in a diffusion-controlled growth the  $\text{Mo}_5\text{Si}_3$  and  $\text{Mo}_3\text{Si}$  grow simultaneously with a parabolic rate law already at an early annealing stage. They also found that Si is the primary diffuser in the  $\text{Mo}_5\text{Si}_3$  phase, as Byun et al. described in their work [74].

Only Byun et al. [74] and Lassner et al. [78] found the  $\text{Mo}_3\text{Si}$  layer which is situated between the Mo and  $\text{Mo}_5\text{Si}_3$  layers. They mentioned three different possible mechanism of the formation of a  $\text{Mo}_3\text{Si}$  layer [74]: First the decomposition reaction of the  $\text{Mo}_5\text{Si}_3$  phase into the  $\text{Mo}_3\text{Si}$  and Si phases at the interface of  $\text{Mo}_5\text{Si}_3/\text{Mo}_3\text{Si}$ . Second is the diffusion of Si through the  $\text{Mo}_3\text{Si}$  phase to the interface  $\text{Mo}_3\text{Si}/\text{Mo}$ . The third one is the reaction of Si with the Mo substrate to form a new  $\text{Mo}_3\text{Si}$  phase.

It has to be considered that the  $\text{MoSi}_2$  suffers from extreme brittleness and gains from its oxidation resistance. Further on, the electrical and thermal conductivities of  $\text{MoSi}_2$  are high. Most of the industrial applications of  $\text{MoSi}_2$  relate to its excellent corrosion and oxidation resistance, in particular for the production of protecting films against

oxidation. This protective ability is due to the volatility of  $\text{MoO}_3$  which volatilises at  $750^\circ\text{C}$ , leaving behind an amorphous  $\text{SiO}_2$  film which is a coating in the  $\text{MoSi}_2$  matrix and will protect the underlying metals from oxidation from  $600^\circ\text{C}$  to above  $1700^\circ\text{C}$  ( $5\text{MoSi}_2 + 7\text{O}_2 \rightarrow \text{Mo}_5\text{Si}_3 + 7\text{SiO}_2$ ). However, below  $600^\circ\text{C}$  decomposition may occur due to oxidation when the formation of  $\text{MoO}_3$  competes with  $\text{SiO}_2$  formation ( $2\text{MoSi}_2 + 7\text{O}_2 \rightarrow 2\text{MoO}_3 + 4\text{SiO}_2$ ). Some studies have shown that decomposition occurs through the transport of oxygen into the internal surface of the material where it reacts to form  $\text{MoO}_3$  and  $\text{SiO}_2$ . The internal stress resulting from the formation of  $\text{MoO}_3$  is sufficient to cause the material to disintegrate. They further showed that the silicon-rich mixtures do not have this weakness. Thus it can be appreciated that the high temperature protection afforded by  $\text{MoSi}_2$  is dependent to a large extent on the presence of an atmosphere containing a sufficient partial pressure of oxygen. In the absence of such conditions it is likely that  $\text{MoSi}_2$  will lose its excellent resistance to oxidation. Some advantages of  $\text{MoSi}_2$  are for example that coating systems can be designed to form a protective silica-rich film at temperatures from  $500$  to  $1500^\circ\text{C}$ .  $\text{MoSi}_2$  offers a top-end temperature increase of about  $300^\circ\text{C}$  over existing silicide coatings.  $\text{MoSi}_2$  furnace elements operate successfully up to  $1700^\circ\text{C}$ .

The mechanical properties and high temperature strength of  $\text{MoSi}_2$  have been improved by incorporating  $\text{SiC}$  whiskers in  $\text{MoSi}_2$  composites.

The thermal behaviour of Mo-Si powder mixtures has been examined by Wiltner et al. [79]. It was observed that with increasing Si amount the reaction temperatures were more affected by Si particle size and milling-mixing times. Increased milling-mixing time and powder mixture homogeneity resulted in forced diffusion behaviour. The more Si was available the more pronounced exothermic behaviour was observed

One of the project partners, Almut Wiltner, investigated the stability of Mo in contact with  $\text{MoSi}_2$ , which is a highly crucial item for Mo components with  $\text{MoSi}_2$  surface coatings. The investigation of the Mo- $\text{MoSi}_2$  interface stability is important since the diffusion of Si into Mo from the Si rich side ( $\text{MoSi}_2$ ) leads to the formation of silicides with lower Si content and lower stability in oxidizing environment ( $\text{Mo}_5\text{Si}_3$  and  $\text{Mo}_3\text{Si}$ ). The Mo in inner parts of future components is needed for enhanced ductile properties whereas the  $\text{MoSi}_2$  at outer regions gives raised mechanical properties at high temperatures together with self-passivating behaviour in oxidative environments. The other silicides differ in their oxidation behaviour (poor stability) and mechanical properties compared to  $\text{MoSi}_2$ . Therefore the interface Mo- $\text{MoSi}_2$  has to be improved in order to retard the Si diffusion.

If the initial content of  $\text{MoSi}_2$  is high enough (approximately  $> 50 \text{ Vol}\%$ ),  $\text{MoSi}_2$  is remaining after heating at  $1100^\circ\text{C}$  and 6h. In other case  $\text{MoSi}_2$  is consumed under formation of firstly  $\text{Mo}_5\text{Si}_3$  followed by  $\text{Mo}_3\text{Si}$ . It was also observed by Wiltner that  $\text{MoSi}_2$  is remaining if compaction is fast enough (via SPS at  $1300^\circ\text{C}$  for example compared to standard heating rates of about  $10 \text{ K/min}$  by powder sintering route).

The following conclusions could be drawn from these observations. Either the initial  $\text{MoSi}_2$  content has to be high enough or a diffusion barrier for Si migration has to be included

in order to increase the long-time stability of a graded material. The most promising results were observed by Wiltner using  $\text{TiB}_2$ . Small interdiffusion zones within Mo –  $\text{MoSi}_2$  and Mo –  $\text{TiB}_2$  –  $\text{MoSi}_2$  samples could be observed. The B interlayer suppressed Si diffusion into Mo coupon.

Another partner, Ludger Weber, asserted that the diffusion coefficients of the silicides differ depending on the literature that is found. With changing diffusion coefficient also

the stability (calculated) of the silicides is changing dramatically especially for the low silicides.

### 1.3.1.1 Properties

In tab. 1 some properties of the known silicides are listed compared to Mo. Molybdenum and MoSi<sub>2</sub> have many technical applications, and this is the reason why more data could be found in the literature.

**tab. 1.: summary of some properties of Mo, MoSi<sub>2</sub>, Mo<sub>5</sub>Si<sub>3</sub> and Mo<sub>3</sub>Si**

material	melting point / °C	density/g/cm <sup>3</sup>	CTE / K <sup>-1</sup> (20°C)	therm. conductivity W/mK (20°C)	el. Resistivity/ Ω m	fracture toughness MPa.m <sup>1/2</sup>
Mo	2623	10.28	4.8 x 10 <sup>-6</sup>	138	5.5 x 10 <sup>-8</sup>	
MoSi <sub>2</sub>	2030	6.24	6.5 x 10 <sup>-6</sup>	66 (23°C)	45 x 10 <sup>-8</sup>	3-6
Mo <sub>5</sub> Si <sub>3</sub>	2180	8.24				
Mo <sub>3</sub> Si	2025	8.90				

Yao et al. [71] summarised some physical properties of MoSi<sub>2</sub> which are the high melting point of 2030 °C and high temperature oxidation resistance due to the protective silica layer. MoSi<sub>2</sub> exhibits a brittle-to-ductile transition in compression in the range of 1000 °C. It has a high thermal conductivity, high temperature oxidation resistance (similar to SiC), maximum oxidation rates in MoSi<sub>2</sub> actually occur at a temperature of 500 °C. The thermal expansion coefficient is close to that of Al<sub>2</sub>O<sub>3</sub>. The low fracture toughness of MoSi<sub>2</sub> results in fracturing in a brittle manner. In the case of high temperature creep mechanism, MoSi<sub>2</sub> deforms via matrix dislocation glide and climb at high stresses, and grain boundary sliding at low stresses.

### 1.3.1.2 Oxidation mechanism

There are two different oxidation mechanisms. At low temperatures below 600 °C low temperature oxidation occurs which is called “pesteing”. At temperatures above 600 °C high temperature oxidation takes place where the material is protected by SiO<sub>2</sub> formation. No “pesteing” can be observed. The exact mechanisms are described below.

#### **Low temperature oxidation behaviour:**

MoSi<sub>2</sub> disintegrates to a powder when subjected to oxidizing environments at 400 - 600 °C. This disintegration during low temperature oxidation is known as “pest” or “pesteing” effect. A high Si content will not influence the oxidation resistance at low temperatures since the formation of a protective SiO<sub>2</sub> layer at this temperature region is slow compared to the loss of Mo by the formation and volatilization of MoO<sub>3</sub> [8,80].

It is suggested that the cause is grain boundary embrittlement produced by short - circuit diffusion of O<sub>2</sub> and subsequent dissolution into the grain-boundary areas. There are two possible oxidation reactions for MoSi<sub>2</sub>. The first possible reaction is 2MoSi<sub>2</sub> + 7O<sub>2</sub> --> 2MoO<sub>3</sub> + SiO<sub>2</sub>. The second possible reaction is 5MoSi<sub>2</sub> + 7O<sub>2</sub> --> Mo<sub>5</sub>Si<sub>3</sub> + 7SiO<sub>2</sub>. Both



reactions are thermodynamically feasible, but the first reaction is favoured, which results in pesting between 400 - 600 °C. It could be shown that the pesting of MoSi<sub>2</sub> is associated with a substantial volume expansion, and the disintegrated powdery product contains mainly crystalline MoO<sub>3</sub> whiskers or platelets, amorphous SiO<sub>2</sub> clusters, and residual MoSi<sub>2</sub> crystals. The pest reaction apparently has nucleation and growth stages. Pesting also involves volume and grain boundary diffusion of oxygen. Grain boundary diffusion of oxygen causes preferential oxidation of intergranular interfaces and the formation of protruding MoO<sub>3</sub> whiskers. These would result in the formation of internal tensile stresses, which destroy intergranular bondings [71,81,82,83].

The pest reaction initially nucleates in the form of blisters. The fact that most blisters were burst open suggesting that the internal stresses developed during pest oxidation are significant. The internal stresses may arise from three sources. The first is the volume expansion by oxidation (internal tensile stresses at grain boundaries, causing intergranular decohesion). The second is the vapour pressure of MoO<sub>3</sub> (the volatilization of MoO<sub>3</sub> was believed to serve as the driving force for the initial formation of the blisters) and the third is the different thermal expansion between the Si - O - Mo (= oxide layer containing more oxygen than silicon and molybdenum) formed on the substrate and the MoSi<sub>2</sub> substrate. The preferential formation of protruding MoO<sub>3</sub> whiskers at grain boundaries can also produce uneven stress states between grains. This would further open up the structure and accelerate the disintegration of MoSi<sub>2</sub>. Once the internal structure of a sample is opened up and more interfaces are produced and exposed to oxygen, pest of the sample through the volume diffusion of oxygen is conceived to be accelerated [81,84,85]. Hansson et al. described in their work the influence of oxygen and water on the oxidation behaviour of MoSi<sub>2</sub> in the low temperature range (400-550 °C). They found that the rate of depletion of Mo from the oxide scales during oxidation increases with increasing temperature and water vapour content [86]. Lee et al. [87] reported that a very significant mechanism at the lower temperatures where pesting is observed is that the oxidation product does not form a protective silica layer as it does at higher temperatures. Pesting oxidation of MoSi<sub>2</sub>, therefore, occurs at a linear rate.

### ***High temperature oxidation behaviour:***

No pesting has been observed in MoSi<sub>2</sub> during oxidation above 600 °C. The reaction  $5\text{MoSi}_2 + 7\text{O}_2 \rightarrow \text{Mo}_5\text{Si}_3 + 7\text{SiO}_2$ , which does not produce volatile MoO<sub>3</sub>, appears dominant (SiO<sub>2</sub> as outer layer, Mo<sub>5</sub>Si<sub>3</sub> beneath). Both static and cyclic oxidation characteristics of MoSi<sub>2</sub> materials have been studied by Yao et al. [71]. Isothermal oxidation experiments have been conducted on specimens exposed in air for 24 h at 800 to 1500 °C. MoSi<sub>2</sub> composites have significant isothermal oxidation resistance compared to intermetallic compounds based on titanium, niobium and tantalum composites and the single-crystal nickel base superalloy. The protective silica layers are excellent barriers to oxidative attack because of low oxygen permeation rates. MoSi<sub>2</sub> is known to exhibit excellent high temperature oxidation behaviour up to 1600 °C [71].

Sharif et al. [88] tested the oxidation behaviour of MoSi<sub>2</sub> in the temperature range of 1400 - 1700 °C. Spallation of the SiO<sub>2</sub> scale did not occur at any temperature, and Mo<sub>5</sub>Si<sub>3</sub> formation did not happen below 1700 °C. It could be observed that at temperatures approaching the melting temperature of SiO<sub>2</sub>, there is a change in oxidation mechanism of MoSi<sub>2</sub> when compared to lower temperatures. The activation energy for oxidation decreases from 340 kJ/mol at lower temperatures to 204 kJ/mol above 1550 °C. Sharif et al. [88] could explain the outstanding oxidation resistance of

MoSi<sub>2</sub> up to 1700 °C by the formation of a protective silica (SiO<sub>2</sub>) layer above the pesting temperature. This is typical of all SiO<sub>2</sub>-forming materials. Above the pest oxidation temperature range of 500 - 800 °C, oxidation behaviour of MoSi<sub>2</sub> is identical to that of Si up to 1400 °C. During oxidation at higher temperatures than 800 °C, a continuous SiO<sub>2</sub> layer forms on MoSi<sub>2</sub>, which acts as a barrier against further oxidation. Lee et al. [87] reported that above 800 °C the oxidation of silicon is accompanied by the formation of the silicide Mo<sub>5</sub>Si<sub>3</sub>, between the MoSi<sub>2</sub> and outer SiO<sub>2</sub> layer. Further oxidation is limited because of slow diffusion of reactants through the existing oxide layer. It is believed that the rate limiting factor is the diffusion of oxygen anions through the oxide. Below 800 °C, MoSi<sub>2</sub> oxidizes to form SiO<sub>2</sub> and MoO<sub>3</sub> as final products. Above 800 °C this reaction is no longer favoured because MoO<sub>3</sub> boils off [87,83]. The formation and growth of the oxide layer on MoSi<sub>2</sub> is governed by transport of the oxidizing species to the outer surface of the oxide layer for absorption, diffusion of the oxidant through the oxide layer, and oxidant reaction with the bulk MoSi<sub>2</sub> to form SiO<sub>2</sub>. The linear rate is a consequence of interfacial reaction control at short times, and diffusion of the reactants is the controlling mechanism at longer times in the parabolic regime [88].

Melsheimer et al. [89] carried out some oxidation resistance tests with MoSi<sub>2</sub> between 1100 and 1400 °C. Contrary to the observations before, he could observe that MoSi<sub>2</sub> forms volatile MoO<sub>3</sub> above 600 °C which attains a vapour pressure of 1 atmospheric pressure at 1160 °C. The MoO<sub>3</sub> formation could not be fully explained, but he had a theory which could explain it by the following mechanism. Mo is dissolved to MoO<sub>2</sub> in SiO<sub>2</sub> in the transition zone MoSi<sub>2</sub>/SiO<sub>2</sub>, it is migrating through the oxide layer and only if the activity of oxygen is high enough in the SiO<sub>2</sub> layer MoO<sub>2</sub> is oxidised in this layer to MoO<sub>3</sub>. At the transition zone SiO<sub>2</sub>/gas the MoO<sub>3</sub> evaporates.

Hansson et al. [90] investigated the influence of water vapour between 600 and 700 °C on the oxidation behaviour of MoSi<sub>2</sub> - based composites. During oxidation of MoSi<sub>2</sub> without water vapour the MoO<sub>3</sub> species is evaporating out of the specimen surface. With water vapour - MoO<sub>2</sub>(OH)<sub>2</sub> is formed, which has a higher vapour pressure and is increasing even more with increasing water vapour content and results in more Mo loss. Then the pure SiO<sub>2</sub> heals the pores from the Mo loss, and a protective scale is established. The vapour pressures of the volatile species increase with temperature and/or water vapour content in the exposure atmosphere, which leads to a more rapid Mo loss from the oxide. A shorter time then elapses before the oxide scale is transformed into the relatively Mo-free protective SiO<sub>2</sub> scale, which results in less oxide being formed.

### 1.3.1.3 Wetting and infiltration

For the infiltration of porous Mo bodies the wetting of Si is of importance. Some factors have to be examined to determine if a porous body will be infiltrated by silicon. Eustathopoulos et al. [91] have made some studies on the wetting and infiltration behaviour of graphite and silicon nitride porous bodies by silicon.

Spontaneous (pressureless) infiltration of a liquid in a porous medium occurs when the equilibrium contact angle of the liquid on the pore walls is much lower than 90° [92,93]. Kaptay et al. [92] dealt with capillary pressures corresponding to different morphologies of the porous solid and to the way the infiltrating liquid behaves. They found that non-perfectly wetting liquids will not be able to infiltrate porous solids without remaining porosity. This new relationship provides a new functional dependence of the threshold pressure of infiltration on the contact angle.

Although wetting and infiltration both involve the motion of a triple line, the geometry of the region around this line in these two processes is very different.

Eustathopoulos et al. [91,94], and Landry et al. [95] argued that spreading on a solid surface and infiltration in a porous preform in the Si/graphite and Si/Si<sub>3</sub>N<sub>4</sub> systems are governed by the reactions occurring at the solid/liquid/vapour triple lines of these systems.

In the Si/graphite couple at temperatures close to the Si melting point, wetting and infiltration kinetics in neutral gas are controlled by the local chemical process at the triple line moving on the solid surface or on the pore walls. In this system, the geometry has a limited influence on the triple line velocity, the infiltration rate being lower than the spreading rate. In high vacuum, the transport of Si atoms through the vapour phase can modify the surface chemistry of graphite in front of the triple line and thus enhance wetting and infiltration rates even at temperatures close to the Si melting point. A similar effect is expected to occur under inert gas but at much higher temperatures. When Si is present in the liquid as alloying element, long range diffusion of the reactive solute from the preform entrance to the infiltration front can also affect and even control the reactive infiltration. However, a transition from reaction to diffusion control is expected to occur with increasing temperature for any alloy/ceramic system, since the activation energy of diffusion in metallic liquids is one order of magnitude smaller than the activation energy for reaction-controlled reactive infiltration. In the Si/silicon nitride couple, the progress of the interfacial reaction at the triple line needs the removal ahead of the infiltration (or the wetting) front of a gaseous species (SiO) produced by the deoxidation reaction. As a consequence, in this case, the geometry strongly influences the triple line velocity, leading to infiltration rates several orders of magnitude lower than the spreading rate. Such pronounced effects are expected to appear every time a gaseous species is involved in the reaction at the triple line.

Mortensen et al. [96] examined the kinetics of diffusion limited spreading of sessile drops in reactive wetting. Sessile drop experiments on metal/ceramic systems have shown that a sufficient condition for improving wetting of a given substrate by a given metal is to alloy the metal with a chemical species which reacts with the substrate to form a dense layer of solid reaction product that is better wetted by the metal than the original solid substrate. The metal drop is first formed on a solid substrate, it deforms rapidly, opposed only by viscous forces, to form an initial wetting angle, corresponding to the contact angle of the liquid on the original unreacted substrate surface. Thereafter, the droplet spreads while the reaction between metal and substrate progresses, to reach a final stable value. The rate at which the droplet spreads is determined not by viscous resistance, but by the rate of reaction product formation at the triple line.

Oro et al. and Bernardo et al. [97,98,99] described the wetting behaviour at high temperatures on a steel substrate by copper. A proper wetting angle of the liquid phase on the substrate surface as well as the infiltration of this liquid in the pore skeleton at the common sintering temperatures are critical for obtaining high homogenization levels and diffusion of the alloying elements. Therefore, the high temperature wettability and the interfacial reactions that take place due to the compatibility of compositions play a crucial role in sintering and infiltration process with liquid phase presence. The dynamic wetting phenomena can be even more complicated when the substrate is not inert and can be dissolved by the liquid metal because of the composition compatibility. For a surface covered by thin oxide films, it has been seen how the wetting is strongly improved by intermetallic formation reactions leading to replacement of the oxidized surface by a clean one of an intermetallic compound [100]. The evolution of the drop geometry (with time and temperature) depends on the dissolution between the drop and the substrate. A fast spreading of the liquid metal would be attributed to dissolution of



the substrate into the molten alloy. As the liquid becomes enriched by the substrate composition (when  $\Theta$  tends towards very small angles) the spreading rate decreases because the composition of the drop is changing. Besides, when substrates with open pores are considered, some capillarity phenomena should be taken into account as well. When diffusion mechanism occurs (or some solution), the contact angle will evolve since the composition of the liquid in contact will change. In addition, the interface between the drop and the substrate is shifted from the initial position towards the substrate. Formation of different layers can occur. If the thermal expansion coefficients are different between substrate and drop and also due to solidification shrinkage as liquid turns to solid, cracks can occur in the interface and in the volume of the drop. Furthermore, if the diffusion is governed by vacancy mechanism, and if the diffusion fluxes of the different species at the boundary are different, then the vacancies flow is not compensated and can condense to form pores.

Considering the fluidity of the liquid metals, the behaviour is also determined by the reactivity of the drop. In case of Cu, although the contact angle is higher, the low interaction with the iron compacts substrate enables the liquid to penetrate completely into the pore skeleton. On the other hand it should also be mentioned that the pores can also clog if the liquid solidifies in the pores. No further infiltration is then possible. Summarising it can be said that the wettability and the spreading of the liquid phase occur only when the reaction takes place with negative free enthalpy (for example the formation of reaction layers and solid solution).

#### 1.3.1.3.1 Coatings of silicon on molybdenum

Some authors have reported about protective coatings for molybdenum. Henne et al. [101] reported about the possibility of layers that are prepared by low pressure plasma spraying (LPPS). Important is that the thermal expansion coefficient of the layer is similar to that of the substrate. Therefore it is not possible to plasma spray  $\text{MoSi}_2$  on Mo substrate. A "connecting" layer of mullite ( $= 3\text{Al}_2\text{O}_3 \cdot 2\text{SiO}_2$ ) between these two has to be sprayed on the substrate before the  $\text{MoSi}_2$  is put on. Another possibility is to mix some additives to the  $\text{MoSi}_2$  like mullite which adapt the thermal expansion coefficients. Cox et al. [102] reported about the addition of Cr or Fe to  $\text{MoSi}_2$  coatings which extend the thermal cyclic life of the materials by a factor of three. It was observed furthermore that the stability of the silicide coatings is decreased when used at varying temperatures. Zamoum et al. [103] and Chao et al. [104] reported that it is possible to prepare some oxidation resistant coatings by pack cementation. Zamoum et al. proposed a co-deposition of Cr, Fe and Si to form  $\text{MoSi}_x\text{Cr}_y\text{Fe}_z$  while Chao et al. proposed a co-deposition of Ta+Si, or V+Si or Nb+Si. Both agreed that pack cementation technique enables to prepare stable silicide coatings on Mo. Another type of protective coatings are the SIBOR® coatings from Plansee Group which will be discussed in the following chapter.

Ramberg et al. [105] reported that the standard free energies of formation ( $\Delta G^\circ_f$ ) of oxides are useful to compare their chemical stability with that of silica. The oxides of molybdenum and tungsten are much less stable than  $\text{SiO}_2$  and are easily reduced by silicon. In the competition for oxygen which occurs at the silicide/silica interface, the disilicides of molybdenum could be expected to form only a silica scale. The best kinetic barrier to the oxidation of silicides is a protective scale that inhibits the diffusion of oxygen or metal to or from the scale/silicide interface. Pure silica ( $\text{SiO}_2$ ) is one of the most impermeable oxides at high temperatures; and disilicides that form silica scales

exhibit the best oxidation resistance at high temperatures. The low activation energy for the diffusion of oxygen in  $\text{SiO}_2$  results in a more protective oxide scale at temperatures above  $1080^\circ\text{C}$ . Passive layers are more protective with decreasing diffusivity of oxygen.

Lin et al. [106] reported about the oxidation of  $\text{MoSi}_2$  in  $\text{O}_2$ , air, or oxygen-inert gas atmospheres. However, in combustion products as  $\text{CO}_2(\text{g})$  and  $\text{H}_2\text{O}(\text{g})$  corrosion of  $\text{MoSi}_2$  has not as yet been thoroughly evaluated. Combustion environments are commonly encountered in a wide variety of industrial applications, such as glass melting and metal heat treating.  $\text{MoSi}_2$  has demonstrated distinctly different oxidation behaviour depending on oxygen partial pressure and temperature. At high temperature and oxygen partial pressure, e.g.  $1420^\circ\text{C}$  and  $>104\text{ Pa}$ , it has been reported that  $\text{MoSi}_2$  oxidizes to form volatile molybdenum trioxide and amorphous silica. Continued exposure leads to the formation of a silica surface layer through which molecular oxygen must diffuse. As the protective coating coarsens, the oxygen concentration gradient is reduced and thus oxidation is retarded. This is referred to as a passive oxidation behaviour [106].

Modelling showed that  $\text{MoO}_3(\text{g})$  forms only in presence of  $\text{O}_2$ . The thermodynamic modelling assumed access of a near-infinite quantity of gaseous oxidizing species to come in contact with  $\text{MoSi}_2$ , resulting in complete oxidation of the silicon component of the compound. As the silica coating coarsened, consuming silicon at the  $\text{Mo}_5\text{Si}_3/\text{SiO}_2$  interface, no  $\text{Mo}_3\text{Si}$  was detected using XRD. Due to the high mobility of silicon, the  $\text{Mo}_5\text{Si}_3$  interface coarsened by conversion of  $\text{MoSi}_2$  to  $\text{Mo}_5\text{Si}_3$ , providing diffusing silicon to the  $\text{Mo}_5\text{Si}_3/\text{SiO}_2$  interface to form  $\text{SiO}_2$ . This passive oxidation revealed that the oxygen affinity of  $\text{MoSi}_2$  was high enough to compete with  $\text{H}_2$  and  $\text{CO}$  for oxygen [106].

Zhu et al. [155] investigated the early stage of oxidation of  $\text{MoSi}_2$  since a significant portion of the powder is oxidized before the formation of passive  $\text{SiO}_2$  film. The experiments have been carried out at  $1100^\circ\text{C}$ , and the phases formed during oxidation were characterised by XRD. They found that at temperatures above  $900^\circ\text{C}$  (up to  $1100^\circ\text{C}$ ),  $\text{Mo}_5\text{Si}_3$  phase was formed first and was subsequently oxidized to solid  $\text{SiO}_2$  and volatile  $\text{MoO}_3$ , resulting in an initial weight gain (at short oxidation times) followed by subsequent weight loss. This has been observed for the early stage of oxidation before the self healing protective  $\text{SiO}_2$  layer was covering the whole surface. Alam et al. [156] investigated also the oxidation behaviour of  $\text{MoSi}_2$  on Mo substrates. Short time oxidation experiments have been carried out at  $1500^\circ\text{C}$  for 1 h. They revealed the oxidation to the cracks in the coating. The cracks were generated due to the mismatch of coefficient of thermal expansion between the coating and the substrate, localized oxidation of the substrate below the cracks occurred. Gradual transformation of the  $\text{MoSi}_2$  phase into lower Mo-silicides occurred below the coating during high temperature oxidation exposure.

### 1.3.2 Molybdenum silicides and boron

There are some selected cases where a refractory metal is in equilibrium with binary silicide and boride phases and also in a few cases with a ternary intermetallic. The most notably system is the  $\text{Me}_5\text{SiB}_2$  (T2 phase) + Me two phase region where Me is Nb or Mo. [107,108]. A ternary phase diagram is given in fig. 1.5 where the T2 phase is pointed out. Concerning material properties for high-temperature applications, the

combination of Nb or Mo with a silicide phase seems to be the most favourable. The development in the field of Mo-Si-B alloys is summarized in an excellent review by Perepezko [109].

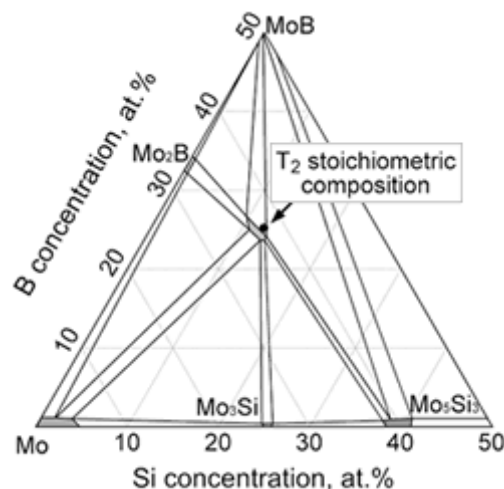


**fig. 1.5.: Isothermal section through the Mo - Si - B ternary system at 1600 °C according to Perepezko et al. [8]. In the Mo-rich corner are the binary phases  $\text{Mo}_2\text{B}$ ,  $\text{MoB}$ ,  $\text{Mo}_3\text{Si}$ ,  $\text{Mo}_5\text{Si}_3$  (T1) and the ternary isotype of this, the T2-phase  $\text{Mo}_5\text{SiB}_2$**

Multiphase microstructures based on Mo+ $\text{Mo}_3\text{Si}$ +T2 three phase alloys appear to offer a good balance of high temperature performance (mechanical properties and oxidation resistance) [110,111,112,113,114,115] and processability due to in-situ toughening.

In terms of oxidation resistance the addition of boron to metal rich binary silicides enhances the performance significantly [116], and the Mo phase together with the equilibrium T2 phase offer a ductile phase toughening. Krüger et al. [117] reported that mechanical alloying is beneficial as an interim manufacturing step to prepare three-phase Mo-Si-B alloys with a continuous  $\alpha$ -Mo matrix containing embedded, uniformly distributed intermetallic particles. Kestler et al. [118] reported that the establishment of a continuous Mo solid solution matrix with finely dispersed intermetallic phases is crucial for fracture toughness at ambient temperature, and hot working of such alloys at temperatures typical for refractory metals requires an ultrafine microstructure.

The formation of protective  $\text{SiO}_2$  layers at high temperatures in Mo-Si-B system also results in useful oxidation resistance [114]. The addition of small amounts of alloying elements may influence oxidation performance further. Thus it was reported that the addition of 1 at% Zr to Mo+ $\text{Mo}_3\text{Si}$ +T2 improves the oxidation resistance below 1200°C but was not beneficial at higher temperatures [119]. Heilmaier et al. [120] reported that by the addition of Zr to such Mo - Si - B alloy the fracture toughness and the grain boundary strength can be improved. The low oxidation resistance below 1200 °C could also be confirmed. The reason for that peculiar behaviour is that the monoclinic zirconia incorporated into the forming scale undergoes a phase transformation towards tetragonal crystal structure at temperatures beyond 1150 °C accompanied by a distinct volume reduction. This causes damage to the scale and gives access to the substrate beyond 1200 °C [120,121]. Also the substitution of Ti for Mo was found to offer useful options for improved oxidation resistance [120]. Heilmaier et al. [120] reported that Ti addition influences the oxidation behaviour of Mo - Si - B alloys as a consequence of

the presence of the hexagonal  $\text{Ti}(\text{Mo})_5\text{Si}_3$  phase and because of the high Ti solubility. Due to some oxidation tests carried out at 1100 °C for 100 h it could be observed that a duplex layer of borosilicate and rutile under a  $\text{TiO}_2$  surface layer was formed. This porous duplex layer, which mainly consists of  $\text{TiO}_2$ , does not serve as an effective barrier to oxidation. The main reason is that oxygen can easily penetrate through the rutile particles as the mobility of oxygen in  $\text{TiO}_2$  is significantly higher than in  $\text{SiO}_2$ . That results in an increasing volume fraction of  $\text{TiO}_2$  within the duplex layer with increasing time and/or temperature and facilitates the inward transport of oxygen as well as the formation of pores through which oxygen can reach the substrate easily and  $\text{MoO}_3$  can evaporate.

Nevertheless the boron-to-silicon ratio is the dominating factor that controls the constitution, viscosity and oxygen diffusivity of the in-situ formation of  $\text{SiO}_2\text{-B}_2\text{O}_3$  passive layer upon oxidation [122]. Lowering the B to Si ratio leads to the formation of an  $\text{SiO}_2$  rich protective layer resulting in higher oxidation resistance at high temperatures. The oxidation process of Mo-Si-B alloys is characterized by a rapid mass loss due to evaporation of  $\text{MoO}_3$  during first contact with oxygen at elevated temperatures (approx. 700°C). After some time the borosilica originating from the  $\text{Mo}_5\text{SiB}_2$  and  $\text{MoSi}_3$  phases extends to cover the surface of the material with the consequence of a reduced inward oxygen diffusion. However, Mo-Si-B alloys suffer from catastrophic oxidation in a temperature range of 700°C-800°C since there is no passivation at these temperatures [123]. Additionally the volatility of  $\text{B}_2\text{O}_3$  at temperatures above 1200°C is an issue. Burk et al. [119] tried to suppress the oxidation of Mo-Si-B by lowering the oxygen partial pressure between 820-1200 °C. An oxidation partial pressure of  $10^{-6}$  -  $10^{-4}$  bar (in the mentioned T °C range) is problematic for the oxidation of Mo-Si-B alloys. This can be attributed to the evaporation of the  $\text{B}_2\text{O}_3$  and the simultaneous formation of silica and Mo oxides. Fluxing of the silica scale and the formation of a homogeneous scale is retarded. Local silica droplet formation is observed. Therefore the development of robust and compatible oxidation resistant coatings is necessary.

In order to form phases with higher stability against oxidation at the surface of the material, a coating process which provides an applying of B/Si with controlled ratio is essential. A uniform enrichment of the local B and Si concentration at the surface results in the formation of an oxidation resistant  $\text{MoSi}_2$  layer [124] on top additionally to the stabilization of a continuous layer of borosilicide and/or boride phases underneath. This can be achieved by a co-deposition of Si and B onto the Mo-Si-B alloys followed by an annealing process at 1200-1400°C [124]. During oxidation the  $\text{MoSi}_2$  phase is consumed to form  $\text{Mo}_5\text{Si}_3$  (T1 phase). Such protective coatings are already used by Plansee SE for production of SIBOR® coatings on molybdenum as reported by Januschewsky [125] and some others before like Martinz et al. [126], Jehanno et al. [127], Martinz et al. [128] and Martinz et al. [129]. An Si-B-C mixture is plasma sprayed and subsequently short time annealed in  $\text{H}_2$ , a transient silicide/boride layer system develops which comprises a thick layer of  $\text{MoSi}_2$  at the surface followed by thinner films of  $\text{Mo}_5\text{Si}_3$ ,  $\text{MoB}_2$  and  $\text{MoB}$  respectively. Upon further annealing, Mo - diffusion from the Mo - substrate transforms the initial silicides and borides eventually into thermodynamically stable Mo-rich compounds like the ternary T2-phase  $\text{Mo}_5\text{SiB}_2$ . During exposure to air, a protective and self-healing silica layer develops at the surface. The phase transformation in the silicideboride layer system below the surface occurs concurrently with the oxidation, but is basically unaffected by the presence of oxygen. The stability and the self-healing capability are controlled by the composition of the Mo-silicide phase. While the silica layer is stable in the presence of  $\text{MoSi}_2$ , the

transformation of  $\text{MoSi}_2$  into  $\text{Mo}_5\text{Si}_3$  and later into  $\text{Mo}_3\text{Si}$  reduces the stability of the silica layer drastically. Thus, the oxidation shielding of SIBOR® relies on the presence of a continuous  $\text{MoSi}_2$  layer beneath the protecting silica layer, and hence depends largely on the transformation kinetics of the initial silicide/boride layer system.

As the outer T1 phase is always in contact with MoB or T2 borosilicide phase a saturation of T1 phase with boron is guaranteed. This phase is reported to have excellent oxidation resistance [130]. Furthermore any damage to the outer T1 layer can be recovered by the T2 + MoB layer underneath which leads to a self-healing system. The coating system also provides effective protection at low temperatures (approx. 700°C).

Besides resistance against oxidation by oxygen also oxidation resistance against water vapour may be an important property for materials used in combustion engines, as was reported by Perepezko [109]. It was shown that by partly substituting Si with B in the pack powder mixture, a continuous layer of MoB can be stabilized underneath the silicide layer coating (of  $\text{MoSi}_2$ ) onto the Mo-3Si-1B wt% substrate. This coated Mo-Si-B alloys (by pack cementation) also show significantly better performance here compared to uncoated alloys. During oxidation tests of the (B+Si)-pack alloys, the initial  $\text{MoSi}_2$  outer layer is consumed by formation of the T1 ( $\text{Mo}_5\text{Si}_3$ ) phase. With continued elevated temperature exposure during oxidation, the outer T1 phase layer would eventually be consumed by dissolution into the substrate. However, part of the initial transient stage of reaction that yields the T1 phase from the inward flux of Si and B also leads to the development of the T2 ( $\text{Mo}_5\text{SiB}_2$ ) borosilicide and/or boride phase layer. The relative amounts of the T2 and MoB phases below the T1 phase region depend on the B/Si ratio of the powder sources. The T1 phase is always in contact with the MoB or T2 borosilicide phase, which guarantees B saturation in the T1 phase. Furthermore, since the T1 phase that is saturated with B has excellent oxidation resistance and the loss of Si is blocked by the underlying diffusion barrier (i.e. the borosilicide and boride phases), the T1 layer thickness change can be arrested. Further, any damage to the outer T1 layer can be recovered from the underlying T2 + MoB layer. In effect, the in-situ reaction that yields the T2 + MoB layer also provides a kinetic bias that allows for the continued existence of the outer T1 layer and also yields a self-healing characteristic of the coating. The Si and B co-deposition treatment can also be applied to commercial Mo alloys such as the TZM alloy or pure Mo, which do not have any B or Si content. A relatively thick  $\text{MoSi}_2$  + MoB coating (50  $\mu\text{m}$ ) can form on the Mo sample at relatively low temperature (900°C) after 48 hours that provides a robust integrated coating structure that offers an excellent oxidation protection for Mo-base systems. Indeed, the capability to provide a robust oxidation protection for pure Mo at 1600°C for at least 100 hours demonstrates the remarkable advantage of the coating design [109].



## 1.4 Niobium

In addition to molybdenum, also niobium has to be considered as high temperature material. Its high melting point makes it suitable for applications at high temperatures. The chemistry and some properties of niobium are summarised below. Since pure niobium does not withstand high temperatures due to oxidation, the issue of protection from oxidation is described, especially protection by silicon.

### 1.4.1 Properties

Niobium is a refractory metal of group Va with a body-centred cubic crystal structure and a melting point of 2468°C. Niobium is a rare element and does not occur in nature in pure form. Due to similar ionic radius Niobium always occurs in the presence of Tantalum. The most important Nb-containing minerals are Columbite ( $(\text{Fe}, \text{Mn})(\text{Nb}, \text{Ta})_2\text{O}_6$  which is also known as Niobite or Tantalite dependent on the content of the elements – frequently termed “Coltan” - and Pyrochlor ( $\text{NaCaNb}_2\text{O}_6\text{F}$ ). Main producers of concentrated ore are Brazil and Canada.

The separation of Nb and Ta is done by digesting and following fractioned crystallization or solvent extraction. Another method uses the fractionized distillation of the chlorides  $\text{NbCl}_5$  and  $\text{TaCl}_5$  which are obtained by the reaction of the ore with coke and chlorine at high temperatures.

Among all refractory metals Niobium features the highest low temperature ductility and the lowest specific weight (8,4 g/cm<sup>3</sup>). Furthermore it is characterized by the highest solubility of interstitial elements and the least sensibility of ductile properties to their content. Due to this profile of properties Niobium was considered as a very promising structural material for high temperature applications for example in aerospace engineering. Up to now the main application field for Niobium is the use as alloying element in steels to increase strength and ductility. It also features some other interesting technological properties such as the ability to form superconducting alloys or a proper biocompatibility for medical applications like implants. In the present work the focus on Niobium and its base alloys is put on the application as high temperature strength construction materials.

### ***Sintering of pure Niobium***

Manufacturing of Niobium and Nb-based alloys is frequently done by the powder metallurgy route. Nb has to be sintered in high vacuum at temperatures up to 2000°C for proper degassing of oxygen and nitrogen. Sintering at high temperatures on the other hand leads to enhanced grain growth due to increased boundary mobility. As a consequence isolated pores may remain in the microstructure hindering further densification.

Sandim et al. [131] investigated the formation of microstructure (grain growth and orientation, porosity) in dependence on isothermal sintering for 1 h at 1000°C and 2000°C. They found significant coarsening of the grain structure above a sintering temperature of 1800°C, resulting in an abnormal grain growth above 1900°C. Misorientation histograms from EBSD analysis showed that whereas a random distribution of orientation was found in specimens sintered below 2000°C the fraction of low-angle boundaries increased in the specimens sintered at 2000°C. The increase in low-angle boundaries is explained by the coalescence of the grains.

Excessive grain growth at a sintering temperature of 2000°C for 2 h was also observed by Aggarwal et al. [132]. They investigated the influence of sintering temperature and time as well as sintering atmosphere on the processing of Nb by PIM (powder injection moulding) technology. It was shown that densities above 90% of theoretical density can only be achieved at sintering temperatures of  $0,75 \times T_{\text{melt}}$  Nb. Sintering in low vacuum ( $10^{-3}$  torr) at 2000°C for 2 h led to a density of 98% whereas a low partial pressure oxygen atmosphere gave a density of 94% at the same sintering temperature. In any case NbC was found in the microstructure of the specimen (from the organic binder).

The influence of compaction pressure for the preparation of green compacts on microstructure was investigated by Zilnyk et al. [133]. They used pressures of 200 MPa and 1500 MPa to produce green compacts which were sintered at 2000°C in high vacuum for various sintering times. From the results of metallographic investigations they concluded that high pressures for compaction of green bodies lead to a more pronounced grain growth. This effect was explained by a primary recrystallization process taking place at the early stage of sintering which increases the driving force for further normal grain growth. According to the authors, this recrystallization happens because of the intense grain fragmentation during cold compaction at high pressures.

An investigation by Schulze et al. [134] deals with the possibility of liquid phase sintering of Nb. They describe a fast sintering process with the help of a disappearing liquid Nb-oxide phase. If Nb powder is exposed to air, a layer of Nb<sub>2</sub>O<sub>5</sub> is formed on the surface of the powder with an approximate thickness of 5-10 nm. The application of an extremely high heating rate up to 1500°C leads to melting of Nb<sub>2</sub>O<sub>5</sub> ( $T_{\text{melt}} = 1495^{\circ}\text{C}$ ) before it can transform to NbO and NbO<sub>2</sub> and the oxygen can dissolve in the bulk. Due to the formation of a liquid phase, contact zones between Nb particles can be built up very quickly. Furthermore the oxygen from the melt immediately diffuses into the Nb particles resulting in only one Nb-O-mixed phase in the microstructure. According to the authors a heating rate of >5000 K/min is necessary for this sintering mechanism. In their experiments they used an electron beam to achieve such high heating rates.

### ***Nb-based alloys***

To increase high-temperature strength and improve resistance against oxidation at operating temperatures >1000°C various Niobium-base alloys were developed during the 1960s and 1970s [135,136].

Besides an aspired long time service at operating temperatures also a high workability has to be achieved. To increase the high-temperature strength of Nb-alloys, common methods of strengthening may be applied, such as the solid solution method, alloying by interstitial and substitutional elements, precipitation or dispersion strengthening and also the creation of special structures. Sheftel et al. gave a good overview on the design of high-temperature strength Nb-base alloys especially by the strengthening by oxides, carbides and nitrides [137]. The influence of alloying elements like Ti, Zr, Al, Cr, W, Mo, Fe, Ni, Co on the resistance against oxidation is summarized in an overview article by Loria et al. [136].

The alloying of Nb by these elements respectively combinations leads to an improvement in resistance against oxidation (expressed as average oxidation rate by weight gain) by at least 6 to 10 fold compared to unalloyed Niobium.

New developments of Nb-based materials for high-temperature applications focus on Nb-silicide based composites which are treated separately below.



## 1.5 Niobium and silicon

Niobium silicide based composite materials may serve as structural materials for enhanced aeroengine turbine applications due to their low density, high melting point and high strength and creep resistance at operating temperatures exceeding 1200°C. However binary Nb-Si phases suffer from low fracture toughness and poor resistance against medium and high temperature oxidation, due to the formation of non-protective oxides. In fig. 1.6 the binary phase diagram of Nb-Si is shown. The most important technological materials correspond to the two-phase-area Nb/Nb<sub>5</sub>Si<sub>3</sub> which is marked yellow in fig. 1.6. Such structural materials consist of two components, the high strength Nb<sub>5</sub>Si<sub>3</sub> component and the ductile Nb matrix. In the binary phase diagram in fig. 1.3 can be seen that only a small amount of Si can be dissolved in Nb.

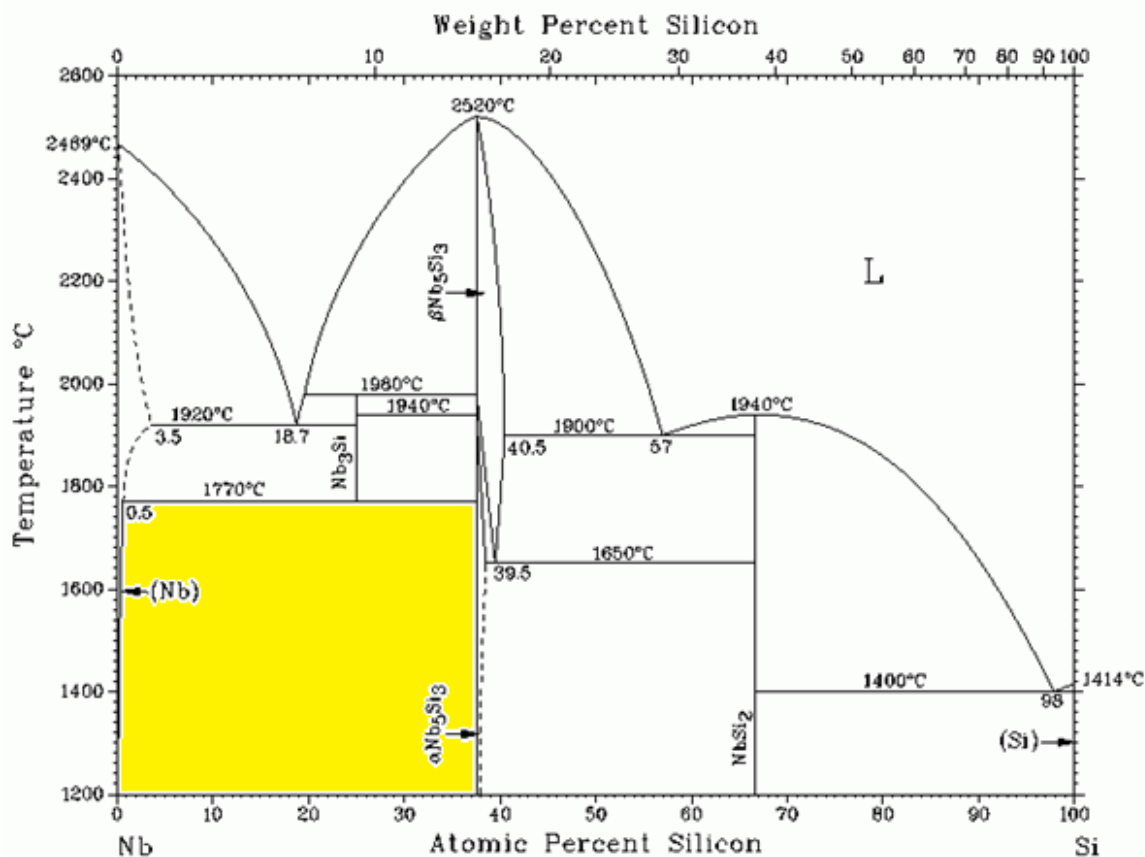
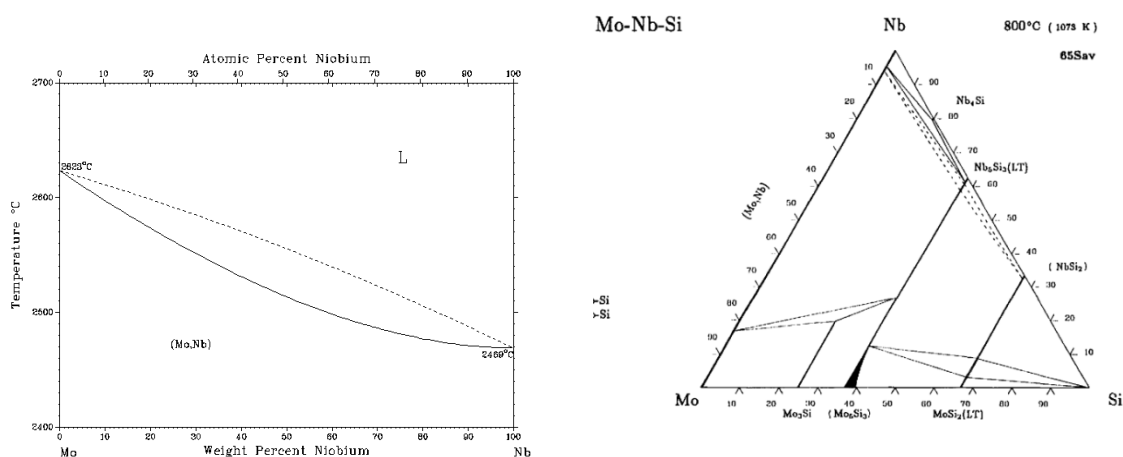


fig. 1.6.: Binary phase diagram of Nb-Si

Exposure to high temperatures leads to an oxidation of Nb to Nb<sub>2</sub>O<sub>3</sub> and also the Nb<sub>5</sub>Si<sub>3</sub> phase undergoes a transition from Nb<sub>5</sub>Si<sub>3</sub> to Nb<sub>2</sub>O<sub>3</sub> in a temperature range of 700°C to 1000°C [138]. The formation of Nb<sub>2</sub>O<sub>3</sub> leads to high stresses in the metal-oxide interface as the molar volume of Nb<sub>2</sub>O<sub>3</sub> is significantly higher compared to Nb [139]. Additionally the lower CTE (coefficient of thermal expansion) of Nb<sub>2</sub>O<sub>3</sub> compared to Nb<sub>5</sub>Si<sub>3</sub> (approximately one fourth) leads to residual tensile stresses inside of the oxide scale.

Alloying elements such as Ti and Cr can improve mechanical properties as well as oxidation resistance. Bewlay and co-workers [140,141] designed a family of Nb-silicide



The requirement for high temperature structural materials, specifically for applications in turbine blades operating at temperatures above 1000 °C, has led to significant research in the area of multicomponent Nb-silicide based alloys with high melting temperatures, impressive mechanical properties and adequate oxidation resistance. The microstructures of the Nb-silicide based alloys consist of either Nb<sub>ss</sub> (Nb solid solution with a small amount of Si, solubility less than 1 at.%) or Nb<sub>5</sub>Si<sub>3</sub> as the primary phase, and a eutectic mixture of Nb<sub>ss</sub> and Nb<sub>5</sub>Si<sub>3</sub>. High temperature strength of Nb-silicide based alloys is governed by the volume fraction of Nb<sub>5</sub>Si<sub>3</sub>, whereas their low temperature fracture toughness is a function of the amount of Nb<sub>ss</sub>, having limited ability for plastic deformation. Studies on ternary additions of Mo to the Nb–Si alloys by Kim et al. [147,148] and Chattopadhyay et al. [149] have established its positive role in increasing the elastic modulus, microhardness of the constituent phases, strength and fracture toughness, provided the composition and volume fraction of the constituent phases is optimised (fig. 1.7). Furthermore, Kim et al. have shown that alloying with Mo inhibits the eutectic reaction leading to the formation of Nb<sub>ss</sub> and Nb<sub>3</sub>Si and promotes the formation of Nb<sub>ss</sub> and Nb<sub>5</sub>Si<sub>3</sub>. As a consequence, although metastable Nb<sub>3</sub>Si is observed in the binary Nb–Si alloys, it has been reported to be absent in the

Nb–Si–Mo alloys. The microstructure and mechanical behaviour of Mo - Si - Nb alloys have also been studied by Ma et al. [150] and Nakano et al. [151]. The results from Kim et al. and Chattopadhyay could be confirmed.

Zhang et al. [152] have described the oxidation behaviour of the  $(\text{Mo}_{1-x}\text{Nb}_x)\text{Si}_2$  pseudo-binary system over a wide composition range ( $x=0-0.6$ ) at different temperatures between 1473 and 1773 K. Compared with binary  $\text{MoSi}_2$ , a small amount of Nb substitution results in an improved oxidation resistance in the single-phase region.  $(\text{Mo}_{0.7}\text{Nb}_{0.3})\text{Si}_2$  displays the lowest weight gain and thus has the best oxidation resistance at all investigated temperatures. The oxidation tests carried out by Chattopadhyay et al. [153] showed that among the Nb-Si-Mo alloys, those with a lower concentration of Mo have shown a higher gain in mass (higher oxidation), compared to those having a higher Mo content.

Nevertheless, all described compositions have been prepared by arc melting. There is barely literature available about sintering in solid state of Mo - Nb alloys. Yao et al. [154] studied the interdiffusion behaviour in the Nb/ $\text{MoSi}_2$  system by solid–solid diffusion couples annealed at 1250–1400 °C for 120 h. Two intermediate phases,  $\text{Nb}_5\text{Si}_3$  and  $(\text{Nb},\text{Mo})_5\text{Si}_3$  have been detected in the Nb/ $\text{MoSi}_2$  diffusion couples. The integrated interdiffusion coefficients and the average interdiffusion coefficients in  $\text{Nb}_5\text{Si}_3$  phase have been determined from the interdiffusion fluxes. Strong diffusional interaction between Nb and Mo in  $(\text{Nb},\text{Mo})_5\text{Si}_3$  phase has been detected.

As can be seen, some more work has to be done on the sintering behaviour of Mo with Nb as one bulk material. In particular the influence of sintering atmosphere on the properties of specimens thus prepared has to be examined more carefully.

## **Aim of this thesis**

The aim of the work was the preparation of a novel composite material comprising a continuous metallic skeleton fully covered by a silicide surface area that gradually transforms into the metallic core material, whereas continuous refractory metal will improve the fracture toughness, ductility and creep resistance and the silicide grants the oxidation resistance at high temperatures. A self-healing silica or complex oxide coating should be automatically formed at the surface of composite in oxidising environment at HT without danger of its premature evaporation.

As metallic skeleton, molybdenum and also niobium were chosen. The preparation of specimens was carried out by powder pressing and sintering of the metal powders at TUW. Such preforms have to be characterised for their density, open porosity and mechanical properties. The open porosity is controlled by pressing and sintering parameters. The particle size of the initial powder is also deciding for the resulting open porosity. Additional to the TUW experiments with powder metallurgical preparation route of Mo preform, also electron beam sintering was carried out by the partner KE. In both cases further experiments are carried out where some Si was added to Mo during porous preform preparation.

Such continuous porous skeletons of refractory metal (Nb, Mo) were then sent to be infiltrated with molten silicon by IMSAS or by CVI by ATL.

During Si infiltration, partial reactions between melt/gas and refractory metal take place, forming silicides predominantly in the vicinity of the surface of the porous precursor, leaving less free silicon for formation of silicides inside the porous structure, thus making in situ functionally graded materials with gradiently increasing metal content towards the core of composite. To ensure sufficient mechanical strength, porous and thus infiltrable near-surface area and fully dense core were regarded as optimum preforms.

## 2 Sample preparation and characterisation methods

### 2.1 Preparation

#### 2.1.1 Starting powders used

##### 2.1.1.1 Molybdenum from Plansee

In fig. 2.1 the molybdenum powder from Plansee SE is shown (grade “<32  $\mu\text{m}$ ”). This powder was used only for some experiments in the beginning. It was an Mo powder which had been stored for a long time and as it was consumed it was not possible to buy further powder of the same grade. It was subsequently replaced by the Chemie Metall powder. Octahedral particles of different sizes can be observed. The particles stuck together which can be seen in fig. 2.1. A reason might be the oxides on the surface (present due the long storage). Even though the powder was sieved before using for experiments they stuck again. The largest particles do not exceed 4  $\mu\text{m}$ .

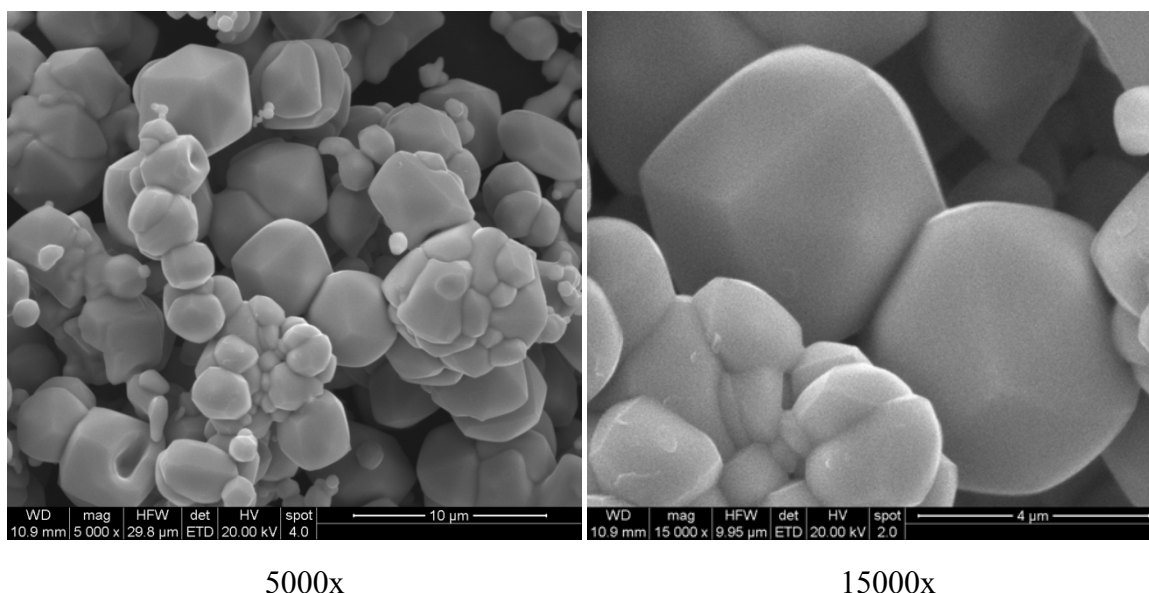


fig. 2.1.: Molybdenum powder from Plansee SE at 5000x and 10000x magnification; depicted as a “<32  $\mu\text{m}$ ” powder

##### 2.1.1.2 Molybdenum from Chemie Metall

In fig. 2.2 the molybdenum powder from Chemie Metall can be observed. At 5000x magnification can be seen that most particles are below 5  $\mu\text{m}$  even though the powder was sold as a “ $\leq 63 \mu\text{m}$ ” powder. Just a few particles are bigger than 5  $\mu\text{m}$ . As can be observed in fig. 2.2 most of the fine grained particles are agglomerated. Before implementation of this powder for experiments, it was sieved to disintegrate possible agglomerates. Some of the fine particles are adhered forming a kind of “rope”, which passed the sieve and did not disintegrate. Due to the fact that the Mo powder from Chemie Metall is very similar to the one from Plansee SE, it replaced the Plansee SE powder (after the Plansee SE powder was used up).

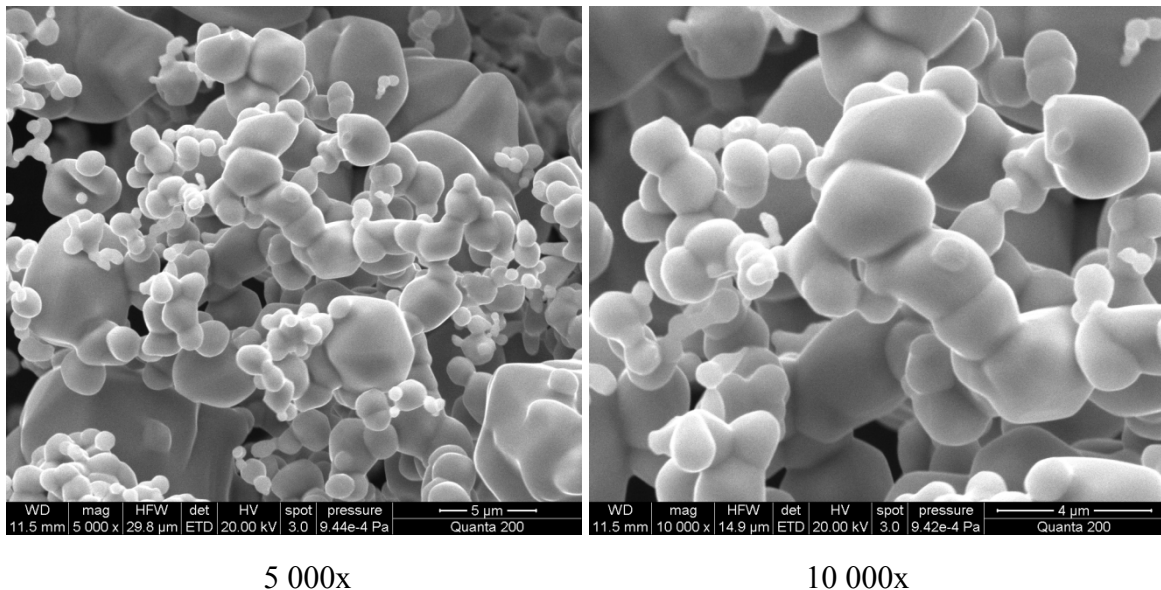


fig. 2.2.: Chemie Metall powder at 5 000 x and 10 000 x magnification; nominal particle size  $\leq 63 \mu\text{m}$

In fig. 2.3 the results from the particle size measurement on a Sympatec particle size analyzer are given. These data were supplied by Chemie Metall. From fig. 2.3. can be seen very well that  $d_{50}$  is in the range of  $10 \mu\text{m}$ , i.e. the powder is much finer than the nominal designation  $<63 \mu\text{m}$ .

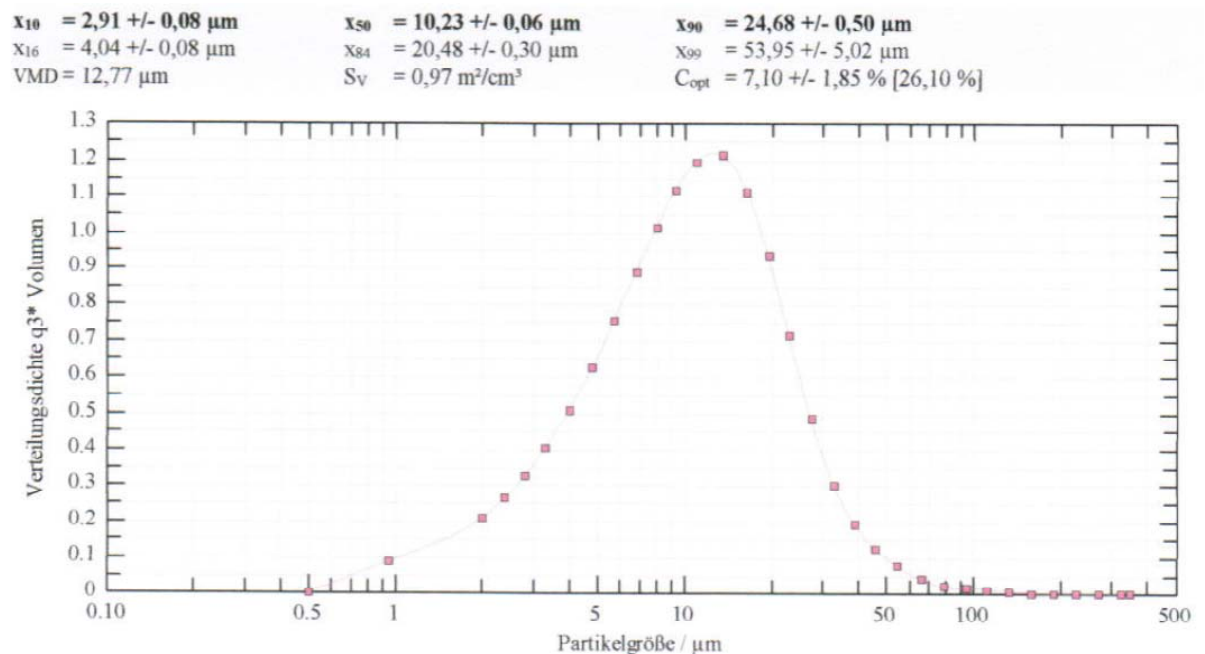


fig. 2.3.: Particle size distribution of Chemie Metall Mo powder as measured on Sympatec laser particle size analyzer (data from Chemie Metall);

### 2.1.1.3 Molybdenum powder from Goodfellow

In fig. 2.4 the Mo powder from Goodfellow is shown. Already in the 50 x magnification it can be seen that the particles are very coarse. This powder was sold as a coarse Mo powder with particle size  $< 355 \mu\text{m}$ . At 1500 x magnification one particle is shown in



detail. It can be seen that one large particle consists of many small ones which were sintered together. Apparently after sintering the material was crushed, and the coarse particles were obtained this way.

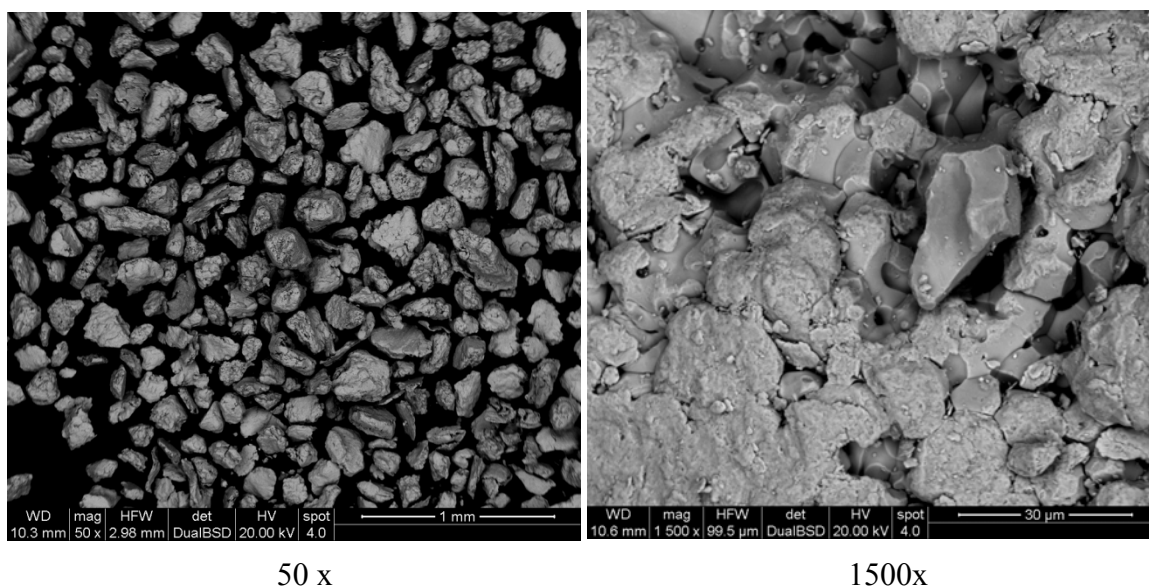


fig. 2.4.: Coarse molybdenum powder from Goodfellow at 50 x and 1500x magnification

#### 2.1.1.4 MoO<sub>2</sub> from Chemie Metall (CM)

The shape and size of the MoO<sub>2</sub> powder is shown in the SEM images summarized in fig. 2.5. The particles are very angular and form plates. For the MoO<sub>2</sub> powder from Chemie Metall (obtained through the project partner KE) an oxygen content of  $18.3 \pm 0.1$  mass% was measured by Leco. Stoichiometric calculations resulted in 25 mass% of oxygen to be expected. A much lower amount was measured on Leco, which is probably due to the fact that it is quite difficult to measure volatile materials on Leco. Some of the volatile MoO<sub>2</sub> sublimated in the LECO tester during heating up (even if the heating is very quick) and therefore this amount could not be reduced and measured in Leco.

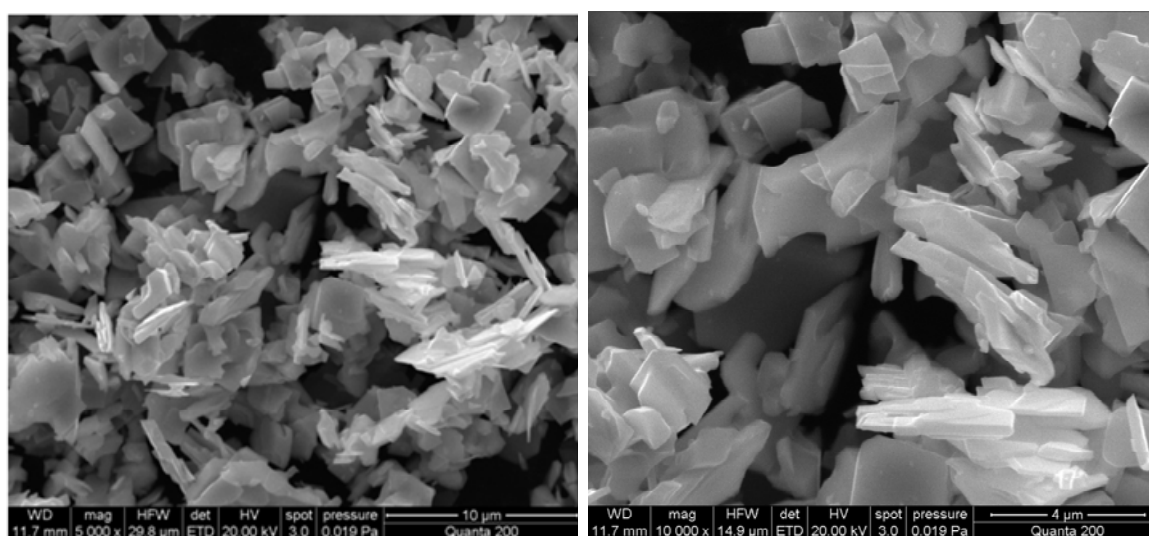


fig. 2.5.: SE images of the MoO<sub>2</sub> from CM; left: 5000x and right: 10 000x magnification



By XRD it could be shown (in fig. 2.6) that the whole powder is pure MoO<sub>2</sub> (Tugarinovit).

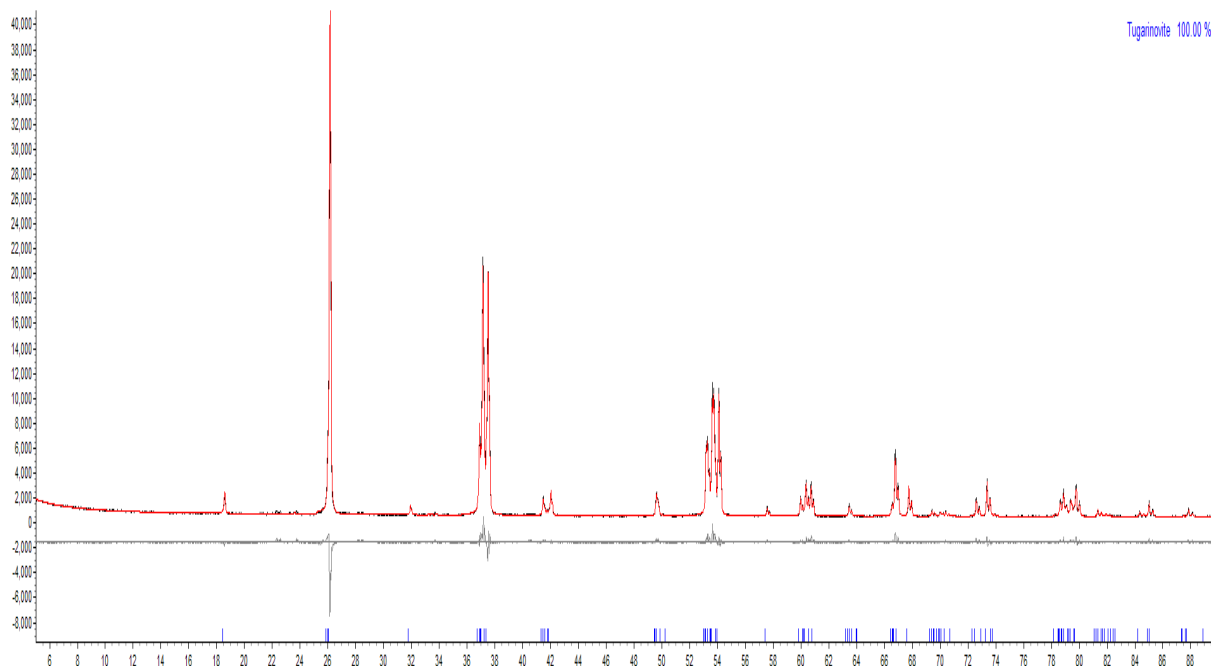


fig. 2.6.: XRD pattern of Chemie Metall MoO<sub>2</sub> powder; x axis: 2θ; y axis: intensity in arbitrary units

#### 2.1.1.5 Niobium powder from H. C. Starck - Amperit 30/10 μm

The Nb powder was bought from H. C. Starck under the designation "Amperit 30/10 μm". In fig. 2.7 SEM images at 400 x and 1500 x magnification of the Nb powder are demonstrated. The particles are sharp edged and of different sizes between 10 and 50 μm. At 1500 x magnification it can be recognized that the powder was apparently prepared by crushing of ingots.

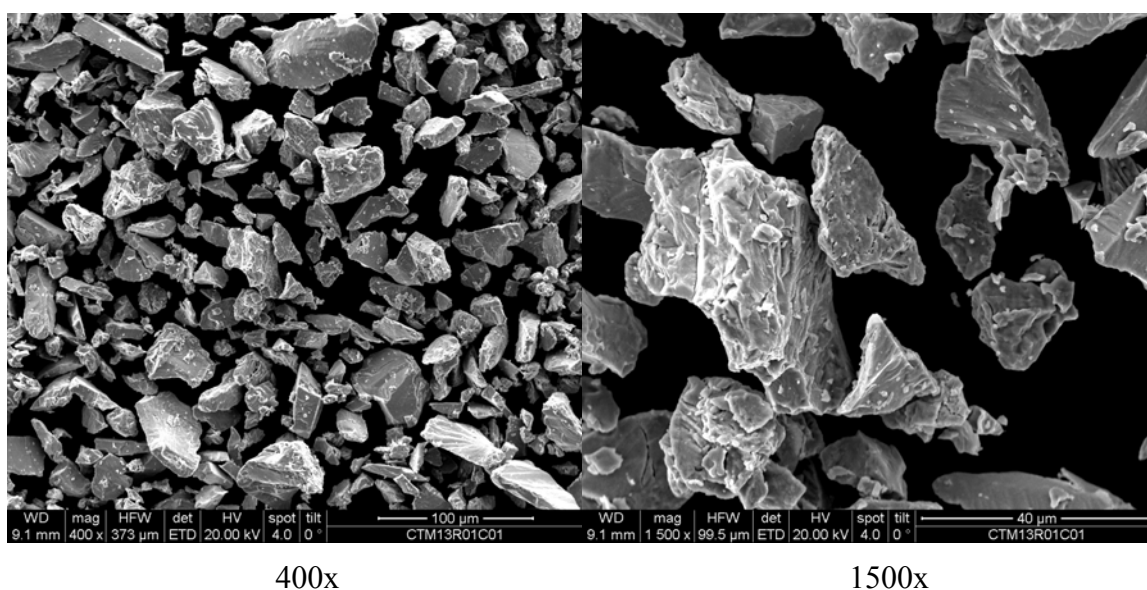
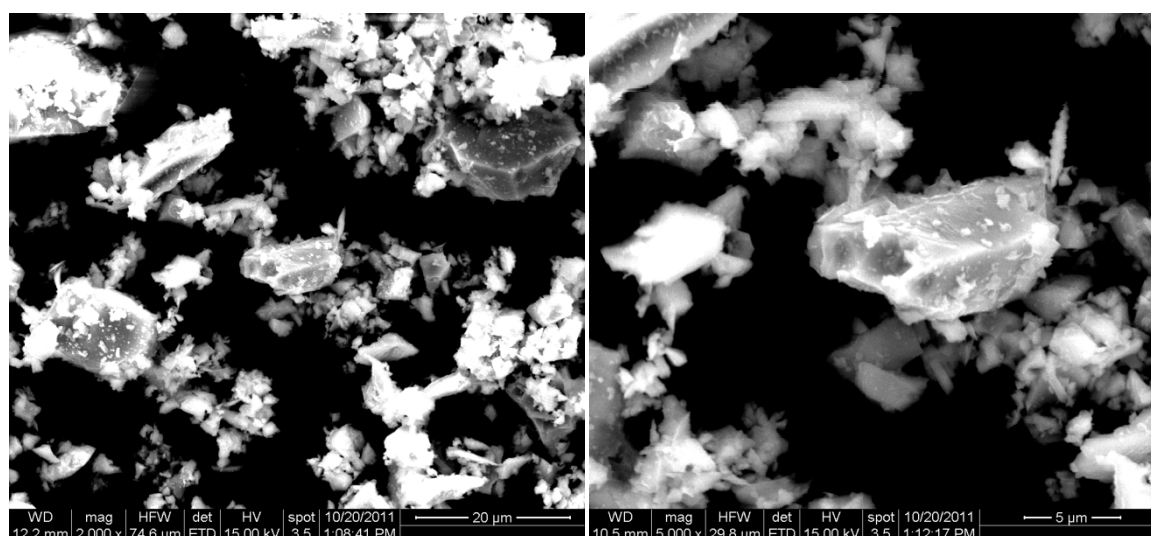


fig. 2.7.: Nb powder from H.C. Starck - Amperit 10/30 μm

### 2.1.1.6 Silicon from Ecka

In fig. 2.8 two SEM images of the Ecka silicon powder are shown. It was difficult to prepare focused images. The powder was stored for a long time at TU Wien and therefore a lot of oxygen was adsorbed at the surface impeding the SEM measurement. The oxygen content was measured on Leco and was determined as 0.96% oxygen which is a quite high amount. This can explain the low conductivity (of electrons during SEM measurement) and the blurred images. The powder consists of particles of different shape and size, with small particles in the range of 1  $\mu\text{m}$  and some bigger ones in the range of 10  $\mu\text{m}$ .



2000x

5000x

fig. 2.8.: Silicon powder from Ecka at 2000 x and 5000 x

### 2.1.1.7 Nickel powder

In fig. 2.9 - 500x magnification, a lot of very small Ni particles from Carbonyl Ni INCO 123 are demonstrated. In the 5000x magnification it can be seen that the small round particles from 500x magnification consist of even smaller particles.

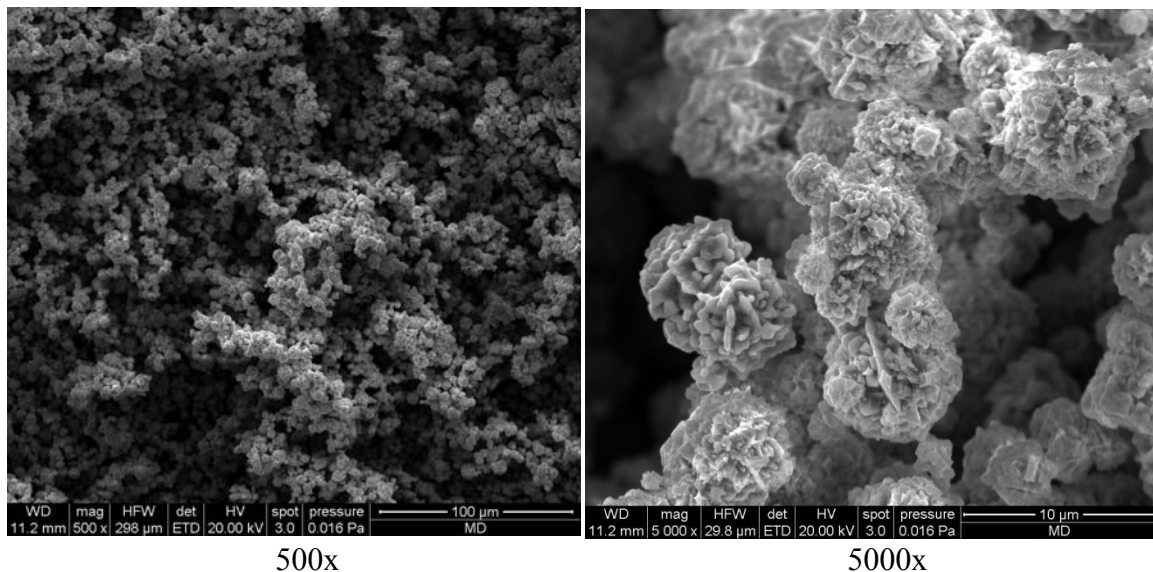


fig. 2.9.: Nickel powder from INCO 123

### 2.1.1.8 Space holder - wax Kenolube P11

Kenolube P11 is a lubricant wax which reduces the friction during pressing. It consists of 22.5 wt% zinc stearate and 77.5 wt% of amide wax. For the compaction of very coarse Mo or Nb powders, Kenolube P11 was used as a lubricant helping to reduce the friction. For some experiments it was also used as space holder. Different amounts of Kenolube P11 wax, up to 5 wt%, were mixed into the Mo powder.

## 2.1.2 Manufacturing of samples

### 2.1.2.1 Mixing of powders

The relevant starting powders were weighed in PE containers (500 ml) and dry mixed in a tumbling mixer for 3 h. The frequency was 100 rpm. Some steel grinding balls and a spiral were added to enhance mixing and destroy agglomerates.

For some experiments a wax was added. After 3 h premixing of the powders a preset amount of the wax was weighed into the powder mixture and mixed in the tumbling mixer for another 30 min. This stepwise mixing was chosen to prevent formation of agglomerates.

### 2.1.2.2 Pressing

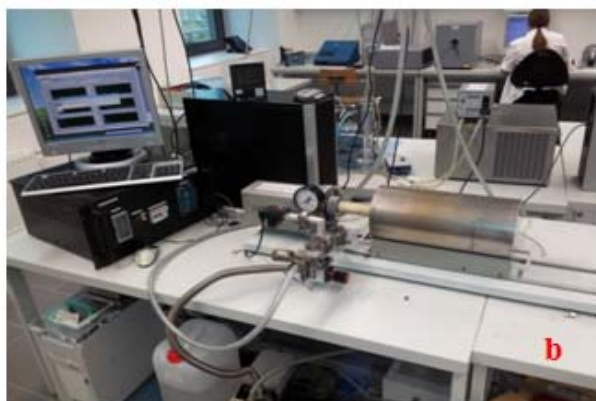
In this work three different presses were used. The first one was a hydraulic press supplied by Jessernigg & Urban ( $F_{\max} = 1500 \text{ kN}$ ). Charpy rods of  $55 \times 10 \times \text{ca. } 8 \text{ mm}$  were pressed with a defined compacting pressure. This kind of press is not too accurate at low pressing forces and tends to overpress the set pressure. Therefore the green densities of specimens pressed on this press are a little bit higher.

The second press was a hydraulic press manufactured by Amsler. The shape of the specimens could be defined by the tool used. For this work only cylindrical specimens (20 mm or 11.27 mm diameter) were pressed on this machine. It was possible to set accurate values for the pressing force on this press, therefore the values differ (are lower) from the ones pressed on the Jessernigg & Urban press. However, since the green densities were routinely measured, any discrepancies of the compacting pressure were immediately recognized.

The third press was a cold isostatic press from P. O. Weber, type PW 40. The shape of the specimen was preset by a silicon mould which was put into the press liquid. In this work cylindrical ( $\varnothing 20$  mm and 10 mm; 15-20 mm height) and rectangular specimens (55 x 10 x 8 mm) were prepared on this press.

### 2.1.2.3 Sintering

The removal of the wax Kenolube P11 was carried out in an AHT – push type furnace with a retort consisting of heat-resistant steel (W Nr. 1.4841). The Kenolube P11 wax was used as binder for the very coarse Mo powder and as space holder for some experiments carried out with Mo. The delubricating atmosphere was  $N_2$  (5.0 purity = 99.999%; 2 l/min gas flow) for 1 h soaking period at 600 °C. Afterwards the specimens were pushed into the cooling zone (shown left in fig. 2.10) and cooled down with  $\sim 0.5$  K/min.





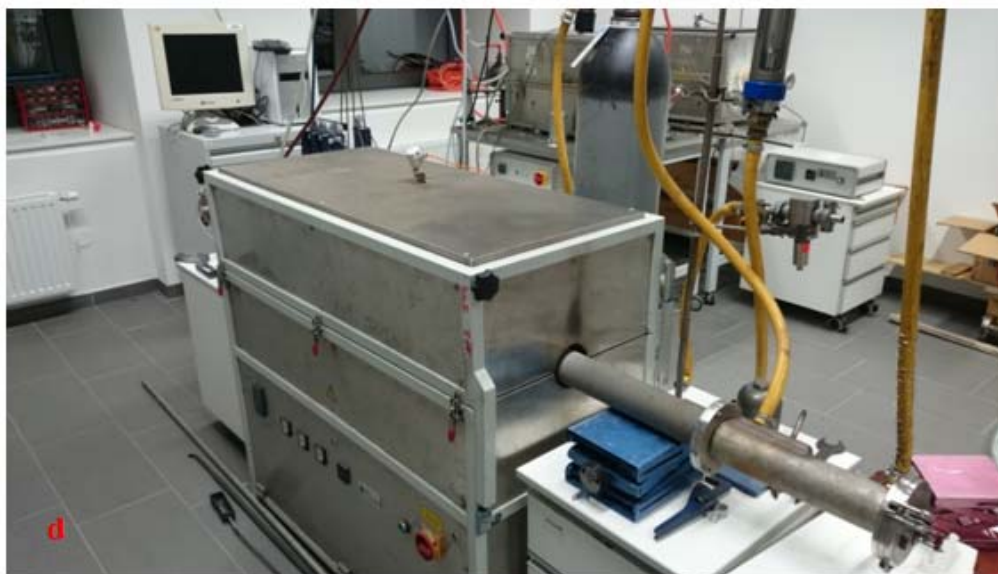


**fig. 2.10.: a: AHT push type furnace with heat resistant retort; left: cooling zone – cooled by water; b: Bähr DIL 801 for sintering in vacuum; c: KCE hot press; d: AHT - SiC pushtype furnace with a gas-tight superalloy muffle**

Sintering was carried out in a high temperature furnace. This furnace is a pushtype furnace (type AHT-SiC) with gas-tight superalloy muffle. The heating elements are silit rods. The furnace tube is a dispersion strenghtened Kanthal superalloy APM (Fe-22%Cr-7%Al). The highest operating temperature is 1300 °C.

The furnace was heated up to 1300 °C, the sintering boat was placed in the preheating zone for 10 min. Afterwards, the sintering boat was inserted in the center of the furnace, - in the hottest zone for sintering. Sintering of molybdenum was always carried out in reducing atmosphere in hydrogen (5.0 purity; 2 l/min gas flow).

Further sintering experiments were carried out in a Nabertherm pushtype furnace with a Kanthal superalloy retort. The highest operating temperature is 1300 °C, too. A difference to the AHT pushtype furnace is the size of the retort. The Nabertherm has a much wider retort. The sintering atmosphere was also hydrogen (5.0 purity; 2 l/min gas flow).

The sintering experiments of sintering Mo - Nb compacts were carried out in a Nabertherm MoSi<sub>2</sub> heated furnace with a Al<sub>2</sub>O<sub>3</sub> retort. The difference to the AHT pushtype furnace is only the type of retort and the higher operating temperature of 1500 °C. Furthermore, the experiments have been carried out in vacuum. A rotary vane pump was connected to the Al<sub>2</sub>O<sub>3</sub> retort.

Hot pressing was carried out in a KCE hot press. For heating a graphite heating element was used. Maximum operating temperature is 1800 °C. Pressure can also be applied during sintering. The maximum pressure is 100 kN. The specimens were placed in the center of the KCE press, in the center of the graphite heating elements. The temperature measurement started at 600 °C (set point of the pyrometer). From this temperature the pressure was slowly increased up to 50 kN at 1800 °C. This temperature and pressure were held for 2 h soaking period. During cooling down, no pressure was applied.

The KCE hot press was also used in some experiments for pressureless sintering at 1800 °C. The specimens were placed in a cylindrical graphite die without using any punches. The graphite die was placed in the center of the KCE press and heated up to 1800 °C without applying any pressure. The soaking period was 2 h.

For sintering at 1500 °C a dilatometer Bähr DIL 801 was used with an Al<sub>2</sub>O<sub>3</sub> measuring system and a protecting tube closed on one end. The sintering could be carried out in vacuum only. The vacuum was applied by an oil-sealed vacuum rotary vane pump. The furnace was water cooled during the whole sintering process. The maximum run temperature is 1500 °C. The specimen was placed into the specimen holder, the Al<sub>2</sub>O<sub>3</sub> tube was closed, the sliding furnace was pushed in position and the system was evacuated until the atmosphere reached  $4 \cdot 10^{-2}$  bar. Afterwards, the sintering run was started. The temperature of 1500 °C was held for 2 h soaking period.

Sintering of the first Nb specimens was carried out in a "MF - recipient - induction furnace" ("MF-Rezipienten-Induktionsofen") which can be seen in fig. 2.11. For the sintering all Nb specimens were put into an Mo cup which was placed in the center of the furnace. The Mo cup was surrounded by a heating coil. Under the Mo cup and above a radiant panel out of Mo was placed. The function of the radial panels was to ensure a homogeneous distribution of the temperature in the Mo cup and the furnace. The temperature was measured with a pyrometer. The temperature was controlled by an electronic temperature controller from Eurotherm. The heat was produced by a generator - MF-Generators PS 12/18 (Frequency range 14-40 kHz, maximum power 18kW, from company: EFD Induction).



**fig. 2.11.: inside of the MF - recipient - induction furnace**

The oxidizing experiments of the FGM specimens were carried out in an AHT pushtype furnace with  $\text{Al}_2\text{O}_3$  tube which was open at both ends. On one end a gas burner was placed which introduced the combustion gases (natural gas and oxygen mixture- burned in a flame) into the furnace. The highest operating temperature was 1300 °C. The specimen was placed on a mullite sintering support plate in the hot zone of the furnace. During the heating up and cooling of the furnace, the specimen was in the furnace the whole time. The furnace was feeded with combustion gas already during heating up and during the soaking period of 3 h. For cooling of the furnace, only atmosphere gas (air) was used.

#### **2.1.2.4 Infiltration of Mo and Nb specimens by partners**

##### **CVI by ATL**

ATL carried out the infiltration process with Si by a chemical vapour infiltration process (CVI). As Si source  $\text{SiCl}_4$  was used. The specimens were placed in a furnace and heated up to temperatures between 850 and 1000 °C and isothermally held for 120 min. During this soaking period the  $\text{SiCl}_4$  was inserted into the furnace. Two ways of how the gas was fed into the furnace were chosen. In the first experiments the gas was filled into the furnace, and it remained in the reaction chamber during the whole infiltration process until cooling. In some further experiments the furnace was constructed in this way that the  $\text{SiCl}_4$  passed during the whole soaking period.

##### **Liquid infiltration by IMSAS**

IMSAS carried out the infiltration process in an induction furnace. Only 3 specimens could be infiltrated at the same time (in one experiment). The specimens were placed in a graphite die and the calculated amount of Si fragments was poured at each specimen. As Si source, molten Si which had been crushed after cooling was used. The graphite die was placed in a quartz tube. Outside the tube, at the position where the graphite die inside was situated, an induction coil surrounded the tube and heated up the furnace to about 1500 °C (melting point of Si is at 1410 °C, - due to the long way of energy transfer between the induction coil and specimens a higher temperature was chosen). After all Si was molten, which was observed from outside, the heating was stopped and the furnace was cooled down.

#### **2.1.2.5 Metallographic preparation**

The sintered specimens were cut along the height (= axially) on a Struers Accutom 50 with a  $\text{Al}_2\text{O}_3$  cutting wheel. Hot pressed Mo+wt%Si specimens have been cut with a diamond cutting disc. After cutting the samples were hot embedded in bakelite, so that the cross section was visible.

The grinding and polishing of the cross section was carried out on a Struers TegraPol31 polishing machine. The specimens were fixed in the machine and the grinding and polishing was carried out automatically. In the first step a MD Piano 220 disc for grinding was taken and the specimens were ground for 20 min with water cooling. In the next step a MD Allegro disc was used and a 9 µm diamond suspension was added drop by drop for 10 min until the first polishing step was finished. In the last polishing



step a MD Dac disc was used with a 3  $\mu\text{m}$  diamond suspension which was also added drop by drop during the whole 20 min of polishing.

After completing of the polishing all samples were put into a ultrasonic bath for cleaning of the surface and at the end the surface of the specimens was rinsed with isopropanol and dried with a hair dryer.

### 2.1.3 Measurement of physical and mechanical properties

#### 2.1.3.1 Measurement of the density

##### 2.1.3.1.1 Green density

The green density was calculated through eq. 2 from the volume and mass of the green bodies. The volume was measured with a sliding caliper (precision 0.02 mm) and calculated with eq. 1. Afterwards the weight of the specimens was measured and the density calculated.

$$V_G = l_G * w_G * h_G \quad \text{eq. 1}$$

$l_G$  length of the green compacts [cm]  
 $w_G$  width of the green compacts [cm]  
 $h_G$  height of the green compacts [cm]

$$\rho_G = \frac{m_G}{V_G} \quad \text{eq. 2}$$

$\rho_G$  density of the green compacts [ $\text{g}/\text{cm}^3$ ]  
 $m_G$  mass of the green compacts [g]  
 $V_G$  volume of the green compacts [ $\text{cm}^3$ ]

##### 2.1.3.1.2 Sintered density

The sintered density was measured by Archimedes method (DIN ISO 3369). Therefore the specimens were weighed in air, impregnated with a Erdal water stop spray, and the dry specimens were weighed in water. The density was calculated with eq. 3. The buoyancy effect in air was neglected.

$$\rho^s = \frac{m_a}{m_a - m_w} \cdot \rho_w \quad \text{eq. 3}$$

$\rho_s$  sintered density [ $\text{g}/\text{cm}^3$ ]  
 $\rho_w$  density of water [ $\text{g}/\text{cm}^3$ ]  
 $m_a$  mass of sample in air [g]  
 $m_w$  mass of sample in water [g]

### 2.1.3.2 Measurement of the He – pycnometer density

He - pycnometry was used for measuring the density and in further step for calculation of the open porosity. More accurately, the volume of solids which may be regularly shaped, porous or non-porous, monolithic, powdered, granular or in some way comminuted is measured. The volume of the solid is calculated from the measured drop in pressure of a known amount of gas which is allowed to expand into a chamber containing the sample. The density is then calculated as the ratio of mass (measured by weighing) to volume. The volume measured in a gas pycnometer is that volume which is inaccessible to the used gas. Therefore the volume measured considering the finest scale of surface roughness will depend on the atomic or molecular size of the gas. Helium therefore is most often used as the measurement gas, not only because of its small atom size but also because of its inert and most ideal gas behaviour. Closed pores, which means those that do not communicate with the surface of the solid, are included in the measured volume. Open porosity then may be calculated in reference to the volume including total porosity which can be measured for example by Archimedes method.

### 2.1.3.3 Measurement of the porosity

The open porosity can be calculated from the density measured with He - pycnometry and Archimedes density or measured with immersion method.

In the first case the open porosity was calculated from the density measured with Archimedes and the density measured with He – Pycnometry. In the measurement of the Archimedes density the closed and open porosity are included in the resulting values for the density. By measuring the density with He Pycnometry only the closed porosity is included in the resulting values for the density (the open porosity can be penetrated by He). By the subtraction of the He – pycnometry values from the Archimedes values the resulting density is considering only the open porosity. For the calculation the theoretical density of each specimen was needed. The theoretical density was calculated (for the silicon containing Mo specimens) from the silicides formed (amount of each phase was measured by XRD).

For the measurement of the open porosity by the immersion method the specimen weight in air was taken ( $w_{\text{dry}}$ ). Afterwards the specimen was situated in an exsiccator in a glass bowl and evacuated for 10 min (to avoid any residue gas in the pores of the specimen). The vacuum pipe was closed and the water supply was opened. The specimen was covered and partially infiltrated with water. The exsiccator was evacuated again to produce some underpressure and afterwards air was inserted abruptly to the exsiccator which pressed the water into the pores of the specimen. The wet specimen was taken out of the exsiccator, the surface was carefully wiped with a towel (avoiding stopping with the towel in one position not to absorb the water from the pores), and the weight of the saturated specimen was taken ( $w_{\text{sat}}$ ). The weight of saturated specimen immersed in water again was taken ( $w_{\text{wet}}$ ). Now the open porosity could be calculated by

$$P = \left( \frac{w_{dry} - w_{sat}}{w_{dry} - w_{wet}} \right) * 100$$

#### 2.1.3.4 Measurement of the pore size with Hg porosimetry

By applying pressure to a sample immersed in mercury, the mercury is forced into pores and cavities and thereby the sizes of these pores and cavities can be determined. Mercury porosimetry can determine a wide range of data e.g.: Total pore volume, total pore surface area, differential volume. Mercury intrusion porosimetry involves placing the sample in a special sample cup (penetrometer), then surrounding the sample with mercury. Mercury is a non-wetting liquid to most materials and resists entering voids, doing so only when pressure is applied. The pressure at which mercury enters a pore is inversely proportional to the size of the opening to the void. As mercury is forced to enter pores within the sample material, it is depleted from a capillary stem reservoir connected to the sample cup. The incremental volume depleted after each pressure change is determined by measuring the change in capacitance of the stem. This intrusion volume is recorded with the corresponding pressure or pore size. The mercury measurement was carried out externally on a Pascal 140 equipment from Porotec, and only the results have been received.

#### 2.1.3.5 Measurement of the electrical conductivity

The electrical conductivity was measured by Foerster Sigmatest 2.067 and by "semi-automatic resistance device".

The Foerster Sigmatest 2.067 determines the conductivity by measurements based on the complex impedance of nonferromagnetic materials. Test frequency was 60 kHz. The Sigmatest 2.067 was calibrated by measuring 2 conductivity standards and positioning the indicator to the corresponding electrical conductivity value. This procedure was continued until the right conductivity values were shown for both standards. Electrical conductivity measurements were carried out on Charpy samples (55x10x10 mm) and cylindrical specimens with 20 mm diameter. At least four points on the samples were measured and the mean value was calculated. For good absolute values at least a sample diameter of 16 mm is recommended since edge effects can show an influence on the measurement results. Therefore the absolute electrical conductivity values may not be completely correct for the Charpy specimens which are only about 10 mm wide. However, due to the fact that all samples were measured in the same way a relative comparison was possible.

The resistance was also measured with a "semi-automatic resistance device", operating through the 4-point method and custom-built by the technician Wolfgang Tomischko. For the measurement all dimensions of the rectangular specimen were noted and the

cross section  $C$  calculated [ $\text{mm}^2$ ]. The specimen was placed in the device and contacted with four metal rods. The distance between the contacts was 30 mm. The device was switched on and the resistance [ $\mu\Omega$ ] could be read for each tested specimen.

The electrical conductivity was calculated from the cross section of the sample [ $\text{mm}^2$ ], the distance between the electrical contacts ( $l$ ) [m] (which touch the specimen) and the measured values for the resistance  $R$  [ $\mu\Omega$ ]. The electrical conductivity  $\sigma$  [ $\Omega^{-1}\text{m}^{-1}$ ] could be calculated from

$$\sigma = \frac{l}{R * C} \quad \text{eq. 5}$$

#### **2.1.3.6 Carbon analysis by LECO**

The carbon measurement was carried out using a LECO CS230 combustion analyzer in which the carbon is determined by infrared adsorption. The analysis begins by weighing a sample into a ceramic crucible. Accelerator material (tungsten chips) is added, the crucible is inserted to the system and the analysis starts. After the system has been purged with oxygen, oxygen flow through the system is restored, and the induction furnace is turned on. The inductive elements of the sample and accelerator couple interact with the high frequency field of the furnace. The pure oxygen and the heating cause the specimen to burn. During combustion, carbon present in the specimen reacts with the oxygen to form CO and CO<sub>2</sub>. Carbon is measured as carbon dioxide, CO being converted to CO<sub>2</sub> in the catalytic heater assembly, and the CO<sub>2</sub> is detected in the IR cell.

#### **2.1.3.7 Oxygen analysis by LECO**

The oxygen measurement was carried out in a Leco TC 400 analyser. The oxygen is measured by infrared detection as carbon dioxide in an IR cell. The analysis begins by placing an empty graphite crucible on the electrode. The crucible is purged and after it, the specimen is dropped by the system into the crucible and the system starts the measurement by heating the crucible in He. The oxygen released from the sample reacts with the carbon from the crucible to form carbon monoxide and small amounts of carbon dioxide. Any CO formed in this fusion is first passed through heated rare earth copper oxide, which converts CO to CO<sub>2</sub>. The carbon dioxide is measured by the IR cell.

#### **2.1.3.8 DTA analysis**

DTA is a method that monitors the temperature difference between a sample and a reference material as a function of time and/or temperature assuming that both sample and reference are subjected to the same environment at a selected heating or cooling rate. The difference in temperature,  $\Delta T$ , between the sample and a reference material is recorded while both are subjected to the same heating programme. These analyses were performed to identify eventual recrystallisation or reaction temperatures as well as mass loss during heat treatment, thermobalance measurements being possible in parallel.

In the present work, the tests were performed on a simultaneous thermoanalyser coupled with quadrupol mass spectrometer (NETZSCH STA449C Jupiter®+QMS403 Aëolos®). All TG/DTA analyses were performed in Ar 5.0 (99.999%) atmosphere with a flow rate of about 50 ml/min. The heating and cooling rate was 20 K/min, and the specimens were heated up to 1600°C (no soaking period), then were cooled to room temperature.

#### **2.1.3.9 Dilatometry**

The dilatometry was carried out using a Netzsch dilatometer DIL 402 C with Al<sub>2</sub>O<sub>3</sub> measuring system (as stated above, the Bähr dilatometer was also used, but mainly as a sintering device). The sintering behaviour of Mo and Mo+wt% Si were examined through the length change. The Netzsch dilatometer is a pushrod dilatometer.

The measurements were carried out at 1500 °C in H<sub>2</sub> atmosphere (50 ml/min flow rate; 5.0 purity) for Mo and Mo+wt%Si. The heat-up ramp was set with 10 K/min to 1500 °C and the soaking time was 120 min. The cooling was as fast as possible, which was approximately 50 K/min between 1500 °C and 500 °C. Analysis of the gathered data was done with Proteus software from Netzsch. The dilatometry experiments with Nb and Nb+wt%Si were carried out in the Bähr DiL 801 dilatometer with an Al<sub>2</sub>O<sub>3</sub> measuring system and a protecting tube in vacuum ( $2 \cdot 10^{-2}$  mbar). The dilatometer was already described in chapter 2.1.2.3. The heat up ramp was set with 10K/min to 1500 °C and the soaking period was 2 h.

#### **2.1.3.10 XRF analysis**

The elemental composition of the materials was measured on a WDS XRF analyzer (Panalytical Axios Advanced, with Rh K<sub>α</sub> radiation). The analysis of major and trace elements in materials by x-ray fluorescence is made possible by the behavior of atoms when they interact with radiation. When a primary x-ray excitation source from an x-ray tube hits a sample the x-ray can either be absorbed by the atoms or scattered through the material. The process in which an x-ray is absorbed by an atom by transferring all of its energy to an innermost electron is called the "photoelectric effect". During this process, if the primary x-ray had sufficient energy, electrons are ejected from the inner shells creating vacancies. These vacancies present an unstable condition for the atom. As the atom returns to its stable condition electrons from the outer shells are transferred to the inner shells and this process gives off a characteristic x-ray whose energy is the difference between the two binding energies of the corresponding shells. Because each element has a unique set of energy levels, each element produces x-rays at a unique set of energies allowing a non-destructive measurement of the elemental composition of a sample. The quantification was carried out with Omnian software from Panalytical as standardless quantification.

### **2.1.3.11 SEM and EDAX**

The scanning electron microscope (SEM) images shown in this thesis have been carried out on an SEM FEI Quanta 200. The SEM analysis enables the investigation of specimens with a resolution down to the nanometer scale. An electron beam is generated by an electron cathode and the electromagnetic lenses of the column and finally swept across the surface of a sample. The path of the beam describes a raster which is correlated to a raster of gray level pixels on a screen. The conventional scanning electron microscope operates in high vacuum. The specimen has to be electrically conductive or has to be coated with a conductive layer. Pure molybdenum or niobium cross sections (after metallographic preparation) were uncoated. By the addition of Si to Mo or Nb it was necessary to coat the sample cross section with carbon. Due to the fact that all cross sections of the specimens had to be prepared metallographically, they were embedded in bakelite. This embedding material is not conductive, therefore the specimens had to be conducted with a further Cu foil with the metallic specimen holder.

The main signals which are generated by the interaction of the primary electrons of the electron beam and the specimen's bulk are secondary electrons (SE) and backscattered electrons (BSE) and furthermore X-rays. They come from an interaction volume in the specimen which differs in diameter according to different energies of the primary electrons (typically between 200 eV and 30 keV). All specimens described in this work were analysed with 20 keV. The SE come from a small layer on the surface and yield the best resolution to be realized with a scanning electron microscope. The well known topographical contrast delivers micrographs which resemble conventional light optical images, but up to much higher magnification and depth of field. The BSE come from deeper regions of the investigated material thus giving a lower resolution. However, the typical compositional contrast gives material specific information since the signal is brighter for regions of a higher average atomic number of the investigated area.

As a byproduct of the image-giving signals, X-rays are produced. They result from ionization processes of inner shells of the atom leading to electromagnetic radiation. The characteristic X-rays give information about the chemical composition of the material. The energy dispersive X-ray analysis (EDAX) enables the detection of chemical elements from boron to Uranium in a qualitative and even quantitative manner. The analysis is less precise than XRF regarding quantification but enables laterally resolved analysis.

### **2.1.3.12 Determination of Vickers hardness**

The macrohardness was measured by the Vickers method on a tester EMCO (Hallein/Österreich) Type Test M4U-25. The hardness was calculated from the length of the two diagonals of the pyramid indentation. The calculation was done by the machine and the calculated values of the hardness were given.

The microhardness was carried out on a testing device from AHOTEC (type: eco HARD XM 1270A). The calculation was done by the testing device. The resulting values for the hardness were summarised in a list in the software.

### 2.1.3.13 Measurement of the impact strength

The impact strength was measured following the Charpy method on rectangular specimens (ISO 5754) with a pendulum impact hammer (Wolpert,  $W_{\max} = 50 \text{ J}$ ). According to the Charpy method for PM materials (ISO 5754), unnotched samples were broken perpendicular to the pressing direction, and the absorbed energy (in J) was measured. The impact energy values thus determined were related to  $1 \text{ cm}^2$  cross section. The impact strength can be calculated with eq. 6 in  $\text{J/cm}^2$ .

$$\alpha_k = A/S \quad \text{eq. 6}$$

$\alpha_k$  impact strength [ $\text{J/cm}^2$ ]  
 $A$  impact energy [J]  
 $S$  cross section of the specimen [ $\text{cm}^2$ ];  $S = \text{width} * \text{height}$

### 2.1.3.14 Measurement of the 3-point bending strength

The 3-point bending strength was measured with a Zwick 1474 universal testing machine. The support distance  $L_s$  was 25 mm. The 3-point bending strength  $\sigma_{fM}$  [MPa] can be calculated with eq. 7 while  $F_{\max}$  [kN] is the maximum load which is applied in the moment of the cracking.

$$\sigma_{fM} = \frac{(3/2) * F_{\max} * L_s}{b * h^2} \quad \text{eq. 7}$$



## 3 Results

### 3.1 Mo specimens from commercially available Mo

The work was started with a Plansee SE Mo powder (designated as  $\leq 32 \mu\text{m}$ ) that was readily available but had been on storage at the University of Technology in Vienna (TUW) for quite some time. After this long period of storage it was needed to sieve the powder to achieve a defined maximum particle size by disintegrating agglomerated particles. As the Plansee Mo powder was consumed for the experiments, another Mo from Chemie Metall was bought and used for further studies. This powder was designated as  $\leq 63 \mu\text{m}$ , and as can be seen in chapter 2.1.1.1 (SEM images of Plansee SE Mo powder) and in chapter 2.1.1.2 (SEM images of Chemie Metall Mo powder) there is visually no difference between the powders. Some experiments in the beginning compared the sintered densities and open porosities of specimens prepared with the same compaction pressures out of these two powders. No significant difference could be observed in the results. Therefore, no distinction was made between these two Mo powders in the following chapter.

Two fractions have been sieved (from the commercially available Mo powder from Chemie Metall) differing in particle size distribution. One was designated as “particle size  $\leq 63 \mu\text{m}$ ” and the second one “ $\leq 45 \mu\text{m}$ ”. In the following, first the results for the density, open porosity and hardness (in dependence of compacting pressure, sintering temperature and soaking period) are discussed for the sieved  $\leq 45 \mu\text{m}$  powder and afterwards they were compared with those achieved for the  $\leq 63 \mu\text{m}$ .

#### 3.1.1 Influence of some factors on density and porosity of molybdenum samples

The influence of particle size, compacting pressure and sintering temperature on the resulting properties (hardness, density and porosity) was explored.

Both powders were uniaxially pressed on Amsler (hydraulic press) to samples with cylindrical geometry of 20 mm diameter and approx. 10 mm height, applying different compacting pressures of 70 / 130 / 200 / 230 / 270 MPa. The specimens were sintered at 1200 / 1250 / 1300 °C with defined soaking periods of 30 min and 90 min isothermal in  $\text{H}_2$  atmosphere (5.0 purity; 2 l/min gas flow).

A summary of all achieved values for density and open porosity of samples prepared from Mo powder  $\leq 45 \mu\text{m}$  can be found in tab. 2. The ones for the  $\leq 63 \mu\text{m}$  are summarised in tab. 3.

**tab. 2.: Density and open porosity of samples prepared from Mo (CM) powder  $\leq 45 \mu\text{m}$  after sintering at different sintering temperatures and soaking periods**

sintering conditions	compacting pressure [MPa]	Sintered density /g*cm <sup>-3</sup>	Immersion method open Porosity /%	He - Pycnometry open Porosity/%	calc. total Porosity /%
1200°C-30min	70	5,14	49	49,6	50,4
	130	5,82	42	42,9	43,9
	200	6,3	38	38,3	39,4
1200°C-90min	70	5,52	46	45,4	45,8
	130	5,83	43	42,6	43,1
	200	6,31	37	37,7	38,7
1250°C-30min	170	6,11	40	39,4	40,1
	200	6,42	37	36,9	37,6
	230	5,73	44	43,5	44,2
	270	5,93	42	41,9	42,4
1250°C-90min	170	6,30	38	37,9	38,4
	200	6,55	36	35,9	36,8
	230	5,81	43	42,6	43,3
	270	6,01	42	41,0	41,7
1300°C-30min	170	6,52	35	35,8	36,5
	200	6,74	32	34,1	35,1
	220	7,32	30	28,2	29,0
	230	6,13	38	40,1	41,8
1300°C-90min	170	6,62	35	34,3	34,9
	200	6,92	32	32,1	33,2
	220	7,21	29	32,7	33,5
	230	6,33	38	38,0	38,7

The values for the open porosity measured with He - pycnometry and immersion method differ by less than 1 % from each other. The difference is very small, so it can be concluded that the values are representing very well the values for open porosity. Comparing the open porosity (both the He - Pycnometry and the immersion method) with the calculated total porosity it can be observed that there is barely a difference between the values for the open and the total porosity. The difference is mostly below 1%. That means that there is barely a closed porosity in the specimens, as is desirable for infiltration purposes.

### 3.1.1.1 Influence of compacting pressure

Up to 220 MPa compacting pressure the density is increasing while the values for the density of samples pressed with more than 220 MPa are decreasing. It could be shown that 200 MPa is the compacting pressure limit for the powder used, since overpressing and pressing defects occur at higher pressures. One exception are specimens sintered at 1300 °C (for 30 and 90 min soaking period). For these specimens, 220 MPa is the compacting pressure limit after which overpressing occurs. With increasing sintering temperature the density is increasing, too. Furthermore, when comparing the same

sintering temperatures with different soaking periods it can be observed that samples sintered for 90 min (higher) soaking period show also higher densities. In fig. 3.1 the values from tab. 2 are plotted.

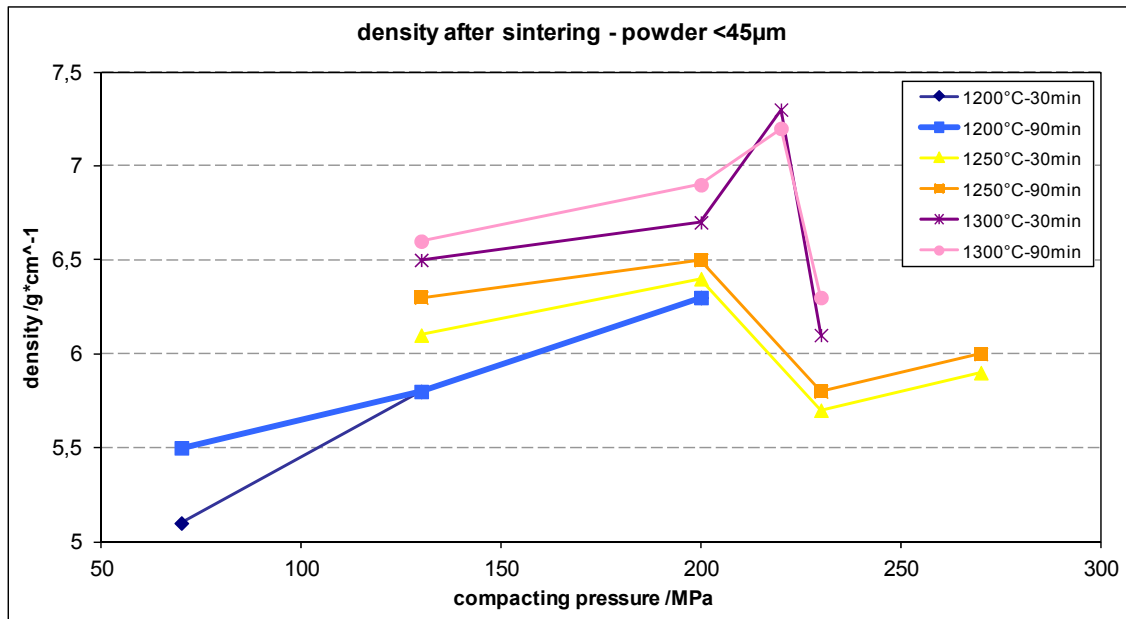


fig. 3.1.: Sintered density of samples from Mo powder  $\leq 45 \mu\text{m}$  as a function of the compacting pressure;  $\text{H}_2$  atmosphere (5.0 purity; 2l/min gas flow)

The lowest value for the open porosity was shown by samples pressed with 220 MPa and sintered for 90 min at 1300°C in  $\text{H}_2$  atmosphere which can be observed in fig. 3.2. The highest values for the open porosity were offered by samples pressed with 130 MPa and sintered for 30 min and 1200°C. With increasing density both the open porosity and total porosity are decreasing.

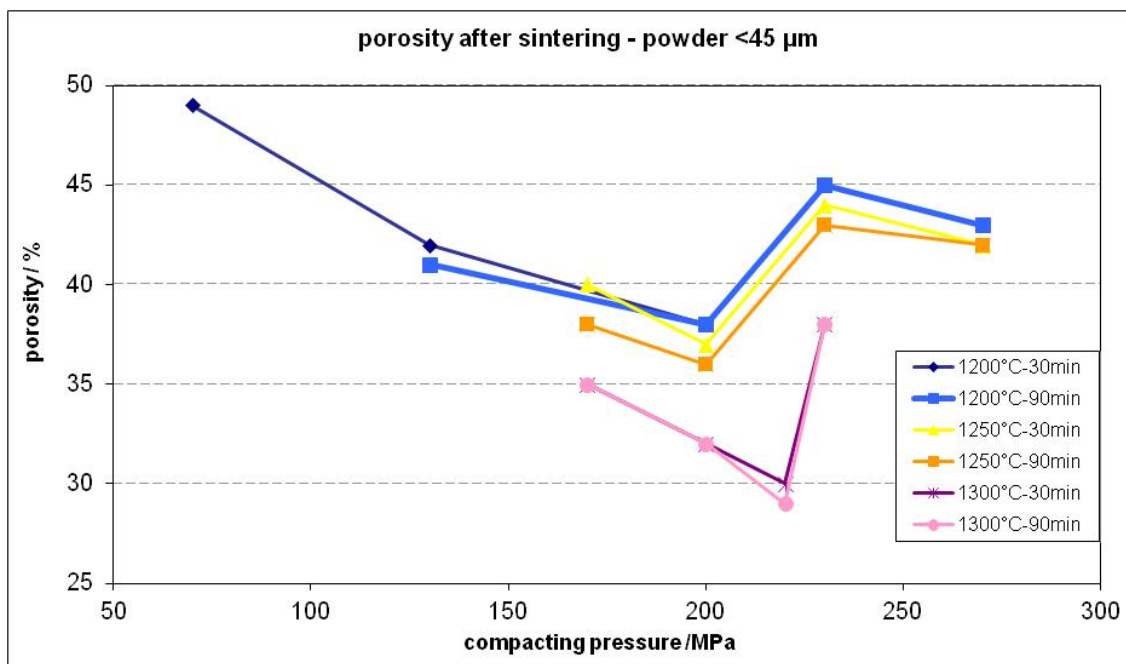


fig. 3.2.: Open porosity measured with He- pycnometry of samples prepared from powder  $\leq 45 \mu\text{m}$  as a function of the compacting pressure, sintered in  $\text{H}_2$  atmosphere (5.0 purity; 2 l/min gas flow).

### 3.1.1.2 Influence of the sintering temperature

The influence of sintering temperature on the density can be observed very well in fig. 3.3. In this experiment, specimens (out of  $\leq 45 \mu\text{m}$  Mo powder) have also been sintered at higher temperatures than  $1300^\circ\text{C}$ . A dilatometer furnace was available at this time of project, which enabled sintering at temperatures up to  $1500^\circ\text{C}$ . Samples sintered between  $1200^\circ\text{C}$  and  $1500^\circ\text{C}$  (in  $50^\circ\text{C}$ -steps) are presented and the densities visualized in fig. 3.3. With increasing temperature the values for the density are increasing, too. Specimens sintered at  $1200^\circ\text{C}$  and 90 min soaking period show much lower densities (blue line in fig. 3.3) than samples sintered at  $1500^\circ\text{C}$  and 90 min soaking period (grey line in fig. 3.3). All specimens have been sintered in  $\text{H}_2$  (5.0 purity; 2 l/min gas flow) atmosphere.

Pressing with higher compacting pressures than 200 MPa (220 MPa for specimens sintered at  $1300^\circ\text{C}$  which could be shown in fig. 3.1) resulted in lower densities. Above 200 MPa compacting pressure, moulding (pressing) defects are occurring, which lowers the density. Therefore specimens which have been sintered at  $1350^\circ\text{C}$  and higher temperatures were not pressed at higher compacting pressures than 200 MPa as it was done for specimens sintered at lower temperatures.

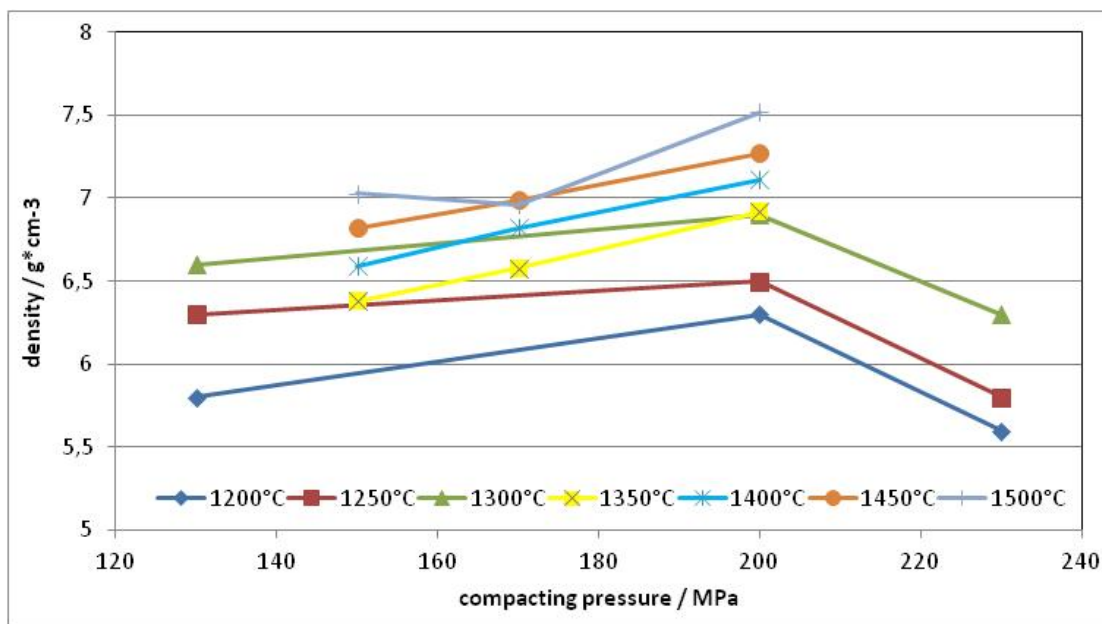


fig. 3.3.: Influence of sintering temperature on density of specimens; all specimens were sintered with 90 min soaking period;  $\text{H}_2$  atmosphere (5.0 purity; 2l/min gas flow)

In fig. 3.4 the influence of the sintering temperature (with soaking period of 90 min for all samples) on the open porosity is shown. With increasing sintering temperature the open porosity is decreasing. The highest value of open porosity was measured for samples sintered at the lowest sintering temperature of  $1200^\circ\text{C}$  with 90 min soaking period. The lowest value of open porosity, which is shown in fig. 3.4, could be achieved with a sample sintered at  $1500^\circ\text{C}$  and pressed with 200 MPa compacting pressure. As mentioned already for the density it could be shown that above 200 MPa compacting pressure the density is decreasing and for this reason the open porosity is increasing. The reason is the occurring of the moulding (pressing) defects which cause cracks. These cracks were measured as open pores with He-pycnometry.

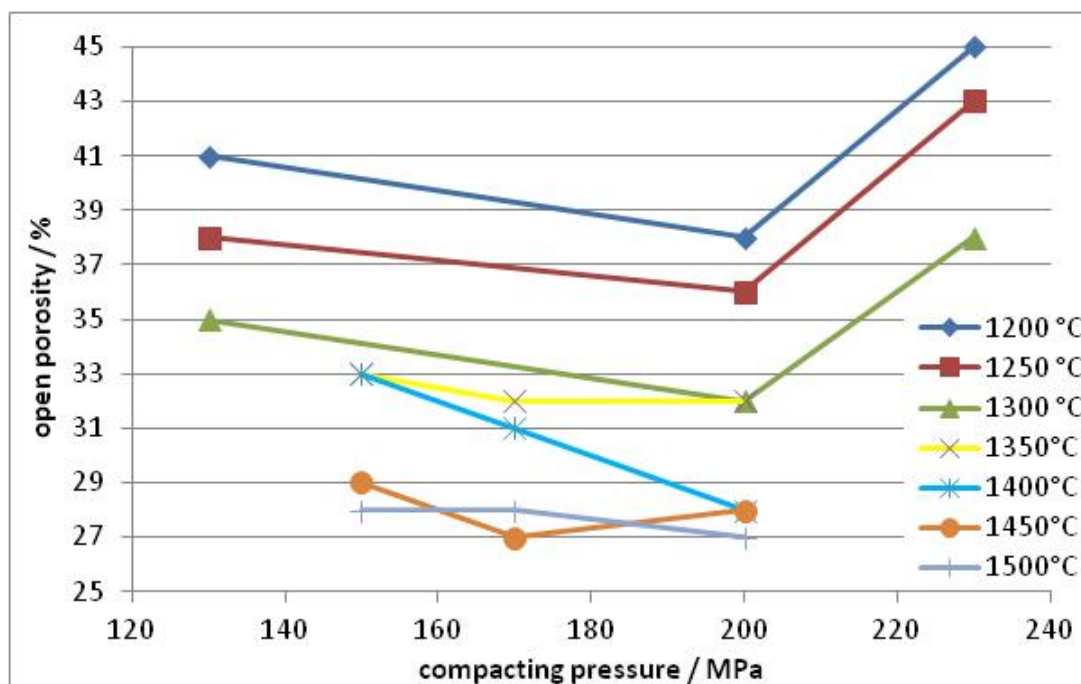
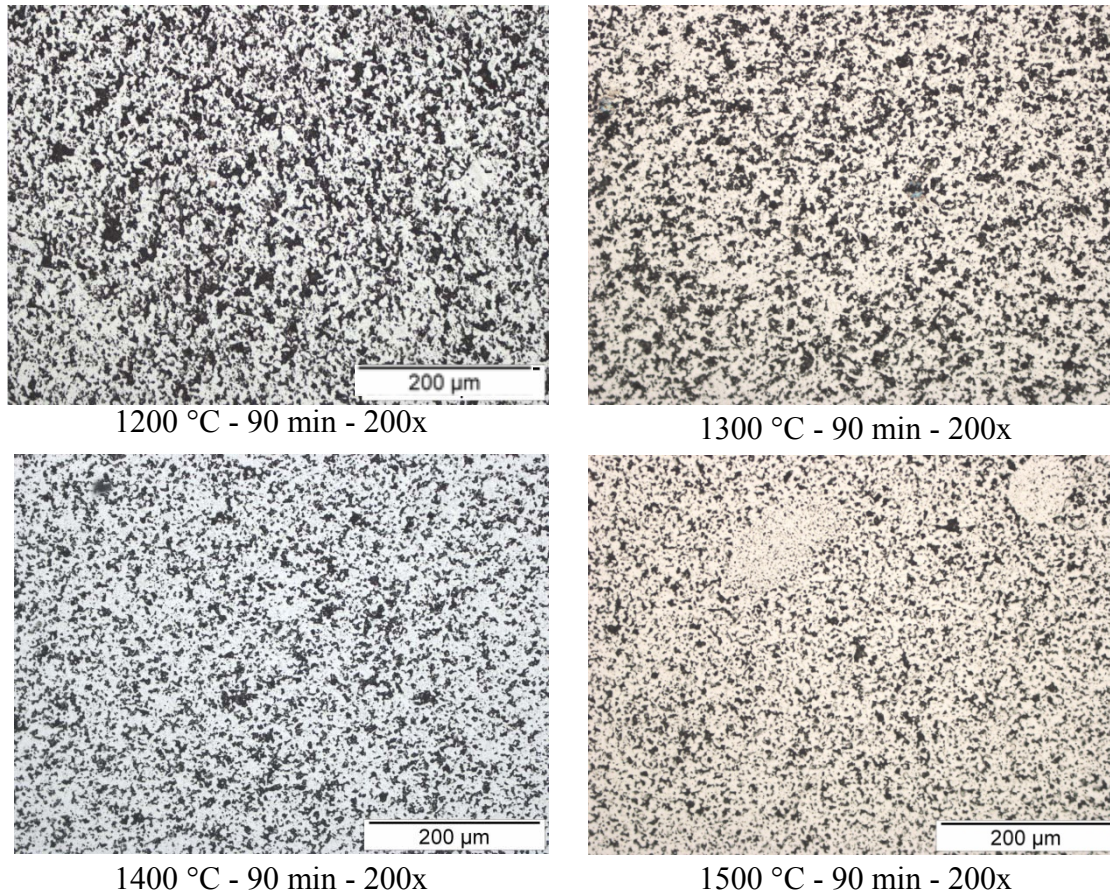


fig. 3.4.: Influence of sintering temperature on open porosity, all specimens were sintered with 90 min soaking period in H<sub>2</sub> (5.0 purity; 2 l/min gas flow)

#### 3.1.1.2.1 LOM images of Mo samples from Mo fraction $\leq 45 \mu\text{m}$ sintered at different temperatures

In fig. 3.5 images of polished cross sections of sintered Mo specimens are demonstrated. The first specimen was sintered at 1200 °C, the next one at 1300 °C, 1400 °C and the last one at 1500 °C. The soaking period was 90 min for all samples and the atmosphere was H<sub>2</sub> (5.0 purity; 2 l/min gas flow). With increasing sintering temperature the porosity is decreasing which can be observed very well in the images in fig. 3.5. While many bigger pores are pervading the sample sintered at 1200 °C the pores are mostly of reduced scale after sintering at 1500 °C. In the right lower image (1500 °C - 90 min - 200x) in the upper part of the image two "clusters" of smaller particles can be identified. Some smaller particles might agglomerate after sieving, grow together during sintering and form agglomerated centers.





**fig. 3.5.:** LOM images of Mo samples sintered at four different temperatures for 90 min soaking period; H<sub>2</sub> atmosphere (5.0 purity; 2l/min gas flow)

### 3.1.1.3 Different powder fractions

Beside samples prepared from molybdenum  $\leq 45 \mu\text{m}$  also specimens from powder  $\leq 63 \mu\text{m}$  have been prepared. A summary of the density and open porosity is given in tab. 3. Samples sintered at the same temperature but with 30 min and 90 min soaking period have been compared. There is barely a difference in the values for the density and open porosity between the specimens sintered for different soaking periods. Samples pressed with 70 MPa show about 50% open porosity (immersion method) while with increasing compacting pressure of 200 MPa the porosity decreased to 39% (immersion method).



**tab. 3.: Density and open porosity for samples prepared from Mo powder  $\leq 63 \mu\text{m}$  after sintering at different sintering temperatures and soaking periods in  $\text{H}_2$  atmosphere (5.0 purity; 2 l/min gas flow).**

sintering conditions	compacting pressure [MPa]	Sintered density / $\text{g}\cdot\text{cm}^{-3}$	Immersion method open Porosity /%	open Porosity He - Pycn./%	total porosity He - Pycn. /%
1200°C-30min	70	5,1	51	48,9	49,7
	130	5,7	43	43,6	44,6
	200	6,2	39	38,8	39,9
1200°C-90min	70	5,4	50	46,5	47,1
	130	5,7	43	43,3	43,8
	200	6,2	39	38,0	38,3

In fig. 3.6 the density of samples prepared from Mo powder  $\leq 63 \mu\text{m}$  (results tab. 3) is compared with samples pressed out of Mo  $\leq 45 \mu\text{m}$  (tab. 2). All samples were sintered at the same temperature of 1200°C but for two different soaking periods in  $\text{H}_2$  atmosphere (5.0 purity; 2 l/min). It can be seen that with a longer soaking period of 90 min the density could be increased. Furthermore, samples prepared from Mo  $\leq 45 \mu\text{m}$  show higher values for the density compared to samples from  $\leq 63 \mu\text{m}$  at the same temperature and soaking period. The most pronounced difference is observed for the samples pressed with 70 MPa compacting pressure. Specimens sintered at 1200 °C for 90 min (for both powder fractions) show higher densities than samples sintered just for 30 min. At higher compacting pressures the same values for the density have been measured for samples out of Mo powder  $\leq 45 \mu\text{m}$  independent of the soaking period. The same was observed for specimens of Mo  $\leq 63 \mu\text{m}$ .

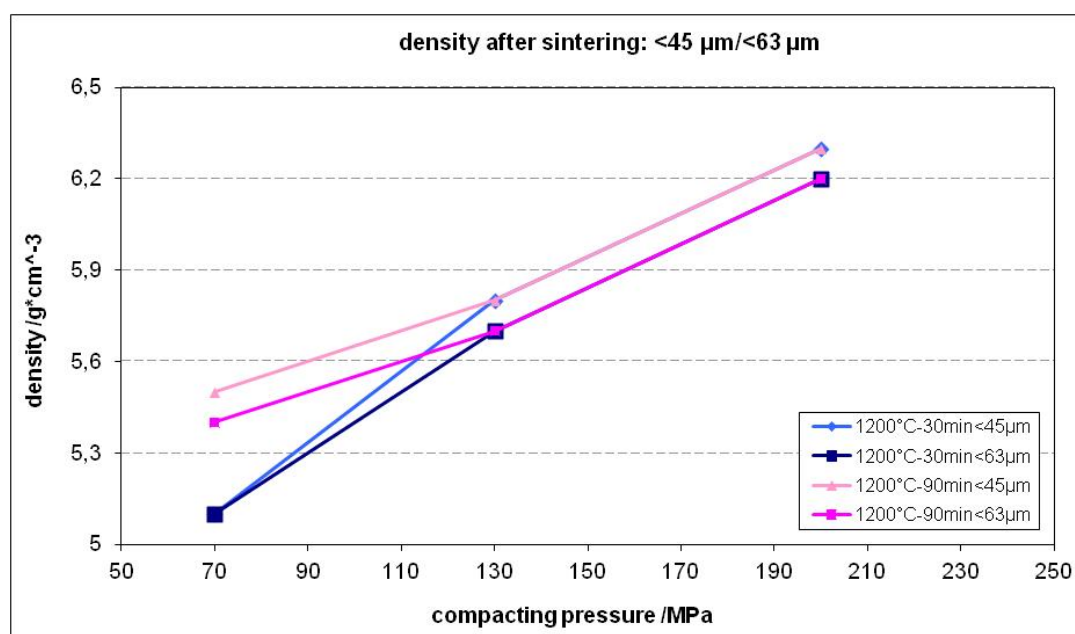


**fig. 3.6.: Sintered density of samples prepared from powder  $\leq 63 \mu\text{m}$  as compared to powder  $\leq 45 \mu\text{m}$  as a function of the compacting pressure; all specimens were sintered in  $\text{H}_2$  (5.0 purity; 2 l/min flow rate)**

The porosity of samples prepared from powder  $\leq 45 \mu\text{m}$  was compared with samples from powder  $\leq 63 \mu\text{m}$ . As shown in tab. 3 (compared with values for porosity of powder  $\leq 45 \mu\text{m}$ , shown in tab. 2) the porosity is differing by about 1%. Further on, as tab. 3 illustrates, values for calculated porosity (He-pycnometry) and those measured by the immersion method are differing up to 1% maximum.

The values illustrated in fig. 3.7 are the values for the open porosity measured for powder  $\leq 63 \mu\text{m}$  (tab. 3) and  $\leq 45 \mu\text{m}$  from tab. 2

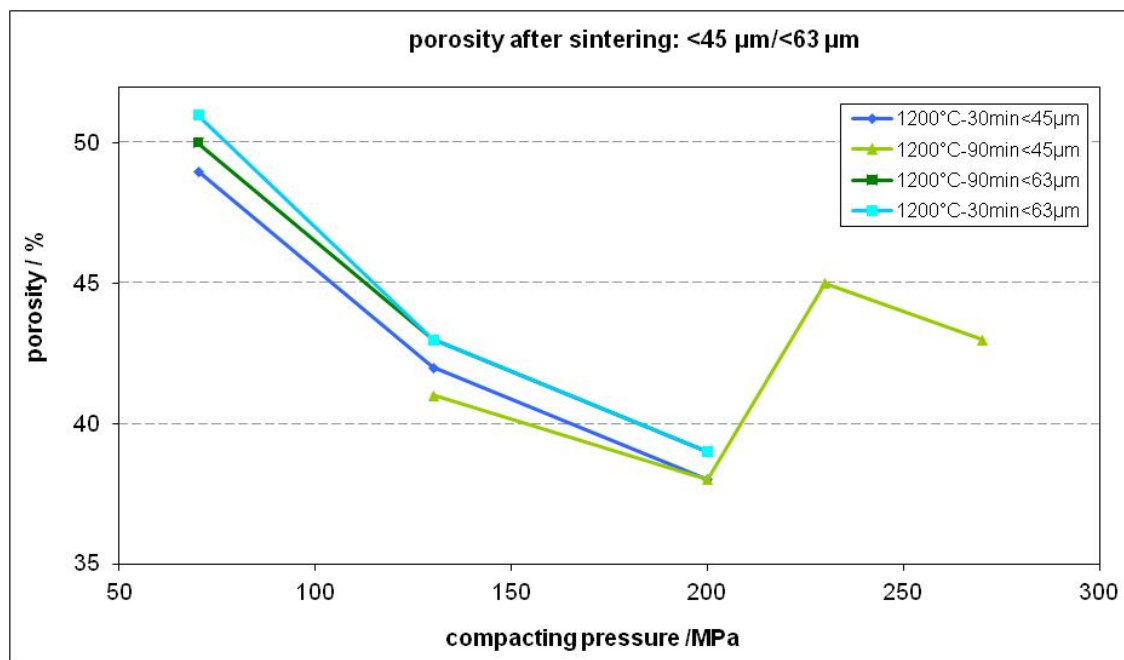


fig. 3.7.: Open porosity measured with He pycnometry after sintering of samples prepared from powder  $\leq 63 \mu\text{m}$  compared with powder  $\leq 45 \mu\text{m}$  as a function of compacting pressure; all specimens were sintered in  $\text{H}_2$  (5.0 purity; 2 l/min gas flow)

#### 3.1.1.4 Resulting hardness

The hardness was measured with 10 kp indentation load and the data are summarized in tab. 4. Samples sintered at 1200 / 1250 / 1300 / 1350 / 1400 / 1450 / 1500 °C with 230 / 200 / 170 / 150 / 130 MPa (in  $\text{H}_2$  atmosphere; 5.0 purity; 2 l/min gas flow) were characterized for their hardness. With increasing compacting pressure up to 200 MPa the hardness is increasing. Specimens pressed with higher compacting pressures than 200 MPa showed a drop of the hardness to levels lower than those measured for samples pressed with 130 MPa compacting pressure. Comparing the sintering temperatures it can be observed that with increasing sintering temperature the hardness is increasing too. The hardness value for the specimen sintered at 1400°C and pressed with 200 MPa compacting pressure is much higher than for specimens sintered at higher temperatures, which is an outlier. In tab. 4 the results for the hardness of samples prepared from Mo powder  $\leq 45 \mu\text{m}$  are presented. Specimens from Mo  $\leq 63 \mu\text{m}$  were not presented in tab. 4 because only samples sintered at 1200°C have been prepared from this powder, and the values for the hardness were identical to those for specimens from Mo powder  $\leq 45 \mu\text{m}$ .

**tab. 4.: HV 10 of samples prepared from Mo powder  $\leq 45 \mu\text{m}$ , differently compacted and sintered at different temperatures between 1200°C and 1500°C in  $\text{H}_2$  atmosphere (5.0 purity; 2 l/min flow rate)**

sintering temperature / °C	compacting pressure [MPa]	HV 10
1200	130	36
1200	200	48
1200	230	29
1250	130	39
1250	200	43
1250	230	29
1300	130	50
1300	200	53
1300	230	37
1350	150	78
1350	170	81
1350	200	94
1400	150	81
1400	170	81
1400	200	88
1450	150	94
1450	170	91
1450	200	95
1500	150	102
1500	170	91
1500	200	99

In fig. 3.8 the values from tab. 4 are graphically presented. It can be very well observed that with increasing sintering temperature the values for the hardness are increasing too. The highest values for the hardness were achieved for samples pressed with 200 MPa compacting pressure. The lowest values are attained for the samples pressed with 230 MPa. At 230 MPa the density of the specimens was already decreased due to moulding defects (which can be observed in fig. 3.1). Due to the decreased density the macro hardness decreased too. These moulding defects were in part immediately visible from outside, in part they were discernible in the cross section, as long cracks or as very small cracks between some particles.

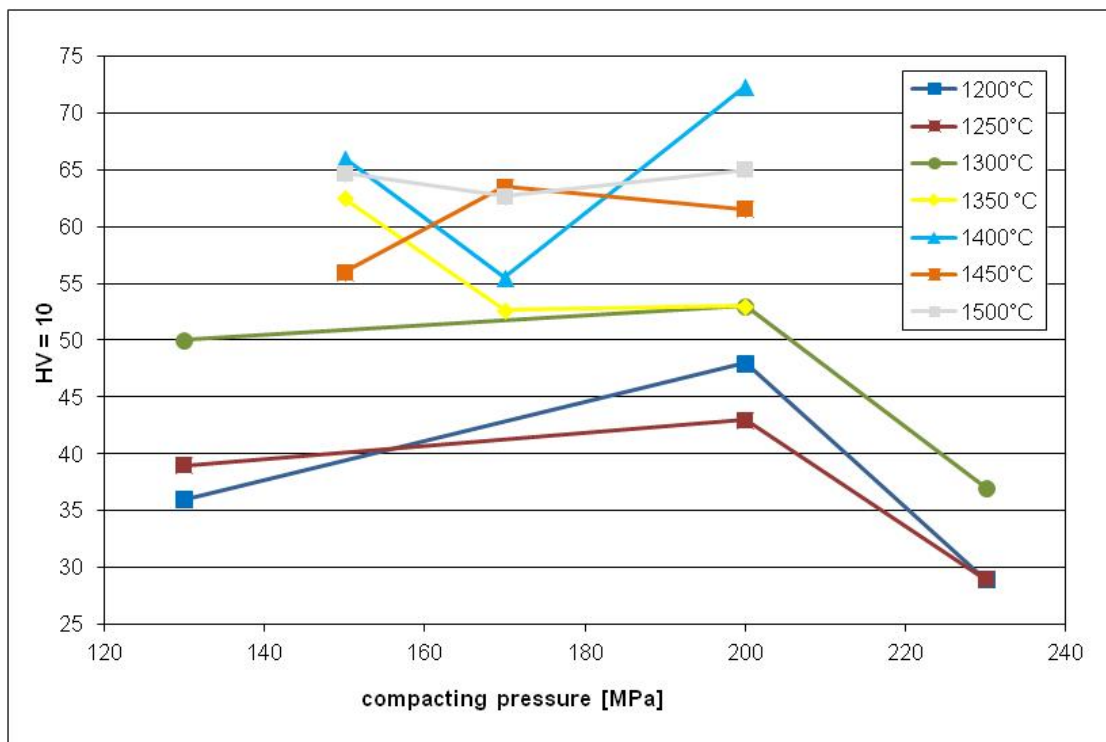


fig. 3.8.: Hardness HV 10 of samples sintered at different temperatures between 1200°C and 1500°C (with 50°C steps) as a function of the compacting pressure. Sintered in H<sub>2</sub> atmosphere (5.0 purity; 2 l/min flow rate)

### 3.1.1.5 Open porosity measured by Hg porosimetry

#### 3.1.1.5.1 Uniaxially pressed samples

Specimens prepared from two Mo powder fractions ( $\leq 45 \mu\text{m}$  and  $\leq 63 \mu\text{m}$ ) were characterised for their open porosity after sintering at three temperatures. The compacting pressure of all compared specimens was 200 MPa. Also the sintered density was characterised, and all values were compared in fig. 3.9. It can be observed that with increasing sintering temperature the open porosity is decreasing. Specimens sintered at 1200°C and prepared from two different powder fractions have been compared for their open porosities. It can be seen that the open porosity of specimen from powder  $\leq 63 \mu\text{m}$  is (surprisingly) lower than from Mo powder  $\leq 45 \mu\text{m}$ . Both powders have been sieved before implemented into the experiments. Due to the fact that the used Mo powders have been sieved, the low amount of coarse particles (in the initial commercially available Mo powder) was removed during sieving with  $\leq 45 \mu\text{m}$  and  $\leq 63 \mu\text{m}$ . The remaining particles were all considerably smaller than 45  $\mu\text{m}$  or 63  $\mu\text{m}$ .

The sintered density was characterised too. It can be observed that with increasing sintering temperature the density is increasing too. An exception in density shows the specimen sintered at 1250°C, which was measured twice. The value for the density should be higher than the one for the specimen sintered at 1200°C. This value for the density of the  $\leq 63 \mu\text{m}$  powder is an outlier which can only be explained by "mis-measurement" of the machine.

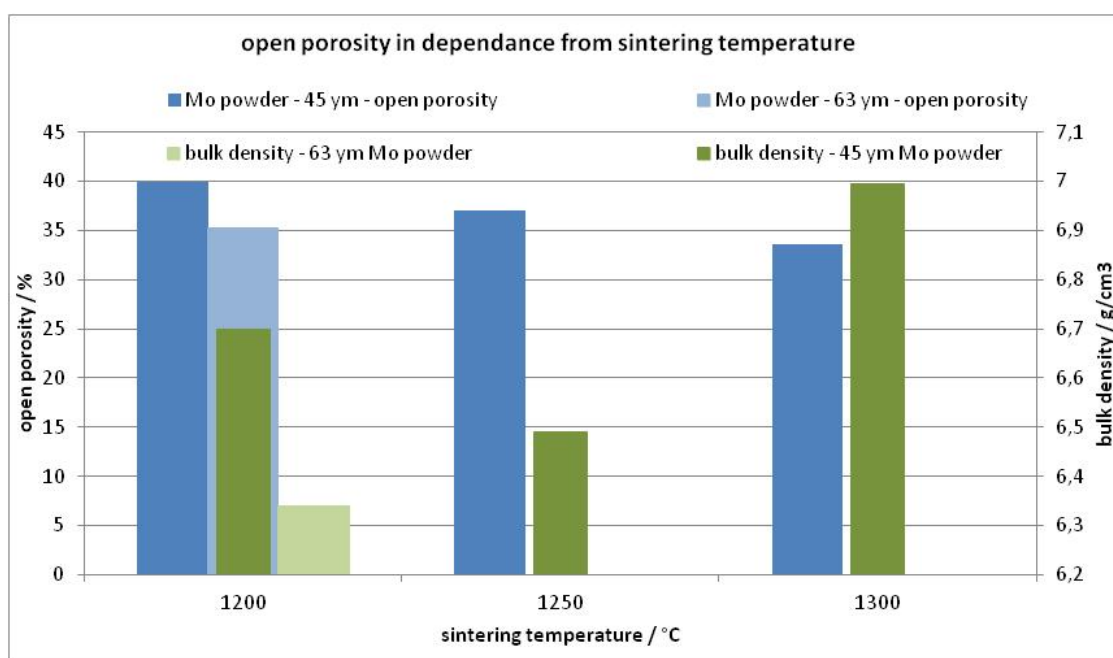


fig. 3.9.: Open porosity and sintered density of specimens pressed with 200 MPa uniaxially sintered at different temperatures in  $\text{H}_2$  atmosphere (5.0 purity; 2 l/min gas flow)

At lower sintering temperatures the values for the open porosity are higher than for specimens sintered at higher temperatures. For comparison the open porosity, measured by Hg porosimetry, of the specimens sintered at 1200°C is higher than the one for samples sintered at higher sintering temperatures (fig. 3.10). Specimens sintered at 1300°C show an average pore size of  $\sim 1 \mu\text{m}$ , and for the specimens sintered at 1200°C and 1250°C a lower average pore size of  $\sim 0,8 \mu\text{m}$  was measured, which may be explained by pore coarsening at higher temperatures.

The average pore size of specimens prepared from  $< 63 \mu\text{m}$  Mo powder is in the size range of  $0,72 \mu\text{m}$  while the one for the specimen out of the  $< 45 \mu\text{m}$  is about  $0,79 \mu\text{m}$ . The difference in the pore size is quite small and can be regarded as being within the experimental scatter.

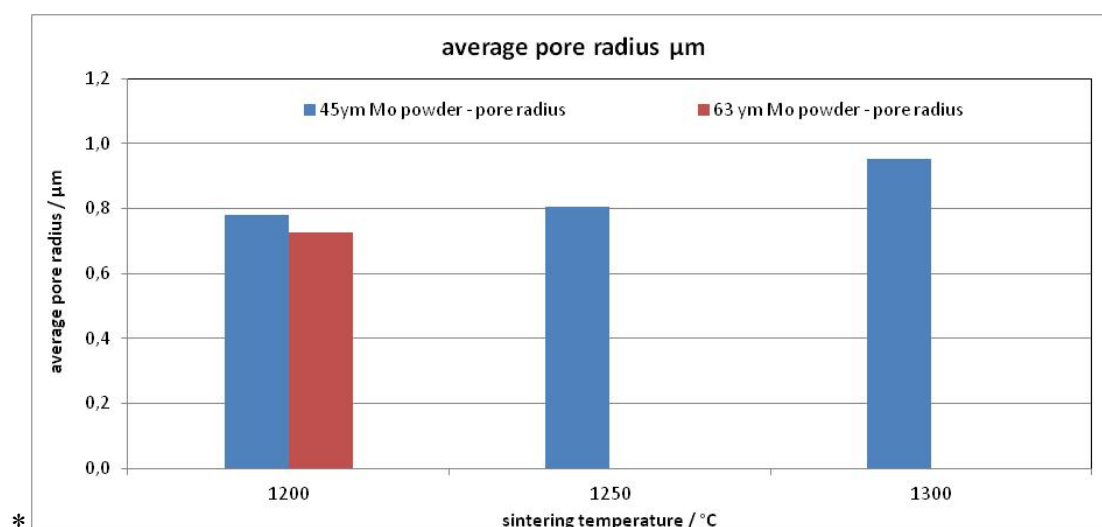


fig. 3.10.: average pore radius in  $\mu\text{m}$  of specimens prepared from  $\leq 45 \mu\text{m}$  and  $\leq 63 \mu\text{m}$  Mo powders

### 3.1.1.5.2 Cold isostatically pressed samples

Samples from Mo <63  $\mu\text{m}$  have been pressed also cold isostatically to compare the values with those of samples pressed uniaxially. Three different sintering temperatures were chosen. In fig. 3.11 the values for the open porosity and sintered density are shown. It can be observed that with increasing sintering temperature the open porosity is increasing. It is contrary to the expectations that with increasing sintering temperature the open porosity would decrease while the sintered density is increasing. Well, the density was increased, which can be observed very well in fig. 3.11. Therefore, the value of the open porosity of the specimen sintered at 1200 °C is quite too low and can be defined as an outlier. The increase in open porosity between 1200 °C and 1250 °C is quite high, with 32 % specimen sintered at 1200 °C and 35,5 % for specimen sintered at 1250 °C. There is barely a difference for the open porosity between samples sintered at 1250 °C and 1300 °C. The open porosity is 35,5 % for the specimen sintered at 1250 °C which is a little bit lower than for the specimen sintered at 1300 °C (35,8 %). The same applies for the sintered density. The open porosity should decrease while the density should increase with increasing temperature. Well, only one specimen of each sintering temperature was measured with Hg- porosimetry (due to the high operating costs). Therefore, the lower value for the density of the specimen sintered at 1300 °C can be explained as an outlier which might be corrected by further Hg - porosimetry measurements.

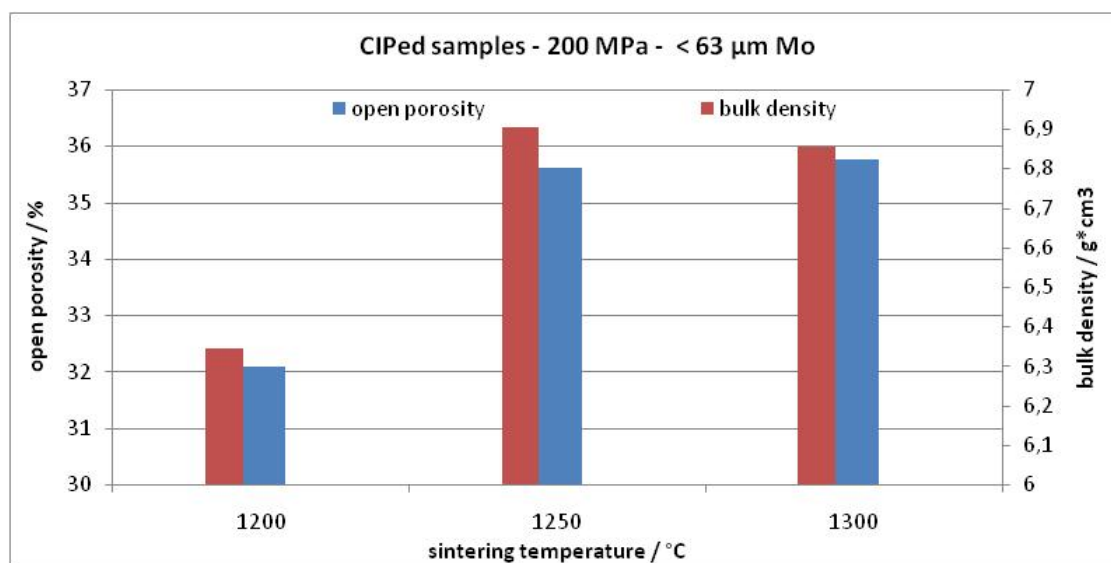


fig. 3.11.: Open porosity and density of CIPed samples after sintering at different temperatures; sintered in H<sub>2</sub> atmosphere (5.0 purity; 2 l/min gas flow) with 90 min soaking period

In fig. 3.12 the values for the pore radius and the density are shown. With increasing sintering temperature the average pore size is decreasing. It can be observed in fig. 3.12 that the sintered density increased with increasing sintering temperature. One exception is the value of the density for the specimen sintered at 1300 °C, which has already been discussed before. Furthermore, it is surprising that the pore size of the specimen sintered at 1200 °C is bigger than for all other specimens sintered at higher temperatures and the value for the open porosity is quite low at this time. This result for the pore size is contrary to the values for the amount of open pores demonstrated in fig. 3.9. On the other hand it confirms the assumptions that the value for the open porosity (demonstrated in fig. 3.9) for the specimen sintered at 1200 °C is too low (apparently due to a measurement error).



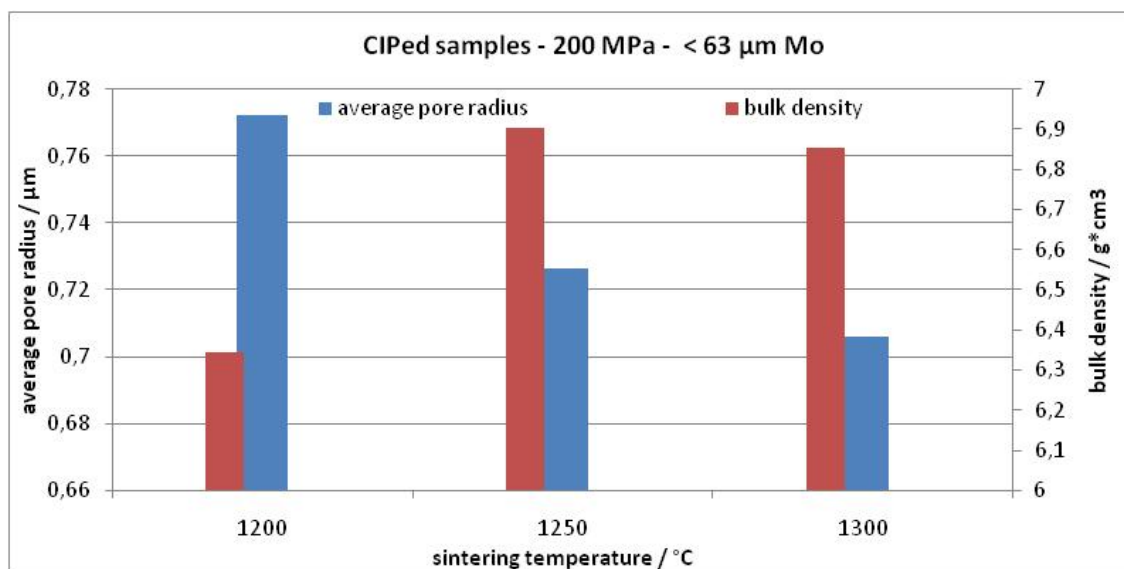
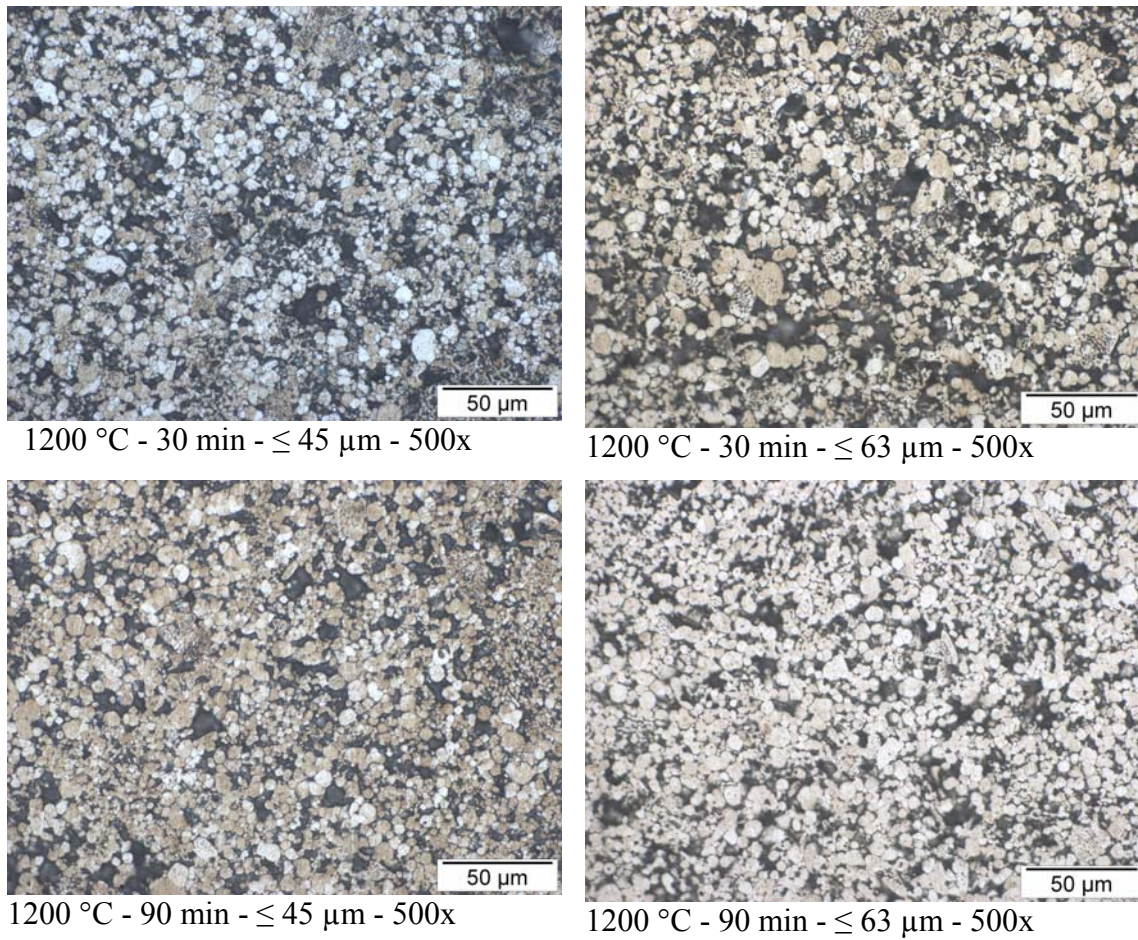


fig. 3.12.: average pore size of Mo < 63 μm specimens sintered at different temperatures, sintered in H<sub>2</sub> atmosphere (5.0 purity; 2 l/min gas flow) with 90 min soaking period

### 3.1.1.6 Characterisation by LOM and SEM

In fig. 3.13 the microstructures of Mo samples sintered at 1200 °C are compared. The two upper images show Mo specimens prepared from different powder fractions ( $\leq 45$  μm and  $\leq 63$  μm) sintered at the same temperature of 1200 °C for 30 min. In the two lower images Mo samples are shown which were sintered for 90 min instead of 30 min. All samples were etched with Murakami I+II (1:1) for 60 s and polished afterwards carefully on an Al<sub>2</sub>O<sub>3</sub> disc for about 10 s. A longer polishing resulted in polishing away the etched surface, and only pores but not grain boundaries could be observed. The short polishing explains the brown colour of the surfaces caused by the Murakami mixture. Between all samples barely a difference can be observed. In each sample the same amount on porosity can be seen. The pore size appears smaller in the top left image (1200°C - 30 min -  $\leq 45$  μm) than in the top right image (1200 °C - 30 min -  $\leq 63$  μm). It could be shown in fig. 3.9 that open porosity of the < 63 μm specimen is higher than the one of specimen from  $\leq 45$  μm. When comparing the right top and right bottom images (specimens from Mo  $\leq 63$  μm) it can be seen that with increasing soaking period the size of pores is decreasing. In fig. 3.9 it was also demonstrated that the porosity decreased a little bit with increasing soaking period.



**fig. 3.13.:** LOM images of Mo samples prepared from  $<45 \mu\text{m}$  and  $<63 \mu\text{m}$  fractions sintered at  $1200 \text{ }^{\circ}\text{C}$  for 30 and 90 min in  $\text{H}_2$ ; etched with Murakami I+II - 60 s

For comparison the same specimens from fig. 3.13 are shown again before etching with Murakami (in fig. 3.14). The grain boundaries cannot be seen anymore but the porosity can be observed very well. Specimens which were sintered at  $1200 \text{ }^{\circ}\text{C}$  for 30 min out of  $\leq 45 \mu\text{m}$  Mo powder are the one with the highest open porosity. The porosity of all the other demonstrated specimens looks comparable to each other. The porosity of the specimen sintered at  $1200 \text{ }^{\circ}\text{C}$  for 30 min out of  $\leq 63 \mu\text{m}$  (fig. 3.14) seems to be lower than the one demonstrated in fig. 3.13. During polishing, broken out particles might clog some pores. After etching they could be cleaned easily out of the pores.



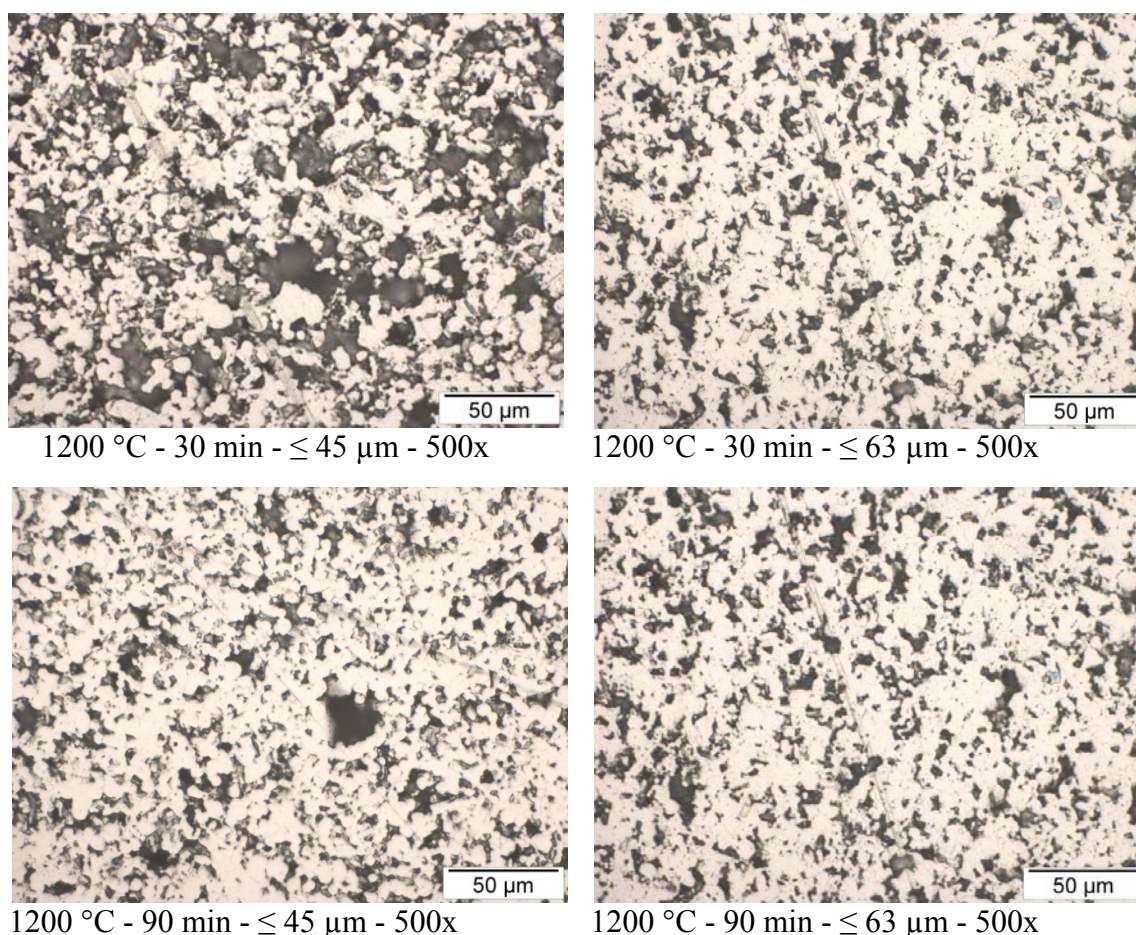


**fig. 3.14.: LOM images of Mo samples prepared from <45 µm and <63 µm fractions sintered at 1200 °C for 30 and 90 min in H<sub>2</sub>; without etching**

### 3.1.1.7 Dilatometry

The dilatometer curve shown in fig. 3.15 describes the length change of an Mo specimen pressed with 200 MPa uniaxially on Amsler hydraulic press to a cylinder with 11.27 mm diameter and 10 mm height. The specimen was prepared from CM Mo powder (as delivered) and was sintered in the Netzsch dilatometer at 1500 °C with 60 min soaking period in H<sub>2</sub> (5.0 purity; 2l/ min gas flow). The green density of the described sample is 6,72 g/cm<sup>3</sup>. The length measurement was done parallel to the pressing direction, i.e. axially. The change in the length can be observed in fig. 3.15. At about 700 °C a peak can be observed in the first derivative. That might be an evidence for an expansion of the sample. At 880 °C the sintering process starts which can be observed in the curve progression where the curve starts to drop. At this point shrinkage of the sample starts. At about 1297 °C the curve drops more strongly up to 1464 °C where the strongest decrease can be observed. The total shrinkage of the sample is 4.63 % in length.

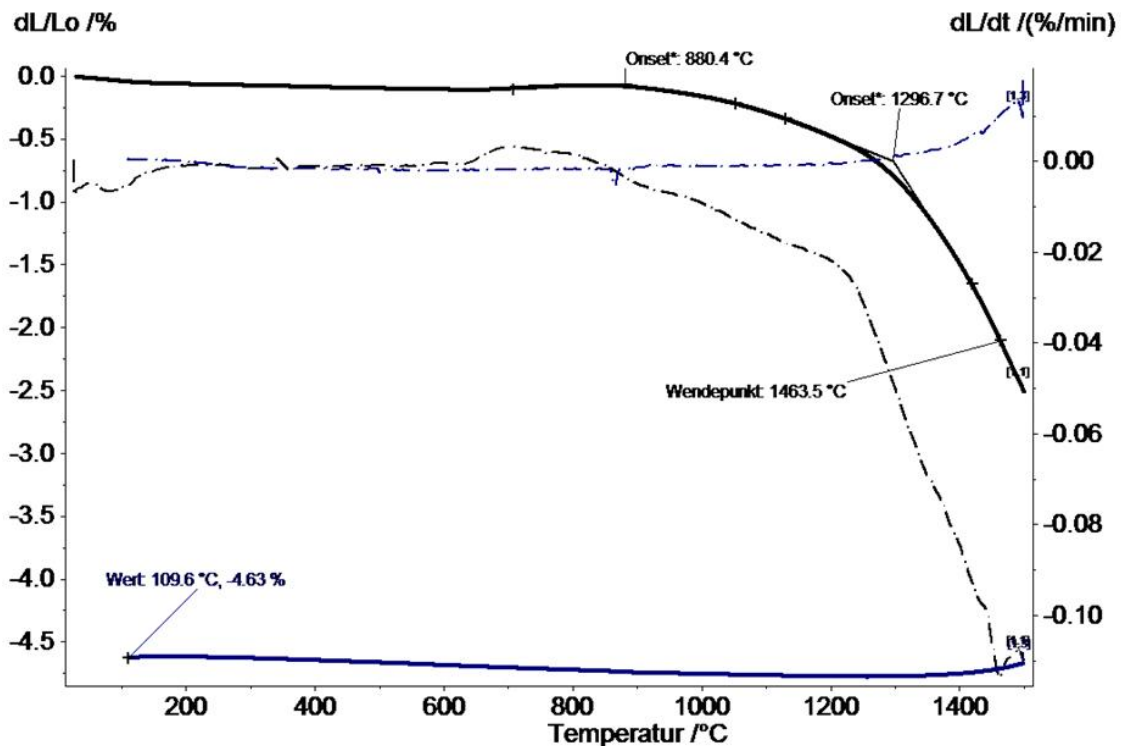


fig.3.15.: Dilatometric graph of Mo specimen pressed at 200 MPa; sintered at 1500 °C; 60 min soaking period; heating rate 10 K/min, H<sub>2</sub>

In a further analysis the gaseous compounds were measured by MS spectrometry. In fig. 3.16 can be seen that at 121 / 338 and 714 °C the peak maxima of H<sub>2</sub>O formation occur (blue line), indicating reduction processes. At 323 / 794 and 1187 °C peaks of mass 28 were found, which can only be N<sub>2</sub> (red line). No additives like organic waxes (for example Kenolube P11), were used for pressing, only lubricant oil for the die which evaporated as CO<sub>2</sub> at about 320 °C (pink line)

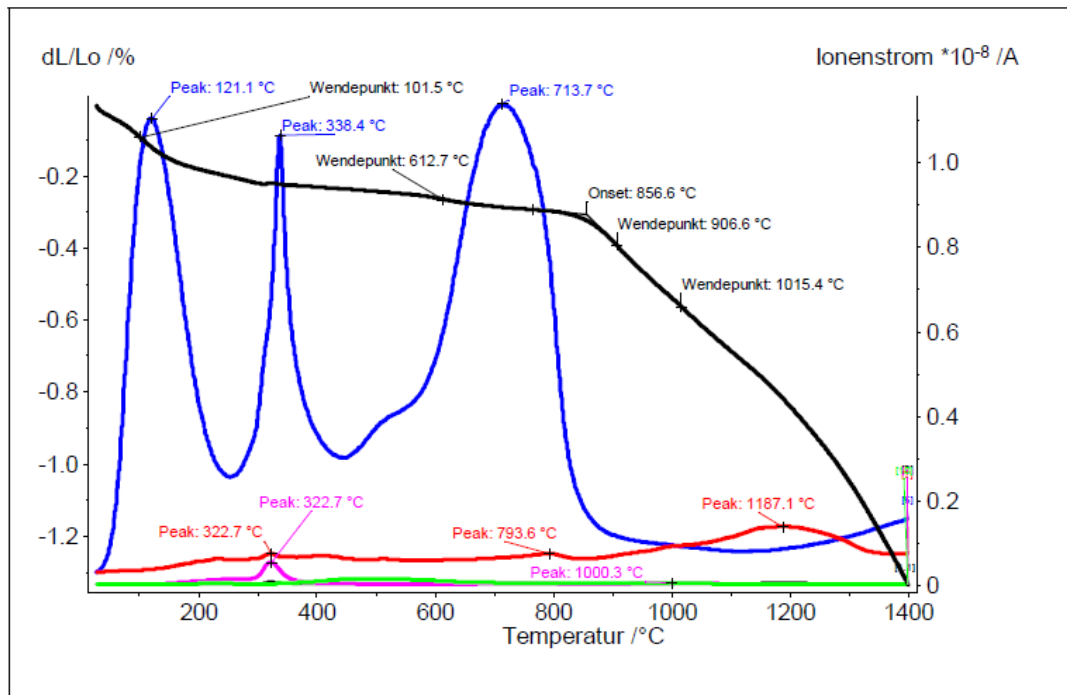


fig.3.16.: Dilatometer measurement with MS analysis; blue line - mass 18: H<sub>2</sub>O; red line - mass 28: N<sub>2</sub>; pink line - mass 44: CO<sub>2</sub>

For a better overview the shrinkage of the sample is demonstrated in fig. 3.17 as a function of the sintering time. The most pronounced shrinkage of the sample can be observed between 1000 °C and 1400 °C. During the cooling process an expansion of about 0.2% can be observed which is however an artifact, resulting from the contraction of the Al<sub>2</sub>O<sub>3</sub> measuring system the CTE of which is higher than that of Mo (about  $7.9 \cdot 10^{-6}/\text{K}$  compared to about  $5.1 \cdot 10^{-6}/\text{K}$  at 20°C for Mo).

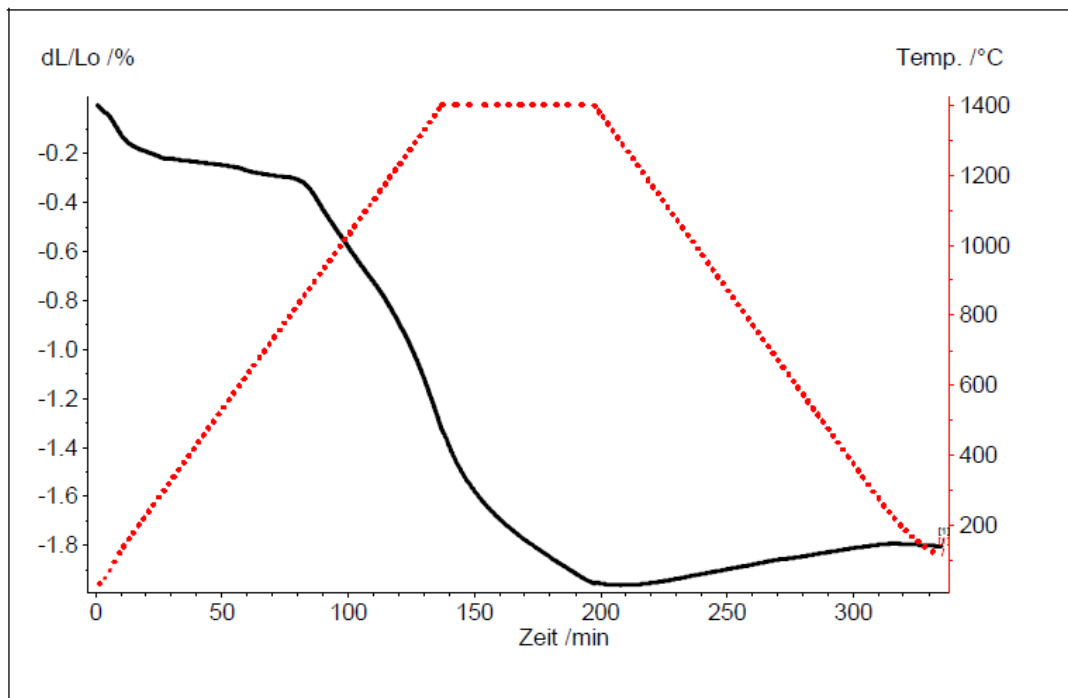
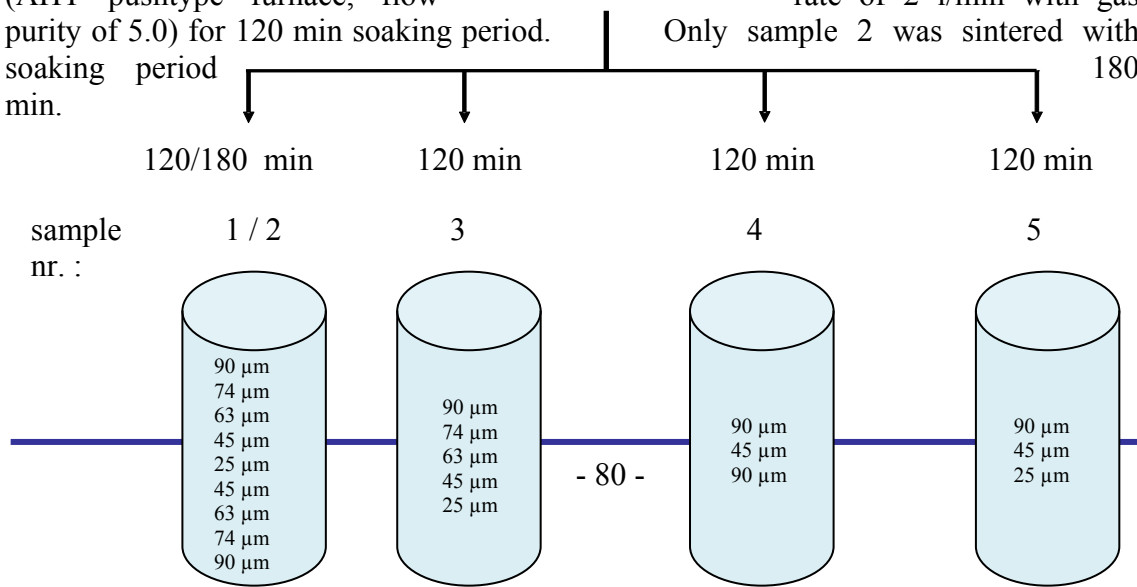


fig.3.17.: Length change of Mo powder compact as a function of time during the dilatometric run

### 3.1.2 Preparation of layered samples for gradient porosity

#### 3.1.2.1 Multiple layer samples

Samples with layered structure have been prepared from different powder fractions. The composition of the layers can be seen in fig. 3.18. All samples were of cylindrical geometry with 11,27 mm diameter. For better understanding, the design of the first (left) sample is discussed. Powders with different particle size were stepwise filled into a cylindrical mould. The filling was started with the powder with particle size  $\leq 90\mu\text{m}$ , followed by  $\leq 74\mu\text{m}$ ,  $\leq 63\mu\text{m}$ ,  $\leq 45\mu\text{m}$  and  $\leq 25\mu\text{m}$  in the centre of the sample. Finally the filling of the mould was continued with powder  $\leq 45\mu\text{m}$  up to  $\leq 90\mu\text{m}$  at the end. The composition of all the other samples is written in the blue cylinders in fig. 3.18. Then this “multilayer” powder body was compacted in one single step and sintered. Such specimen was about 20 mm high. All samples were pressed uniaxially with 200 MPa on Amsler hydraulic press, sintered **1300 °C - H<sub>2</sub> - 2 l/min** at 1300°C in hydrogen (AHT pushtype furnace, flow rate of 2 l/min with gas purity of 5.0) for 120 min soaking period. Only sample 2 was sintered with soaking period 180 min.





**fig. 3.18.: Description of layered samples prepared from different Mo fractions, sintering at 1300°C for indicated time**

In tab. 5 a summary is given of the values measured for density, calculated open (He-pycnometry measured)/total porosity and hardness HV10. It has to be considered here that the density and porosity data are integral values, including all the layers together. The hardness was measured in the cross section along the height in all layers. Because there was no difference in hardness between the layers, only one value for each sample is listed in tab. 5. By increasing the sintering time from 120 min to 180 min the density is increasing too. Calculated open porosity is below 41%, which level is shown by all the other samples. As clearly evident the porosity is almost totally open, which is of course desirable for subsequent infiltration. The hardness measured with 10 kp indentation load (HV 10) is at about 30 for all layered samples. The hardness of sample 2 is a little bit higher which is due to the longer soaking period of 180 min instead of 120 min. Specimens which were pressed out of the same powder with 200 MPa and sintered at 1300 °C showed higher values for the hardness (HV 10) which was demonstrated in fig. 3.8. The hardness was about 55 HV10. The specimens prepared before were only 10 mm high and the ones described in this experiment are twice as high. It is expected in this case, that due to the increased height of the specimen, the density is not homogeneously distributed in the specimen.

**tab. 5.: Archimedes density, calc. open and total porosity and HV 10 of cylindrical multilayer samples after sintering at 1300 °C with two different soaking periods in H<sub>2</sub>**

sample number	sintering time at 1300°C	density /g*cm <sup>-3</sup>	calc. open Porosity/%	calc. total Porosity /%	hardness HV=10
1	120	5,95	41,5	41,7	31±1
2	180	6,18	39,1	39,4	34±2
3	120	5,99	41,1	41,3	31±1
4	120	5,98	41,1	41,4	32±1
5	120	6,02	41,4	41,8	31±3

All values for open porosity and hardness measured with 10 kp are shown in fig. 3.19. It can be clearly seen that the variation between the values is very small. Only the value for the open porosity and hardness of Mo sample sintered for 180 min differs. The open porosity is lower and the hardness higher compared to samples sintered with 120 min soaking period.

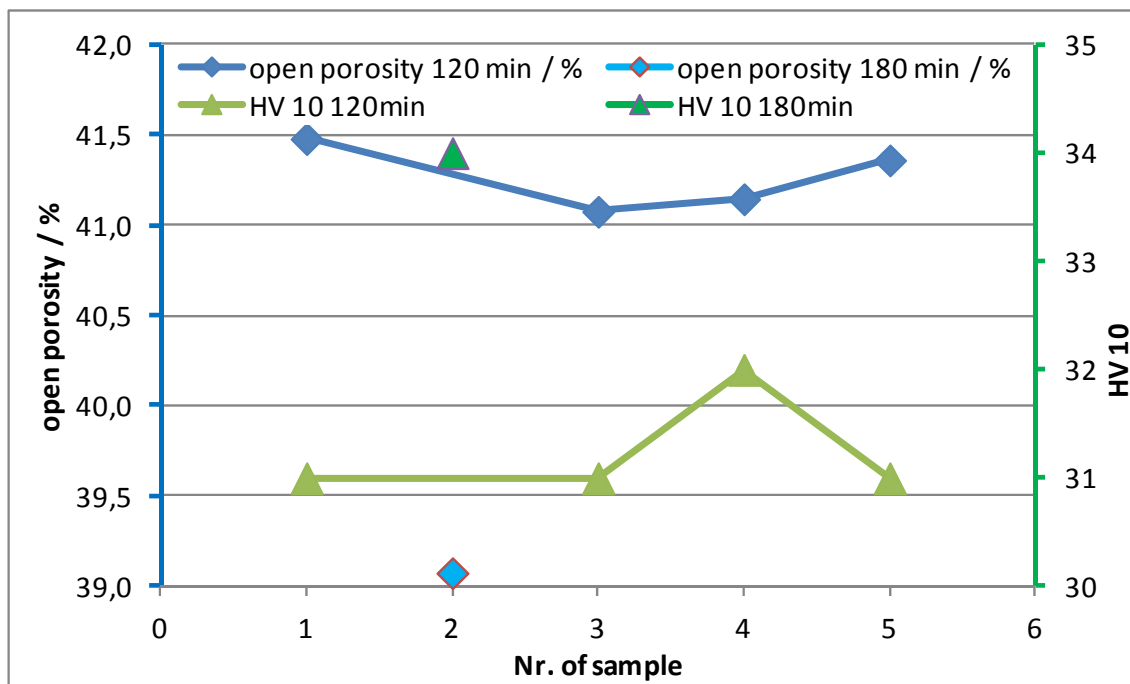


fig. 3.19.: Hardness and open porosity of each layered Mo sample after sintering in  $H_2$  at  $1300^\circ C$  and soaking period of 120 min or 180 min

#### 3.1.2.1.1 LOM images of multilayer samples after sintering at $1300^\circ C$ for 120/ min soaking period

The images in fig. 3.20 depict multilayer Mo samples. In the LOM it was not possible to recognize the transition zone (the interlayer) between the layers. The powders were sieved for the multi layer sample preparation. The low amount of coarse particles was separated by sieving, the particles which passed each sieve were about  $10\ \mu m$  in size (as was measured and demonstrated in fig. 2.3). Therefore, each layer contained mostly  $10\ \mu m$  particles and not primarily particles as big as the size of the sieve that was chosen. The cross sections (cut along the height of each specimen - for better demonstration of layer composition) in fig. 3.20 are demonstrating a representative part of each sample. Each layer was about 2mm high. Barely a difference can be observed in the pore size and distribution between the samples.

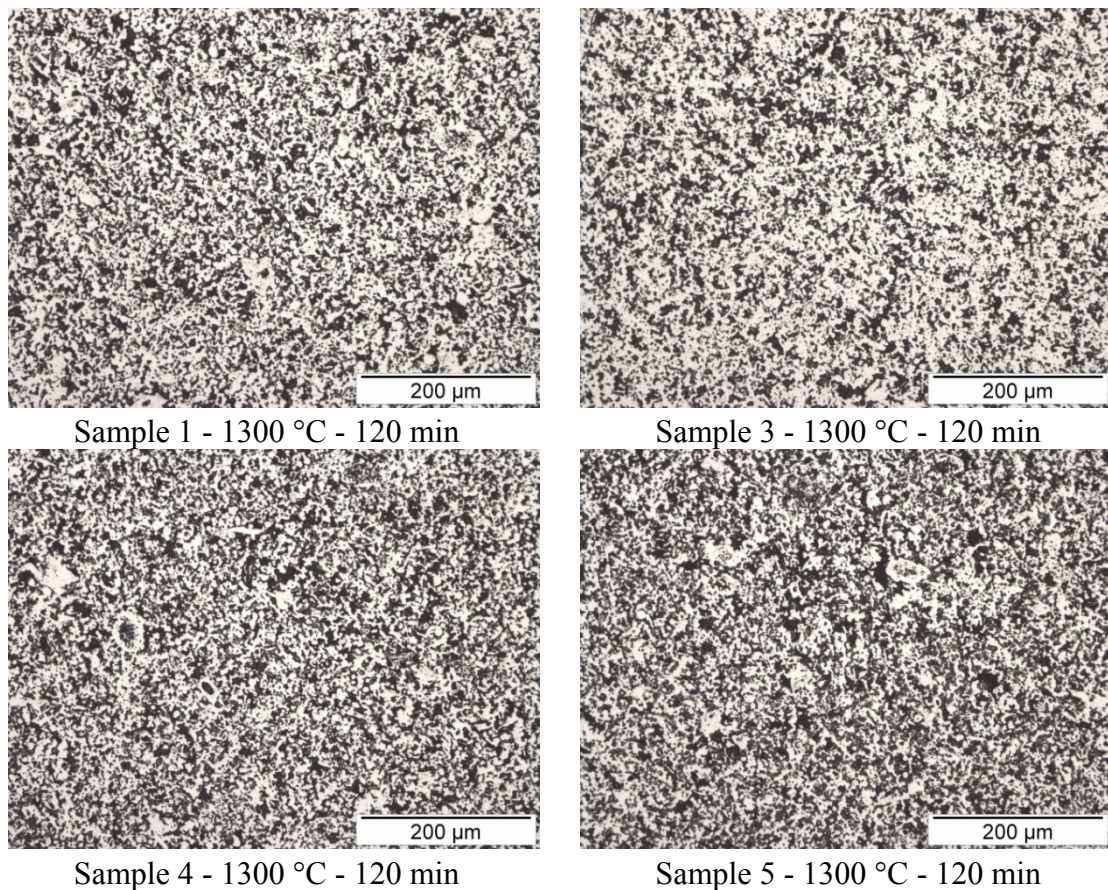


fig. 3.20.: LOM images of layered Mo samples after sintering at 1300 °C with 120 min soaking period

### 3.1.3 Characterisation of samples after Si CVI treatment

The CVI process was carried out by the project partner ATL. The samples for the CVI process have been prepared at TUW, and after the CVI treatment the Si content was analyzed by XRF, the distribution of silicides by light microscopy and scanning electron microscopy (SEM), and the phases formed were investigated by XRD.

The specimens were pressed as cylinders, both by uniaxial (11.27 mm diameter) die compaction on Amsler hydraulic press and by CIP (10 mm diameter), and sintered in the push-type furnace (type AHT-SiC) with gas-tight superalloy muffle. The pressing and sintering parameters are listed in tab. 6. The sintering atmosphere was hydrogen (5.0 purity) with 2 l/min flow rate. Parameters for the CVI process are also given in tab. 6.

**tab. 6.: Parameters for pressing and sintering of the samples before sending to ATL for CVI; CVI parameters as given by ATL**

sample name	pressed at [MPa]	sintered at [°C]	sintering time [min]	sintered density [g/cm <sup>3</sup> ]	CVI conditions
<i>e1078_1</i>	200 uniaxial	1300	120	7,04	850°C 4 mbar 10 l/min 120 min
<i>e1078_2</i>	200 CIP	1300	120	-	
<i>e1078_3</i>	170 uniaxial	1300	120	6,78	
<i>e1078_4</i>	200 uniaxial	1200	180	6,45	
<i>e1078_5</i>	200 CIP	1200	180	-	
<i>e1078_6</i>	170 uniaxial	1200	180	5,79	
<i>e1080_1</i>	200 uniaxial	1300	120	7,07	925°C 2 mbar 10 l/min 120 min
<i>e1080_2</i>	200 CIP	1300	120	-	
<i>e1080_3</i>	170 uniaxial	1300	120	6,72	
<i>e1080_4</i>	200 uniaxial	1200	180	6,48	
<i>e1080_5</i>	200 CIP	1200	180	-	
<i>e1080_6</i>	170 uniaxial	1200	180	5,83	
<i>e1082_2</i>	200 uniaxial	1300	120	7,00	825°C 2 mbar 5 l/min 360 min
<i>e1082_3</i>	170 uniaxial	1300	120	6,81	
<i>e1082_4</i>	200 uniaxial	1200	180	6,43	
<i>e1082_6</i>	170 uniaxial	1200	180	5,74	

The content of deposited silicon was measured twice. First measurement was done by ATL by taking the mass of the samples before and after the CVI process. The (hypothetical) value for the silicon content in the sample is obtained by subtraction of the two masses. The values thus obtained for the content of silicon are summarized in tab. 7. It has to be considered that clusters of silicon or silicides were adsorbed (observed at TUW after receiving the specimens) at the surface of the molybdenum samples. It seemed like a nucleus was formed at which the Si from CVI nucleated and started to grow in form of clusters which covered the surface irregularly. These clusters were very fragile and disintegrated by touching. They were removed by slight touching of the surface and were not taken for any analysis. The results obtained by XRF include the Si content only inside the specimen, without the clusters. Indeed the effective concentration of silicon inside the molybdenum samples must be expected to be much lower than the weight gain. Furthermore, all other reactions that affect the mass (reduction, oxidation ...) also affect the results.

The second measurement of the Si concentration inside the molybdenum samples was carried out by TUW. The concentration of Si and O was measured in the cross section of the molybdenum samples by X-ray fluorescence (XRF) analysis. The results are summarized in tab. 7. It should be noted that these are integral values, i.e. the entire cross section of the specimens has been analyzed. The Si concentration at or near the surfaces may be much higher, but since also the method used by ATL, i.e. the weight gain, is an integral method, the integral XRF was regarded as a sound reference.

Both values are compared in the last column. As expected the content of silicon measured through the weight gain after CVI is much higher than that measured by XRF, with one exception (→ samples “e1082”, which shows very low weight gain). Furthermore it should be noted that the samples were exposed to air during and after cutting until they have been measured by XRF. Therefore the measured oxygen might be some molybdenum oxide on the surface (XRF is fairly sensitive to the surface since



the penetration depth of the Rh K $\alpha$  radiation used is limited, in particular in case of a heavy element such as Mo).

tab. 7.: Measurement of Si content after CVI process; measurement by XRF vs. mass gain

<i>Sample Name</i>	<i>XRF Si [%]</i>	<i>XRF O [%]</i>	<i>Mass gain by CVI Si [%]</i>	<i><math>\Delta</math> XRF/CVI</i>
<i>e1078_1</i>	0,09	0,62	0,3250	0,2368
<i>e1078_2</i>	0,04	0,91	0,2049	0,1602
<i>e1078_3</i>	0,04	0,57	0,4214	0,3852
<i>e1078_4</i>	0,03	0,58	0,4959	0,4676
<i>e1078_5</i>	0,05	0,76	0,2916	0,2412
<i>e1078_6</i>	0,05	0,60	0,4755	0,4300
<i>e1080_1</i>	0,04	0,20	0,3047	0,2616
<i>e1080_2</i>	0,07	0,84	0,4282	0,3612
<i>e1080_3</i>	0,06	0,39	0,4326	0,3742
<i>e1080_4</i>	0,05	0,70	0,3968	0,3454
<i>e1080_5</i>	0,07	0,91	0,3912	0,3195
<i>e1080_6</i>	0,05	0,74	0,4621	0,4161
<i>e1082_2</i>	0,07	0,64	0,0212	-0,0455
<i>e1082_3</i>	0,04	0,81	0,0162	-0,0245
<i>e1082_4</i>	0,04	0,80	0,0370	-0,0013
<i>e1082_6</i>	0,04	0,85	0,0380	-0,0031

fig. 3.21 depicts the values measured by XRF from tab. 7. Green encircled values indicate samples pressed with 170 MPa, red encircled values those that were cold isostatically pressed (CIPed) with 200 MPa. Values in fig. 3.21 that are not encircled indicate samples pressed uniaxially with 200 MPa. The ones that were cold isostatically pressed show higher concentration on silicon inside the sample (after the CVI process) than samples that were pressed with 170 MPa. Samples pressed uniaxially have only two areas (the bottom and top area, i.e the punch surfaces) with completely accessible open porosity, while the porosity of the area on the side (the die surface) might be partially closed because of the friction (shear) forces during the uniaxial pressing, esp. during ejection. At least for sintered steels this has been definitely shown [157]. During the cold isostatic pressing, in contrast, the forces act equally from all directions (without any friction forces). Therefore the pores remain accessible/open from all sides.

Apart from the first sample 1080\_1 (fig. 3.21 and according to tab. 7) it can be seen that samples at which the CVI process was carried out at 925°C (target: SiC) show the highest concentration of silicon. Samples for which the CVI was carried out at 825°C show higher concentration of silicon than samples after CVI at 850°C. The CVI process for the first mentioned samples (825°C) was carried out with lower gas pressure in the reaction chamber but for longer time (360 min instead of 120 min) which can be taken as an indicator that time plays a more important role for the CVI process than temperature. Generally, however, the integral Si contents are relatively low.

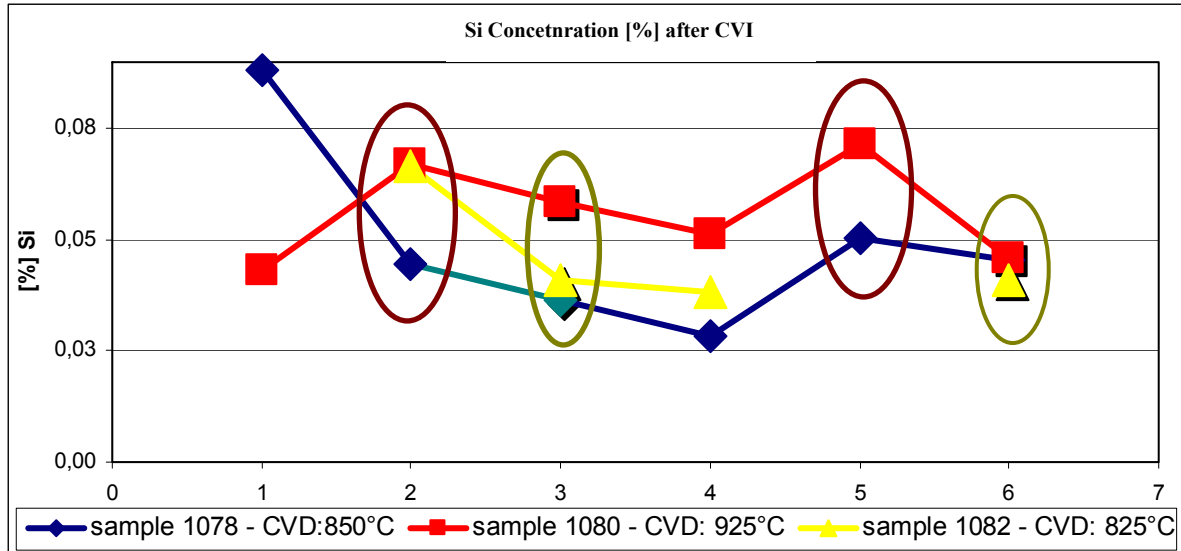


**fig. 3.21.: Concentration of silicon after CVI as measured by XRF (cross section); samples pressed uniaxially with 170 MPa are encircled in green, samples pressed cold isostatically with 200 MPa are encircled in red. Samples pressed uniaxially with 200 MPa were not encircled.**

Some light microscopic images from Mo specimens on which CVI was carried out by ATL will be presented in this chapter. The amount of Si in each sample was listed in tab. 7. As can be seen in tab. 7 many specimens were characterized after CVI treatment. Not all LOM images will be shown here. From each CVI experiment, only from one specimen the LOM images are shown. There have been three experiments carried out at three different temperatures, different soaking periods and chamber pressures, which was summarized in tab. 7 (different colours have been chosen to distinguish the different CVI experiments).

#### ***Sample "e1078\_1" from first CVI experiment: 850 °C - 4 mbar - 120 min***

In fig. 3.22 the cross section of specimen "e1078\_1" is depicted at two magnifications. This specimen was prepared by TU Vienna while the CVI treatment was carried out by ATL at 850 °C and 120 min soaking period at 4 mbar chamber pressure and 10 l/min  $\text{SiCl}_4$  flow. By XRF method 0.09 % Si were measured and by taking the weight 0.33 % Si mass gain were deduced (tab. 7). A light blue layer can be seen on one side of the sample. This blue area was analyzed by energy dispersive X-ray analysis (EDAX) on the scanning electron microscope. The blue band was identified as silicon enriched molybdenum. In fig. 3.22 (200x image) the two areas where silicon had penetrated the sample were encircled in red. One part of the silicon was adsorbed at the surface and the other part penetrated some micrometers below the sample surface. No gradient in concentration on silicon can be observed. Furthermore it can be observed that the blue silicon band appears only on one side of the sample (fig. 3.22 - 100 x - left vertical base shows a blue layer extending over the whole length). Possibly the position of the specimen in the CVI apparatus has some effect here.



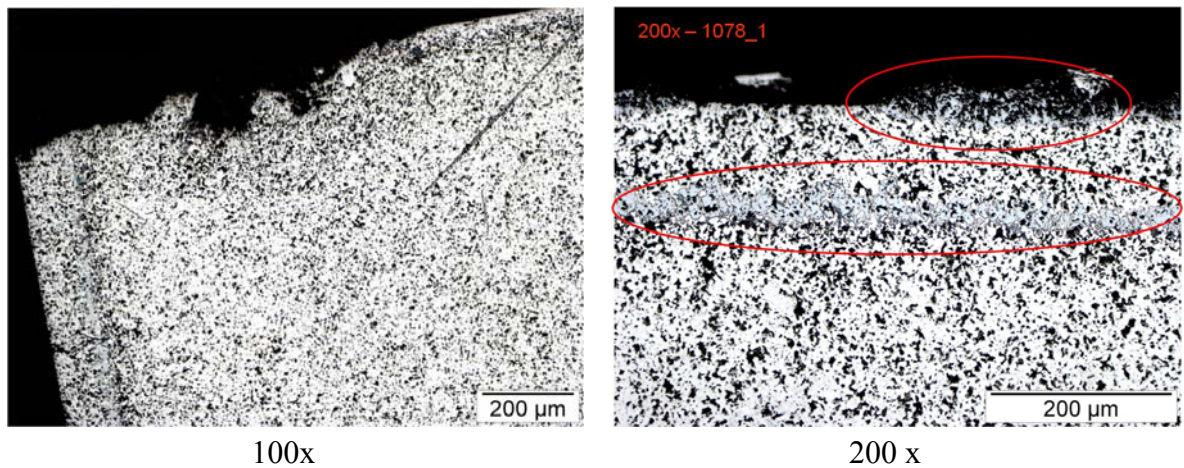


fig. 3.22.: LOM of Mo specimen after CVI at 850 °C for 120min at 4 mbar and 10l/min of  $\text{SiCl}_4$

***Sample "e1080\_5" from second CVI experiment: 925 °C - 2 mbar - 120 min***

In fig. 3.23 the cross section of specimen "e1080\_5" is shown at two magnifications. The Mo preform was prepared by TU Vienna while CVI was carried out by ATL at 925 °C and 120 min soaking period at 2 mbar chamber pressure and 10 l/min  $\text{SiCl}_4$  flow. By XRF, 0.07 % Si and by taking the weight 0.32 % Si mass gain were measured (tab. 7). Comparing the cross section images from specimen "e1080\_5" (fig. 3.23) with the "e1078\_1" (fig. 3.22) no blue area or a blue band can be observed. All areas look very similar to each other, no "islands" of Si deposited at the surface could be observed. The surface of the cross section shown in fig. 3.23 looks very uniform with no visible Si. The 0.07 % Si measured by XRF is a very low amount of Si, therefore it is quite difficult to recognize it in the LOM images of the cross section.

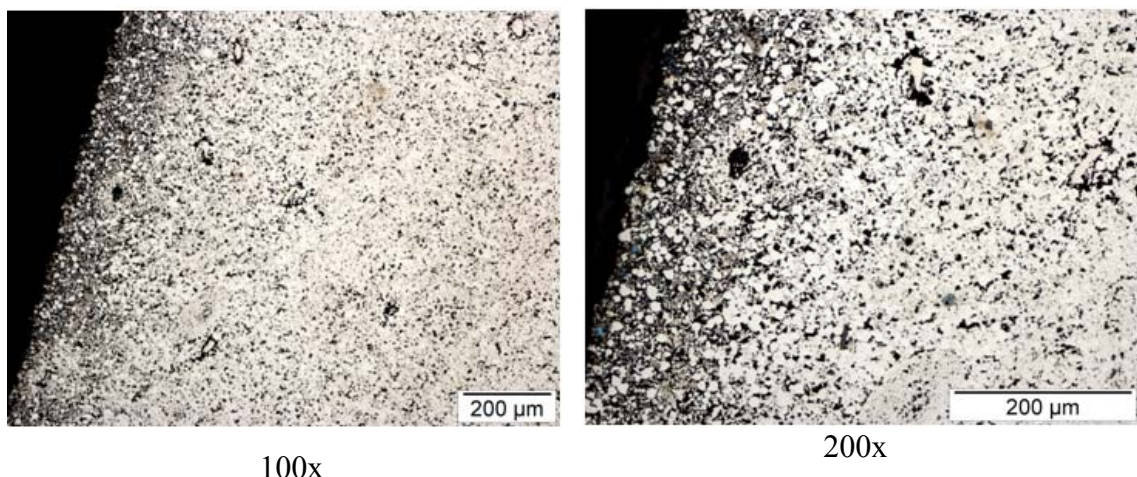


fig. 3.23.: LOM of Mo specimen after CVI at 925 °C for 120 min at 2 mbar and 10 l/min of  $\text{SiCl}_4$

**Sample "e1082\_2" from third CVI experiment: 825 °C - 2 mbr - 360 min**

In fig. 3.24 the left top part of the sample "e1082\_2" is shown. CVI was carried out by ATL at 825 °C and 360 min soaking period in 2 mbar chamber pressure and 5 l/min  $\text{SiCl}_4$  flow. The reaction temperature is lower than in specimen "e1080\_5" but the reaction time is 3 times longer. By XRF method 0.07 % Si and by taking the weight 0.02 % Si mass gain were measured (tab. 7). A curved, more porous area is pointed out. This area forms a ring around the centre of the sample. Within the ring large pores were observed. The boundary of the pores and the pores themselves were oxidized during CVI which might explain the ring. This area of the sample seemed less resistant to oxygen, and the grey colour might come from oxidized molybdenum.

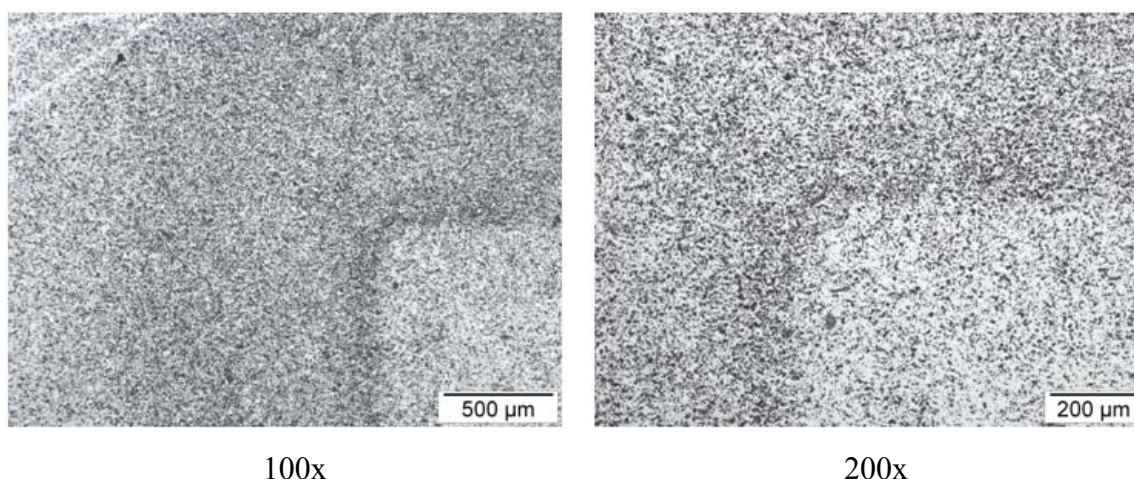


fig. 3.24.: LOM of Mo specimen after CVI at 825 °C for 360 min at 2 mbar and 5 l/min of  $\text{SiCl}_4$

### 3.1.3.2 Scanning electron microscope (SEM) investigations

Sample "e1078\_1" was already discussed before with the LOM images. Some SEM images are depicted in fig. 3.25. All images are backscattered electron images (BSE). In comparison to light microscope images it is possible to identify silicon around the band (green encircled). Furthermore the dark grey band (which appears light blue in the LOM images - fig. 3.22) was analysed by EDAX. The result from the EDAX analysis is shown too in fig. 3.25. About 37% Si content was measured in this area.



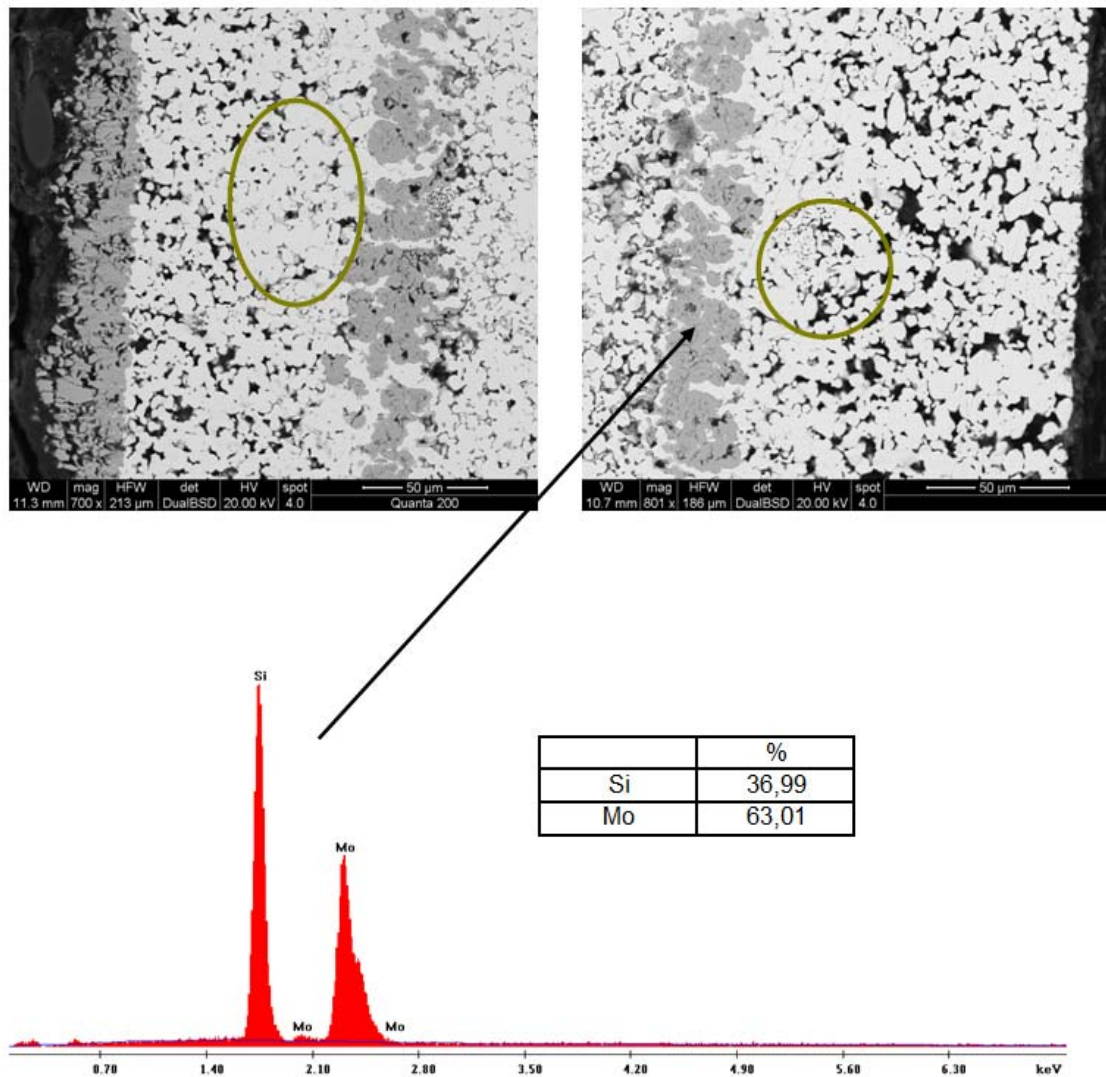


fig. 3.25.: Back scattered images (BSE) from specimen "e1078\_1" from cross section after CVI

### 3.1.4 Summary: molybdenum samples prepared from commercially available Mo

For the experiments, commercially available molybdenum powder (designated as < 63 $\mu$ m from CM) was used. Two fractions have been sieved differing in particle size distribution. One was designed as particle size < 63  $\mu$ m and the second one < 45  $\mu$ m. The influence of particle size, compacting pressure and sintering temperature on mechanical properties like hardness, density and porosity was explored. For the experiments, specimens with cylindrical geometry of 20 mm diameter and approximately 10 mm height were pressed uniaxially with different compacting pressures. The compacting pressure was chosen between 70 and 270 MPa and the sintering temperature was 1200 / 1250 / 1300  $^{\circ}$ C with 30 min and 90 min soaking

period. It could be observed that the density of the compacts is increasing with increasing compacting pressure up to 200 MPa. At higher compacting pressures the density is decreasing. Samples pressed at 220 MPa and 270 MPa show noticeably lower density. So it could be shown that 200 MPa is the optimum compacting pressure for the powder used. The reason for these compacting problems is the emergence of pressing defects in the material, due to overpressing. The lowest density was measured for samples pressed with the lowest compacting pressure of 70 MPa. With increasing density the open porosity and total porosity are decreasing. The highest values for the open porosity were measured for samples compacted at 70 MPa (the lowest pressure). Due to the pressing defects the open porosity is increasing with higher compacting pressures than 220 MPa. The influence of sintering temperature on density can be observed very well in fig. 3.3. All specimens were sintered between 1200°C and 1500°C in 50 °C steps. With increasing sintering temperature the values for the density are increasing while the open porosity is decreasing. It can be observed that specimens pressed at 200 MPa and sintered at 1500 °C show the highest density. The lowest density was achieved for samples sintered at the lowest temperature of 1200 °C.

Samples from Mo powders < 45 µm and < 63 µm have been compared. It could be observed that specimens pressed out of < 45 µm Mo powder tend to higher sintered densities compared to samples pressed out of < 63 µm Mo powder.

The hardness was increasing with higher sintering temperature for all specimens up to 200 MPa compacting pressure, before pressing defects occurred.

Samples sintered at three different temperatures (1200°C; 1250 °C; 1300°C) were compared for their pore diameter, which was measured with Hg - porosimetry, as a function of the sintered density (fig. 3.9). It could be seen that with increasing sintering temperature the average pore size is increasing too (fig. 3.10). The average pore size of specimens sintered at 1200°C (uniaxially) was 0.78 µm and for specimens sintered at 1300 °C it increased to 0.95 µm. It should also be mentioned that every specimen could be measured only once, because, as the pores were filled up with Hg, the specimens had to be disposed of after every measurement. While the average pore radius increased, also the density was increasing with higher sintering temperature. Furthermore, observing specimens prepared at the same conditions but pressed cold isostatically are showing lower values for the average pore radius (fig. 3.11). With increasing sintering temperature the size of the open pores was decreasing. The average pore size of specimens sintered at 1200°C was 0.77 µm while the pore size of specimens sintered at higher temperature of 1300°C decreased to 0.71 µm. With increasing sintering temperature the size of pores decreased.

Multilayer samples have been prepared. These are specimens prepared layerwise from different Mo powder fractions. Between the specimens prepared from different powder fractions barely any difference in open porosity could be measured. Furthermore, it was not possible to see any interlayer/interface between the layers. The powders used seemed not to differ in particle size distribution. There have not been many coarse particles and most coarse particles were sieved away, therefore only the fine particles remained. The open porosity (measured integral including all layers) was between 40 and 41%. Samples sintered for longer time of 180 min showed a lower open porosity of 39% compared to specimens sintered for 120 min. The hardness HV10 was in the range of 31 for samples sintered for 120 min and 34 for samples sintered for 180 min.

The LOM images of Mo specimens have also been shown. The light microscopy images of Mo specimens prepared from < 45 µm and < 63 µm powders and sintered for 30 min and 90 min soaking period were compared (fig. 3.13). Between all sections in fig. 3.13 barely a difference can be observed.

By a careful look it could be observed that with increasing soaking period the size of the pores is decreasing (fig. 3.13; compared 1200°C - 90 min - < 45 µm and 1200 °C - 30 min - < 45 µm). Furthermore it can be seen that specimens from coarser Mo powder show larger pores. It can be said that, as expected, coarser particles result in larger pores.

LOM images of cross sections of Mo specimens from < 45 µm Mo powder sintered at 1200 / 1300 / 1400 / 1500 °C were compared. The soaking period was 90 min for all four specimens. It could be observed that with increasing sintering temperature the size of the pores is decreasing.

In fig. 3.20 multilayer Mo specimens from different powder fractions were compared. The transition zone between the layers was not visible in the LOM. The difference in particle sizes was too small to see any difference. Pores of very similar size are uniform distributed through the whole cross section without any difference.

In the dilatometry a Mo specimen with a green density of 6,72 g/cm<sup>3</sup> was sintered at 1400 °C for 60 min soaking period. The length change during sintering was measured parallel to the pressing direction and can be observed in fig. 3.15. Sintering starts at 880 °C. The total shrinkage during sintering (with respect to cooling) is 4,63 %.

The MS spectroscopy (fig. 3.16) helped to understand the processes during sintering like the formation of H<sub>2</sub>O, N<sub>2</sub> and CO<sub>2</sub> gases. During heating up considerable amounts of H<sub>2</sub>O were detected, as a consequence of reduction of surface oxides. A negligibly small amount of CO<sub>2</sub> was formed, probably from pressing oil (used for die wall lubrication).

In chapter 3.1.3 some Mo specimens were characterised which were prepared by TUV and then CVI treated with SiCl<sub>4</sub> by the partner ATL. The weight gain after infiltration was taken by ATL as an indicator for the silicon deposited. TUV carried out XRF analysis of the cross section of the sample bodies. The difference in mass gain between the two methods was quite high. The mass gain by ATL considered Si clusters absorbed on the surface as well as possible oxygen pickup. The TUV XRF method was measuring the silicon content inside of the specimen because the Si clusters were pulled away and were not included in the measurement. The values are listed in tab. 6. The oxygen content was measured too (tab. 7). The content was below 1 % but it should be noted that the specimens were exposed to air during cutting in water (until they were measured by XRF) therefore the measured oxygen might be some molybdenum oxide on the surface.

When comparing differently pressed specimens, it can be seen that samples that were CIPed show higher concentration of silicon inside the sample. The difference is however very small, +/- 0,02, which might be experimental scatter.

Apart from the first sample 1080\_1 (fig. 3.23 and according to tab. 6) it can be seen that samples at which the CVI process was carried out at 925°C show the highest silicon content. Samples on which the CVI was carried out at 825°C show higher concentration of silicon than samples after CVI at 850°C. The reason is that also other parameters were changed: The CVI process for the first mentioned samples (825°C) was carried out with lower gas pressure in the reaction chamber but for longer time (360 min instead of 120 min) which can be taken as an indicator that the time plays a more important role for the CVI process than the temperature. Generally, however, the integral Si contents are relatively low, due to too small pores or the pores closed already after some minutes of infiltration disabling further Si to enter.

### 3.1.5 Molybdenum with Ni as sintering activator

The first infiltration experiments done by the project partners had shown that the structural strength of standard sintered Mo compacts was too low to sustain the loads during Si infiltration, with the consequence that the specimens simply disintegrated. Therefore, higher strength, i.e. better interparticle bonding, was regarded necessary. In addition to sintering at significantly higher temperatures, also activation of the sintering process was regarded an interesting option.

To gain information about the influence of nickel – the most common sintering activator for W and Mo - on the sintering behaviour of the molybdenum preforms, samples were prepared of molybdenum with different wt% Nickel and analysed. In a further experiment Mo samples were doped with 0.1 wt% Ni and sintered at four different temperatures. All experiments carried out were done using Chemie Metall molybdenum powder <63  $\mu\text{m}$  (nominally). The nickel powder used for the activated sintering experiments was INCO type 123 carbonyl nickel powder. It should be further mentioned that the addition of a sintering activator like Ni is just a supporting method for sintering. In fact, as has already been discussed in the literature, Ni deteriorates the high temperature properties of molybdenum. It would not be possible to introduce Ni into Mo and infiltrate the material in a further step with Si without fatal consequences for the high temperature properties such as creep strength.

#### 3.1.5.1 Influence of Ni content on the open porosity in Mo bodies

##### 3.1.5.1.1 Influence of sintering temperature on Mo doped with 0.1 wt% Ni

In the starting experiments the influence of the sintering temperature on density, open porosity and hardness of molybdenum doped with 0.1 wt % Ni as sintering activator was examined. The sintering temperatures were 1000 / 1100 / 1200 and 1300 °C. The soaking period at all temperatures was 120 min. All specimens were compacted with 200 MPa uniaxially to cylinders with 20 mm diameter and about 12 mm height. Mo from Chemie Metall with particle size  $\leq 63 \mu\text{m}$  was chosen.

In tab. 8 can be seen that the lowest density and hardness and the highest degree of open porosity was measured for the specimen sintered at 1000 °C. The highest density of 6,03 g/cm<sup>3</sup> was measured for the sample sintered at 1300 °C. The open porosity was 28 %. The specimens have been pressed on the Amsler press. It was quite difficult to adjust the compacting pressure. That might explain the smaller densities of the sintered bodies compared to those achieved for samples pressed with the same pressure and sintered at the same temperature which were summarised in tab. 2.

**tab. 8.: Measured density, hardness and calculated open porosity for nickel doped Mo samples**

sintering temperature/ °C	compacting pressure/ MPa	density/ g/cm <sup>3</sup>	measured - He - pycn. open porosity/ %	HV 10
1000	200	5,38	47,5	47
1100	200	5,88	44,0	51
1200	200	5,99	42,1	55
1300	200	6,33/6,00*	32,3/37,2*	83/72*

\* measured values for reference samples sintered at 1300°C without addition of nickel



Values from tab. 8 are graphically shown in fig. 3.26 and were compared with samples without nickel. It can be seen that by adding nickel the porosity is decreasing while the hardness is increasing. A difference to undoped samples can be observed very well, although the difference is not too pronounced, indicating that the Ni content chosen here might have been slightly too low.

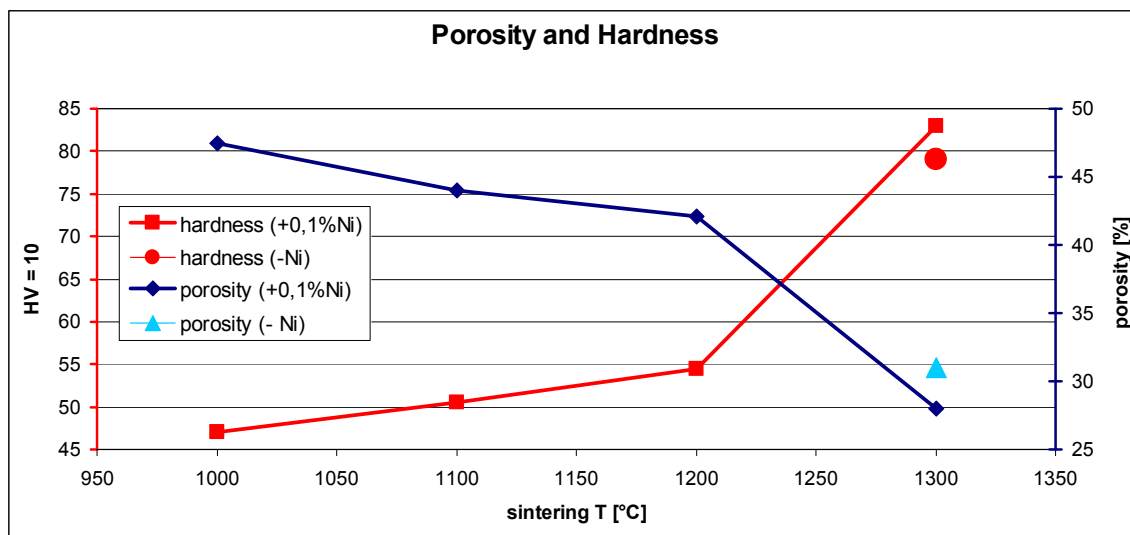


fig. 3.26.: Open porosity and hardness (HV 10) with 0.1 wt% Ni and without Ni as a function of the sintering temperature. Compacted 200 MPa, sintered 2 h in H<sub>2</sub>

By controlling the sintering temperature and the addition of a very small amount of sintering activator it is possible to influence the resulting density and open porosity of the material. The sintering activator, in this case Ni, increases the density and decreases the open porosity. That means that instead of going to very high sintering temperatures just an exact amount of sintering activator is needed.

#### 3.1.5.1.2 Influence of different amounts of Ni on the physical and mechanical properties of Mo

As stated above, the effect of 0.1%Ni on sintering was not too pronounced. In further experiments, therefore, higher amounts of sintering activator have been added, to examine the influence of different amounts of Ni on the physical and mechanical properties. Batches with different contents of nickel in molybdenum were prepared. As a reference, no nickel was added to the first powder batch.

The powder blends prepared contained 0.1 wt%, 0.5 wt%, 1 wt% and 5 wt% nickel. Each batch was homogenised for 2 h in a tumbling mixer and pressed on the Jessernigg & Urban press with 200 MPa to samples of rectangular geometry. The dimension of the rectangles was 55\*10\*7 mm (l\*w\*h). As was already mentioned, this press is not accurate at low pressures, which might result in higher pressures than the one that was

set. This explains the higher values for the porosity achieved compared to the ones that were measured in tab. 1 or tab. 7.

For this test run the samples were sintered at 1300°C in hydrogen (5.0 purity and 2 l/min gas flow) at a soaking period of 120 min in the AHT SiC-rod heated push-type furnace.

After sintering the physical and mechanical properties of the samples were measured to define the influence of nickel in molybdenum. The change in open porosity was of particular interest, open porosity being a must to ensure the infiltrability. To explore the physical properties, the geometrical density, density after Archimedes and open porosity (by water impregnation method) were measured. He-pycnometry was not possible because of the sample geometry – long, thin bars - and no suitable analysing cell being available. However, as shown above, the water impregnation method yields results that differ only marginally from those of the He pycnometry.

The mechanical properties were characterized by 3-point bending test, Charpy impact strength testing and Vickers hardness measurement with 10 kp indentation load (HV10). Furthermore the electrical conductivity of the sintered samples was determined. The sintered specimens were cut, embedded in bakelite and the cross sections were metallographically prepared and characterised on the LOM.

### ***Physical properties***

The density of the specimens was measured by the Archimedes method (water displacement) after impregnating the samples with a commercial waterstop spray. Open porosity was measured by immersion method with water (filling of open pores) according to DIN EN 623. The measurement of the conductivity was carried out in two ways, first on a Dr. Förster - Sigmatest 2.067. Each rectangular sample was measured on three points along the length of the sample punch surface. Attention was paid how the sensor was held during the measurement on the surface of the sample. For an accurate measurement the sensor should terminate within the sample border. The second measurement was carried out on "Halbautomatisches Widerstandsmessgerät" (short: HAWM) (see Chapter 2.1.3.5). In the literature values for the conductivity were found. Fully dense Molybdenum<sup>1)</sup> has a conductivity of  $18.2 \cdot 10^6 \Omega^{-1} \cdot \text{m}^{-1}$  and Nickel<sup>1)</sup>  $14.5 \cdot 10^6 \Omega^{-1} \cdot \text{m}^{-1}$ . With increasing number of sintering bridges the conductivity should increase, but as can be seen in tab. 9 the conductivity is in fact decreasing with increasing amount of Ni. The knowledge of conductivity let us understand something about the sintering effect. By addition of nickel the sinterability of molybdenum is increasing. By addition of the highest amount of nickel the highest sinterability of molybdenum is expected. By the addition of Ni, the density is increasing, and further on also the amount and size of sintering bridges. These results achieved are contrary to the expectations.

All results from the experiments are summarized in tab. 9.

tab. 9.: Density, open porosity and electrical conductivity of Mo-x%Ni. Compacted 200 MPa, sintered 2 h 1300°C in H<sub>2</sub>

results	[ ]	[wt%] Nickel				
		0	0,1	0,5	1	5
<b>geometrical density</b>	g/cm <sub>3</sub>	7,31±0,07	7,24±0,03	8,31±0,04	8,73±0,06	8,85±0,03
<b>Archimedes density</b>	g/cm <sub>3</sub>	7,40±0,02	7,28±0,02	8,38±0,03	8,84±0,02	8,98±0,01
<b>open porosity</b>	%	31,12 ±0,6	24,82±0,9	14,05±0,7	3,72±0,9	0,82±0,3
<b>total porosity</b>	%	32,70±0,4	28,70±0,4	17,80±0,7	5,40±0,4	3,20±0,3
<b>Conductivity - Förster / HAWM</b>	(μΩ. m) <sup>-1</sup>	8,09±0,3 / 8,19±0,1	6,28±0,2 / 7,63±0,2	5,60±0,2 / 6,36±0,1	5,38±0,1 / 6,18±0,1	5,43±0,1 / 5,37±0,1

As the amount of nickel was increasing the open porosity was decreasing, as can be seen very well in tab. 9. Apart from all samples, the sample that was doped with 0,1 wt% nickel shows a lower density than the one without nickel, which can only be explained that this value is an outlier. With increasing density (Archimedes) and amount of Ni as sintering activator the open porosity was decreasing. The lowest value for the open porosity (0.8 % open porosity) was measured for Mo sample containing 5 wt% Ni. Furthermore the values for the conductivity can be found in tab. 9. Two values for each Ni content are listed. Each first value is the conductivity measured with the Förster tester and the second value is the one measured by "Halbautomatisches Widerstandsmessgerät". It can be seen that the values for the conductivity measured with both methods are quite similar. It was expected that with increasing amount of Ni the sintering activity is increasing, the material gets more dense (more and thicker sintering bridges) and therefore the electrical conductivity is increasing. However, it can be seen in tab. 9 that the electrical conductivity in fact decreases with higher Ni content. Very small amount of Ni might have diffused into Mo and formed solid solution which shows a lower conductivity than the pure metal. (There is just a very small solubility of Ni in Mo of about 2 % at 1362 °C.). Furthermore, also the formation of the intermetallic phase MoNi at the sintering contacts might have occurred, which may also lower the conductivity. Nevertheless it is surprising that this effect outweighs the densification.

An illustration of the increasing density with higher amount of nickel and of the simultaneous decreasing of open porosity is shown in fig. 3.27.

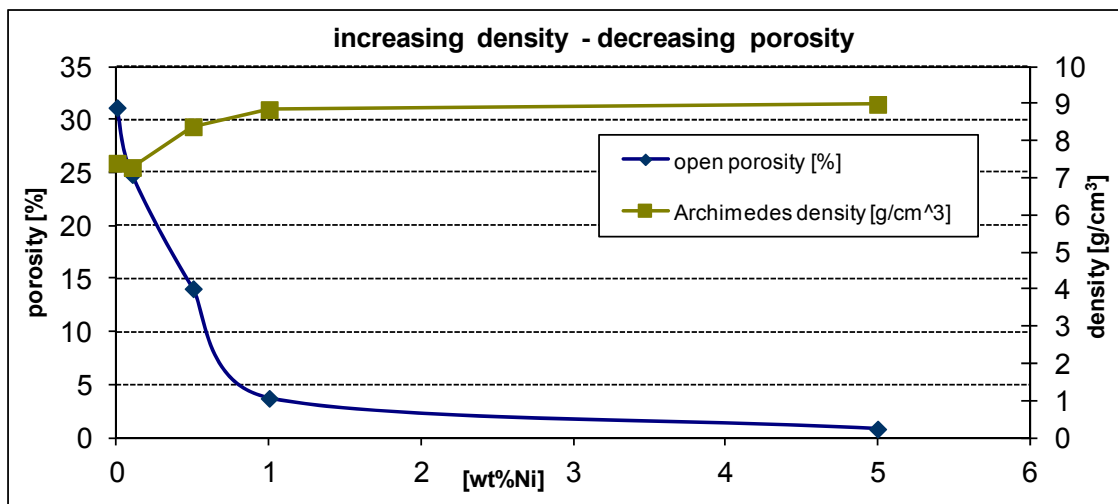


fig. 3.27.: Density and open porosity of Mo-Ni as a function of the Ni content. Compacted 200 MPa, sintered 2 h 1300°C in H<sub>2</sub>

In fig. 3.28 the electrical conductivity in dependence of sintered density is shown. With increasing density the electrical conductivity is decreasing too. As stated above, it was expected that with increasing density the conductivity is also increasing because of more sintering bridges. A higher degree of sintering bridges gives more ways for the electrons to flow. However, molybdenum and nickel form a solid solution which inhibits electron movement.

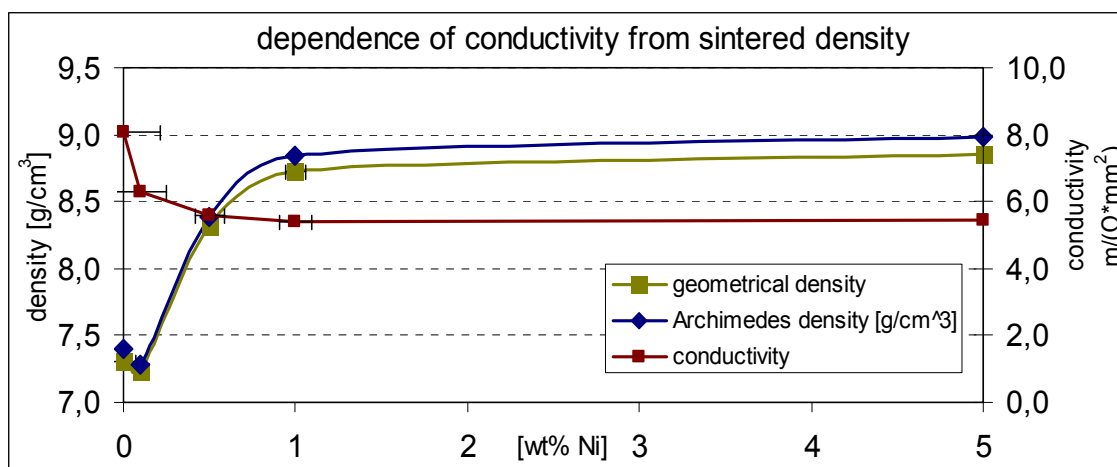


fig. 3.28.: Electrical conductivity and density of Mo-Ni as a function of the Ni content. Compacted 200 MPa, sintered 2 h 1300°C in H<sub>2</sub>

### *Mechanical properties*

The hardness was measured by the Vickers method with 10 kp indentation load (HV10), using a hardness tester EMCO M4U-025.

While the open porosity decreased with higher amount of nickel the hardness increased. It was possible to increase the hardness five times by addition of 5 wt% nickel to molybdenum (fig. 3.29).

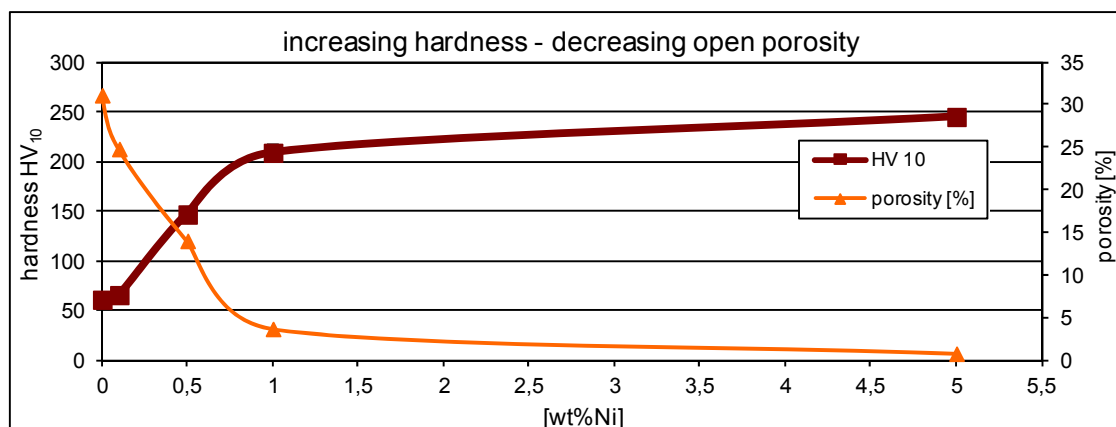


fig. 3.29.: Hardness (HV 10) and open porosity of Mo-Ni as a function of the Ni content.  
Compacted 200 MPa, sintered 2 h 1300°C in H<sub>2</sub>

The bending strength was measured in 3-point testing. The crosshead speed was 0.5 mm/min. By increasing addition of nickel as sintering activator the bending strength is increasing too. It was already observed for the density and open porosity (in fig. 3.27 and tab. 9) that by addition of 0.1 wt% nickel the values for the density were increasing while the open porosity was decreasing. The same can be observed with the bending strength. Because of a lower density measured at samples with 0,1 wt% nickel the bending strength is also lower (fig. 3.30). The scatter of the bending fracture of Mo specimen with 0,1 wt% Ni was quite low. However, it should be noted that the value for the density is quite low. It should be higher than the one for the specimen from plain Mo (or at least at the same level if 0,1 wt%Ni were below the threshold for activation).

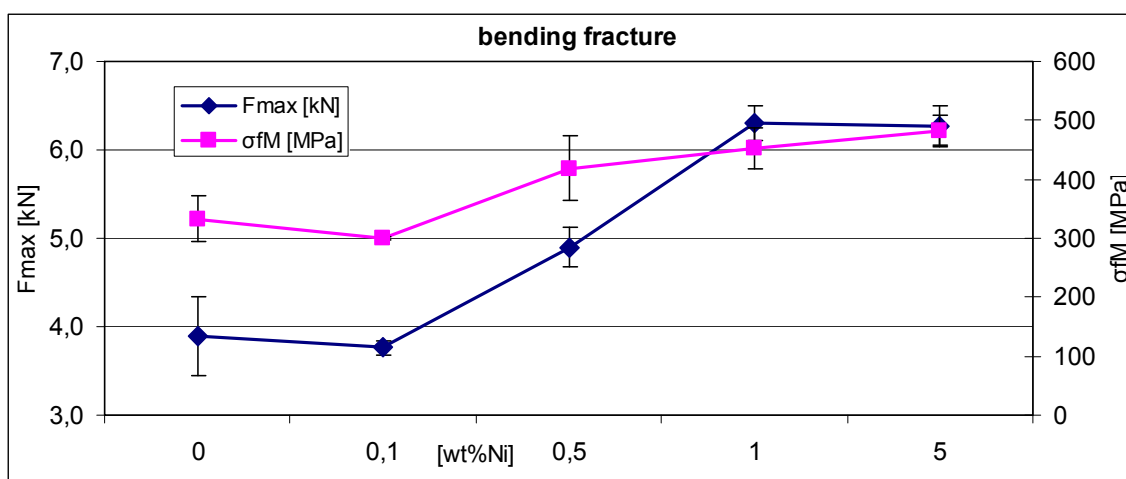


fig. 3.30.: 3-point bending strength measured in a 3-point test of Mo-Ni as a function of the Ni content.  
Compacted 200 MPa, sintered 2 h 1300°C in H<sub>2</sub>

The Charpy impact energy test was carried out on a 50 Joule tester. With increasing amount of nickel in the molybdenum matrix the impact strength was also increasing (fig. 3.31). In contrast to the bending strength, here 0,1 wt%Ni has a positive effect.

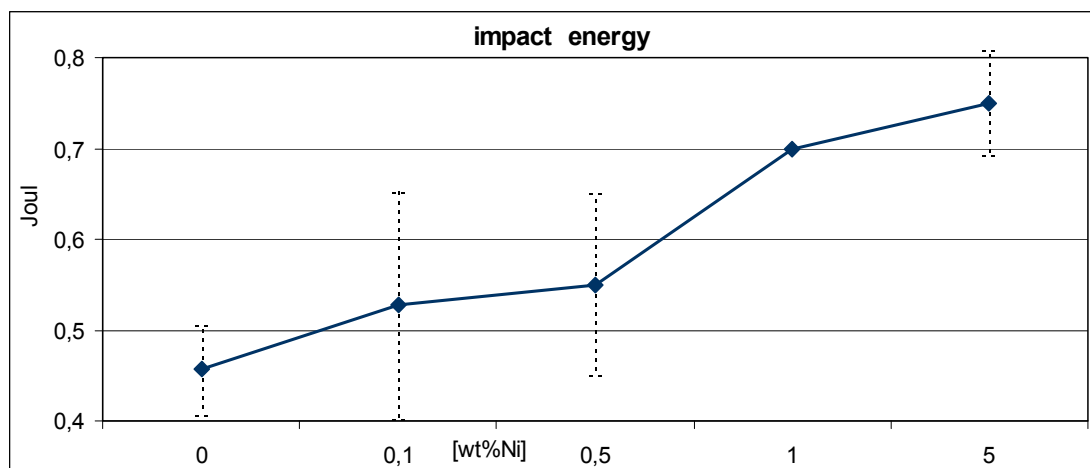


fig. 3.31.: Impact energy of Mo-Ni as a function of the Ni content. Compacted 200 MPa, sintered 2 h 1300°C in H<sub>2</sub>

In tab. 10 a brief summary is given of hardness (HV 10), bending strength and impact energy. It can be observed very well that with increasing Ni content in Mo the hardness, bending strength and impact energy are increasing due to higher density of the material and better interparticle bonding, due to higher sintering activity of Mo with increasing content of Ni.

tab. 10.: Summary of hardness, bending strength and impact energy

Results	[ ]	[wt%] Nickel				
		0	0,1	0,5	1	5
HV10	-	61	70	157	223	271
Fmax	kN	3,89	3,76	4,90	6,27	6,31
$\sigma_F$	MPa	332,9	301,0	418,3	452,7	482,2
impact energy	Joul	0,46	0,53	0,55	0,70	0,75

### *Light optical microscopy*

For microstructural characterization, the rectangular samples were cross cut. One cross section was embedded in bakelite so that it was possible to see the complete cross section of the sample. Polishing was carried out in three steps. First of all any bakelite present on the section surface was polished away on a coarse 220 grid diamond bonded disc. In the last two steps the scratches were polished off first with 9  $\mu$ m than with 3  $\mu$ m diamond suspension.

### *Molybdenum with different amounts of Ni*

Some images of the cross section of each Mo (+/- Ni) are summarized in fig. 3.32. It can be seen very well that between Mo sample without and the one with 0.1 wt% Ni there is barely any difference in the amount and size of pores. The first difference can be observed at the Mo sample doped with 0.5 wt% Ni. There are obviously smaller pores than those observed in LOM image of Mo doped with 0.1 wt% Ni. With



increasing Ni content the size of the pores is decreasing, as can be observed in fig. 3.32 - Mo + 5 wt% Ni.

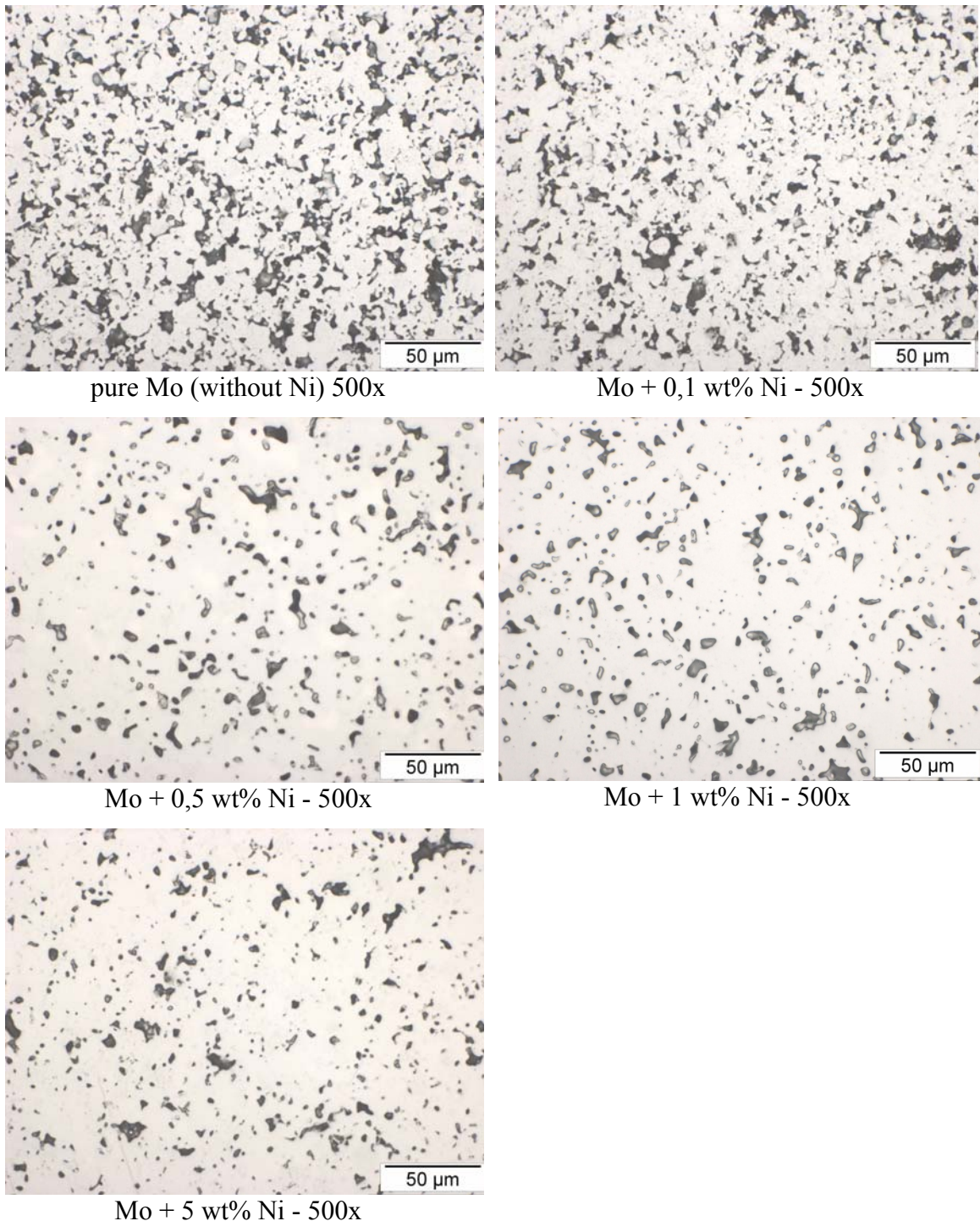
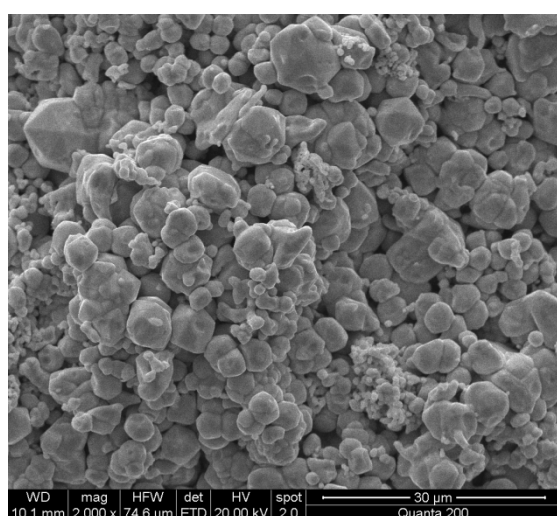


fig. 3.32.: Metallographic cross section of Mo-Ni with different amount on Ni; all images: 200x magnification

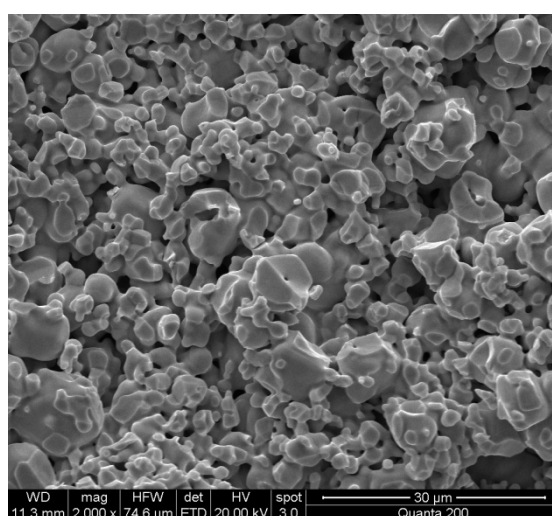
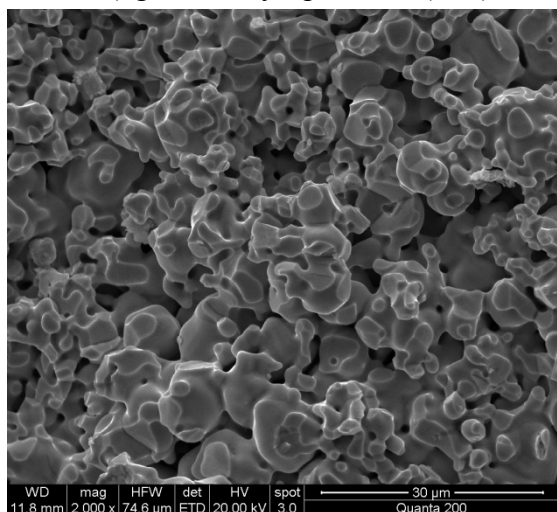
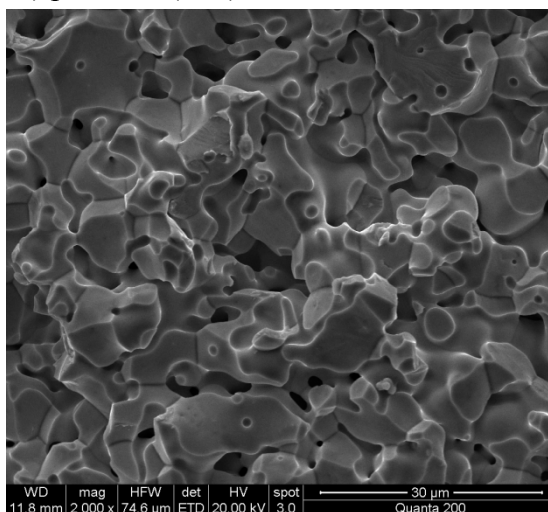
### *Fracture surfaces*

The fracture surface is giving some information about the sintered material. The amount and the size of the sintering bridges gives information about the sintering stage of the material. Depending on the sintering temperature, the soaking period and of the material itself the sintering bridges can be more or less distinctive. For example, sintering

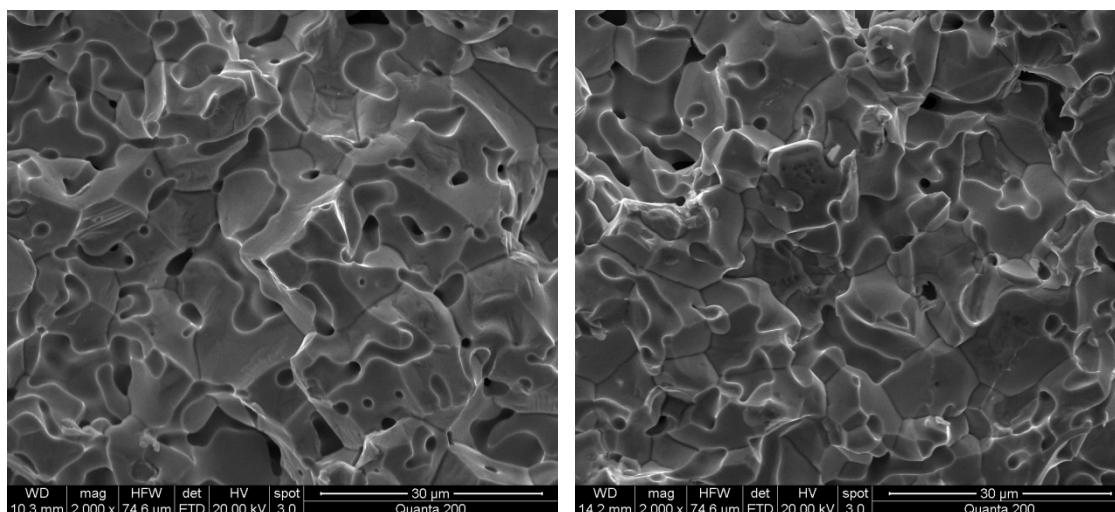
molybdenum with x wt% Ni as sintering activator should result in pronounced sintering bridges. In fig. 3.33 the fracture surface of a green body, of plain Mo after sintering at 1300°C for 2 h and of Mo with different amounts of Ni as sintering activator is shown. It can be observed very well that starting with the SEM image where no sintering bridges can be seen and moving to sintered plain Mo and to Mo specimens with increasing amount of Ni the amount and size of sintering bridges is increasing too. Mo without Ni has only very thin sintering bridges, and the pores in-between the particles can be seen very well. Already after addition of 0.5 wt% Ni the cavities between the particles are shrinking, and the sintering bridges have grown to nearly the size of the particles. After doping Mo with 1 wt% or 5 wt% Ni no difference between particles and sintering bridges can be observed. The pores have decreased already to a size that cannot be recognized easily.



a) green body - pure Mo (CM)

b) pure Mo (CM) - 1300 °C - 120 min - H<sub>2</sub>c) Mo + 0,1 wt Ni - 1300 °C - 120 min - H<sub>2</sub>d) Mo + 0,5 wt Ni - 1300 °C - 120 min - H<sub>2</sub>





e) Mo + 1 wt Ni - 1300 °C - 120 min - H<sub>2</sub>    f) Mo + 5 wt Ni - 1300 °C - 120 min - H<sub>2</sub>

**fig. 3.33.: Fracture surface of Mo specimens +/- Ni; (a) Mo sample (without Ni) before sintering - without sintering bridges; (b) sintered plain Mo; (c-f) Mo + x wt% Ni; (b-f) after sintering at 1300 °C for 2h soaking period in H<sub>2</sub>**

The fracture surface was analysed using the Pixcal image analyzing software for the amount of fractured contacts in the surface. An SEM image of 2000 x magnification was taken for the analysis. Each broken sintering contact was marked up by the user and the program plotted the percentage of fractured surface in relation to the whole analysed 2D surface. In tab. 11 the results of the fracture surface measurement on Pixcal were summarised. It can be seen very well that with increasing amount of Ni the percentage of broken sintering contacts in the entire fracture surface is increasing, too, which could be observed very well in fig. 3.33. By the addition of 1 wt% Ni and 5 wt% Ni the Mo particles sintered almost completely together and barely any pores and channels in-between the particles remained. For Mo specimen containing 5 wt% Ni the measured fracture surface was 89 % which means that only 11 % of the fracture surface remained as pores.

**tab. 11.: Quantitative fractography by Pixcal**

Mo + [x] wt% Ni	Broken neck area of surface [%]
0	32 ± 2
0,1	42 ± 4
0,5	65 ± 1
1	79 ± 3
5	89 ± 2

### 3.1.5.2 Molybdenum with different amounts of Ni introduced in aqueous solution

In another experiment it was tried to dope molybdenum with nickel by adding  $\text{NiNO}_3$  dissolved in water. A better distribution of nickel in molybdenum was expected in a liquid phase.

A specified amount of  $\text{NiNO}_3$  was dissolved in distilled water. Four liquids with different amounts of  $\text{NiNO}_3$  were prepared. The following liquids contained 0,1 wt%, 0,5 wt%, 1 wt% and 5 wt% nickel (relating to the Mo amount). To each of the liquids, molybdenum powder from Chemie Metall was added and stirred for about 15 minutes. The wet powder was dried in a drying chamber at  $100^\circ\text{C}$ . The dry powder agglomerated during the drying process. Therefore the powder was deagglomerated with some steel milling balls (8 mm diameter) in a tumbling mixer for 1 h. The obtained powder was very hygroscopic therefore it was not possible to leave the powder packed until pressing some days later. The powder was therefore pressed on the same day with 200 MPa to samples with rectangular geometry (55x10x7 mm). The sintering process was carried out in the silicon-rod heated furnace. The samples were heated up with 10 K/min to  $1300^\circ\text{C}$  with a soaking period of 120 min in  $\text{H}_2$  (5.0 purity and 2 l/min gas flow). The specimens have been slowly heated up in the furnace from RT to the sintering temperature to avoid cracks. During the sintering process, however, the samples were destroyed by many cracks (fig. 3.34). A possible reason for the destruction might be the  $\text{NO}_x$  production or, as another explanation, drying cracks (because of the very hygroscopic powder) during the heating.



fig. 3.34.: Macroscopic view of sintered specimens. During sintering cracks occurred which destroyed the samples

This experiment showed that on one hand the addition of Ni as  $\text{NiNO}_3$  might result in a homogeneously distributed additive but on the other hand the preparation of such powder is a time-consuming activity. Furthermore the powder has to be dried very carefully to avoid drying cracks during sintering. Even then, cracks can occur during sintering as has been shown. Due to the fact that the prepared powder is very hygroscopic, humidity cannot be avoided (except doing the entire processing in a glove box, which is impractical) as well as the  $\text{NO}_x$  formation, which are the possible reasons for the described destruction of the material.

### 3.1.5.2.1 Summary: Mo samples with Ni as sintering activator

In the first experiments the influence of sintering temperature on the sintering activator was determined. Molybdenum specimens with 0.1 wt% Ni were sintered at 1000 / 1100 / 1200 and 1300 °C for 2 h soaking period in hydrogen (5.0 purity and 2 l/min flow rate). With increasing sintering temperature the density and hardness (HV10) of the material could be slightly increased. The open porosity decreased from 47.5 % (1000 °C) to 28 % (1300 °C) for Mo specimens with 0.1 wt% Ni. A reference Mo sample without Ni was sintered, too. The open porosity of this specimen was 37 % after sintering at 1300 °C.

It could thus be shown that the amount of a sintering activator does change the physical and mechanical properties of the material. By increasing the amount of Ni in Mo with unchanged sintering temperature it was possible to set the percentage of open porosity. On the other hand it could be shown that also the open porosity can be adjusted by increasing the sintering temperature while doping just a small amount of sintering activator (0.1 wt%), although this content seems to be rather low for a pronounced activating effect.

Therefore, the influence of the amount of Ni as sintering activator was determined. Molybdenum from Chemie Metall was mixed with different amounts – 0,1 wt%, 0,5 wt%, 1 wt% and 5 wt% - Carbonyl nickel. After blending for 2 h in a tumbling mixer the powders were pressed to rectangular Charpy bars. Sintering was carried out at 1300 °C in hydrogen (5.0 purity and 2 l/min gasflow) at a soaking period of 120 min.

Physical and mechanical properties are listed in tab. 9 and tab. 10. With increasing content of sintering activator the density and hardness (HV10) of the material increased while the total and open porosity and, somewhat surprisingly, the electrical conductivity were decreasing. A plain Mo specimen with 7,4 g/cm<sup>3</sup> density and ~ 31 % open porosity showed a conductivity of ~ 8,15  $\mu\Omega^{-1}\cdot m^{-1}$ . By the addition of 5 wt% Ni the density increased to ~ 9 g/cm<sup>3</sup>, the open porosity decreased to < 1% and also the electrical conductivity decreased to 5,4  $\mu\Omega^{-1}\cdot m^{-1}$  which was contrary to the expectations. With increasing Ni content, the density increased which means that also the amount and size of sintering bridges increased. These effects should also increase the conductivity. There is just a very small solubility of Ni in Mo of about 2 % at 1362 °C. A small amount of Ni can be dissolved in Mo already at 1300 °C forming solid solution, and also an intermetallic phase on the Mo grains can be formed, which apparently lowered the conductivity of the material.

The hardness could be increased from 61 HV10 measured at plain Mo samples to 271 HV10 at Mo specimens doped with 5 wt% Ni. The impact energy increased from 0.46 J (plain Mo) to 0.75 J (Mo + 5 wt% Ni). The bending strength was increasing too with increasing Ni content, which could be shown in fig. 3.30 and tab. 10.

The influence of the sintering activator could be observed very well in the LOM images in fig. 3.32. Metallographic cross sections are shown for each Mo + x wt% Ni specimen after preparation. Molybdenum sample without Ni and with 0.1 wt% Ni showed barely any difference in the structure. By the addition of 0.5 wt% Ni the pores decreased. Between specimens with 1 wt% Ni and 5 wt% Ni a significant difference could be shown, esp. less and smaller pores. In the fracture surfaces the sintering progress could be described. A green Mo body, plain Mo specimen and Mo with different wt% Ni were demonstrated in fig. 3.33. The increase of the number of sintering contacts and their thickness with increasing amount of sintering activator could be observed very well. Mo specimens doped with 1 wt% and 5 wt% Ni showed only a very small amount of pores in-between the particles. Their sintering contacts were virtually as large as the grains



itself. Furthermore, by using Pixcal, a software for quantitative fractography through manual plotting of the sintering contacts, it could be seen again that the amount and size of the sintering contacts grew with increasing amount of Ni in Mo. About 90 % of the fracture surface consisted of sintering contacts after addition of 5 wt% Ni as sintering activator. The remaining 10 % are pores.

In a further experiment it was tried to dope molybdenum with  $\text{NiNO}_3$  dissolved in water instead of adding Ni powder. A better distribution of nickel in molybdenum was expected through adding it in a liquid phase. The following liquids contained 0.1 wt%, 0.5 wt%, 1 wt% and 5 wt% nickel (relative to Mo). The preparation was a time-consuming activity resulting in destruction of the material. The prepared powder was hygroscopic and after sintering cracks occurred, which makes this method impractical.

### **3.1.5.3 Porous layered samples with different amounts of Ni**

Specimens containing two layers with different Ni content in each layer were prepared. One layer was doped with 0.1 wt% Ni while the second was not doped. For the beginning only a small amount on sintering activator was chosen, to avoid a strong shrinkage of one of the layers (of the doped layer with a high amount of sintering activator) which could destroy the specimen. The powder was poured into a cylindrical die of 20 mm diameter starting with the pure Mo powder. After a layer of about 10 mm had been filled, a second layer doped with 0.1 wt% Ni followed. Afterwards the specimens were pressed with 200 MPa uniaxially and sintered at 1300°C for 2 h soaking period in  $\text{H}_2$ . For comparison, further two layered samples without a Ni containing layer were prepared and sintered also at 1300 °C but for a longer soaking period of 180 min. The effect of sintering activator addition should be demonstrated in comparison to undoped specimens. In comparison to experiments carried out with multilayer samples, by preparing samples out of only two layers a higher total content of Ni is guaranteed in the sample, and the differences between doped and undoped materials could be expected to stand out more clearly since the nickel doped layer is taller and wider than in case of multilayered specimens. Furthermore a better visualization of the transition zone was expected. The layout of the two-layer samples is schematically depicted in fig. 3.35. The pressed samples had the geometry of a cylinder with 20 mm diameter and about 15 mm height. Different powder fractions have been chosen, primarily to increase the open porosity by using coarser fractions. As has been already discussed, also in fractions which were designated as  $> 63 \mu\text{m}$  barely any coarse particles can be found. Due to the fact, that no coarser powders were available at this time, experiments with the commercial Mo (from CM), which was sieved into fractions, were carried out.

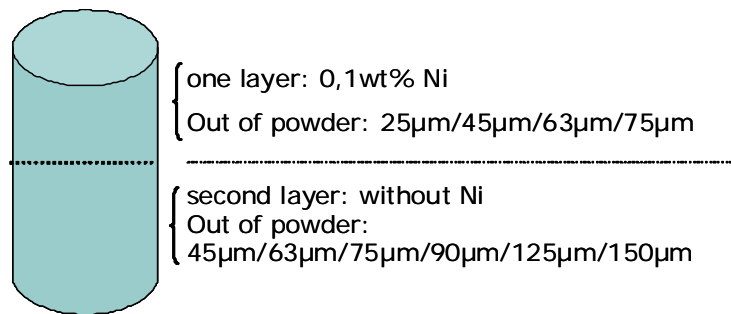


**fig. 3.35.: Structure of the two layer sample; one layer is containing 0,1 wt% Ni, the second layer is without Ni; both layers have been prepared from different Mo powder fractions**

An overview of the composition of the layers in one sample is given in tab. 12. The composition of the first sample will be discussed as an example. The first layer of sample has been made of powder  $\leq 25 \mu\text{m}$  and is doped with 0,1 wt% nickel. The second layer was prepared from powder  $\leq 45 \mu\text{m}$  and does not contain any nickel. In total, 12 samples have been prepared.

**tab. 12.: Overview of powder fractions used for the layers. One layer is Mo + 0,1 wt% Ni - combined with a second layer without Ni**

Mo [ $\mu\text{m}$ ] + 0,1 wt% Ni layer	layer without Ni			
<25	<45	<63	<75	<150
<45	<63	<75	<90	
<63	<75	<90	<125	<150
<75	<90			

After sintering, the density, porosity and hardness were measured in each layer, and the results are listed in tab. 14. The green densities are listed in the table in tab. 13. The green densities for specimens without Ni sintered for 120 min were lower by about  $0,4 \text{ g/cm}^3$  than the sintered ones. The increase in sintered density (compared to the green one) for specimens sintered with Ni for 120 min and without Ni sintered for 180 min was about  $1 \text{ g/cm}^3$ . It can be observed that the lowest densities are shown by specimens without Ni doping and sintered at  $1300^\circ\text{C}$  for 180 min soaking period. The density is about  $6 \text{ g/cm}^3$ . These samples show also the highest open porosity of  $\sim 40\%$  and lowest hardness HV 10 of  $\sim 32$ . Molybdenum specimens that contained one layer with 0,1 wt% Ni and were sintered for 120 min at  $1300^\circ\text{C}$  show very similar values for density, porosity and hardness as the Mo specimens without Ni sintered at  $1300^\circ\text{C}$  but for 180 min. It can be said that the addition of 0,1 wt% Ni results in the same physical properties than for the Mo specimens without any sintering activator but sintered for a longer time. Comparing the two layered specimens it can be seen that the values for density, open porosity and hardness do not differ from each other. There is barely a difference in density, open porosity and HV 10 between, for example, 45/25\* and 63/25\* (both containing Ni). It was expected that the open porosity is higher for specimens from a fine grained layer (for example  $25 \mu\text{m}$ ) and a layer from coarse powder of  $150 \mu\text{m}$  size (due to coarser particles of the  $150 \mu\text{m}$  particle layer resulting in bigger open porosity). Entirely it can be said, that no difference could be found which

was suspected because of the low amount of coarse particles in each fraction. Observing the values for the hardness (HV 10; tab. 14) for the layer "120 min (+Ni)" with those for "180 min (-Ni)" it can be seen that the values are very similar. The addition of 0,1 wt% Ni to Mo resulted in the same effect as sintering for a longer time without a sintering activator. Furthermore, the values for the hardness are quite low, which can not be explained. They are similar to the ones which were already discussed in tab. 8, The densities are comparable to the ones demonstrated in tab. 8.

**tab. 13.: Green densities of two-layer samples in which one layer contains 0,1 wt% Ni; "\*" is marking the Ni containing layer**

Layer	green density g*cm <sup>-3</sup>		
	120min (-Ni)	120min (+Ni)	180min (-Ni)
63/45*	5,53	5,95	6,08
45/25*	5,72	5,96	6,15
75/45*	5,65	6,01	6,15
90/75*	5,56	6,02	6,08
90/45*	5,52	5,94	6,08
63/25*	5,64	6,00	6,09
75/25*	5,67	5,98	6,10
90/63*	5,54	6,03	6,06
125/63*	5,51	5,88	6,02
150/63*	5,56	5,89	6,03
75/63*	5,48	6,01	6,06
150/25*	5,61	6,00	6,03

**tab. 14.: Open porosity, HV 10 and density of two-layer samples in which one layer contains 0,1 wt% Ni; "\*" is marking the Ni containing layer; all specimens were sintered at 1300 °C**

Layer	density g*cm <sup>-3</sup>			calc. open Porosity/%			hardness HV=10		
	120min (-Ni)	120min (+Ni)	180min (-Ni)	120min (-Ni)	120min (+Ni)	180min (-Ni)	120min (-Ni)	120min (+Ni)	180min (-Ni)
63/45*	5,96	6,91	7,07	40,9	29,7	29,9	32	58	66
45/25*	6,11	6,95	7,24	39,6	31,9	28,5	33	65	63
75/45*	6,03	6,93	7,18	40,1	29,7	28,8	32	63	60
90/75*	6,01	6,92	7,09	40,2	29,8	30,1	32	64	60
90/45*	5,96	6,90	7,11	41,2	30,6	29,8	31	65	63
63/25*	6,09	6,91	7,14	40,0	30,3	29,4	31	72	61
75/25*	6,01	6,93	7,15	40,7	31,1	29,1	30	64	59
90/63*	5,93	7,02	7,02	41,8	30,5	30,9	30	60	62
125/63*	5,93	6,85	7,01	41,3	31,2	30,7	31	60	58
150/63*	5,94	6,84	7,06	41,8	31,4	29,8	31	60	58
75/63*	5,93	6,94	7,03	41,8	30,7	30,7	32	61	57
150/25*	6,00	6,94	7,16	41,3	31,1	29,1	32	70	63

### **SEM images**

After sintering, cracks occurred between the layers. These cracks occurred only in samples where one layer was doped with nickel. This crack could be observed only in samples where the difference in particle size distribution between the layers is high, for example in 150/25\* sample (tab. 14, fig. 3.36) where one layer is from powder  $\leq 25\mu\text{m}$  + 0,1 wt%Ni and the other of  $\leq 150\mu\text{m}$  without a sintering activator. Furthermore these cracks occurred in the center of the sample, near the axis, not near the surface. It seems that the two layers did not sinter together in some areas in the transition zone. Another possibility is that the two layers started to sinter (and shrink) at different times, which could also cause these cracks.

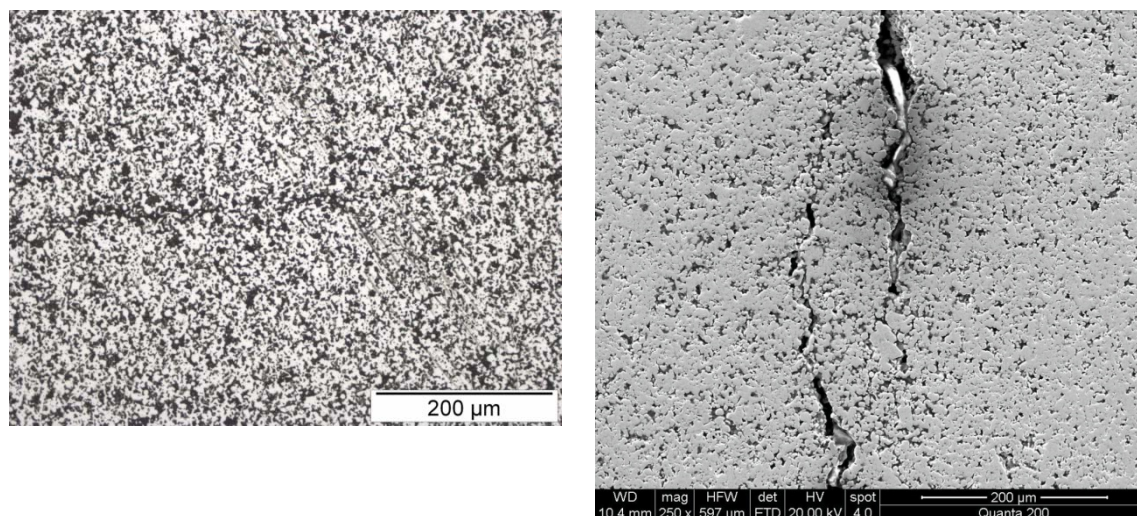


fig. 3.36.: Left: light microscope image from sample 150/25\* (1300°C-120min (+Ni)) – 200x; right: SEM image from the same sample – 250x

### 3.1.5.4 Two-layer samples with high amount of sintering activator

To examine the influence of the sintering activator content on the layer cohesion, two-layer samples with higher amount of nickel than before were manufactured. Two variants of two-layer samples were prepared. The first ones contain one layer with 5 wt% Ni and the others contain only 0,1 wt% Ni as sintering activator. The second layer was in both cases a pure Mo layer. These two species of samples were compared.

The way how the two layers were compacted together can be seen in tab. 15. Three samples were built containing a  $\leq 45\mu\text{m}$  (+0,1 wt% Ni) layer. This layer was combined with  $\leq 90\mu\text{m}$ , in the next sample with  $\leq 125\mu\text{m}$  and in the last sample with  $\leq 150\mu\text{m}$  layer without Ni. Samples with the same constitution of layers were pressed again differing in  $\leq 45\mu\text{m}$  layer which was doped with 5 wt% Ni.

The last 6 samples were pressed the same way but instead of  $\leq 45\mu\text{m}$  layer a  $\leq 63\mu\text{m}$  layer was used. All of the 12 samples were pressed with 200 MPa. These samples were sintered at 1300°C in hydrogen (5.0 purity and 2 l/min flow rate) with 180 min soaking period.

tab. 15.: Overview of layer composition; One layer is Mo + 5 wt% Ni - combined with a second layer without Ni, prepared from different fractions

Mo [ $\mu\text{m}$ ] + 5 wt% Ni layer	layer without Ni		
<45	<90	<125	<150
<63	<90	<125	<150

The results for the density, measured (He pycnometry) open porosity and the hardness HV10 are summarized in tab. 16. As has been expected, with higher amount of sintering activator the density is increased. Resulting from a higher density the open porosity is



lower. Hardness was differing depending in which layer the measurement was carried out. In the layer of the sample containing 0,1 wt% Ni only  $\frac{1}{4}$  of the hardness was measured in comparison to the layer containing 5 wt% Ni. The hardness in the Ni - free layer was just a little bit lower than the hardness measured in the 0,1 wt% Ni layer.

**tab. 16.: Density, open porosity and hardness for two-layer samples**

Sample name	density g/cm <sup>3</sup>		Open porosity (pycnom.)/%		hardness HV10		
	1300°C-180+ 0,1 wt%Ni	1300°C-180+5 wt%Ni	1300°C-180+ 0,1wt%Ni	1300°C-180+ 5wt%Ni	1300°C-180+ 0,1wt%Ni	1300°C-180 +5 wt%Ni	
						layer (-5wt%)	layer (+5wt%)
90-45	6,73	7,87	33	20	51	57	222
125-45	6,65	8,04	34	18	49	53	208
150-45	6,58	7,86	35	20	46	58	216
90-63	6,72	7,72	34	20	52	57	204
125-63	6,72	7,48	33	24	50	57	215
150-63	6,68	7,91	34	18	49	55	232

The data of tab. 16 for porosity are graphically shown in fig. 3.37

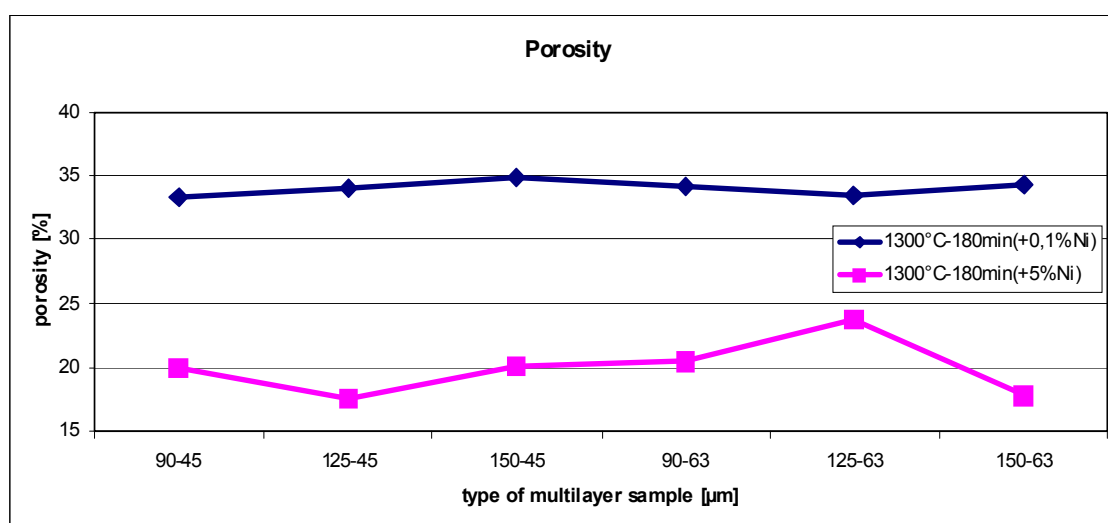


**fig. 3.37.: Values from tab. 16 are demonstrating the difference in porosity as a function of sintering activator content**

Hardness data from tab. 16 are shown in fig. 3.38. A large difference in hardness between the two layers in the sample containing 5 wt% Ni can be seen.

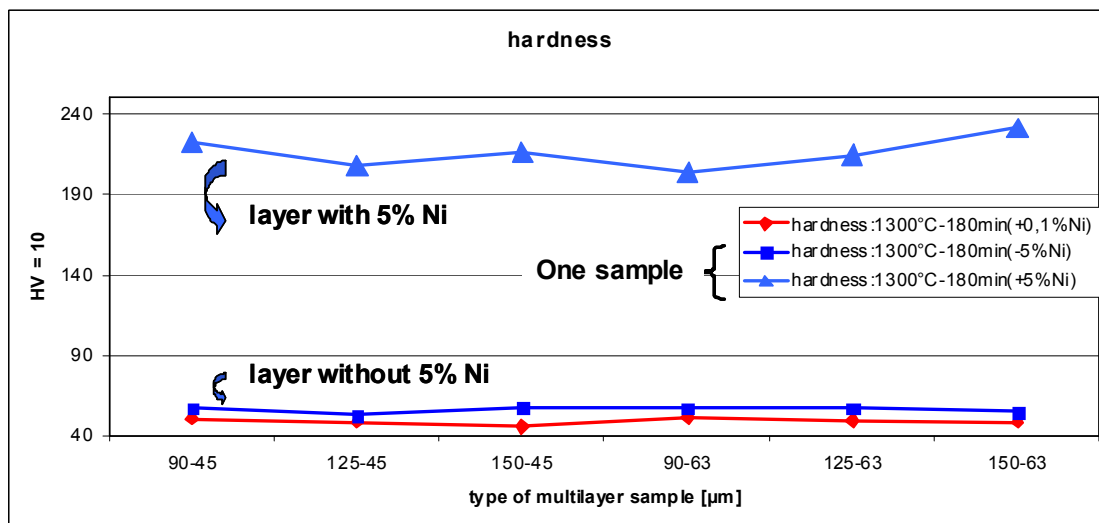


fig. 3.38.: Hardness of samples with different sintering activator content

This large difference in hardness of the two layers in the sample containing 5 wt% Ni results from the higher density of the doped layer. The sintering activator in this layer causes a higher density resulting in higher hardness. Furthermore a big crack in the transition zone occurred. This crack started from the surface and was crossing half of the sample. The reason was the large difference in shrinkage between the layers and the resulting stresses in the transition area. It was possible to see the difference in shrinkage without a microscope. Also the crack was visible.

### 3.1.5.5 Summary

Molybdenum two layer samples were prepared. One layer was doped with 0,1 wt% Ni and the second layer consisted of pure Mo. Furthermore both layers were prepared from different Mo powder fractions. For comparison, specimens with the same composition were prepared but without doping with Ni. All specimens were pressed uniaxially with 200 MPa in a cylindrical 20 mm die. Sintering was carried out at 1300 °C for 120 min soaking period. In a third experiment undoped two-layer samples were sintered for 180 instead of 120 min. It could be observed that the resulting density, open porosity and HV 10 did not vary in-between the different two layer samples. It made no difference which layers were combined together. A difference was recognised between specimens doped with 0,1 wt% Ni, the undoped ones and the specimens which were sintered with a soaking period of 180 min. The densities of all specimens where no layer was doped with Ni were in the range of 6 g/cm<sup>3</sup> (tab. 14). The open porosity was about 40 % and 30 HV 10. Molybdenum specimens which were doped with 0,1 wt% Ni and the ones that were not doped but sintered for 180 min showed very similar values for density, porosity and hardness. In both cases the density was ~ 7 g/cm<sup>3</sup>, the open porosity ~ 30 % and the hardness ~ 60-65 HV 10 (tab. 14). Considering the results it can be summarized that by doping Mo with 0,1 wt% Ni the sintering time could be shortened from 180 min to 120 min. This means, that the addition of a sintering activator shortens

the soaking period by 30 %. Comparing the green with the sintered densities it could be observed that specimens without Ni sintered for 120 min increased their density after sintering only by 0,4 g/cm<sup>3</sup>. The ones containing Ni and sintered also for 120 min and the ones without Ni but sintered for 180 min increased their densities by 1 g/cm<sup>3</sup>.

By the observation on LOM (fig. 3.36) of the cross sections of the specimens, cracks were found between the layers with a big difference in particle size between the layers. It seems that the two layers did not sinter together in some areas in the transition zone. Another possibility is that the two layers started to sinter (and shrink) at different time, which could also cause these cracks.

Also some experiments with a higher amount of sintering activator were carried out. Again Mo specimens out of two layers were prepared in which one layer contained 5 wt% Ni. All layers were built up out of different particle fractions (tab. 15). It could be observed that by the addition of such high amount of sintering activator the density was increased significantly to a value of 7,8 g/cm<sup>3</sup>. The open porosity decreased to 20 % and the hardness was increased to 210 HV 10 measured in the Mo + 5 wt% Ni layer. Molybdenum specimens doped with 0,1 wt% Ni had a density of ~ 6,7 g/cm<sup>3</sup>, an open porosity of ~ 33% and 50 HV10. Due to the addition of Ni to Mo, the sintering activity increased and the density increased, too, which resulted in a higher shrinkage of the material. Big cracks occurred between the layers and the specimens were deformed due to the different diameter of the Ni - free and 5 wt% Ni layers.

### **3.1.6 Preparation of highly porous molybdenum samples with bigger open pores**

It could be shown that the preparation of porous specimens from molybdenum powder by different pressing and sintering techniques did not result in specimens with a high amount of open porosity which could be infiltrated effectively (homogeneous distribution of Si). Furthermore the addition of a sintering activator could in fact influence the porosity but the pore size remained very small. The amount of total open porosity was quite high (in the range of about 35 %) but the pores themselves were still small.

Further options were tried to prepare specimens with high and defined open porosity. In the following chapter three different techniques have been tried. In the first step, different amounts of a space holder, an organic wax, were added. After pressing the specimens were debinded to remove the wax and leave open porosity.

In another experiment loose powder bed specimens were prepared by gravity sintering. By pouring the molybdenum into a ceramic cup without pressing, most particles form a network of open pores. By sintering afterwards the particles approach each other but still leave considerable pore space open.

In the last experiment a polymer sponge was dipped into a powder-binder mixture. After drying the sponge was burnt out, i.e. thermally decomposed, leaving a molybdenum matrix which was sintered afterwards forming a Mo network with big pores in between.

### 3.1.6.1 Molybdenum with wax as space holder

The production of samples with defined and gradient porosity can be done by using space holders. It should be possible to introduce these space holders into the green body and to get them out after sintering without any residue. For the following experiments, two types of wax have been used. One type was a “Hoechst wax” (Microwax C, ethylene bisstearamide) and the second one a “Kenolube P11” (EBS + 25% Zn stearate). Both are common pressing lubricants especially in ferrous powder metallurgy. Eight powder fractions with these two types of wax have been prepared. Four powder fractions with different wt% (3/5/7/10) of wax were used. The samples were produced with two layers. One layer was plain molybdenum powder from Chemie Metall ( $<63\mu\text{m}$ ) and the second layer was from the same powder but containing wax. In another experiment, a cylindrical sample was prepared with two layers where both layers contained wax, 7 wt% and 10 wt% wax, respectively. These powders were stepwise filled into a cylindrical die and pressed at 200 MPa on Amsler (hydraulic press). The structure is schematically shown in fig. 3.39.

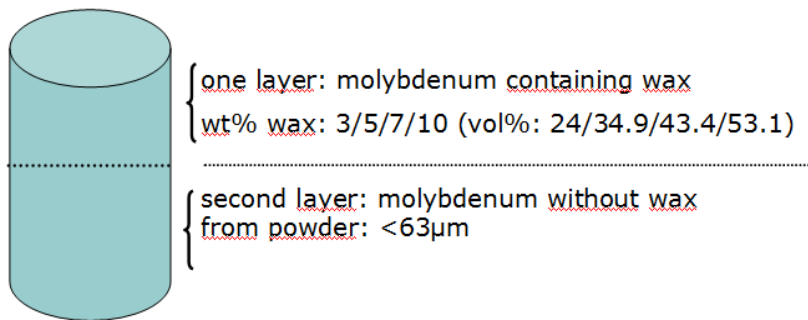


fig. 3.39.: Schematic picture of the two layer samples

The samples were debinded at  $600^{\circ}\text{C}$  in  $\text{N}_2$  with a heating and cooling rate of 1 K/min and a soaking period of 90 min. After debinding the samples were sintered in the AHT silicon-rod heated furnace, for 120 min at  $1300^{\circ}\text{C}$  in  $\text{H}_2$  (5.0 purity and 2 l/min gas flow).

Those samples where one layer contained Höchst wax were destroyed by cracks after sintering (fig. 3.40). Furthermore, the wax showed inhomogeneous distribution in the molybdenum matrix. In some areas big pores remained after debinding.



fig. 3.40.: Specimen Mo + 5 wt % EBS after sintering covered with cracks

The best results in homogeneity and debinding process (no cracks occurred) were obtained with the “Kenolube P11 wax” with low amounts of wax (lower than 7 wt% wax). Samples with one layer containing higher amounts like 7 wt% or 10 wt% wax showed a very coarse surface after debinding, and the two layers split (fig. 3.41 left). The sample built out of two layers which both contained wax (7 wt% wax one layer, second layer 10 wt% wax), was destroyed, too, by cracks after debinding (fig. 3.41 right).

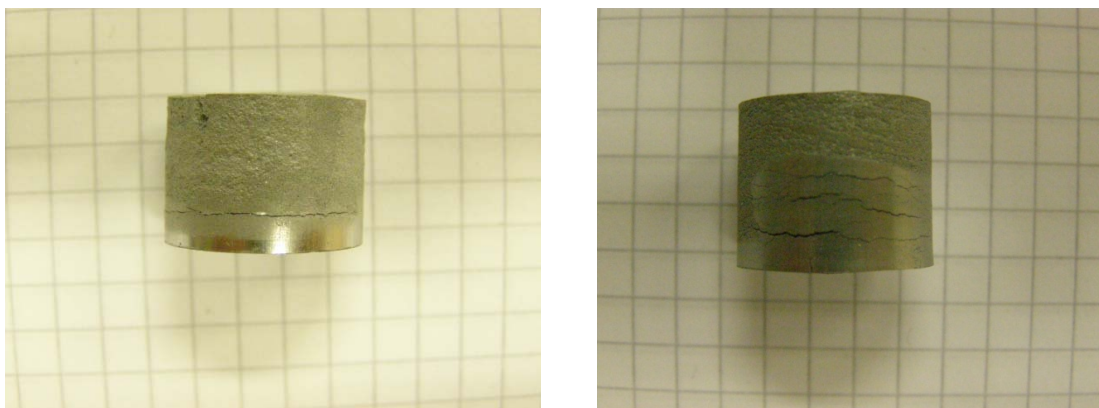


fig. 3.41.: Left: sample containing 7 wt% wax in one layer and no wax in the other; right: sample out of 2 layers where both layers contained wax (7 wt% Kenolube and 10 wt% Kenolube)

Those two layer samples that contained 3 wt% or 5 wt% wax survived and were analysed for the hardness, density and open porosity. The hardness was measured as well in the pure molybdenum layer as in the space holder layer. As expected a lower hardness was measured in the space holder layer. With increasing amount of space holder the open porosity is increasing, too, which is shown in the sample containing 5 wt% wax (tab. 17).

tab. 17.: Density, open porosity and hardness for two-layer samples

Sample	Archimedes density [g/cm <sup>3</sup> ]	open porosity (He-pycn.) [%]	HV 10	
			+ wax	pure Mo
3wt % P11/ pure Mo	7,01	32,96	58 ± 1	61 ± 2
5 wt % P11/ pure Mo	6,53	38,23	42 ± 3	63 ± 1

As expected, the hardness (HV10) is decreasing with increasing amount of open porosity and increasing amount of added space holder. In can be also seen in tab. 17



that the difference in hardness between spaceholder (3 wt% P11) and spaceholder-free specimen is quite low. By addition of a higher amount of space holder (5 wt% P11) the difference in hardness between the layers increased.

### 3.1.6.2 Characterisation of space holder samples after Si treatment by ATL

It has been seen after the characterisation of the space holder specimens that the open porosity is quite high and the hardness is acceptable. Therefore some specimens, prepared with a spaceholder wax Kenoblube P11, have been prepared by debinding and afterwards sintering, and were sent to ATL for CV infiltration. The specimens for ATL were out of one layer with the highest possible amount of space holder (5 wt%). After CVI at ATL the specimens have been sent back to TUW for characterisation.

The samples were pressed from Mo containing 5 wt% wax (as required by the partner) and debinded at 600°C for 2 h in N<sub>2</sub>. After debinding, first cracks occurred. The samples were then sintered at 1300°C in the AHT silicon-rod heated furnace for 2 h in H<sub>2</sub> (5.0 purity; 2 l/min). After chemical vapour infiltration at ATL one sample out of this batch was sent back to TUW for further characterisation. A macroscopic image of the sample after CVI is shown in fig. 3.42. Before cutting the sample, the geometrical and Archimedes density were measured. The open porosity was measured by He – Pycnometry. The geometrical density is 5,88 g/cm<sup>3</sup>. Because of cracks the punch face got a bulging surface, so the dimensions of the sample might not be too reliable. The Archimedes density was measured as 6,189 g/cm<sup>3</sup>. By measuring the density by He - Pycnometry it was possible to calculate the open porosity to be 37.2%. The closed porosity was measured as 0.9%. This sample was cut along the diameter (horizontal). In the cross section some dark elongated areas could be observed. fig. 3.42 shows this described area.

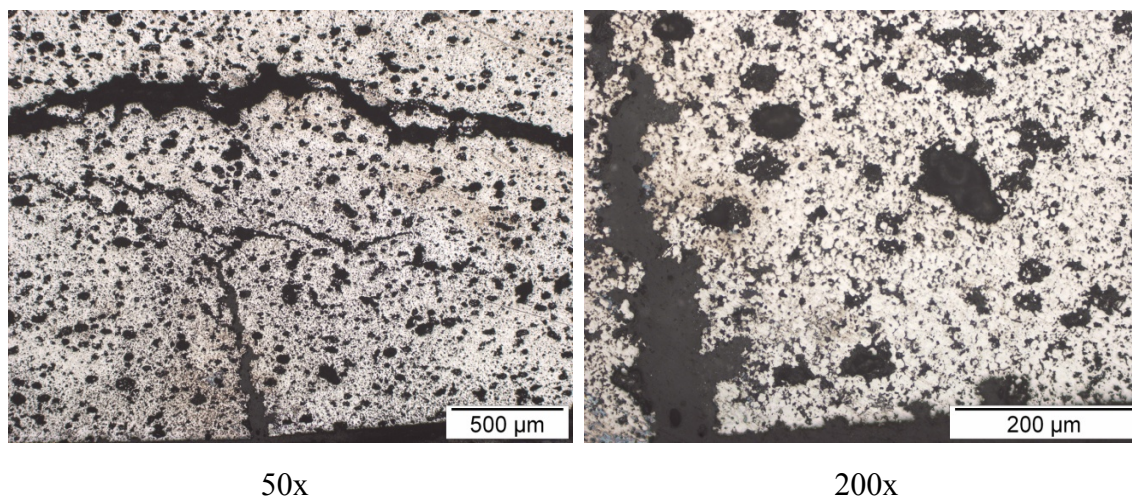


fig. 3.42.: camera picture of the cross section of Mo specimen with 5 wt% space holder sintered

The sample was prepared by polishing the surface and characterised by light microscopy and by SEM.

#### 3.1.6.2.1 Light optical microscopy

In fig. 3.43 the cross section of the Mo sample after CVI (at ATL) is shown. Cracks could be observed over the whole cross section. These occurred during the debinding process due to the very high amount of wax. Here the considerable springback effect due to the high volume fraction of wax combined with its low Young's modulus should be considered.



**fig. 3.43.: Light microscopy images of cross section of Mo (5 wt % Kenolube P11 space holder) sample after CVI**

#### 3.1.6.2.2 SEM

In fig. 3.44 some BSE images of the cross section of the Mo sample (which was prepared with 5 wt% Kenolube P11) after CVI are shown. Cracks can be observed, and some larger pores can be seen, too. They occurred after metallographical preparation of the sample because some grains were broken out during grinding and polishing of the surface. It is possible that during the homogenisation of Kenolube P11 and the Mo, some wax was agglomerated. Using such high amount of organic wax resulted in a "sticky" powder, that adsorbed easily on the inside of the PE container (which was used for homogenisation) influencing and causing some homogenisation problems. The dark grey areas were analysed by EDAX. They occurred on the same places that could be observed before in the camera image (fig. 3.42). It was expected that it might be Si locally introduced by CVI but the EDAX analysis of the elements has shown that there is no difference in the Si content between the light and darker areas. In the darker areas more carbon was found (by EDAX measurement) which could be attributed to problems during debinding and some remaining wax. Also this can be taken as an indicator that too high wax content is detrimental and should be avoided.

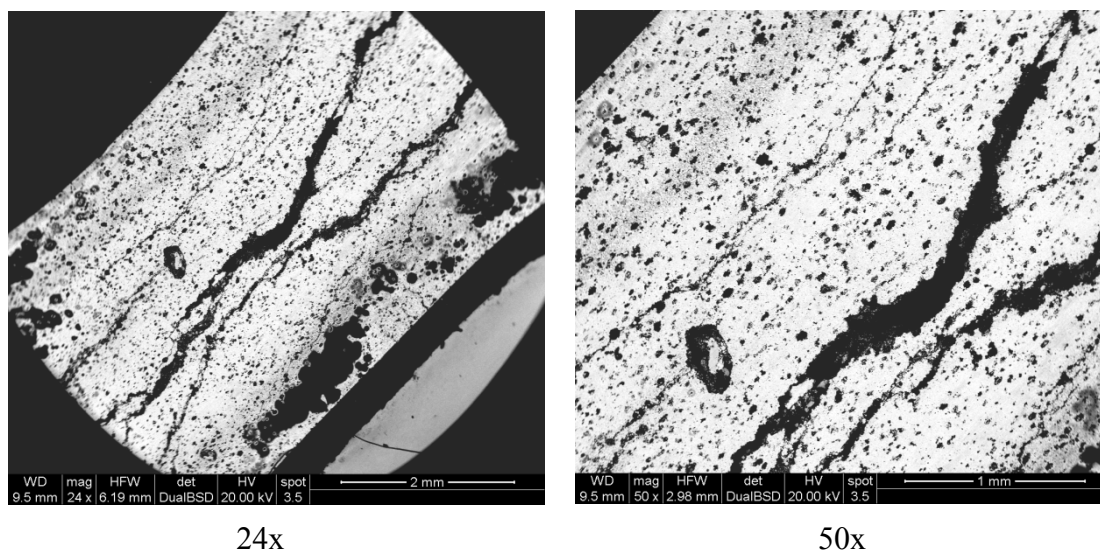


**fig. 3.44.: BSE images of the cross section of Mo sample after CVI of an Mo specimen containing 5 wt % Kenolube P11;**

### 3.1.6.2.3 Elemental mapping

One area of the cross section of the sample was analysed for Si distribution. In fig. 3.45 the area that was taken for the element distribution in EDAX was marked in red. As can be seen there is barely any Si detectable near the surface.

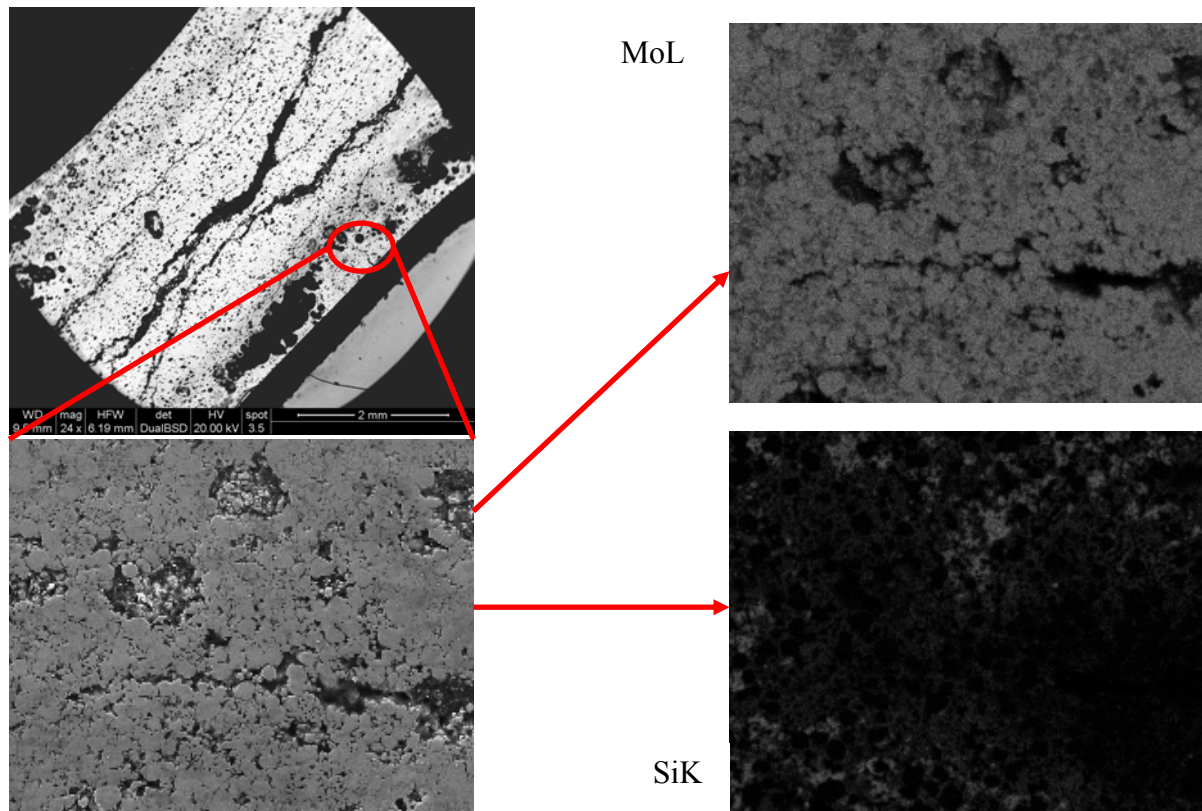


**fig. 3.45.: One area taken out of the EDAX image from Mo specimen which was prepared with 5 wt% Kenolube P11, after CVI at ATL; EDAX mapping with MoL and SiK**



### 3.1.6.2.4 Microhardness

The microhardness was measured in the cross section area of the sample. The hardness was measured with 100 g indentation load along the length and width of the embedded cross section. There is barely a difference in the hardness between the near-surface area and the core of the sample. The hardness decreased from 96 HV0.1 at the surface to 79 HV0.1 in the core. Some darker areas have been observed near the surface at 200x magnification. In this areas the hardness increased to 224 HV0.1. These areas did not contain much Si. These darker areas were located near the surface. Due to some debinding problems some wax remained (measured by EDAX) forming carbides resulting in higher hardness.

The measurement of the hardness along the length of the sample has shown that there are differences in the hardness. All hardness values were measured in one line parallel to the surface (in press direction) line. They differ between 50 and 108 HV0.1. Differences in colour resulted also in different values of hardness. Darker areas showed higher values for the hardness than lighter one.

### 3.1.6.3 Loose powder (gravity) sintering

A further option for preparation of samples with a high degree of open porosity is to sinter a loose powder in a mould ("gravity sintering"). For this experiment the powder was poured into a cylindrical  $\text{Al}_2\text{O}_3$  cup (as a mould). No pressing was carried out, therefore the most pores/space between the particles remained. Two ways of sintering the samples were chosen. In the first experiment the molybdenum powder was doped with nickel as sintering activator. Different amounts of nickel were added (0,1 / 0,5/ 1 wt% nickel). In the second experiment instead of a sintering activator, a space holder was used. For the space holder the wax "Kenolube P11" was used. The cylindrical cups with the powder were sintered in the AHT silicon-rod heated furnace at 1300°C for 120 min in  $\text{H}_2$  (5.0 purity; 2 l/min gas flow). Samples containing the wax had to be debinded before sintering. This was carried out at 600°C with heating and cooling rate of 1 K/min and a soaking period of 90 min in  $\text{N}_2$ .

During the debinding process first cracks occurred in the specimens containing P11. During the sintering the cracks increased, therefore no further work was done on these samples.

Gravity sintered samples with nickel activator were characterized for open porosity and hardness. Samples with 0,1 wt% nickel or less did not sinter in the core. There was no explanation found until now. Therefore it was not possible to measure the hardness. Best values for open porosity and the hardness were measured for the gravity sintered sample with 1 wt% nickel as sintering activator. Results for the open porosity of all samples and hardness HV10 for the 0,5 wt% Ni and 1 wt% Ni containing Mo specimens are listed in tab. 18. A gravity sintered Mo specimen containing 1 wt% Ni had an open porosity of 44 % and a hardness of 45 HV 10 (tab. 18). Comparing this sample with one of the pressed ones (200 MPa) and sintered at the same conditions it can be observed, that – not surprisingly - the open porosity of the loose powder bed sintered specimen is higher. In tab. 9 the open porosity of such pressed and sintered Mo specimen with 1 wt% Ni is given. The open porosity was measured as 3.7 % while the hardness was

about 200 HV10. The hardness was four times higher. The density of the samples was measured, too. Plain Mo specimen without any sintering activator showed the lowest density with  $2,72 \text{ g/cm}^3$ , while the open porosity was very high with 72 %.

A light microscopy image of the gravity sintered Mo-1wt% Ni sample is shown below (fig. 3.46). The sample contains a huge network of open pores. Very coarse and also smaller pores can be observed.

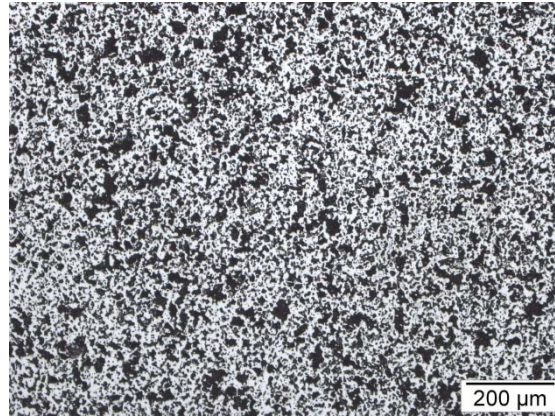


fig. 3.46.: Cross section of a gravity sintered sample Mo-1 wt% Ni. Sintered 2 h  $1300^\circ\text{C}$  in  $\text{H}_2$

tab. 18.: Open porosity and hardness of gravity sintered specimens

Sample wt% Ni	Density - Archimedes [ $\text{g/cm}^3$ ]	Open porosity [%]	HV10
0	2,72	72	-
0,1	3,19	67	-
0,5	4,86	51	$19 \pm 2$
1	5,64	44	$45 \pm 2$

Three of the Mo specimens containing 1 wt% Ni were sent for infiltration experiments to IMSAS. The experiment was carried out in an induction furnace where the specimen was placed in the center of the furnace tube with some Si plates ( $<1 \text{ mm}$ ; fragments of broken Si wafers). The infiltration temperature was reached when all Si plates had melted. During this experiment, all gravity sintered specimens disintegrated completely due to the low stability of the sintering contacts. The disintegrated specimens were not sent to TUW for characterisation.



### 3.1.6.4 Very porous molybdenum sponge preparation

In the following experiment an Mo skeleton with very coarse pores in-between was prepared. For a successful infiltration of the Mo body, very coarse pores are needed and also a stable Mo network.

For this experiment a polymer sponge (fig. 3.47) (Polyurethane sponge) was dipped into a binder/powder mixture. As binder, Methylan (wallpaper glue) was taken. The powder mixture was a molybdenum powder ( $<63\ \mu\text{m}$  from Chemie Metall) with 0.5 wt% nickel (INCO type 123 nickel) in one experiment and 1 wt% nickel in the second experiment. This powder was mixed with the Methylan carefully so that agglomerates could be avoided. Into this binder/powder mixture the polymer sponge was dipped. Before the burnout process, the sponge was dried with a hair dryer for about 30 min. Already in this stage it was difficult to keep the pores open. A toothpick was taken to break through the sticky binder/powder walls during the drying process. This dry sponge was burnt out at  $700^\circ\text{C}$  for 90 min in  $\text{N}_2$  (2 l/min gas flow). That was followed by a sintering process in the AHT silicon-rod heated furnace at  $1300^\circ\text{C}$  for 180 min in  $\text{H}_2$  (5.0 purity; 2 l/min gas flow).

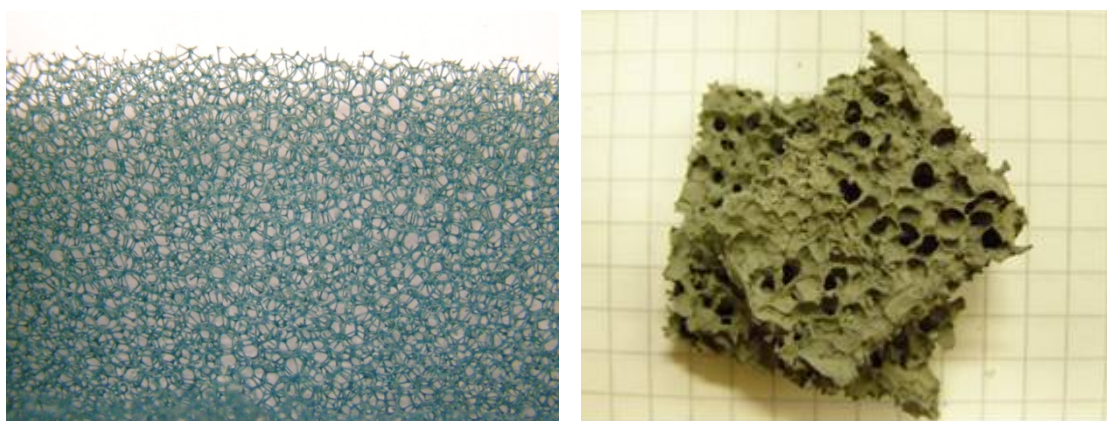


fig. 3.47.: Left: polymer sponge before dipping into the polymer/powder mixture; right: molybdenum structure after sponge burnout and sintering (Mo-1wt% Ni)

After sintering both sponges (with different amounts of nickel) collapsed. There was no mechanical stability of the sponges. Just by slightly touching the surface of the sponge it disintegrated to powder. A possible reason could be the formation of  $\text{Mo}_2\text{C}$  during debinding and sintering. The carbon content was measured as 4% on the Leco CS 230.

### 3.1.6.5 Summary: preparation of high porosity molybdenum samples

Two-layer Molybdenum specimens with wax as space holder in one layer have been prepared (3.1.6.1). By mixing 3 wt% and 5 wt% of Microwax C and, in a further experiment, Kenolube P 11 lubricant with Mo (from Chemie Metall) and pressing with 200 MPa, cylindrical bodies of 20 mm diameter were obtained. After a very slow debinding at 600 °C with a cooling and heating rate of 1 K/ min in N<sub>2</sub>, first cracks occurred in specimen mixed with Microwax C. Specimens mixed with 7 wt% and 10 wt% of wax P11 suffered from cracks, too. The sintering process was carried out at 1300 °C for 120 min in H<sub>2</sub>. For the characterisation only specimens with 3 wt% wax and 5 wt% Kenolube P11 were taken. The density of specimens with 3 wt% wax layer was 7 g/cm<sup>3</sup> and the open porosity was 33 %. With a sample containing a 5 wt% wax layer the density decreased to 6.5 g/cm<sup>3</sup> and the open porosity was increased to 38 %. This specimen was sent to ATL for CVI treatment and received back for characterisation. First cracks were observed (fig. 3.43). EDAX with mapping of Mo(L) and Si(K) have been carried out (fig. 3.44). Hardly any Si could be found near the surface. In the cross section, areas with different colours could be observed. Different HV 10 values were obtained depending on the colour. The dark region showed of 224 HV 10 and the lighter one 50 – 108 HV 10. The hardness was not constant within the cross section. A reason is the different distribution of Si due to cracks passing the specimen which might facilitate Si to pass other ways and react on other places than just at the surface.

In a further experiment loose powder (gravity) sintered specimens were prepared from Mo with 0 / 0,1 / 0,5 / 1 wt% Ni (3.1.6.3). The powder mixture was carefully filled into an Al<sub>2</sub>O<sub>3</sub> cup without pressing and sintered at 1300 °C for 120 min in H<sub>2</sub>. After sintering the density and hardness were measured. The hardness of samples with 0 wt % Ni and 0,1 wt% Ni could not be measured, because the stability of the sintering contacts was very low. The open porosity of a 45 specimen with 0,5 wt% Ni was 51 % while the hardness was very low at 19 HV 10. A specimen containing 1 wt% Ni had an open porosity of 44 % and a hardness of 45 HV 10. Comparing this specimen to one pressed at 200 MPa and sintered at the same conditions it could be observed that the pressed one had much higher densities and the hardness was 223 HV 10 which is more than four times higher than that one of gravity sintered Mo + 1 wt% Ni.

This specimen was sent to IMSAS for Si infiltration. During the infiltration process the specimen however disintegrated due to weak sintering bridges and very large specific surface.

In a further experiment a metal sponge was prepared (3.1.6.4). A polymer sponge was dipped into a powder-binder mixture containing Mo + 0,5 wt% Ni. The sponge was burnt out, and the metal skeleton was sintered at 1300 °C for 120 min soaking period in H<sub>2</sub>. After sintering the specimen was very fragile, apparently due to Mo<sub>2</sub>C formation, and disintegrated when slightly touched.

## 3.2 Molybdenum with Si

In this chapter, different experiments will be introduced which helped to understand the reactivity between molybdenum and silicon. As stated in the introductory chapter, the aim of the work was to prepare molybdenum specimens with gradient open porosity ready for infiltration with silicon. Previous infiltration tests which were carried out on Mo specimens (described in the above chapters) had shown that most of them have been destroyed or deformed due to the strongly exothermic reaction between Mo and Si and the ensuing volume changes. Some experiments have been carried out to obtain some more information about the reactivity of these two components. At the beginning, molybdenum and Si powders were mixed in different ratios and sintered. A silicon wafer was placed on the surface during the sintering. Silicon was added as powder to Mo to lower the reactivity of Mo and Si during subsequent Si infiltration. The idea was to let Mo pre-react with small amounts of Si, to form silicides, which avoid fatal exothermic reaction during the following infiltration with liquid Si. The Si wafer was put on the surface as source for liquid silicon. The sintering temperature was chosen above the eutectic temperature. In further experiments, two-layer specimens have been prepared where one layer was plain Mo and the second one contained Si. In all experiments the sintering conditions have been varied and the resulting material properties were described.

### 3.2.1 Reactivity of molybdenum with different amounts of Si

Samples of molybdenum with varying contents of silicon were pressed and sintered at 1300°C. On one side of the sample a silicon wafer was placed on the top. Both sides were analysed with regard to phase composition. Furthermore it was necessary to analyse how much of Mo and Si react to a  $\text{Mo}_x\text{Si}_y$  composition. The diffusion of Si from the Si wafer into the sample was also of interest.

Next, two-layer samples were prepared and analysed. One layer contained Si in the Mo matrix and the second layer was prepared from plain Mo. The diffusion of Si from the Si containing layer into the plain Mo layer was characterised. Also the diffusion of Si from the wafer into the Mo + Si layer was described.

#### 3.2.1.1 Different wt % Si and Si wafer

Rectangular samples (55 x 10 x 5 mm) from Mo (Chemie Metall) containing different amounts - 0 / 2 / 5 / 10 / 15 / 25 / 37 wt% - of Si (from Ecka) were characterised. The prepared powder mixtures were blended in a tumbling mixer for 3 h. All powders were pressed uniaxially with 150 MPa on Jessernigg & Urban hydraulic press and sintered with a Si wafer on top of the sample at 1300°C for 8 h in  $\text{H}_2$ . The specimens were pressed with a lower compacting pressure of 150 MPa (as stated above, 200 MPa have been taken for compaction of Mo specimens), because at higher pressures the specimens disintegrated during ejection from the die. The springback effect was too high at compacting pressures above 150 MPa. All samples were characterised by XRD on both

sides of the sample (+ / - Si wafer) and by light microscopy. In fig. 3.48 a schematic figure depicts the experimental setup.

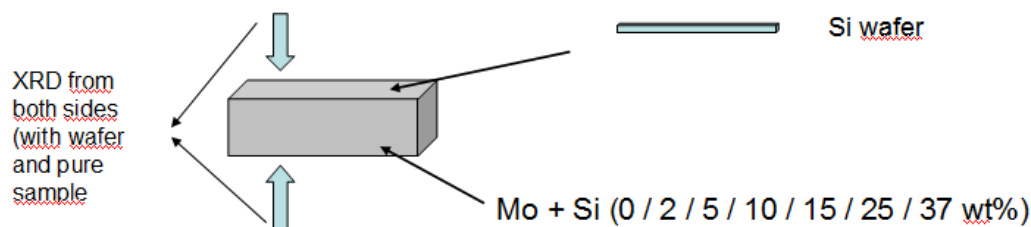


fig. 3.48.: Schematic presentation of the specimen assembly

#### 3.2.1.1.1 XRD

Both sides of the sample were analysed by XRD. The Si wafer peeled off after sintering - not having fully reacted with the substrate - and a dark area remained. Some Si seemed to react with the specimen forming the dark area but still a thin Si wafer remained. The whole surface within this dark area was analysed. In fig. 3.49 the two areas that were characterised by XRD are pointed out.

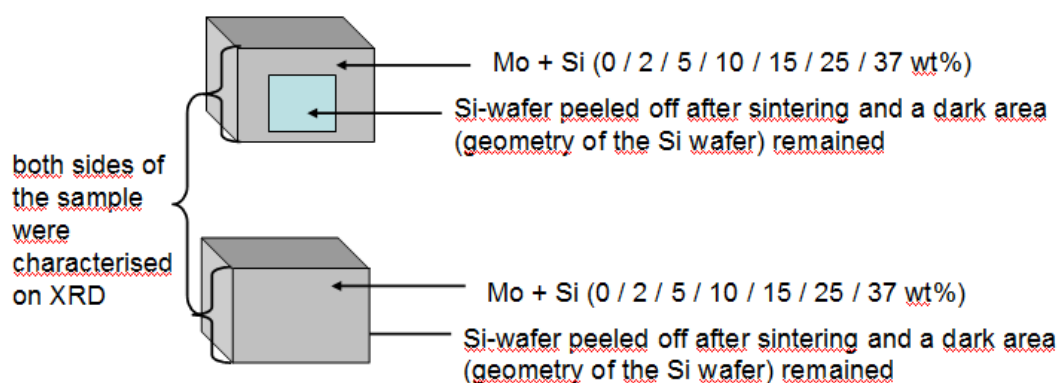


fig. 3.49.: Both sides of the specimen, one side (top image) with Si wafer on the surface; (bottom image) without Si wafer

In fig. 3.50 the XRD patterns of the plain Mo sample, i.e. the reference without admixed Si, is shown. The blue line shows the pure Mo side of sample. The red line characterises that side of sample where the Si wafer had peeled off after sintering.

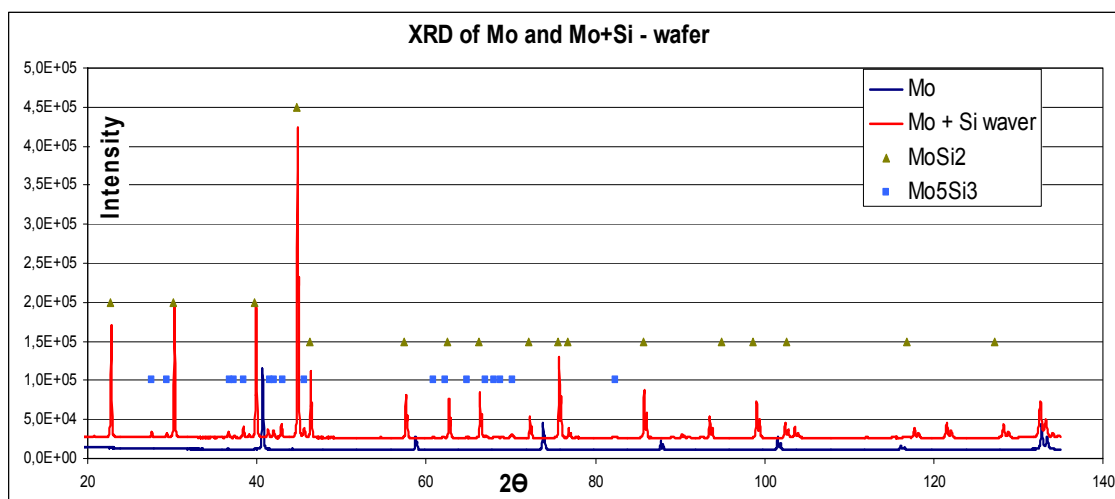


fig. 3.50.: XRD pattern of reference specimen from plain Mo (CM) after sintering at the same conditions as the Mo + x\*wt% Si specimens; on one side the Si wafer was placed - red graph; other side without Si wafer - blue graph

All samples were characterised by their phase composition as summarised in tab. 19. MoSi<sub>2</sub> was detected by XRD after sintering at 1300°C for 8 h in H<sub>2</sub> but only on that side of sample where the Si-wafer was situated. One exception was the sample containing 37 wt% Si (in Mo). About 45% MoSi<sub>2</sub> was measured on the wafer-free side. As can be seen in fig. 3.49 the top of the sample was not fully covered by the Si wafer. The values (on the Si wafer side) given in tab. 19 are average values including the area of the Si wafer and that around the wafer. All reflexes given in the XRD could be well explained and calculated by the Topas software (Rietveld analysis).

tab. 19.: All Mo<sub>x</sub>Si<sub>y</sub> phases detected by XRD after sintering with (+) and without (-) Si wafer on the surface

Si [%] in Mo	0		2		5		10		15		25		37	
wafer	-	+	-	+	-	+	-	+	-	+	-	+	-	+
Mo	97	2,5	31	0,02	36,7	1,2	15,4	7,9	37,9		47,7			
MoSi <sub>2</sub>		86		71		59,9		44,8	0,1	81,9		97,2	45,1	78,7
Mo <sub>5</sub> Si <sub>3</sub>		11		23		38,1	61,9	45,9	58,7	17,7		2,3	54,2	21,3
Mo <sub>3</sub> Si			69	5,6	42,9	0,7	22,7	0,7	3,3	0,4	52,3	0,5	0,7	
MoO <sub>2</sub>					20,4									

### 3.2.1.1.2 Light optical microscopy

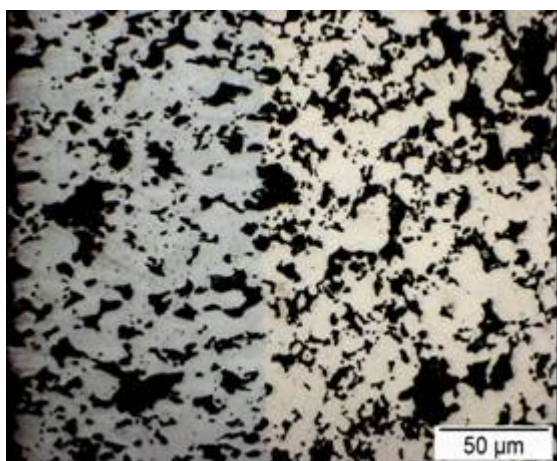
#### *Different wt% Si in Mo – Si wafer side; sintering 8 h at 1300°C in H<sub>2</sub>*

In all samples shown in fig. 3.51 a light blue layer occurs on that side of the sample where the Si wafer was put on before. The blue colour comes from Si which diffused into the sample. It is a Mo-silicide layer which was formed during the infiltration

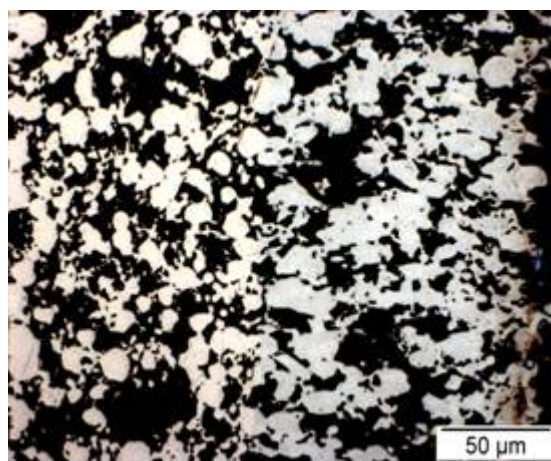


process. In all cases the silicide layer has a thickness of  $\sim 120 \mu\text{m}$ . No Si – layer can be seen in “0 / 10 wt% Si in Mo” sample.

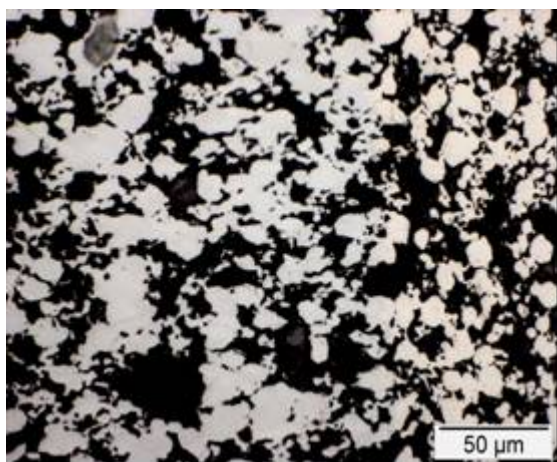
Furthermore, a lot of pores can be observed in the cross section. They come from Kirkendall porosity that emerges through the reaction between Mo and Si during pressureless sintering.



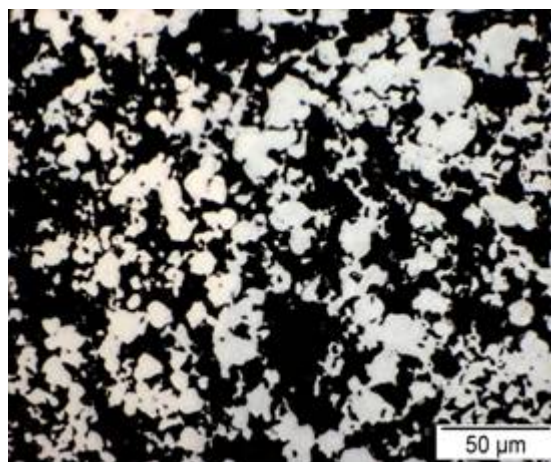
Mo + 2 wt% Si - wafer side - 500x



Mo + 5 wt% Si - wafer side - 500x



Mo + 15 wt% Si - wafer side - 500x



Mo + 25 wt% Si - wafer side - 500x

**fig. 3.51.: LOM images of Mo + x\*wt% Si specimens sintered at 1300 °C for 8 h in H<sub>2</sub>; surface near area; 500x magnification;**

In the centre of the samples no Si can be seen. Already after sintering there was barely cohesion between the Mo and Si particles. The higher the amount of Si in Mo was, the more difficult was the handling of the specimens. Therefore, the green bodies were placed very carefully in the furnace. After sintering the specimens were easier to handle but the first problems occurred during metallographic specimen preparation. During the sample preparation a lot of molybdenum silicides broke out. The centre seems to be more porous and brittle (fig. 3.52). It seemed that Mo did not react completely with Si during sintering, therefore only some parts of the specimen were sintered. During sample preparation a lot of particles broke out. With increasing content of Si, more particles broke out of the cross section during preparation.

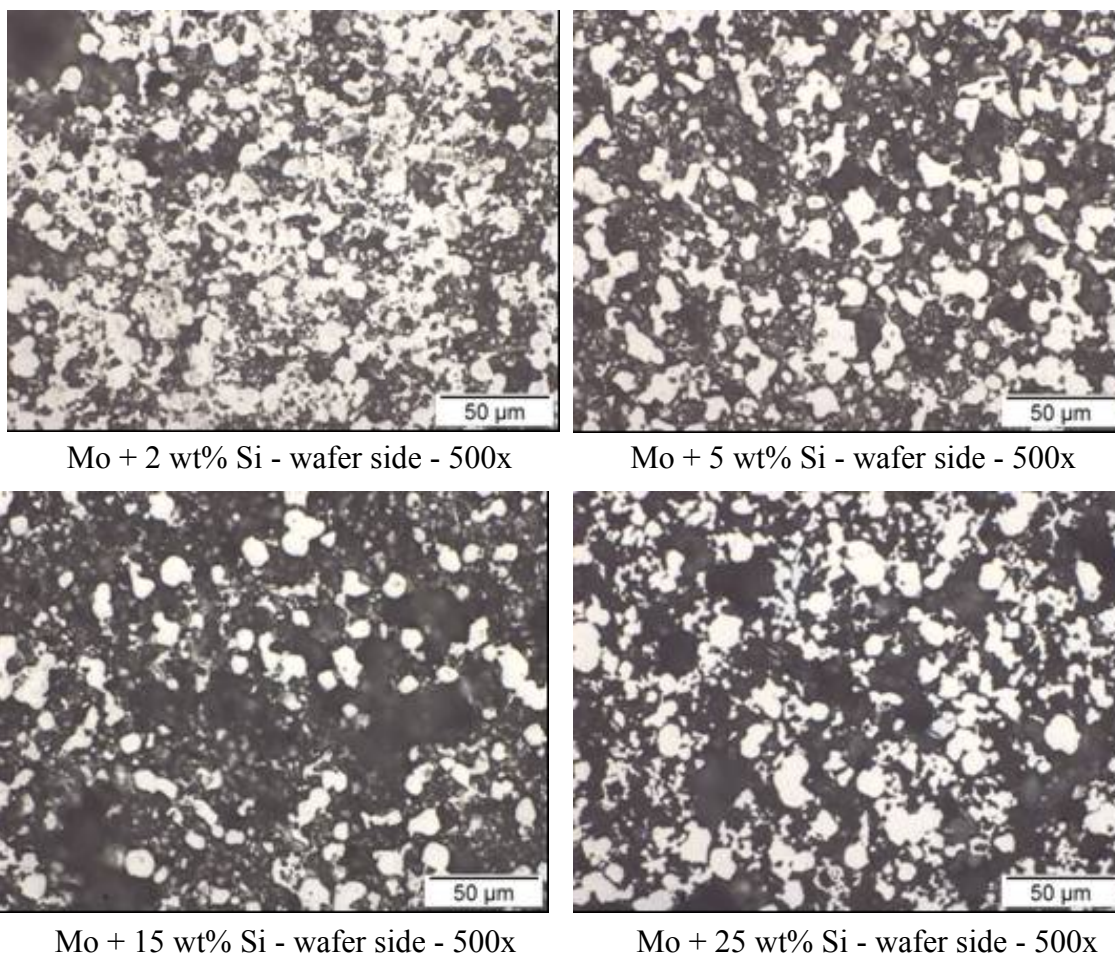
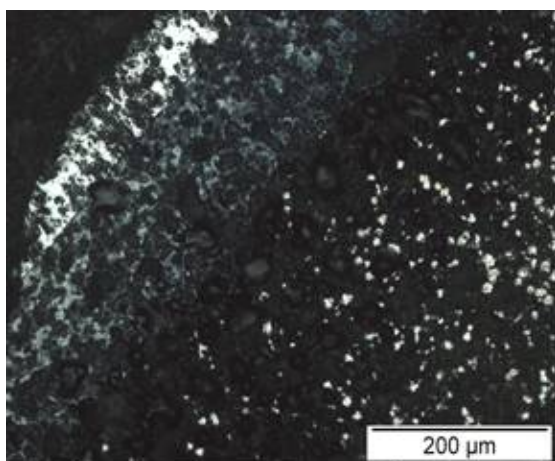


**fig. 3.52.: LOM images of Mo + x\*wt% Si specimens sintered at 1300 °C for 8 h in H<sub>2</sub>; center of the sample; 500x magnification;**

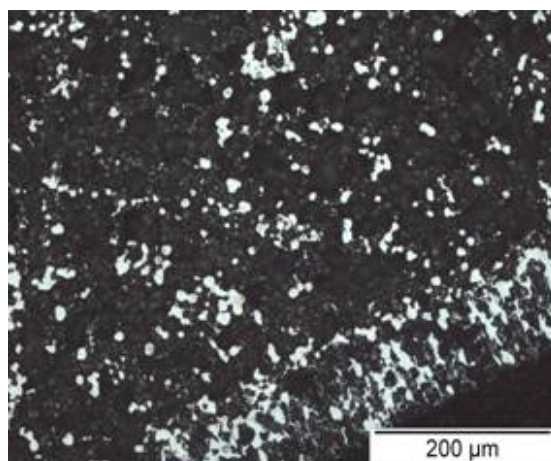
### ***Different wt% Si in Mo – Si wafer side; sintering 2 h at 1300°C in H<sub>2</sub>***

In this following experiment specimens prepared by the same way have been sintered again but for a shorter soaking period of 2 h (instead of 8 h). This step should be a pre sintering step at 1300 °C (below the eutectic temperature of Mo-Si) to take away some reactivity before sintering at the eutectic temperature where the reaction is very exothermic. In a further step the specimens were then sintered a second time at 1420 °C which is above the eutectic temperature (1414°C) of Mo and Si. Samples for this experiment were pressed with 150 MPa and sintered at 1300°C in H<sub>2</sub> but for a shorter time of 2 h instead of 8 h. The samples were analysed in the light microscope (fig. 3.53) if a Si layer can be observed in or near the surface of the sample. After characterisation a second sintering step followed at 1420 °C for 2 h soaking period in vacuum.

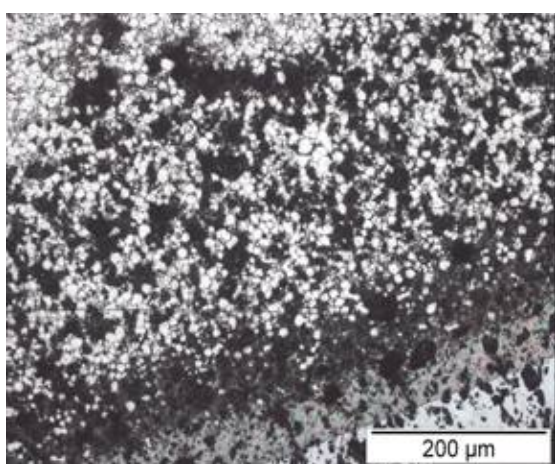




Mo + 2 wt% Si - wafer side - 500x



Mo + 5 wt% Si - wafer side - 500x



Mo + 25 wt% Si - wafer side - 500x

**fig. 3.53.: LOM images of Mo + x\*wt% Si specimens sintered at 1300 °C for 2h in H<sub>2</sub>; surface near area - this side of specimen where Si wafer was placed;**

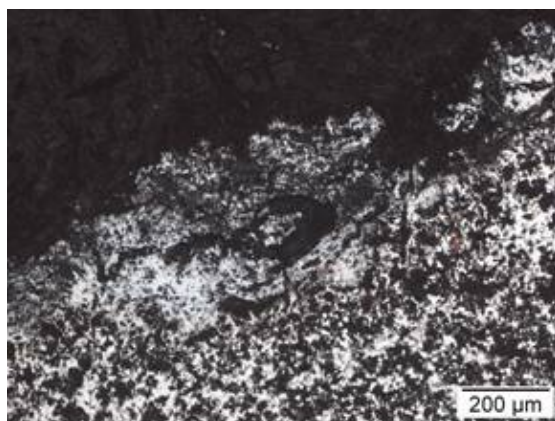
No Si-rich layer can be observed for samples containing „0 / 10 / 15 wt% Si in Mo“. The same samples (one exception is the sample with 15 wt% Si in Mo) did not show any Si layer also after 8 h sintering.

Comparing the light microscopy images of samples sintered at 1300°C for **8 h** in H<sub>2</sub> with samples sintered at 1300°C but only for **2 h** (H<sub>2</sub>), the blue layer showed similar thickness of ~ 120 μm. The only difference is that the samples sintered for a shorter time show less mechanical stability, which indicates that the sintering time (and temperature - less reactivity was observed between the particles) was slightly on the low side. Higher sintering temperatures or re-sintering at higher temperatures might be advantageous. Re-sintering tests were done accordingly, also to study the reactivity of the Si wafer at higher temperatures.

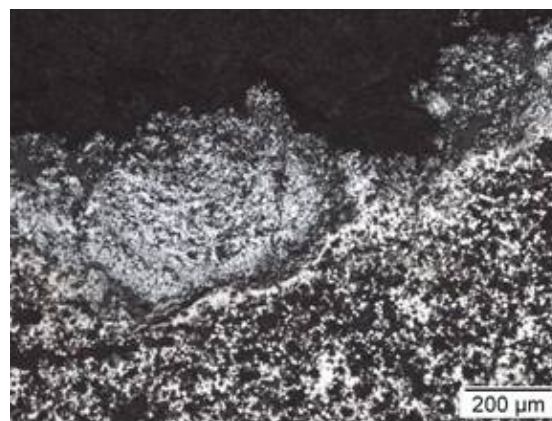
Again, a lot of pores can be observed in the cross section of the specimen. They come from Kirkendall porosity that emerges through the reaction between Mo and Si during pressureless sintering.

***Second step: Re-sintering for 2h at 1420°C in vacuum***

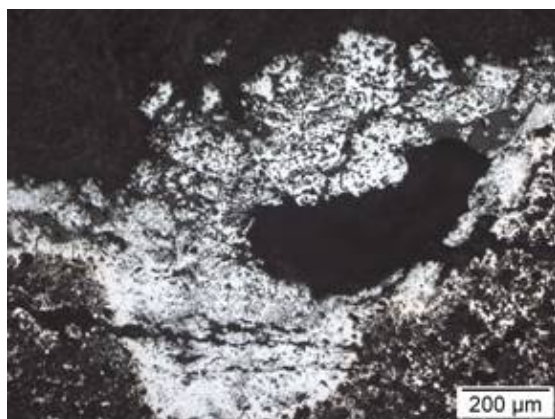
Samples that were sintered before at 1300°C in H<sub>2</sub> for 2 h were re-sintered at a temperature of 1420°C (above the eutectic temperature) for 2 h in vacuum. A Si wafer was put on one side on the top of the sample. After sintering three samples were chosen for characterisation by light microscopy (in fig. 3.54).



Mo + 2 wt% Si - wafer side - 500x



Mo + 5 wt% Si - wafer side - 500x



Mo + 10 wt% Si - wafer side - 500x

**fig. 3.54.: LOM images of Mo + x\*wt% Si specimens sintered at 1300 °C for 2 h in H<sub>2</sub> + sintered again at 1420 °C for 2h in vacuum; surface area magnification, 500x;**

Comparing the light microscopy images of samples sintered at 1300°C for 2 h in H<sub>2</sub> with those resintered 1420°C for 2h in vacuum, a big difference in the stability of the layer could be observed. At sintering temperatures above the eutectic temperature (=1414°C) the Si containing layer was destroyed by uncontrolled exothermic reaction. The Si wafer was lying on the top of the sample but as sort of foam and was mechanically very unstable. By touching this foam the wafer was destroyed. This suggests that the full reaction between Mo and the Si wafer requires temperatures above the Mo-Si eutectic to start, but then the reaction is uncontrollable. Apparently solid state diffusion is too slow to cause significant exothermic effects, only melting can afford this.

### 3.2.1.2 Diffusion of Si in Mo-Si multilayer samples

Two-layer samples of cylindrical geometry with 20 mm diameter were pressed uniaxially with 150 MPa compacting pressure on Amsler hydraulic press. One layer was prepared from plain Mo (from Chemie Metall) and the second layer contained different amounts of Si (0,5 / 1 / 1,5 / 2 wt% Si) in Mo. A Si wafer was situated on the top of the layer containing silicon. In fig. 3.55 a schematic of the two layer samples is depicted.

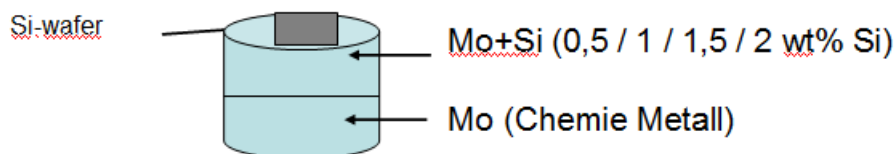


fig. 3.55.: Assembly of the two-layer samples with Si wafer on the top

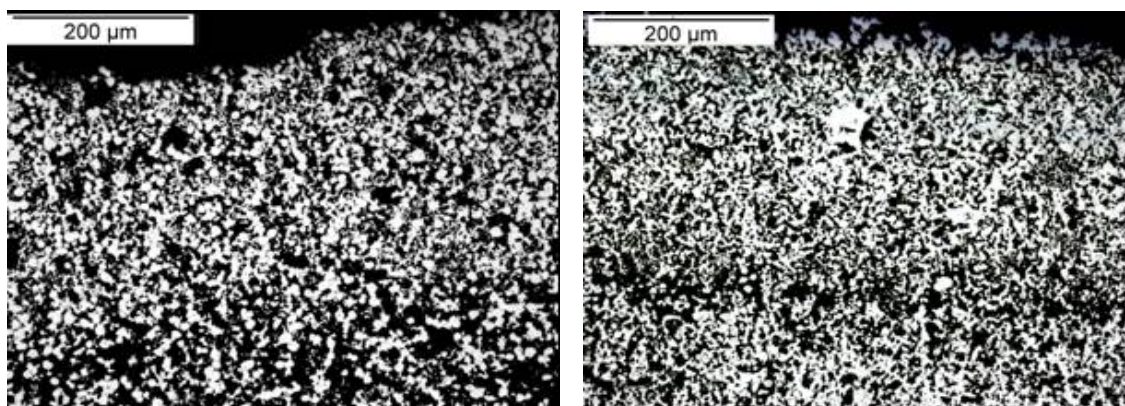
All samples were sintered at 1300°C for 2 h in H<sub>2</sub> and characterised by light microscopy. They were sintered for a second time at 1420°C for 2 h in vacuum and characterised again by light microscopy and SEM-EDX elemental maps.

Some observations after sintering showed that the Mo layer is poorly connected with the Mo+Si (0,5 / 1 / 1,5 / 2 wt% Si) layer. After sintering at 1300°C for 2 h in H<sub>2</sub>, first cracks and separation between the layers occurred. After the second sintering at 1420°C separation of the layers grew until they fell apart when taking the specimen into the hand.

#### 3.2.1.2.1 Light optical microscopy

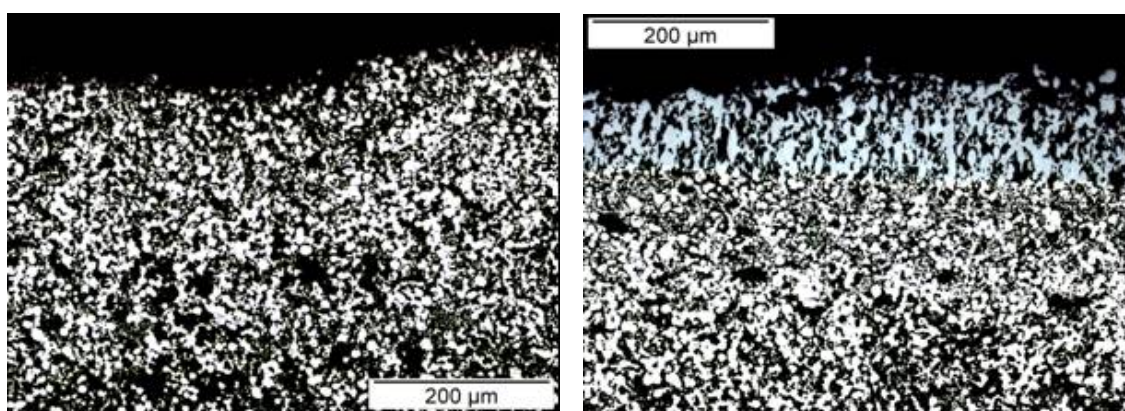
In fig. 3.56 some light microscopy images are shown of Mo-Si specimen with different amounts of Si sintered at 1300 °C for 2h in H<sub>2</sub>. That side of sample is shown where the Si wafer was situated. Only in fig. 3.56 right top and bottom image (Mo with 1 wt% Si and the one with 2 wt% Si) a thin blue layer near the surface can be observed. This blue layer comes from Si from the wafer due to reaction during sintering.





Mo+0,5 wt% Si - 1300°C wafer side - 500x

Mo+ 1 wt% Si - 1300°C wafer side - 500x



Mo+1,5 wt% Si - 1300°C wafer side - 500x

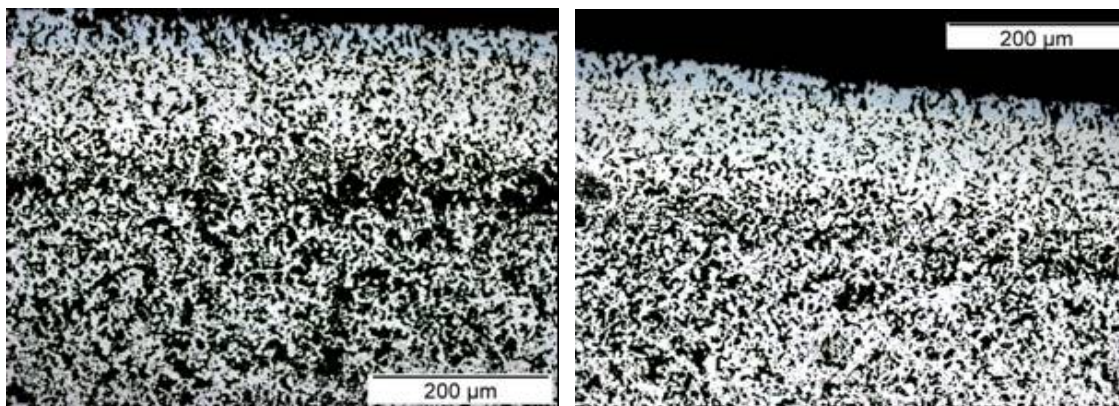
Mo+2 wt% Si - 1300°C wafer side - 500x

**fig. 3.56.: Mo (-Si) samples with different amounts of Si; sintered at 1300 °C - 2h - H<sub>2</sub> with Si wafer on top of the surface**

Specimens which have been sintered before at 1300 °C for 2 h in H<sub>2</sub> and shown in fig. 3.56 were sintered a second time at a higher temperature in the range of the eutectic temperature of Mo and Si. The second sintering was carried out at 1420 °C for 2 h in vacuum. For the second sintering step a new Si wafer was placed on the surface of the Mo specimen, at the same place as the wafer for the first sintering.

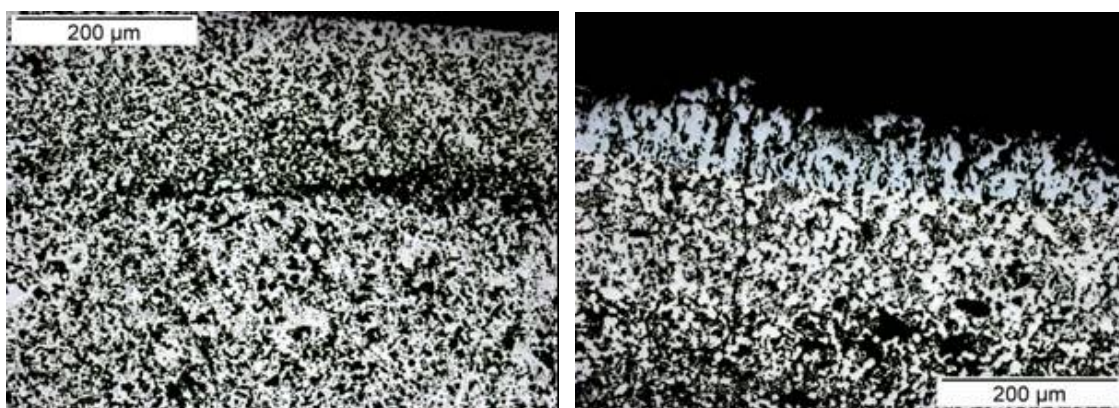
There is no eye-catching difference in Si-layer (coming from Si-wafer) thickness between sample sintered just at 1300°C and the one sintered for a second time at 1420°C (fig. 3.57).

Both types of described samples, also the two layer samples described above (1300°C – 2 h - H<sub>2</sub> + 1420°C - 2h - vacuum) were re-sintered at 1420°C for 2 h in vacuum. Despite the same reaction conditions and sample constitution, only the samples from the first experiment (1300°C - 2h - H<sub>2</sub> + 1420°C - 2h - vacuum) have been destroyed on the surface (due to exothermic reaction of the Si wafer with the sample). There is no explanation why in some cases the surface was destroyed and in another case the Si diffused into the sample without any damage to the sample. The temperature in the furnace was measured with a thermocouple (PtRh-Pt) near the specimen and recorded on the computer. So, it was possible to compare the temperature preset and displayed on the furnace to the real one measured near the specimen.



Mo+0,5 wt% Si - 1420°C wafer side - 500x

Mo+1 wt% Si - 1420°C wafer side - 500x



Mo+1,5 wt% Si - 1420°C wafer side - 500x

Mo+2 wt% Si - 1420°C wafer side - 500x

**fig. 3.57.: Mo (-Si) samples with different amounts of Si; sintered first time at 1300 °C - 2h - H<sub>2</sub> and a second time at 1420 °C for 2h - vac.; with Si wafer on top of the surface**

### 3.2.1.2.2 SEM and mapping

In the scanning electron microscope some elemental maps have been prepared to reveal the distribution of Si in the sample. For the visualisation the EDAX software of the SEM was used. Of primary interest was the diffusion path of Si coming from the Si wafer. In fig. 3.58 an SE image of the cross section of sample “Mo+2wt%Si” can be seen which was sintered at 1300°C for 2 h in H<sub>2</sub> and a second time at 1420 °C for 2 h in vacuum with an Si wafer lying on the surface. On the right side in fig. 3.58 the distribution of Si and Mo can be observed.



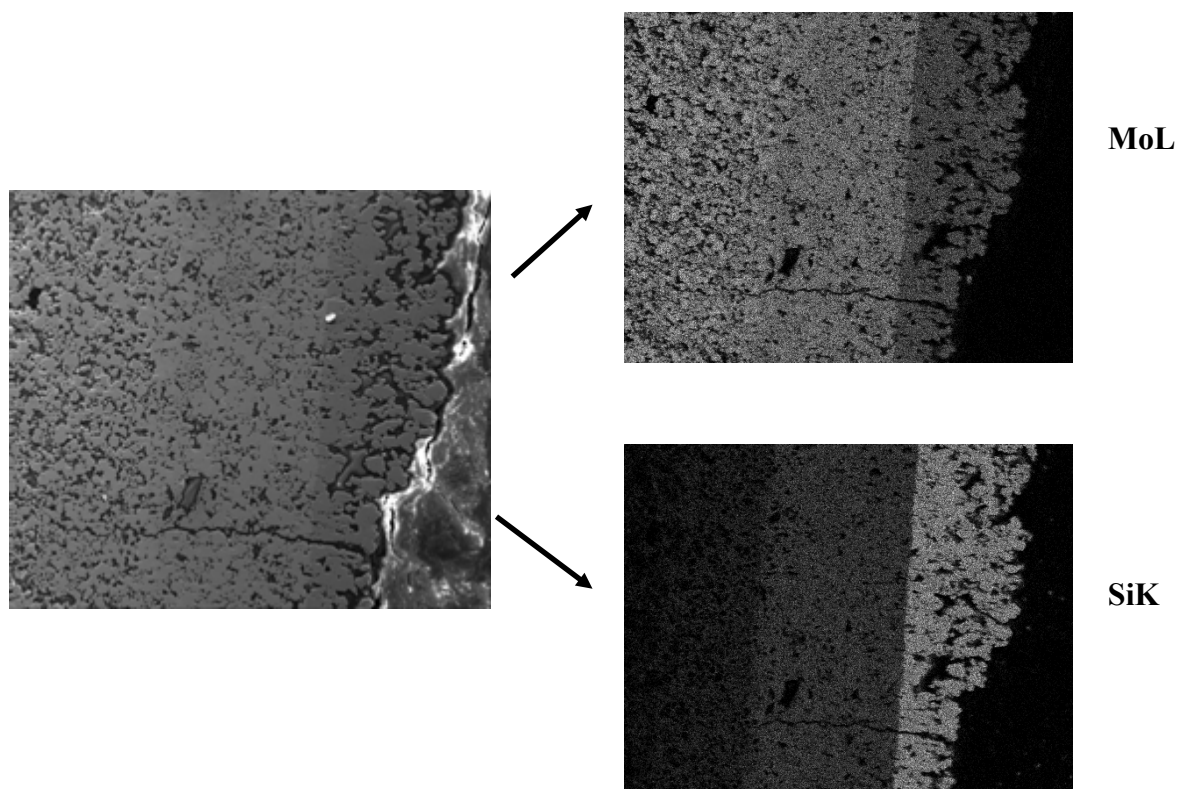


**fig. 3.58.: SE image and elemental mapping of Mo + 2 wt % Si after second sintering at 1420 °C - 2h - vacuum; 300x magnification**

It can be clearly seen in fig. 3.58 bottom right that the highest Si content is present near the surface at which the Si wafer was lying during sintering. Towards the sample core, less Si is in there. Three colours can be observed which correspond to the amounts on Si in Mo. The lightest layer is the one with the highest Si level while the darkest one is with lowest amount on Si.

Concluding these sintering experiments of Mo + x\*wt% Si with wafer, it can be said that the sintering activity of blended Mo-Si compacts was very low (surprisingly!), which is the reason why it was difficult to sinter this material. Therefore some DTA analysis was carried out to find out something about the reactivity of the system Mo - Si.

### **3.2.1.3 Reactivity of molybdenum with silicon measured by DTA**

To prove the reactivity of Mo from Chemie Metall and Si from Ecka, some experiments were prepared in the DTA and TG. Mo was dry mixed with 2 / 15 / 37 wt% Si for 2 h in a tumbling mixer and the mix was afterwards taken (as loose powder) for the DTA analysis. Each powder was heated up at 20 K/min to 1600°C in Argon and cooled down at the same rate (no soaking period). In fig. 3.59 the DTA/TG analysis of Mo sample containing 2 wt% Si can be seen. In fig. 3.60 and fig. 3.61 the DTA graphs of Mo with 15 and 37 wt% Si are shown. The black line is showing the results of the DTA measurement, the blue one those from TG measurement. Plain Mo was measured, too, as a reference and taken for the calculation of the following curves, i.e. the graphs in the

following show the difference between the signals for Mo-Si and Mo specimens, respectively.

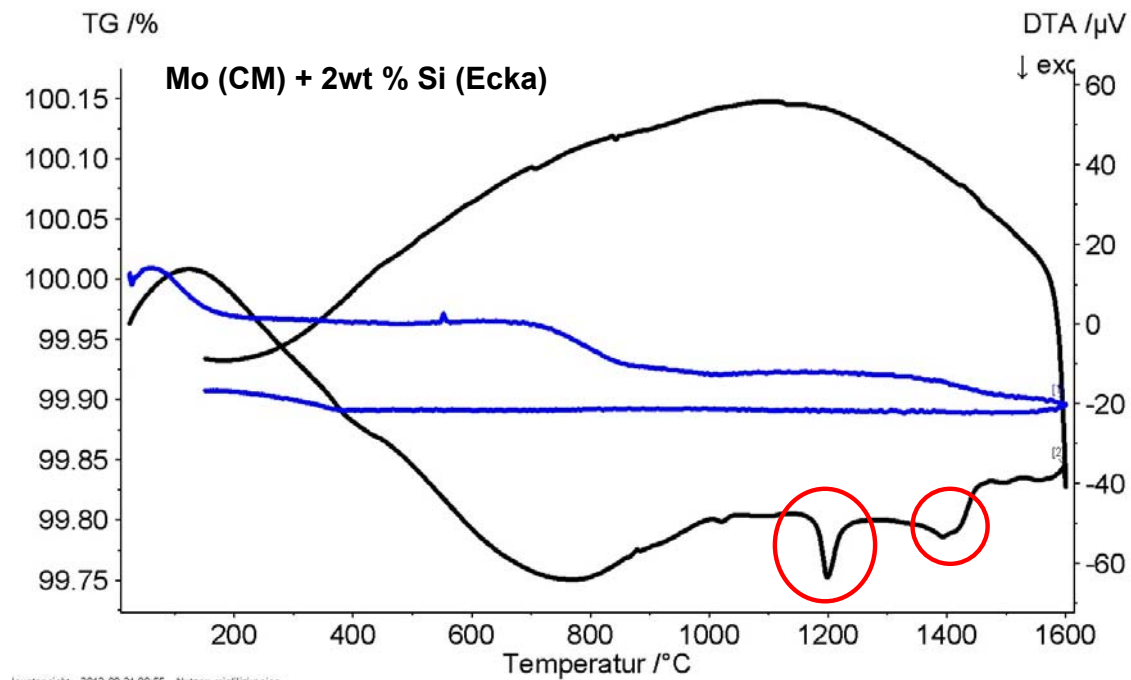


fig. 3.59.: DTA analysis of Mo sample containing 2 wt% Si; heating up at 20 K/min to 1600°C in Argon

In the DTA graph the first exothermic peak can be observed at 1200°C and a small second one at 1400°C (fig. 3.59). At 1200°C Mo might react with Si exothermically by forming some  $\text{Mo}_x\text{Si}_y$ . The TG analysis shows that the specimen lost 0,1 wt% of its mass between 700 and 800 °C, probably by evaporating of surface oxides.

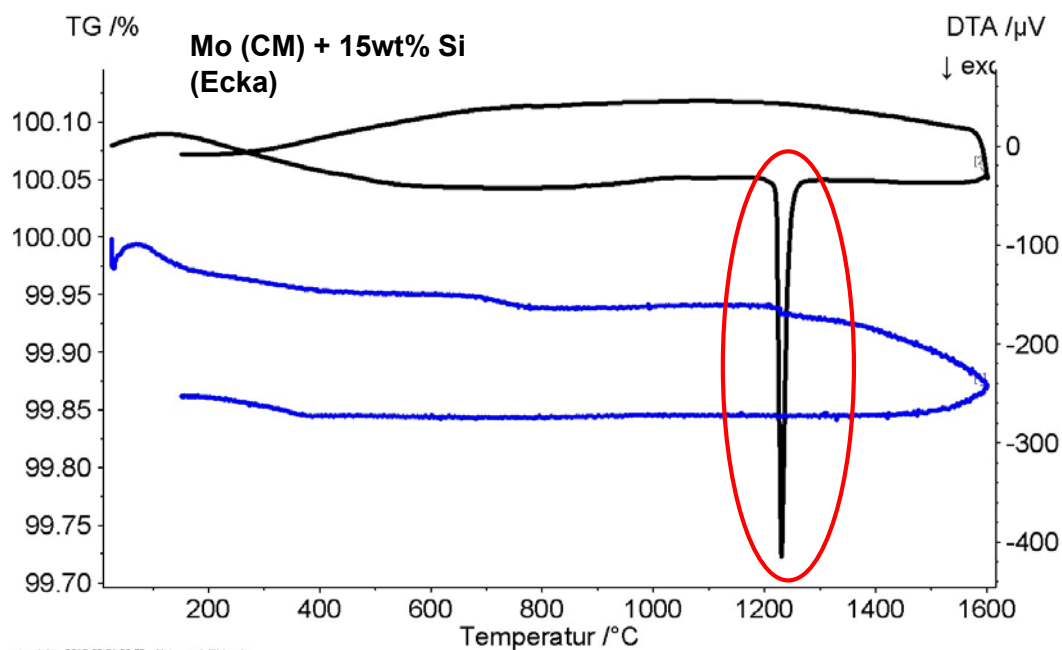


fig. 3.60.: DTA analysis of Mo sample containing 15 wt% Si; heating up at 20 K/min to 1600°C in Argon

In fig. 3.60 can be seen that the exothermic peak of the Mo sample containing 15 wt% Si was shifted to 1230°C (approx.) but with a higher intensity. Furthermore, only one peak can be observed. The second peak that came at 1400 °C in specimen containing 2 wt% Si cannot be seen anymore. It seems that the reaction is finished at 1230 °C. Molybdenum reacted completely with Si at this temperature. The mass loss measured by TG analysis is the same as in the first specimen containing 2 wt% Si where 0,1 wt% mass was lost, but the respective mass loss at the various temperature “windows” was slightly different.

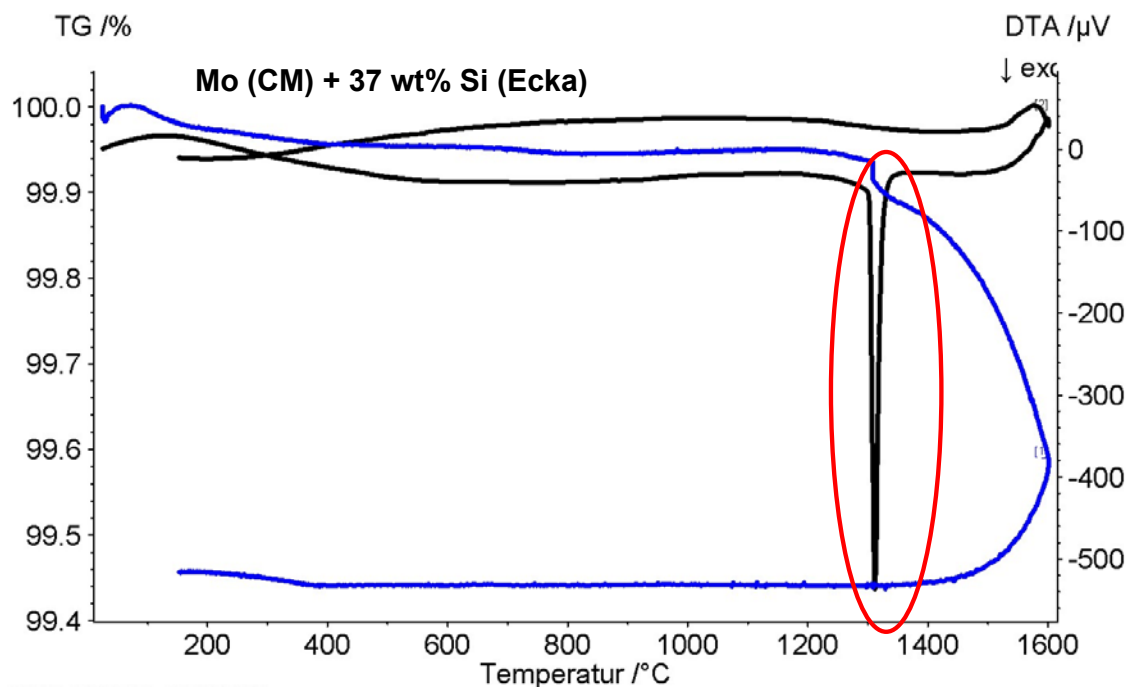


fig. 3.61.: DTA analysis of Mo sample containing 37 wt% Si

By the addition of 37 wt% Si to Mo the exothermic peak which was observed at 1200°C in the first run (for Mo + 2 wt% Si) moved to 1300°C (fig. 3.61). Furthermore it can be observed that, as expected, with higher amount of Si in Mo the intensity of the exothermic peak is growing. Also for this specimen containing 37 wt% Si in Mo no peak at 1400 °C can be observed. Due to the very exothermic reaction at 1300 °C the material reacted completely (without unreacted Mo or Si) therefore no further peak occurs. The TG analysis (blue line) shows that the specimen lost 0,5 wt% of its mass, probably by evaporating of surface oxides.

The DTA studies prove that a reaction between molybdenum and silicon takes place. Apparently the problem is not the low reactivity but the low sintering activity of the two components. Therefore experiments to increase the sintering activity were performed.



### 3.2.1.4 Activation of sintering in Mo-Si compacts

The sintering activity of blended Mo-Si compacts was very low (surprisingly!), for which reason it was difficult to sinter this material. It was necessary to increase the sintering activity of the Mo and Si powders. A possible way was to increase the sinterability by a better homogenisation of the powders. Therefore, Mo and Si were mixed in a tumbling mixer for 2 h with some steel balls. In the following experiments molybdenum was mixed with silicon in cyclohexane in two ways. The idea was to increase the homogeneity of the mixture by a preceding milling process and thus increase the sintering activity.

Two different milling experiments were carried out. In the first experiment the Mo was wet mixed with Si in cyclohexane in a ball mill with hardmetal grinding elements (geometry was something between a cylinder and a ball). In the second experiments the two powders were homogenized in a “Turbula” mixer with 80 rpm, also in cyclohexane, with steel grinding balls. The main difference in the methods was the input energy to the mixing process and the hardness of the grinding elements.

#### *Experimental*

Mo from Chemie Metall ( $\leq 63 \mu\text{m}$ ) was mixed with 5 wt% Si from Ecka in cyclohexane. For homogenisation the two mixing techniques were carried out for 3 h. Afterwards the cyclohexane was decanted and the residue dried in a drying chamber for 12 h. The dried powder mixture was cold isostatically pressed to cylindrical samples with 20 mm diameter at 200 MPa compacting pressure. The samples were presintered at 900 °C for 2 h in  $\text{H}_2$ . A further sintering step followed at 1500°C for 2 h in vacuum (in the KCE hot press furnace).

#### 3.2.1.4.1 SEM of powders

The two homogenised powders were characterised in the SEM. In fig. 3.62 the two prepared powders are shown at 3000x magnification. After homogenisation in a ball mill the particles were more flat while after homogenisation in a “Turbula” no difference in shape to the initial state can be observed. The biggest particles show still an octahedral shape.

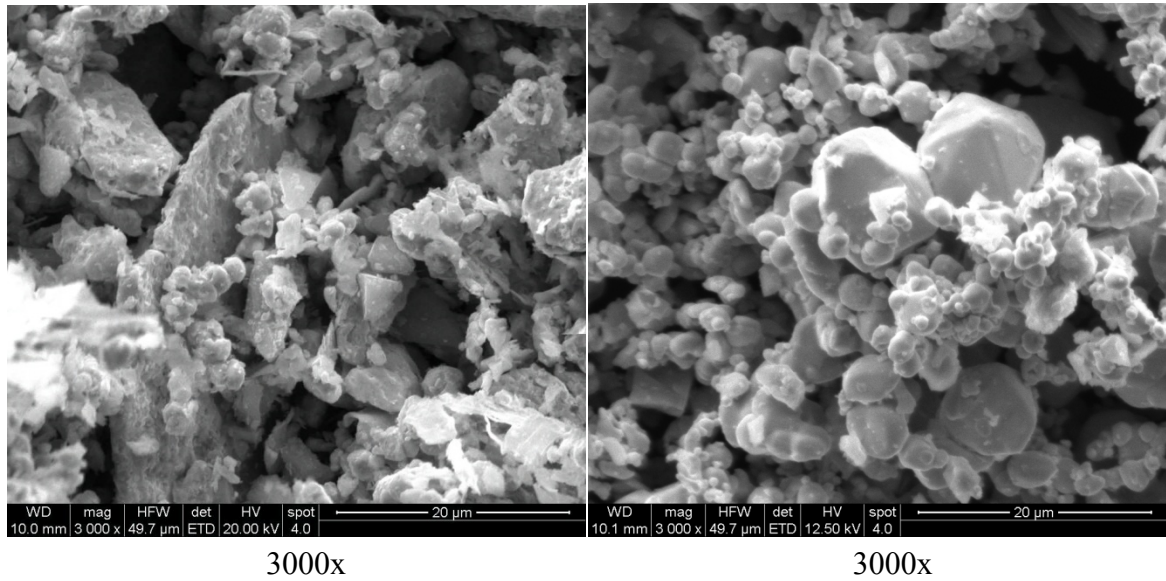


fig. 3.62.: Mo + 5wt%Si wet mixed in cyclohexane, left: in a roller mill; right: in “Turbula”

#### 3.2.1.4.2 LOM

In fig. 3.63 the cross sections of two samples prepared from differently homogenised powders are shown. As could be already observed in fig. 3.62 the powder shape varies due to different homogenisation ways. In fig. 3.63 on the left side the cross section of the sample prepared from the powder homogenised in the ball mill can be observed. The flat particles can be seen. On the other hand the powder shape of the powder homogenised in the “Turbula” remained round, which can be observed in fig. 3.63 right.

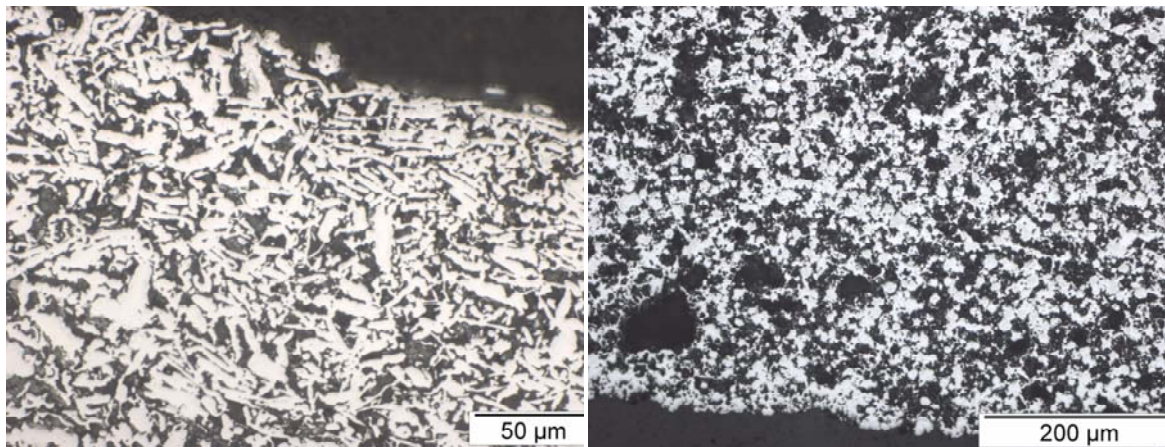


fig. 3.63.: Mo + 5 wt%Si sample – sintered at 900°C for 2 h in H<sub>2</sub> + 1500°C for 2 h in vacuum; left: from powder prepared in a roller mill; right: from powder prepared in “Turbula”; both magnifications 500x

### 3.2.1.4.3 Density, open porosity and hardness

The density of the sample from powder prepared in the roller mill was  $5,7 \text{ g/cm}^3$  while the open porosity was 41%. The density of the sample from powder prepared in the “Turbula” was  $7,1 \text{ g/cm}^3$  and the open porosity was 33%.

The hardness with 1 kp indentation load was measured for both samples. A lower indentation load was chosen this time (comparing to experiments before where 10 kp indentation load was measured). The reason is that the specimens prepared from these two powders did not sustain the higher load of the macro hardness measurement. The corners of the indentation pyramid could not be seen clearly.

The ball milled sample showed a hardness of  $69 \pm 4 \text{ HV1}$  while the “Turbula” sample showed a much higher hardness of  $141 \pm 8 \text{ HV1}$ . Evidently ball milling of  $\text{Mo} + 5 \text{ wt\%Si}$  resulted in a much lower sintered density and higher porosity than Turbula mixing, as a consequence of unfavourable particle shape. Therefore also the hardness of the former sample is much lower. Generally it showed that the treatment in the ball mill changes the shape of the powder particles, apparently rather severely, and the sinterability was not noticeably affected which could be seen in the low density after sintering.

### 3.2.1.5 Summary - examination of reactivity between Mo and Si

The reactivity between Mo and Si was studied. Mo specimens with various contents of Si (0/2/5/10/15/25/37 wt%Si) were pressed with 150 MPa and sintered at  $1300^\circ\text{C}$  for different soaking periods in  $\text{H}_2$ . On the top of each specimen a Si wafer (as Si source) was placed. In the first experiment a soaking period of 8 h was chosen. XRD measurement on the Si wafer side and the opposite side without a wafer, were carried out.  $\text{MoSi}_2$  was only detected on that side of the specimen where the Si wafer was placed during sintering. In Mo sample which contained 37 wt%Si,  $\text{MoSi}_2$  was also measured on the Si wafer free side. In the LOM images a lot of porosity in the specimen was recognised which might come from Kirkendall effect during sintering. A light blue layer near the surface could also be seen, which came from the Si wafer. In the center of the specimen no blue colour (no Si) could be seen. Furthermore, there was barely a cohesion between the particles, and the handling with the specimen got even worse with increasing amount of Si.

Specimens of the same composition have been prepared for a second time. A first sintering step was carried out at  $1300^\circ\text{C}$  for a shorter soaking period of 2 h (in  $\text{H}_2$ ). In the LOM images a light blue layer near the surface was visible only in specimens containing 2 / 5 / 25 wt%Si, but there was barely a mechanical stability in the compact. A second sintering at  $1420^\circ\text{C}$ , which is above the eutectic temperature ( $1414^\circ\text{C}$ ) of Mo and Si, was carried out with a new Si wafer on the top. Comparing now specimens sintered at  $1300^\circ\text{C}$  for 2 h in  $\text{H}_2$  with those sintered above the eutectic temperature, less stability of the Si-rich layer can be observed. The layer was destroyed by uncontrolled exothermic reaction.

Diffusion of Si in Mo-Si multilayer samples was characterised in two layer specimens where one layer contained Si. Different amounts of Si were chosen with 0,5/1/1,5/2 wt% Si in Mo. The specimens were pressed uniaxially with 150 MPa and sintered twice. For each sintering step a Si layer was placed on the top. The first sintering was carried out at  $1300^\circ\text{C}$  for 2h and  $\text{H}_2$  and the second sintering was carried out at  $1420^\circ\text{C}$

for 2h in vacuum. It could be observed that there was barely a cohesion between the layers. Already after the first sintering step, first cracks occurred which propagated and after second sintering the layers separated. Only two of the specimens (the one with 1 and 2 wt% Si) showed a very thin light blue layer near the surface where the Si wafer was situated. After sintering a second time no eye-catching difference in the layer could be observed.

DTA analysis was carried out on Mo specimens containing 2/15/37 wt% Si at 1600 °C in argon to study the reactivity between Mo and Si. The results showed two exothermic peaks at 1200 °C and 1400 °C for Mo specimen containing 2 wt% Si. The peaks are less pronounced. Specimen which contained 15 wt% Si showed only one exothermic peak at 1250 °C which is however more distinctive. This peak was shifted to 1300 °C for the specimen containing 37 wt% Si. The DTA studies proved that a reaction between Mo and Si takes place.

Due to the fact that the sintering activity of Mo-Si compacts was very low, it was tried to increase the sintering activity by a better homogenisation of the powders. In two experiments, Mo and Si (5 wt%) were mixed in a tumbling mixer for 2 h with steel balls and in another experiment in a Turbula mixer with hardmetal grinding elements. In both cases the mixing was carried out in cyclohexane. From the powders, specimens were pressed with 200 MPa and sintered in two steps, first at 900 °C for 2h in H<sub>2</sub> and in a further step at 1500 °C for 2 h in vacuum. The density, open porosity and hardness were examined. In both cases the achieved densities have been quite low, with 5,7 g/cm<sup>3</sup> for the specimen from roller milled powder and in the second case 7,1 g/cm<sup>3</sup> was measured for the specimen from the Turbula mixer. In the LOM images it could be seen that the treatment in the ball mill changed the shape of the powder particles, with adverse effect on the compactibility, but the sinterability was not noticeably affected for specimens from both mixing experiments.

### **3.2.2 Pressure-assisted sintering at higher temperatures**

#### **3.2.2.1 Mo + x wt% Si after hot pressing at 1800 °C and 50 kN**

In the following experiment the reactivity of Mo with Si at higher sintering temperatures was studied, in particular the role of external pressure. Investigations by the project partner EADS had shown that consolidation of fully reacted porous silicide structures was virtually impossible even by HIP because the silicide structure is too rigid and creep resistant also at high temperatures. By applying pressure during the reaction, better densification was expected.

For the characterisation of the reactivity between Mo and Si some specimens were hot pressed and characterised afterwards. Molybdenum with different amounts of silicon was hot pressed at 1800 °C for 120 min applying 50 kN. Molybdenum powder was mixed with 3 / 5 / 15 / 37 wt% Si for 2 h in a tumbling mixer. Afterwards each powder mixture was poured into a graphite die of 50 mm diameter and a height of the bulk powder of approximately 30 mm. After hot pressing the height decreased to approx. 10



mm due to densification. Both ends of the cylindrical die were closed by graphite punches. Between the punches and the powder mixture some carbon foil, coated with BN, was placed to facilitate the separation of specimen from the tool components after hot pressing.

After hot pressing all specimens were characterised for their physical and mechanical properties. Some LOM images showed the cross sections. Out of the sintered discs, rods were cut on a Struers Accutom 50 using a diamond blade. From one disc with 50 mm diameter it was possible to cut 3 rods with 35 mm length, 10 mm width and 7 mm height. These rods were used for 3 - point - bending strength experiments.

### 3.2.2.1.1 Physical and mechanical properties

In tab. 20 physical and mechanical properties of the hot pressed samples are listed. It can be observed that the density (Archimedes) of the specimens is decreasing with increasing amount of silicon. The theoretical density is also given in tab. 20. and was calculated from tab. 21. The amount of each phase was known from the XRD analysis and the theoretical density of each phase was taken from the literature [162;163]. It can be seen that the theoretical density from literature is higher than the one measured by Archimedes method (the density of the specimens is lower than the one from literature). The open porosity was measured with He - pycnometry and was very low. The total porosity was calculated from the theoretical density of the phases compared to the measured one (the difference in % is resulting in total porosity). Due to the fact that a carbon plate was put on the surface of each specimen (which sintered to the specimen during hot pressing), the pores might be closed and therefore the measurement of the open porosity with He-pycnometry resulted in lower values. The hardness was measured as HV1. Plain Mo specimen showed the lowest hardness with 162 HV1 while it increased to 1259 HV1 for Mo specimen containing 37 wt% Si. The bending strength is decreasing with increasing silicon content. By the addition of silicon to molybdenum, some silicides are formed which results in higher hardness of the material. It can also be observed in tab. 20 that with increasing hardness the bending strength of a material was decreasing.

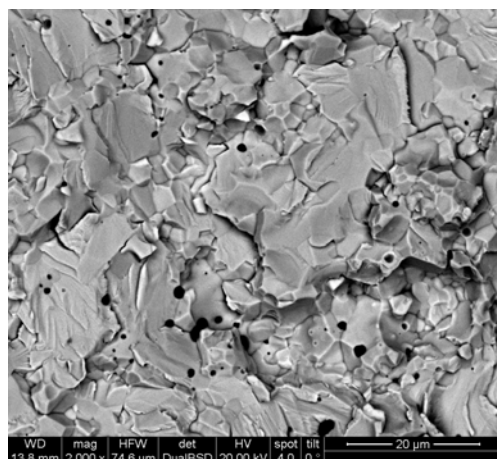
**tab. 20.: Density, open porosity (*He-pycnometry*) HV 1, F max and  $\sigma_{fm}$  of Mo specimens containing different amounts of Si; HP at 1800 °C for 120 min in vacuum with 50 kN; \*) theoretical density calculated; and calculated theoretical total porosity**

Mo + x wt% Si	Density [g/cm <sup>3</sup> ]	Open porosity [%]	HV 1	F max [N]	$\sigma_{fm}$ [MPa]
<b>0 wt% Si</b>	9,58/10,2*	2/6,1*	162	3978,4	603,7
<b>3 wt% Si</b>	8,96/9,84*	2/8,9*	738	3665,7	524,3
<b>5 wt% Si</b>	7,94/9,49*	1/16,3*	1009	2745,3	382,1
<b>15 wt% Si</b>	7,72/8,48*	2/8,9*	1123	1546,7	211,7
<b>37 wt% Si</b>	6,93/7,06*	0/1,8*	1259	1398,3	174,3

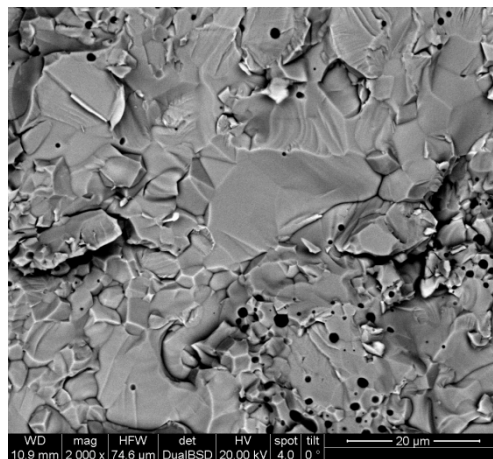
Some BSE images from fractured surface are summarised in fig. 3.64. It is quite difficult to recognize the grain boundaries because due to the high sintering temperature



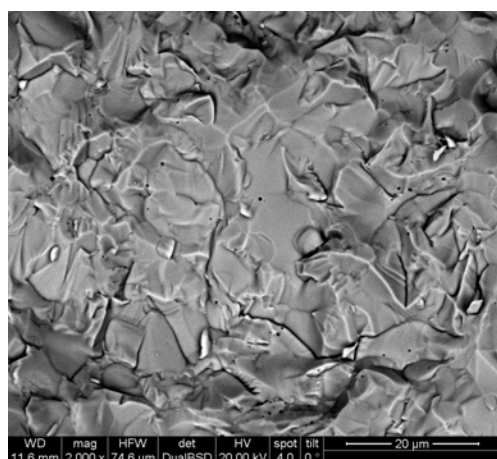
and applied pressure, the powder was pressed and sintered together. In the BSE image from Mo specimen containing 15 wt% Si, first light spots can be observed, which grow to bigger areas in the Mo + 37 wt% Si specimen. This light areas are formed silicides, which might be  $\text{MoSi}_2$  because about 35,2 % Si and 64,8 % Mo were measured with EDAX.



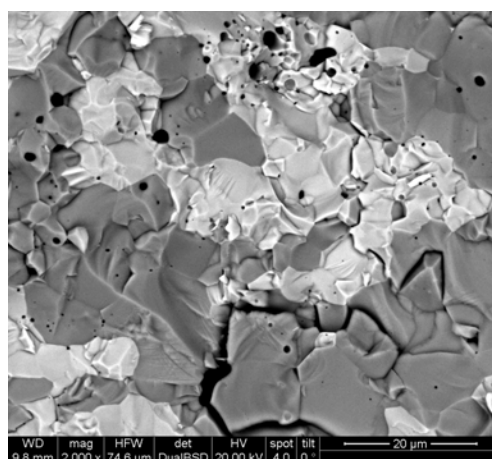
Mo + 3 wt% Si



Mo + 5 wt% Si



Mo + 15 wt% Si



Mo + 37 wt% Si

**fig. 3.64.: 3-point bending fracture surfaces of Mo specimens containing 3 / 5 / 15 / 37 wt% Si after hot pressing at 1800 °C and 50 kN in vacuum;**

### 3.2.2.1.2 XRD

In fig. 3.65 XRD diffraction patterns are given. All five Mo specimens with different amounts of Si were measured, and the different phases which were formed are depicted.

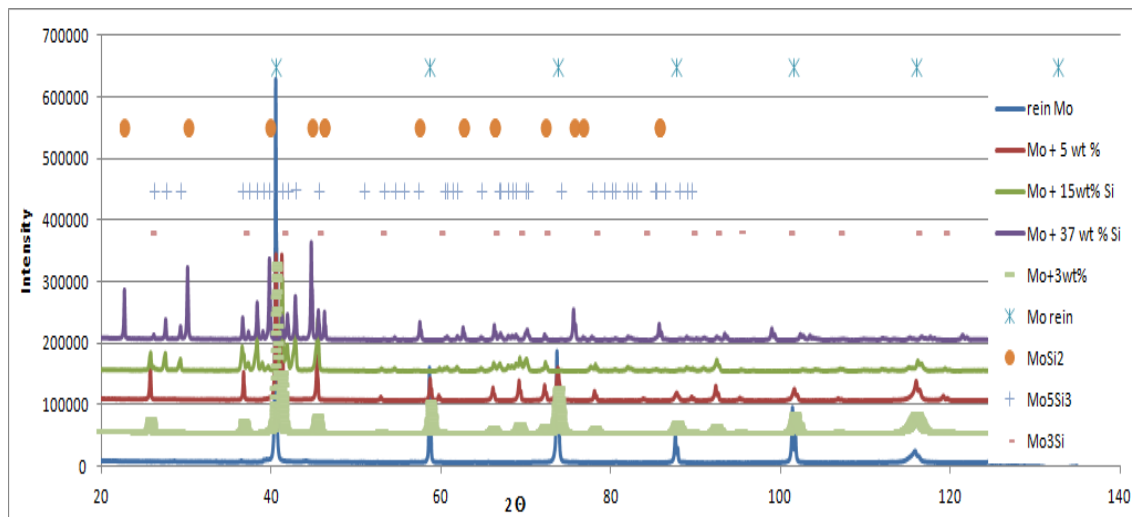


fig. 3.65.: XRD analysis of all specimens Mo + x\*wt% Si - hot pressed at 1800 °C for 2 h and 50 kN

In fig. 3.65 as well as in tab. 21 the phases formed during hot pressing of Mo with different amounts of Si can be observed very well. The measurement was carried out by XRD, and the amount of each phase (and the phase composition) was calculated on Topas, which is a software for Rietveld analysis. The molybdenum specimen which contained 5 wt% Si after hot pressing resulted in 45 % Mo and 55 % Mo<sub>3</sub>Si. The specimen Mo-15 wt% Si resulted in 37 % Mo<sub>3</sub>Si and 63 % Mo<sub>5</sub>Si<sub>3</sub>. The hot pressed sample Mo-37 wt% Si contained 59 % MoSi<sub>2</sub> and balance Mo<sub>5</sub>Si<sub>3</sub>. This was the only specimen containing MoSi<sub>2</sub>. Due to the fact that by the addition of 37 wt% Si to Mo the stoichiometric composition of MoSi<sub>2</sub> should be achieved, it is surprising that the measured amount of MoSi<sub>2</sub> is lower. Furthermore, the values for the Mo<sub>5</sub>Si<sub>3</sub> for Mo + 15wt% Si specimen are quite low. According to the phase diagram a Mo specimen containing 15 wt % Si should consist out of 100 % Mo<sub>5</sub>Si<sub>3</sub>.

tab. 21.: Phases in all hot pressed specimens Mo + x\*wt% Si of XRD

	Mo	Mo <sub>3</sub> Si	Mo <sub>5</sub> Si <sub>3</sub>	MoSi <sub>2</sub>
<b>Mo</b>	100			
<b>Mo + 3wt% Si</b>	72	28		
<b>Mo + 5wt% Si</b>	45	55		
<b>Mo + 15wt% Si</b>		37	63	
<b>Mo + 37wt% Si</b>			41	59

### 3.2.2.1.3 LOM

In fig. 3.66 some LOM images of hot pressed Mo specimens with different amounts of silicon are shown. The cross sections were etched with Murakami I+II for 50s after metallographic preparation. Near the surface a thin layer can be recognised. It has to be remembered that the specimens were pressure sintered in a graphite die. The near-surface area was therefore penetrated with carbon. On the punch surfaces a carbon foil was situated. Near the surface a thin layer can be observed. In this layer some carbon might have penetrated. A micro hardness (HV1) measurement was not possible, because

the layer was too thin. Some blue colour can be recognised too. This colour comes from Si.

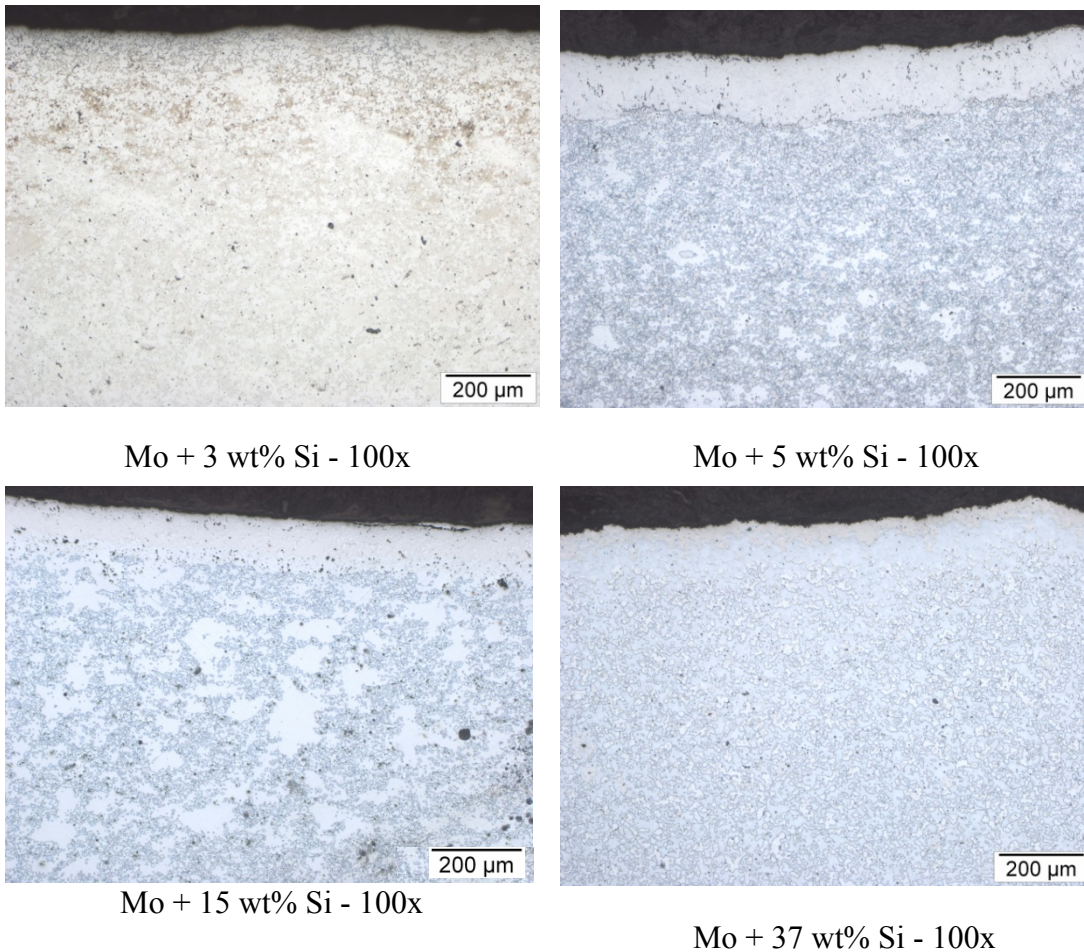


**fig. 3.66.: LOM images of Mo specimens (surface near area from punch surface) with different amounts of Si; etched with Murakami I+II; 50s**

#### 3.2.2.1.4 SEM with mapping

In fig. 3.67 some SEM-BSE images of the cross section of the Mo + 37 wt% Si specimen are shown. It can be seen that the structure is not homogeneous. In the elemental maps the distribution of Mo and Si is shown. There are three different shades of the Si distribution, which means that there are different silicides formed. The darker colour means that there is more silicon. The lighter one in the maps stands for less silicon.



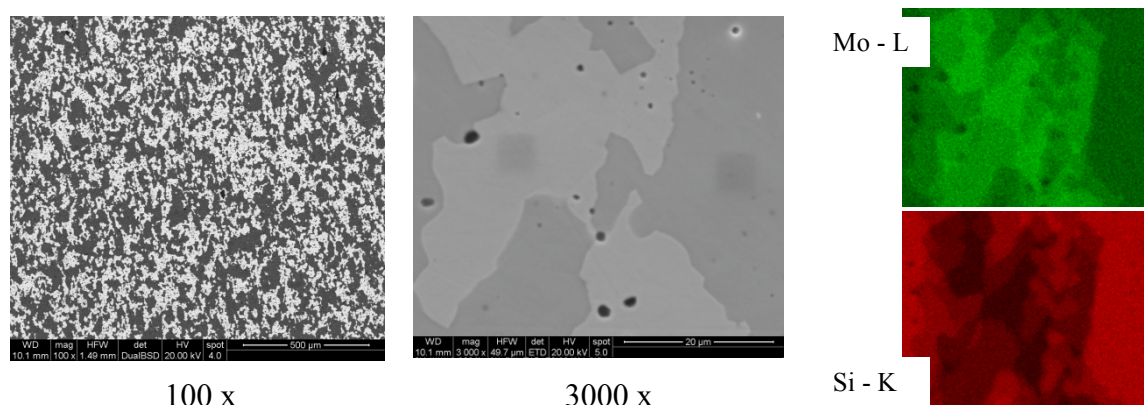


**fig. 3.67.: Left and center image: overview of the cross section of specimen Mo + 37 wt% Si; right: elemental mappings of this specimen**

### 3.2.2.1.5 Summary

Mo-Si specimens containing 3/5/15/25/37 wt% Si were hot pressed at 1800 °C for 120 min with 50 kN in a cylindrical die with 50 mm diameter. Out of the sintered plates bars were cut and used for 3 - point - bending strength measurements. The density was decreasing with increasing amount of Si which can be related to the fact that different silicides were formed with lower densities. The theoretical density of the specimens was also calculated from the values for silicide from literature and from the XRD results, where the amount of each phase was given. It could be seen that the Archimedes density measured was lower than the one from literature. After hot pressing barely any open porosity could be measured with He - Pycnometry. The total porosity was also calculated from the theoretical achievable density. Due to the fact that the carbon foil which was used for hot pressing sintered to the specimens, the pores may have been blocked and the values measured with He - Pycnometry were too low. The open porosity was determined to be between 0 and 2% which is still high for a hot pressed specimen. Plain Mo specimen showed the lowest hardness with 162 HV1 while it increased to 1259 HV1 for Mo specimen containing 37 wt% Si. XRD (fig. 3.65) pointed out which phases were formed.  $\text{MoSi}_2$  was only formed in specimen Mo + 37 wt% Si. In the LOM images (fig. 3.66) a thin layer was observed near the surface which might come from carbon that penetrated the specimen during the hot pressing. In SEM images (fig. 3.67) the distribution of Mo and Si was shown. It could be seen that different phases were formed. Comparing the hot pressed specimens with those which were pressureless sintered, good sinterability and densification of the Mo-Si mixes could be observed, Molybdenum sintered with Si forming a compact without Kirkendall porosity.

### 3.2.2.2 Sandwich – structured sample after hot pressing of [Mo / Mo+15 wt%Si / 37 wt%Si]

Since the investigations with layered structures described above had shown that pressureless sintering easily results in cracking at the interfaces, layered specimens were also prepared by hot pressing, in order to check if this method can yield defect-free specimens. Molybdenum was mixed in two fractions with 15 wt% Si and 37 wt% Si,

respectively. A structured sample out of three layers was built up: one layer without Si, with plain Mo, the second layer containing 15 wt% Si in Mo and the third layer with 37 wt% of Si in Mo (to result in  $\text{MoSi}_2$ ). The powders were successively filled up into a slightly conical graphite die until the powder bed reached a height of 30 mm. Two graphite punches were limiting the powder bed, one at the top and the second one at the bottom. The graphite cone with the two punches was placed into the hot press, and the pressure sintering process was started. The furnace was heated up to  $1800^\circ\text{C}$  with 10 K/min in vacuum. The soaking period was 2 h. The pressure of 10 kN was applied at  $600^\circ\text{C}$  and was increased to 50 kN at  $1800^\circ\text{C}$  and held during the soaking period. After cooling the sample stuck to the graphite cone and could not be removed without breaking the graphite cone. In fig. 3.68 left the broken graphite cone with the sticking sample is shown while on the right side the sample can be observed. The silver colour of the surface comes from Mo that had reacted with BN. Some dark areas can be observed in the surface area (left fig. 3.68) which is carbon from the graphite die.



**fig. 3.68.: Left: hot pressed sandwich-structured sample embedded in graphite die; right: disc-shaped structured sample after HP without carbon die (punch surface)**

The disc sample was cut along the axis, embedded in bakelite and prepared metallographically. The sample was characterized by LOM and SEM, and the hardness was measured in all layers and also in the interface zone between the layers.

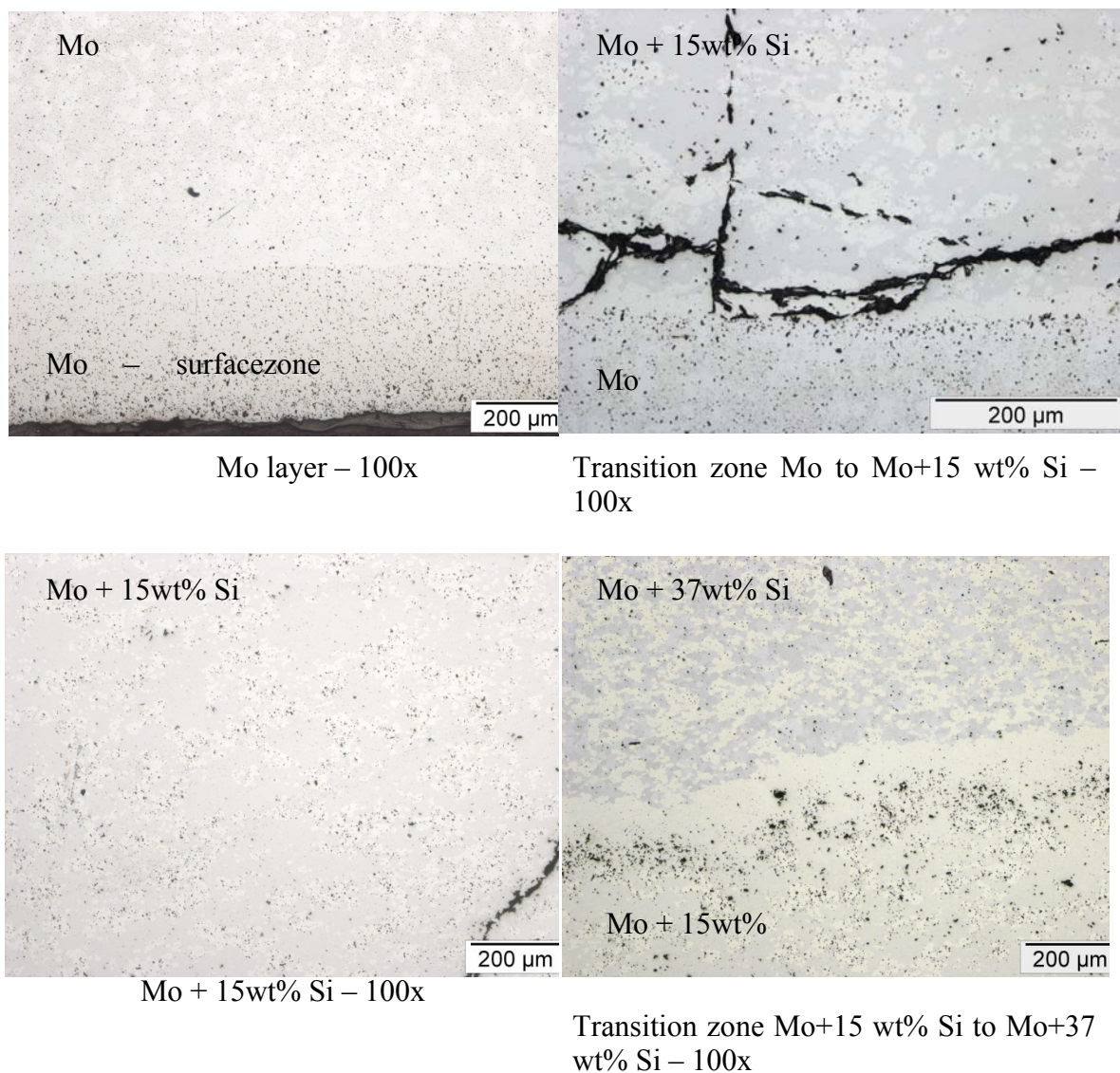
#### 3.2.2.2.1 LOM

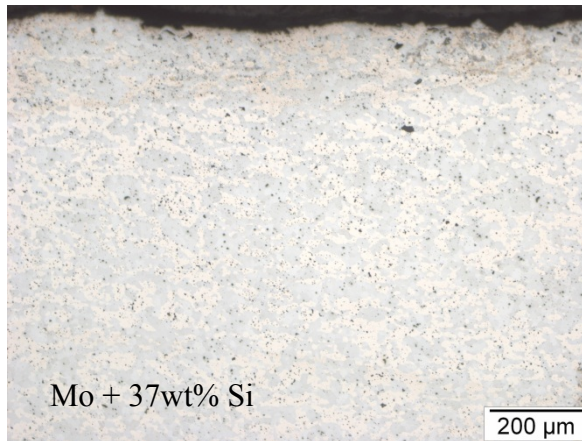
In fig. 3.69 some SEM images of the structured sample are depicted. Each layer and the transition zone between the layers are shown. Some cracks can be observed in fig. 3.69 – image “Transition zone Mo to Mo+15 wt% Si – 100x”. The cracks start in the intersection between the Mo layer and Mo-15 wt% Si. There might be a big difference in the stresses between the two layers. Furthermore the cracks could have been induced during the cutting process, although cutting had been done with a diamond disc with a



small feed (of 0,02 mm/s). In fig. 3.69 “Transition zone Mo+15 wt% Si to Mo+37 wt% Si – 100x” some light blue area in the Mo+37 wt% Si layer (upper layer) can be observed. The blue color comes from different silicides.

The microstructures of all 3 areas - Mo, Mo-15Si and Mo-37Si - look virtually dense. Hot pressing, or, correctly speaking, pressure sintering, thus seems to be a suitable way to eliminate the porosity that was encountered when consolidating Mo-Si through the classical press-and-sinter route. Apparently the Kirkendall porosity that emerges through the reaction between Mo and Si during pressureless sintering is avoided here, while the pressure is apparently effective in a state of the sintering process in which there is not yet a rigid silicide skeleton. Otherwise the structure would most probably resist densification in the same way as encountered by EADS during the HIP experiments. The blended elemental approach for Mo-Si thus can be regarded to be not suited for pressureless sintering but it is highly attractive for the hot pressing approach.





Mo + 37 wt% Si – 100x

**fig. 3.69.: Pressure sintered structured sample consisting of three Mo layers with different Si content.**

#### 3.2.2.2.2 SEM

In fig. 3.70 left an overview of the structured sample is given through a BSE image. Cracks occurred starting in the Mo+15 wt%Si layer at the interface to plain Mo. One big crack propagates even into the Mo+37 wt% Si layer. In the Mo layer (right in fig. 3.70) a darker area near the surface could be observed. This band was penetrated by carbon during the pressure sintering in a graphite die. The right two images are showing elemental maps with the distribution of Mo and Si, depicting the interfacial area Mo-15Si to Mo-37Si. Also in the SEM the structures appear pore-free, which corroborates the findings of LOM.

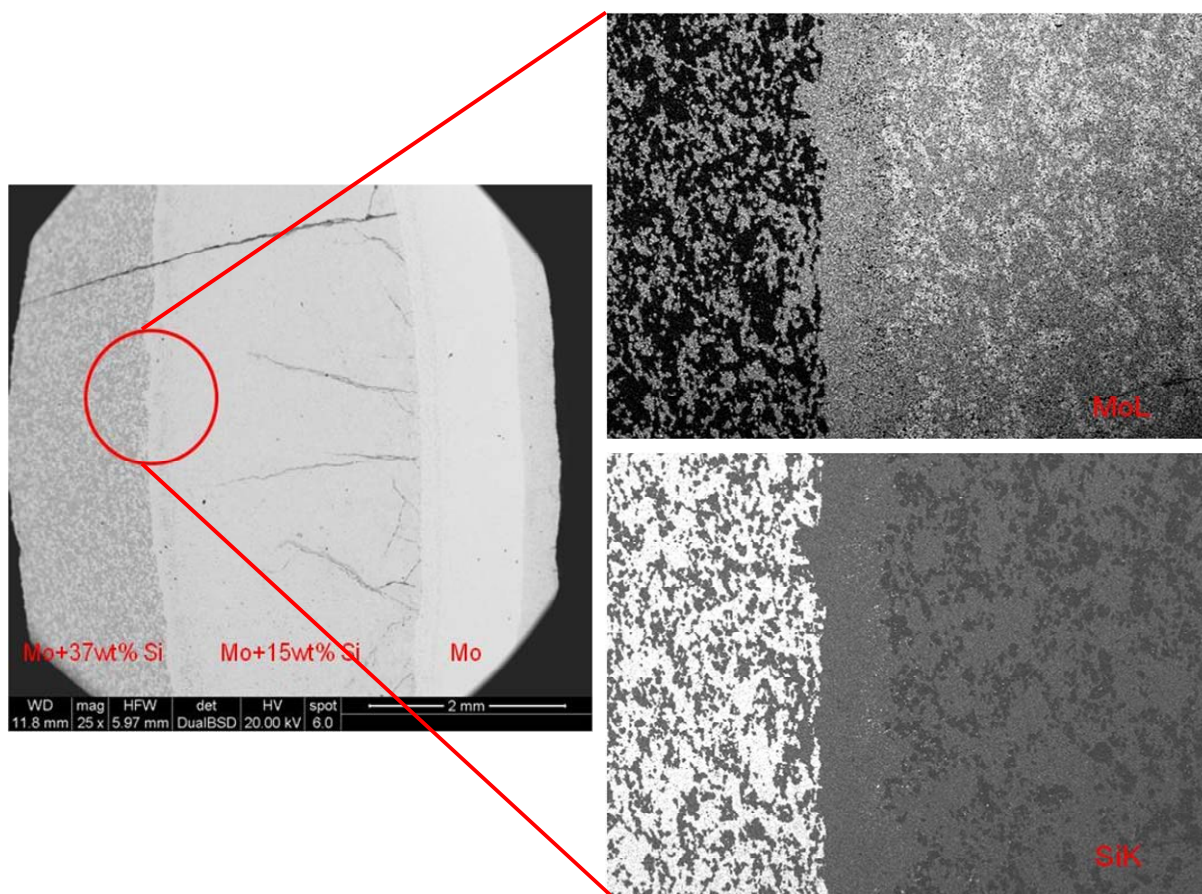


**fig. 3.70.:** Left: an overview of the structured layers; right: distribution of Si and Mo in the layers – magnification of transition zone between Mo layer containing 15 wt% Si (right hand side) and the layer with 37 wt% Si (left hand side)

It can be observed that the silicon distribution is not homogeneous. There are areas with concentrated Si.

### 3.2.2.2.3 Hardness

The hardness was measured with 1 kg indentation load (HV1). The embedded sample is schematically plotted in fig. 3.71 with all three layers. The dark grey area surrounding the sample is bakelite. The hardness was measured in all three layers and in the transition zone. With increasing content of Si the hardness increased too. The lowest hardness was measured in the pure Mo layer with 192 HV1 while it increased to 1068 in the 15 wt% Si layer and was on the highest level in the Mo + 37 wt% Si layer. A very high hardness was measured near the surface in the pure Mo layer with 958 HV1. In fig. 3.69 can be observed that the near-surface area is darker than the core. Some carbon might have penetrated the sample during the hot pressing process (in a graphite die).



The lubrication of the carbon die with hBN as a separating agent apparently does not help to stop the carbon from penetrating into the sample.

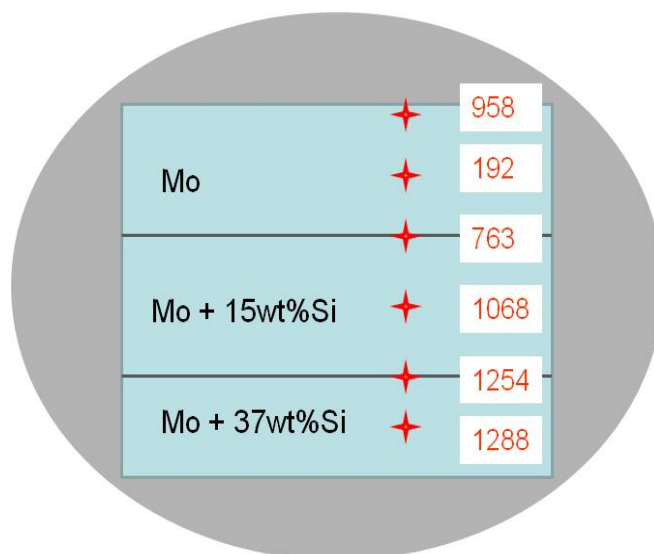


fig. 3.71.: Scheme of embedded sample with the three layers and measured hardness in the layers with differing Si content

#### 3.2.2.2.4 Summary

A sandwich structured specimen was prepared out of three layers. One layer was pure Mo, the second one contained 15 wt% Si and the third one 37 wt% Si in Mo. A structured sample was built up with these three powders beginning with the Si-free layer to the one with 37 wt% Si. This powder structure was pressure sintered at 1800 °C and 50 kN for 2 h in vacuum. In the LOM images the microstructure of all three layers looked virtually dense. Apparently the Kirkendall porosity that emerges through the reaction between Mo and Si during pressureless sintering is avoided. Some cracks could be observed in the 15 wt% Si layer which might occur during cutting due to high stresses induced. In the BSE images a darker layer near the surface could be detected which came from carbon which penetrated during sintering (due to the graphite die). The hardness was measured with 1 kp indentation load. It was observed that the hardness is increasing with increasing amount of Si in Mo. In the Mo layer the hardness was 192 HV1 and it increased to 1288 HV1 in the 37 wt% Si layer.

### 3.3 Mo specimens prepared from coarse powder

It could be shown after the infiltration of Mo specimens which were prepared out of fine Mo powders (CM - Mo, commercially available) that the specimens disintegrated during infiltration experiments. Some specimens survived but the pores were blocked by silicide formation, and no further infiltration was possible. Therefore, Mo specimens were needed with thick sintering contacts – i.e. mechanical stability - and a low specific surface – low reactivity with Si - which would enable infiltration with Si without disintegration. The following experiments concentrated on coarse Mo powders which will lower the specific surface.

Molybdenum from Chemie Metall (CM) with an average particle size of 10  $\mu\text{m}$  ( $\leq 63 \mu\text{m}$  was the specification by the company) has been used so far, in part also Plansee Mo powder with similar particle size. The amount of open porosity could be increased to 40 % in specimens out of CM Mo powder by control of compacting pressure or sintering conditions such as the sintering temperature [ $^{\circ}\text{C}$ ] or soaking period [min]. However, for a successful infiltration the pore size of the open pores is a crucial parameter. Until now the pores have been very small, so the reaction of Si with Mo took place before the Si could penetrate the material. Therefore the open pores near the surface were blocked before the whole Mo skeleton was covered with Si.

An advantage was expected by application of a very coarse Mo powder. It was difficult to find such coarse powders on the market. Molybdenum powders like the one from Chemie Metall with  $\leq 63 \mu\text{m}$  (average particle size  $< 10 \mu\text{m}$ ) was a standard available powder. One provider, Goodfellow, was found offering a  $\leq 355 \mu\text{m}$  Mo powder, but for a price 10 times higher than the one from Chemie Metall.

Some specimens of such coarse powder were prepared, characterised and sent to partners for infiltration.

### **3.3.1 Molybdenum from Goodfellow**

Molybdenum powder from Goodfellow (particles  $\leq 355 \mu\text{m}$ ) was mixed with 1 wt% Ni and 1 wt% wax (Kenolube P 11) for 3 h in a tumbling mixer. From previous experiments it was known that it is not possible to press compacts out of coarse Mo (from Goodfellow) without an additive such as e.g. a wax. The powder was pressed uniaxially in a cylindrical die (11.27 mm diameter) with 200 MPa compacting pressure on Amsler hydraulic press. To remove the wax out of the compacts, the specimens were debinded at 600  $^{\circ}\text{C}$  for 2 h in  $\text{N}_2$  and presintered at 1100  $^{\circ}\text{C}$  for 2 h in  $\text{H}_2$  (5.0 purity; 2 l/min gas flow). The sintering process was completed by increasing the temperature to 1300  $^{\circ}\text{C}$  for 4 h soaking period in the same atmosphere ( $\text{H}_2$ ).

The properties of compacts are defined by the properties of the chosen Mo powder. Some characteristics are summarised in the following.

#### **3.3.1.1 Characterisation of samples from coarse Mo powder**

It could be observed after sintering that the specimen was still very brittle. It was necessary to handle it very carefully. The Archimedes density was measured as 7,26  $\text{g}/\text{cm}^3$  and the open porosity was 28 %. The microhardness was measured with 0,01 kp indentation load in the sintering contacts and in the grains itself. The sintering contacts were very thin, therefore many values had to be taken and the average of all of them was  $287 \pm 26 \text{ HV } 0,01$  while the hardness in a grain was  $340 \pm 12 \text{ HV } 0,01$ .

##### **3.3.1.1.1 LOM**

After cutting and metallographic preparation the cross section of the Mo (Goodfellow Mo powder  $\leq 355 \mu\text{m}$ ) was examined. The microstructure can be observed very well in fig. 3.72. There are many very coarse particles (fig. 3.72 left image: 50x) and only a low amount of small particles. Very coarse pores are pervading the specimen. In the right image in fig. 3.72 barely any sinter contacts can be observed.



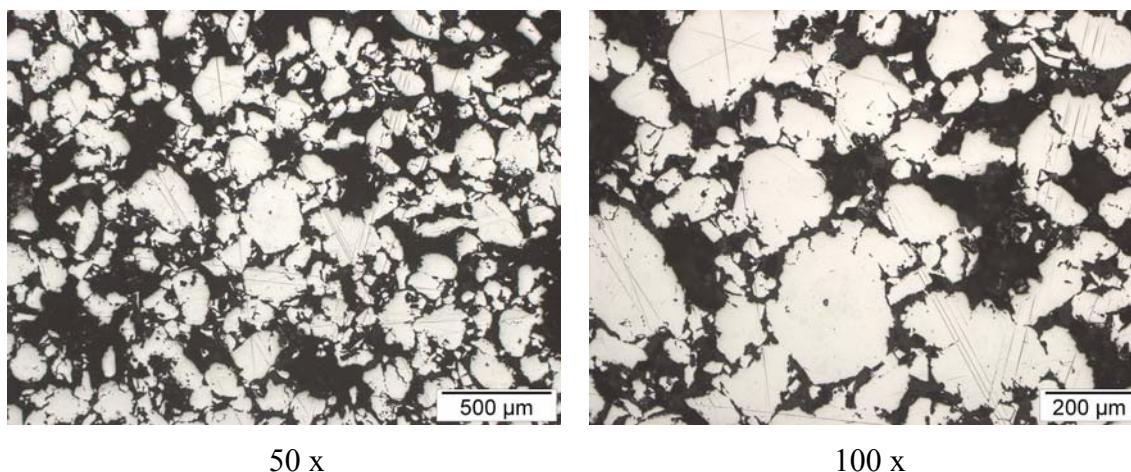


**fig. 3.72.: LOM images from Mo specimen of Goodfellow powder ( $\leq 355 \mu\text{m}$ ) + 1 wt% Ni + 1 wt% P11 Kenolube after debinding and sintering ; left image: 50x; right image: 100x magnification;**

It could be shown that by increasing the particle size it is possible to increase the size of the pores. Molybdenum from Goodfellow is produced probably by pre-sintering of Mo compacts from a fine grained powder and crushing afterwards. That might be the reason for the low sintering activity of the Goodfellow Mo powder and the small amount and size of the sintering bridges.

### 3.3.1.2 Si penetration of compacts from coarse Mo powder

The aim of this experiment was to explore if Si can better penetrate Mo samples prepared from a very coarse powder where the open pores are much wider. As stated above, in earlier experiments a fine grained Mo powder (from Chemie Metall or Plansee) was used where the resulting open porosity was high but the pores themselves were small. In this experiment the coarse Mo powder from Goodfellow ( $\leq 355 \mu\text{m}$ ) was used. This powder was mixed with 1 wt % Ni and 1 wt% wax (Kenolube P11) in a tumbling mixer for 2 h. Afterwards two cylindrical (20 mm diameter) samples were pressed uniaxially with 200 MPa on Amsler hydraulic press. With these two prepared samples two different experiments were carried out.

In the first experiment Si powder was pressed on the top of the surface of the sample. In the second experiment a Si wafer was placed on top of the surface. Both samples were sintered at  $1420^\circ\text{C}$  – i.e. above the eutectic temperature - for 2 h soaking period in vacuum (in Bähr DiL 801). After sintering each sample was cut across the height, embedded and polished.

For better visualisation of the depth of penetration of Si into the molybdenum body, each sample was analysed by SEM-EDAX.

### 3.3.1.2.1 SEM-EDAX of sample with Si powder pressed on it

In fig. 3.73 some BSE images with elemental mapping can be observed. The cross section of the Mo sample with pressed Si powder on the top of the surface after sintering at 1420°C for 2 h in vacuum can be seen. The depth of Si penetration into the Mo body is about 200  $\mu\text{m}$ . Furthermore the Si covered the Mo grains very well. Moreover it has to be said, that no dramatic exothermic reaction could be observed, therefore the specimen retained its shape without disintegration. This means that lowering the specific surface of the Mo perform is a suitable way to control Si infiltration and silicide formation.

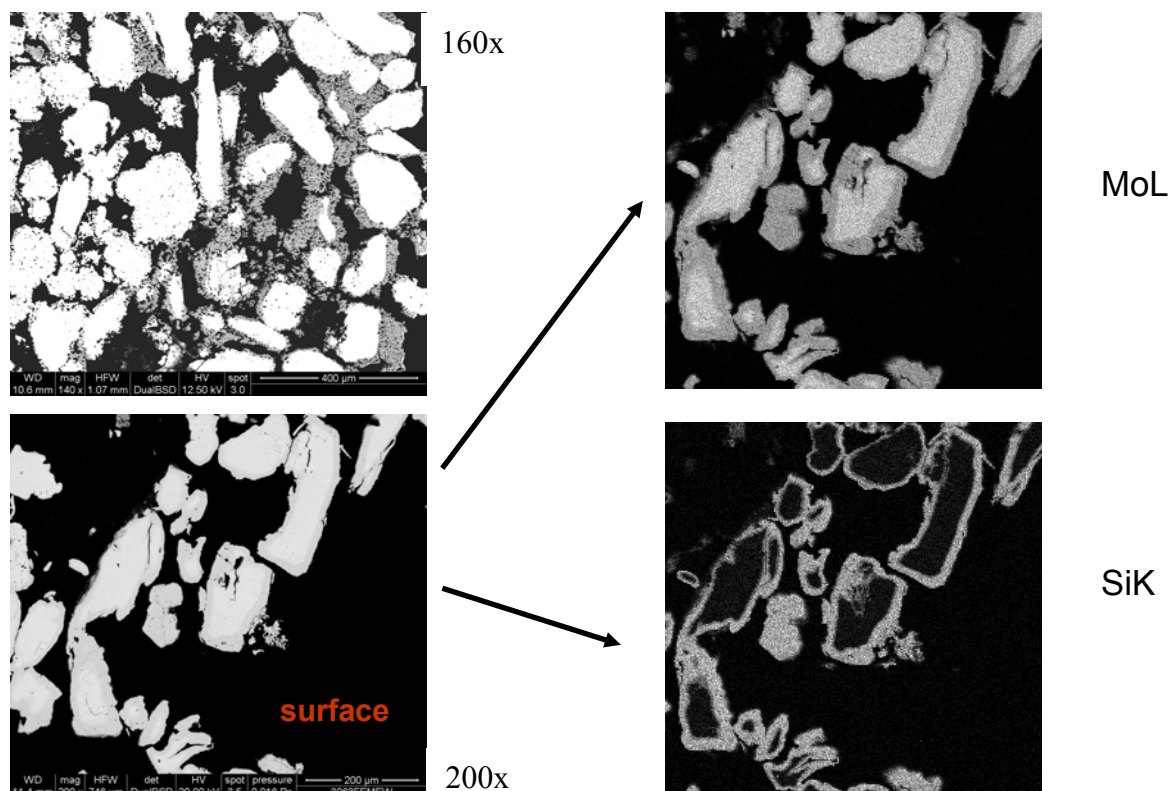


**fig. 3.73 Penetration of Si into the Mo body after pressing of Si powder on top of the Mo surface and sintering 1420°C for 2 h in vacuum; left: SE images; right side: Mo/Si mapping with elemental distribution**

### 3.3.1.2.2 SEM-EDAX of sample with Si wafer placed on the top of the surface

In fig. 3.74 some BSE images with elemental mapping can be observed. A Mo sample of Goodfellow Mo with Si wafer placed on top of the surface after sintering at 1420°C for 2 h in vacuum is demonstrated. It can be seen that the Si penetrated into the Mo body for 20  $\mu\text{m}$  depth. It is less than the infiltration by Si that was pressed as powder on the surface. Furthermore the Si does not cover the Mo grains very well. A concentration

gradient can be seen in fig. 3.74 in the elemental mapping of Si. The highest Si concentration can be seen near the surface.

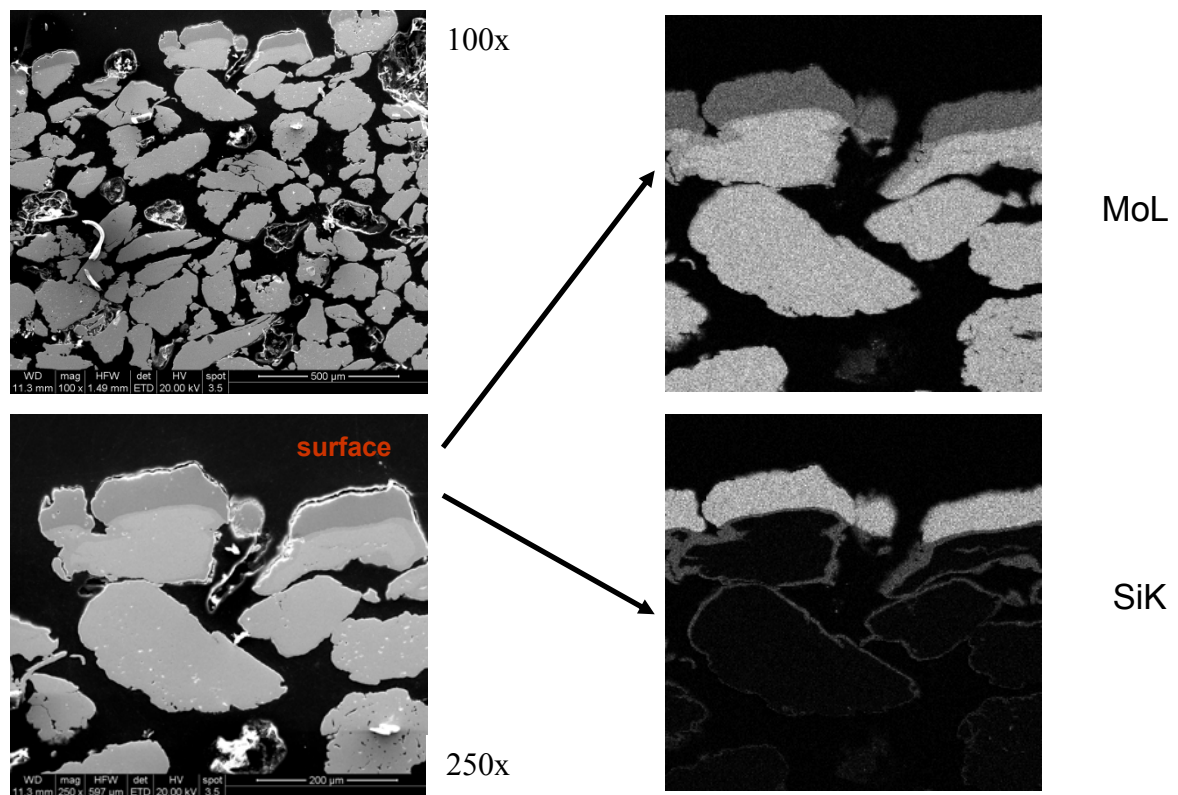


**fig. 3.74.:** Penetration of Si into the Mo body after placing an Si wafer on top of the Mo surface and sintering 1420°C for 2 h in vacuum; left: SE images; right side: Mo/Si mapping with elemental distribution

The explanation why the pressed Si powder covered the Mo grains better is that by pressing the powder on the surface of the Mo body, it was easier for the Si to enter the cavities (pores) of the specimen. When Si starts to melt, it can move very easily through the pores in vertical direction.

Nevertheless it could be shown that with enough big pores it is possible for Si to infiltrate the pores of a Mo body before reacting and closing the pores for further infiltration.

### 3.3.1.3 Mixtures of Goodfellow coarse Mo and fine grained Mo (CM)

In chapter 3.3.1 could be shown that it is possible to prepare Mo specimens with coarse pores which can be penetrated by Si without closing the pores before reaction. However, it was observed that the sintering contacts are very thin which resulted in disintegration during infiltration by liquid Si at IMSAS. The specimen was completely destroyed. The reason was that the coarse Mo particles from Goodfellow have a low

sintering activity due to low specific surface, and the compacted specimen had to be sintered for a longer period to achieve some mechanical stability. It was needed to insert a kind of binder into the Mo network which helps to get some stability. One possibility is to insert some fine grained Mo (which acts as a kind of binder with high sintering activity) into the coarse powder.

For this reason some samples were prepared from a bimodal mix from two Mo powders with different powder particle size. The first powder was the coarse Mo powder grade from Goodfellow with particle size  $\leq 355\mu\text{m}$ . The second powder was the Mo powder from Chemie Metall with a smaller particle size of  $\leq 63\mu\text{m}$ , according to the supplier's specification.

Both described powders were mixed at a ratio of 50 wt% of the coarse Mo powder from Goodfellow to 50wt% Mo (fine grained) powder from Chemie Metall. Both powders were mixed in a tumbling mixer for 2 h. Out of this powder mix five Charpy bars (55\*10\*10mm) were pressed uniaxially at 200 MPa compacting pressure on Jessernigg & Urban hydraulic press. The bars were presintered in hydrogen (2 l/min gas flow;  $\text{H}_2$  5.0 purity) at 1100°C and 2 h soaking period. Afterwards the samples were sintered in vacuum (KCE vacuum hot press, graphite heater, pressureless) at 1800°C for 2 h soaking period. After sintering all samples were characterised.

### 3.3.1.3.1 Mechanical properties

The density was measured by the geometrical dimensions and by Archimedes. The open porosity was calculated out of the values for the Archimedes density and the He-pycnometry density. The specific conductivity was measured on the "WT-Halbautomatisches Widerstandsmessgerät" at TUW and is given here both as absolute value and relative to the theoretical conductivity of Mo (18.2 MS/m). The fracture surface was characterised in the SEM and afterwards the broken sintering bridges were quantified using the "pixcal" program, the effective load bearing cross section  $A_c$  being determined [158]. By division of the area of broken sintering bridges in an image through the total image shown area, the percentage of sintered contacts can be calculated, the low deformation fracture required for reliable  $A_c$  values being given here. All values are summarised in tab. 22.

**tab. 22.: Some characteristics of the samples; literature values for the conductivity 18,2 MS/m (t.c)**

Sample	$\rho_{\text{geometrical}}$ [g/cm <sup>3</sup> ]	$\rho_{\text{geometrical}}$ [g/cm <sup>3</sup> ]	open porosity [%]	impact energy [J/cm <sup>2</sup> ]	spec. conductivity [MS/m]	L.B.cross section $A_c$ [%]
50 wt% CM : 50 wt% GF	$7,7 \pm 0,1$	$7,9 \pm 0,1$	$22,5 \pm 0,1$	$0,9 \pm 0,1$	$8,4 \pm 0,4$ 46 % t.c.	$20 \pm 0,3$
Mo from CM	$8,3 \pm 0,1$	$8,5 \pm 0,1$	$16,8 \pm 0,1$	$1,9 \pm 0,2$	$11,9 \pm 0,3$ 65 % t.c.	$60 \pm 0,2$

As can be observed in tab. 22 the density (geometrical and Archimedes), impact energy, specific conductivity and the L. B. cross section  $A_c$  of the mixed samples decreased compared to reference samples prepared from fine grained Mo only, as a consequence of the lower sintering activity of the mixed powder. Half of the powder is out of a



coarse Mo powder (GF) which has a lower sintering activity (due to the fact that this powder was apparently prepared out of ingots which were crushed after melting). The open porosity of the described samples increased. Not only the percentage increased but also the size of the pores. Because of the high amount of porosity and low load bearing cross section the impact energy of the measured samples is very low. An example of such a quantitative fracture surface analysis is given in fig. 3.75, the areas identified as broken contacts being depicted in blue.

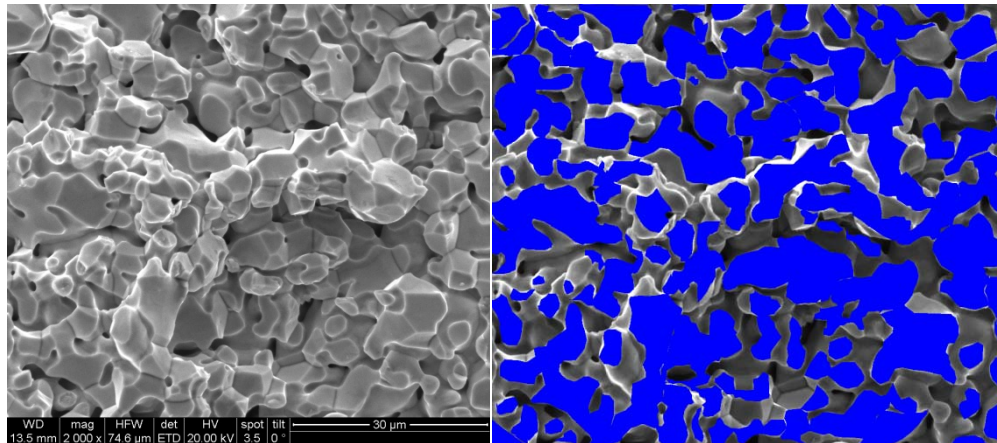


**fig. 3.75.: Fracture surface of a Mo sample (from Chemie Metall powder); left: SEM image – 2000x; right: SEM image after „pixcal“ quantification of the sintering contacts – blue colour;**

fig. 3.76 two fracture surfaces can be observed. All bars were presintered at 1100°C in H<sub>2</sub> (purity 5.0 and 2 l/min gas flow) for 2 h and sintered at 1800°C in vacuum with 2 h soaking period. On the left side the fracture surface of a bar prepared from the fine grained Mo from Chemie Metall can be seen. On the right side another fracture surface is shown, of a sample prepared from mixed powder (50 wt% Mo from Chemie Metall and 50 wt% Mo from Goodfellow). In the fracture surface of the mixed powder some big particles surrounded by small ones can be observed.

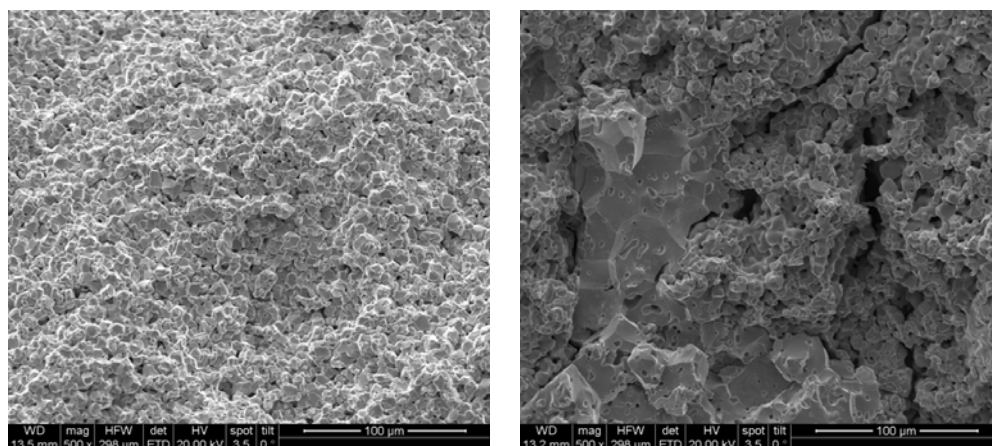


**fig. 3.76.: Fracture surface of Charpy bars ( 55\*10\*10 mm) from different powders - after presintering at 1100°C – 2h – H<sub>2</sub> and afterwards sintering at 1800°C – 2h – Vacuum; left: Chemie Metall powder; right: Goodfellow powder**



In the LOM images in fig. 3.77 the cross section of such a Mo specimen prepared out of 50 wt% coarse Mo from GF and 50 wt% fine Mo from CM described in tab. 22 were shown. Very big pores and also very small ones can be observed.

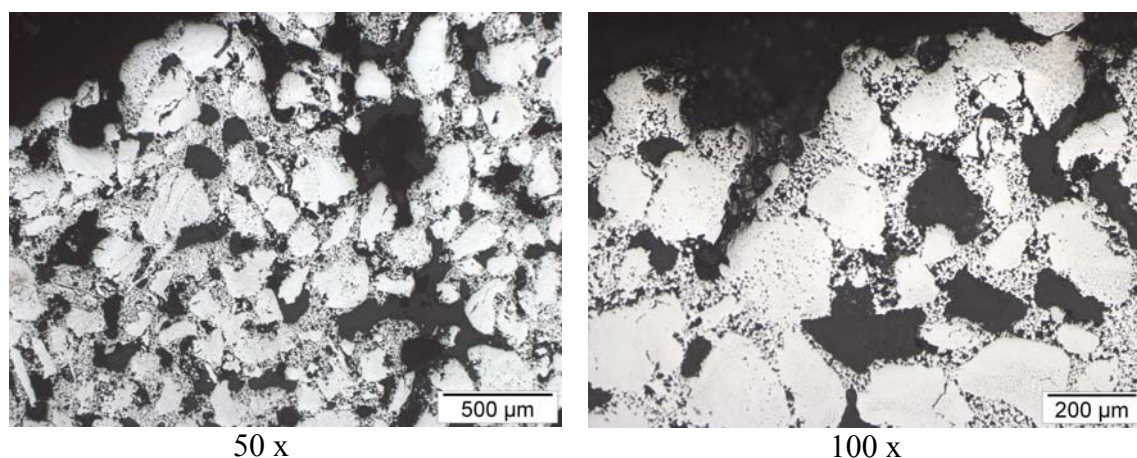


**fig. 3.77.: LOM images of cross section of Charpy bars ( 55\*10\*10 mm) from specimen prepared out of 50 wt% CM and 50 wt% GF molybdenum - after presintering at 1100°C – 2h – H<sub>2</sub> and afterwards sintering at 1800°C – 2h – Vacuum; left: 50 x and right: 100 x**

### 3.3.1.4 Characterisation of samples after Si treatment by partners

#### *Sample from batch 1378*

The sample was prepared at TUW from two molybdenum fractions and sent afterwards for CVI to ATL. The two Mo fractions were mixed 50:50 for further sample preparation. One fraction was Chemie Metall Mo ( $\leq 63\mu\text{m}$ ) and the second one was Goodfellow Mo ( $\leq 355\mu\text{m}$ ), as described in chapter 3.3.1.3. These two Mo powders were mixed for 2 h on a tumbling mixer. The sample was pressed with 200 MPa uniaxially in a cylindrical die ( $\varnothing=11,27$  mm) on Amsler hydraulic press. Afterwards the sample was presintered at 1100°C for 2 h in H<sub>2</sub> (5.0 purity; 2 l/min gas flow) and sintered at 1800°C for 2 h in vacuum. The density of the specimens was 7.7 g/cm<sup>3</sup> and the open porosity 23 %.

For analysis of the CVI treated specimens it was necessary to cut the sample along the diameter. The sample was embedded in Araldite, ground and polished.

#### 3.3.1.4.1 LOM

In fig. 3.78 some LOM images of the polished microsection of the sample are shown. Near the surface a light blue layer appeared. It can be seen in the 50x magnification image that the layer is not uniformly distributed around the sample. At 500x magnification a grain is demonstrated that is surrounded by a light blue layer. Some small blue particles are around. The small particles come from the fine grained Mo particles (from CM) that reacted with Si.

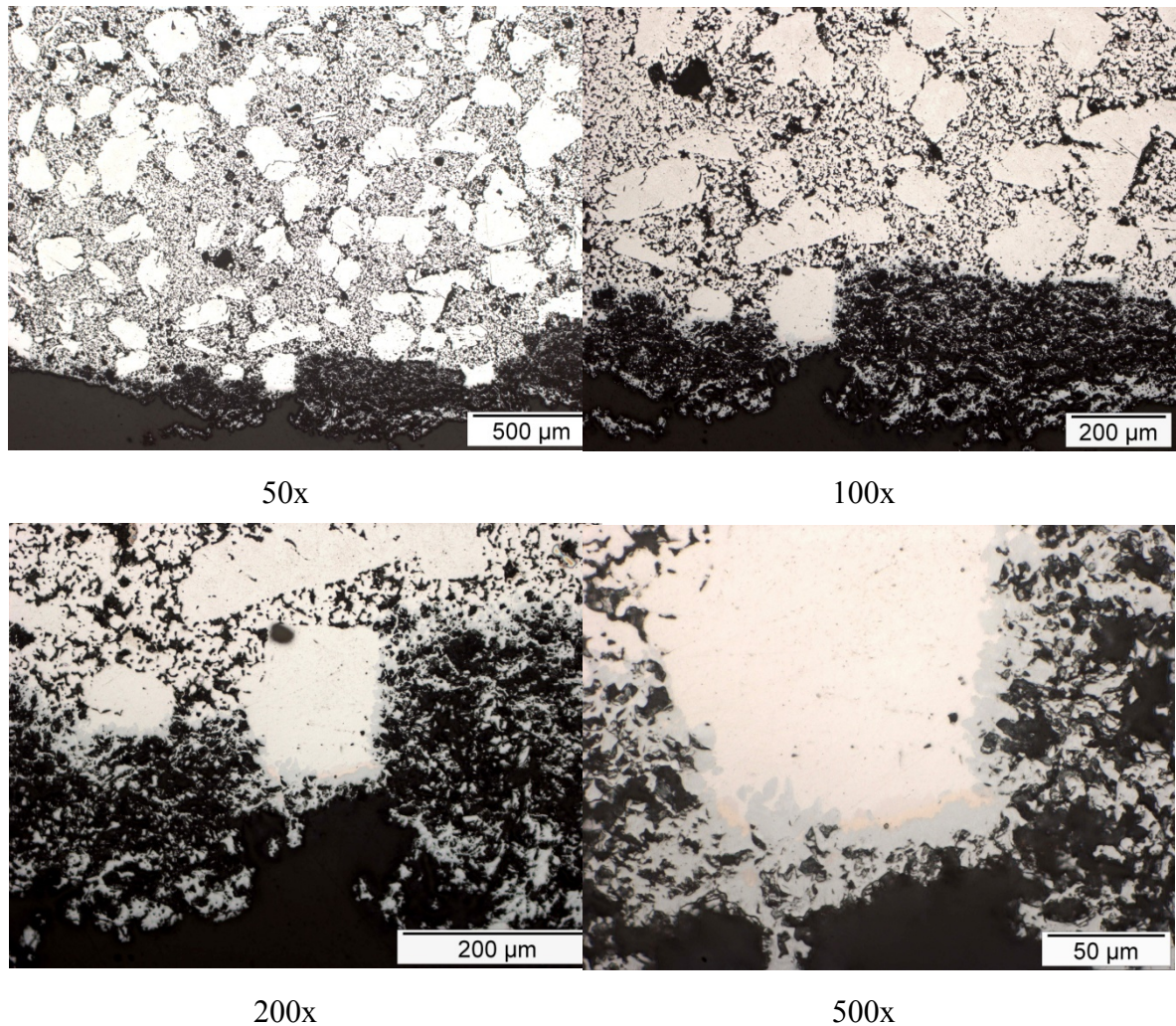


**fig. 3.78.: LOM images of Mo sample after CVI at ATL**

#### 3.3.1.4.2 SEM

In fig. 3.79 some BSE images of a polished microsection depicting a Mo specimen from TUW after CVI at ATL are shown. A grey layer can be observed (in LOM a blue layer). This layer was analysed on the EDAX. It can be seen very well that the darker grey layer is somehow destroyed. A sponge-like structure is formed due to exothermic reaction and volume changes due to formation of silicides. The Kirkendall porosity plays also a major role.



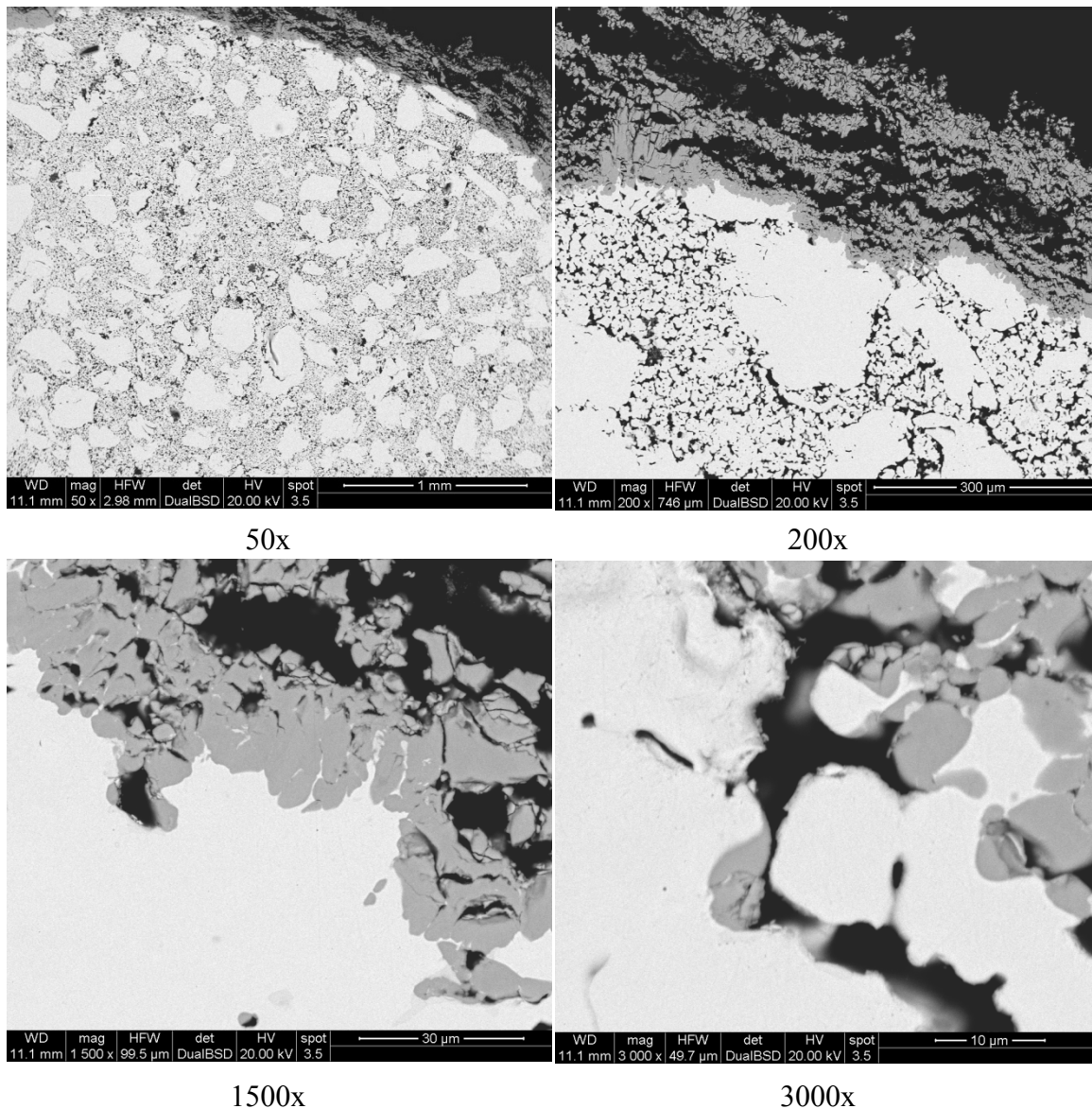


fig. 3.79.: BSE images of Mo sample after CVI at ATL

### 3.3.1.4.3 EDAX

In fig. 3.80 one part of the sample was zoomed out and analysed by EDAX. In the darker grey area about 38% Si was measured ( $\sim\text{MoSi}_2$ ) and in the light area just 0,5% Si. Furthermore an elemental mapping was prepared to reveal the distribution of Si and Mo. There is a clear boundary line between the silicon rich part and the “pure” Mo. It is surprising, that no further silicides were found between these two layers.

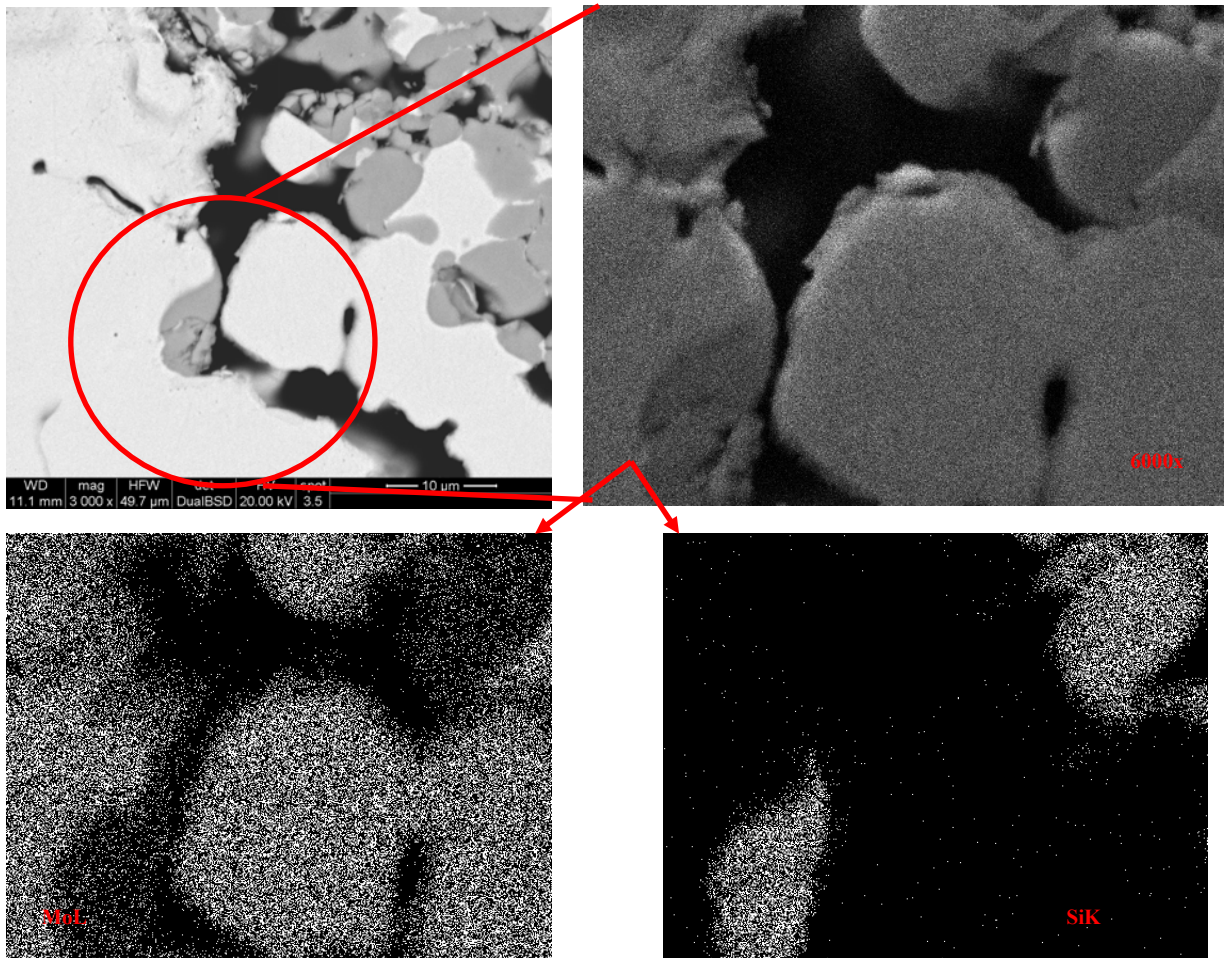


fig. 3.80.: EDAX analysis of Mo sample after CVI at ATL

#### 3.3.1.4.4 Hardness

The hardness was measured with 0.5 kp indentation load (HV0,5) near the surface. The measurement was taken in the Si layer around a Mo grain and inside the grain. In the Si layer the hardness was  $1135 \pm 26$  HV0,5 and in the grain it decreased to  $169 \pm 16$  HV0,5. It has to be mentioned that the microhardness of the Si containing layer was measured in the grains themselves not in the Si containing layer which surrounds the specimen (this one was too brittle for measurement).

### 3.3.1.5 Compacts from bimodal Mo powders infiltrated with Si by IMSAS

The sample preparation was the same as already described in chapter 3.3.1.3. One Mo sample out of two different Mo powder sizes was prepared. One was the fine grained Mo from Chemie Metall and the second Mo powder was the coarse Mo (Goodfellow). Both powders were mixed at a ratio of 50 wt% Mo CM to 50 wt% Mo GF. The sample out of this powder mixture was pressed uniaxially in a cylindrical die ( $\varnothing=11,27$  mm). The specimen was presintered at 1100 °C for 2 h soaking period in H<sub>2</sub> (purity 5.0; gas flow 2 l/min) and sintered afterwards in vacuum at 1800 °C (2 h soaking period). The sample was sent to IMSAS for infiltration with Si.

After infiltration at IMSAS the sample was sent back to TUW for further characterization. In fig. 3.81 the embedded sample is shown. Three layers can be observed. There is a thin outer layer followed by a thick intermediate layer and the core in a dark colour. The sample was characterized by LOM and SEM and EDAX.



fig. 3.81.: Embedded sample; 3 different layers can be observed

#### 3.3.1.5.1 LOM

All three layers can be observed in the light microscope. The layers and the transition zone between the layers were characterized as described in the following.

##### ***Outer part – near-surface layer***

The outer part of the sample can be observed in fig. 3.82. There is a difference in colour. The outer layer appears darker and more porous. There are some big pores or rather some spalled parts of Mo<sub>x</sub>Si<sub>y</sub> due to exothermic reaction during infiltration. Nevertheless it is evident that the specimen did not disintegrate during infiltration, as had been the case with previous compacts that had been sintered at lower temperature. This indicates that sufficiently intense sintering results in specimen strength that enables withstanding the stresses during reaction with liquid Si. Probably also the lower specific surface, as a consequence of using coarser powders, is also helpful in lowering the reactivity towards the Si melt.



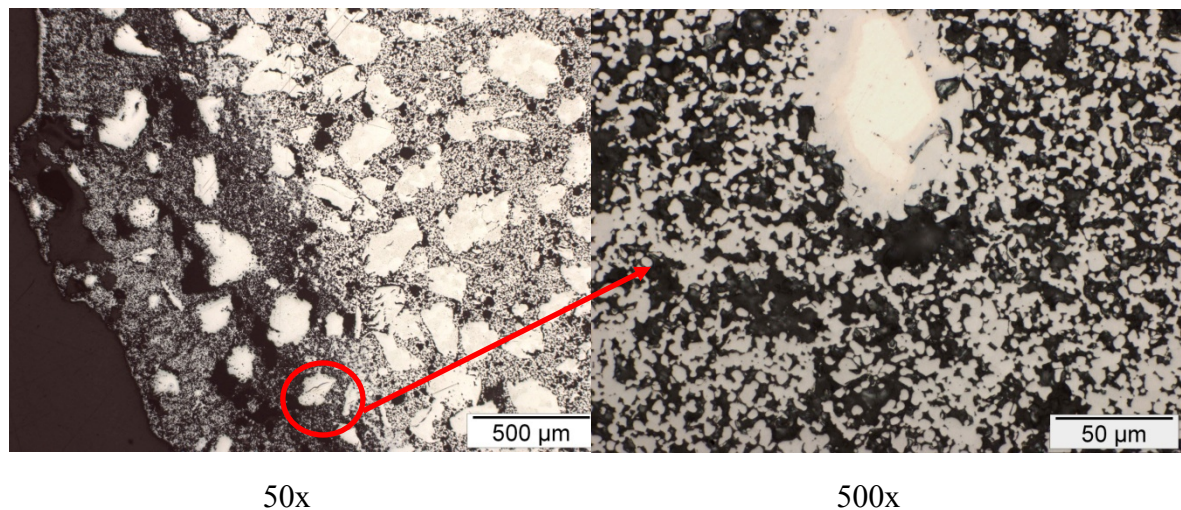


fig. 3.82.: LOM of the near-surface layer

#### *Intermediate part – between surface layer and core*

The intermediate area and the transition zone to the core can be observed in fig. 3.83. The intermediate area still shows porosity. In fig. 3.83 at 50x magnification the transition zone and the core on the right side of the image can be seen. The transition zone appears more porous in this image. One explanation can be given that during the cutting and metallographic preparation more particles broke out of the transition zone matrix. In this part of the specimen more Si is inside, therefore more silicides  $\text{Mo}_x\text{Si}_y$  were formed. The difference in hardness is bigger between silicides and Mo. Due to mechanical stresses during cutting or metallographic preparation some of the silicides broke out. On the other hand, the pores could remain after infiltration with Si. It is quite surprising that the core of the specimen appears dense. Before infiltration the porosity was uniformly distributed along the whole specimen, which can be seen in fig. 3.77.

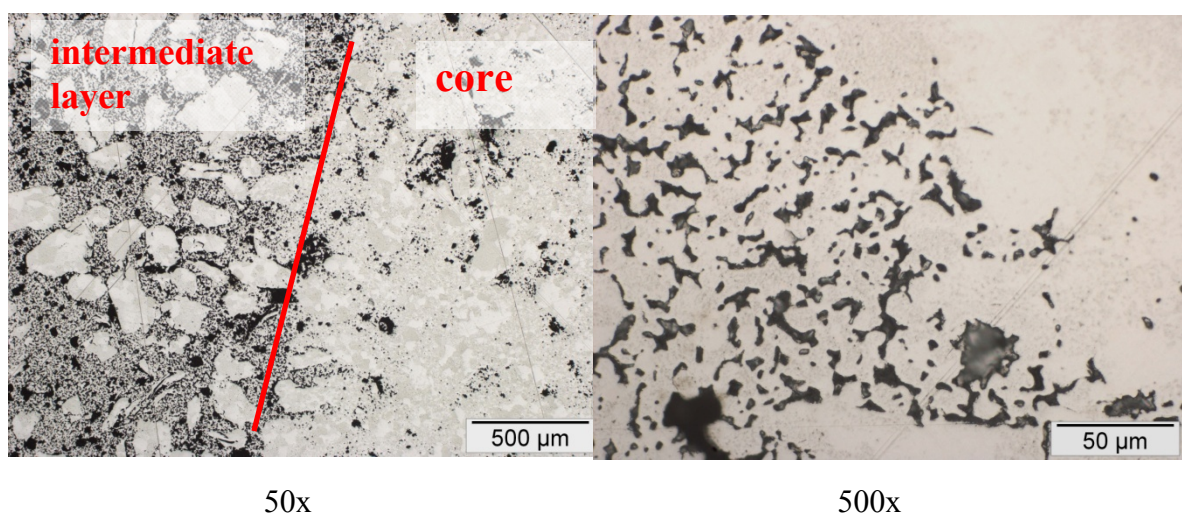


fig. 3.83.: LOM of the intermediate layer



### Core

In the core (fig. 3.84) there are still some regions containing pores but compared to the other layers it is the most compact one.

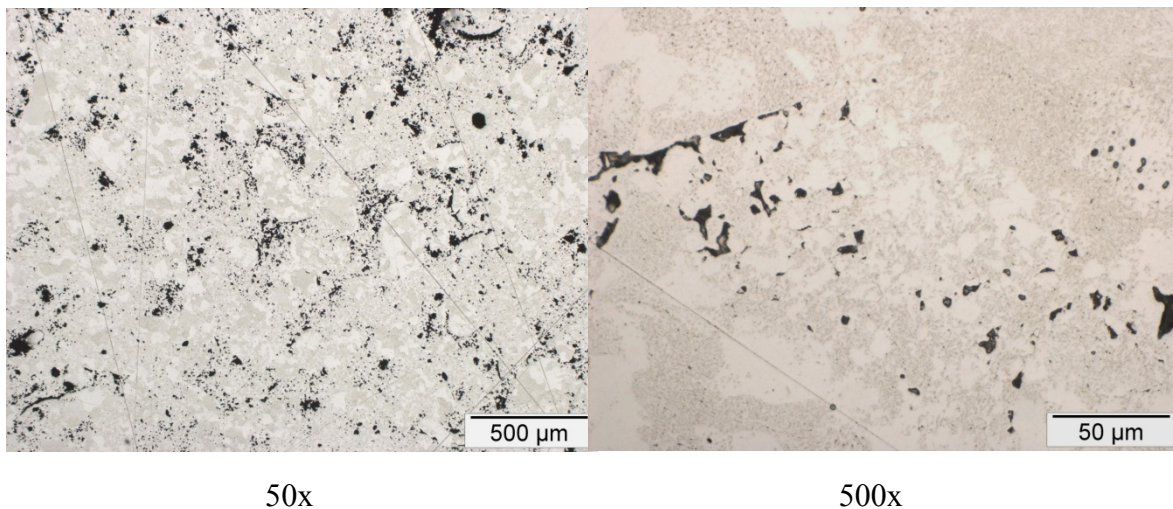


fig. 3.84.:LOM of the core layer

### 3.3.1.5.2 SEM

In fig. 3.85 two magnifications of the sample cross section can be observed. At 50x magnification all three layers can be observed. At 100x magnification the partially spalled-off parts of the outer layer can be seen.

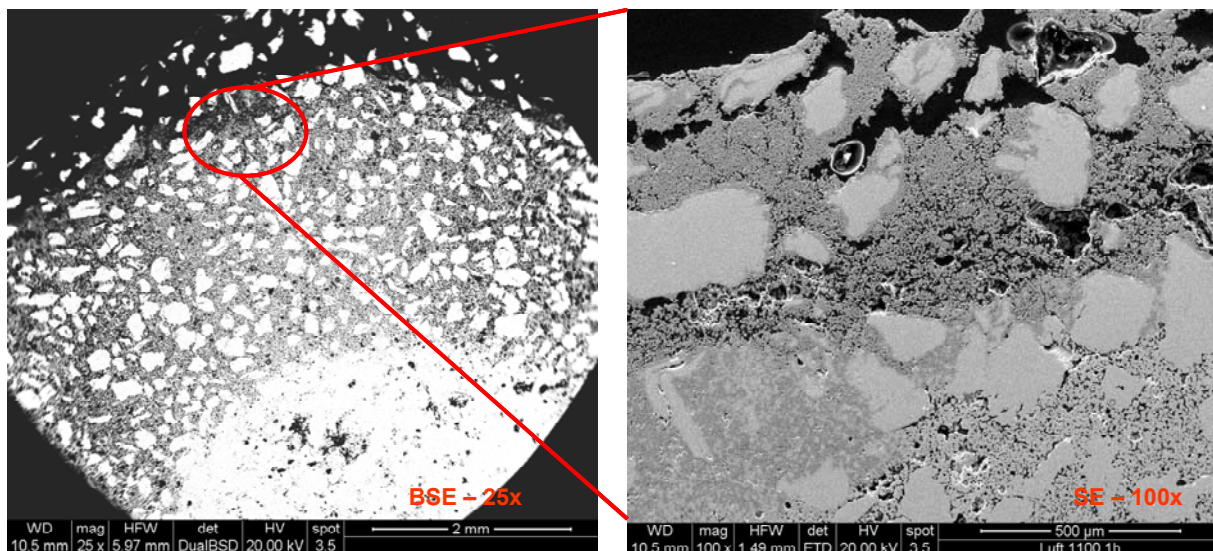


fig. 3.85.: BSE images of the three layers of the infiltrated specimen

## 3.3.1.5.3 EDAX analysis

By EDAX analysis it was possible to describe the different parts of the sample that occur in fig. 3.86 in different colours. The darkest particles with ~36 wt% Si are  $\text{MoSi}_2$ , the lighter one with ~16 wt% Si are  $\text{Mo}_5\text{Si}_3$  and the lightest particles which form the core of some big grains show a very low value of Si, with 0,3 wt% Si. It can be observed that the core of each particle is very well covered by  $\text{Mo}_5\text{Si}_3$  and  $\text{MoSi}_2$  as outer shell.

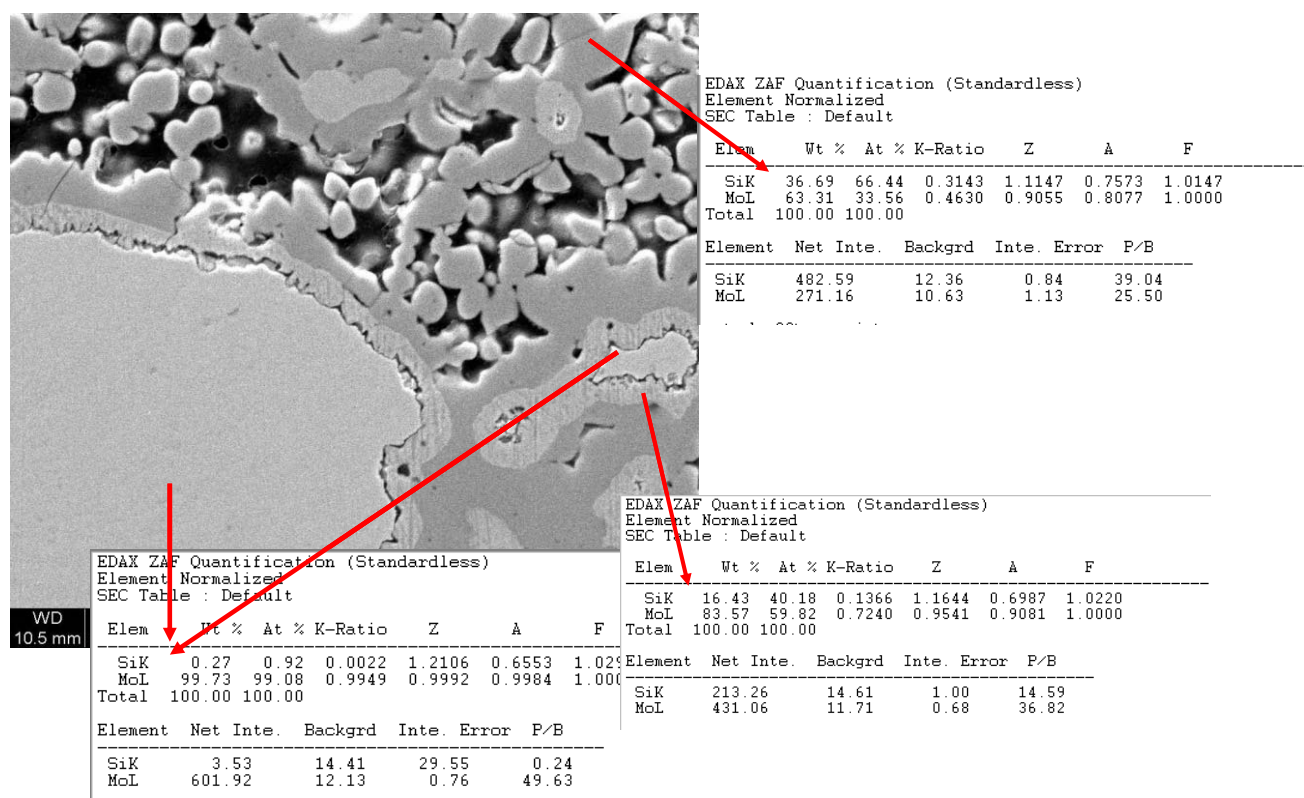


fig. 3.86.: EDAX analysis of one infiltrated part of Mo specimen after infiltration at IMSAS



### 3.3.1.5.4 Mapping

The distribution of silicon and molybdenum could be visualised by an elemental mapping (fig. 3.87). No diffusion zone between the layers can be observed. There is a sharp separation of the layers, indicating formation of discrete phases, which agrees well with the Mo-Si phase diagram.

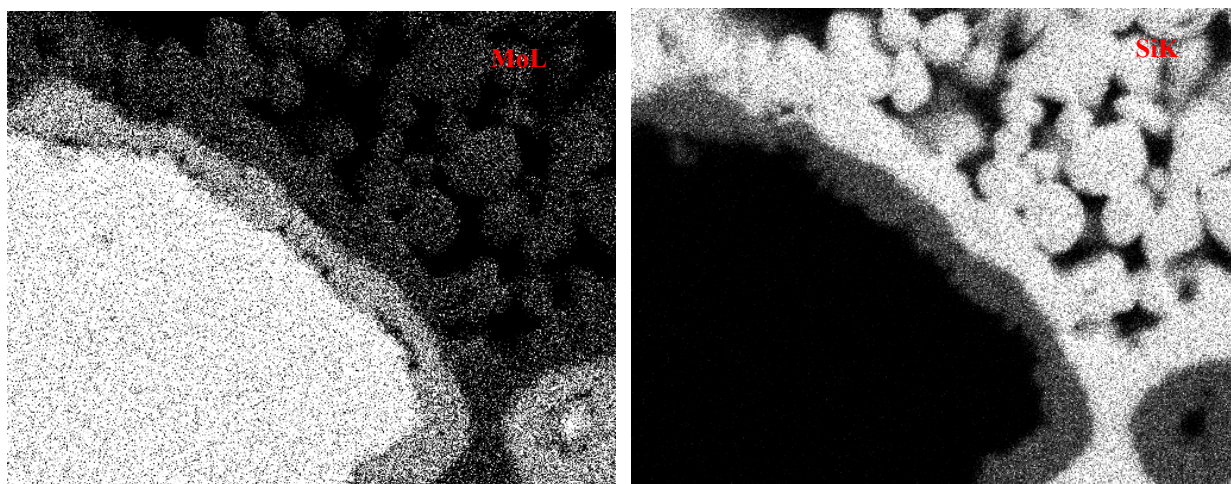


fig. 3.87.: Elemental mapping (1600x)

### 3.3.1.6 Summary: molybdenum samples from Goodfellow powder < 355 $\mu\text{m}$

In the first experiment the properties of a Mo specimen out of a very coarse Mo powder were examined. Some previous experiments were carried out to press the specimen. It was quite impossible to press a specimen of such coarse powder without additive. Therefore a wax was added. The Goodfellow Mo (< 355  $\mu\text{m}$ ) was mixed with 1 wt% Kenolube P11 wax and 1 wt% Ni as sintering activator. The pressing was carried out in a cylindrical die with 11,27 mm diameter and 200 MPa uniaxially. After debinding at 600 °C for 2 h in  $\text{N}_2$ , sintering followed at 1300 °C for 2 h soaking period in  $\text{H}_2$ . In the LOM images (fig. 3.72) the cross section after sintering could be observed. Very coarse pores could be seen and less sintering contacts. The microhardness was measured, too. The sintering contacts were weaker with  $287 \pm 26 \text{ HV } 0,01$  than the grains with  $340 \pm 12 \text{ HV } 0,01$ . After Si infiltration by IMSAS such a specimen disintegrated due to the weak sintering bridges.

In a further experiment the reaction vs. infiltration was examined. Specimens described above were taken as skeleton out of Mo and in the first experiment Si powder was pressed on the sample surface and in the second experiment a Si wafer was placed on the surface. After heating up to 1420 °C (> eutectic temperature) and cooling down, the specimen were cut and the cross sections were metallographic prepared and observed on the LOM (fig. 3.73 and fig. 3.74). It could be seen very easily that the Si powder could penetrate deeper into the specimen due to the fact that the powder particles were smaller and could fill up better the pores. In both cases the Si did not react exothermically

destroying the specimen. Furthermore the infiltration by Si occurred at first before the reaction.

For a better cohesion of the very coarse Mo particles a binder was needed. A fine grained Mo powder was inserted at a ratio 50 wt% fine grained Mo from Chemie Metall to 50 wt% coarse Mo from Goodfellow. The specimen was pressed with 200 MPa and presintered at 1100 °C for 2 h in H<sub>2</sub> followed by sintering at 1800 °C for 2 h soaking period in vacuum. In tab. 22 some characteristics compared to a specimen which was out of a fine grained Mo are given. The density with 7,7 g/cm<sup>3</sup> was lower and the open porosity with 22,5 % higher than the one from Mo specimen out of a fine grained powder. The fracture surface was analysed for the amount of sintering contacts (in [%]) of both specimens. The sample body out of the mixed powder showed more big pores and less sintering contacts between the particles, therefore the load bearing cross section was measured as 20 % instead of 60 % in the fine grained one.

Such Mo sample that was prepared at TUW (out of mixed Mo – 50 wt% coarse Mo with 50 wt% fine grained Mo; presintered at 1100°C in H<sub>2</sub> followed by sintering at 1800°C in vacuum – 2 h) was infiltrated with Si by CVI at ATL and in a further experiment by Si melt infiltration at IMSAS.

Both specimens were cut along the diameter and investigated by LOM and SEM.

In the CVI specimen from ATL a sponge-like outer layer in darker grey colour could be observed in the LOM (fig. 3.79). The EDAX analysis (fig. 3.80) helped to analyse the different coloured areas. The dark grey one contained about 38 wt% Si (~MoSi<sub>2</sub>) while the lighter one area contained just 0,5 wt% Si. There is a clear boundary line between the silicon rich part and the plain Mo. Surprisingly, no intermediate silicides were found.

The hardness was measured with 0,5 kp indentation load (HV0,5) near the surface. The hardness of the Mo containing Si-layer (dark grey appearing) was 1135 ± 26 HV 0,5 and in the grain it decreased to 169 ± 16 HV 0,5.

In the Mo specimen infiltrated with Si by IMSAS after cutting along the diameter the three different layers could be observed that varied in colour and Si content. The outer layer was the most brittle one, with the highest Si content, the surface tending to spall off due to the exothermic reaction. The core with barely any Si was the most stable part of the particle. EDAX analysis in fig. 3.86 near the surface showed some diffusion of Si into the particles. Different Mo<sub>x</sub>Si<sub>y</sub> phases were formed. Some parts were containing 36 wt% Si (MoSi<sub>2</sub>), some 16 wt% Si (Mo<sub>5</sub>Si<sub>3</sub>) and in the core of some big particles only 0,3 wt% Si could be measured, indicating virtually plain Mo.

In any case, however, these experiments showed that porous Mo compacts can be infiltrated with liquid Si without disintegration if they have been well sintered. Furthermore, also the use of coarser Mo powder, which results in lower specific surface, may be helpful to better control the reaction between Mo and the Si melt.



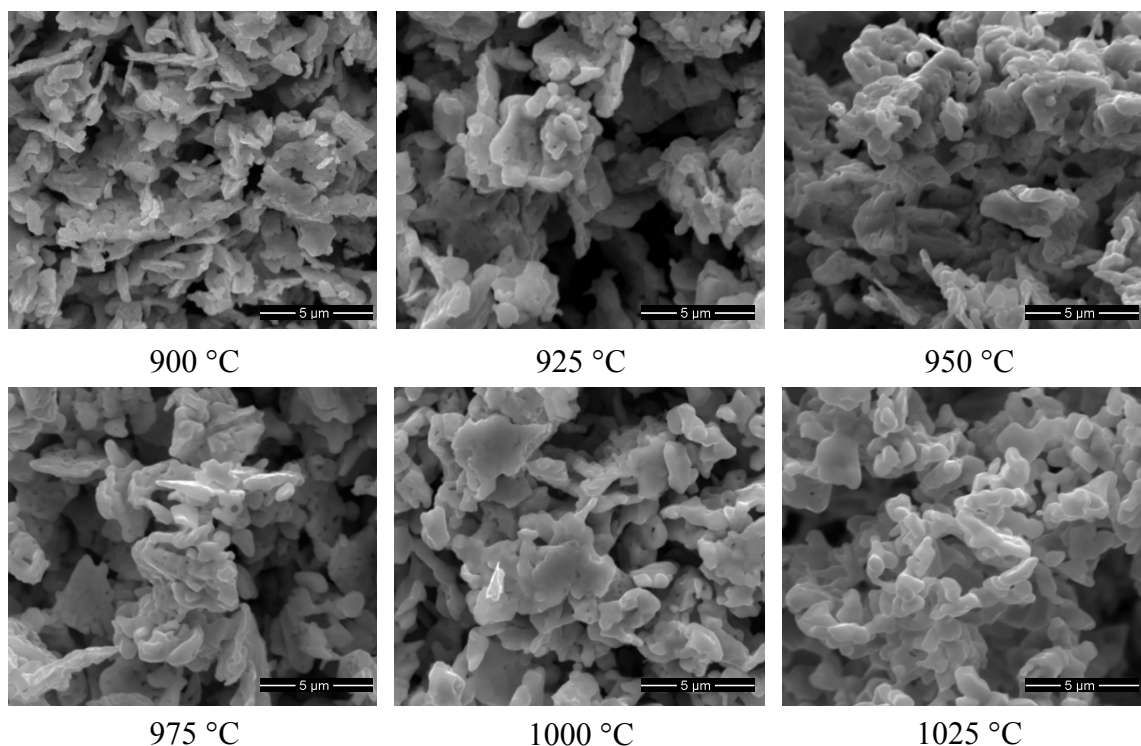
### 3.3.2 Preparation of coarse molybdenum powders and samples

#### 3.3.2.1 Reduction of MoO<sub>2</sub>

From reduction experiments of tungsten it was known that by control of atmosphere conditions and reduction temperature, it is possible to receive a coarse tungsten powder. It was assumed from tungsten experiments that also the morphology of Mo powders can be influenced by the different partial pressures of water compared to hydrogen (in the MoO<sub>2</sub> --> Mo stage). The higher the partial pressure of the water vapour, the coarser are the resulting particles. The reduction process was discussed in detail in the literature (chapter 1.2.2). Related to the literature about the coarsening of tungsten by reduction, similar experiments with reduction of MoO<sub>2</sub> were carried out. An MoO<sub>2</sub> powder from KE (information from KE: Chemie Metall MoO<sub>2</sub>) was reduced in two ways, in dry and in humid H<sub>2</sub> atmosphere. As reducing agent hydrogen (5.0 purity) was taken. The particle size and shape of Mo obtained by reduction in dry and humid atmosphere were compared. For the MoO<sub>2</sub> powder (from KE) an oxygen content of 18,3±0,1% was measured on Leco. Images of the MoO<sub>2</sub> can be found in fig. 2.5 and the XRD in fig. 2.6.

##### 3.3.2.1.1 Reduction in dry H<sub>2</sub> atmosphere

The MoO<sub>2</sub> powder from KE was filled into an Mo boat and reduced at different temperatures [°C] for 1 h soaking period in dry H<sub>2</sub> (5.0 purity; 2 l/min gas flow). The height of such powder was about 15 mm, which is equivalent to a weight of app. 70 g Mo powder. The reduction temperature was varied between 900 and 1100°C in steps of 25°C. During the heating, cooling and soaking periods H<sub>2</sub> was passing through the furnace tube. All reduced powders were characterized in the SEM (fig. 3.88) and by measuring the oxygen content.



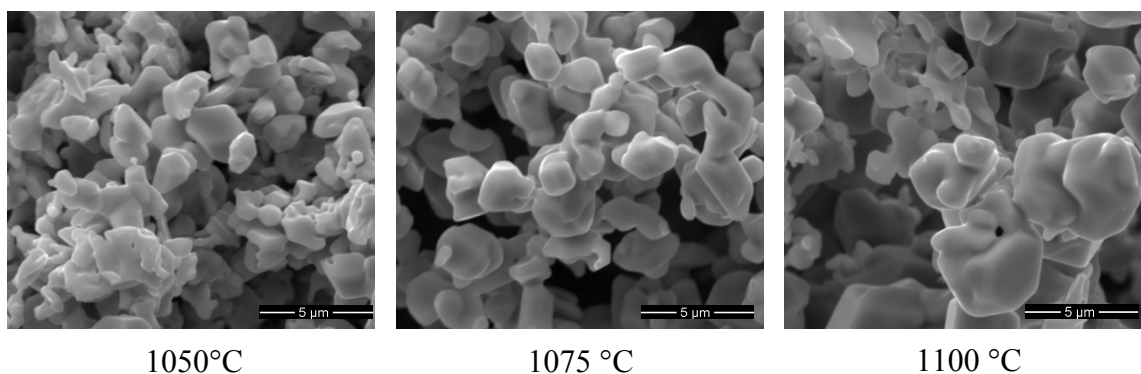


**fig. 3.88.:** SEM images of  $\text{MoO}_2$  reduced at different temperatures between 900 and 1100 °C in 25 °C steps; all magnifications are 10000x; soaking period 2 h; atmosphere:  $\text{H}_2$  dry

It can be seen very well in fig. 3.88 that by increasing the reduction temperature the shape of the resulting particles is changing. After reduction at 900 °C the shape of the Mo particles remained in plate form. By increasing the temperature the edges of the particles rounded up which can be observed very well in fig. 3.88 - after 1000 °C reduction. The plates can still be recognised but the edges lost their shape. The first round shape can be recognised in the powder reduced at 1025 °C. After reduction at 1100 °C round particles of different sizes can be recognised. The biggest particles are about 5 µm in diameter.

#### ***Measurement of the oxygen content***

The O content was measured on the LECO analyzer TC-400. All values of the O content measured for each powder are summarized in tab. 23. All values are an average of three parallel measurements.

**tab. 23.:** Content of oxygen and nitrogen in Mo after reduction in  $\text{H}_2$

reduction temperature [°C]	oxygen [%]	nitrogen [%]
900	$0,357 \pm 0,14$	$0,061 \pm 0,006$
925	$0,241 \pm 0,03$	$0,064 \pm 0,013$
950	$0,184 \pm 0,02$	$0,048 \pm 0,009$
975	$0,202 \pm 0,05$	$0,048 \pm 0,005$
1000	$0,132 \pm 0,01$	$0,033 \pm 0,005$
1025	$0,146 \pm 0,00$	$0,042 \pm 0,002$
1050	$0,162 \pm 0,08$	$0,022 \pm 0,010$
1075	$0,199 \pm 0,03$	$0,001 \pm 0,015$
1100	$0,229 \pm 0,10$	$0,026 \pm 0,006$

The values from tab. 23 are graphically shown in fig. 3.89. With increasing temperature up to 1000°C the oxygen content is decreasing. Above 1000°C the oxygen content is increasing again. Above 1000 °C the partial pressure of the water vapour is changing in the atmosphere and the reduction of  $\text{MoO}_2$  is less favoured.

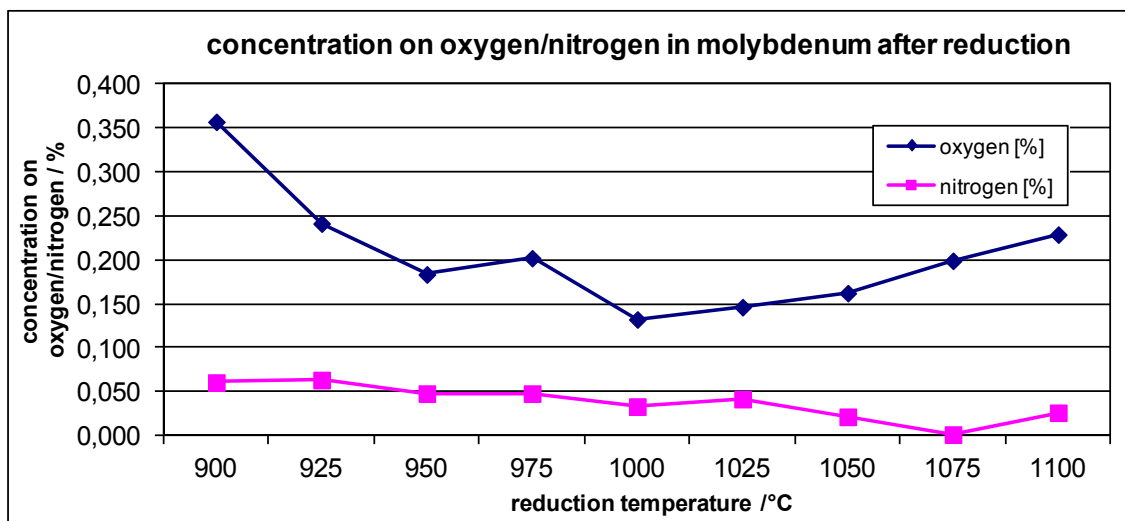
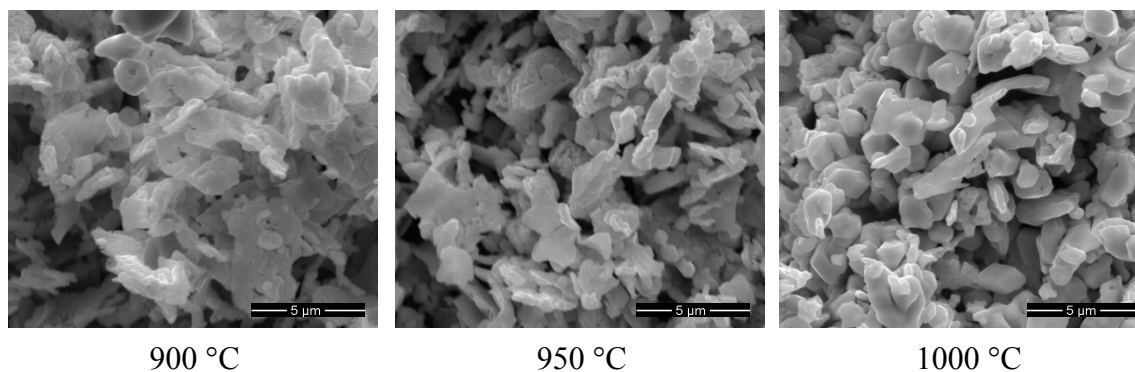


fig. 3.89.: Oxygen/nitrogen content of Mo reduced from MoO<sub>2</sub> as a function of the reduction temperature

The best reduction temperature to achieve a low oxygen Mo powder (a pure Mo without oxides) is 1000 °C.

#### 3.3.2.1.2 Reduction in humid H<sub>2</sub> atmosphere

All powders were reduced between 900 °C and 1100 °C in 50 °C steps for 1 h in H<sub>2</sub>. Before the H<sub>2</sub> entered the superalloy retort of the AHT furnace it passed a gas-washing bottle filled with water. In a further experiment the layer bed height, i.e. the thickness of the bulk Mo oxide powder in the boat, was changed from 15 mm to about 35 mm. A higher MoO<sub>2</sub> loose powder bed results in a higher humidity inside the powder bed. For tungsten it has been observed that with higher humidity the particle size of the reduced powder increases. In the last experiment the reduction was carried out in a mixture of Ar:H<sub>2</sub> = 95:5, which should result in still higher humidity in the powder bed, at least in a still higher ratio H<sub>2</sub>O/H<sub>2</sub>. For the characterisation of the powders SEM images were taken (fig. 3.90) and the oxygen content was measured on the LECO analyzer.



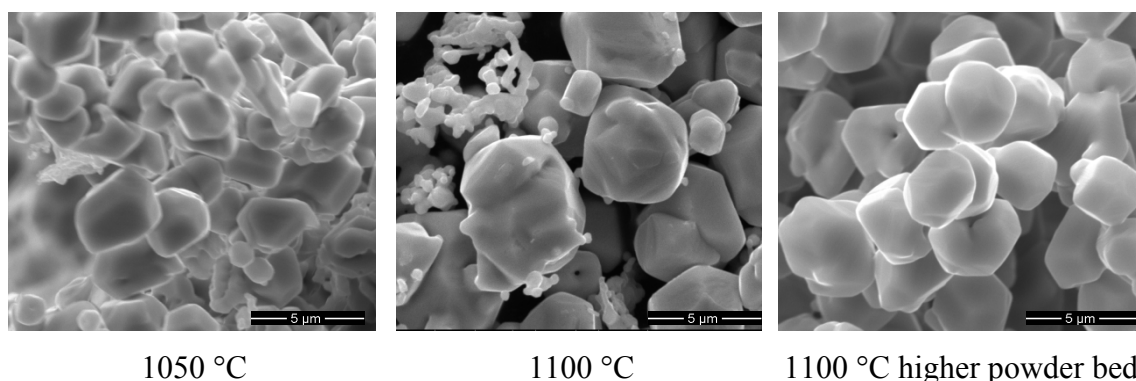


**fig. 3.90.:** SEM images of MoO<sub>2</sub> reduced at different temperatures between 900 and 1100 °C in 50 °C; all magnifications are 10000x; soaking period 2 h; atmosphere: H<sub>2</sub> humid

With increasing reduction temperature the shape of the particles is changing, too, which can be observed very well in fig. 3.90. At 900°C reduction temperature the particles are still very angular. Already at 1000°C the edges of the particles start to be rounded. At 1050°C most particles are octahedral with round edges. By increasing the temperature to 1100°C all particles are round shaped. Furthermore a bimodal distribution of the particle size can be observed. The biggest particles are about 5 µm. In fig. 3.90 - 1100 °C higher powder bed the particles are all of the same size of ~ 5 µm. Compared to the Mo powder which was reduced at the same temperature but in a lower powder bed it can be seen now that the particles are more uniform and not bimodal. However, the size of the biggest particles could not be increased comparing with particle size of Mo reduced in a dry H<sub>2</sub> atmosphere.

### ***Oxygen content of the reduced powders***

The oxygen content of the powder after reduction was measured on LECO TC400. After reduction the oxygen content decreased to 1% oxygen and below. By increasing the loose bed height the oxygen content of the powder dropped. The reduction in Ar with 5% H<sub>2</sub> does not work as expected. Only the outer part of the powder could be reduced. The inner part was still MoO<sub>2</sub>. Apparently the amount of H<sub>2</sub> offered for reduction was too low to reduce also the core of the powder bed. To reduce 1 g MoO<sub>2</sub> 0,0156 mol H<sub>2</sub> will be necessary. About 100 g MoO<sub>2</sub> have been filled in to the boat which means that 1.56 mol H<sub>2</sub> are needed. For the equilibrium of the reduction twice as much H<sub>2</sub> is needed. Theoretically an excess of H<sub>2</sub> was used. Only the outer part of the powder bed was analysed for the oxygen content. The analysed powder showed an oxygen content of about 12% which is only 6% below the value (measured also on LECO) for the KE MoO<sub>2</sub> powder. In tab. 24 a summary of all measured oxygen values is given.

**tab. 24.:** Oxygen concentration of Mo after reduction in humid H<sub>2</sub>

temperature of reduction [°C]	oxygen [%]	nitrogen [%]
900	1,04 ± 0,07	0,00 ± 0,04
950	1,05 ± 0,14	0,00 ± 0,01
1000	0,70 ± 0,18	0,03 ± 0,02
1050	0,56 ± 0,07	0,02 ± 0,01
1100	0,51 ± 0,04	0,03 ± 0,02
1100 (↑ layer height)	0,39 ± 0,12	0,03 ± 0,03
1100-(Ar:H <sub>2</sub> =95:5)	12,2 ± 3,75	0,02 ± 0,04



The nitrogen concentration of each powder is very low. The oxygen content of the powder is decreased by increasing the temperature of reduction. The lowest oxygen content was measured for the powder reduced at 1100°C in a higher layer bed. In fig. 3.91 the oxygen content of all powder is graphically shown in dependence of the reduction temperature. Comparing the results for the reduction of  $\text{MoO}_2$  in dry hydrogen, it can be observed that the oxygen content of Mo (from dry  $\text{H}_2$  reduction) is much lower than the results achieved during humid  $\text{H}_2$  reduction. At 900 °C the oxygen content of dry  $\text{H}_2$  reduced Mo was 0,35% while the one for the humid  $\text{H}_2$  reduced Mo was higher at 1 %. The oxygen content of Mo reduced in dry  $\text{H}_2$  atmosphere could be lowered to 0,2 % at 1100 °C while in the Mo from humid  $\text{H}_2$  reduction still 0,5 % oxygen remains. Cooling down after reduction was carried out in dry hydrogen, therefore reoxidation should be excluded. Furthermore, no change in colour on the surface could be seen.

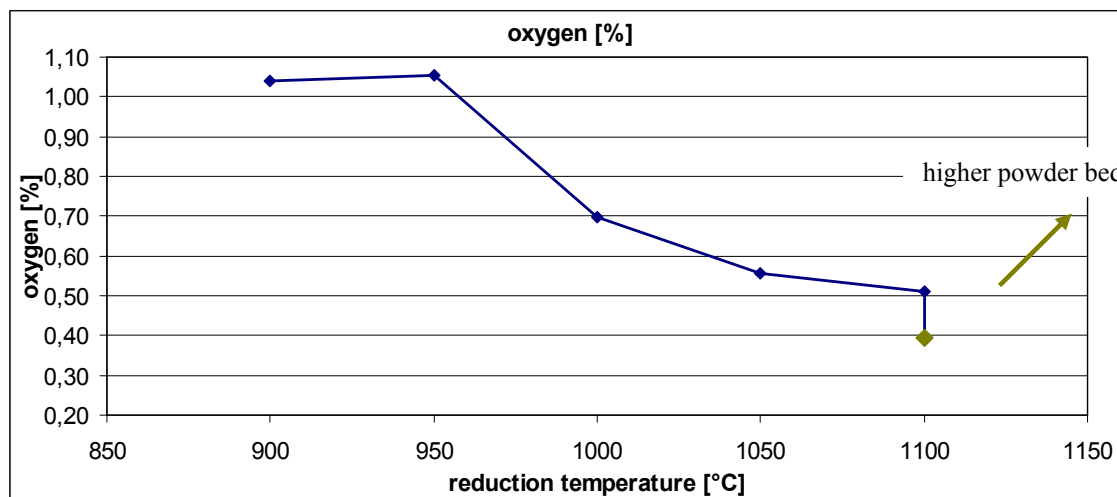


fig. 3.91.: Oxygen content as a function of the reduction temperature

Based upon the previous reduction experiments of  $\text{MoO}_2$  in humid  $\text{H}_2$  atmosphere, another experiment with a higher degree of humidity of  $\text{H}_2$  was carried out. The reduction of  $\text{MoO}_2$  goes through the gas phase and the formation of  $\text{MoO}_2(\text{OH})_2$  which was discussed in the literature. The higher the amount of water in  $\text{H}_2$  the coarser Mo particles are expected after reduction due to more of the volatile compound  $\text{MoO}_2(\text{OH})_2$  being available.

$\text{MoO}_2$  (from Chemie Metall; KE) was filled into a Molybdenum sintering boat at a powder bed height of about 30 mm. The sintering boat was placed in the AHT tube furnace at 1100°C in flowing  $\text{H}_2$ . Before entering the furnace the  $\text{H}_2$  had to pass a gas-washing bottle filled up with distilled water which was heated up (to boiling temperature). The  $\text{H}_2$  was thus saturated with hot water vapour and conducted through pipes into the furnace. Three experiments were carried out. In the first reduction experiment the pipes were not insulated, so that most of the water condensed in the pipes, and the humidity degree was probably fairly low in the furnace. In the second experiment the pipes were insulated by aluminum foil. Barely any water condensed while passing the pipes. About 60°C dew point was expected in the furnace. In the last experiment the second experiment was repeated but with an integrated three-way-cock

for separating the wet  $H_2$  reduction gas from the dry cooling  $H_2$ . After reduction all three Mo powders were characterized in the SEM.

### SEM

In fig. 3.92 Mo powder is shown after reduction at  $1100^\circ\text{C}$  for 2 h soaking period in humid  $H_2$  (5.0 purity; 2 l/min gas flow). Two different magnifications are showing the particle size and their distribution. Two different particle sizes can be observed. Small particles can be seen of approximately  $1\ \mu\text{m}$  diameter and bigger ones of about  $5\ \mu\text{m}$ .

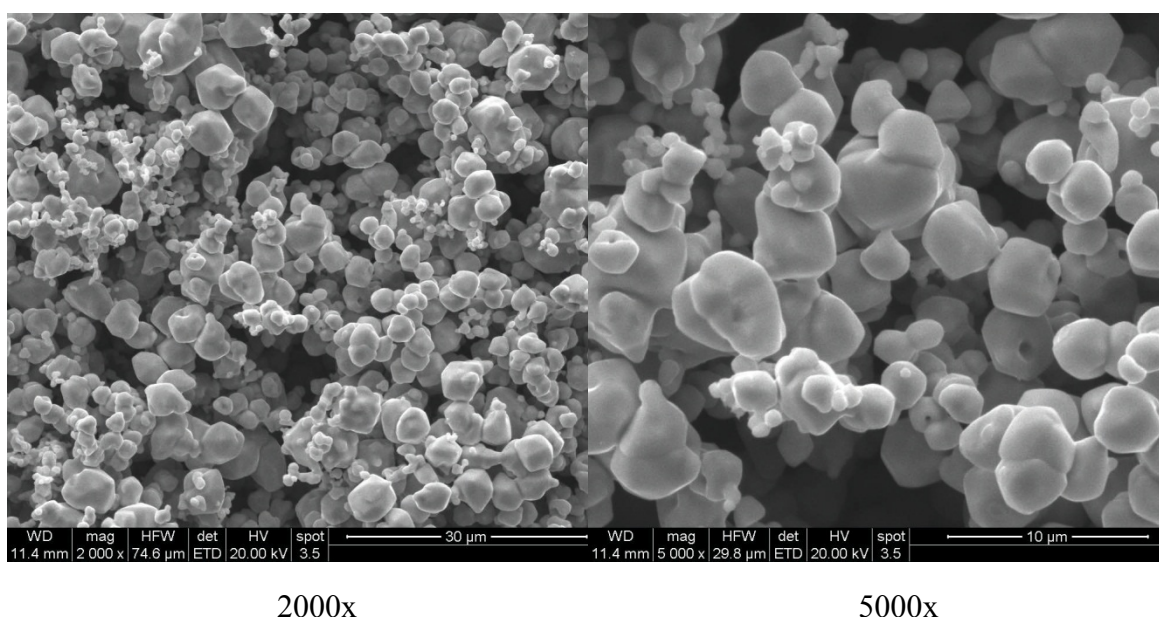


**fig. 3.92.:** SE images of Mo powder after reduction at  $1100^\circ\text{C}$  – 2 h –  $H_2$  (humid), non-insulated piping; left: 2000x; right: 5000x

It can be observed in fig. 3.93 that the Mo powder which was reduced at the same conditions as the one from fig. 3.92 but with a better insulated gas piping resulted in slightly larger particles. The homogeneity does not change. There are particles of two different sizes. The biggest particles are approximately  $8\ \mu\text{m}$  in diameter. The smallest particles do not exceed  $2\ \mu\text{m}$ .

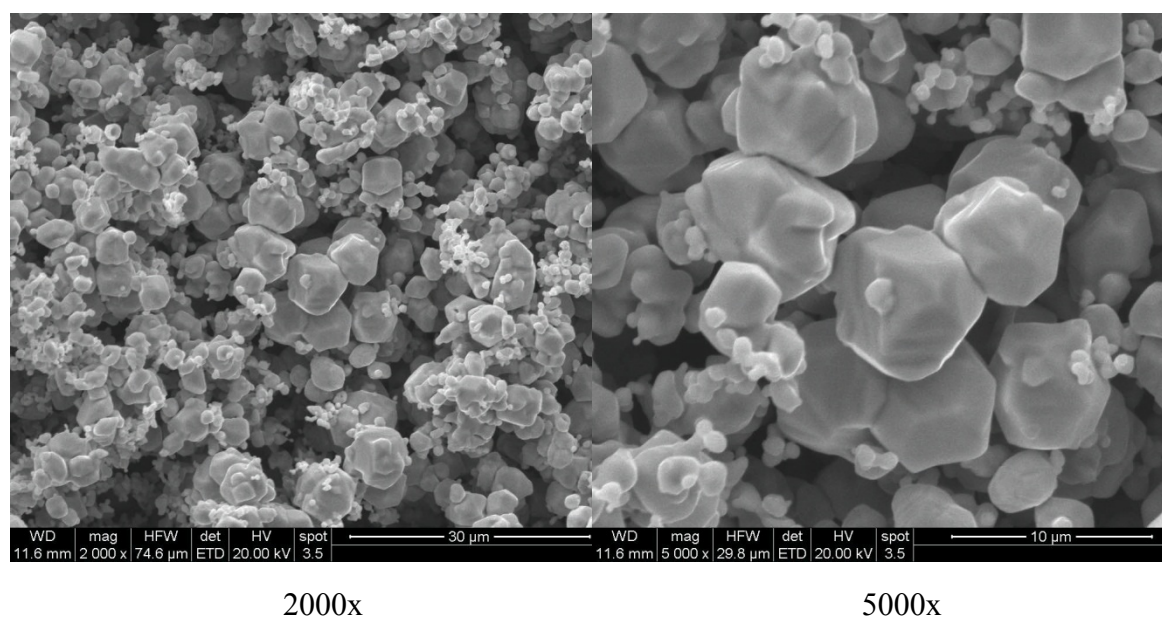


**fig. 3.93.: SE images of Mo powder after reduction at 1100°C – 2 h – H<sub>2</sub> (humid) with insulated gas tubes; left: 2000x; right: 5000x**

The third experiment was carried out at the same conditions as the second one. The gas tubes were also insulated. The difference was the three-way cock which enabled to feed the furnace alternating with wet (for reduction process) or dry gases during heating or cooling processes. In fig. 3.94 can be observed that there are barely very small particles of about 2 µm as were obtained in the experiment before. The biggest particles are about 8 µm which size did not change compared to the previous experiment.

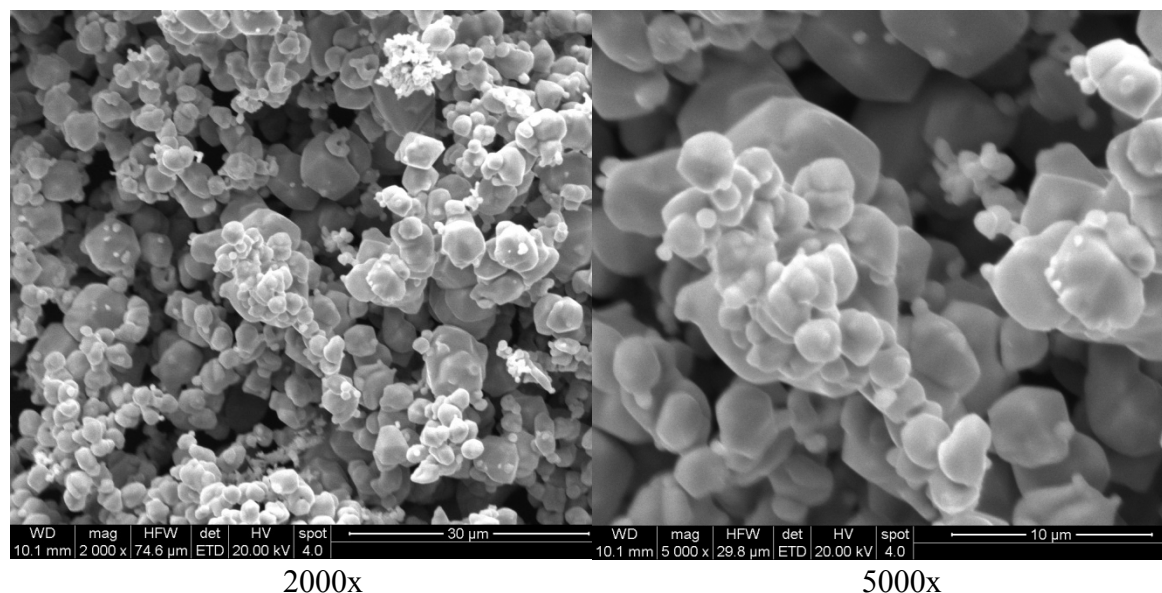


**fig. 3.94.: SE images of Mo powder after reduction at 1100°C – 2 h – H<sub>2</sub> (humid) with insulated gas tubes and 3-way-cock; left: 2000x; right: 5000x**

### 3.3.2.2 Reduction of LiOH doped MoO<sub>2</sub>

Another possibility might be the reduction of MoO<sub>2</sub> that was doped with LiOH before. This is based on work done by Roland Haubner [159] in which he has mixed tungsten with different alkaline elements. Best results, that means a coarsening of the powder, was observed with LiOH doping. A further positive aspect is that only a small amount of LiOH (in wt%) is needed due to its low atomic weight.

For the experiment MoO<sub>2</sub> (from Chemie Metall) was mixed with 250 ppm LiOH in distilled water. This mixture was stirred for about 10 min mechanically. The wet powder mixture was put into a drying chamber at 120 °C for 10h (air). A crust was formed which was sieved through a 355 µm sieve. The resulting powder was reduced at the same conditions as the MoO<sub>2</sub> before. A high powder bed of about 25 mm height (about 100 g) out of this powder was put into a Mo sintering boat and reduced at 1100 °C in wet H<sub>2</sub> atmosphere (5.0 purity; gas flow: 2 l/min) for 2 h. The heating and cooling processes have been carried out in H<sub>2</sub> atmosphere. Some SEM images of the powders are shown in fig. 3.95. The unreduced powders are more angular. After reduction, round uniform particles can be observed in the size of ~ 3 µm.

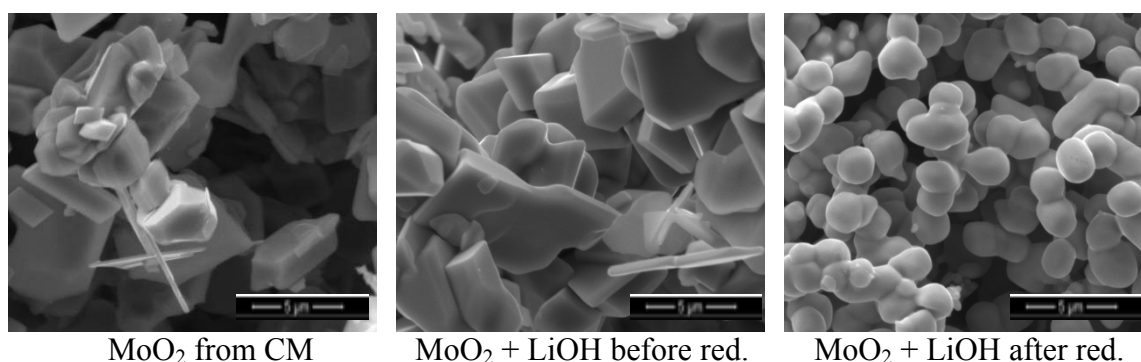


fig. 3.95.: Left: MoO<sub>2</sub> before reduction; middle: MoO<sub>2</sub> doped with LiOH before reduction; right: MoO<sub>2</sub> + LiOH after reduction;

The SEM images of the reduced MoO<sub>2</sub> particles show that the Li-induced coarsening does not occur for Mo. It worked for tungsten as has been described in the work of Haubner [159] but not for molybdenum as had been expected.

### 3.3.2.3 Granulation of Mo (CM) with camphor and Ni

The idea behind the described experiment was that the Mo-Ni granules sinter together through internal densification. The cavities between the granules grow during sintering and form a continuous network of open porosity. A material with large pores and a moderate specific surface can be achieved through this way of production. The idea of production of such a granulated powder was read in the doctoral thesis of H. Danninger [160].

For the experiments, molybdenum powder from Chemie Metall ( $\leq 63\mu\text{m}$ ) was sieved through a 63 µm sieve to avoid particles that might be bigger than the specified size. Molybdenum was mixed with 1 wt% Camphor (Fluka) and 1 wt% nickel (Ecka, 4-5 µm). This powder mixture was wet mixed in cyclohexane for 3 h in a tumbling mixer. Cyclohexane was evaporated in a drying/ vacuum box. The still humid powder mix was



granulated through a 500  $\mu\text{m}$  sieve and dried again in a drying chamber for about 12 h at 120  $^{\circ}\text{C}$ . Afterwards an annealing process was carried out at 1000  $^{\circ}\text{C}$  for 2 h in  $\text{H}_2$ .

### SEM

The powder was analysed by scanning electron microscopy (SEM) in fig. 3.96. Secondary electron (SE) images were taken. In two different magnifications the very low size of the particles can be observed. Most particles are very small. Agglomerates can be seen only here and there in the 3000x magnification and they are very small. The biggest observed particles are in the range of 10  $\mu\text{m}$ .

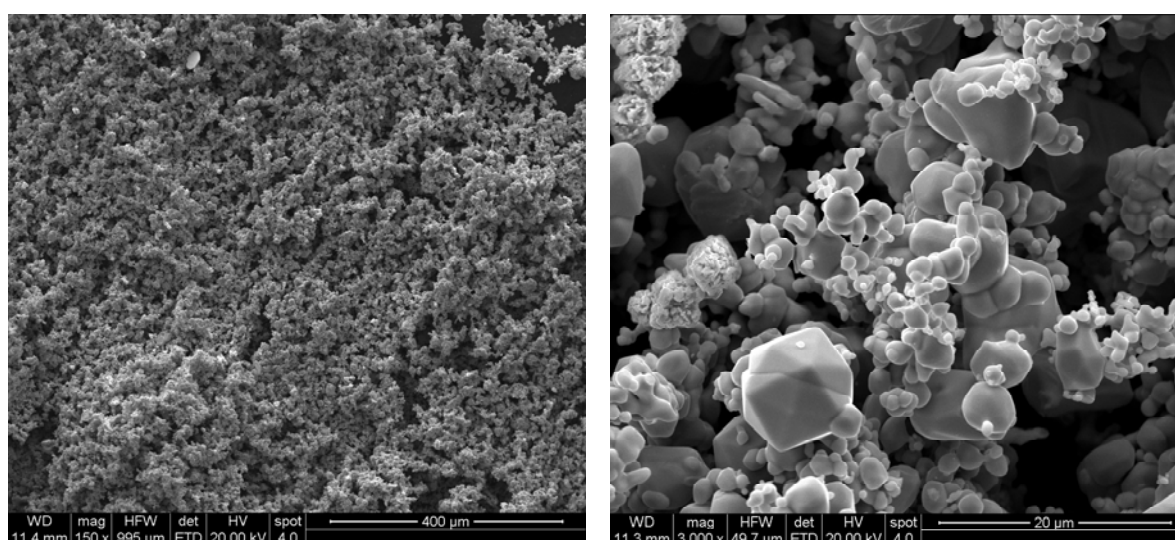


fig. 3.96.: SEM images of agglomerated Mo powder with Ni and Camphor

### Laser particle size analysis (CILAS)

In tab. 25 the particle size distribution of the granulated powder is summarized. About 100% of all particles are < 25  $\mu\text{m}$  and 50% of all particles are below 10  $\mu\text{m}$ .

tab. 25.: Summarized particle size distribution of campher granulated MoNi powder

x	0.04	0.10	0.50	1.00	2.00	3.00	4.00	6.00	8.00	10.00
Q3	0.03	0.15	0.85	1.67	4.90	8.53	12.80	23.67	36.71	50.41
x	12.00	15.00	20.00	25.00	40.00	63.00	90.00	125.0	250.0	500.0
Q3	62.89	77.83	92.20	97.82	100.00	100.00	100.00	100.00	100.00	100.00

In fig. 3.97 the summarized distribution of the granulated particles is graphically shown.

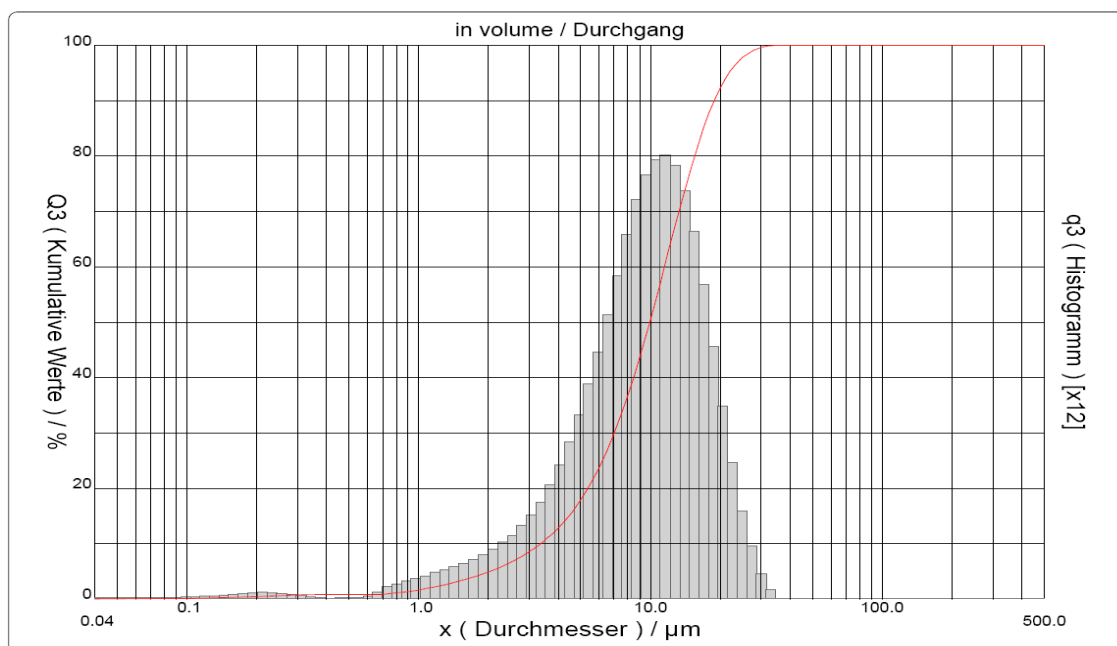


fig. 3.97.: Particle size distribution of Mo-Ni granulated powder

It could be shown in the SEM images and measurements by CILAS that the granulation of the molybdenum powder was less effective than expected. Only the smallest particles form granules locally. There are hardly any particles bigger than 25  $\mu\text{m}$ . 50% of all particles are < 10  $\mu\text{m}$ . One reason for the insufficient granulation might be the very low strength of the granules. During handling, disintegration of the granules might have occurred.

#### Summary of preparation of coarse Mo powders

In the first experiments  $\text{MoO}_2$  was reduced in dry and in a further experiment in a humid  $\text{H}_2$  atmosphere (but the cooling process was carried out in dry  $\text{H}_2$  atmosphere). From reduction experiments from tungsten it was known that by control of atmosphere conditions and reduction temperature it is possible to prepare a coarse tungsten powder. Firstly  $\text{MoO}_2$  was reduced in dry  $\text{H}_2$  atmosphere in the temperature range between 900 and 1100  $^\circ\text{C}$  (with 25  $^\circ\text{C}$  steps) for 1 h soaking period. From the SEM images it could be seen that with increasing temperature the shape of the particles is changing. The edges of the particles rounded up. The biggest particles do not exceed 5  $\mu\text{m}$ . The oxygen measurement had shown that with increasing temperature up to 1000  $^\circ\text{C}$  the oxygen content of the powders decreased. Between 1025 and 1100  $^\circ\text{C}$  the oxygen content increased a little bit, due to the fact that the pressure of the water vapour is changing and the reduction of  $\text{MoO}_2$  is less favoured.

The same  $\text{MoO}_2$  powder grade was reduced between 900 and 1000  $^\circ\text{C}$  (in 50  $^\circ\text{C}$  steps) in a further test series but this time in humid  $\text{H}_2$  atmosphere. The gas had to pass a gas washing bottle filled with water before entering the furnace. For cooling down the atmosphere was changed to dry  $\text{H}_2$  to avoid reoxidation. In a further experiment an  $\text{MoO}_2$  powder was reduced at 1100  $^\circ\text{C}$  in humid  $\text{H}_2$  but in a higher powder bed. In the last experiment the reduction was carried out in a mixture of  $\text{Ar}:\text{H}_2=95:5$ , which should result in still higher humidity in the powder bed. In the SEM images it could be seen

that the shape of the particles was changing from angular particles in the beginning to round uniform particles after reduction at 1100 °C in a higher powder bed. The particles did not exceed 5 µm. The oxygen content of each powder was measured by Leco. With increasing reduction temperature the oxygen content was decreasing. The lowest amount was measured for powder reduced at 1100 °C in a higher powder bed (in humid H<sub>2</sub> atmosphere). Reduction in Ar:H<sub>2</sub> atmosphere resulted in a very high amount of oxygen of 12,2 %, due to incomplete reduction.

Some further reduction was carried out at 1100 °C for 2 h in humid H<sub>2</sub> atmosphere but in better insulated tubes. The gas had to pass a gas washing bottle filled with boiling water before entering the furnace. The gas should be more saturated with gas vapour. In the SEM images however no significant difference in particle size or distribution to the previous runs could be observed.

Next, some MoO<sub>3</sub> was doped with 250 ppm LiOH in water and after drying and sieving through a 355 µm sieve reduced afterwards at 1100 °C in humid H<sub>2</sub> atmosphere for 2 h. The resulting powder consisted out of round particles which were uniformly distributed but the size of the particles did not exceed 3µm. This showed that the coarsening effect of alkaline element doping that had been observed with W does not apply for Mo.

For producing Mo powder granulates, Mo (commercially available designated as ≤ 63 µm) was mixed with 1 wt% Camphor and 1 wt% nickel. This powder mixture was blended in cyclohexane in a tumbling mixer for 3 h. The cyclohexane was evaporated and the wet mixture granulated through a 500 µm sieve. After drying at 120 °C in a drying chamber the granules were sintered at 1000 °C for 2h in H<sub>2</sub>. In the SEM images hardly any agglomerates could be seen; the biggest observed particles did not exceed 10 µm.

### **3.3.3 Powder prepared from presintered Mo(CM) powder compacts**

For economical reasons it was tried to prepare coarse grained Mo powder like the one from Goodfellow. This Mo powder of an average powder size of ≤355µm is very expensive and costs 10 times more than the relatively cheap fine grained Mo powder (≤63µm) from Chemie Metall. Some SEM images (fig. 2.4) have indicated that the coarse Mo powder acquired from Goodfellow might have been prepared by presintering of a fine grained Mo powder and subsequent crushing and milling of the sintered samples. In the following experiment it was tried to prepare a coarse powder similar to the one sold by Goodfellow following the sintering-milling route.

#### **3.3.3.1 Preparation**

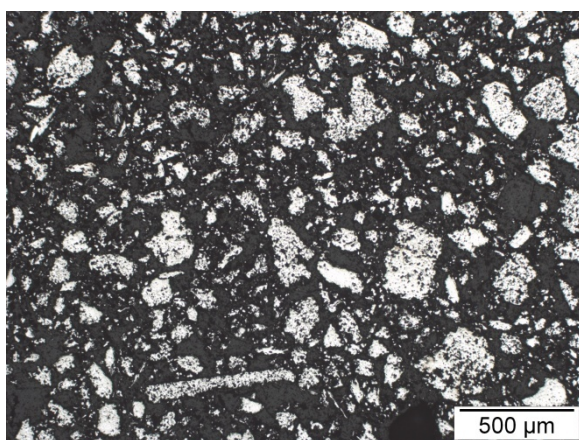
Fine grained Mo powder from Chemie Metall (≤63 µm) was pressed uniaxially at 200 MPa to Charpy bars (55\*10\*10 mm) on Jessernigg & Urban hydraulic press. These bars were sintered for 2 h at different temperatures of 1200/1300/1400/1500 °C in H<sub>2</sub> (5.0 purity; 2 l/min gas flow). After sintering the bars were crushed in liquid N<sub>2</sub> and afterwards milled in a knife (coffee) mill. The powder granulate thus obtained was sieved through a ≤355µm sieve. The sieved powder was embedded in bakelite, ground



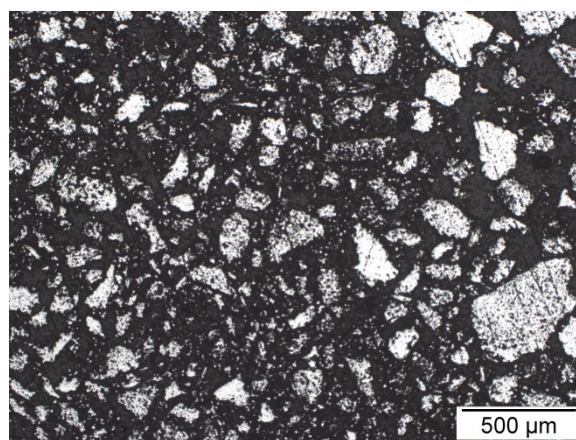
and polished. All embedded powders were characterised by optical microscopy (LOM) and SEM.

### 3.3.3.2 LOM

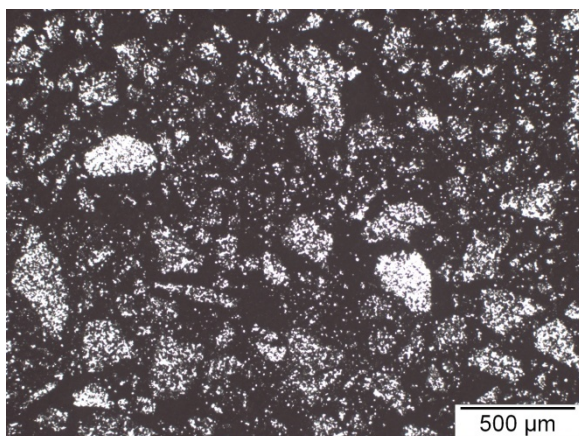
In fig. 3.98 a comparison of the particle shape and size of the different Mo powders that were embedded in bakelite and prepared metallographically is given. Each powder was prepared from compacts sintered at a specific temperature. As can be seen (fig. 3.98) the shape and size of the particles depend on the sintering temperature.



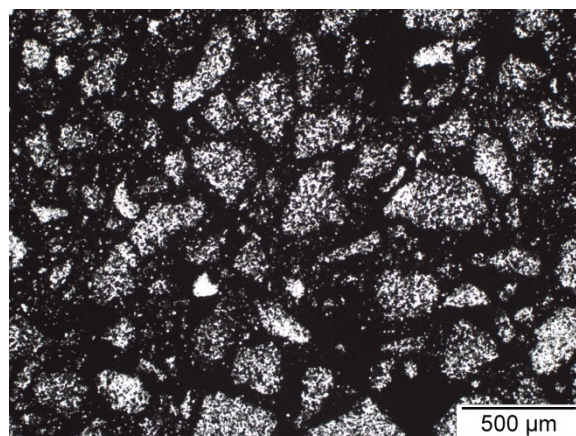
50x – sintered at 1200°C



50x – sintered at 1300°C



50x – sintered at 1400°C



50x – sintered at 1500°C

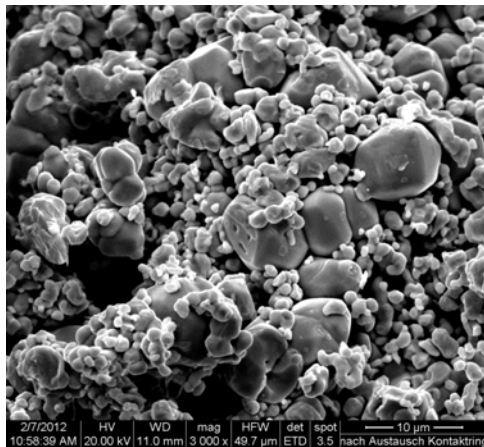
**fig. 3.98.: LOM images from the different Mo powders prepared by crushing sintered bars**

It could be observed in fig. 3.98 that the largest particles were achieved after presintering the Mo bars at 1500 °C. Molybdenum bars that were sintered for example at 1200 °C contained much more of fine particles compared to those sintered at 1500 °C.

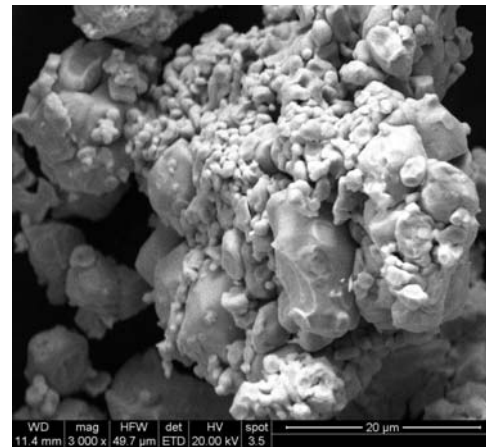


### 3.3.3.3 SEM

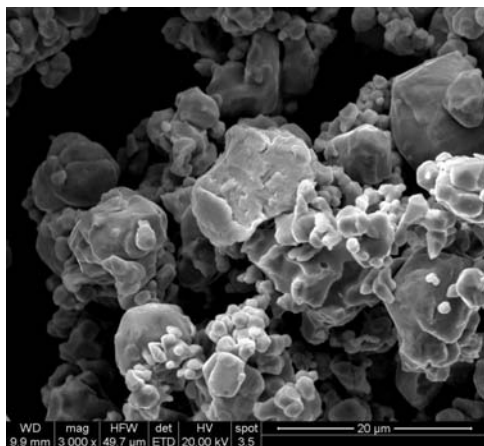
In fig. 3.99 images at 3000x magnification of all four prepared powders are summarized. Powders sintered at 1100°C and 1200°C have a higher amount of fine particles while powders sintered at higher temperature, 1400 °C and 1500 °C, mostly consist of coarser powder. The powder sintered at 1500°C for 2 h exhibits distinctive sintering bridges which were broken during milling. These distinctive bridges indicate that the granules are strongly bonded. This shows that “thermal granulation”, i.e. pressing, sintering and milling, is a more promising approach to manufacture coarse Mo powders, although of course also these coarse particles contain internal porosity.



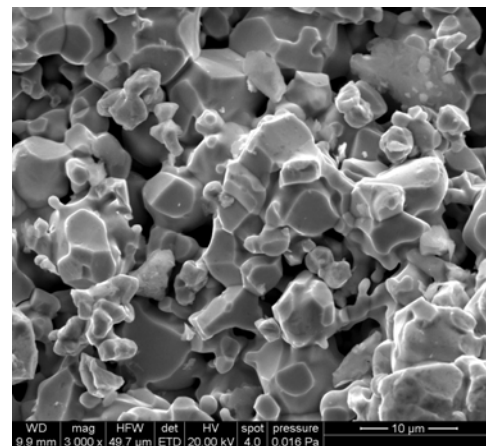
1100°C



1200°C



1400°C



1500°C

**fig. 3.99.: Coarse Mo powder prepared from Chemie Metall Mo powder; pressed, sintered and milled at 1200 / 1300 / 1400 / 1500 °C; 2 h soaking period; vacuum ; 3000x magnification**

### 3.3.4 Sample preparation from coarse Mo powder

For the following experiment a coarse Mo fraction with <355µm was used (prepared as described in 3.3.3) taken from compacts sintered 2 h at 1500°C and then milled, and

some samples have been prepared. The powder was mixed with 2 wt% wax (Kenolube P11) and pressed at 200 MPa in a cylindrical die with 11.3 mm diameter on Amsler hydraulic press. Then the samples were dewaxed at 600 °C in N<sub>2</sub> for 2 h. It proved to be necessary to presinter the sample (at 1100 °C for 2 h in H<sub>2</sub>) in the dewaxing furnace to prevent any damage during moving the specimens between the furnaces. All samples were sintered afterwards in a dilatometer (Bähr 801) at 1500 °C for 5 h in rotary pump vacuum, the heating rate being set at 10 K.min<sup>-1</sup>.

### ***Macroscopic images***

In fig. 3.100 some photos of the sintered specimen were taken with a digital camera and shown. The images clearly reveal the very coarse particles of the sample.



**fig. 3.100.: Digital camera images of a pressed sample and sintered specimen prepared from coarse Mo powder (fraction <355 µm); sintered at 1500 °C – 5 h soaking period; vacuum**

#### **3.3.4.1 Properties of the samples**

The density measured by Archimedes is 5.8 g/cm<sup>3</sup>. The open porosity as measured by He-pycnometry gives a value of 43% and the one of total porosity gives a value of 44%, i.e. the porosity is almost fully open, which is the desirable state for infiltration. It also shows that there is virtually no closed internal porosity in the coarse powder particles. The microhardness was measured too with 50 g indentation load in the particle cores and also in the sintering bridges. The hardness in the grains was  $165 \pm 10$  HV0.05 and that measured in the sintering bridges was  $62 \pm 3$  HV0.05. Of course the indentations in the bridges do not reveal the hardness of Mo as such since there is always some displacement of Mo during indentation, but the relative hardness of the necks can be regarded as an at least tentative indicator for their thickness (and thus strength).

The samples were cut and hot embedded in bakelite. During the grinding and polishing some grains broke out of the center of the sample. Therefore the whole cross section was impregnated with Loctite 420 (it is a cyanoacrylate glue).

### 3.3.4.2 Light microscopy

In fig. 3.101 some light microscopy images are shown. The very coarse grains of the sample can easily be seen. Some sintering bridges between the grains can also be observed, although the degree of sintering is only moderate (as also indicated by the fairly low hardness of the necks). I.e. sintering at higher temperatures is definitely recommendable here.

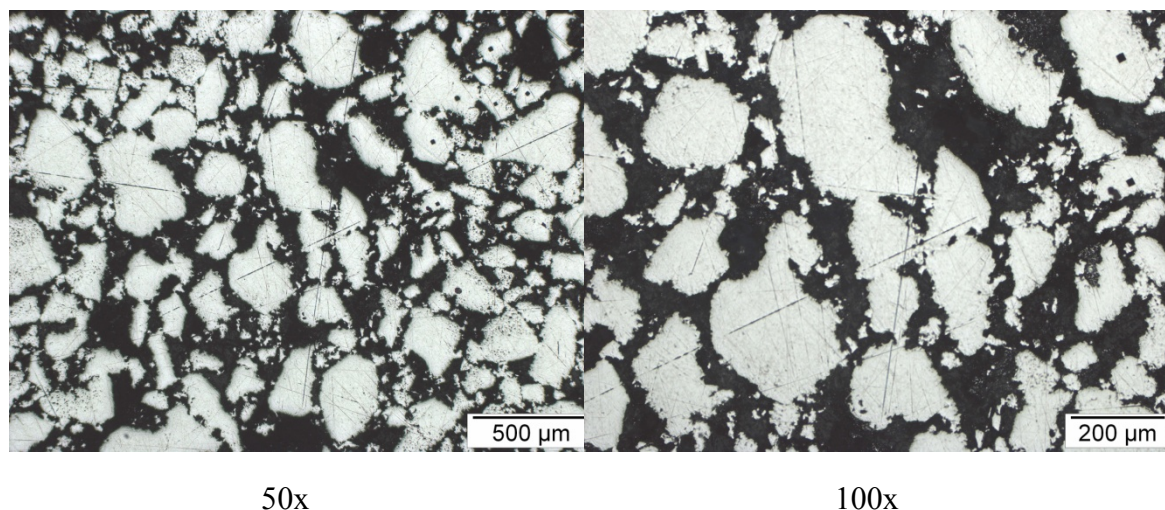


fig. 3.101.: Light microscopy images of a sample prepared from coarse powder  $<355\mu\text{m}$ , sintered at  $1500^\circ\text{C}$  for 2h

### 3.3.4.3 Addition of Si in different contents

Coarse Mo powder prepared from fine powder by pressing and presintering at  $1500^\circ\text{C}$  (2 h soaking period) and crushing afterwards, (as described in 3.3.3) was used for the following experiment. The powder size of the Mo was  $\leq 355\mu\text{m}$ . This powder was mixed with different amounts of fine silicon powder from Ecka (particle size 4-5  $\mu\text{m}$ ). Mixtures of Mo with varying Si contents, 2 / 5 / 10 / 15 / 25 / 37 wt% Si, were prepared. The powders were dry mixed in a tumbling mixer for 2 h and pressed uniaxially with 150 MPa in a cylindrical die ( $\varnothing = 11.27\text{ mm}$ ) without any lubricant. Afterwards the compacts were presintered at  $1100^\circ\text{C}$  for 2 h soaking period in  $\text{H}_2$  (5.0 purity; 2 l/min gas flow). Afterwards all samples were sintered at  $1800^\circ\text{C}$  in vacuum for 2 h.

#### 3.3.4.3.1 Characterisation of density and open porosity

The density was measured by Archimedes after impregnation, and the results are summarized in tab. 26. Furthermore the density was also measured by He pycnometry (which as stated above records the closed but not the open pores). The open porosity was then calculated from Archimedes and He pycnometry data and is summarized, too, in tab. 26.

**tab. 26.: Measured density (Archimedes) and open porosity (He pycnometry) of Mo-x%Si prepared from coarse Mo <355  $\mu\text{m}$** 

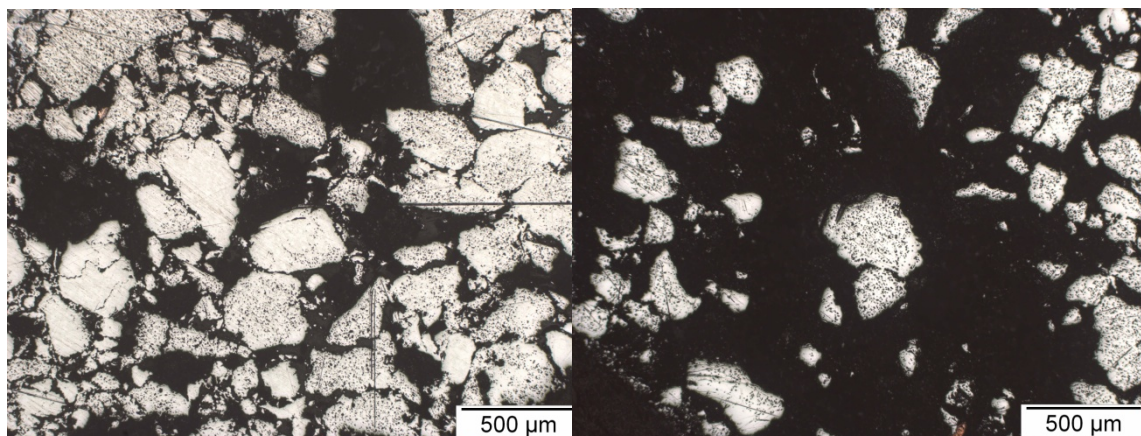
Mo + %wt Si	$\rho_{\text{Archimedes}} [\text{g/cm}^3]$	open porosity [%]	total porosity [%]
2	$6,5 \pm 0,1$	$34 \pm 0,3$	$35 \pm 0,1$
5	$6,1 \pm 0,1$	$33 \pm 0,2$	$35 \pm 0,1$
10	$5,2 \pm 0,2$	$37 \pm 0,4$	$40 \pm 0,6$
15	$4,8 \pm 0,1$	$40 \pm 0,4$	$42 \pm 0,2$
25	$3,8 \pm 0,1$	$49 \pm 0,6$	$53 \pm 0,3$
37	$3,3 \pm 0,2$	$50 \pm 0,5$	$53 \pm 0,1$

It can be observed in tab. 26 that with increasing Si content the density (Archimedes) is decreasing. With decreasing density the open porosity is increasing. The total porosity is about 1-3 % higher (which is equivalent to closed porosity) than the one measured for the open porosity, which mean that most pores are open. It could be furthermore observed that the mechanical stability (handling of the sample) was very difficult with increasing content of Si. The samples were very brittle. In fig. 3.102 some LOM images of Mo samples containing different amounts of Si are shown. All images were taken in the surface-near area. LOM images of the Mo specimens out of a coarse powder were compared with the one which have been prepared out of a commercially available CM Mo, both specimens pressed with different amounts of Si. The specimens out of the CM Mo were sintered in the first experiment at 1300 °C for 8h in  $\text{H}_2$  and in a further experiment they were presintered at 1300 °C in  $\text{H}_2$  (2h) and afterwards sintered at 1420 °C (above the eutectic temperature) for 2 h in vacuum (chapter 3.2.1.1; fig. 3.54 + fig. 3.54). In both cases it could be observed in the LOM images that the porosity of the specimens was very high after sintering and a lot of grains broke out during metallographic preparation. The sintering activity was very low. Specimens prepared out of coarse Mo with different amounts of Si were presintered at 1100 °C in reducing atmosphere and sintered again at 1800 °C in vacuum for 2 h. The sintering temperature is much higher than the one chosen for the fine grained specimens. However, the resulting porosity is very high. Furthermore, the sintering activity was also very low for this powders, resulting in few and weak sintering bridges. A lot of particles broke out during preparation which can be observed in the LOM images.

### 3.3.4.3.2 LOM

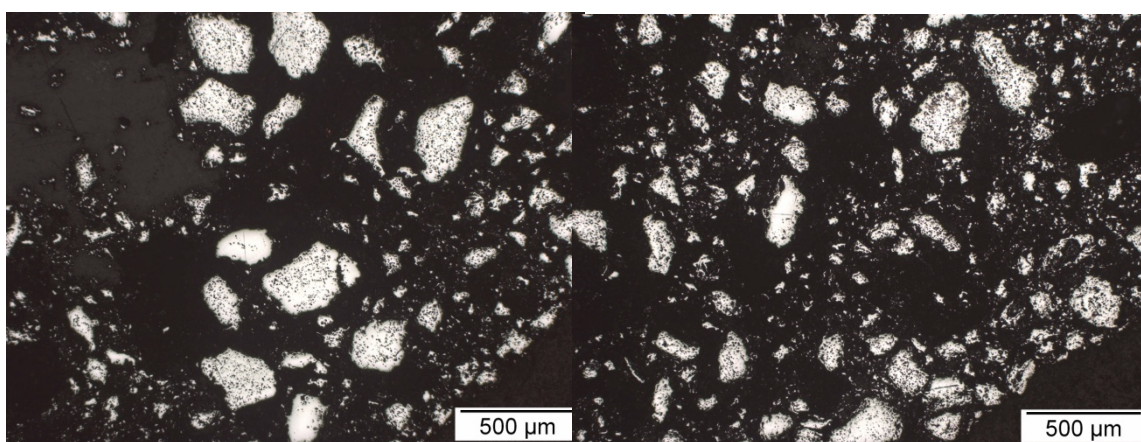
The sintered samples were embedded in Araldite and ground. Afterwards it was necessary to infiltrate the samples with some Araldite again to stabilize the structure of the samples. After curing of the resin the samples were polished. Even though they were infiltrated with Araldite before, they were very brittle, and the polishing was therefore carried out manually.





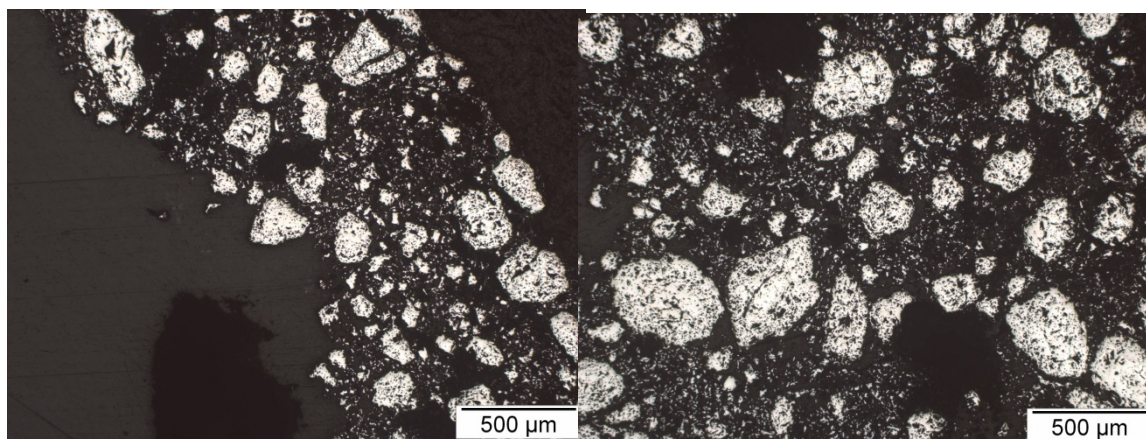
50x – 2 wt% Si in Mo

50x – 5 wt% Si in Mo



50x – 10 wt% Si in Mo

50x – 15 wt% Si in Mo



50x – 25 wt% Si in Mo

50x – 37 wt% Si in Mo

**fig. 3.102.: LOM of polished microsection of Mo samples (from powder <355 μm) with different amounts of Si**

It can be seen in fig. 3.102 that with increasing content of Si in Mo the cohesion of the particles is lower. In the 50x magnification of the Mo sample containing 25 wt% of Si there is only a thin layer of about 1 mm of sintered particles located near the surface forming a ring around the core. The core of the sample broke out during polishing. All samples were very brittle and fragile and difficult to handle.

### 3.3.4.4 Summary of specimens prepared from coarse Mo powder

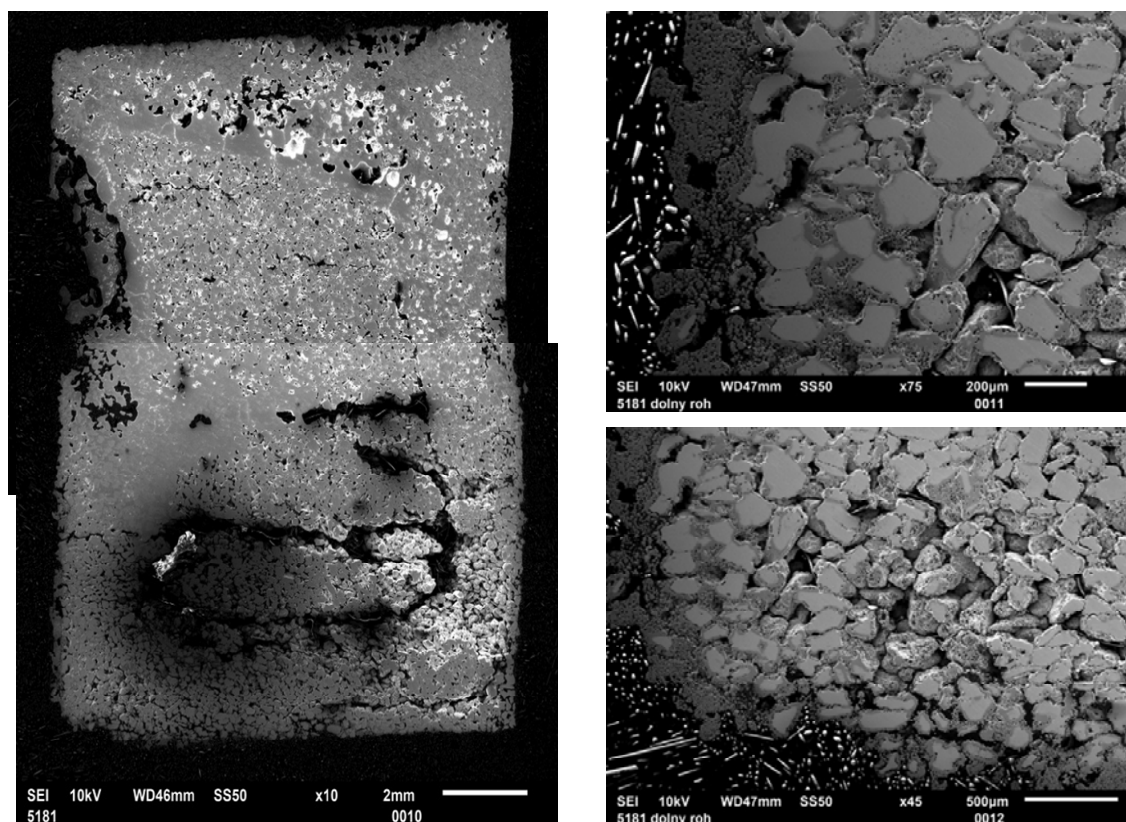
Due to the fact that the commercially available coarse Mo powder from Goodfellow is quite expensive, it was started to prepare some coarse Mo from commercially available fine grained Mo (from CM). Charpy bars were pressed with 200 MPa out of this fine Mo and sintered at four temperatures 1200/1300/1400/1500 °C for 2 h in H<sub>2</sub>. After sintering, the bars were crushed in liquid N<sub>2</sub> and sieved through a 355 µm sieve. The four powders were embedded in bakelite and characterised on LOM and SEM. It could be observed in LOM and SEM that the biggest particles were achieved from bars which were sintered at 1500 °C (2 h; H<sub>2</sub>). This powder was taken for further experiments and mixed with 2 wt% Kenolube P11 and pressed at 200 MPa to cylindrical specimens with 11,27 mm diameter. The specimens were dewaxed at 600 °C in N<sub>2</sub> for 2 h and presintered afterwards at 1100 °C for 2 h in H<sub>2</sub>. A second sintering step at a higher temperature was carried out at 1500 °C for 2 h in vacuum. The resulting density was 5,8 g/cm<sup>3</sup> with 43 % open porosity. The hardness was measured in the grains and in the sintering bridges. In the grains 165 HV 0.05 were measured while in the sintering bridges the hardness decreased to 62 HV0.05.

The same coarse Mo powder was used for the following experiment. The powder size of the Mo was ≤355µm. This powder was mixed with different amounts of fine silicon powder from Ecka. Mixtures of Mo with varying Si fractions, 2 / 5 /10 /15 / 25 / 37 wt% Si, were prepared. Afterwards the compacts were pressed with 150 MPa and presintered at 1100°C for 2 h soaking period in H<sub>2</sub>. Afterwards all samples were sintered at 1800°C in vacuum for 2 h. The density of the compacts decreased with higher Si content. At the same time the open porosity was increasing. LOM images of the Mo specimens out of a coarse powder were compared with the one which have been prepared out of a commercially available CM Mo, both specimens pressed with different amounts of Si. The specimens from the fine CM Mo were sintered in the first experiment at 1300 °C for 8 h in H<sub>2</sub> and in a further experiment they were presintered at 1300 °C in H<sub>2</sub> (2 h) and afterwards sintered at 1420 °C (above the eutectic temperature) for 2 h in vacuum. In both cases it could be observed in the LOM images that the porosity of the specimens was very high after sintering and a lot of grains broke out during metallographical preparation. The sintering activity was very low. Specimens prepared out of coarse Mo with different amounts of Si were presintered at 1100 °C in reducing atmosphere and sintered again at 1800 °C in vacuum for 2 h. The sintering temperature is much higher than the one chosen for the fine grained specimens. However, the resulting porosity is very high. Furthermore, the sintering activity was also very low for this powders resulting in low amount and weak sintering bridges. A lot of particles broke out during preparation which can be observed in the LOM images. This confirms that Mo-Si specimens that have been at least partially transformed to silicides do not sinter well, which agrees with their resistance to densification by HIP.



### 3.3.5 Characterisation of samples after Si treatment by partners

A molybdenum specimen prepared at TUW from coarse Mo powder was sent to IMSAS for a further infiltration experiment. The coarse Mo powder had been prepared from fine one (the bars were presintered at 1500 °C for 2 h soaking period and crushed afterwards) as described in chapter 3.3.3. Specimen preparation was done as described in chapter 3.3.4 by presintering at 1100 °C for 2 h in H<sub>2</sub> and sintering at 1500 °C for 2 h in vacuum. The specimen was infiltrated in an induction furnace. It was placed in the centre of the coil in a graphite die. The required amount of Si (as fragments from crushed and milled Si) was poured over the specimen and some fragments of the Si were lying around the specimen. The induction furnace was heated up to 1500 °C until the Si melted and held at temperature for 3 min. After cooling the specimen was cut axially and the cross section was analysed by SEM (at IMSAS). In fig. 3.103 the cross section and the elemental mapping of Mo and Si can be seen. After infiltration with Si a lot of pores remained in the Mo bulk material, as can be observed very well in fig. 3.103 top images. In the 75x magnification can be seen that the particles are covered with Si but many pores remained. Furthermore a lot of particles broke out, which effect can be related to the cutting process of the specimen due to mechanical stresses. The elemental maps of the Si and Mo distribution showed very well two Si containing layers around the Mo core. The first layer surrounding the Mo core is a Mo<sub>5</sub>Si<sub>3</sub> layer, and the outer one of each particle is a MoSi<sub>2</sub> layer. In particular from the Si mapping it can be seen that the sintering contacts between the coarse Mo particles have mostly been transformed to Mo<sub>5</sub>Si<sub>3</sub>, which indicates that the contacts are still too small to remain metallic during infiltration. This confirms once more that the sintering activity of the coarse powders is too low.



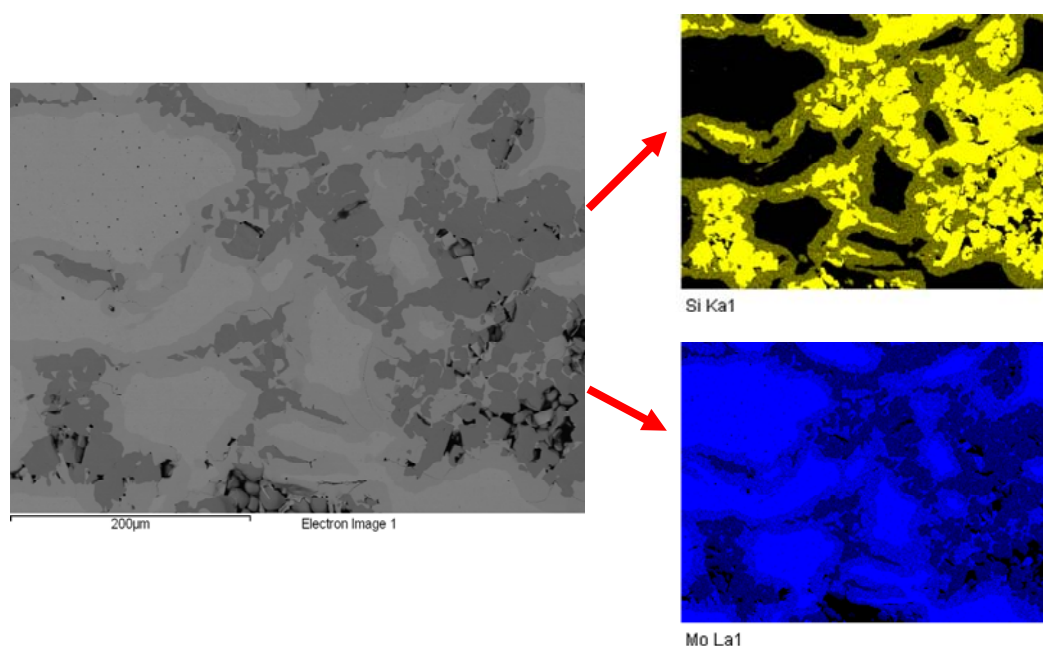


**fig. 3.103.: Top: cross section of Si infiltrated specimen from coarse Mo; bottom: elemental mapping of Si and Mo distribution**

### 3.3.5.1 Specimens from bimodal mixtures of coarse and fine Mo powders

The preparation of the coarse Mo has already been described in chapter 3.3.3. The bars out of fine Mo powder were presintered at 1500 °C (for 2 h soaking period; H<sub>2</sub>) and crushed afterwards. Three different fractions of this Mo powder were sieved -  $\leq 355 \mu\text{m}$ ,  $\leq 250 \mu\text{m}$  and  $\leq 125 \mu\text{m}$ . From all grades the finest particles were retained, i.e. the fractions contain in fact coarse as well as fine particles. Each fraction was mixed with the original Mo powder from Chemie Metall in varying ratios. 90/80/70/60/50 wt% of coarse Mo ( $\leq 355 \mu\text{m}$ ,  $\leq 250 \mu\text{m}$  or  $\leq 125 \mu\text{m}$ ) were mixed with fine Mo from Chemie Metall in a tumbling mixer for 2 h. Cylindrical samples of 11,27 mm diameter were pressed in the CIP with 200 MPa. The samples were sintered at 1300°C in hydrogen (5.0 purity; 2 l/min gas flow) for 2 h. A second sintering step was carried out at 1800°C in vacuum for 2 h in the hot press furnace with a graphite die. The samples were characterised by the open porosity, HV 0.1, LOM and carbon content on Leco.

#### 3.3.5.1.1 Open porosity

The open porosity was calculated from Archimedes density and He-Pycnometry density. The values of the calculated open porosity of samples sintered at 1300 °C for 2 h in H<sub>2</sub> (5.0 purity; 2 l/min gas flow) are summarized in tab. 27 for the very coarse Mo powder  $\leq 355\mu\text{m}$ , in tab. 28 for the  $\leq 250\mu\text{m}$  and in tab. 29 for the  $\leq 125\mu\text{m}$  powder. Samples with a high ratio of coarse powder ( $\leq 355\mu\text{m}$ ) to fine show the highest values for the open porosity. For example, the sample pressed out of 90% coarse Mo  $\leq 355\mu\text{m}$  with 10% of fine Mo (Chemie Metall) shows about 44% open porosity. With decreasing particle size of the coarse fraction the open porosity is slightly decreasing too, as can be seen for the sample from 90% of  $\leq 125\mu\text{m}$  coarse Mo powder with 10% fine Mo powder (about 40% of open porosity was measured). The density (Archimedes) is decreasing with increasing amount of total and open porosity independently of which coarse Mo



fraction was used ( $\leq 355\mu\text{m}$ ,  $\leq 250\mu\text{m}$  and  $\leq 125\mu\text{m}$ ). The highest densities were achieved for specimens prepared from 50 % coarse and 50 % fine Mo fraction. As for the open porosity already observed, samples with a high ratio of coarse powder ( $\leq 355\mu\text{m}/\leq 250\mu\text{m}/\leq 125\mu\text{m}$ ) to fine show the lowest values for the density.

**tab. 27.: Open porosity (pyc.) of specimens prepared from a mix of coarse ( $\leq 355\mu\text{m}$ ) and fine grained Mo**

powder fraction	Mixture of [%]		Density Archimedes [g/cm <sup>3</sup> ]	Open porosity [%]	Total porosity [%]
	coarse Mo	fine Mo			
$\leq 355\mu\text{m}$	50	50	7,21	38	39
	60	40	6,85	40	40
	70	30	6,74	39	41
	80	20	6,55	40	41
	90	10	6,32	44	45

**tab. 28.: Open porosity (pyc.) of specimens prepared from a mix of coarse ( $\leq 250\mu\text{m}$ ) and fine grained Mo**

powder fraction	Mixture of [%]		Density Archimedes [g/cm <sup>3</sup> ]	Open porosity [%]	Total porosity [%]
	coarse Mo	fine Mo			
$\leq 250\mu\text{m}$	50	50	7,19	34	36
	60	40	7,13	34	35
	70	30	6,91	37	37
	80	20	7,06	33	34
	90	10	6,67	39	40

tab. 29.: Open porosity (pyc.) of specimens prepared from a mix of coarse ( $\leq 125\mu\text{m}$ ) and fine grained Mo

powder fraction	Mixture of [%]		Density Archimedes [ $\text{g}/\text{cm}^3$ ]	Open porosity [%]	Total porosity [%]
	coarse Mo	fine Mo			
$\leq 125\mu\text{m}$	50	50	7,00	36	37
	60	40	6,77	38	40
	70	30	6,97	35	37
	80	20	6,98	36	37
	90	10	6,69	40	42

In fig. 3.104 the values for the open porosity of all three coarse powders are plotted. The highest and most regular open porosity could be achieved for the samples from the coarsest powder. Specimens out of the two other coarse powders show lower values than the  $\leq 355\mu\text{m}$  specimens, and both reached similar values for the open porosity. The open porosity was measured twice with He - Pycnometry for each sample. In some cases even more parallel runs were done. The diameter of the specimens was quite small for the He - Pycnometer, and some specimens had to be measured several times to achieve reproducible values for open porosity.

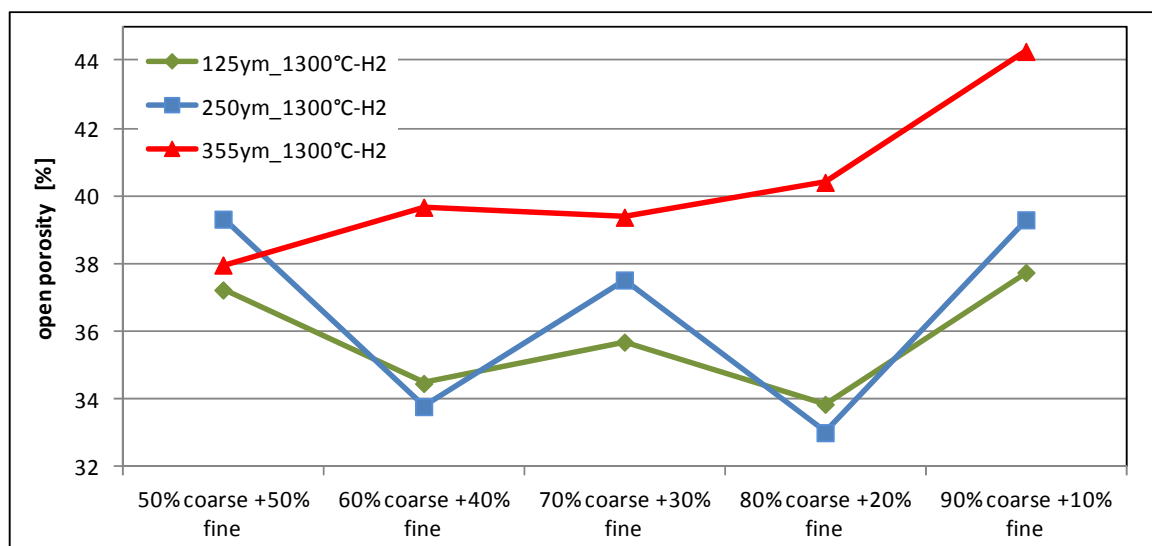


fig. 3.104.: Open porosity for sintered specimens from bimodal Mo powder mixes (different coarse fractions). CIPed at 200 MPa, sintered 2 h 1300°C in  $\text{H}_2$  + 2 h 1800°C in vacuum

## 3.3.5.1.2 Hardness

The hardness was measured with 0,1 kp indentation load (HV0,1). The microhardness was measured inside of a particle. The sintering bridges were mostly too thin to measure the hardness within them. The hardness data are summarised in tab. 30, tab. 31 and tab. 32.

**tab. 30.: Hardness HV0.1 of samples from coarse Mo  $\leq 125\mu\text{m}$  mixed with fine grained Mo**

powder fraction	Mixture of [%]		HV 0,1
	coarse Mo	fine Mo	
$\leq 125\mu\text{m}$	50	50	94
	60	40	106
	70	30	108
	80	20	130
	90	10	155

**tab. 31.: Hardness HV0.1 of samples from coarse Mo  $\leq 250\mu\text{m}$  mixed with fine grained Mo**

powder fraction	Mixture of [%]		HV 0,1
	coarse Mo	fine Mo	
$\leq 250\mu\text{m}$	50	50	115
	60	40	155
	70	30	161
	80	20	136
	90	10	154

**tab. 32.: Hardness HV0.1 of samples from coarse Mo  $\leq 355\mu\text{m}$  mixed with fine grained Mo in different ratios**

powder fraction	Mixture of [%]		HV 0,1
	coarse Mo	fine Mo	
$\leq 355\mu\text{m}$	50	50	129
	60	40	177
	70	30	153
	80	20	164
	90	10	148

A graphic overview is given in fig. 3.105. By trend it can be seen that the hardness is higher with increasing particle size of the coarse particles. Furthermore it can be observed that samples from 90% coarse particles show similar values for the hardness of about 150 HV0.1 with 40% open porosity, independent of the coarse powder fraction used.

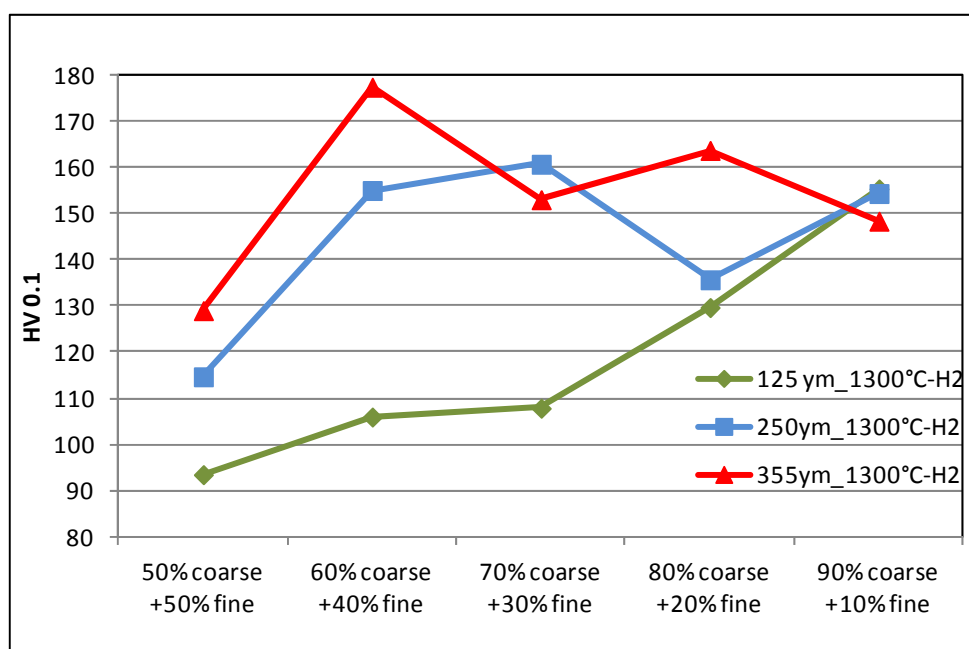
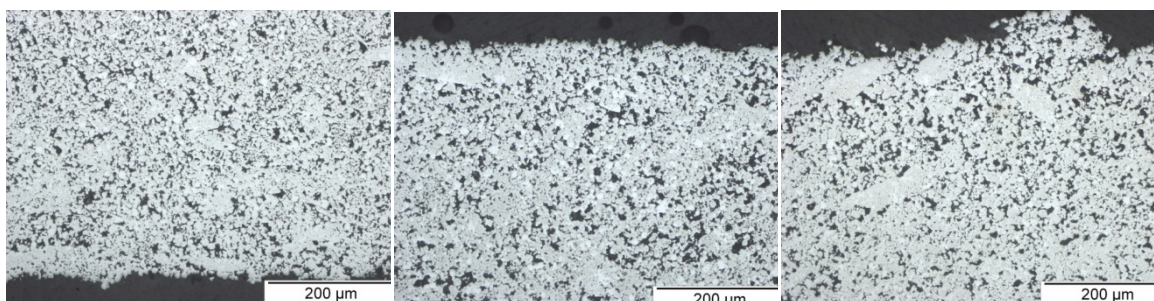


fig. 3.105.: Hardness HV0,1 of sintered Mo prepared from different particle size fractions. CIPed at 200 MPa, sintered 2 h 1300°C in H<sub>2</sub> + 2 h 1800°C in vacuum

### 3.3.5.1.3 LOM

In fig. 3.106 - fig. 3.108 some images of samples prepared from different coarse Mo powders mixed in different ratios with fine grained Mo were compared. All samples were sintered at 1300 °C for 2 h in H<sub>2</sub> (5.0 purity; 2 l/min). The increasing amount of coarser particles can be observed in fig. 3.106. Furthermore, the bigger the particles of the coarse powder the more pronounced the particle growing and agglomeration during sintering. On the other hand it is evident that the materials prepared from fraction <125 μm contain more fines in general, which originates from the fact that for preparing this fraction the coarser fractions were re-crushed. Apparently disintegration down to relatively fine particle size was thus attained, and the fraction of large particles seems to be relatively low even in the specimen with nominally 90% coarse fraction.

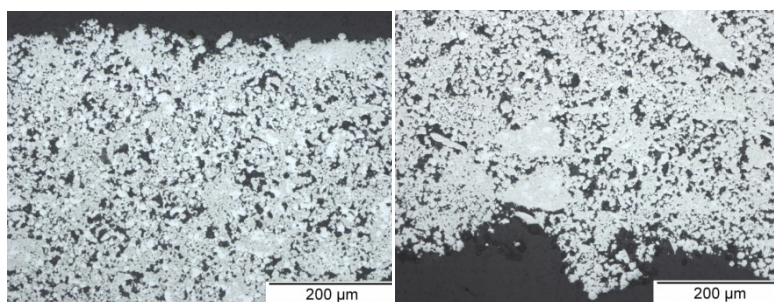


50% ≤125 μm Mo : 50%  
CM

60% ≤125 μm Mo : 40%  
CM

70% ≤125 μm Mo : 30%  
CM

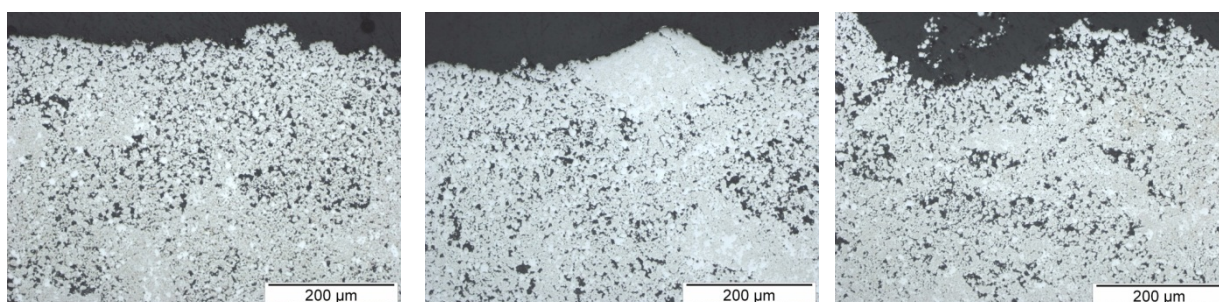




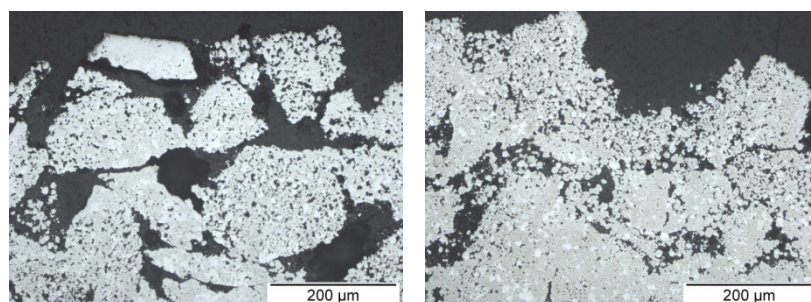
80%  $\leq 125 \mu\text{m}$  Mo : 20% CM      90%  $\leq 125 \mu\text{m}$  Mo : 10% CM

**fig. 3.106.:** Metallographic sections of samples prepared from coarse Mo powder  $\leq 125 \mu\text{m}$  mixed in different ratios with a fine grained Mo from Chemie Metall. CIPed at 200 MPa, sintered 2 h 1300°C in  $\text{H}_2$  + 2 h 1800°C in vacuum

In fig. 3.107 the LOM images of specimens prepared from  $\leq 250 \mu\text{m}$  coarse Mo powder mixed with fine Mo (CM) are shown. With increasing ratio of the coarse fraction (80 and 90 % of the  $\leq 250 \mu\text{m}$ ) powder the fine powder cannot be recognized in the LOM images. There is also a lower adhesion between the particles due to lower amount of the "binder", - the fine grained Mo fraction, indicating a mechanically weaker structure.



50%  $\leq 250 \mu\text{m}$  Mo : 50% CM      60%  $\leq 250 \mu\text{m}$  Mo : 40% CM      70%  $\leq 250 \mu\text{m}$  Mo : 30% CM



80%  $\leq 250 \mu\text{m}$  Mo : 20% CM      90%  $\leq 250 \mu\text{m}$  Mo : 10% CM

**fig. 3.107.:** Metallographic sections of samples prepared from Mo powder  $< 250 \mu\text{m}$  mixed in different ratios with a fine grained Mo from Chemie Metall. CIPed at 200 MPa, sintered 2 h 1300°C in  $\text{H}_2$  + 2 h 1800°C in vacuum

In fig. 3.108 the same phenomena as before could be observed. With increasing amount of the coarse fraction, in this case the  $\leq 355 \mu\text{m}$  coarse Mo fraction, the adhesion

between the big particles is lower due to less amount of the fine grained fraction, which acts as binder, being available.

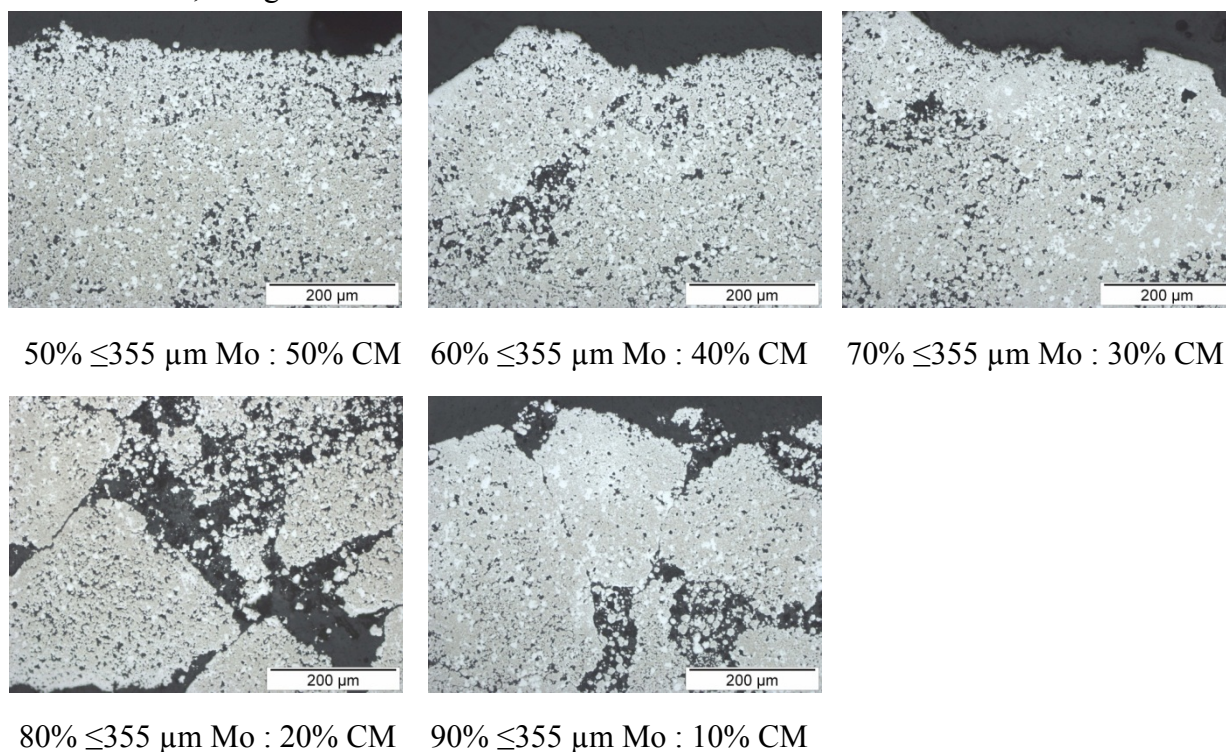


**fig. 3.108.: Metallographic sections of samples from coarse Mo powder  $\leq 355 \mu\text{m}$  mixed in different ratios with a fine grained Mo from Chemie Metall. CIPed at 200 MPa, sintered 2 h  $1300^\circ\text{C}$  in  $\text{H}_2$  + 2 h  $1800^\circ\text{C}$  in vacuum**

Samples sintered out of coarse Mo powder  $\leq 355 \mu\text{m}$  show furthermore larger spaces between the big particles which are mostly filled with fine particles and can be observed in fig. 3.108 very well. For a better adhesion between such big particles, more fine grained particles, which act as binder, are needed.

### 3.3.6 Testing of FGM for oxidation resistance

The intended application of the Si infiltrated Mo specimens is for such components that are mechanically loaded at high temperatures and in oxidizing environment, e.g. in combustion gases. Therefore, oxidation resistance is an essential requirement for these materials. In the last period of the project, Si treated molybdenum specimens were tested for their oxidation resistance. Three different specimens were received from partners. Two of the specimens were laser sintered Mo specimens from KE (the source powder for the laser sintering was a Mo powder with small amounts of Si). The third specimen was prepared from bunched Mo wires which were infiltrated with Si by IMSAS.

The oxidation experiments were carried out in an AHT pushtype furnace with  $\text{Al}_2\text{O}_3$  tube. The oxide ceramic tube was open on both ends. The specimen was placed in the center of the furnace at the hottest zone in the tube. On one end of the  $\text{Al}_2\text{O}_3$  tube a Bunsen burner burning natural gas with air supply was placed to supply combustion gases, in particular water vapour which otherwise is difficult to introduce in sufficiently



high quantities. The furnace temperature was preset to 1100 °C, and exposure time at temperature was 3 h.

Before the experiment was carried out the weight of each sample was taken. During heating up and cooling the specimen was in the furnace tube all the time. At the end of the experiment the weight of the tested specimen was taken and the each specimen characterised by LOM and SEM.

### 3.3.6.1 First specimen from KE (batch 1427\_12)

#### 3.3.6.1.1 Characterisation before oxidation

The demonstrated specimen is a laser sintered specimen. A Mo powder which was prealloyed with a low amount of Si was used as starting material for the laser sintering. Due to the fact that the specimen was not covered with a MoSi<sub>2</sub> protective layer (the amount of prealloyed Si was too low to form such a layer), it was not expected that this specimen will be oxidation resistant. The specimen was characterised on the stereomicroscope (fig. 3.109) and SEM with EDAX. In the stereomicroscope the structure, typical for a laser sintered specimen, can be observed already at 7,5 x magnification. The weight of the specimen was taken before the oxidation experiment. The weight was 15,2322 g.



fig. 3.109.: image of specimen from stereomicroscope; 7,5 x magnification

#### *SEM and EDAX analysis of the specimen as received*

In fig. 3.110 the structure of the elongated particles of the laser sintered sample can be observed in detail. Some open pores can be seen. The laser sintered particles are covered by very small particles which can be seen better at 3000x magnification. Each elongated particle (50x magnification) is built up out of several finer particles sintered together (3000x magnification). With EDAX analysis, Si was also identified since, as stated above, the source powder for the laser sintering process was a Mo powder

containing small amounts of Si. In some parts of the specimen higher amounts of Si were found, which were locally concentrated.

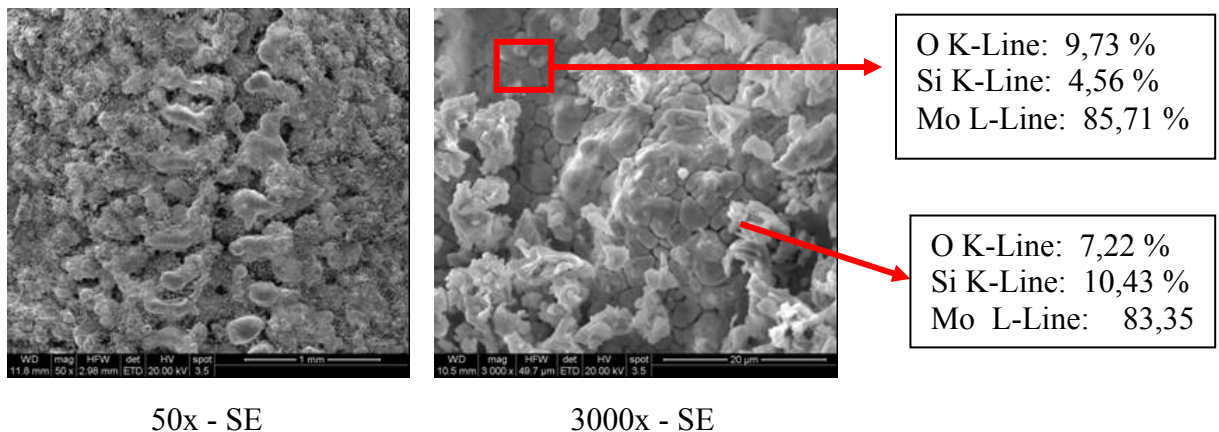


fig. 3.110.: Left: SEM image of laser sintered Mo-Si specimen. as received; right EDAX analysis

### 3.3.6.1.2 During oxidation

During oxidation the sample started to evaporate as can be observed in fig. 3.111 (left image). In the right image yellow needles in the furnace tube can be observed: Molybdenum that had been oxidized and had evaporated condensed as  $\text{MoO}_3$  in a cooler part of the furnace.

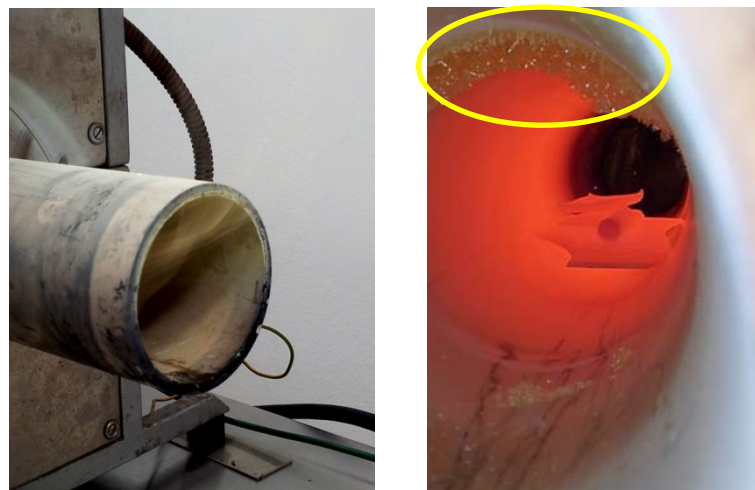


fig. 3.111.: left:  $\text{Al}_2\text{O}_3$  tube -  $\text{MoO}_3$  evaporating during oxidation; right: evaporated  $\text{MoO}_3$  condensed as needles in a cooler part of the furnace

### 3.3.6.1.3 After oxidation

After the oxidation experiment the sample was characterised by weight and on the stereomicroscope, SEM with EDAX. The weight after oxidation was 1,2175 g which is only about 8% of the original weight. This means almost all of the specimen had been lost through oxidation and evaporation of the  $\text{MoO}_3$  formed.



### ***Stereomicroscope***

The surface of the oxidized sample can be observed very well in the stereomicroscope in fig. 3.112. No shining (typical for metals) is visible, and the sample appears white in the 7,5x magnification. At higher magnifications (20x magnification) no structure is noticeable and no elongated particles (like in fig. 3.110) can be observed. The structure seems to be spongy.

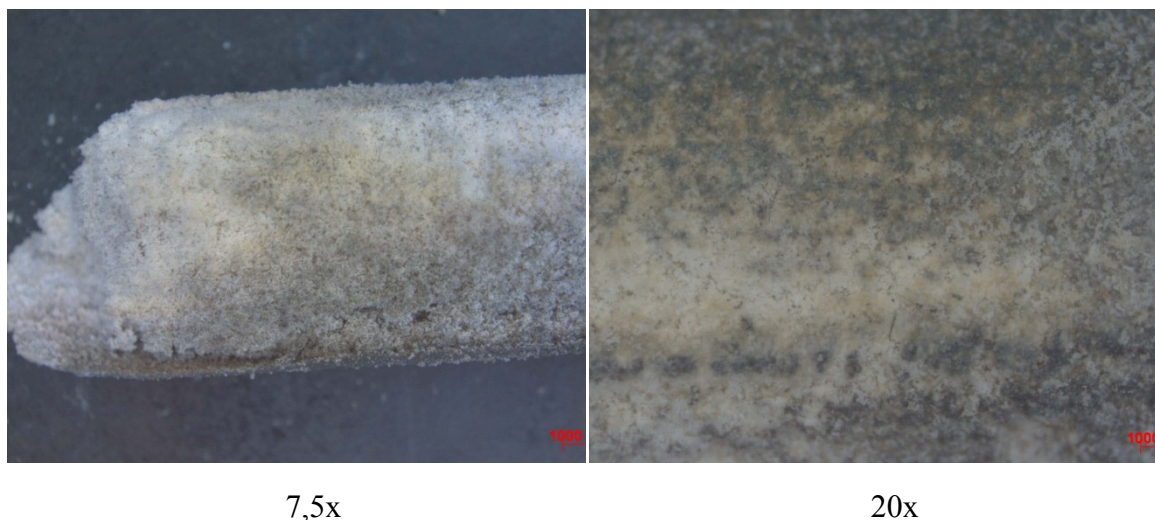


**fig. 3.112.: Laser sintered Mo (with small amounts of Si) specimen after oxidation experiment characterised on the stereomicroscope; spongy structure of the specimens visible**

### ***SEM and EDAX after oxidation test***

The specimen was sputtered with C for 10s and afterwards characterised in the SEM. In the images in fig. 3.113 the structure is difficult to recognise. Silicides and oxides (which were formed during the oxidation experiment) do not conduct electrons, and the material was charged.

The composition after the oxidation experiment was analysed by EDAX. It could be observed that the molybdenum content dropped to 0.5% from 85% before the oxidation experiment and the oxygen content increased to 45%. Most Mo evaporated during the experiment and the remaining Mo formed different oxides. The remaining material is almost completely Si and oxygen. Beside  $\text{Mo}_x\text{O}_y$  a lot of  $\text{Si}_x\text{O}_y$  was formed and remained in the material, forming a spongy shape. Because of the high amount and the insulating character of silicon oxide, it was difficult to get the particles in the image to focus.

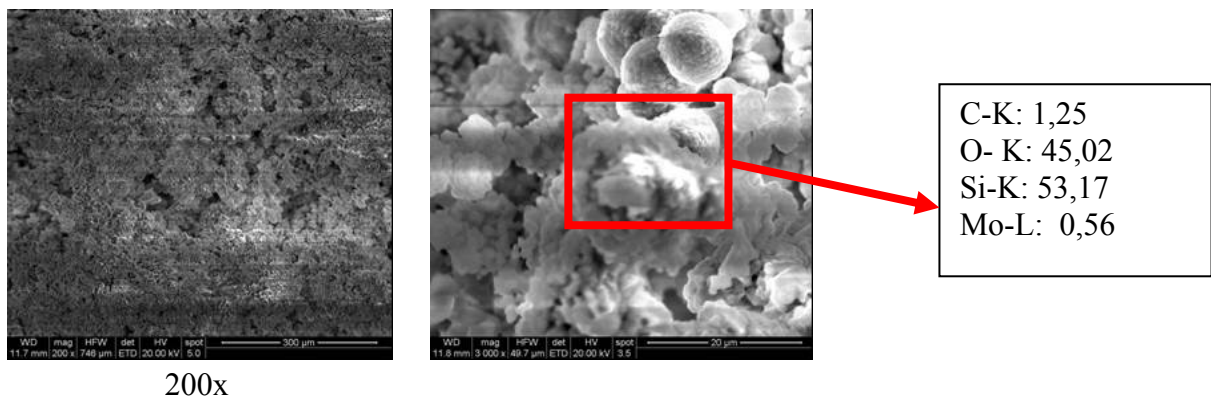


fig. 3.113.: Left and center image: SEM images of oxidised Mo specimen; right: results from EDAX analysis

### *SEM of the sample after oxidation and polishing*

One piece of the sample was cut carefully with a knife. The sample was very brittle and did not show any mechanical stability. Therefore, the small piece was embedded carefully in araldite. After the embedding material had been cured, the sample was infiltrated with super glue Loctite 404® to stabilise the structure. After hardening, the embedded sample was polished very carefully and characterised a second time on the SEM. It can be observed that the round particles consist of fine ones which were sintered together forming round particles (3000x magnification in fig. 3.114).

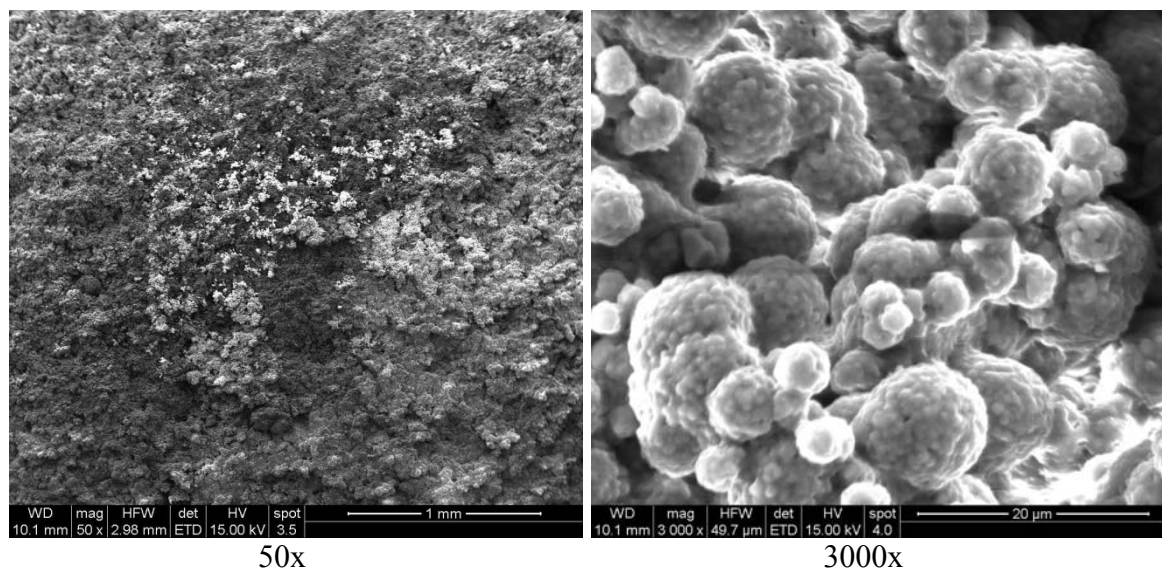


fig. 3.114.: SEM images of sample after oxidation; left: 50x magnification; right: 3000x magnification

### 3.3.6.2 Summary

A laser sintered sample with the description “batch 1427\_batch12” was tested for oxidation. The laser sintering was carried out with a Mo powder which was alloyed with some Si. Before testing the oxidation resistance of this sample, characterisation by stereomicroscope, SEM with EDAX and weighing were done. The EDAX analysis showed that the sample consists of molybdenum with silicon (between 5 to 10 wt%) and about 10 wt% oxygen. The original mass of the specimen was 15,2322 g. During the oxidation experiment molybdenum evaporated from the sample as  $\text{MoO}_3$  and condensed as needles on some cooler parts of the furnace tube.

After exposing the specimen for 3 h to an oxidising atmosphere at 1100 °C for 3 h the weight of 1,2175 g was recorded. 92% of the sample had evaporated as  $\text{MoO}_3$  during the oxidation experiment. The remaining specimen was very brittle and difficult to handle. In the stereomicroscope a spongy shape could be identified. The EDAX analysis of the element composition resulted in barely any molybdenum, just <0,5 wt%, about 50 wt% silicon and the same amount of oxygen. The residual structure is an Si-O network with Mo in traces. Apparently the amount of Si was too low in the original sample to form enough  $\text{MoSi}_2$  which is the reason why the material does not survive the oxidation test. No gas-tight silicide layer was formed. In summary it can be said, that the delivered material is not resistant against oxidation.

### 3.3.6.3 Second specimen - EPFL specimen 5

#### 3.3.6.3.1 Characterisation before oxidation

The specimen demonstrated in the following is a laser sintered specimen from KE. After laser sintering the specimen was sent to EPFL for infiltration with Si-Mg-Al. Some infiltration experiments with Mg- and Al-diluted Si have been carried out by EPFL to reduce the reactivity during infiltration with pure Si (between Si and Mo). Weighing before the oxidation experiment showed a mass of 46,2805 g.

#### ***SEM and EDAX of the specimen as received***

##### *smooth side*

In fig. 3.115 the SEM images show the surface of the smooth side of the Mo sample. The rough side of the specimen is demonstrated later. At the 3000x magnification some needles growing in-between the particles can be observed. In the EDAX analysis the surface (fig. 3.115) was characterised. About 10 wt% Mg, 14 wt% C (can only be explained by impurities; The specimen was touched by many partners during meeting for purpose of specimen observation and it seems like cleaning in isopropanol was not enough), about 8 wt% O, 11 wt% Si and traces of Al (~0,6 wt%) were found. Molybdenum was measured as 55 wt%. Residual Mg (quite high) was found inside, which indicates that the evaporation of Mg after infiltration (by EPFL) was not completely successful.

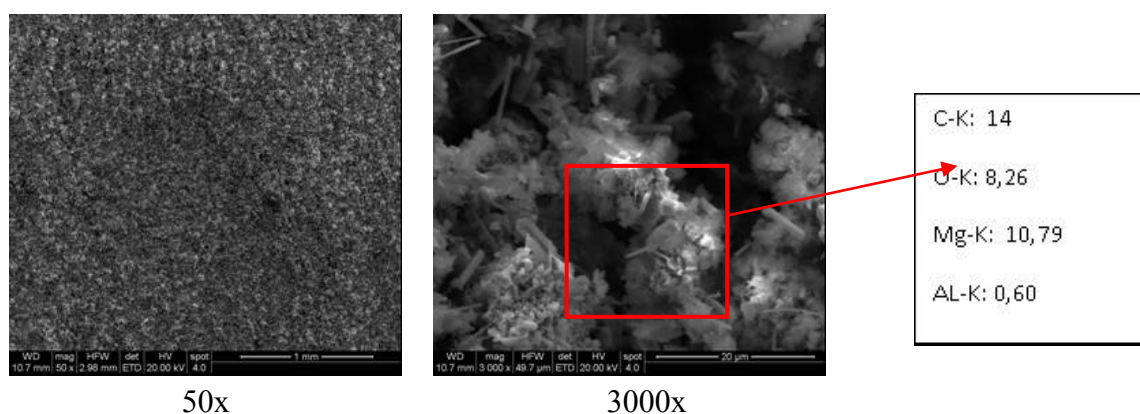


fig. 3.115.: Left and center image: SEM characterisation of specimen before oxidation test; right image: EDAX analysis

### *rough surface*

In fig. 3.116 the rough side of the sample is shown in SEM images. Compared to the smooth side (fig. 3.115) no needles can be seen. In fig. 3.116 also the results from the EDAX analysis of the sample are given. No needles can be seen but the composition is similar to that of the smooth side (fig. 3.115). About 5 st% Mg, 29 wt% Si, about 11 wt% O and traces of Al were found. Molybdenum was measured as 54%. A lot of Mg was found, which indicates that the Mg was not evaporated fully.

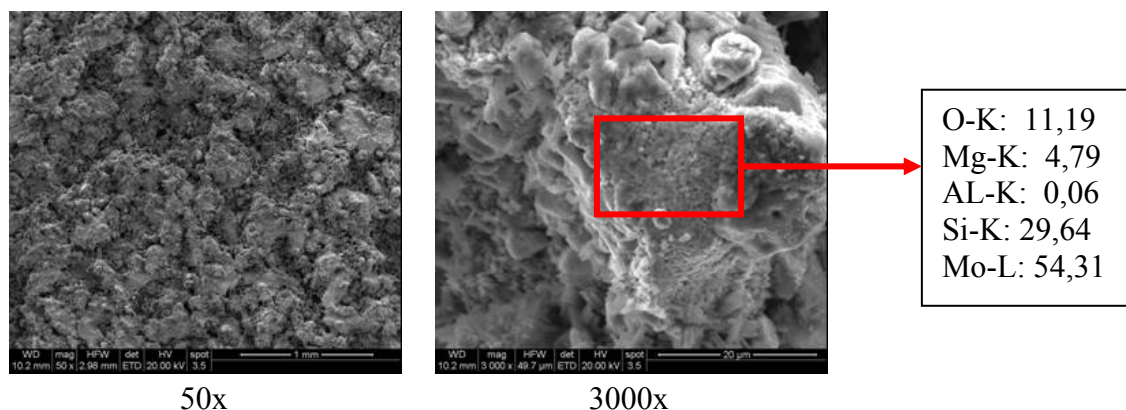


fig. 3.116.: Left and center images: SEM characterisation of specimen before oxidation test; right image: EDAX analysis

### 3.3.6.3.2 During oxidation

During the oxidation experiment the sample started to sublime. One part of the evaporated molybdenum condensed as  $\text{MoO}_3$  needles in some cooler parts of the furnace, and the residual evaporating material was trapped in a metal bucket (which was located on one end of the furnace tube). The specimen showed very similar behavior to the one described in chapter 3.3.6.1 and the images in fig. 3.111.

### 3.3.6.3.3 After oxidation



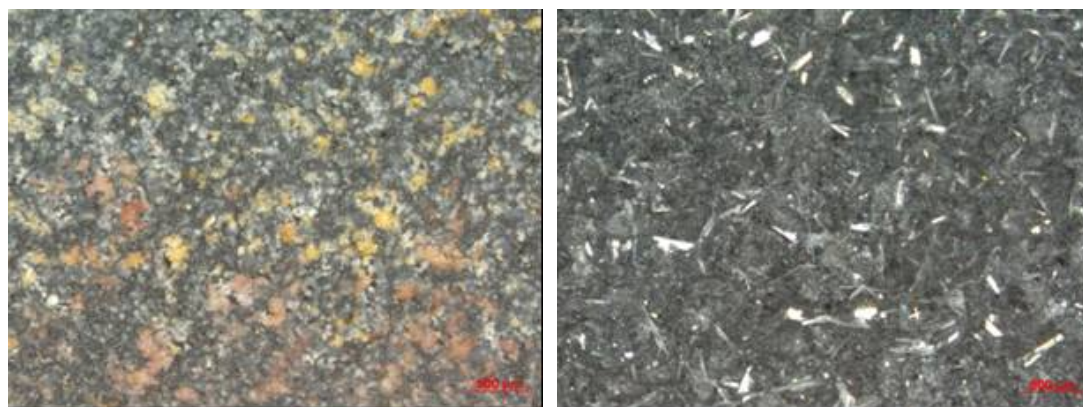
After the oxidation experiment the residual sample was weighed to gain the weight change. The weight was decreased to 37,4481 g which is 81% of the original weight (46,2805 g). Furthermore a profound change in colour on the sample surface was observed. Some yellow and red regions occurred (fig. 3.117).



fig. 3.117.: Photo camera image of the specimen after oxidation test

### *Stereomicroscope*

In fig. 3.118 - left the smooth surface of the sample is shown. Different colours like yellow and red can be identified. Except of the colours no other change to the unoxidised state can be observed on the stereomicroscope. On the rough side (fig. 3.118 - right image) much more needles could be observed after oxidation. Before oxidation these needles could be seen only in SEM images on the smooth side of the specimen (fig. 3.115 - middle image). As consequence of oxidation the needles grew to an optically visible scale.



Smooth surface - 30 x

Rough surface - 30 x

fig. 3.118.: Left image: smooth surface of Mo specimen after oxidation experiment - different colours occurred; right image: rough side of oxidised specimen with needles

### *SEM and EDAX characterisation after the oxidation test*

*smooth surface*

The areas of the specimen that appeared red and yellow in the stereomicroscope images (fig. 3.119) were characterized by SEM and EDAX too.

The red region (fig. 3.119) can be observed with some dots. No needles can be seen. Some regions with smooth surface could be observed in the SEM. These regions showed a high content of oxygen (36,6 wt%), about 42 wt% silicon and 21 wt% of molybdenum. In contrast, regions which appeared more rough in the SEM showed less silicon (of about 35 wt%), almost the same amount of oxygen and molybdenum but traces of elements like Na, Mg and Al.

In the yellow region in contrast to the red region some “needles” and grains with sharp edges can be seen at 800x magnification in the SEM. These needles and grains were analysed in EDAX, and it can be seen that they contain 12-14 wt% Mg. The bulk material contains <0.5 wt% Mg. Well, as it was already mentioned in the beginning, the infiltration of the bulk Mo with Si-Mg-Al should help to handle the strong exothermic reaction which occurs during infiltration with Si (between Mo and Si, where Mo is dissolved in Si). Mg and Al dilution should lower the the temperature increasing during infiltration with Si. On the other hand, it could be shown with the EDAX analysis that the Mg could not be completely evaporated after infiltration with Si.

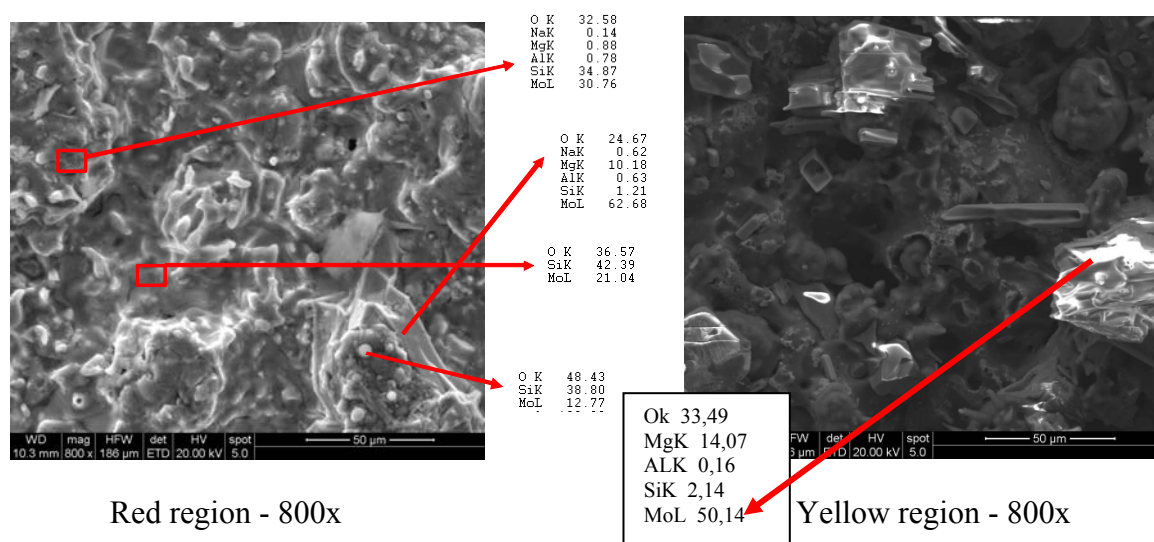


**fig. 3.119.: SEM and EDAX characterisation of the two surfaces of Mo specimens; left: red region; right: yellow region**

*rough surface*

On the rough side of the sample many needles could be observed in fig. 3.120. By a closer look at 1500x magnification needles all over the surface can be seen.

In fig. 3.120, too, some results from the EDAX analysis are shown. The bulk material contains <0,5 wt% Mg, about 1 wt% Al, about 7,5 wt% silicon, and the main component is molybdenum with 23 wt% oxygen. The analysis of the needles gave as result a higher amount on silicon (35 wt%) and oxygen (46 wt%) and less molybdenum (18 wt%).

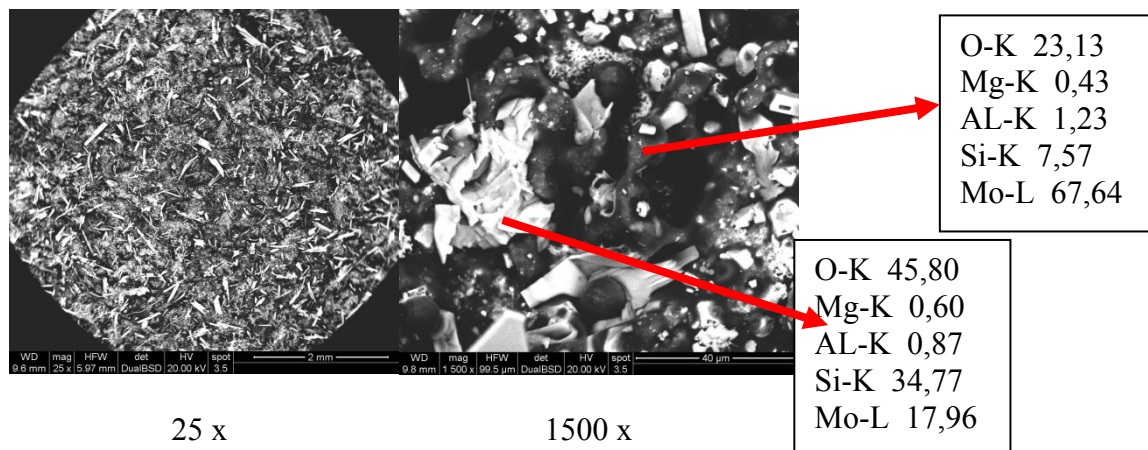


fig. 3.120.: Left and center image: rough surface of specimen after oxidation test; right image: EDAX analysis of the rough surface

### *Sample after polishing after oxidation resistance testing: SEM and EDAX*

The embedded and polished cross section (cut along the height) of the sample is shown in fig. 3.121. At 1600x magnification the three different occurring colours (grey shades) can be seen very well. The core of a particle is much brighter than the other shells around. The center shell covers the core completely while the outer shell is discontinuous with differing width of the shell.

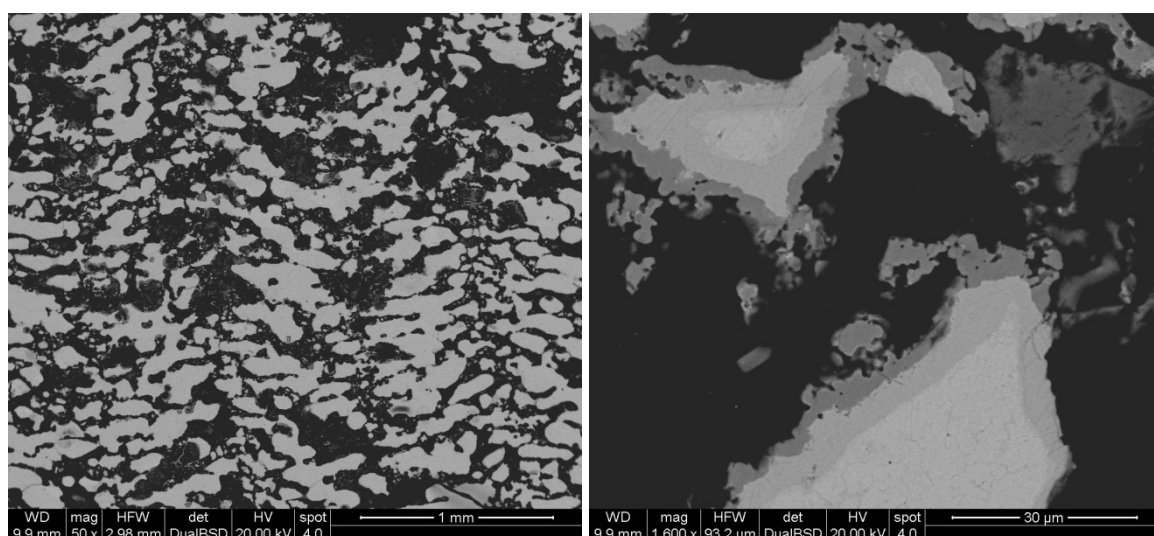


fig. 3.121.: BSE images of embedded and polished sample; left: 50x; right: 1600x magnification

All three zones were characterized on EDAX (fig. 3.122). The core of the particle (bright grey) has the lowest amount of silicon, with 2%. The intermediate shell contains



15 wt% Si and the outer shell contains the highest amount of Si with 34,1 wt% Si. 5.5-7 wt% oxygen could be measured in each shell. It can be furthermore observed (in fig. 3.122 at 3000x magnification) that the outer shell is discontinuous.

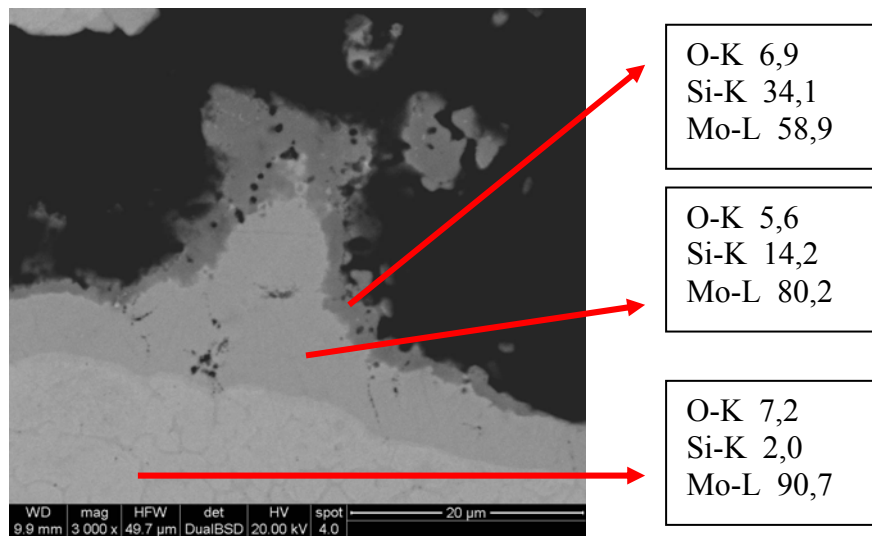
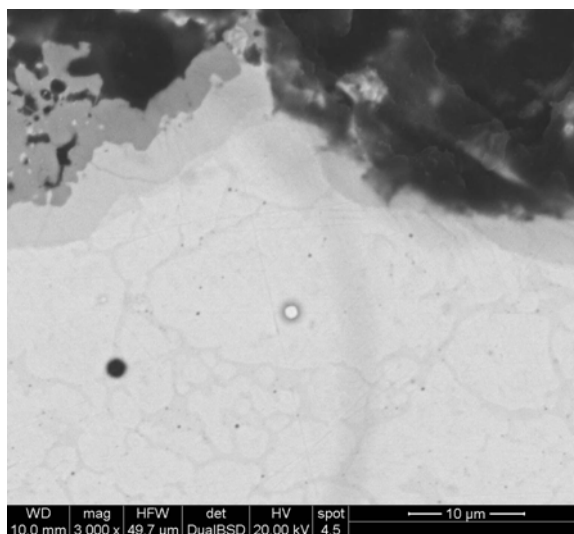


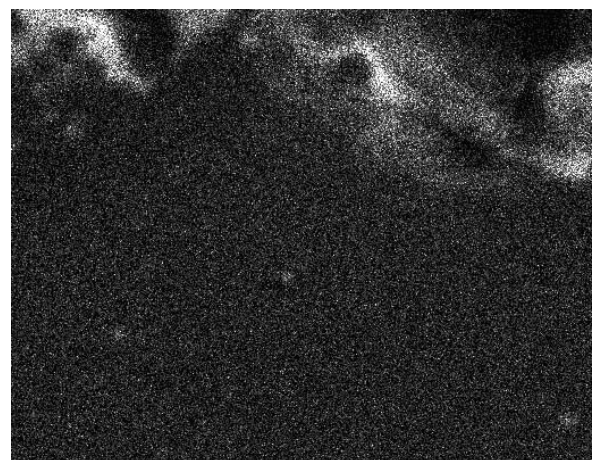
fig. 3.122.: EDAX analysis of the specimen after oxidation test; 3000x magnification

### Mapping

The distribution of silicon, molybdenum and oxygen after the oxidation test was determined by preparing an element mapping. It can be seen in fig. 3.123:  $O(K_{\alpha})$  image, that the outer shell of the illustrated grain contains the highest amount of oxygen. This leads to the conclusion that this part was oxidized. Furthermore the highest Si content was measured in the outer shell. Inside of the one big grain (light grey core shown in fig. 3.123 BSE image), Si is located around smaller grains and thin Si-veins are passing through the big grain.



BSE image



$O(K_{\alpha})$



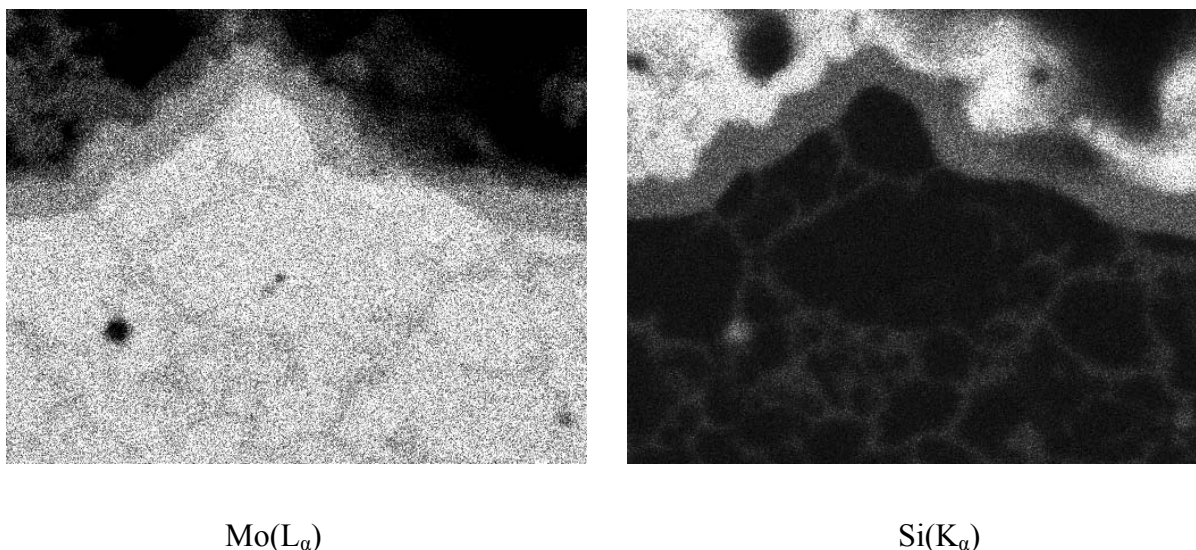


fig. 3.123.: SEM-EDAX elemental mapping: distribution of Mo, Si and O in specimen after oxidation experiment; 3000x magnification

### 3.3.6.4 Summary

A laser sintered sample out of Mo which was infiltrated with Si- Mg - Al (Mg and Al evaporated during infiltration), was tested for oxidation resistance in combustion gases. Before testing and after the test, some characterisation on stereomicroscope, SEM with EDAX and weighing were done. The specimen had a smooth and a rough side. The EDAX analysis showed that the sample consists of molybdenum with silicon (about 10 wt%), about 8 wt% oxygen and 10 wt% Mg were found. The original weight of the specimen was 46,2805 g. During the oxidation experiment molybdenum evaporated as  $\text{MoO}_3$  from the sample and condensed as  $\text{MoO}_3$  needles on cooler parts of the furnace tube.

After exposing the specimen to an oxidising atmosphere (combustion gases) at 1100°C for 3 h a weight of 37,4481 g was recorded, i.e. 81 wt% of the original weight, which indicates insufficient oxidation resistance also here, although definitely better than with the previous specimen.

In the stereomicroscope, yellow and red coloured areas could be observed on the smooth surface of the specimen. These areas have been characterised by SEM. In the red region some smooth particles were observed which contained about 10% Mg. In the yellow region some angular particles can be found which look like broken needles. These “needles” contained 12-14 wt% Mg, 2-4 wt% Si, about 30 wt% oxygen and 50 wt% Mo (It might be probably  $\text{MgMoO}_4$  which was found in the literature as a stable  $\alpha$  and  $\beta$  phase) [161].

The rough surface was interspersed with needles which were characterized by EDAX. The needles consist of Si (~35 wt%), about 18 wt% Mo and 46 wt% oxygen. The bulk material in this area contains less silicon (~7,6 wt%), less oxygen (23 wt%) but more Mo (wt68%).

In the EDAX analysis three different areas in one grain could be observed. The core of each grain contained the lowest amount of Si with 2%. The outer part contained the most Si (34 wt%) and oxygen was analyzed too in the elemental maps.

In the as-received specimen, i.e. before oxidation, needles growing out of the sample surface were observed (fig. 3.115) on the smooth side of the specimen. These needles

grew during oxidation and after the oxidation experiment the surface was strewn with needles (fig. 3.120). The average Si content was low with 11 wt% which might be too low to form enough protective  $\text{MoSi}_2$ . Furthermore the surface of the particles was not uniformly covered by  $\text{MoSi}_2$  and oxide formation on uncovered particles surface was measured (fig. 3.122 and fig. 3.123). For this reason Mo in form of  $\text{MoO}_3$  evaporated. The specimen thus had to be classified as being not sufficiently resistant against oxidation.

### 3.3.6.5 third specimen - IMSAS sample

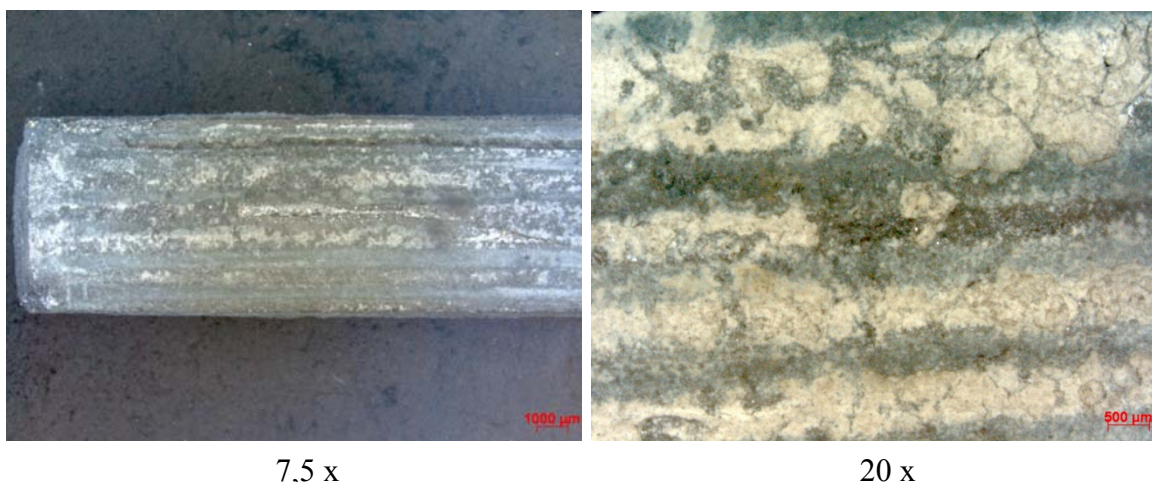
#### 3.3.6.5.1 Characterisation before oxidation

This specimen used for oxidation testing was prepared from bunched Mo wires in a Mo capsule which assembly was then infiltrated with Si by IMSAS. This specimen seems to have been cut before the infiltration process and one part of it was handled out of TUW for testing. Weighing of the specimen showed a mass of 5,2374 g.

The surface of the specimen was characterised in the stereomicroscope and by LOM before the oxidation experiment was started.

#### *stereomicroscope*

In the stereomicroscope image the capsule of the Mo wires can be seen. In the left image in fig. 3.124 a crack can be observed that proceeds along the length of the specimen. In the right image (fig. 3.124), 20 x magnification shows the surface a little bit closer. Some further small cracks can be observed.



7,5 x

20 x

**fig. 3.124.: Mo wires in a capsule, Si infiltrated at IMSAS**

#### *LOM*

In fig. 3.125 the cross section of the Si infiltrated Mo wire can be seen. The specimen was cut by IMSAS before infiltration and was handled over to TUW afterwards for the oxidation resistance experiment. The Mo wires appear in white colour while the  $\text{MoSi}_2$  around the wire appear in light blue colour. The residual Si between the wires

appears also in light blue colour. Some cracks can be recognised in the MoSi<sub>2</sub> layer. A sharp line/space between the wires can also be seen. The silicides which were growing away from one Mo wire did not join with the silicides from the opposite wire.

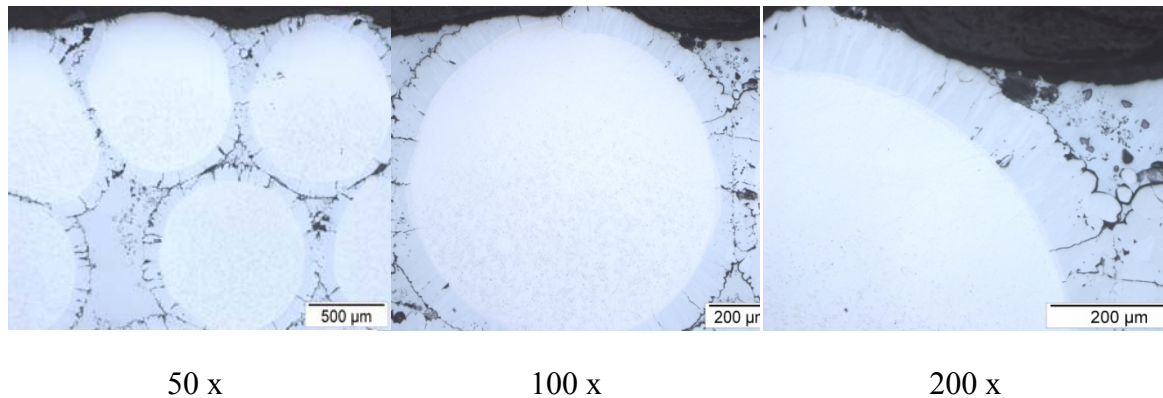


**fig. 3.125.: LOM images of the specimen from Mo wires in a Mo capsule which was infiltrated with Si by IMSAS**

#### 3.3.6.5.2 Characterisation after oxidation

The accurate weight of the specimen after oxidation resistance test was taken. A mass loss of 0,0812 g could be observed. The sample mass after the test was 5,1562 g which means that the specimen lost 1,55 wt% of its mass.

##### *Stereomicroscope*

In fig. 3.126 the surface of the Mo capsule can be observed after the oxidation test. The colour changed but no other difference can be seen. Even the crack which was observed in fig. 3.124 did not grow further.

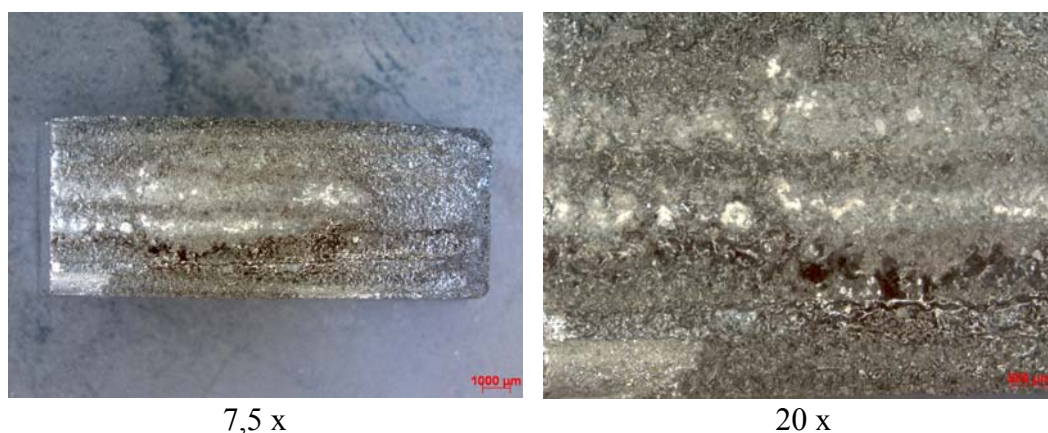


**fig. 3.126.: Both images show the surface of the Mo capsule after oxidation testing**

##### *LOM*



In fig. 3.127 the cross section of the specimen can be observed after the oxidation test. The specimen was etched with Murakami I+II (1:1) for 50s which explains the darker colour in the centre where the Mo wire can be seen. Around the wire  $\text{Mo}_x\text{Si}_y$  can be observed very well, it appears in the LOM in light blue colour. No difference in structure can be observed after the oxidation experiment.

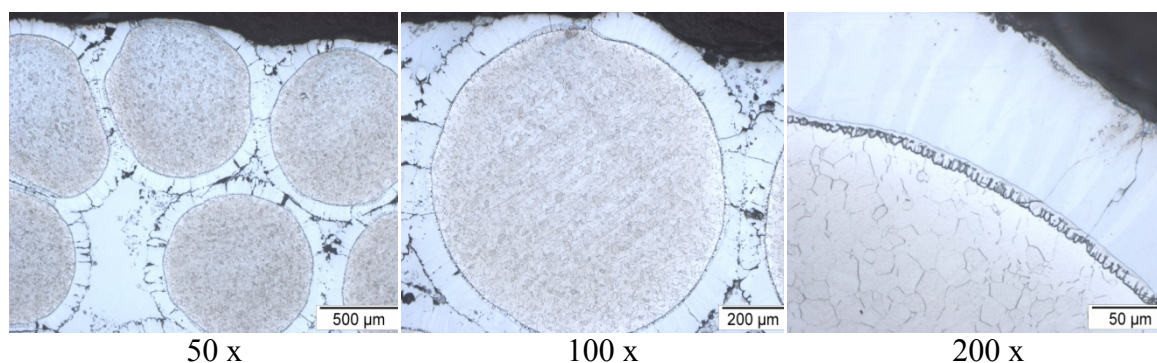


**fig. 3.127.: Cross section of Mo wires in a Mo capsule which were infiltrated with Si; sample was etched with Murakami I+II (1:1) for 50s**

### *SEM and EDAX*

The BSE images in fig. 3.128 are showing the Mo wires after infiltration and the oxidation experiment. As could be already observed in the LOM before oxidation (fig. 3.125) is that cracks occurred in the silicide layer. At 2000x magnification in fig. 3.128 can be observed that the crack propagates through the darkest to the intermediate layer and stops before the Mo core. Some characterisation on EDAX has been prepared too. The composition of each area (which was highlighted by colour in BSE) was analysed by EDAX and the phase which corresponds to the composition was summarised here. The dark layer (fig. 3.128 - 2000x) is  $\text{MoSi}_2$  and the intermediate layer (between the dark one and the Mo core) was characterised as  $\text{Mo}_5\text{Si}_3$ . The distribution of silicon can be seen very well in the elemental maps, in the right image in fig. 3.128. There are always sharp boundary lines between the layers. Furthermore it can be said that there is no noticeable change after the oxidation test compared to the as-delivered state.



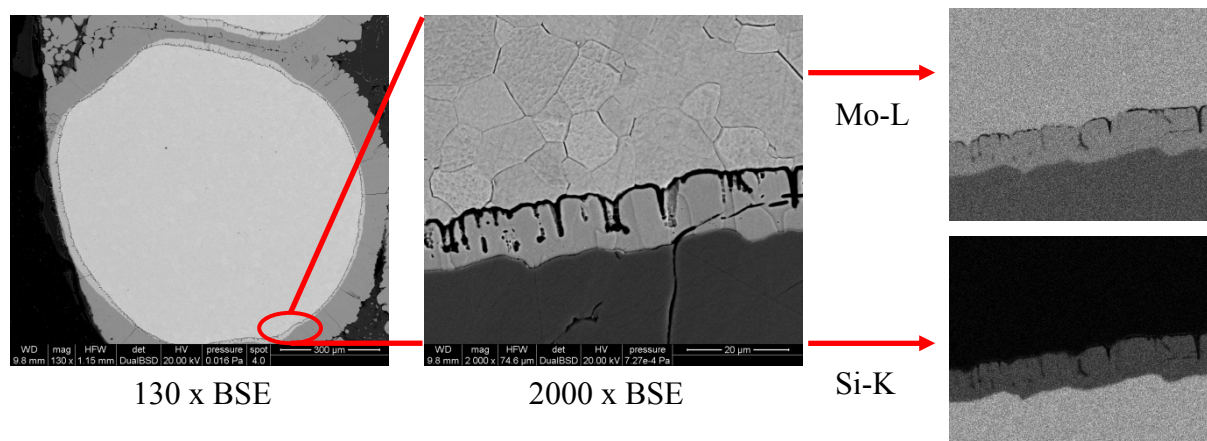


**fig. 3.128.: Left and center image: BSE images of infiltrated Mo wires; right images: elemental mapping of center image showing the Mo and Si distribution**

### 3.3.6.6 Summary

Molybdenum wire bundles were encapsulated and Si infiltrated by IMSAS in Bratislava and were received for oxidation tests. The specimen was weighed before and after the testing. Some investigations by LOM, SEM and stereomicroscope were prepared to characterise the specimen before and after the oxidation test. For the experiment the specimen was exposed to an oxidising atmosphere – air and  $\text{CH}_4$  combustion gases - at  $1100\text{ }^\circ\text{C}$  for 3 h. The specimens mass before oxidation was 5,2374 g after the oxidation experiment the weight decreased to 5,1562 g which is 1,55 wt% mass loss.

The surface of the capsule was characterised on the stereomicroscope before (fig. 3.124) and after (fig. 3.126) the experiment. A crack propagating along the surface in the capsule could be observed before the oxidation experiment. Furthermore the colour of the surface changed after the oxidation tests.

The cross section was investigated too. The Mo wires with  $\text{Mo}_5\text{Si}_3$  around the Mo core and  $\text{MoSi}_2$  enclosing the  $\text{Mo}_5\text{Si}_3$  layer could be observed. Some cracks in the  $\text{MoSi}_2$  and  $\text{Mo}_5\text{Si}_3$  layer were also visible. In all cases they stopped propagating before the Mo core. There was no difference in the cross section after the oxidation experiment compared to the stage before oxidation. Due to the very low mass loss and the cracks in the Mo capsule, the mass loss during the oxidation experiment might come from the capsule, not from the infiltrated Mo wires inside it. In any case, this specimen can be regarded to have sufficient oxidation resistance.

### 3.3.6.7 Fourth specimen: oxidation resistance of Mo + x\*wt% Si hot pressed at 1800 °C with 50 kN

For this experiment specimens from chapter 3.2.2.1 were taken. These are Mo specimens with 3 / 5 / 15 / 25 / 37 wt% Si hot pressed at 1800 °C for 120 min in vacuum with 50 kN load applied. The specimens before oxidation have already been described, therefore only the results after the oxidation test will be presented here.

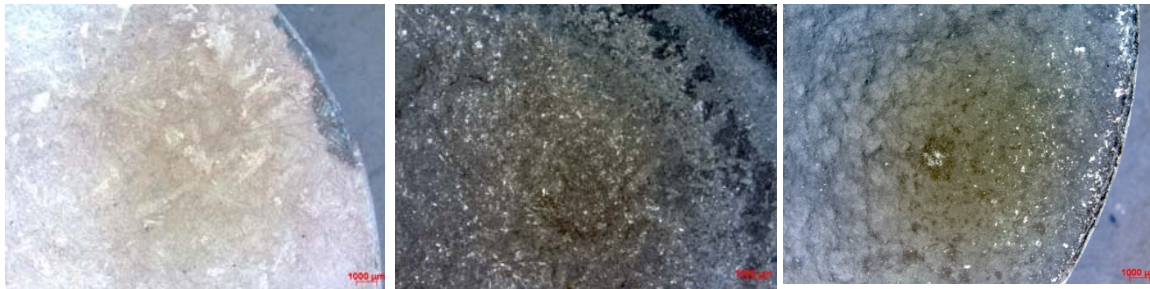
A comparison measurement with fully dense piece of a MoSi<sub>2</sub> heating rod was carried out at the same temperature, time and atmosphere. The specimens weight before and after the oxidation resistance testing was taken. No change in weight after the test could be observed which means that this MoSi<sub>2</sub> specimen is fully protected against oxidation. In tab. 33 the mass of all tested Mo + x\*wt% Si specimens before and after the oxidation experiment is given. It can be seen easily that with increasing amount of Si the weight loss is decreasing. However, even the molybdenum specimen with the highest Si content (37 wt%) still loses 5 % mass during the oxidation test. One can conclude from these results that even this specimen (tab. 21 --> 59 wt% MoSi<sub>2</sub> was formed after hot pressing - 49 % Mo<sub>5</sub>Si<sub>3</sub>) is not fully stable in the oxidising atmosphere. It could be observed already (fig. 3.66) that the structure of the specimen is not single-phase after hot pressing, which means that in addition to the oxidation resistant phase MoSi<sub>2</sub> also the less resistant Mo<sub>5</sub>Si<sub>3</sub> is present, and apparently the latter is in fact progressively oxidized.

tab. 33.: Mass change of all Mo + x\*wt% Si specimens during the oxidation test (3 h 1100°C, combustion gas + air)

sample	before oxidation [g]	after oxidation [g]	weight loss [g]	weight loss [%]
Mo+3%Si	110,2320	78,4630	31,77	29
Mo+5%Si	89,7360	74,0963	15,64	17
Mo+15%Si	67,5782	61,2326	6,35	9
Mo+37%Si	66,6713	63,6181	3,05	5

#### *stereomicroscope*

Some stereomicroscope images in fig. 3.129 show the Mo specimens containing 3/5/37 wt% Si after the oxidation experiments. The left specimen in fig. 3.129 shows the Mo specimen containing 3 wt%. No MoSi<sub>2</sub> was measured by XRD in this specimen (tab. 21). The surface of this specimen is covered with some white shiny needles. These needles are MoO<sub>3</sub> which condensed after cooling down on the surface of the specimen.. In the center image (Mo + 5 wt%Si) less needles can be observed and in the right one, where 51 wt% MoSi<sub>2</sub> were detected by XRD, no needles can be observed even though 5 wt% of the material evaporated.



Mo + 3 wt% Si - 7,5 x

Mo + 5 wt% Si - 7,5 x

Mo + 37 wt% Si - 7,5 x

**fig. 3.129.: Stereomicroscope images of three different specimens after oxidation experiment at 7,5 x magnification**

It could be seen that with increasing amount of Si in Mo, more protective  $\text{MoSi}_2$  was formed, which explained why less material was lost during the oxidation experiment. Nevertheless even in Mo containing 37 wt% Si – i.e. the stoichiometric composition of  $\text{MoSi}_2$  - a loss of 5 wt% material could be noted. It is still a high amount compared to a fully dense material from  $\text{MoSi}_2$  where no loss of the material during oxidation tests could be noted.

### 3.4 Niobium preforms

#### 3.4.1 Sintering

In parallel to the sintering of Mo specimens also some Nb samples have been prepared, characterised and compared with Mo. In the beginning two Nb powders, a coarse and a fine grained one, have been analysed. Small amounts of these powders were stored at TUW. The third powder was bought and also characterised. The third Nb powder was also a coarse grade and also one from the same company. They differ merely in the supplier designation, which can be explained by the time lag between the dates the powders were bought.

First niobium samples were prepared from H. C. Starck powders. One powder was a fine grained H. C. Starck 3050 powder and the second one was a very coarse powder also from H. C. Starck, grade 2944. Both powders were pressed uniaxially at 200 MPa in a cylindrical die ( $d = 11,27$  mm) on Amsler hydraulic press. Each sample was sintered in a Bähr 402C dilatometer at  $1400^{\circ}\text{C}$  for 60 min in rotary pump vacuum, with 10 K/min heating and cooling rate.

##### 3.4.1.1 Dilatometry

In fig. 3.130 the dilatometer curves of the two sintered samples can be seen. The blue curve shows the change in length for the sample prepared from the coarse powder whereas the black curve shows the sample from the fine grade. Up to  $900^{\circ}\text{C}$  both samples are expanding. From this temperature the sintering process starts, and the samples are shrinking. Only marginal densification could be observed. The expansion and shrinkage of the fine grained specimen was more distinctive. The maximum shrinkage for the latter specimen (out of fine grained powder) was  $\sim 1,1$  % and for the one specimen out of a coarse one about 0,6 % shrinkage have been measured. The curves shown below are uncorrected curves, i.e. a curve for the thermal expansion of the  $\text{Al}_2\text{O}_3$  holder material has not been subtracted. The thermal expansion coefficient of  $\text{Al}_2\text{O}_3$  is  $6,5\text{--}8,9 \cdot 10^{-6}/\text{K}$  while that for Nb is  $7,1 \cdot 10^{-6}/\text{K}$ . If the curves beneath will be corrected a higher expansion would be observed.



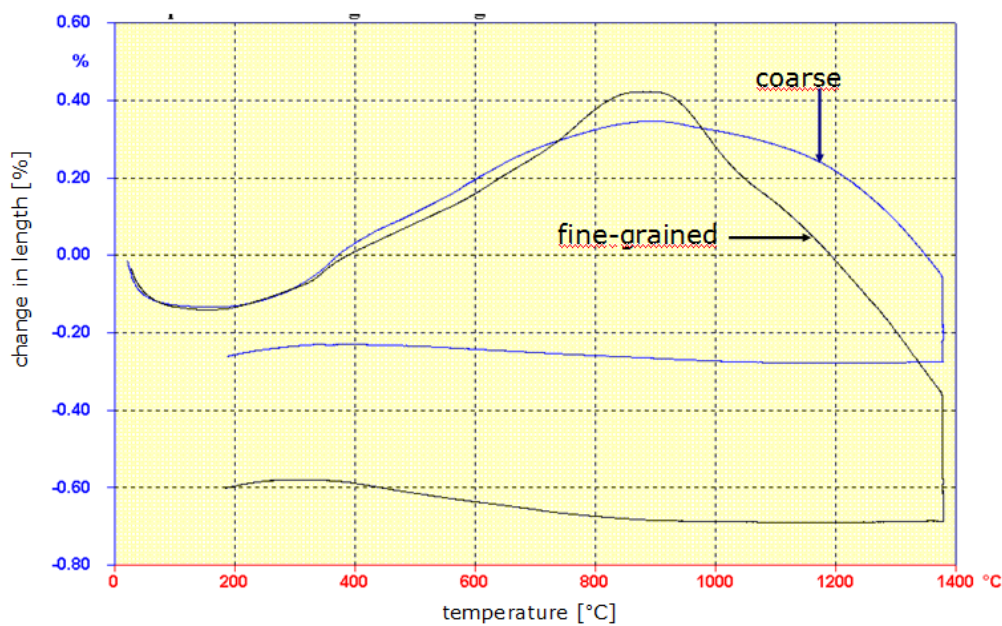
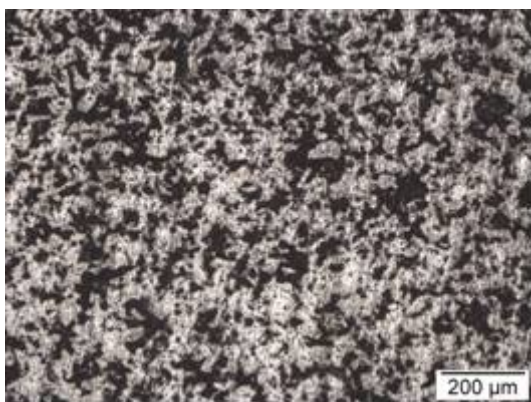


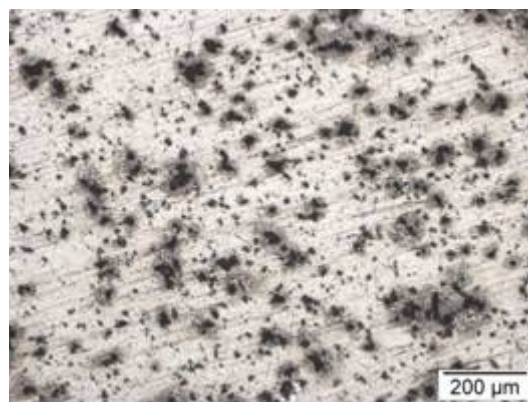
fig. 3.130.: Sintering of Nb compacts from coarse and fine powders. Isothermal hold at 1400°C for 60 min in vacuum (uncorrected curves)

### 3.4.1.2 Light microscopy

Metallographic cross sections of two Nb specimens were prepared, see fig. 3.131. A lot of big pores surrounding the grains can be observed in the specimen from coarse powder. The specimen from fine powder shows less and smaller pores. Around the pores a grey area can be observed which comes from local oxidation during sample preparation. The specimen might have been oxidized during grinding in water or even at polishing with diamond suspension. It was quite difficult to dry the specimen (drying with a hair dryer and in a drying chamber at 50 °C for 3 h have been tried). Some exuding liquids might also oxidise the specimen.



coarse Nb (H.C. Starck 2944) - 100x



coarse Nb (H.C. Starck 3050) - 100x

fig. 3.131.: left: sample cross section out of coarse Nb powder; right: sample cross section out of fine grained Nb powder

The open porosity was measured by He-Pycnometry and the hardness as HV10; the results are listed in tab. 34. A marginal difference in density and open porosity could be observed between the two powders even though it was expected to see a much higher difference in density in the cross section. The hardness differs significantly. The sample from coarse niobium powder shows a significantly lower hardness with  $40 \pm 1$  HV10 than the sample from fine powder with  $56 \pm 2$  HV10.

**tab. 34.:** Density, open porosity and hardness of the sintered niobium samples

Nb - powder	Density [g/cm <sup>3</sup> ]	Open Porosity [%]	HV 10
coarse	5,85	31	$40 \pm 1$
fine - grained	5,95	29	$56 \pm 2$

Due to the fact that for infiltration with Si, wide pores and a high degree of open porosity are needed, a coarse Nb powder was bought from H.C. Starck. It was a Nb grade "Amperit 30/10  $\mu\text{m}$ " which is about as coarse as the H. C. Starck 2944 powder. Further experiments with the new coarse powder were carried out by varying compacting pressures and sintering temperatures. Cylindrical samples with 11.27 mm diameter and about 15 mm height have been pressed uniaxially with three different compacting pressures (150/170/200 MPa). The compacted samples were sintered in a "MF - recipient - induction - furnace " at four different temperatures starting at 1350°C and increasing the temperature by 50 °C each. All samples were sintered in vacuum (at about  $2,5 \cdot 10^{-2}$  bar the sintering process was started) in an induction furnace with 60 min isothermal soaking time.

The density, open porosity, hardness (HV10) and microstructures are summarised in the following.

Some physical and mechanical properties as a function of the sintering temperature and compacting pressure are listed in tab. 35. The green densities could not been measured, due to the fact that the green compacts were very brittle and it was difficult to handle them without destroying the specimens.

**tab. 35.:** Density, hardness and open porosity of sintered Nb specimens (Amperit 30/10 powder)

sintering temperature [°C]	compacting pressure [MPa]	density [g/cm <sup>3</sup> ]	HV 10	total porosity [%]	open porosity [%]
1350	150	5,80	36	31	30
	170	6,04	36	29	28
	200	6,30	42	26	25
1400	150	5,84	38	31	30
	170	6,01	39	29	28
	200	6,31	45	26	24
1450	150	5,97	48	30	29
	170	6,17	49	28	26
	200	6,37	51	25	24
1500	150	6,04	49	29	28
	170	6,16	57	27	26
	200	6,41	60	25	23

With increasing compacting pressure and sintering temperature the density (measured with Archimedes method after impregnation) is increasing too. The highest Archimedes density was measured for the sample that was compacted with 200 MPa and sintered at 1500 °C. While the density is increasing, the open porosity is decreasing. In any case it showed that even for the highest compacting pressure and sintering temperature the porosity remained almost completely open, which with regard to infiltrability is a very positive result.

With increasing density the hardness (HV10) is increasing too. The values summarised in tab. 35 are graphically shown in fig. 3.132– fig. 3.134.

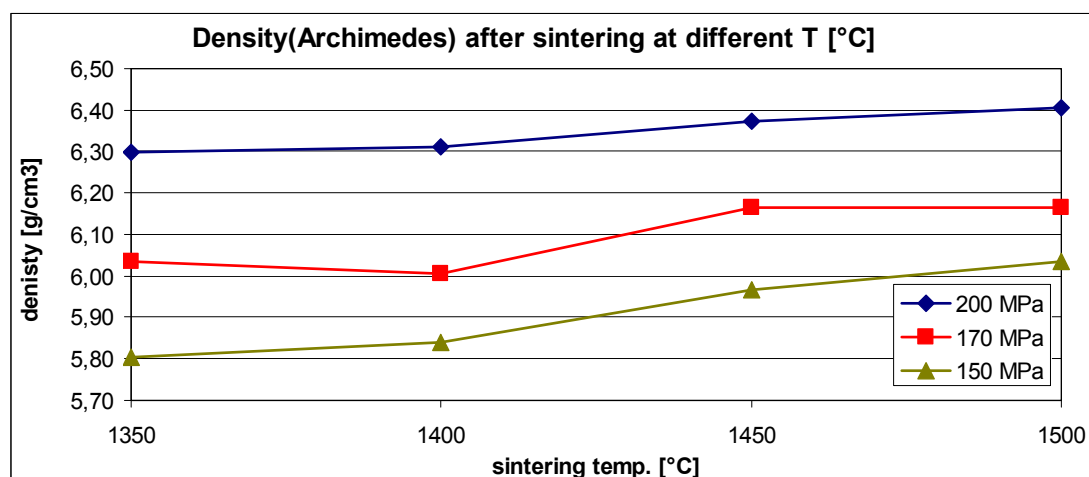


fig. 3.132.: Sintered density of Nb samples (Amperit 30/10 powder) pressed with different compacting pressures and sintered at different temperatures

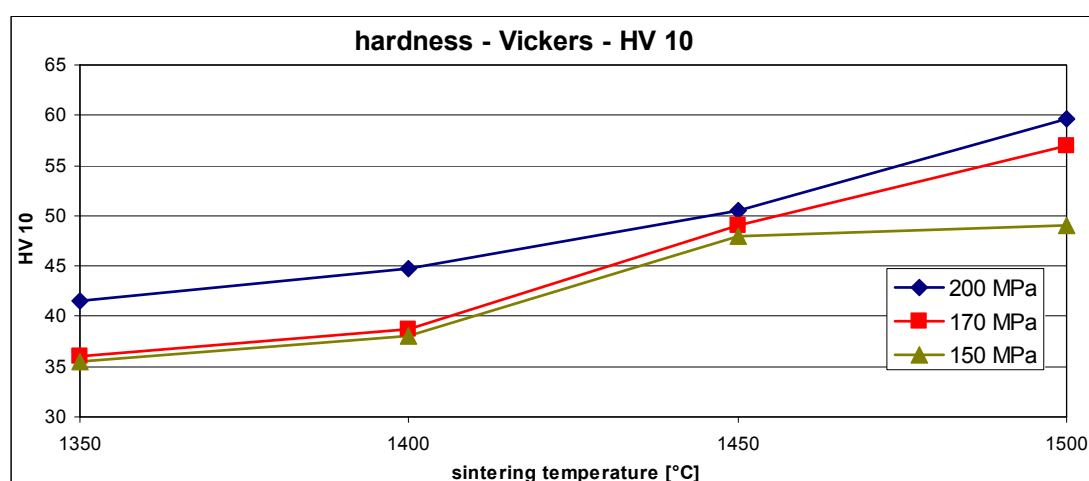


fig. 3.133.: Hardness HV 10 of Nb specimens (Amperit 30/10 powder) pressed with different compacting pressures and sintered at different temperatures

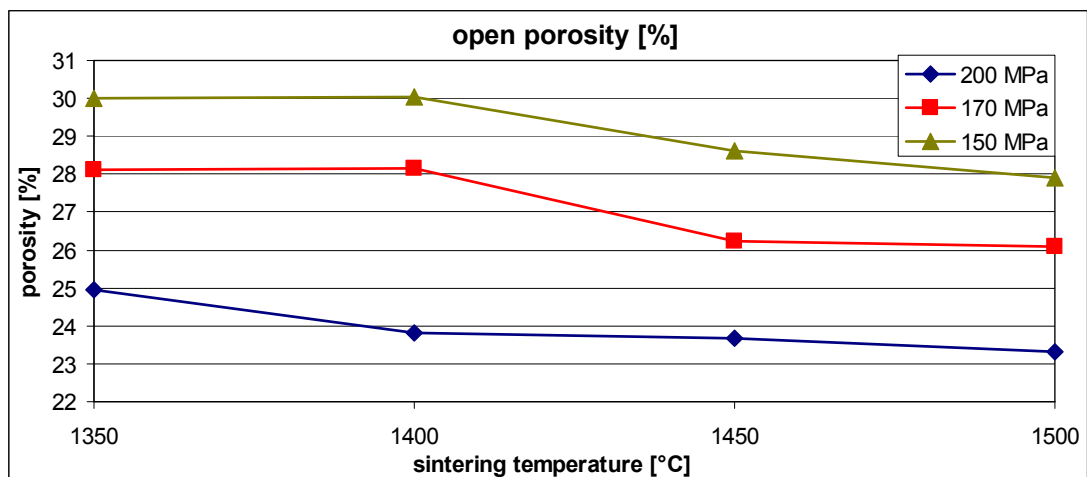
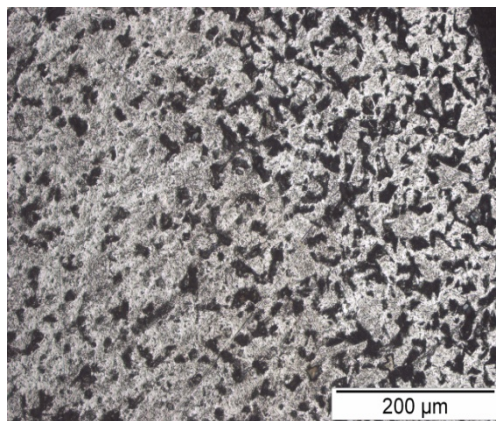


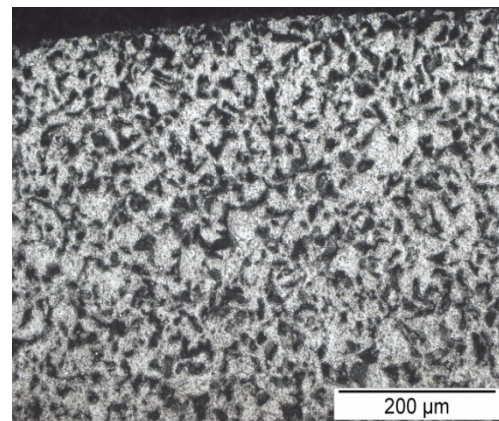
fig. 3.134.: Open porosity after sintering of Nb compacts; different sintering temperature and compacting pressures (Amperit 30/10 powder)

### 3.4.1.3 Light microscopy

In fig. 3.135 some images are shown from samples pressed with 200 MPa and sintered at different temperatures.



1350 °C - 200x



1400 °C - 200x



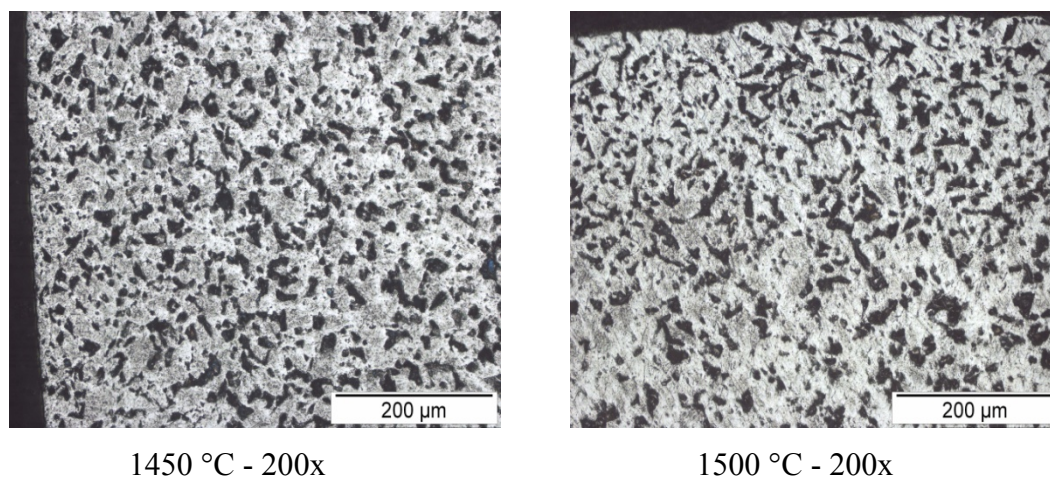


**fig. 3.135.: LOM images of cross sections of Nb specimens (from Amperit 30/10 powder) sintered at different temperatures, Compacted at 200 MPa**

It can be seen that there is barely any difference in porosity visible in the cross sections of the specimens in fig. 3.135. The porosity seems to be the same independent of the sintering temperature. It can also be seen very well in tab. 35 that there was barely a difference measured in open porosity.

### 3.4.2 Reactivity with Si

For the investigation of the reactivity between Nb and Si, Nb-Si specimens containing different amounts of Si were pressed, sintered and characterised.

The H.C.Starck- Amperite 30/10 $\mu$ m niobium powder was used. The particle fractions of the niobium powder were obtained by sieving in different fractions (in 45-63  $\mu$ m and 63-90  $\mu$ m). This was used as the base material, and then the powders were mixed in a tumbling mixer for 60 min with different amounts, 5 / 10 / 15,4 / 25 / 38 wt%, of Si powder (Ecka, 4-5  $\mu$ m).

Rectangular test specimens 55\*10\*10 mm (Unnotched impact test bar – ISO 5754) were compacted in cold isostatic press P.O. Weber PW40 in CIP tools at 200 MPa. Afterwards they were sintered in a dilatometer (Bähr 801 with SiC tube heated furnace) at 1500°C for 2 h soaking period in rotary pump vacuum.

Nb-Si specimens were very brittle, and after CIP pressing they broke in the die, and it was also very difficult to transport the samples because they were so fragile. With increasing amount of Si the specimens became even more brittle. It was very difficult to measure the green density, because by touching the specimens with a sliding caliper, already some particles broke out of the specimen.

The green and sintered density, dimensional change, porosity and electrical conductivity were measured and summarised in tab. 36. The porosity data have to be regarded with some caution since the theoretical density data that were used for calculating the porosity were obtained through the rule of mixture which holds for powder mixtures but not for reacted systems.

**tab. 36.: Properties of specimens from powder mixes Nb-x%Si, compacted at 200 MPa (CIP), sintered at 1500°C, 120 min in vacuum**

<b>Materials</b>	<b>Atmosphere</b>	<b>theoretical density [g/cm<sup>3</sup>]</b>	<b>Sintered density [g/cm<sup>3</sup>]</b>	<b>Porosity [%]</b>	<b>Electrical Conductivity [MS*m<sup>-1</sup>]</b>
Nb	<b>Vacuum</b>	8,57	7,04	18,19	4,1
Nb+5%Si		8,06	5,68	28,34	1,9
Nb+10%Si		7,6	4,61	38,9	1,2
Nb+15,5%Si		7,16	3,62	49	0,8
Nb+25%Si		6,38	3,04	51,41	0,7
Nb+38%Si		5,53	2,08	62,85	
Nb45μm+5%Si		8,06	5,71	30,94	1,8
Nb45μm+10%Si		7,6	4,6	37,48	1,2
Nb45μm+15,5%Si		7,16	3,66	47,66	0,7
Nb45μm+25%Si		6,38	2,91	55,24	
Nb45μm+38%Si		5,53	2,14	61,74	
Nb63μm+5%Si		8,06	5,68	27,61	2
Nb63μm+10%Si		7,6	4,57	38,32	1,2
Nb63μm+15,5%Si		7,16	3,55	48,73	
Nb63μm+25%Si		6,38	3,67	53,46	
Nb63μm+38%Si		5,53	2,3	55,44	

It can be observed very well in tab. 36 that with increasing content of Si in Nb the sintered densities (measured with Archimedes) are decreasing. Due to the fact that the density of Si is lower than the density of Nb it is not surprising that the densities are decreasing with increasing Si content. The theoretical (from literature available densities for the phases have been calculated with the composition of specimens compared with the phase diagram) densities have also been calculated and summarised in the table. With increasing Si content the theoretical densities are decreasing, but not as much as the sintered densities as measured through the Archimedes method. The very high decrease in the measured density can be explained by the Kirkendall effect, similar to the results obtained with sintering of Mo-Si. With decreasing density the open porosity is increasing, as can be observed very easily in the tab. 36.

Furthermore it can be seen that with increasing content of Si the dimensional change is increasing. The more Si was mixed into the Nb compacts the more expansion occurred during sintering. It is well known that electrical conductivity/resistivity of sintered materials is closely related to its microstructure. This was measured by WT (semiautomatic resistance meter). It could not be measured for all specimens because some of them were broken many times so the remaining pieces were too small. From the remaining pieces of the compacts can be seen that with increasing content of Si in Nb the electrical conductivity was decreasing.

The comparison of the theoretical and sintered density is shown in fig. 3.136. The difference between the measured and the theoretical density is quite high and it is growing with higher Si content.

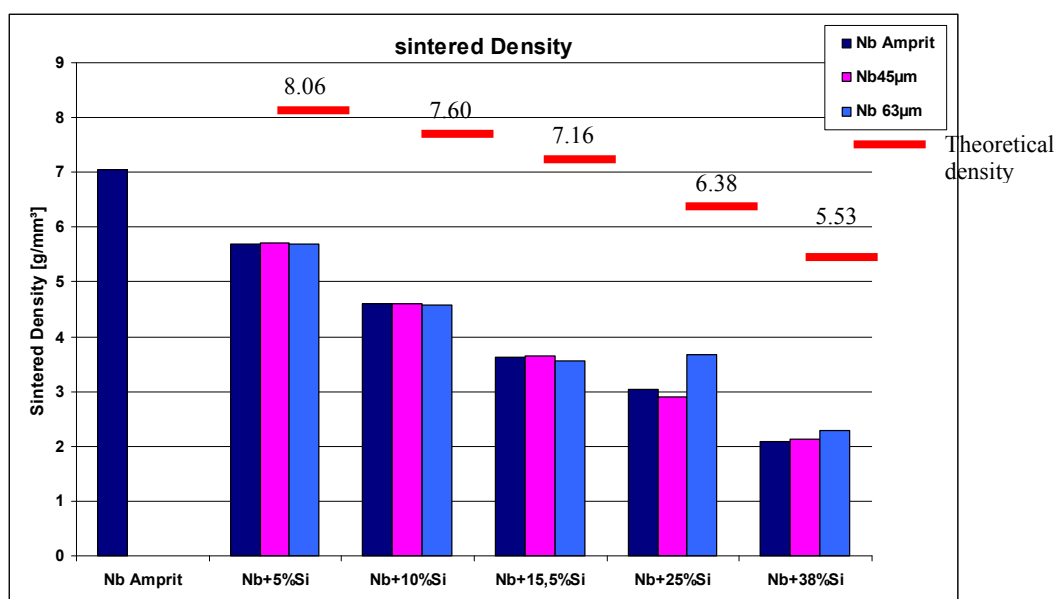


fig. 3.136.: sintered density and theoretical density (calculated through the rule of mixture) of Nb powder (different fractions) mixed with different amounts of Si compacted at 200 MPa (CIP), sintered at 1500°C, 120 min in vacuum

The fracture surfaces of the sintered compacts were also characterised by SEM and are shown in fig. 3.137. The images reveal that with increasing silicon content in the Nb compacts the sintering contacts of the samples decrease and the porosity increases. In specimen containing 10 / 15,5 / 25 / 38 wt% Si in Nb no sintering contacts can be observed. Their fracture surfaces look like powder.

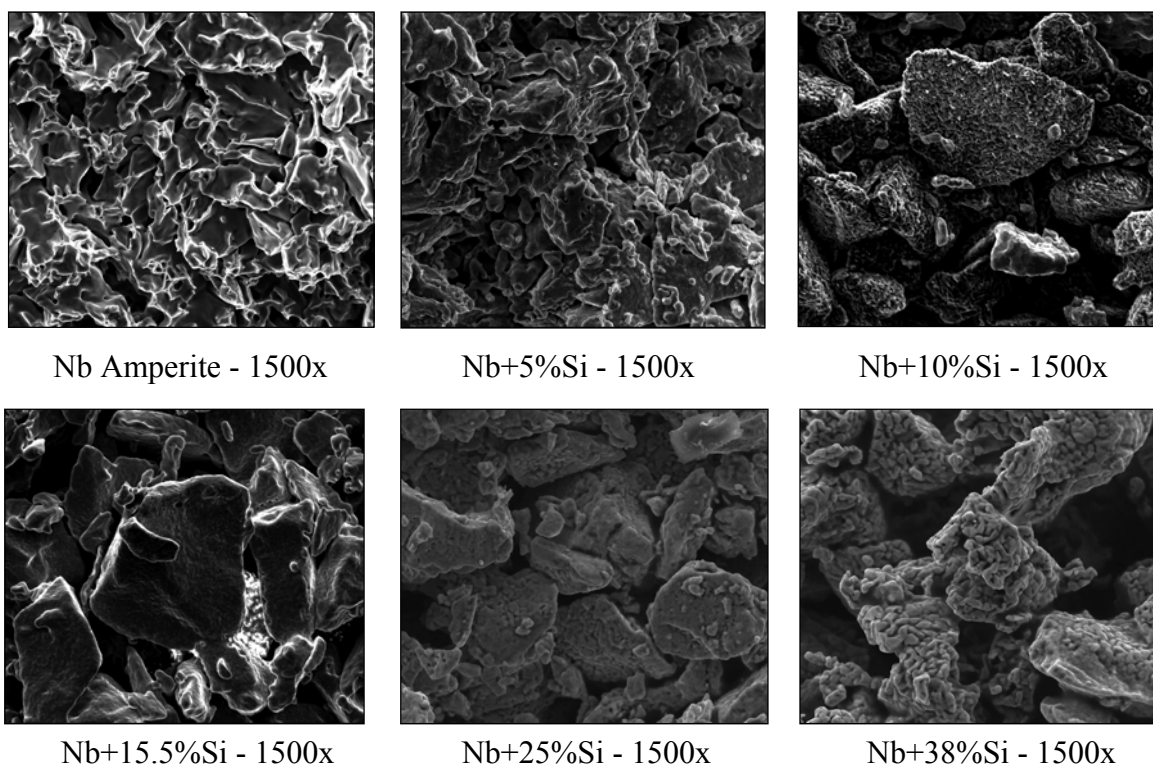


fig. 3.137.: Fracture surfaces of the samples of Nb amperite mixed with different amounts of Si compacted at 200 MPa (CIP), sintered at 1500°C, 120 min in vacuum



During these experiments it was observed that the Nb + x\*wt% Si compacts are quite difficult to handle and even after sintering they never reach the stability of a sintered Mo - Si compact, for example (which was not too good either). Furthermore, the resulting densities are lower than for Mo-Si with equivalent amounts of Si, and Nb is more tricky to sinter. It could be observed that the specimens (Nb and Si) barely sintered together. Therefore some reactivity experiment were prepared in the DTA/TG.

### 3.4.2.1 Microstructures

In fig. 3.138 some metallographic sections of Nb-x%Si are shown. All specimens were compacted with 200 MPa and sintered at 1500 °C for 180 min. It can be seen that with increasing amount of Si the specimens are getting more porous. The samples are less stable, and during metallographic preparation a lot of particles break out.

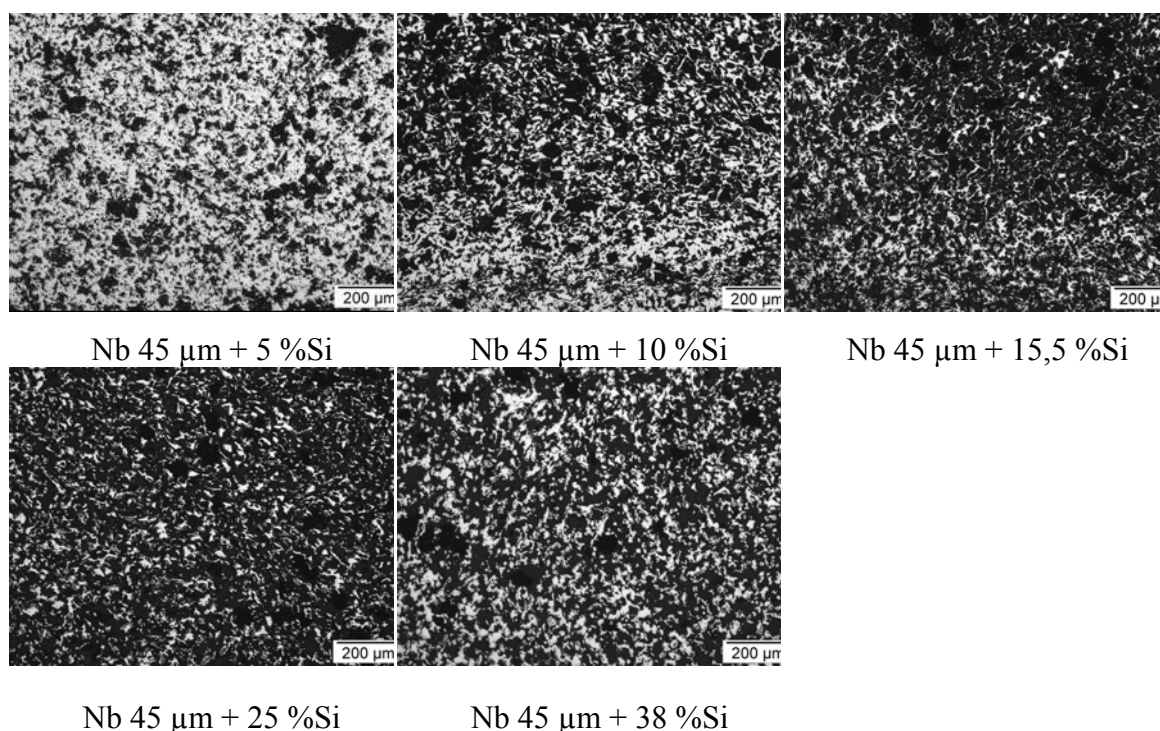


fig. 3.138.: Microstructures of Nb (45 μm)+x%Si powder, compacted at 200 MPa (CIP), sintered 180 min at 1500°C in vacuum

### 3.4.2.2 DTA/TG analysis of Nb + x\*wt% Si

The tests were performed on a simultaneous thermoanalyser coupled with quadrupol mass spectrometer (NETZSCH STA449C Jupiter®+QMS403 Aëolos®). All TG/DTA analyses were performed in Ar (5.0 purity) atmosphere with a flow rate of about 50 ml/min. For this analysis, specimens were pressed at 200 MPa by CIP. Then the compacts were crushed to small pieces. The mass of the studied specimens was about 500 mg for each sample.



The heating and cooling rate was the same in all cases, 20 K/min, and the specimens were heated up to 1600°C (no soaking period), then after dwelling at the temperature were cooled to room temperature.

The curves in all cases were plotted as corrected, i.e. the graphs for the empty run (crucible without specimen) has been subtracted. DTA results are shown for the samples in fig. 3.139. The reaction between Nb and Si is exothermic, as is that between Mo and Si. The exothermic reaction was observed in the heating section. As can be seen in the image with more Si, the exothermic peak of the DTA samples is shifted to higher temperature, and the reaction comes later but the intensity of the peak was higher with increasing Si content. I.e. also in that respect the reaction behaviour between Nb and Si is similar to that of Mo-Si.

tab. 37 shows the temperature of the peak maxima of the exothermic peaks (peak one and two) for compacts prepared from the different fractions of Nb powder. As can be seen the difference is negligible, i.e. the Nb particle size is not relevant. With more Si (38 wt %) two exothermic reaction peaks are observed. By addition of 25 wt% Si the first time NbSi<sub>2</sub> occurs. At 38 wt% Si the stoichiometric composition of NbSi<sub>2</sub> is reached.

For pure Nb specimen a peak at 865.1 °C was observed. No reaction is expected, it is a disorder of the measuring system.

**tab. 37.: Characteristic maxima of the peaks of DTA of compacts from different fractions of Nb powder mixed with different amount of Si (wt%) compacted at 200 MPa (CIP)**

samples	Temperature °C	
	1	2
<b>Nb</b>	865,1	-
<b>Nb+5%Si</b>	1061,1	-
<b>Nb45µm+5%Si</b>	1069,9	-
<b>Nb63µm+5%Si</b>	1070,1	-
<b>Nb+10%Si</b>	1083,4	-
<b>Nb45µm+10%Si</b>	1084,1	-
<b>Nb63µm+10%Si</b>	1078,5	-
<b>Nb+15.5%Si</b>	1098	-
<b>Nb45µm+15.5%Si</b>	1110,8	-
<b>Nb63µm+15.5%Si</b>	1096,7	-
<b>Nb+25%Si</b>	1141,4	-
<b>Nb45µm+25%Si</b>	1145,6	-
<b>Nb63µm+25%Si</b>	1172,3	1386,2
<b>Nb+38%Si</b>	1210,3	1391
<b>Nb45µm+38%Si</b>	1212,9	1388,3
<b>Nb63µm+38%Si</b>	1270,8	1388,4

The thermogravimetry (TG) curves of the Nb, Nb-Si samples with 5 / 10 / 15.5 / 25 / and 38 %Si are shown below (black graphs). There is some slight mass loss in the temperature range about 400°C. All the other curves (Nb - 45  $\mu$ m and 63  $\mu$ m) are not shown. The values of the temperature where the peaks occurred are given in tab. 37.

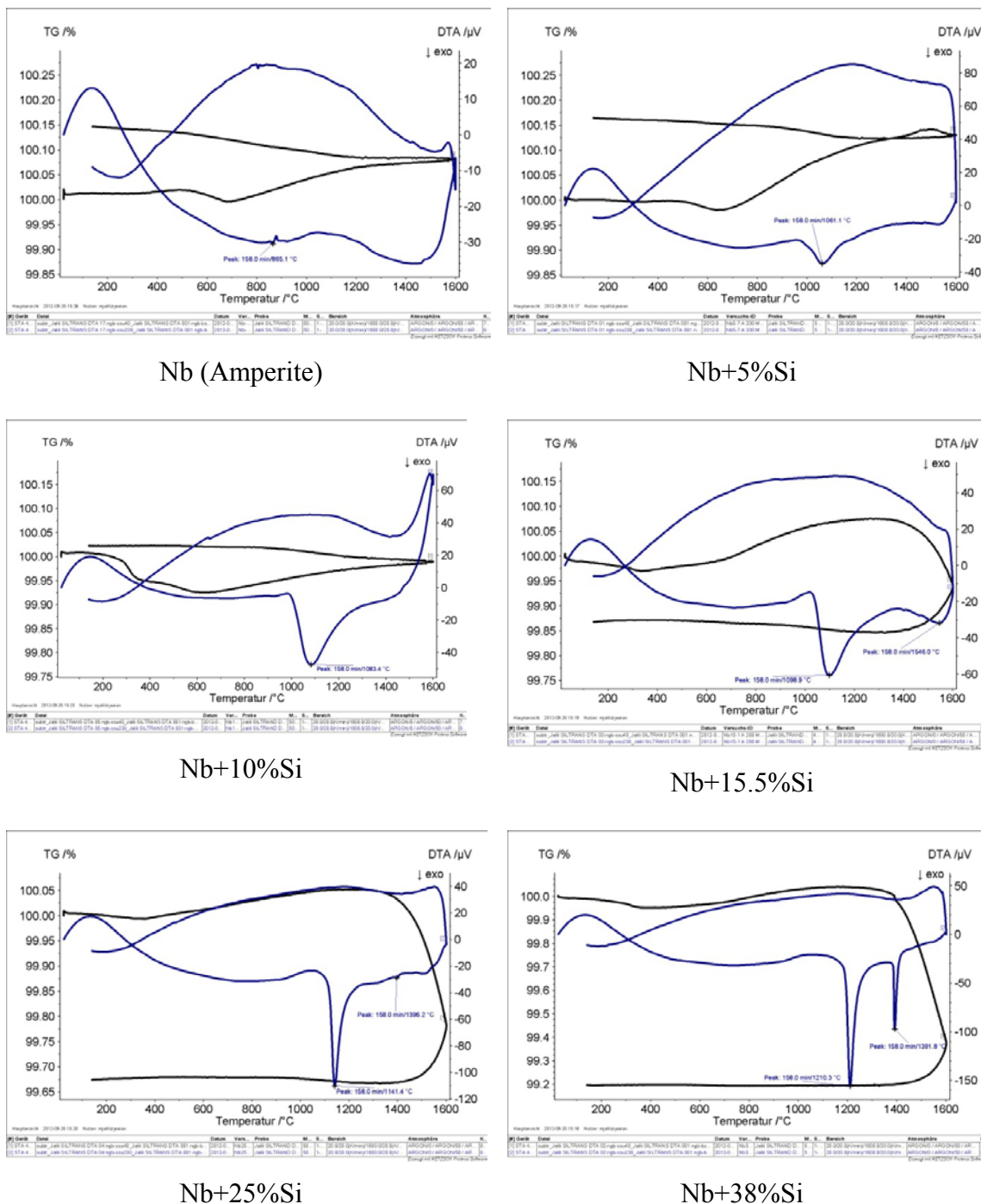


fig. 3.139.: DTA/TG graphs of the Nb Amperite samples mixed with different amounts of Si.  
Heating/cooling rate 20 K/min, Ar

It could be observed very well in fig. 3.139 that some exothermic reaction between Nb and Si occurs. Although there was reaction in the DTA observed, no sintering of these specimens (pressed specimens discussed before) was observed. They cracked already

after pressing and after sintering and some of the compacts were still very difficult to handle. Even after very careful polishing a lot of pores (from broken-out particles) remained.

### 3.4.3 Si infiltration of Nb preforms by partners

A niobium specimen from Nb powder (H.C. Starck Amperit 30/10  $\mu\text{m}$ ) was pressed uniaxially with 150 MPa in a cylindrical die ( $d=11,27$  mm). The green compact was sintered at 1500  $^{\circ}\text{C}$  for 2 h in vacuum. This sample was Si infiltrated at IMSAS in Bratislava. For the infiltration experiment the specimen was put into a graphite die and some defined mass of Si (as fragments) was poured on the specimen. Afterwards the assembly was heated up to 1500  $^{\circ}\text{C}$ , held for some seconds and cooled down. The specimen was partly destroyed on the surface due to the exothermic reaction.

#### 3.4.3.1 LOM

In fig. 3.140 two images show the cross section of the infiltrated Nb specimen. In the 50 x magnification can be observed that part of the specimen was destroyed by exothermic reaction forming a hole and dissolving some Nb particles. In the 100 x magnification a light blue line proceeding along the surface can be observed. It is some silicon that reacted with the Nb during the infiltration process forming silicides. An EDAX analysis was carried out, and the light blue area showed  $\sim 21$  % Si, about 12 % O and 67 % Nb.

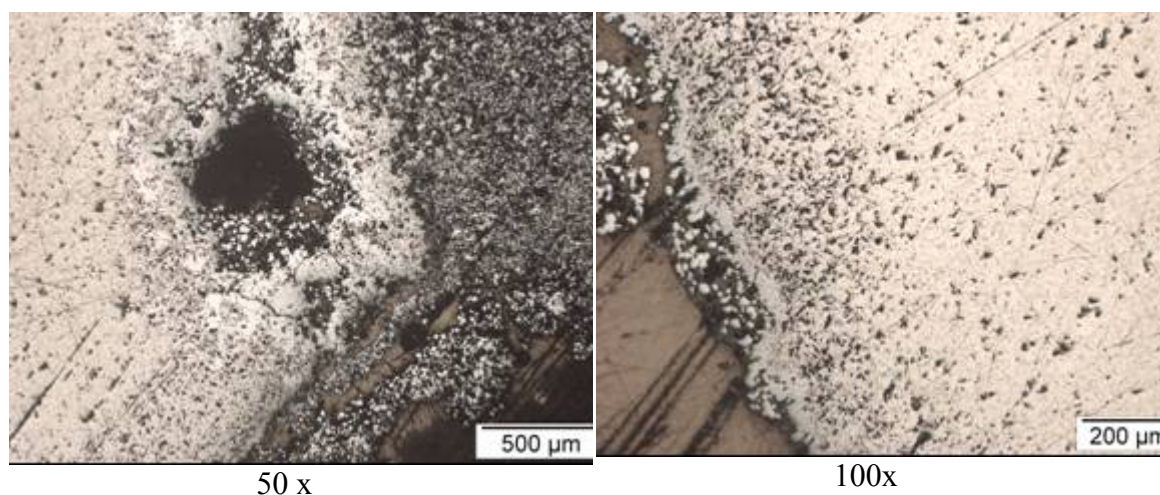


fig. 3.140.: both images are showing the surface near area of a Nb specimen after infiltration with Si;

#### 3.4.3.2 SEM and elemental mapping

In fig. 3.141 some BSE images of the Nb specimen after infiltration with Si are shown. In the 25x magnification can be seen that only some parts have been infiltrated. Some parts were destroyed by the exothermic reaction. The elemental maps of Nb and Si

show the distribution of Si after the infiltration process. They were taken in the infiltrated part of the specimen (left bottom corner - 25 x).

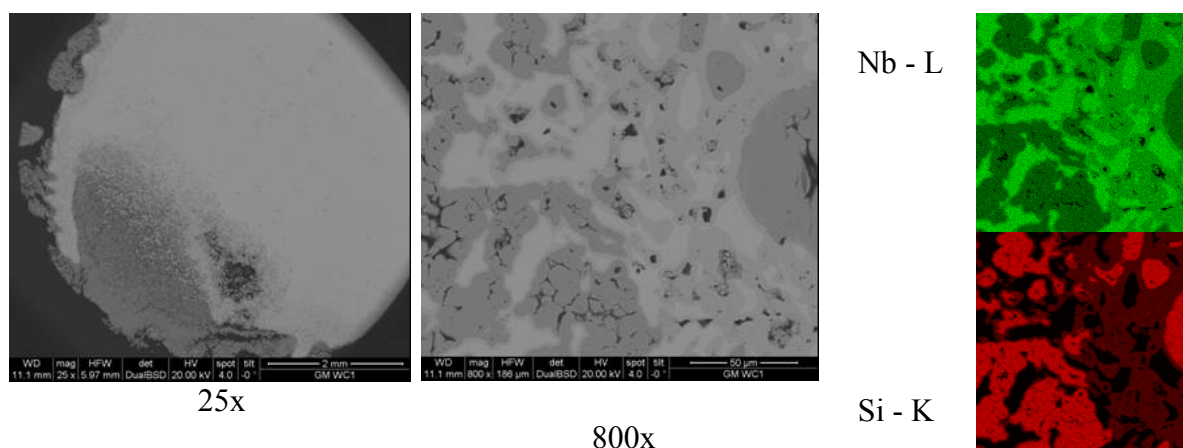


fig. 3.141.: left and center images showing BSE images of Nb specimen after infiltration with Si; at 25x - only parts infiltrated; some parts dissolved; right images: mappings from 800x image

The macrohardness of the specimen was measured, too. The measurement was started near the surface where the hardness was measured with 140 HV10, which is quite low for a silicide. Considering the low mechanical stability of the specimens after sintering at TUW, it is clear that it can not be increased by Si infiltration and the resulting hardness is quite low. Going towards the core where no Si was observed the hardness decreased to 78 HV10.

Generally it can be said that the reaction of niobium with silicon is very exothermic. The specimen was partly destroyed due to this reaction. Some parts which were not destroyed could be analysed by LOM and SEM. With both methods some dissolved regions could be observed. Apart from the exothermic reaction some infiltrated zones could be identified and are shown in the elemental maps of Nb and Si.

### 3.4.4 Summary and discussion of Niobium

Nb compacts were prepared from a fine and a coarse Nb powder from H.C. Starck and characterised after sintering. The powders were pressed uniaxially in a cylindrical die at 200 MPa. The specimens were sintered at 1400 °C for 60 min in vacuum. The dilatometry curves (fig. 3.130) showed that up to 900 °C the specimens are expanding and afterwards the shrinkage starts. The total shrinkage was about 1,1 % for the fine grained specimen and lower for the coarse one. In the LOM (fig. 3.131) less pores could be observed in specimen from the fine grained powder. Some darker areas around the pores could be seen, due to some corrosion.

Further specimens have been prepared from a coarse Nb powder from H.C. Starck (Amperit 30/10 µm) and sintered at temperatures between 1350 and 1500 °C in vacuum. The specimens were pressed with 150 / 170 / 200 MPa. It could be shown in tab. 34 that with increasing compacting pressure and sintering temperature the density is increasing, too. The highest density was achieved for specimens pressed with 200 MPa and sintered at 1500 °C. With increasing density the open porosity decreased and the hardness (HV 10) increased. In the metallographic cross sections barely any difference, in terms of sintering temperature, was observed.

Some experiments about the reactivity between Nb and Si were carried out. Compacts from Nb (fractions  $\leq 45$  µm and  $\leq 63$  µm) with 0 / 5 / 10 / 15,5 / 25 / 38 wt% Si were



pressed with 200 MPa cold isostatically and sintered at 1500 °C for 120 min. After sintering the density, open porosity, dimensional change and electrical conductivity were measured (tab. 35). It could be observed that with increasing amount of Si in the Nb specimens the density is decreasing and the open porosity increasing. The more Si was in the samples the more was the difference in density between the compacts and the theoretical density (fig. 3.136). Furthermore, the dimensional change after sintering is also depended on the Si content. With more Si the expansion after sintering was larger. The electrical conductivity could be measured only in some few specimens that did not crack after sintering. Those were specimens from as-received Nb with different amounts of Si. The higher the content of Si was, the lower was the electrical conductivity, which can be explained by the formation of silicides. Some SEM images of fracture surfaces are shown in fig. 3.137. Only in specimens containing 5 wt% Si or less some sintering bridges could be observed. Specimens containing more Si look like a powder, and no cracked sintering bridges could be found. This explains why the specimens were more difficult to handle with increasing amount of Si. In the LOM (fig. 3.138) images a lot of pores could be seen. Due to the fact that with increasing amount of Si in Nb the density decreased and the specimen became more fragile it does not surprise that the specimens became difficult to handle and to prepare metallographically. A lot of particles broke out even though the preparation was made by hand.

It could be shown in chapter 3.4.2 that the sintering activity of the specimens is low, therefore the reactivity of the specimens was tested by DTA/TG analysis (fig. 3.139). At about 1100 °C the exothermic reaction peaks were recorded. With increasing amount of Si in Nb the peaks were bigger because the exothermic reaction got also more intense, but the occurrence of the exothermic peaks was almost at the same temperature.

Some Nb specimens from coarse Nb from H.C. Starck (Amperit 30/10 µm, 2944) were sent to IMSAS for Si infiltration. The specimens were pressed with 150 MPa and sintered at 1500 °C for 2h in vacuum. The infiltration experiment was carried out in an inductive coupled furnace where the specimen was placed in a graphite die in the centre of the tube. As Si source some melted and crushed Si was taken which was poured over the specimen. For the experiment the specimen with the Si were heated up to 1500 °C with no soaking period. After cooling it could be seen that the exothermic reaction between the Nb and Si was so intense that parts of the specimen were destroyed. In the LOM images (fig. 3.140) the near-surface area could be observed. A big hole and some dissolved Nb-Si particles can be seen. In the SEM and mapping images (fig. 3.141) the distribution of the Si can be observed. There are different colours indicating the Si distribution according to the reaction of Nb with Si and what was formed. Higher hardness of 140 HV10 was measured in the Si containing part of the specimen. In the centre, where barely a Si could be found, the hardness dropped to 78 HV 10.

Generally it can be said that the reaction between Nb and Si is very exothermic. As could be shown in the DTA/TG analysis, the more Si is added the more intense is the reaction. That is the reason why the specimens which were infiltrated by Si were partly destroyed. On the other hand specimens which were mixed with Si and sintered between 1350 °C - 1500 °C do not suffer from cracks but are less stable which could be observed in the LOM images (fig. 3.138) after metallographical preparation.

### 3.5 Sintering of Niobium – Molybdenum compacts

The aim of this study was to characterise the sintering behaviour of molybdenum-niobium powder mixes. There is barely any literature available about the sintering mechanism of the two metals, only for each metal separately.

For the experiments, molybdenum powder from Chemie Metall was mixed with niobium powder from HC Starck, in the ratios 100/80/60/40/20/0 wt% Mo. Each powder mixture was blended in a tumbling mixer for 2 h with steel grinding elements. Afterwards cylindrical samples with 20 mm diameter were pressed in a CIP (P. O. Weber type PW40) with 200 MPa pressure (without any lubricant) from each powder mix. Samples of each mix were sintered in a Nabertherm furnace with a  $\text{Al}_2\text{O}_3$  retort, with three different sintering profiles which are summarized in tab. 38 and demonstrated in fig. 3.142.

tab. 38.: Sintering profiles for Mo/Nb samples

Profile	$T_1$ [°C]	$t_1$ [min]	Atm <sub>1</sub>	$T_2$ [°C]	$t_2$ [min]	Atm <sub>2</sub>
profile 1	1300	120	vac.	-	-	-
profile 2	1100	60	$H_2$	1300	120	vacuum
profile 3	400	60	$H_2$	1300	120	vacuum

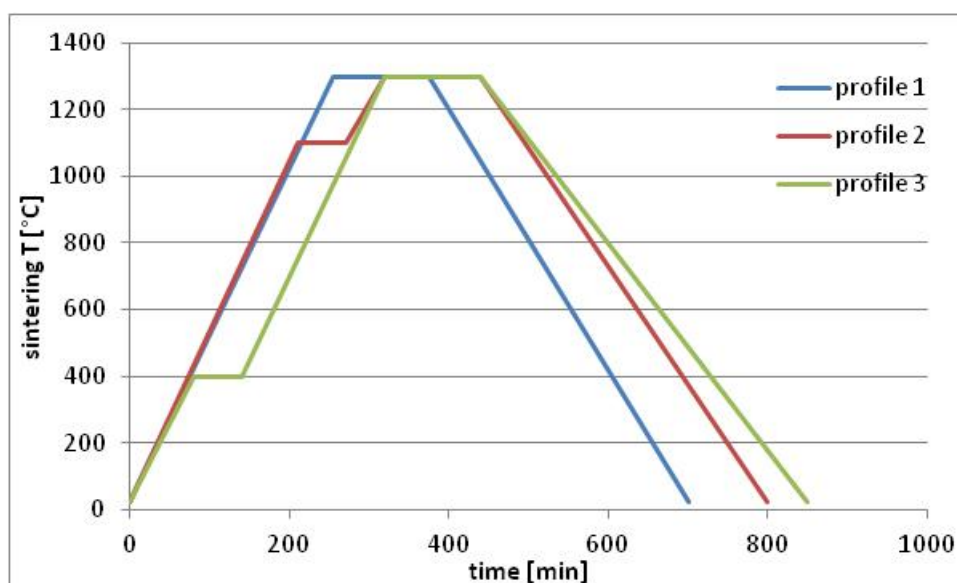


fig. 3.142.: Temperature-time profile for sintering of Mo-Nb specimens

A parallel experiment was carried out where molybdenum and niobium were co-pressed to two layer samples with an interface in-between. A schematic of the sample is given in fig. 3.143. The samples were uniaxially pressed (without a lubricant) in a cylindrical die with 20 mm diameter with 200 MPa, and sintered for comparability with the same sintering profiles given in tab. 38 and in the same Nabertherm furnace with  $\text{Al}_2\text{O}_3$  retort. All samples were characterised by hardness, C on LECO CS 230 combustion analyser and O on LECO analyzer TC-400.

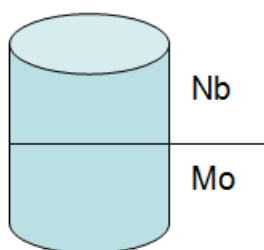


fig. 3.143.: Scheme of co-compressed sample from Mo and Nb for the parallel experiment

### 3.5.1 Appearance of specimens

The samples prepared from mixed powders did not show any noticeable change after pressing or sintering. The two layer samples, which were sintered as prescribed in profiles 2 and 3, sustained cracks after sintering. Some images are given in fig. 3.144. The samples sintered as described in profile 1 in tab. 38 (vacuum) did not suffer from cracks. A possible reason is that these samples were not reduced due to absence of hydrogen. Therefore they did not suffer from shrinkage.

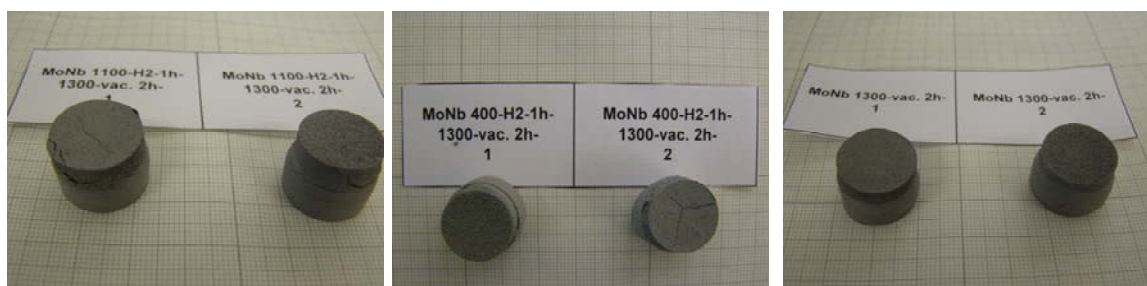


fig. 3.144.: left and center image: layered samples which suffered from cracks after sintering (sintering profiles 2 + 3); right image: samples sintered in vacuum without any cracks (sintering profile 1)

### 3.5.2 Carbon measurement

The carbon analysis was carried out on the LECO CS 230 combustion analyzer.

#### 3.5.2.1 Mixed powder samples

In fig. 3.145 the results of the carbon measurement by Leco are shown for the three sintering profiles of the mixed Mo/Nb powder samples.

It can be observed in fig. 3.145 that samples which were sintered in the first step in hydrogen (sintering profile 2 + 3, tab. 38) and contain between 60 and 80wt% Nb show the highest amount of carbon. All other samples do not differ in the carbon content. It is not clear where the carbon comes from.

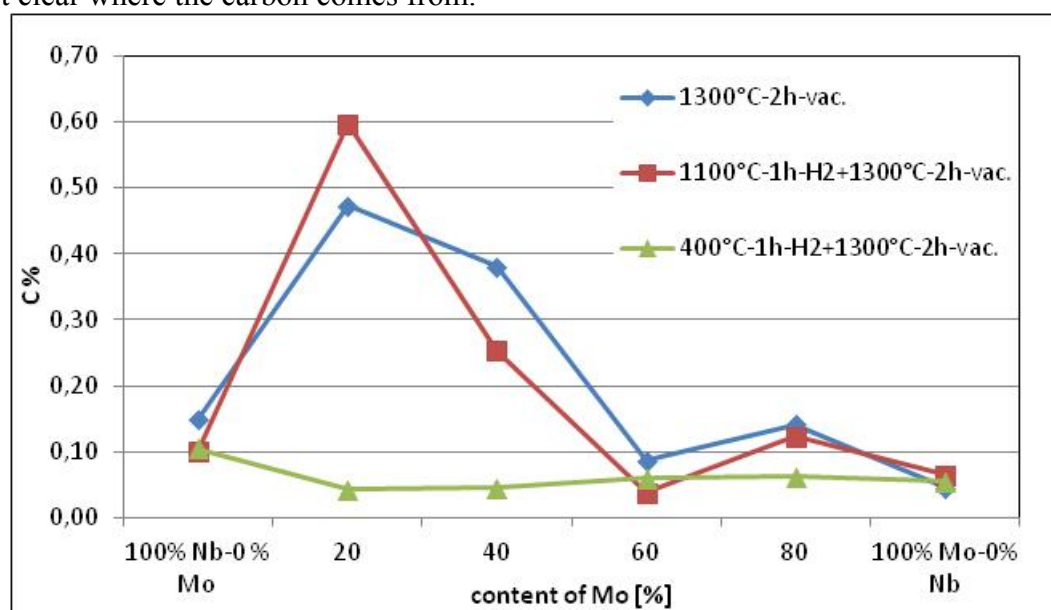


fig. 3.145.: carbon content of samples prepared from Mo-Nb powder mixes

#### 3.5.2.2 Two layer samples

For the carbon measurement in the two layer sample, the specimen was cut along the height and both layers were measured at the same time. The measured carbon content was between 0,1 and 0,2 %C for all three of the two layer specimens.

### 3.5.3 Oxygen measurement

The oxygen analysis was carried out on LECO analyzer TC-400.

#### 3.5.3.1 Mixed powder samples

Samples from plain niobium showed the highest amount of oxygen independent of the sintering (profile) which can be observed very well in fig. 3.146. With increasing amount of molybdenum in the sample the oxygen content decreased. The lowest oxygen



content was measured for the samples from 60/80 %Mo and sintered at profile 1 (1300°C – 2 h – vacuum). The oxygen content measured in plain Nb samples was about 0.1-0.15 % O independent of the sintering process, which is a bit surprising. It was expected that the presintering in H<sub>2</sub> would lower the oxygen content considerably.

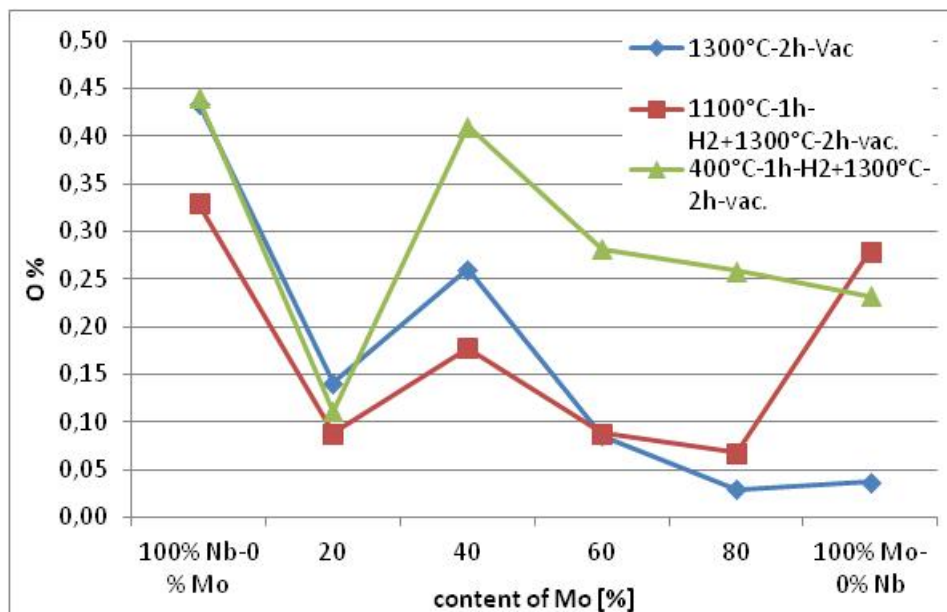


fig. 3.146.: content of oxygen measured in Mo/Nb samples after three sintering runs following different profiles with differing temperatures and atmospheres

### 3.5.3.2 Two layer samples

The content of oxygen measured in the two layer samples was between 0.35 and 0.45% oxygen for all samples and for all three sintering profiles independent of sintering temperature and atmosphere.

### 3.5.4 Hardness of the mixed samples

The hardness was measured as HV1. The results are given in fig. 3.147. It can be observed that the highest hardness was measured in the sample containing 60 % Nb. In fig. 3.145 was shown that this specimen also contains the highest amount of carbon, which explains the increase in hardness.

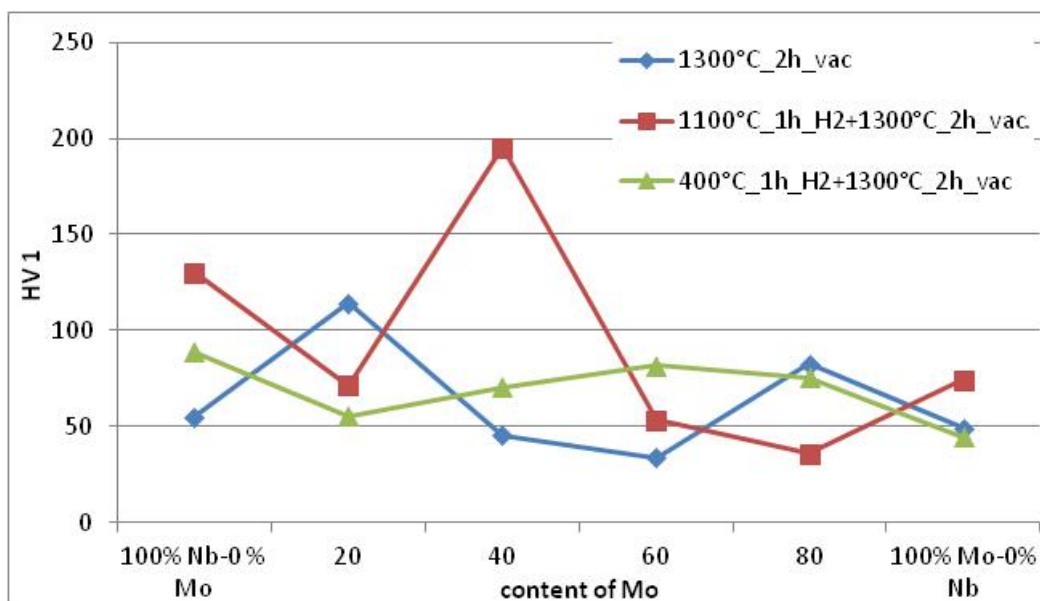


fig. 3.147.: hardness measured in Mo/Nb specimens after different sintering routes

### 3.5.5 Hardness for the two layer samples

The hardness was measured with 1 kp indentation load. A summary of all hardness values is given in tab. 39.

tab. 39.: HV1 measurement in the two layer sample in each layer

sintering	Mo layer	Nb layer
profile 1	$48 \pm 9$	$52 \pm 3$
profile 2	$62 \pm 3$	$72 \pm 8$
profile 3	$55 \pm 6$	$65 \pm 3$

The highest hardness was measured in the sample sintered with sintering profile 2. In this case the hardness was 62 HV1 for the plain Mo and 72 for Nb. Samples sintered at sintering profile 1 and 3 had a hardness of about 50 HV1. Niobium was by trend about 10 HV1 higher than molybdenum. The difference in hardness was not as big between the sintering profiles as was observed in specimens from mixed powders.

### 3.5.6 Summary and discussion of niobium-molybdenum specimens

The sintering behavior of Mo mixed with Nb was characterized since literature is scarce on this topic. Therefore samples out of Mo mixed with different wt% of Nb have been sintered and characterised. Three different sintering profiles were chosen with different sintering temperatures and atmospheres.

Summarising this chapter it can be said that the sintering of two layer specimens was quite difficult. The Nb and Mo layer separated during sintering. In specimens which were prepared from powder mixtures of Mo and Nb no difference between green and sintered bodies was observed. The carbon content was quite high for samples containing 80 % Nb and sintered at 1300 ° for 2 h in vacuum (0,5 % C) and the ones presintered at 1100°C for 1 h in H<sub>2</sub> and sintered afterwards at 1300 °C for 2 h in vacuum (0,6 % C). The two layer specimens from Nb and Mo showed lower values for the carbon content of 0,1 - 0,2%.

The oxygen content was higher for specimens containing more Nb. The plain Nb specimen showed the highest amount of oxygen. With increasing content of Mo the oxygen amount was decreasing. Contrary to expectations the presintering in hydrogen did not decrease the content of oxygen in the specimens, probably due to the “internal getter” effect. The oxygen which was reduced from molybdenum was caught by Nb and oxidized it. Furthermore it was observed that the sintering profile with presintering at 400 °C for 1 h in H<sub>2</sub> and sintering afterwards at 1300 °C for 2 h in vacuum resulted in the highest amount of oxygen (0,4 % for specimen with 80 % Nb decreasing with increasing amount of Mo). The oxygen content of the two layer specimens was 0,35 - 0,45 % constantly for all three sintering profiles.

The highest values for the hardness (HV1) were measured for the same specimen that showed already high values for carbon content. It was the specimen containing 80 % Nb. All the other values were in the range 50 – 100 HV1. Furthermore the two-layer specimens showed also very similar values for hardness as most Mo/Nb mixed specimens in the range of 50-70 HV1.

These results show that Mo-Nb alloys prepared by the blended elemental approach are tricky to sinter due to the widely different reactivity of Mo and Nb towards interstitials. Nb tends to pick up both C and O much more readily than Mo.

## 4 Summary of the work

The aim of the work in the beginning was the preparation of porous Mo preforms which could be infiltrated with Si as further step. The work was started with the examination of the influence of compaction pressure, sintering temperature and particle size on density, open porosity and hardness. A molybdenum powder that is commercially available was taken for the experiments. In the beginning a Plansee SE Mo was used, which was designated as  $a \leq 32 \mu\text{m}$ . As this powder was consumed another one was bought which was very similar to the Plansee SE powder. The new Chemie Metall Mo powder was designated as  $a \leq 63 \mu\text{m}$  (in practice it is rather  $< 10 \mu\text{m}$ ). Two fractions differing in particle size distribution have been sieved from these two powders. One was designated as  $\leq 63 \mu\text{m}$  and the second one as  $\leq 45 \mu\text{m}$ .

The experiments started with the  $\leq 45 \mu\text{m}$  Mo fraction. Specimens were pressed with 70 / 130 / 200 / 230 / 270 MPa and sintered at 1200 / 1250 / 1300 °C for 30 and 90 min (chapter 3.1.1.1). The results were compared, and it could be seen that with increasing compacting pressure, sintering temperature and soaking period the density of the specimens increased, too. Specimens pressed with 200 MPa and sintered at 1300 °C for 90 min showed the highest density of 7,2 g/cm<sup>3</sup>. The open porosity was at about 33 % which was a desired value. Specimens which were compacted at pressures higher than 200 MPa showed lower values for the density because the first pressing defects occurred. While the density increased the open porosity was decreasing (fig. 3.4).

The influence of the sintering temperature was examined, too. Mo specimens pressed the same way have been sintered at 1200 - 1500 °C in 50 °C steps (chapter 3.1.1.2). It could be observed very well that the density was increasing with increasing sintering temperature. The highest values for the density were achieved for specimens pressed with 200 MPa and sintered at 1500 °C. The density was 7.5 g/cm<sup>3</sup> and the open porosity 27 %. The density was increasing up to a compacting pressure of 200 MPa and afterwards it was decreasing due to pressing defects and overpressing. In the LOM images of cross sections of Mo specimens out of fine grained  $< 45 \mu\text{m}$  Mo powder could be observed, that with increasing sintering temperature the size of the pores was decreasing.

In a further experiment the influence of the powder fraction was examined. Specimens out of the  $\leq 45 \mu\text{m}$  Mo fraction have been compared to those out of the  $\leq 63 \mu\text{m}$  fraction (chapter 3.1.1.3). All specimens were pressed with 70 / 130 and 200 MPa and sintered at 1200 °C for 30 and 90 min. It could be observed that specimens out of  $\leq 45 \mu\text{m}$  Mo showed slightly higher density values (of about 0,1 g\*cm<sup>-3</sup> for all three different compacting pressures and the two soaking periods). That means that using coarse powders results in somewhat lower densities and higher porosity. The hardness was increasing with higher sintering temperature and compacting pressure (up to 200 MPa) (tab. 4). Specimens sintered at 1500 °C and pressed with 200 MPa had a hardness of 99 HV 10 while the hardness of specimens sintered at 1200 °C and pressed with 200 MPa was quite low, at 48 HV 10.

The pore size diameter in dependence of the sintered density was compared for specimens compacted with 200 MPa uniaxially and sintered at 1200°C, 1250 °C and 1300°C (chapter 3.1.1.5.1). Furthermore, specimens out of  $\leq 45 \mu\text{m}$  Mo fraction were compared with regard to sintered density and pore size with those prepared out of  $\leq 63$



$\mu\text{m}$  Mo fraction. Due to the fact that the powder fractions have been sieved, the low amount of coarse particles was removed during sieving and the remaining particles were all considerably smaller than 45 or 63  $\mu\text{m}$ . That is the only possible explanation for the lower value for open porosity of specimens from  $\leq 63 \mu\text{m}$  Mo fraction than those out of  $\leq 45 \mu\text{m}$  Mo fraction. Also the sintered density of Mo specimens out of  $\leq 63 \mu\text{m}$  powder was lower than expected. For specimens out of  $\leq 45 \mu\text{m}$  Mo the open porosity was decreasing with increasing sintering temperature. It was furthermore observed that the pore radius was increasing with higher sintering temperature, which was contrary to expectations.

The open porosity, bulk density and pore size of cold isostatically pressed specimens were characterised (chapter 3.1.1.5.2). The specimens have been pressed with 200 MPa and sintered also between 1200 and 1300 °C. The sintered density of specimen sintered at 1200 °C was too low, which was an outlier. The open porosity decreased with higher sintering temperature, as was observed for the uniaxially pressed specimens. While the open porosity decreased, the sintered density increased with increasing temperature. It was also observed that the average pore size decreased to 0,71  $\mu\text{m}$  at 1300 °C compared to the specimen sintered at 1200 °C (0,77  $\mu\text{m}$ ). Both specimen types out of the two powder fractions have been observed in the LOM and barely a difference in the microstructures could be observed. Between  $\leq 45 \mu\text{m}$  and  $\leq 63 \mu\text{m}$  the difference in particle size is too low to see a significant difference, in particular since the bulk of the starting powder is  $\leq 25 \mu\text{m}$  for both fractions.

Further experiments dealt with the preparation of specimens with gradient porosity. The aim of this experiment was to build up a gradient layer specimen out of different powder fractions, which were sieved out of the commercially available Mo powder (chapter 3.1.2). Different powder fractions ( $\leq 25$ ,  $\leq 45$ ,  $\leq 63$ ,  $\leq 74$  and  $\leq 90 \mu\text{m}$ ) were used for such layered specimens. The specimens were pressed with 200 MPa and sintered at 1300 °C (in  $\text{H}_2$ ) for 2 h and 3 h soaking period. The density and open porosity were measured as integral values including all layers. Barely a difference in open porosity could be measured between the specimens out of different powder fractions. The open porosity was between 40 and 41 %. Samples sintered for a longer soaking period of 180 min showed lower open porosity of 39 %. In the metallographic sections no interface between the layers could be seen. The initial Mo powder had a low amount of coarse particles, and after sieving most of them were removed. The remaining powder consists out of fine particles. Therefore it was hard to find a visual difference between the layers. The hardness was measured with 10 kp indentation load and was in the range of 31 HV 10 for samples sintered with 120 min soaking period and 34 HV 10 for samples sintered for 180 min. The increase of the soaking period did not result in much higher hardness.

Some dilatometry measurements of a Mo specimen pressed with 200 MPa helped a little bit more to understand the sintering process of Mo. The green density of the described sample is 6,72  $\text{g}/\text{cm}^3$ . The sintering temperature was 1400 °C with a soaking period of 60 min and the atmosphere was  $\text{H}_2$ . At about 880 °C the sintering process started and the shrinkage of the sample was initiated. The total shrinkage of the sample was 4,63 % in the length. The MS spectroscopy measured the formation of  $\text{H}_2\text{O}$ ,  $\text{N}_2$  and  $\text{CO}_2$  gases. Three distinctive peaks for water have been found, which was related to the reduction of the oxides (Mo surface oxides).

Specimens prepared from the commercially available Mo were sent to ATL for chemical vapour infiltration with Si (CVI). Afterwards, they were sent back to TUW for further investigation (chapter 3.1.3). The weight gain after infiltration was taken by

ATL as an indicator for the silicon concentration, including the clusters of Si sticking on the surface of each specimen. These clusters were observed by TUV and by touching the surface they were removed easily. It seemed that a nucleus was formed at which the Si from CVI nucleated and started to grow in form of clusters which covered irregularly the surface. After removing of the residual Si sticking, some XRF analysis of the cross section of the sample bodies was carried out.

Samples that were CIPed show higher concentration on silicon inside the sample. Samples pressed uniaxially have only two areas (the bottom and top area, i.e. the punch surfaces) with completely accessible open porosity, while the porosity of the area on the side (the die surface) might be partially closed because of the friction (shear) forces during the uniaxial pressing. During the cold isostatic pressing, in contrast, the forces act equally from all directions (without any friction forces). Therefore the pores remain accessible/open from all sides.

Apart from the first sample 1080\_1 it was found that samples after CVI at 925°C show the highest concentration of silicon. Samples after CVI at 825°C show higher concentration of silicon than samples after CVI at 850°C. The reason is that the CVI process for the former samples (825°C) was carried out with lower gas pressure in the reaction chamber but for longer time (360 min instead of 120 min) which can be taken as an indicator that the time plays a more important role for the CVI process than the temperature. Generally, however, the integral Si contents are relatively low. In the LOM images a thin Si layer near the surface and some Si clusters on the surface could be observed. In some specimens no Si area/band could be observed. No correlation between specimen preparation or CVI conditions and the existence of a Si layer could be found.

After first infiltration experiments with liquid Si, insufficient strength of the Mo compacts was observed, and they did not sustain the loads during Si infiltration, i.e. expansion through silicide formation and strongly exothermic reaction. Therefore, higher strength with sound interparticle bonding was needed. In addition to sintering at significantly higher temperatures, also activation of the sintering process was regarded. It has to be mentioned that the addition of Ni is an activation method for sintering but it has to be considered that in fact, Ni lowers the high temperature properties of Mo.

It could be shown in chapter 3.1.5.1.1 for Mo with 0,1 wt% Ni that with increasing sintering temperature the density and hardness could be increased without increasing the content of sintering activator. The open porosity decreased from 47,5 % (1000°C) to 28 % (1300 °C) for Mo specimen with 0,1 wt% Ni. A reference Mo sample without Ni was sintered too. The open porosity of this specimen was 37 % after sintering at 1300 °C.

The influence of the amount of Ni as sintering activator was determined in chapter 3.1.5. Molybdenum from Chemie Metall was mixed with 0,1 wt%, 0,5 wt%, 1 wt% and 5 wt% Nickel from INCO. After blending for 2 h in a tumbling mixer the powders were pressed to rectangular Charpy bars. Sintering was carried out at 1300 °C for 120 min in hydrogen. It was observed that with increasing content of sintering activator the density and hardness (HV10) of the material increased while the open porosity and electrical conductivity were lowered. A specimen out of pure Mo with 7,4 g/cm<sup>3</sup> and ~ 31 % open porosity showed a conductivity of ~ 8,15 Ω<sup>-1</sup>\*mm<sup>-1</sup>. By the addition of 5 wt% Ni the density increased to ~ 9 g/cm<sup>3</sup>, the open porosity decreased to < 1% and also the electrical conductivity decreased to 5,4 · 10<sup>6</sup> Ω<sup>-1</sup>\*m<sup>-1</sup>. The hardness (HV10) could be increased from 61 HV10 measured at pure Mo samples to 271 HV10 at Mo specimens doped with 5 wt% Ni. The impact strength increased from 0,46 J (Mo pure) to 0,75 J (Mo+ 5 wt% Ni). The bending strength was increasing too with higher content of Ni.

In the LOM images it could also be observed that with increasing amount of Ni the pore size decreases. By SEM observation of the fracture surfaces the sintering progress could be described. A green Mo body, pure Mo specimen and Mo with different wt% Ni were investigated. The increase of sintering contacts and their thickness with higher amount of sintering activator could be observed very well. Mo specimens doped with 1 wt% and 5 wt% Ni showed only a very small amount of pores in-between the particles. Their sintering contacts were as big as the grains itself.

In a further experiment it was tried to dope molybdenum with  $\text{NiNO}_3$  dissolved in water instead of Ni (chapter 3.1.5.2). A better distribution of nickel in molybdenum was expected due to dissolving of  $\text{NiNO}_3$  in water. The following liquids/water contained 0,1 wt%, 0,5 wt%, 1 wt% and 5 wt% nickel. The preparation was a time consuming activity and resulted in destruction of the specimens. The prepared powder was hygroscopic and after sintering cracks occurred and destroyed the specimens which made this method impractical.

Molybdenum two layer samples where one layer was doped with 0,1 wt% Ni and the second layer was out of pure Mo were prepared. Furthermore both layers were prepared from different Mo powder fractions. By the addition of Ni as sintering activator and by the difference in powder fraction, gradient porosity specimens were tried to prepare. For comparison, specimens from the same fractions were prepared but without doping with Ni. All specimens were pressed uniaxially with 200 MPa in a cylindrical 20 mm die. Sintering was carried out at 1300 °C for 120 min. In a third experiment undoped two layer samples were sintered instead 120 min for 180 min. It could be observed, that the resulting density, open porosity and HV 10 did not vary in-between the different two layer samples. It made no difference which layers were combined together. A difference was recognised between specimens doped with 0,1 wt% Ni, the undoped ones and the specimens which were sintered with a soaking period of 180 min. The densities of all specimens, where no layer was doped with Ni, were in the range of 6 g/cm<sup>3</sup>. The open porosity was about 40 % and the hardness 30 HV10. Molybdenum specimens which were doped with 0,1 wt% Ni and the ones that were not doped but sintered for 180 min showed very similar values for density, porosity and hardness. In both cases the density was ~ 7 g/cm<sup>3</sup>, the open porosity ~ 30 % and the hardness ~ 60-65 HV 10. Considering the results it can be summarized that by doping Mo with 0,1 wt% Ni the sintering time could be shortened from 180 min to 120 min. Furthermore, to increase the open porosity, another, much coarser powder is needed.

In the metallographic cross sections, cracks were found to occur between some layers. The layer containing Ni as sintering activator might have sintered at different time than the one without Ni, which caused stresses between the layers and they cracked.

Some further experiments with a higher amount of sintering activator were carried out. Again Mo specimens out of two layers were prepared where one layer contained 5 wt% Ni. All layers were built up out of different particle fractions. It could be observed that by the addition of such high amount of sintering activator the density was increased significantly to a value of 7,8 g/ cm<sup>3</sup>. The open porosity decreased to 20 % and the hardness was increased to 210 HV 10 measured in the Mo + 5 wt% Ni layer. Molybdenum specimens doped with 0,1 wt% Ni had a density of ~ 6,7 g/cm<sup>3</sup>, an open porosity of ~ 33% and 50 HV10. Due to the addition of Ni into Mo, the sinterability increased and the density increased too which resulted in a higher shrinkage of the material. However, big cracks occurred between the layers. The specimen was deformed due to the different diameter in the Ni - free and 5 wt% Ni layer.

It could be observed until now, that the size of the pores was still too small for infiltration with Si. Si blocked the pores during infiltration (due to reaction with Mo), and no further penetration of pores was possible. As was observed in the specimens from commercially available Mo, just a very small amount of Si could penetrate and react with Mo. IMSAS reported even that the specimens disintegrated after infiltration due to highly exothermic reaction of Mo with Si and the weak sintering bridges. In the following experiments it was tried to widen the open pores by adding some space holder like an organic wax, or by sintering of a loose powder bed or by sintering of an immersed sponge.

Molybdenum specimens out of two layers with wax as space holder in one layer were prepared (chapter 3.1.6.1). By mixing 3 wt% and 5 wt% of "Hoechst" wax and in a further experiment "Kenolube P 11" wax with Mo (from Chemie Metall) and pressing with 200 MPa, cylindrical bodies of 20 mm diameter were achieved. After a very slow debinding at 600 °C with a cooling and heating rate of 1 °C/ min in N<sub>2</sub> first cracks occurred in specimens mixed with "Hoechst" wax. Specimens which were mixed with 7 wt% and 10 wt% of wax P11 suffered from cracks, too. The sintering process was carried out at 1300 °C for 120 min in H<sub>2</sub>. For the characterisation only specimens with 3 wt% wax and 5 wt% "Kenolube" wax were taken. The density of specimen with 3 wt% wax layer was 7 g/cm<sup>3</sup> and the open porosity 33 %. Comparing to sample with 5 wt% wax layer the density decreased to 6,5 g/cm<sup>3</sup> and the open porosity was increased to 38 %. This specimen was sent for CVI to ATL. During characterisation at TUW of the CV infiltrated body, first cracks could be observed. EDAX with mapping of Mo(L<sub>α</sub>) and Si(K<sub>α</sub>) was carried out, and barely any Si could be found near the surface. Different colours of the cross section could be observed. The hardness analysis gave different HV10 values for the colours. The dark region showed HV10 of 224 and the lighter one 50 - 108. The hardness was not constant within the cross section. A reason is the different distribution of Si due to cracks (which might occur during the debinding process) passing the specimen which might facilitate Si to pass other ways and react on other places than just the surface.

In a further experiment loose powder (gravity) sintered specimens out of Mo and 0 / 0,1 / 0,5 / 1 wt% Ni were prepared (chapter 3.1.6.3). The powder mixture was carefully filled into an Al<sub>2</sub>O<sub>3</sub> cup without pressing and sintered at 1300 °C for 120 min in H<sub>2</sub>. After sintering the density and HV 10 were measured. Samples with 0 wt % Ni and 0,1 wt% Ni were not stable, therefore no hardness could be measured. The open porosity of specimen with 0.5 wt% was 51 % while the hardness was very low at 19 HV 10. Specimen containing 1 wt% Ni had a open porosity of 44 % and a hardness of 45 HV 10. Comparing this specimen to one which was pressed with 200 MPa and sintered at the same conditions it could be observed, that the pressed one had higher densities and the hardness was much higher with 223 HV 10.

This specimen was sent for infiltration to IMSAS. However, during the infiltration process the specimen disintegrated due to weak sintering bridges, as was reported to TUW.

In a further experiment a metal sponge was prepared (chapter 3.1.6.4). A polymer sponge (PU sponge) was dipped into a polymer/powder mixture out of Mo + 0,5 wt% Ni. The sponge was burnt out and the metal skeleton was sintered at 1300 °C for 120 min soaking period in H<sub>2</sub>. After sintering the specimen was very fragile due to Mo<sub>2</sub>C formation and disintegrated by touching.

The reactivity between Mo and Si was very high during the infiltration process. Exothermic reaction destroyed many specimens. Therefore it was tried to prepare porous Mo specimens with different amounts of Si (which reacts during sintering to



form silicides) to lower the reactivity during infiltration (by anticipating part of the reaction and consuming some energy already during the sintering process). The reactivity between Mo and Si should be investigated (chapter 3.2). Rectangular compacts out of Mo with different amounts of Si (0 / 2 / 5 / 10 / 15 / 25 / 37 wt%) were pressed with 150 MPa. The bars were sintered with a Si wafer put on the one side of the surface and sintered at 1300 °C for 8 h in H<sub>2</sub>. That side of specimen where the Si wafer was placed and the opposite side were characterised on the XRD for their phase composition. In the Mo-37 wt% Si specimen, MoSi<sub>2</sub> was detected (on both sides of the specimen). Apart from this result, MoSi<sub>2</sub> was detected only on that side of sample where the Si wafer was placed. In the LOM images a light blue layer from the Si could be observed in some specimens but only near the surface. In Mo specimens containing 0 / 10 wt% Si no layer was observed. Furthermore no silicon could be observed in the centre of the specimens. Some further specimens were sintered at higher temperature of 1420 °C (above the eutectic temperature) for 2 h. Comparing the light microscopy images of both sintering experiments a difference in the Si wafer stability could be observed. After resintering at temperature above the eutectic temperature the top layer was destroyed due to exothermic reaction.

Two layer samples were pressed out of pure Mo as one layer and the second layer was a Mo + 0,5 / 1 / 1,5 / 2 wt % Si. Not only the reactivity but also the sinterability between an Si containing and a pure Mo layer were investigated (diffusion of Si between the layers). The specimens were pressed with 150 MPa in a cylindrical die and sintered at 1300 °C for 4 h in H<sub>2</sub>. After the first sintering, cracks occurred which grew after a second sintering step at 1420 °C (2h in vacuum). In both sintering steps an Si wafer was placed on the surface. In the LOM images a blue Si rich layer could only be observed in specimens containing 1 or 2 wt% Si. No difference in the LOM could be observed between specimens sintered once at 1300 °C for 4 h in H<sub>2</sub> and the ones sintered for a second time at 1420 °C for 2 h in vac. The only difference was that some specimens which were sintered at 1300 °C for 2 h in H<sub>2</sub> were destroyed on the surface due to exothermic reaction. A mapping of one specimen (Mo + 2 wt% Si after sintering at 1420 °C for 2h in vac.) was prepared. The highest Si content is found near the surface, and in the direction of the core less Si can be found.

It could be shown that the sinterability of Mo and Si is very low. The sintered specimens had low mechanical stability, and during preparation a lot of particles broke out. The reactivity between these two elements was examined in a DTA experiment where Mo with 2 / 15 / 37 wt% Si was heated up to 1600 °C (20 K/min) in Argon. Between 1200 - 1300 °C exothermic reaction peaks could be detected. With increasing amount of Si the exothermic peak moved to higher temperatures. It could be observed that a reaction between Mo and Si takes place. As reactivity is given, the problem might be the low sinterability. It can be assumed that reaction between Mo and Si occurs during the heating process, resulting in expansion, formation of Kirkendall pores and of silicides, and the silicides are too inert to respond to sintering.

To increase the sinterability, two experiments were carried out where Mo was mixed with Si in cyclohexane in two ways. This should increase the homogeneity of the mixture by a preceding milling and homogenisation process. The first experiment was carried out in a roller mill with hard metal grinding elements while the second one was carried out in a "Turbula" with steel grinding elements. Molybdenum with 5 wt % Si was mixed on these two ways and after drying pressed to compacts which were sintered afterwards at 1500 °C for 2 h in vacuum. In the LOM images in fig. 3.63 could be seen

that the particles of compacts out of powder prepared in the roller mill were elongated, the ones from the "Turbula" were round but very small.

The density of the sample out of powder prepared in the roller mill was  $5,7 \text{ g/cm}^3$  while the open porosity was 41%. The density of the sample out of powder prepared in the "Turbula" was  $7,1 \text{ g/cm}^3$  and the open porosity was 33%. The hardness with 1 kp indentation load was measured for both samples. The sample which was prepared out of powder mixed in a roller mill showed a hardness of  $69 \pm 4 \text{ HV1}$  while the sample out of powder mixed in a "Turbula" showed a much higher hardness of  $141 \pm 8 \text{ HV1}$ . For the sample out of Mo + 5 wt%Si powder mixed in the roller mill a much lower density and porosity was measured than for the sample out of the same powder but homogenized in a "Turbula". Therefore also the hardness of the sample (roller mill) is much lower. Generally it showed that the treatment in the roller mill changes the shape of the powder particles, apparently in an adverse way, but the sinterability was not noticeably affected by both mixing techniques.

Since pressureless sintering of Mo-Si powder compacts had not yielded satisfactory results, hot pressing/pressure sintering experiments were carried out. Mo specimens with different amounts of Si 3 / 5 / 15 / 37 wt% were mixed and pressure sintered in a hot press at  $1800 \text{ }^\circ\text{C}$  for 2 h in vacuum (chapter 3.2.2). From the resulting cylindrical specimens, rods were cut out in the size range of  $35 * 10 * 7 \text{ mm}$ . The density, open porosity, HV1 and bending strength were measured. With increasing amount of Si in Mo the density and bending strength decreased but the hardness increased to  $1259 \text{ HV 1}$  for the specimen containing 37 wt% Si. Barely any porosity was measured (0-2%), which clearly shows that applying pressure during the reaction between Mo and Si, before a solid silicide skeleton is formed, is a successful way to obtain low porosity specimens. In the XRD could be shown that only in the specimen containing 37 wt% Si some  $\text{MoSi}_2$  was formed (59 %). In the LOM images a thin layer near the surface could be observed. Due to the fact that the specimens were sintered in a carbon die, this layer comes from the carbon that diffused to the material.

A sandwich sample was prepared where one layer was pure Mo, the second one was Mo + 15 wt % Si and the third layer was Mo + 37 wt% Si (3.2.2.2). The sample was sintered at  $1800 \text{ }^\circ\text{C}$  in vacuum applying 50 kN pressure. In the LOM images some cracks could be observed in the 15 wt% Si layer which occurred possibly during the cutting process due to mechanical stresses. The microstructure looked dense, therefore hot pressing seems to be a suitable way to eliminate pores. Apparently the Kirkendall porosity that emerges through the reaction between Mo and Si during pressureless sintering is avoided here, while the pressure is apparently effective in a state of the sintering process in which there is not yet a rigid silicide skeleton. In the SEM images different areas with silicides distributed could be observed. The highest hardness was measured with  $1288 \text{ HV1}$  in the layer with the highest amount of Si (37 wt%) and the hardness decreased with decreasing amount of Si in the Mo layer.

To increase the size of pores even more and reduce the specific surface of the powder particles, Mo specimens out of a very coarse Mo powder were prepared. The Goodfellow Mo ( $< 355 \text{ }\mu\text{m}$ ) was mixed with 1 wt% Kenolube P11 wax and 1 wt% Ni as sintering activator (chapter 3.3.1). The uniaxially pressing was carried out in a cylindrical die with 11,27 mm diameter and 200 MPa. After debinding at  $600 \text{ }^\circ\text{C}$  for 2 h in  $\text{N}_2$ , sintering followed at  $1300 \text{ }^\circ\text{C}$  for 2 h in  $\text{H}_2$ . In the metallographic sections, very coarse pores could be seen and less sintering contacts. The microhardness was measured too. The sintering contacts were weaker with  $287 \pm 26 \text{ HV 0.01}$  than the grains with 340

$\pm 12$  HV 0,01. After Si infiltration by IMSAS such a specimen disintegrated due to the weak sintering bridges.

In a further experiment the reaction vs. infiltration was examined. Specimens described above were taken as such Mo skeleton body and in the first experiment Si powder was pressed on the sample surface and in the second experiment a Si wafer was placed on the surface. After heating up to 1420 °C (> eutectic temperature) and cooling down the specimens were cut and the cross sections were metallographically prepared and characterised on the LOM. It could be seen very easily that the Si powder could penetrate deeper into the specimen, due to the fact that the powder particles were smaller and could fill up better the pores. In both cases the Si did not react as exothermically as to destroy the specimen. Furthermore the infiltration by Si occurred at first before the reaction.

For a better cohesion of the very coarse Mo particles a binder was needed. For this, fine Mo powder with high sintering activity was used. A fine grained Mo powder from Chemie Metall was added in the ratio 50 wt% to 50 wt% coarse Mo from Goodfellow (3.3.1.3). The specimen was pressed with 200 MPa and presintered at 1100 °C for 2 h in H<sub>2</sub> followed by sintering at 1800 °C for 2 h soaking period in vacuum. The density was lower (7,7 g/cm<sup>3</sup>) and the open porosity higher (22,5 %) than the one from Mo specimen out of a fine grained powder. The fracture surface was analysed for the amount of sintering contacts (in [%]) of both specimens. The sample from the mixed powder showed more big pores and less sintering contacts between the particles, therefore the load bearing cross section in the fracture surface was measured as 20 % instead of 60 % in the fine grained one.

Such Mo samples from bimodal powder prepared at TUW were infiltrated with Si by CVI at ATL and in a further experiment at IMSAS. Both specimens were cut along the diameter and investigated by LOM and SEM. In the CVI specimen from ATL a sponge like outer layer in darker grey colour could be observed in the LOM. The EDAX analysis helped to analyse the differently coloured areas. The dark grey one contained about 38 %Si (~MoSi<sub>2</sub>) while the lighter one area contained just 0,5 %Si. There is a clear boundary line between the silicon rich part and the pure Mo. The hardness was 1135  $\pm$  26 HV 0,5 in the Mo containing Si-layer (dark grey appearing) and in the grain it decreased to 169  $\pm$  16 HV 0,5.

In the Mo specimen infiltrated with Si by IMSAS the three different layers that varied in colour and Si content could be observed after cutting along the diameter. The outer layer was the most brittle one, with the highest Si content, the surface tending to spall off due to the exothermic reaction. The core with barely any Si was the most stable part of the specimens. EDAX analysis near the surface showed some diffusion of Si into the particles. Different Mo<sub>x</sub>Si<sub>y</sub> phases were formed. Some parts were containing 36% Si (MoSi<sub>2</sub>), some 16% Si (Mo<sub>5</sub>Si<sub>3</sub>) and in the core of some big particles only 0,3 %Si could be measured, indicating virtually plain Mo. In any case, however, these experiments showed that porous Mo compacts can be infiltrated with liquid Si without disintegration if they have been well sintered. Furthermore, also the use of coarser Mo powder, which results in lower specific surface, may be helpful to better control of the reaction between Mo and the Si melt.

An alternative to the very expensive coarse Mo from Goodfellow was needed. From the literature it was known at least for W that by different temperatures and humidity of H<sub>2</sub> atmosphere during reduction, it is possible to achieve coarse powders. Therefore MoO<sub>2</sub> powder was reduced in dry and wet atmosphere (chapter 3.3.2.1). In dry H<sub>2</sub> atmosphere

the  $\text{MoO}_2$  was reduced between 900 - 1100 °C in 25 °C steps. The lowest oxygen content was achieved by sintering at 1000 °C. Above this temperature the water vapour pressure changed and the reduction of  $\text{MoO}_2$  was not as favoured as before. In the SEM images could be seen that even at the highest reduction temperature the particles did not exceed 5 µm in size. The reduction in humid  $\text{H}_2$  atmosphere was carried out between 900 - 1100 °C but in 50 °C steps. At 1100 °C a second reduction with a higher powder bed was carried out and a third reduction in an  $\text{Ar:H}_2$  atmosphere. It could be seen from the measured oxygen content that powder sintered at 1100 °C in a higher powder bed showed the lowest degree of oxygen (0,39 %). Furthermore the particles are very uniformly distributed but the diameter does not exceed 5 µm. Contrary to results achieved by [37] in the literature, the particles could be coarsen in humid atmosphere.

Related to a work of Haubner et.al. on reduction of W oxides, an experiment with doping of  $\text{MoO}_2$  with LiOH was carried out. It was expected that the powder will coarsen after reduction.  $\text{MoO}_2$  was mixed with 250 ppm LiOH in distilled water (chapter 3.3.2.2). The wet powder was sieved through a 355 µm sieve. After drying of the powder mixture the reduction process was carried out at 1100 °C in wet  $\text{H}_2$  for 2 h. Contrary to the expectations the reduced powder does not coarsen, and the resulting powder particles do not exceed 3 µm. This shows that results obtained with W cannot be directly transferred to Mo.

Another way was to granulate molybdenum (chapter 3.3.2.3). The expectations were that the Mo-Ni granules sinter together through internal densification and the cavities between the granules grow during sintering and form a continuous network of open porosity. Molybdenum was mixed with 1 wt% Camphor and 1 wt% Ni in cyclohexane for 3 h in a tumbling mixer. The mixture was dried in a drying chamber and the resulting powder sieved through a 500 µm sieve. An annealing process at 1000 °C for 2 h was carried out. The SEM images showed a bimodal powder with very fine and some coarser particles that do not exceed 5 µm.

It could thus be shown that it is not possible to coarsen Mo powder by reduction or by doping with LiOH. Even the granulation process did not succeed. Therefore, new possibilities have been searched to increase the powder size.

For this and some economic reasons it was tried to prepare coarse grained Mo powder like the one from Goodfellow from a fine grained one which was commercially available (3.3.3). Fine grained Mo powder from Chemie Metall ( $\leq 63$  µm) was pressed uniaxially at 200 MPa to Charpy bars (55\*10\*10 mm). These bars were sintered at different temperatures of 1200 / 1300 / 1400 / 1500 °C in  $\text{H}_2$  for 2 h. After sintering the bars were crushed in liquid  $\text{N}_2$  and afterwards milled in a knife (coffee) mill. The powder granulate thus obtained was sieved through a  $\leq 355$  µm sieve. It could be shown in the LOM images that the biggest particles were obtained by sintering at 1500 °C in the size range of 300 - 400 µm. Such prepared powder was mixed with 2 wt% wax (Kenolube P11) and pressed at 200 MPa in a cylindrical die with 11,27 mm diameter (3.3.4). After dewaxing at 600 °C for 2 h it was necessary to presinter the sample to prevent any damage to the specimens during moving them between the furnaces. All samples were sintered afterwards in a dilatometer furnace (Bähr 801) at 1500°C for 5 h soaking period in rotary pump vacuum, the heating rate being set at 10 K.min<sup>-1</sup>. The density measured by Archimedes is 5,8 g/cm<sup>3</sup>. The calculation of the open porosity gives a value of 43 % and the one of total porosity gives a value of 44 %, i.e. the porosity is almost fully open, which is the desirable state for infiltration. The microhardness was measured too with 50 g indentation load in the particle cores and also in the sintering bridges. The hardness in the grains was  $165 \pm 10$  HV 0,05 and that measured in the sintering bridges was  $62 \pm 3$  HV 0,05. Of course the indentations in the



bridges do not reveal the hardness of Mo as such since there is always some displacement of Mo during indentation, but the relative hardness of the necks can be regarded as an indicator for their thickness (and thus strength).

Such coarse Mo powder prepared from fine one was mixed with silicon powder from Ecka with varying Si fractions (2 / 5 /10 /15 / 25 / 37 wt% Si) (chapter 3.3.4.3). The powders were mixed dry in a tumbling mixer for 2 h and pressed uniaxially in a cylindrical die ( $\varnothing = 11,27$  mm). Afterwards they were presintered at 1100°C for 2 h in H<sub>2</sub>. Then all samples were sintered at 1800°C in vacuum for 2 h. The resulting density decreased with higher amounts of Si while the open porosity increased. The density decreased due to formation of silicides, which have lower densities, but also to Kirkendall porosity. The measured densities were compared to those calculated for the theoretical density, and it could be shown that the measured densities decreased much more with higher Si content than the theoretical densities. Furthermore with increasing content of Si the mechanical stability of the compacts was lower. With higher Si level more and more particles broke out of the specimens cross section during preparation.

Such specimens were sent to IMSAS for infiltration experiment with Si (chapter 3.3.5.1). After infiltration some cracks could be seen that occurred due to exothermic reaction but in some parts the infiltrated particles could be recognized very well. The elemental maps of the Si and Mo distribution showed two Si layers around the Mo core. The first layer surrounding the Mo core is a Mo<sub>5</sub>Si<sub>3</sub> layer and the outer layer of each particle is a MoSi<sub>2</sub> layer.

The aim of the further experiments was to find the ideal ratio between coarse and fine Mo powder compacts to achieve specimens with coarse open porosity at the same time with stable sintering bridges. In a further experiment (chapter 3.3.5.1) the very coarse powder prepared at TUW was sieved to fractions of < 355  $\mu\text{m}$ , < 250  $\mu\text{m}$  and < 125  $\mu\text{m}$ . Each fraction was mixed with the original fine grained Mo from CM with 90 / 80 / 70 / 60 / 50 wt% coarse powder. After mixing in a tumbling mixer, compacts out of these powders were prepared with 200 MPa compacting pressure and sintered twice: At first at 1300 °C for 2 h in H<sub>2</sub> and afterwards at 1800 °C for 2 h in vacuum. Specimens out of 80 or 90 % of coarse powder mixed with a low amount of the fine grained one, showed the highest amounts of open porosity of 40 - 44 % (comparing all coarse fractions). Their values for the hardness (HV 0,1) were also much higher than the one for specimens out of for example 50 % coarse and 50 % fine grained powder. The hardness of the coarse powder mixtures was about 150 HV 0,1 while the one for the fine coarse fractions with a lot of fine grained powder was about 100-120 HV 0,1. In some LOM images could be observed that specimens prepared from 80 and 90 % of the coarse fraction contain so much coarse particles that the stability between the particles is lower due to lower amount of binder (fine particles). Comparing the results for the open porosity, HV0,1 and the LOM images, satisfying results have been achieved for < 355  $\mu\text{m}$  out of 60 % coarse and 40 % fine particle fraction. The open porosity was about 40 % while the hardness was quite high (compared with other specimens) at 177 HV 0,1. Furthermore, the LOM images showed that there is still enough binder (fine Mo particles) to stabilize the coarse structure.

One part of the work was also the testing of Mo specimens which were infiltrated with Si, in oxidizing atmosphere. Four different FGM specimens were tested in an oxidizing atmosphere out of air and combustion gas. The experiments were carried out in a furnace with an open Al<sub>2</sub>O<sub>3</sub> tube, natural gas was burned by a Bunsen burner at the one end of the tube, and the combustion gases flowed towards the test specimen. The testing

temperature was 1100 °C for 3 h soaking period. All tested specimens were weighed before and after the experiment to gain information about the mass loss during oxidation experiment. In the first experiment a KE laser sintered Mo specimen was tested (3.3.6.1). It was a specimen out of Mo prealloyed with a low amount of Si (~2 %). The weight before the experiment was 15,2322 g and after oxidation 1,2175 g were left. That means that 92 wt% material were lost during oxidation which could be observed by the evaporating  $\text{MoO}_3$  which condensed on cooler parts of the furnace or just outside in a bucket. The remaining specimen was a network out of  $\text{Si}_x\text{O}_y$ . In the stereomicroscope the spongy structure could be observed very well. In any case, the oxidation resistance of this specimen was completely insufficient.

The second specimen was a laser sintered sample from KE but infiltrated with Si - Mg - Al by EPFL. The Mg evaporated during infiltration and Si reacted with Mo. Mg should lower the reactivity between Mo and Si during infiltration. The specimen had a smooth and a rough side. The EDAX analysis showed that the sample consists of molybdenum with silicon (about 10 %), about 8% oxygen and 10% Mg were found. The original weight of the specimen was 46,2805 g. During the oxidation experiment molybdenum evaporated as  $\text{MoO}_3$  from the sample and condensed as  $\text{MoO}_3$  needles on cooler parts of the furnace tube. After exposing the specimen to the oxidising atmosphere a mass loss of 19% was measured. In the stereomicroscope yellow and red coloured areas could be observed on the smooth surface of the specimen. These areas have been characterised on the SEM. In the red region some smooth particles with 10% Mg, in the yellow region some edged particles can be found which look like broken needles. These “needles” contained 12-14% Mg, 2-4% Si, about 30% oxygen and 50% Mo. The rough surface was interspersed with needles which consist out of Si (~35%), about 18% Mo and 46% oxygen (it might be some  $\text{MgMoO}_4$ ). The bulk material in this area contains less silicon (~7,6%), less oxygen (23%) but more Mo (68%) which could be shown on EDAX. In the EDAX analysis three different areas in one grain of a polished cross section could be observed. The core of each grain contained the lowest amount of Si with 2%. The outer part contained the most Si (34%) and oxygen was analyzed too in the elemental maps.

Before oxidation, needles growing out of the sample surface (rough side), were observed. These needles were growing during oxidation and after oxidation experiment the surface was strewn with needles. The average content of Si was low with 11 % which might be too low to form enough protective  $\text{MoSi}_2$ . Furthermore the surface of the particles was not uniformly covered by  $\text{MoSi}_2$  and oxide formation on uncovered particles surface was measured. For this reason Mo in form of  $\text{MoO}_3$  evaporated. The specimen was not sufficiently resistant against oxidation, either.

A third specimen for testing of oxidation resistance was a specimen out of bunched wires of Mo encapsulated in Mo and infiltrated with Si (chapter 3.3.6.5) by IMSAS in Bratislava and sent for oxidation tests to TUW. This specimen showed a mass loss during the oxidation test of only 1,55 %.

The surface of the capsule was characterised on the stereomicroscope before and after the experiment. A crack propagating along the surface in the capsule could be observed before the oxidation experiment. Furthermore the colour of the surface changed after the oxidation tests. The cross section was investigated too. The Mo wires with  $\text{Mo}_5\text{Si}_3$  around the Mo core and  $\text{MoSi}_2$  enclosing the  $\text{Mo}_5\text{Si}_3$  layer could be observed. Some cracks in the  $\text{MoSi}_2$  and  $\text{Mo}_5\text{Si}_3$  layer could be observed. In all cases they stopped propagating before the Mo core. There was no difference in the cross section after the oxidation experiment (compared to the stage before oxidation) observed. Due to the

very low weight loss and the observed cracks in the Mo capsule, the weight loss during the oxidation experiment might come from the capsule not from the infiltrated Mo wires inside the capsule. In this case the oxidation resistance could be regarded as adequate.

The last specimens were hot pressed specimens out of Mo- 3 / 5 / 15 / 25 / 37 wt% Si (chapter 3.3.6.7). Hot pressing was carried out at 1800 °C for 2h in vacuum applying 50 kN pressure. It could be seen easily that with increasing amount of Si in Mo the weight loss was decreasing. Specimen which contained 37 wt% Si lost 5 % of the mass, which is still high concerning that this specimen contains 59 wt% MoSi<sub>2</sub> and 41 wt% Mo<sub>5</sub>Si<sub>3</sub>. In the stereomicroscope could be seen that the molybdenum specimen which contained 3 wt% Si was covered with MoO<sub>3</sub> needles after oxidation while the specimen with the highest amount of Si did not show any change after oxidation.

Parallel to the sintering of Mo specimens, also Nb compacts have been prepared (chapter 3.4) and characterised for their mechanical properties and also for the reactivity with Si. Test specimens from a fine and a coarse Nb powder from H.C. Starck were prepared and characterised after sintering. The powders were pressed uniaxially in a cylindrical die at 200 MPa. The specimens were sintered at 1400 °C for 60 min in vacuum. The dilatometry curves showed that the total shrinkage was about 1,1 % for the fine grained specimen and lower for the coarse one. Nb specimens from powder from H.C. Starck (Amperit 30/10 µm) were prepared and sintered at temperatures between 1350 and 1500 °C in vacuum. The specimens were pressed with 150 / 170 / 200 MPa. It could be shown that with increasing compacting pressure and sintering temperature the density is increasing too. The highest density was achieved for specimens pressed with 200 MPa and sintered at 1500 °C. With increasing density the open porosity decreased and the hardness (HV 10) increased. In the metallographic cross sections barely any difference was observed.

Some experiments about the reactivity between Nb and Si were carried out. Compacts from Nb (out of  $\leq 45$  µm and  $\leq 63$  µm) with 0 / 5 / 10 / 15,5 / 25 / 38 wt% Si were pressed with 200 MPa cold isostatically and sintered at 1500 °C for 120 min. It could be observed that with higher amount of Si in the Nb specimens the density decreased and the open porosity increased. The more Si was in the samples the more was the difference in density between the compact and the theoretical density (calculated from literature). Furthermore, the dimensional change after sintering also depended on the Si content. With more Si the expansion after sintering was larger. I.e. the sintering behaviour of Nb-Si compacts is similar to that of Mo-Si specimens. The electrical conductivity could be measured only in a few specimens which did not crack after sintering. Those were specimens from as-received Nb with different amounts of Si. The higher the content of Si was, the lower was the electrical conductivity, which can be explained by the formation of silicides. Only in specimens containing 5 wt% Si or less some sintering bridges could be observed in the SEM. Specimens containing more Si look like a powder, and no cracked sintering bridges could be found in the fracture surfaces. This explains why the specimens were more difficult to handle with increasing amount of Si. In the LOM images a lot of pores could be seen. A lot of particles broke out during preparation and the specimens were very fragile without high mechanical stability.

DTA/TG analysis was carried out to test the reactivity between Nb and Si due to the fact that low sinterability was observed (chapter 3.4.2). At about 1100 °C exothermic reaction peaks were recorded. With increasing amount of Si in Nb the peaks were

bigger because the exothermic reaction got also more intense, but the occurrence of the exothermic peaks was almost at the same temperature.

Some Nb specimens from coarse Nb from H.C. Starck (Amperit 30/10  $\mu\text{m}$ , 2944) were sent to IMSAS for Si infiltration. The specimens were pressed with 150 MPa and sintered at 1500 °C for 2h in vacuum. The infiltration experiment was carried out in an inductive coupled furnace. It could be observed after infiltration that the exothermic reaction between Nb and Si was so heavy that parts of the specimen were destroyed. In the LOM images a big hole and some dissolved Nb-Si particles could be seen. In the SEM and mapping images the distribution of the Si could be observed. There were different colours of Si distribution according to the reaction of Nb with Si and what was formed. Higher hardness of 140 HV10 was measured in the Si containing part of the specimen. In the centre, where barely any Si could be found, the hardness dropped to 78 HV 10.

Generally it can be said that the reaction between Nb and Si is very exothermic. That is the reason why the specimens which were infiltrated by Si were partly destroyed. On the other hand specimens which were mixed with Si and sintered between 1350 °C - 1500 °C do not suffer from cracks or have been destroyed by the reaction. On the other hand, they sintered barely together and were mechanically not stable.

The sintering behavior of Mo mixed with Nb was characterized since literature is scarce on this topic. Therefore samples out of Mo mixed with different wt% of Nb have been sintered and characterised. Three different sintering profiles were chosen with different sintering temperatures and atmospheres (chapter 3.4.2).

Summarising this chapter it can be said that the sintering of two-layer specimens was quite difficult. The Nb and Mo layers separated during sintering. In specimens which were prepared from powder mixtures of Mo and Nb no difference between green and sintered bodies was observed. The carbon content was quite high for samples containing 80 % Nb and sintered at 1300 ° for 2 h in vacuum (0,5 % C) and the ones presintered at 1100°C for 1 h in H<sub>2</sub> and sintered afterwards at 1300 °C for 2 h in vacuum (0,6 % C). The two-layer specimens from Nb and Mo showed lower values for the carbon content of 0,1 - 0,2%.

The oxygen content was higher for specimens containing more Nb. The plain Nb specimen showed the highest amount of oxygen. With increasing content of Mo the oxygen amount was decreasing. Contrary to expectations the presintering in hydrogen did not decrease the content of oxygen in the specimens, apparently due to “internal getter” effect. I.e. the oxygen which was reduced from molybdenum was caught by Nb and oxidized it. Furthermore it was observed that the sintering profile with presintering at 400 °C for 1 h in H<sub>2</sub> and sintering afterwards at 1300 °C for 2 h in vacuum resulted in the highest amount of oxygen (0,4 % for specimen with 80 % Nb decreasing with increasing amount of Mo). The oxygen content of the two-layer specimens was 0,35 - 0,45 % constantly for all three sintering profiles.

The highest values for the hardness (HV1) were measured for the same specimen that showed already high values for carbon content. It was the specimen containing 80 wt% Nb. All the other values were in the range 50 - 100 HV1. Furthermore the two-layer specimens showed also very similar values for hardness as most Mo/Nb mixed specimens in the range of 50-70 HV1.

These results show that Mo-Nb alloys prepared by the blended elemental approach are tricky to sinter due to the widely different reactivity of Mo and Nb towards interstitials. Nb tends to pick up both C and O much more readily than Mo.



Concluding the work it can be said that it is beneficial to take molybdenum instead of niobium preforms for preparation and furtheron for infiltration with Si. First of all, Mo is much cheaper on the market than Nb. Furthermore it is easier to press compacts out of Mo, there is a cohesion between the particles of the green bodies and the compacts don't disintegrate just by touching. Due to the fact that Nb has to be sintered in very pure vacuum, which is quite difficult to achieve, it is easier and cheaper to sinter Mo compacts in hydrogen (the gas can be adapted easily to the furnace and the gas itself is quite cheap).

Experiments with different particles sizes of Mo powder have been carried out resulting in different open porosities. Subsequent infiltration experiments with Si had shown, that specimens with big open porosity and small surface are needed to reduce the high exothermic reaction and avoid pore blocking during infiltration with Si. Therefore, Mo bodies out of very coarse Mo powder (Goodfellow or prepared out of a fine grained one by pressing, sintering and crushing) are needed. To increase the cohesion between the particles a fine Mo powder should be inserted acting as a binder in the range of 40 % (60 % coarse Mo powder).

In future some work should be focused on finding some interlayers which increase the stability of  $\text{MoSi}_2$  in presence of Mo.

## 5 References

- [1] B. P. Bewlay, M. R. Jackson, J. C. Zhao, P. R. Subramanian: A review of very-high-temperature Nb-silicide-based composites. *Metall. Mater. Trans.* 34A(10), p. 2043 (2003)
- [2] J.H. Schneibel: Beyond Nickel-Base Superalloys. Metals and Ceramics Division Oak Ridge National Laboratory P.O. Box 2008; Oak Ridge, U.S.A. keynote paper from: M. Gupta, T. S. Srivatsan, C. Y. H. Lim, R. A. Varin: Processing and fabrication of advanced materials XIII, Stallion press 2005
- [3] W. G. Fahrenholtz, G. E. Hilmas: NSF-AFOSR Joint Workshop on Future Ultra-High Temperature Materials. UHTM Workshop Report, 2004
- [4] G. Raisoon: Evolution of PM Nickel base superalloys process and products. *Powder Metallurgy* 51(1), p. 10-13 (2008)
- [5] A. Baldan: Progress in Ostwald ripening theories and their applications to the  $\gamma'$  precipitates in nickel-base superalloys – Part II / Nickel-base superalloy. *Journal of Material Science* 37, p. 2379-2405 (2002)
- [6] F. R. N. Nabarro: Rafting in superalloys. *Metall. Mater. Trans.* 27A, p. 513-530 (1996)
- [7] M. Segersäll: Nickel-Based Single-Crystal Superalloys. Licentiate Thesis No. 1568, Linköping University, SE-58183, Linköping, Sweden, 2013
- [8] J. Perepezko: The Hotter the Engine, the Better. *Science* 326, p. 1068-1069 (2009)
- [9] M. R. Jackson, B. P. Bewlay, R. G. Rowe, D. W. Skelly, A. Lipsitt: High - Temperature refractory metal-intermetallic composites. *JOM* 48(1), p. 39-44 (1996)
- [10] N. P. Padture, M. Gell, E. H. Jordan: Thermal barrier coatings for gas - turbine engine applications. *Material Science* 296, p. 280-284 (2002)
- [11] P. A. Hahn, G. Vees, P. Rödhammer: Thermal shock resistance for refractory metals. *Int. J. Refractory Metals & Hard Materials* 12, p. 269-282 (1994)
- [12] B. Fischer, S. Vorberg, R. Völkl, M. Beschliesser, A. Hoffmann: Creep and tensile tests on refractory metals at extremely high temperatures. *Int. J. Refractory Metals & Hard Materials* 24(4), p. 292-297 (2006)
- [13] Gmelin - Handbuch der anorganischen Chemie; Chapter: Vorkommen und Gewinnung von Mo; E. Schön, E. Haller, M. du Maire, Vol. B2; Verlag Chemie GmbH; 1935
- [14] R. R. Dorfler, J. M. Laferty: Review of molybdenum recovery processes. *JOM* 33; p. 48-53 (1981)

- [15] D. J. Jones: Practical aspects of sintering molybdenum and tungsten. *Journal of Less Common Metals* 2, p. 76-85 (1960)
- [16] R. W. Burman: Molybdenum - a super superalloy. *JOM*, p. 12-17 (1977)
- [17] Gmelin - *Handbuch der anorganischen Chemie*; Chapter: Aktiviertes Sintern; F. Benesovsky; Vol. A1; Springer Verlag; 1977
- [18] B. B. Argent, G. J. C. Milne: The physical properties of niobium, tantalum, molybdenum and tungsten. *Journal of Less Common Metals* 2, p. 154-162 (1960)
- [19] S. R. Agnew, T. Leonhardt: The low-temperature mechanical behavior of molybdenum-rhenium *JOM* 10, p. 26-29 (2003)
- [20] M. Endo, K. Kimura, T. Udagawa, T. Tanabe, S. Seto: The effects of doping molybdenum wire with rare earth elements. *Proceedings of the 12th International Plansee Seminar*, Vol 1, p. 37-52 (1989)
- [21] 21 Sondermetalle; <http://21-sondermetalle.de/pdf/Molybdaen.pdf>
- [22] E. R. Braithwaite, J. Haber: *Molybdenum: An Outline of Its Chemistry and Uses*. Elsevier Science Ltd, New York – Amsterdam, 1994
- [23] P. Garg, S.-J. Park, R. German: Effect of die compaction pressure on densification behavior of molybdenum powders. *Int. J. Refractory Metals & Hard Materials* 25, p. 16-24 (2007)
- [24] T. Sakamoto: Sintering Behavior of Mo Powder Compact Applied SPS Spark Plasma Sintering Method. *J. Jap. Soc. Powder Metall.* 44(9), p. 845 – 850 (1997)
- [25] B. Mouawad, M. Soueidan, D. Fabrègue, C. Buttay, V. Bley, B. Allard, H. Morel: Full densification of Molybdenum powders using Spark Plasma Sintering. *Metall. Mater. Trans.* 43A(9), p. 3402 -3409 (2012)
- [26] S. Shankar, L.E. Murr: Heat treatment of explosively consolidated molybdenum: TEM studies. *J. Mater Sci. Lett.* 3, p. 15-17 (1984)
- [27] R. M. German: Heterodiffusion model for the activated sintering of molybdenum. *Journal of Less Common Metals* 58, p. 61-74 (1978)
- [28] Y. Hiraoka, T. Ogusu, N. Yoshizawa: Decrease in yield strength in molybdenum by adding small amounts of group VIII elements. *Journal of Alloys and Compounds* 381, p. 192–196 (2004)
- [29] S. Majumdar, S. Raveendra, I. Samajdar, P. Bhargava, I.G. Sharma: Densification and grain growth during isothermal sintering of Mo and mechanically alloyed Mo–TZM. *Acta Materialia* 57, p. 4158–4168 (2009)

- [30] O. Blaschko, R. Glas, G. Krexner, P. Weinzierl: Neutron small-angle scattering investigation on the sintering of molybdenum powders. Proceedings of the 13th International Plansee Seminar, Vol. 1, p. 531-543 (1993)
- [31] W. Schatt, K.-P. Wieters, B. Kieback: Pulvermetallurgie - Technologien und Werkstoffe. Springer-Verlag Berlin Heidelberg, 2007
- [32] G. An, R. Z. Liu, J. Li, Y.J. Sun, J. Sun: The effect of molybdenum powder micro-morphology on properties of molybdenum products. Proceedings of the 18th International Plansee Seminar, RM 77, (2013)
- [33] A. R. Poster: Factors Affecting the Compaction of Tungsten Powders. Powder Metallurgy 9, p. 301-315 (1962)
- [34] G.-S. Kim, H. G. Kim, D.-G. Kim, S.-T. Oh, M.-J. Suk, Y. D. Kim: Densification behavior of Mo nanopowders prepared by mechanochemical processing. Journal of Alloys and Compounds 469, p. 401–405 (2009)
- [35] Y. Du, L. X. Yang, B. H. Zhao: Effects of EBS lubricants on compaction and sintered P/M molybdenum and tungsten. Proceedings of the 16th International Plansee Seminar; Powder metallurgical high performance materials, p. 619 – 625 (2005)
- [36] S. M. Tuominen, K. H. Carpenter: Powder metallurgy molybdenum: influence of powder reduction processes on properties. JOM 32, p. 23-26 (1980)
- [37] S. Luidold, H. Antrekowitsch: Wasserstoff - ein Reduktionsmittel mit Zukunft. BHM 152(9), p. 292-295 (2007)
- [38] J. Haber: Kinetics and mechanism of the reduction of VIb transition metal oxides and their oxysalts. Journal of Less Common Metals 54, p. 243-261 (1977)
- [39] W. Thöni, P. Gai, P. B. Hirsch: Direct observation of the reduction of MoO<sub>3</sub> at low temperatures. Journal of Less Common Metals 54, p. 263-271 (1977)
- [40] W. V. Schulmeyer, H. M. Ortner: Mechanism of the hydrogen reduction of molybdenum oxides. Int. J. Refractory Metals & Hard Materials 20, p. 261-269 (2002)
- [41] E. Lalik, W. I. F. David, P. Barnes, J. F. C. Turner: Mechanism of reduction of MoO<sub>3</sub> to MoO<sub>2</sub> reconciled. J. Phys. Chem. 105, p. 9153-9156 (2001)
- [42] F. Yang: New ways to make moly as it enters nano-phase production; Metal powder report 59(2), p. 18–21 (2004)
- [43] R. K. Enneti, R. Cook: Extension of Master Decomposition Curves concepts to model reduction of MoO<sub>3</sub> to Mo. Proceedings of the 18th International Plansee Seminar, RM 103/1, (2013)
- [44] G. Dobos, K. V. Josepovits, A. Böröczki, I. Csanyi, G. Hars: Heat treatment of molybdenum under vacuum conditions. Int. J. Refractory Metals & Hard Materials 27, p. 764-767 (2009)



- [45] C. Edtmaier, W.-D. Schubert, C. Gierl, L. Pilz, A. Plankensteiner, K. Huber: Pre-sintering behaviour of Mo-powder. Proceedings of the 18th International Plansee Seminar, RM 97/1, (2013)
- [46] G.-S. Kim, Y. J. Lee, D.-G. Kim, Y. D. Kim: Consolidation behaviour of Mo powder fabricated from milled Mo oxide by hydrogen reduction. J. of Alloys and Compounds 454, p. 327-330 (2008)
- [47] S. H. Kim, D. - G. Kim, Y. I. Seo, Y. D. Kim: Chemical vapour transport process in hydrogen reduction of ball-milled molybdenum and tungsten oxide powders. Rev. Adv. Mater. Sci. 28, p. 141-144 (2011)
- [48] A. V. Savin: Particle growth during the reduction of tungsten and molybdenum and activation of the sintering of these metals. Soviet Powder Metallurgy and Metal Ceramics 7(9), p. 695-698 (1968); Translated from Poroshkovaya Metallurgiya 9(69), pp. 34-38 (1968)
- [49] R. Haubner, W.D.Schubert, E.Lassner, B.Lux: Die Wolframreduktion. Proceedings of the 11th International Plansee Seminar, Vol. 2, p. 161-79 (1985)
- [50] R. Haubner, W. D. Schubert, E. Lassner, M. Schreiner, B. Lux: Mechanism of technical reduction of tungsten: part 1 and part 2. Int. J. Refractory Metals & Hard Materials 2(3+4), p. 108-115 (part 1); p. 156-163 (part 2) (1983)
- [51] H. Hellmer, W.D. Schubert, E. Lassner, B. Lux: Kinetik der Wolframoxid-reduktion. Proceedings of the 11th International Plansee Seminar, Vol. 3, p. 43-86 (1985)
- [52] R. Haubner: Untersuchung der Einflüsse von geringen Konzentrationen an Alkalimetallen, Aluminium, Eisen, Nickel, Phosphor und Silizium auf die Reduktion von WO<sub>3</sub> zu Wolfram mit Wasserstoff. Doctoral Thesis, Technische Universität Wien, 1985
- [53] R. Haubner, W.D. Schubert, E. Lassner, B. Lux: Der Einfluß von Alkalidotierungen auf die Reduktion von WO<sub>3</sub> zu Wolfram. Proceedings of the 11th International Plansee Seminar, Vol. 2, p. 69-97 (1985)
- [54] H. Danninger, G. Jangg, E. Lassner, B. Lux: Einfluss von Fremdelementen auf das Sinterverhalten und die Eigenschaften von Wolfram-Schwermetallen. High Temperatures - High Pressures 13, p. 541 – 548 (1981)
- [55] H. Danninger, W. Pisan, G. Jangg, B. Lux, W. J. Huppmann: The influence of some trace impurities on properties and porosity of tungsten heavy metals. Int. J. Refractory Metals & Hard Materials 5(3), p. 144-152 (1986)
- [56] H. Mayer, E. Lassner, M. Schreiner, B. Lux: Einfluss geringer Konzentrationen von Fremdelementen auf die Wolframreduktion und die Eigenschaften des Wolframpulvers. Proceedings of the 10th International Plansee Seminar; H. M. Ortner ed., Vol. 2, p. 55-79 (1981)

- [57] R. M. German, Z. A. Munir: Enhanced low-temperature sintering of tungsten. *Metall. Mater. Trans.* 7A, p. 1873 (1976)
- [58] C. W. Corti: Sintering aids in powder metallurgy - the role of the platinum metals in the activated sintering of refractory metals. *Platinum Metals Rev.* 30(4), p. 184-195 (1986)
- [59] H. W. Hayden, J. H. Brophy, J. Wulff: The Final Stages of Densification in Nickel-Tungsten Compacts; *Trans. AIME* 224, p. 797 (1962)
- [60] I. J. Toth, N. A. Lockington; The kinetics of metallic activation sintering of tungsten; *Journal of Less Common Metals* 12, p. 353 (1967)
- [61] G. W. Samsonov, W. I. Jakowlev: Activated sintering of tungsten with nickel addition; *Soviet Powder Metallurgy and Metal Ceramics* 6, p. 606 (1967), p. 621 (1962)
- [62] C. Li, R. M. German. The properties of tungsten processed chemically activated sintering; *Metall. Mater. Trans.* 14A, p. 2031 (1983)
- [63] L. Brewer: High strength materials. Ed. V. F. Zacky - J. Wiley, New York, p. 122 (1965)
- [64] M. Lejbrandt, W. Rutkowski: The effect of grain size of nickel activating the sintering of molybdenum. *Planseeberichte Pulvermet.* 25, p. 3-12 (1977)
- [65] C. I. Pascu, A. Stanimir, I. Vida-Simiti: Study about activated sintering of pseudoalloys based on tungsten powder. *Proceedings Euro PM 2009 Copenhagen*; section "PM functional materials", paper no. 160 (2009), on CD
- [66] K. S. Hwang, H. S. Huang: Identification of the segregation layer and its effects on the activated sintering and ductility of Ni-doped molybdenum. *Acta Materialia* 51, p. 3915-3926 (2003)
- [67] M. V. Raevsakya, E. P. Lashuk, E. F. Kazakova, I. G. Sokolova: The interaction between nickel, molybdenum and palladium at 700 °C and 1000 °C. *Journal of Less Common Metals* 99, p. 15-16 (1984)
- [68] K. S. Hwang, H. S. Huang: The liquid phase sintering of molybdenum with Ni and Cu additions. *Materials Chemistry and Physics* 67, p. 92-100 (2001)
- [69] W. Cao, S. Liang, Y. Xue, X. Wang: Investigation on the diffusion behaviour of Mo-Ni interface. *Advanced Material Research* 52-153, p. 1607-1610 (2011)
- [70] J. T. Smith: Diffusion mechanism of the nickel - activated sintering of molybdenum. *J. of Applied Physics* 36(2), p. 595-598 (1965)
- [71] Z. Yao, J. Stiglich, T. S. Sudarshan: Molybdenum silicide based materials and their properties. *JMEPEG* 8, p. 291-304 (1999)

- [72] D. Sturm, M. Heilmaier, J. H. Schneibel, P. Jehanno, B. Skrotzki, H. Saage: The influence of silicon on the strength and fracture toughness of molybdenum. *Material Science and Engineering A* 463, p. 107-114 (2007)
- [73] S. Ignat, P. Sallamand, A. Nichici, A. B. Vannes, D. Grevey, E. Cicala: MoSi<sub>2</sub> laser cladding - a comparison between two experimental procedures: Mo - Si online combination and direct use of MoSi<sub>2</sub>. *Optics & Laser Technology* 33, p. 461-469 (2001)
- [74] J.-Y. Byun, J.-K. Yoon, G.-H. Kim, J.-S. Kim, C.-S. Choi: Study on reaction and diffusion in the Mo-Si system by ZrO<sub>2</sub> marker experiments. *Scripta Materialia* 46, p. 537-542 (2002)
- [75] P. C. Tortorici, M. A. Dayananda: Growth of silicides and interdiffusion in the Mo-Si system. *Metall. Mater. Trans.* 30A, p. 545-550 (1999)
- [76] P. C. Tortorici, M. A. Dayananda : Diffusion structures in Mo vs. Si solid-solid diffusion couples. *Scripta Materialia* 38(12), p. 1863-1869 (1998)
- [77] J.-Y. Byun, J.-K. Yoon, G.-H. Kim, J.-S. Kim, C.-S. Choi: Simultaneous growth mechanism of intermediate silicides in MoSi<sub>2</sub>/Mo system. *Surface and Coatings Technology* 148, p. 128-135 (2001)
- [78] E. Lassner, R. Püschel, F. Benesovsky: Die Diffusion von Silizium in Molybdän. *Planseeberichte Pulvermet.* 16, p. 91 – 103 (1968)
- [79] A. Wiltner, B. Klöden, T. Weißgärber, T. Hutsch, B. Kieback: Reaction temperature of Mo-Si powder mixtures and their influencing factors. *Int. J. Refractory Metals & Hard Materials* 37, p. 73-81 (2013)
- [80] Y. Q. Liu, G. Shao, P. Tsakirooulos: On the oxidation behaviour of MoSi<sub>2</sub>. *Intermetallics* 9, p. 125-136 (2001)
- [81] T. C. Chou, T. G. Nieh: Pesting of the high-temperature intermetallic MoSi<sub>2</sub>. *JOM* 45(12), p. 15-21 (1993)
- [82] T. C. Chou, T. G. Nieh: Comparative studies on the pest reactions of single- and poly- crystalline MoSi<sub>2</sub>. *Scripta Metallurgica* 27, p. 19-24 (1992)
- [83] K. Hellström, J. E. Tang, T. Jonsson, M. Halvarsson, R. Pompe, M. Sundberg, J. E. Svensson: Oxidation behaviour of a (Mo, W)Si<sub>2</sub> - based composite in dry and wet oxygen atmospheres in the temperature range 350-950 °C; *Journal of the European Ceramic Society*, 29 (10), p. 2105 - 2118 (2009)
- [84] S. K. Ramasesha, K. Shobu: Oxidation of MoSi<sub>2</sub> and MoSi<sub>2</sub> based materials. *Bull. Mater. Sci.* 22, p. 769-773 (1999)
- [85] T. C. Chou, T. G. Nieh: New observations of MoSi<sub>2</sub> pest at 500 °C. *Scripta Metallurgica* 26, p. 1637 – 1642 (1992)

- [86] K. Hansson, M. Halvarsson, J. E. Tang, R. Pompe, M. Sundberg, J.-E. Svensson: Oxidation behaviour of a MoSi<sub>2</sub>-based composite in different atmospheres in the low temperature range (400–550 °C). *Journal of the European Ceramic Society* 24, p. 3559–3573 (2004)
- [87] E. W. Lee, J. Cook, A. Khan, R. Mahapatra, J. Waldman: The oxidation resistance of MoSi<sub>2</sub> composites. *JOM* 43(3), p. 54-57 (1991)
- [88] A. A. Sharif: High-temperature oxidation of MoSi<sub>2</sub>; *J. Mater Sci.* 45(4), p. 865-870 (2010)
- [89] S. Melsheimer, A. Rahmel, M. Schütze: Mechanismus der Hochtemperatur-oxidation von Molybdän- und Titandisilizid. *Proceedings of the 13th International Plansee Seminar, Vol. 1*, p. 939-952 (1993)
- [90] K. Hansson, J. E. Tang, M. Halvarsson, R. Pompe, M. Sundberg, J. - E. Svensson: The beneficial effect of water vapour on the oxidation at 600 °C and 700 °C of a MoSi<sub>2</sub>-based composite. *J. European Ceramic Society* 25, p. 1-11 (2005)
- [91] N. Eustathopoulos, R. Israel, B. Drevet, D. Camel: Reactive infiltration by Si: Infiltration versus wetting. *Scripta Materialia* 62, p. 966–971 (2010)
- [92] G. Kaptay, T. Barczy: On the asymmetrical dependence of the threshold pressure of infiltration on the wettability of the porous solid by the infiltrating liquid – *J. Mater. Sci.* 40, p.2531-2535 (2005)
- [93] K. P. Trumble: Spontaneous infiltration of non-cylindrical porosity: Close-packed spheres. *Acta Materialia* 46(7), p. 2363-2367 (1998)
- [94] N. Eustathopoulos: Reactive wetting of liquid metals on ceramic substrates. *Acta Materialia* 44(2), p. 421-426 (2008)
- [95] K. Landry, C. Rado, R. Voitovich, N. Eustathopoulos: Mechanism of reactive wetting: the question of triple line configuration. *Acta Materialia* 45, p. 3079-3085 (1997)
- [96] A. Mortensen, B. Drevet, N. Eustathopoulos: Kinetics of diffusion-limited spreading of sessile drops in reactive wetting. *Scripta Materialia* 36(6), p. 645-651 (1997)
- [97] R. Oro, M. Campos, A. R. Garcia-Cebadera, J. M. Torralba: Liquid phase sintering optimization in PM steels by studying the wetting behavior at high temperature of master alloys on iron substrates. *Proc. PM2010 Powder Metallurgy World Congress, EPMA, Shrewsbury, Vol.2, Section “sintering of Fe - based alloys”, paper no. 336* (2010), on CD
- [98] R. Oro, M. Campos, J. M. Torralba: New alloying systems for PM Steels: opportunities for the Mn-Si master alloys. *Euro PM2013 - special interest seminar - lean steels*, 2013



- [99] E. Bernardo, M. Campos, J. M. Torralba, C. Gierl, H. Danninger, R. Frykholm: Lean steels modified with a new Cu-based master alloy: influence of process parameters in dimensional and sintering behaviour. Proc. Euro PM2013 Gothenburg, EPMA, Shrewsbury, Vol.3, pp.319-324 (2013)
- [100] R. Oro, M. Campos, C. Gierl-Mayer, H. Danninger, J. M. Torralba: Introduction of oxidation-sensitive elements in low alloyed steels using the master alloy route - key aspects for success. Proc. Euro PM2013 Gothenburg, EPMA, Shrewsbury, Vol.3, pp.337-342 (2013)
- [101] R. Henne, W. Weber: Fortschritte in der Entwicklung hochtemperaturgeeigneter Oxidationsschutzschichten für Molybdän unter Einsatz des Unterdruckplasmaspritzverfahrens. DVS-Berichte 130, p. 37 (1990)
- [102] A. R. Cox, R. Brown: Protection of molybdenum from oxidation by molybdenum disilicide based coatings. Journal of Less Common Metals 6, p. 51-69 (1964)
- [103] F. Zamoum, Y. Cartigny, N. David, J. M. Fiorani, R. Podor, M. Vilasi: First development of complex silicide coatings for molybdenum and Mo-base alloys. Proceedings of the 16th International Plansee Seminar, paper RM90, p. 883-895 (2005)
- [104] P. J. Chao, D. K. Priest, J. R. Myers: Recent progress in protective coatings for molybdenum. Journal of Less Common Metals 2, p. 426-442 (1960)
- [105] C. E. Ramberg, P. Beatrice, K. Kurokawa, W. L. Worrell: High temperature oxidation behaviour of structural silicides. Mat. Res. Soc. Symp. Proc. 322, p. 243 (1994)
- [106] W.-Y. Lin, R. F. Speyer: Surface oxidation mechanism of molybdenum in high-temperature, combustion environments. Mat. Res. Soc. Symp. Proc. 322, p. 267 (1994)
- [107] H. Nowotny, R. Kieffer, F. Benesovsky, Combination of silicides and borides (silicoborides) of transition metals, vanadium, niobium, tantalum, molybdenum and tungsten, Planseeberichte Pulvermet. 5, p. 86 (1957)
- [108] H. Nowotny, F. Benesovsky, E. Rudy, A. Wittmann: Aufbau und Zunderverhalten von Niob-Bor-Silicium-Legierungen. Monatshefte für Chemie und verwandte Teile anderer Wissenschaften 91(5), p. 975-990 (1960)
- [109] J. H. Perepezko: Mo-Si-B alloys for ultra-high temperature applications. Proceedings of the 18th International Plansee Seminar, RM 24/1, (2013)
- [110] R. Sakidja, J. H. Perepezko, S. Kim, N. Sekido: Phase stability and structural defects in high-temperature Mo-Si-B alloys. Acta Materialia 56, p. 5223-5244 (2008)
- [111] J.H. Perepezko, R. Sakidja, S. Kim and J.S. Park: Multiphase Microstructures and Stability in High Temperature Mo-Si-B Alloys. Structural Intermetallics, Eds. K.J. Hemker, D.M. Dimiduk, H. Clemens, R. Darolia, H. Inui, J.M. Larsen, V.K. Sikka, M. Thomas and J.D. Whittenberger, (TMS, Warrendale, PA) p. 505 (2001)

- [112] J. H. Schneibel, R. O. Ritchie, J. J. Kruzic, P. F. Tortorelli: Optimization of Mo-Si-B Intermetallic Alloys. Metall. Mater. Trans. 36A, p. 525-531 (2005)
- [113] M. G. Mendiratta, T. A. Parthasarathy, D. M. Dimiduk: Oxidation behaviour of  $\alpha$ Mo-Mo<sub>3</sub>Si-Mo<sub>5</sub>SiB<sub>2</sub> (T2) three phase system. Intermetallics 10, p. 225-32 (2002)
- [114] P. Jéhanno, M. Heilmaier, H. Kestler, M. Böning, A. Venskutonis, B. Bewlay, M. Jackson: Assessment of a powder metallurgical (PM) processing route for refractory metal silicide alloys. Metall. Mater. Trans. 36A, p. 515-524 (2005)
- [115] J.S. Park, R. Sakidja and J.H. Perepezko: Coating Designs for Oxidation Control of Mo-Si-B Alloys. Scripta Materialia 46, p. 765 (2002)
- [116] M. Akinc, M. K. Meyer, M. J. Kramer, A. J. Thom, J. J. Huebsch, B. Cook: Boron-doped molybdenum silicides for structural applications. Intermetallics 261, p. 16-23 (1999)
- [117] M. Krüger, S. Franz, H. Saage, M. Heilmaier, J. H. Schneibel, P. Jéhanno, M. Böning, H. Kestler: Mechanically alloyed Mo-Si-B alloys with a continuous  $\alpha$ -Mo matrix and improved mechanical properties. Intermetallics 16, p. 933-941 (2008)
- [118] H. Kestler, M. Heilmaier, P. Jéhanno, L. Sigl: Mo-Si-B alloys for ultrahigh temperature structural applications: powder-metallurgical processing as the key for an optimum balance of properties. Proc. Euro PM2009 Copenhagen, EPMA, Shrewsbury, paper no.914, p. 369-374 (2009)
- [119] S. Burk, B. Gorr, H.-J. Christ: High temperature oxidation of Mo-Si-B alloys: Effect of low and very low oxygen partial pressure. Acta Materialia 58, p. 6154-6165 (2010)
- [120] M. Heilmaier, D. Schliephake, M. Krüger: Microalloying of Mo-Si alloys as a key for the development of ultrahigh temperature Mo - Borosilicide alloys. Proceedings of the 18th International Plansee Seminar 2013, RM 18, (2013)
- [121] M. Krüger, D. Schliephake, P. Jain, K. S. Kumar: Effects of Zr additions on the microstructure and the mechanical behavior of PM Mo-Si-B alloys. JOM 65(2), p. 301-306 (2013)
- [122] N. P. Bansal, R. H. Doremus: Handbook of glass properties, Academic Press; Orlando, FL, 1986
- [123] S. Paswan, R. Mitra, S. K. Roy: Oxidation behaviour of the Mo-Si-B and Mo-Si-B-Al alloys in the temperature range of 700 - 1300 °C. Intermetallics 15, p. 1217-1227 (2007)
- [124] R. Sakidja, J. S. Park, J. Hamann, J. H. Perepezko: Synthesis of Oxidation Resistant Silicide Coatings on Mo-Si-B Alloys. Scripta Materialia 53, p. 723 (2005)
- [125] J. Januschewsky, S. Engelhardt, I. Dreiling, M. Kathrein, L.S. Sigl: Long-term behaviour of SIBOR® - an oxidation protection system for Mo and its alloys. Proceedings of the 18th International Plansee Seminar, RM 62, (2013)

- [126] H. P. Martinz, M. Sulik: Oxidation protection of refractory metals in the glass industry. *Glass Science and Technology: Glastechnische Berichte* 73(2), p. 299- 304 (2000)
- [127] P. Jehanno, M. Heilmaier, H. Kestler: Characterization of an industrially processed Mo-based silicide alloy. *Intermetallics* 12(7-9), p. 1005-1009 (2004)
- [128] H. P. Martinz, B. Nigg, J. Matej, M. Sulik, H. Larcher, A. Hoffmann: Properties of the SIBOR oxidation protective coating of refractory metal alloys. *Int. J. Refractory Metals & Hard Materials* 24(4), p. 283-291 (2006)
- [129] H. P. Martinz, B. Nigg, J. Matej, M. Sulik, H. Larcher: The glass related properties of the SIBOR oxidation protective coating on molybdenum alloys. *Advanced Materials Research* 39-40, p. 613-618 (2008)
- [130] M. K. Meyer, M. Akinc: Isothermal Oxidation Behavior of Mo-Si-B Intermetallics at 1450°C, *Journal of the American Ceramic society* 79 (10), p. 2763-2766 (1996)
- [131] H. R. Z. Sandim, A. F. Padilha, V. Randle: Grain growth during sintering of pure niobium. *Proceedings of the 16th International Plansee Seminar 2005*, RM 70, p. 684-695 (2005)
- [132] G. Aggarwal, I. Smid: Powder injection molding of niobium. *Material Science Forum* 475-479, p. 711-716 (2005)
- [133] K. D. Zilnyk, G. S. Leite, H R. Z. Sandim: Pore-boundary interaction in sintered niobium. *Proceedings of the 18th International Plansee Seminar 2013*, RM 49/1 (2013)
- [134] K. Schulze, M. Krehl, G. Petzow: The influence of gas atmospheres on the first-stage sintering of high-purity niobium powders. *Metall. Mater. Trans.* 15A(6), p. 1111-1116 (1984)
- [135] M. V. Zakharov, A. M. Zakharov: High temperature strength alloys. *Metallurgija*, p. 331-335 (1972)
- [136] E. A. Loria: Niobium-base superalloys via powder metallurgy technology. *JOM* 39(7), p. 22-26 (1987)
- [137] E. N. Sheftel, O. A. Bannykh: Niobium - base alloys. *Int. J. Refractory Metals & Hard Materials* 12, p. 303-314 (1994)
- [138] M. R. Jackson, R. G. Rowe, D. W. Skelly: Oxidation of Some Intermetallic Compounds and Intermetallic Matrix Composites. *Mater. Res. Soc. Symp. Proc.* 364, pp. 1339-44. (1995)
- [139] O. Kubaschewski, B.E. Hopkins: Oxidation mechanisms of niobium, tantalum, molybdenum and tungsten. *Journal of Less Common Metals* 2, p. 172-80 (1960)

- [140] B. W. Bewlay, M. R. Jackson, J.-C. Zhao, P. R. Subramanian, M. G. Mendiratta, J. J. Lewandowski: Ultrahigh-Temperature Nb-Silicide-Based Composites. *MRS Bull.* 28, p. 622 (2003)
- [141] B. P. Bewlay, M. R. Jackson, J.-C. Zhao, P. R. Subramanian: A review of very-high-temperature Nb-silicide-based composites. *Metall. Mater. Trans.* 34A, p. 2043 (2003)
- [142] B.P. Bewlay, M.R. Jackson, H.A. Lipsitt: The balance of mechanical and environmental properties of a multielement niobium-niobium silicide-based in situ composite. *Metall. Mater. Trans.* 27A, pp. 3801–08 (1996)
- [143] K.S. Chan: Alloying effects on fracture mechanisms in Nb-based intermetallic in-situ composites. *Mater. Sci. Eng.* A329–A331, p. 513–22 (2002)
- [144] Y. Murayama, S. Hanada: High temperature strength, fracture toughness and oxidation resistance of Nb–Si–Al–Ti multiphase alloys. *Sci. Technol. Adv. Mater.* 3, p. 145–56 (2002)
- [145] P. R. Subramanian, M. G. Mendiratta, D. M. Dimiduk, M. A. Stucke: Advanced intermetallic alloys - beyond gamma titanium aluminides. *Materials Science and Engineering A* 239-240, p. 1-13 (1997)
- [146] K.S. Chan, D.L. Davidson: Effects of Ti addition on cleavage fracture in Nb–Cr–Ti solid-solution alloys. *Metall. Mater. Trans.* 30A, p. 925-39 (1999)
- [147] W. Y. Kim, H. Tanaka, A. Kasama, S. Hanada: Microstructure and room temperature fracture toughness of Nbss/Nb5Si3 in situ composites. *Intermetallics* 9(9), p. 827–834 (2001)
- [148] W. Y. Kim, H. Tanaka, S. Hanada: Microstructure and high temperature strength at 1773 K of Nbss/Nb5Si3 composites alloyed with molybdenum. *Intermetallics* 10, p. 625–634 (2002)
- [149] K. Chattopadhyay, R. Mitra, G. Balachandran, K. K. Ray: Effect of Mo on microstructure and mechanical behaviour of as-cast Nbss-Nb5Si3 composites. *Intermetallics* 14(12), p. 1452-1460 (2006)
- [150] C. L. Ma, J. G. Li, Y. Tan, R. Tanaka, S. Hanada: Microstructure and mechanical properties of Nb/Nb5Si3 in situ composites in Nb–Mo–Si and Nb–W–Si systems. *Materials Science and Engineering A* 386, p. 375–383 (2004)
- [151] T. Nakano, Y. Nakai, S. Maeda, Y. Umakoshi: Microstructure of duplex phase NbSi2(C40)/MoSi2(C11b) crystals containing a single set of lamellae. *Acta Materialia* 50, p. 1781–1795 (2002)
- [152] L.T. Zhang, O. Zhu, F. Zhang, A.D. Shan, J.S. Wu: High-temperature oxidation of Mo-rich (Mo<sub>1-x</sub>Nb<sub>x</sub>)Si<sub>2</sub> pseudo-binary compounds. *Scripta Materialia* 57, p. 305–308 (2007)
- [153] K. Chattopadhyay, R. Mitra, K. K. Ray: Nonisothermal and isothermal oxidation behavior of Nb–Si–Mo alloys. *Metall. Mater. Trans.* 39A, p. 577 – 592 (2008)



- [154] D. Yao, J. Yang, W. Gong, C. Zhou; Interdiffusion behavior between Nb and MoSi<sub>2</sub> intermetallic compound; Materials Science and Engineering A 527, p. 6787–6793 (2010)
- [155] Y. T. Zhu, M. Stan, S. D. Conzone, D. P. Butt: Thermal oxidation kinetics of MoSi<sub>2</sub>-based powders. J. Am. Ceram. Soc. 82(10), pp. 2785-2790 (1999)
- [156] M. Z. Alam, B. Venkataraman, B. Sarma, D. K. Das: MoSi<sub>2</sub> coating on Mo substrate for short-term oxidation protection in air. Journal of Alloys and Compounds 487, pp. 335-340 (2009)
- [157] M. Dlapka, C. Gierl, H. Danninger, H. Altena, G. Stetina, P. Orth: Porosity effects in low pressure carburizing of sintered steels; Proc. PM2010 Florence, EPMA, Shrewsbury, Vol. 2, p. 459-466 (2010)
- [158] H. Danninger, D. Spoljaric, G. Jangg, B. Weiss, R. Stickler; Characterization of pressed and sintered ferrous materials by quantitative fractography. Pract. Metallography 31 No.2, p.56-69 (1994)
- [159] R. Haubner, W.D. Schubert, E. Lassner, B. Lux; Der Einfluß von Alkalidotierungen auf die Reduktion von WO<sub>3</sub> zu Wolfram; 11th Int. Plansee Seminar '85, Mai 1985, Reutte, Proc. Vol.2, 69-97 (1985)
- [160] H. Danninger; Einfluß der Herstellungsbedingungen auf die Eigenschaften von Wolfram-Schwermetallen, Dissertation, Technische Universität Wien (1980)
- [161] J. A. Rodriguez, J. C. Hanson, S. Chaturvedi, A. Maiti, J. L. Brito; Phase transformations and electronic properties in mixed-metal oxides; J. of Chemical Physics; Vol. 112; 2; 2000; p. 935-945
- [162] F. Chu, D. J. Thoma, K.J. McClellan, P. Peralta; Mo<sub>5</sub>Si<sub>3</sub> single crystals: physical properties and mechanical behaviour; Material Science and Engineering; Vol. 261; 1999; p. 44-52
- [163] A. Misra, J. J. Petrovic, T. E. Mitchell; Microstructures and mechanical properties of a Mo<sub>3</sub>Si-Mo<sub>5</sub>Si<sub>3</sub> composite; Scripta Materialia; Vol. 40; 2; 1999; p. 191-196
- [164] W. Schatt: Pulvermetallurgie, Sinter- und Verbundwerkstoffe. 2<sup>nd</sup> Ed., DVG, Leipzig (1985) p.180

## 6 List of abbreviations

ATL - Archer Technicoat Ltd.; Progress Road, Sands Industrial Estate, High Wycombe, HP12 4JD, UK; Partner of Siltrans project - CVI specialist

BSE - Back Scattered Electrons

CM - Chemie Metall; company from which molybdenum powder was purchased

CVI - Chemical Vapour Infiltration

DTA - Differential Thermal Analysis

EDAX - EDS (Energy Dispersive Spectroscopy) analysis system for SEM X-Ray Microanalysis

EPFL - École Polytechnique Fédérale de Lausanne; Route Cantonale, 1015 Lausanne, Switzerland; Partner of Siltrans Project

GF - Good Fellow; company from which coarse molybdenum powder was provided

HIP - Hot Isostatic Pressing

HP - Hot Pressing

HV - Hardness measured with Vickers indentation method

IFAM - "Fraunhofer-Institut für Fertigungstechnik und Angewandte Materialforschung"; Winterbergstraße 28, 01277 Dresden, Germany; Partner of Siltrans Project

IMSAS - "Slovak Academy of Sciences / Institute of Materials & Machine Mechanics"; Račianska 75; 83102 Bratislava; Slovak Republic

LOM - Light Optical Microscopy

MPa - Megapascal

SE - Secondary Electron(s)

SEM - Secondary Electron Microscopy

TG - ThermoGravimetry

TUW - Vienna University of Technology; Getreidemarkt 9; 1060 Wien, Austria

XRD - X-Ray Diffraction

## Curriculum vitae

### **Personal data:**

Academic degree: Dipl.-Ing  
Name: Ewa Dadal  
Date of birth: 30.06.1985  
Place of birth: Mielec/Poland  
Citizenship: Austria  
Matrinal status: unmarried  
E-Mail: ewa.dadal@gmail.com  
Tel. Nr.: 0699 10329890  
Address: Davidgasse 41/12  
1100-Vienna



### **Study:**

02/2010 - Ph.D. thesis in Technical Chemistry at Vienna University of Technology

estimated 02/2014 Doctoral studies at the Institute of Chemical Technologies and Analytics of Vienna University of Technology under the supervision of *Univ.Prof. Dipl.-Ing. Dr.techn. Herbert Danninger* with the title: „*Micro and Nanocrystalline Silicide - Refractory Metals FGM for Materials Innovation in Transport Applications*“

02/2009 - 02/2010 Diploma thesis at the Institute of Chemical Technologies and Analytics of Vienna University of Technology under the supervision of *Ao.Univ.Prof. Dipl.-Ing. Dr.techn. Walter Lengauer* with the title: „*Oxide ceramics for special bearing applications*“ for SKF Steyr

10/2003 - 02/2010 University study of Technical Chemistry - branch of study: Materials Technology and Analytics at Vienna University of Technology

**Elementary education:**

1995 - 2003	Gymnasium "Albertgasse 8" graduated with "Matura"
1993 - 1995	3 and 4 grade Volksschule in Vienna, Austria
1992 - 1993	First grade Volksschule in Poland, second grade skipped

**Other training:**

03/2012	"PM Sintering - Advanced Processes and Materials Course 2012" Helsingborg, Schweden
06/2011	"Powder Metallurgy Training Courses 2011 of European Powder Metallurgy Association (EPMA)" Dresden, Germany
2011 - now	Member of the European Powder Metallurgy Association (EPMA)

**Traineeship:**

10/2008	Project study in anorganic technologies in the research group of metallurgy under the supervision of <i>Ao.Univ.Prof.</i> <i>Dipl.-Ing. Dr.techn.</i> Walter Lengauer, Vienna University of Technology
08/2008	Project study in anorganic technologies in the research group of high-performance ceramics under the supervision of <i>Dipl.-Ing. Dr.techn.</i> Antje Liersch, Vienna University of Technology

**Professional experience:**

01/2009 - 12/2013	Research scientist at Vienna University of Technology
2003-2009	Employment during the studies: sale at "Ströck GmbH"; "Event Company Hasil & Opitz"; sale at Blaschek GmbH; Promotion at "All-in-Marketing";



	Organizational activities during Annual General Meetings -
"MSS	GmbH"
08/2008	Traineeship in a cement factory "SECIL" in Outao, Portugal Activity: Laboratory work
02/2009 - 02/2010	Employed by "SKF AG" Activity: Diploma thesis

### **Scientific publications:**

#### ***papers***

- "Oxide ceramics for special bearing applications - Oxidkeramiken für spezielle Kugellager- Anwendungen" report for SKF Science Report; 2009; 8 S.

#### ***poster presentations***

- Ewa Dadal, Christian Gierl, Herbert Danninger; Lucia Sencekova, Karol Izdinsky, Frantisek Simancik: "*Manufacturing of Mo preforms with defined porosity for subsequent reactive infiltration*"; Poster: 18<sup>th</sup> Plansee Seminar 2013, Reutte; 3-7. 6. 2013
- Ewa Dadal, Christian Gierl, Herbert Danninger; Lucia Sencekova, Karol Izdinsky, Frantisek Simancik: "*Manufacturing of Si infiltrable PM molybdenum preforms with varying porosity characteristics*"; Poster: Euro PM2013 ,Göteborg; 15-18. 9. 2013

### **Languages**

- Polish: native language
- German: 2. native language
- English: fluently
- Spanish: basic knowledge

### **Computer literacy skills**

- Microsoft Office (Word, Excel, Power Point)

### **Other**

- driving licence (B)

### **Hobbies**

Sports, hiking, traveling

---